Communications of the Byurakan Astrophysical Observatory

Բյուրականի աստղադիտարանի հաղորդումներ

Communications of BAO, Vol. 71, Issue 2, 2024, pp. 215-229

Influence of gas-dynamic flows on the evolution of line spectra in a medium with non-stationary energy sources

A. Nikoghossian*

NAS RA V.Ambartsumian Byurakan Astrophysical Observatory, Byurakan 0213, Aragatsotn Province, Armenia

Abstract

The theory we developed in previous papers on temporal variations in the spectral line profiles formed in the media with nonstationary energy sources is generalized to take into account the influence of stochastic velocity fields. The radiation transfer problem is treated for the case of completely incoherent scattering. The limiting regimes of micro- and macro-turbulence are considered under the assumption that the gas-dynamic velocity is described by a Markov process. Comparison of the characteristic features of the evolution of spectral line profiles in these two cases with that observed in the absence of turbulence allows us to make an idea of the nature of turbulence and the values of various parameters describing the primary energy sources and optical properties of the medium.

1. Introduction

Many of the astrophysical objects of considerable interest are known to be far from the state of equilibrium. A great variety of nonstationary phenomena is observed, differing from each other both in their scales and durations. A far from exhaustive list of such objects includes evolution of the shells formed by Novas and Supernovas bursts, solar CMEs and chromospheric outbursts, flare stars, and FUor-like phenomena. Interest in this kind of phenomena is increasing in view of the emergence of new more precise observational capabilities providing sufficiently informative photometric and spectrophotometric data. Spectroscopic studies of sources exhibiting nonstationary manifestations are crucial, as the line profile shapes offer rich information about the physical processes that are occurring at their current stage of evolution.

In a series of papers (Nikoghossian, 2021a,b, 2022a,b, 2023) we considered a range of different physical factors which can make some contribution in the course of the lines evolution such as inhomogeneity of the medium, localization of primary energy sources, scattering and absorption in the continuum, frequency redistribution, etc. In all of these problems, the non-stationarity was assumed to be due to time variations of the energy sources illuminating the medium. The temporal characteristics of the incident radiation were given by the functional forms of either the Dirac delta function or the Heaviside H-function. The importance of the relationships of these two types is obvious: the first one simulates phenomena of short-term explosive character of the type of Nova explosions, and the second one mimics the evolutionary path of the equilibrium state establishment at the inclusion of a more or less constantly acting energy source of the type of FUor-like phenomena or the case of Her Nova 1934 (Gorbatskii & Minin, 1963, Sobolev, 1985). In all of the mentioned cases the active medium is supposed to be static, i.e., it is considered that the structure and dynamics of the medium do not change under the influence of primary energy sources. Meanwhile, in astrophysical context, it is reasonable to assume that at the specified temporal characteristics, assuming a sudden crossing of the boundary of the medium-energy front, one should lead to the appearance of gas-dynamic currents and a field of fluctuating velocities in it, which is actually equivalent to the appearance of turbulent motions. The latter certainly affects the shape of the observed spectrum and its evolution. This paper

*nikoghoss@yahoo.com

doi: https://doi.org/10.52526/25792776-24.71.2-215

is devoted to the study of these questions. We abstract questions related to energy dissipation or to possible changes in the physical characteristics of the medium under consideration and its dynamics during the evolution of the spectra.

We start with the formulation of the time-dependent model problem under consideration. The basic equations are given with a description of the solution methods used. The next section presents numerical results. Their physical interpretation and consequences are given in the final section.

2. Statement of the problem. Solution methods

As in recent works, we consider, for expository reasons, a 1D absorbing and scattering atmosphere of finite optical thickness τ_0 calculated in the center of a given spectral line. One of its boundaries, e.g., $\tau = 0$, is illuminated by the continuous radiation flux $I_0(t)$, which varies in time according to the above-mentioned laws of $\delta(t)$ or $H(t)$ functional forms. When passing through the medium, the radiation in the spectral line is scattered with the probability λ and is also absorbed in the continuous spectrum. The probability of this latter process is described by the value of β given by the ratio of the absorption coefficient in the continuous spectrum to that in the center of the spectral line. The scattering is assumed to be completely incoherent and the frequency redistribution law may be written in the form

$$r(x', x) = \alpha_0\left(x'\right)\alpha_0\left(x\right), \tag{1}$$

where $\alpha_0\left(x\right) = \pi^{-1/4}\alpha\left(x\right)$, and $\alpha\left(x\right)$ is the profile of the absorption coefficient of the spectral line.

In the present work, calculations are carried out for the Doppler profile of the absorption coefficient $(1/\sqrt{\pi})\exp(-x^2)$. The classical problem of diffuse reflection and transmission is posed and solved under the assumption of homogeneous turbulence in the medium (Bellman & Wing, 1973). We are interested in the line-transfer problem to find out the influence of different types of gas-dynamic motions on the shapes of spectral line profiles observed in the resulting reflection and absorption spectra and on the character of their evolution with time. To this end, it is sufficient to limit ourselves to considering two extreme mutually opposite regimes of micro- and macro-turbulence and to compare the results obtained with those obtained in the absence of turbulence. Consideration of a more general problem at intermediate values of the correlation length, which leads to some mathematical complications and was solved in Nikoghossian (2017), is not essential for our goal, especially since often the transition between two limiting regimes in some cases occurs in a sufficiently narrow interval of change of the specified length (Nikoghossian, 2007).

The evolution of spectral lines in the absence of turbulent motions in the medium under the assumption of complete redistribution over frequencies, we considered in Nikoghossian (2022a). Therefore, the results obtained there will serve as a basis for identifying effects due to gas-dynamic motions. At the same time, as in the above work, we use the same method based on the construction of Neumann series to solve the problems. The method dates back to the works of Ganapol (1979), Matsumoto (1967, 1974). We will see below that the Neumann series allows one to construct easily solutions of the corresponding more general problems taking into account turbulence. This is an additional advantage of the method, which is due to the fact that in both cases one starts with the same Neumann expansion for the stationary problem constructed in the above cited paper. In the homogeneous problems it is a series in powers of λ so that for the reflection and transmission coefficients $\rho(x', x, \tau_0)$ and $q(x', x, \tau_0)$ we have

$$\rho\left(x', x, \tau_0\right) = \sum_{n=1}^{\infty}\rho_{\mathrm{n}}\left(x', x, \tau_0\right)\lambda^n, \qquad q\left(x', x, \tau_0\right) = \sum_{n=1}^{\infty}q_{\mathrm{n}}\left(x', x, \tau_0\right)\lambda^n. \tag{2}$$

where x' and x are the dimensionless frequencies (measured in terms of Doppler widths) of incident quantum and reflected or transmitted quanta. Each term of the Neumann expansions obviously have a probabilistic meaning similar to that of reflection and transmission coefficients, relating however to a certain fixed number of scattering events n. Recall that the coefficients in the Neumann expansions we find using the invariant imbedding technique (Bellman & Wing, 1973, Casti & Kalaba, 1976)

doi: https://doi.org/10.52526/25792776-24.71.2-215

and the recurrence method for their determination we suggested in Nikoghossian (1984). In the case of a medium of finite optical thickness we consider, each stage of application of the above method mathematically is reduced to solving some initial-value problem. The discussion of the accuracy of the construction of the corresponding series in Nikoghossian (2022a) remains valid in our problems, and we will not dwell on it here.

The corresponding Eq.(2) Neumann series for spectral line profiles in the absence of turbulence is written in the form

$$R\,(x,\tau_0) = \sum_{n=1}^{\infty} R_n\,(x,\tau_0)\lambda^n, \qquad Q\,(x,\tau_0) = \sum_{n=1}^{\infty} Q_n\,(x,\tau_0)\lambda^n. \tag{3}$$

In the limiting case of micro-turbulence, when the correlation length tends to zero, the absorption coefficient profile in the spectral line $\alpha(x)$ is transformed as follows.

$$\omega\,(x) = \int_{-\infty}^{\infty} \alpha\,(x-u)P\,(u)\,du, \tag{4}$$

where $\omega(x)$ and α are the profile of the absorption coefficients correspondingly in turbulent and static atmospheres, $P(u)$ is the distribution function of turbulent velocities u which under the assumption of a Gaussian velocity distribution has the form

$$P\,(u) = \frac{1}{\sqrt{\pi}u_t}\exp(-u/u_t)^2, \tag{5}$$

where u_t is the mean hydrodynamic velocity measured in terms of thermal speed. In the case of Dopplerian profile, Eq.(1) leads to known result which is the sum of two variances (see also, Gray, 1978).

$$\omega\,(x) = \frac{1}{\sqrt{1+u_t^2}}\exp\left(-\frac{x^2}{1+u_t^2}\right), \tag{6}$$

Thus, the whole course of reasoning carried out in Nikoghossian (2022a), remains in force in the case of micro-turbulence with the replacement of $\alpha(x)$ by $\omega(x)$, while an additional parameter u_t appears. For each of given values of this parameter, the Neumann series is constructed as has been done in the mentioned paper. By introducing the notations R_n^{mic} and Q_n^{mic} for the obtained coefficients, similarly to Eq.(3) we can write

$$R_{mic}\,(x,\tau_0) = \sum_{n=1}^{\infty} R_n^{mic}\,(x,\tau_0)\lambda^n, \qquad Q_{mic}\,(x,\tau_0) = \sum_{n=1}^{\infty} Q_n^{mic}\,(x,\tau_0)\,\lambda^n. \tag{7}$$

Turning to the limiting case of infinite correlation length (macro-turbulence), we note that now it is the spectral line profile that undergoes transformation Eq.(3) (see, for instance, Bellman & Wing, 1973)

$$R_n^{mac}\,(x,\tau_0) = \int_{-\infty}^{\infty} R_n\,(x-u)P\,(u)\,du, \qquad Q_n^{mac}\,(x,\tau_0) = \int_{-\infty}^{\infty} Q_n\,(x-u)P\,(u)\,du, \tag{8}$$

and

$$R_{mac}\,(x,\tau_0) = \sum_{n=1}^{\infty} R_n^{mac}\,(x,\tau_0)\,\lambda^n, \qquad Q_{mac}\,(x,\tau_0) = \sum_{n=1}^{\infty} Q_n^{mac}\,(x,\tau_0)\,\lambda^n. \tag{9}$$

From the point of view of further exposition, the frequency distribution of the coefficients in the Neumann series for spectral line profiles can be obtained from Figs. (1), (2) for lines formed by reflection from the medium and Figs. (3), (4) - for lines formed as a result of passing through it. In fact, the curves in the figures are profiles formed after a certain fixed number of scattering events in

doi: https://doi.org/10.52526/25792776-24.71.2-215

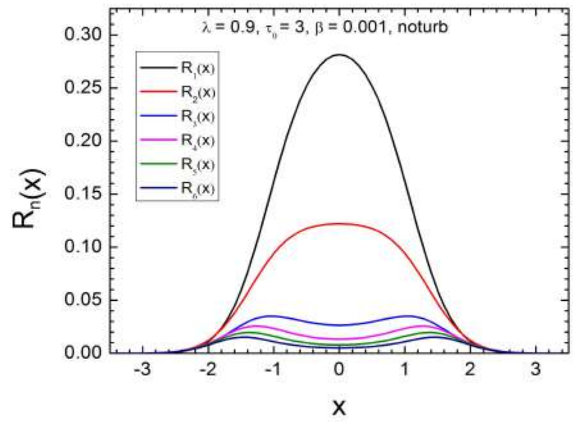

Figure 1. Line profiles formed as a result of reflection after fixed number of scattering events in the medium in the absence of turbulent motions.

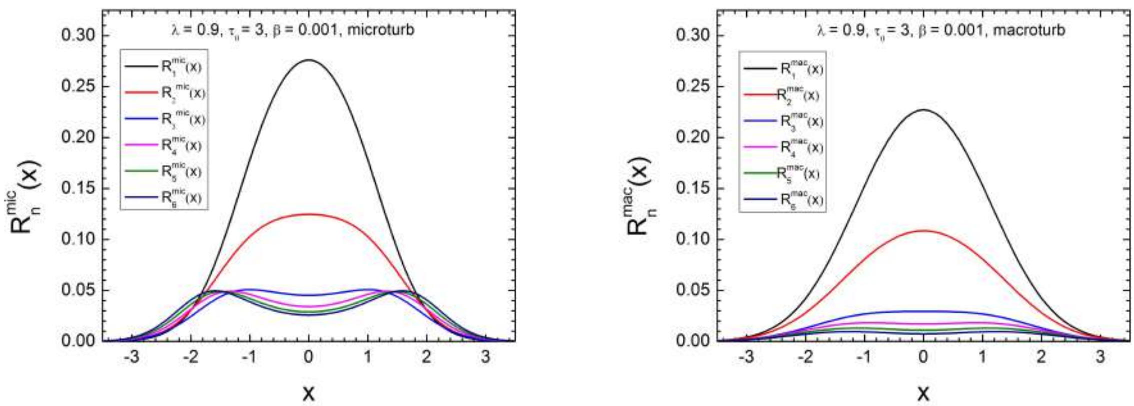

Figure 2. The same as in Fig.1 for the developed micro- (left panel) and the macro-turbulence (right panel) and $u_t = 1$.

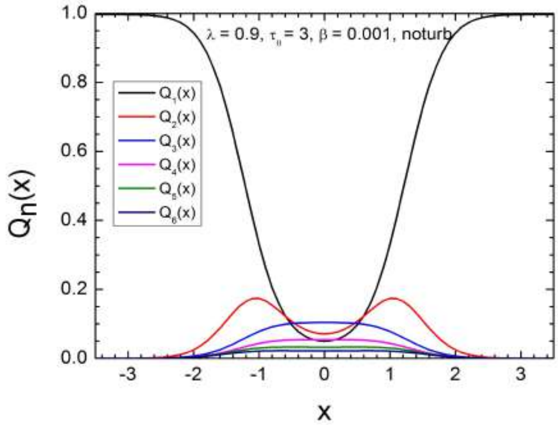

Figure 3. Line profiles formed as a result of transmission through the medium after fixed number of scattering events in the absence of turbulent motions.

doi: https://doi.org/10.52526/25792776-24.71.2-215

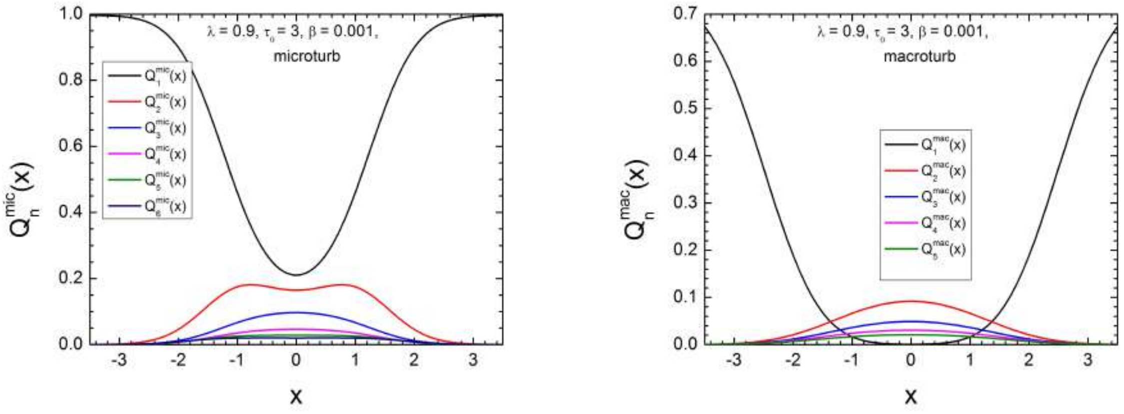

Figure 4. The same as in Fig.3 for the developed micro- (left panel) and the macro-turbulence (right panel) and $u_t = 1$.

the medium and clearly demonstrate the influence of turbulent motions depending on the degree of their development.

The characteristic features of demonstrated profiles are important for interpretation the further considered temporal changes of the discrete spectrum in non-stationary phenomena. The influence of turbulence on the reflectance of the medium is discernible. It is particularly seen that the shapes of the observed profiles of spectral lines are largely determined by processes associated with a small number of scattering acts. Special mention should be made of the rather broad bell-shaped profiles formed in the transmitted spectrum by macro-turbulence. The mechanism of their broadening is similar to that we have in the case of object rotation. Another characteristic feature is the double-peaked profiles appearing in the higher components of both the reflection and transmission functions for the cases of micro-turbulent and absence of it. Especially remarkable is the appearance of the emission double-peaked emission profile in the absorption spectrum formed in transmission of radiation through the medium. In the following, we will return to this question when studying the evolution of spectral line profiles under illumination of the medium by non-stationary energy sources.

3. The evolution of the line profiles

We recall that knowledge of Neumann expansions allows us to write directly the explicit expressions for the required probability density function (PDF) and the cumulative distribution function (CDF).

For the convenience of the reader, we reproduce here these relations, which are basic to the calculations

$$R\,(x,\tau_0,z) = \sum_{n=1}^{\infty} R_n\,(x,\tau_0) F_n\,(z)\,\lambda^n, \qquad Q\,(x,\tau_0,z) = \sum_{n=1}^{\infty} Q_n\,(x,\tau_0) F_n\,(z)\,\lambda^n, \tag{10}$$

where the PDF functions $R(x,\tau_0,z)$, $Q(x,\tau_0,z)$ are introduced such that Rdz and Qdz are respectively the probabilities of observing the given reflected and transmitted lines profiles in the time interval $(z, z+dz)$, and, F_n, as we have shown in recent papers (Nikoghossian, 2021a,b), is the probability density function (PDF) of the total time taken by a quantum at a certain number of n scattering events given by

$$F_n\,(z) = \frac{z^{2n-1}}{(2n-1)!}\mathrm{e}^{-z}, \qquad n = 1, 2, ... \tag{11}$$

which is obtained as a result of addition of two Erlang-n distributions describing the total residence time of atoms in the excited state and the time spent by quanta between two consecutive scattering acts. It is taken into account that the number of free runs of a quantum exceeds by one the number

doi: https://doi.org/10.52526/25792776-24.71.2-215

of its scattering events in the medium. The rates of both distributions for simplicity are assumed for simplicity's sake to be approximately equal, so that the dimensionless time z is read in units of the mean time $\bar{t} = t_1 + t_2$ expressed in terms of t_1 and t_2 representing respectively the mean time for an atom to be in an excited state and the frequency-averaged mean time taken by a quantum to fly between two successive acts of scattering. Note that the value of t_2 depends on the density of scattering centres, which in turn is determined by the physical conditions in the medium. In the simplest cases it is given by formula $t_2 = 1/nkc$, where n is the density of emitting or absorbing atoms, depending on whether the line is in emission or absorption, k is the total coefficient of a given line and c is the speed of light. Sometimes, when it comes to strong lines, usually hydrogen, it is necessary to take into account also the degree of ionisation of these atoms.

The functions F_n taking together describe temporal variations in the profiles of spectral lines formed at the boundaries of the medium when it is illuminated by a δ-function shaped pulse in the continuous spectrum. Note that the take their maximum value at $z = 2n - 1$.

In addition, we also consider the establishment of the equilibrium state regime under prolonged illumination of the medium by a source of the unit jump form given by the Heaviside H-function. The evolution of the line profiles in this case is described by the cumulative distribution function (CDF) given by

$$\tilde{R}\left(x, \tau_0, z_0\right) = \sum_{n=1}^{\infty} R_n\left(x, \tau_0\right) \Phi_n\left(z_0\right) \lambda^n, \qquad \tilde{Q}\left(x, \tau_0, z_0\right) = \sum_{n=1}^{\infty} Q_n\left(x, \tau_0\right) \Phi_n\left(z_0\right) \lambda^n, \tag{12}$$

where

$$\Phi_n\left(z_0\right) = \mathrm{e}^{-z_0} \sum_{k=0}^{\infty} \frac{z_0^{2n+k}}{(2n+k)!} \tag{13}$$

In both illumination cases, the incident radiation in continuum is assumed to be of unit intensity. To identify the influence of turbulent motions, we should consider the cases of micro- and macro-turbulence separately. The reasoning used in the derivation of the basic probability density function (PDF) and cumulative distribution function (CDF) describing the evolution of the observed spectral line profiles remains valid. Now instead of Eqs.(9),(11) we have

$$R_{mic}\left(x, \tau_0, z\right) = \sum_{n=1}^{\infty} R_n^{mic}\left(x, \tau_0\right) F_n\left(z\right) \lambda^n, \qquad Q_{mic}\left(x, \tau_0, z\right) = \sum_{n=1}^{\infty} Q_n^{mic}\left(x, \tau_0\right) F_n\left(z\right) \lambda^n, \tag{14}$$

$$\tilde{R}_{mic}\left(x, \tau_0, z\right) = \sum_{n=1}^{\infty} R_n^{mic}\left(x, \tau_0\right) \Phi_n\left(z\right) \lambda^n, \qquad \tilde{Q}_{mic}\left(x, \tau_0, z\right) = \sum_{n=1}^{\infty} Q_n^{mic}\left(x, \tau_0\right) \Phi_n\left(z\right) \lambda^n, \tag{15}$$

and

$$R_{mac}\left(x, \tau_0, z\right) = \sum_{n=1}^{\infty} R_n^{mac}\left(x, \tau_0\right) F_n\left(z\right) \lambda^n, \qquad Q_{mac}\left(x, \tau_0, z\right) = \sum_{n=1}^{\infty} \bar{Q}_n^{mac}\left(x, \tau_0\right) F_n\left(z\right) \lambda^n, \tag{16}$$

$$\tilde{R}_{mac}(x, \tau_0, z_0) = \sum_{n=1}^{\infty} R_n^{mac}\left(x, \tau_0\right) \Phi_n\left(z_0\right) \lambda^n, \qquad \tilde{Q}_{mac}(x, \tau_0, z_0) = \sum_{n=1}^{\infty} Q_n^{mac}\left(x, \tau_0\right) \Phi_n\left(z_0\right) \lambda^n, \tag{17}$$

where $z_0 = t_0/\bar{t}$, and t_0 is the time interval of the observed variation. Formulas Eqs.(14),(15), as well as Eq.(16) and Eq.(17) allow us to construct the desired PDF and CDF distributions and trace the evolution of the observed spectral line profiles at both considered energy sources.

Turning directly to the description of the obtained results, we continue throughout to give the following figures in pairs (3 panels each) for convenience of comparison by the reader of the results for three limiting cases: absence of gas-dynamic motions, the developed micro- and macro-turbulence.

doi: https://doi.org/10.52526/25792776-24.71.2-215

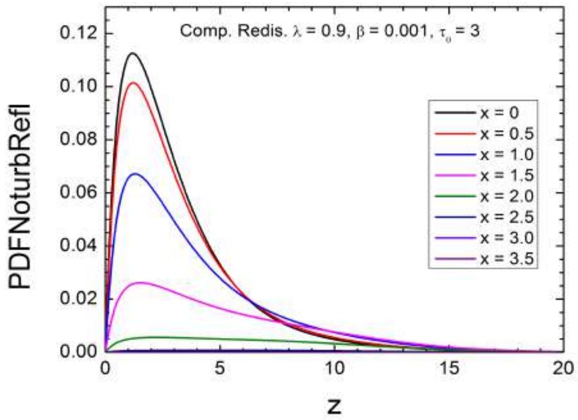

Figure 5. Probability density functions for radiation reflected from the medium of optical thickness $\tau_0 = 3$ and $\lambda = 0,9$ in the absence of turbulent motions.

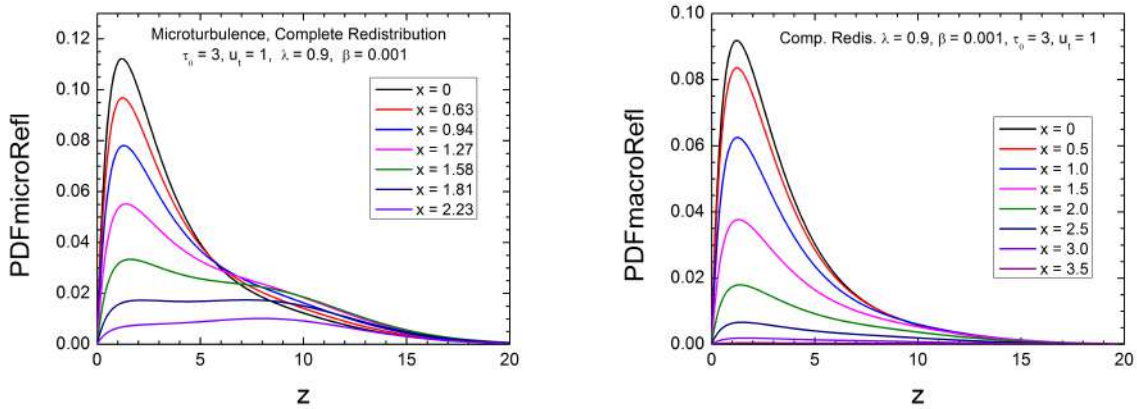

Figure 6. Probability density functions for the developed micro- (left panel) and the macro-turbulence (right panel). In both cases $u_t = 1$

Let us first consider PDF distributions, which allow us to get a general idea of frequency-dependent evolution of spectral lines for the medium illuminated by a source of the form of the $\delta(z)$ pulse. Figs.5,6 concern the reflection spectrum, while Figs.7,8 concern the absorbtion spectrum. Note that in order to achieve satisfactory accuracy in the case of a micro-turbulent medium, the zeros of the Hermite polynomial of the 49th order are chosen as frequency nodes inside the line.

The PDF distributions for both types of spectra contain rich information about the ongoing process that causes the observed changes in the line spectrum. The most important characteristics of these distributions are the location and magnitude of maxima in the centre of the lines. The location of the maxima of the central parts of the spectral lines in a small vicinity of $z = 1$ seems somewhat unexpected in view of the values of z, where the functions $F_n(z)$ reach their maxima. This is due to the magnitude of the functions $R_n(x, \tau_0)$, where the first term is much larger compared to others. Closer to the wings of the lines and in the wings themselves, the maxima are reached later at higher values of z, so that the wings of lines are formed at a later time z and the real time t. This is clearly discernible in Figs.6,8 for the lines formed as a result of reflection in the case of micro-turbulence and lines in the absorption spectrum in the case of macro-turbulence.

Of particular importance are the differences in the real time of the PDF maxima in different lines, which is largely due to the value of t_2. Knowledge of the latter allows us to determine the population of the corresponding level and estimate the optical thickness in the line. Strictly speaking, in certain cases it is necessary to take into account the physical conditions in the medium (such as, for example,

doi: https://doi.org/10.52526/25792776-24.71.2-215

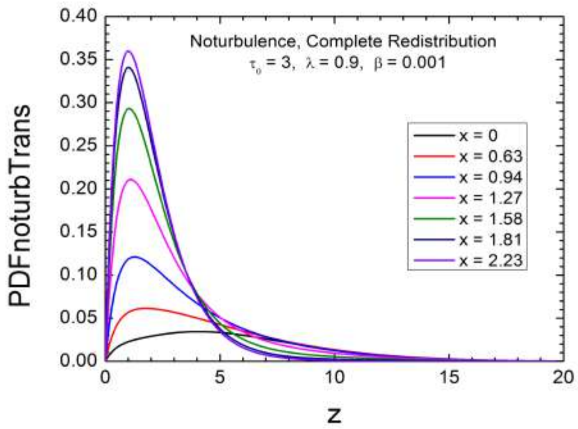

Figure 7. Probability density functions for radiation transmitted through the medium for the above adopted optical parameters in the absence of turbulent motions.

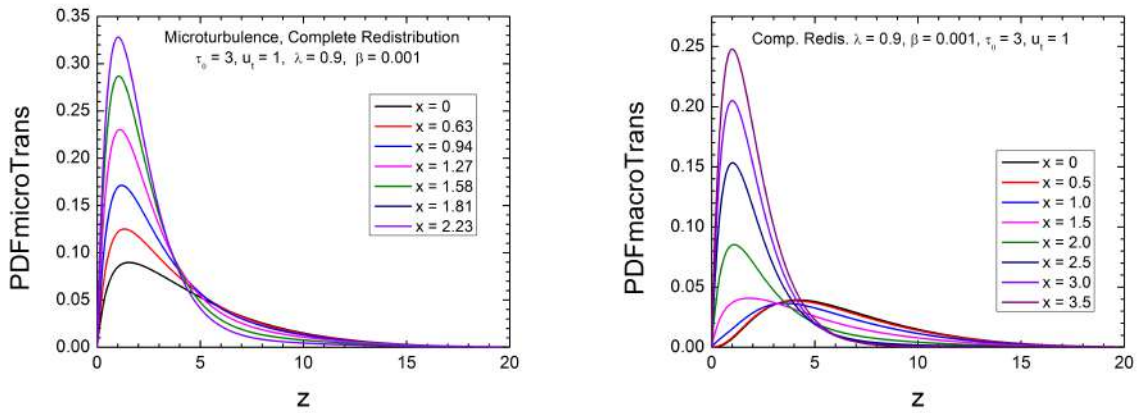

Figure 8. The same as in Fig.7 for the developed micro- (left panel) and the macro-turbulence (right panel).

the degree of ionisation of hydrogen in the case of strong hydrogen lines in the case of giants of the early spectral classes). At low densities of absorbing atoms/ions the quanta scatter less frequently but spend more time in the medium due to the increase of the path length between the scattering acts (Nikoghossian, 2021a,b), which leads to the increase of the real time to reach the intensity maximum even if the z_{max} values are not very different. Thus, the time of reaching the maximum can be regarded as an indicator of the optical thickness in the line under consideration, which, in turn, allows us to judge the chemical composition of the element in question. It should also be noted that different parts of the spectral line profile reach their maximum values at different times, which is most clearly seen in the reflection spectrum in micro-turbulence and the transmission spectrum in macro-turbulence. Usually, the wings of the lines evolve longer than their cores.

Another important characteristic of the PDF distribution is the value of the magnitude of its maximum. This value in addition to optical thickness depends also on the parameter λ (see Nikoghossian, 2022a) so, knowledge of the first one allows us to estimate theoretically the scattering coefficient. Further, the value of the PDF maximum corresponding to the radiation of unit intensity reflected from the medium makes it possible to calibrate the spectrum by comparing it with that for the one of observed lines supposedly possessing similar values of parameters λ and β. A similar possibility of calibration exists also in the absorption spectrum formed as a result of radiation passing through a medium. As it was shown in the above mentioned work, it is due to the asymptotic tendency of the far wings of the spectral line to a continuum, the level of which is determined mainly by the direct passage

doi: https://doi.org/10.52526/25792776-24.71.2-215

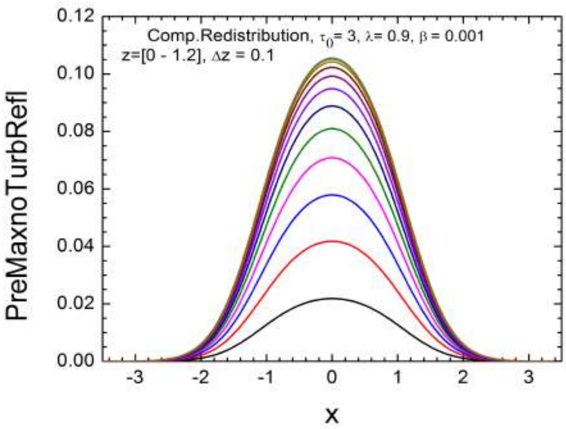

Figure 9. Evolution of the spectral line profiles formed as a result of radiation reflection from the medium until reaching the maximum of the PDF in the absence of turbulence.

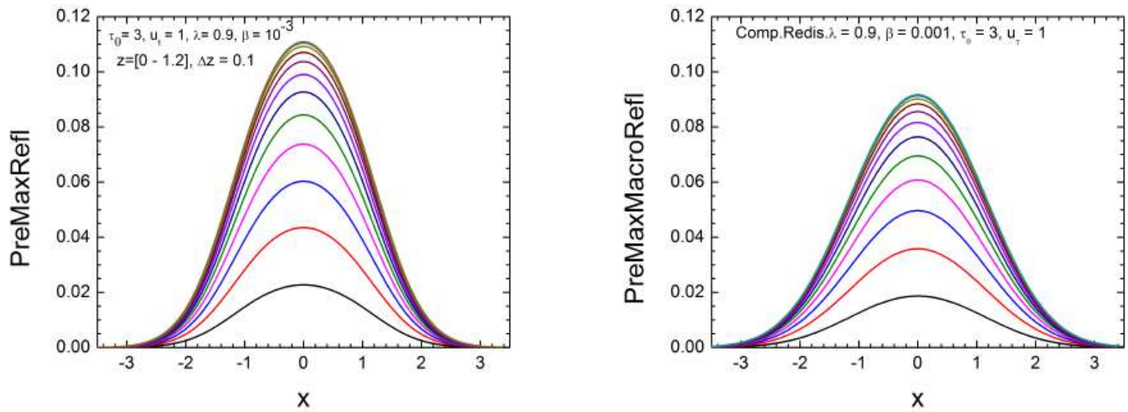

Figure 10. The same as in Fig.9 for the cases of micro-turbulence (left panel) and macro-turbulence (right panel).

of the incident radiation through the medium and is approximately equal to $\mathrm{e}^{-1} = 0.35$. Such calibrations using different lines create a fundamental possibility to study these sources not only in different frequency ranges, but also, importantly, as a function of time. The next characteristic parameter of the PDF distribution is the average duration of line evolution. A comparison of the above plots shows that in the reflection spectrum the line evolves longer in the case of micro-turbulence, while in the absorption spectrum formed as a result of transmission through the medium, the evolution in time is longer in the case of macro-turbulence.

Obviously, the picture of the processes in both reflection and transmission cases depends on both the optical thickness of the medium and the value of the scattering coefficient (the role of β becomes noticeable for strong resonant lines at values of the scattering coefficient sufficiently close to unity). Previously, we have shown that the duration of diffusion in the frequencies of the spectral line can increase if the scattering occurs with redistribution over frequencies (Nikoghossian, 2022b, 2023). The absorption lines produced by the passage of radiation through a medium have a faster time course, which is due to the possibility of direct transmittance without scattering.

Of some interest are the fractions of energy emitted in the lines before they reach their maxima. They are of the order of 20 per cent of the total energy radiated in them during the whole time of their evolution and mainly depend on the optical thickness in the line.

A visual representation of the evolution of spectral line profiles before maximum is given by Figs.9,10 for lines formed by reflection and Figs.11,12 for lines observed as a result of passing through

doi: https://doi.org/10.52526/25792776-24.71.2-215

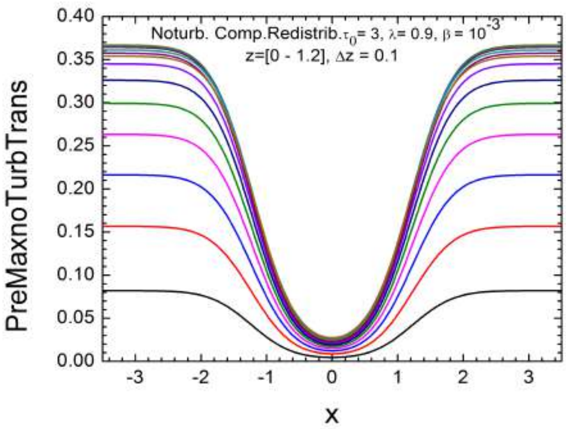

Figure 11. Evolution of the spectral line profiles formed as a result of radiation passing through the medium until reaching the maximum of the PDF in the absence of turbulence.

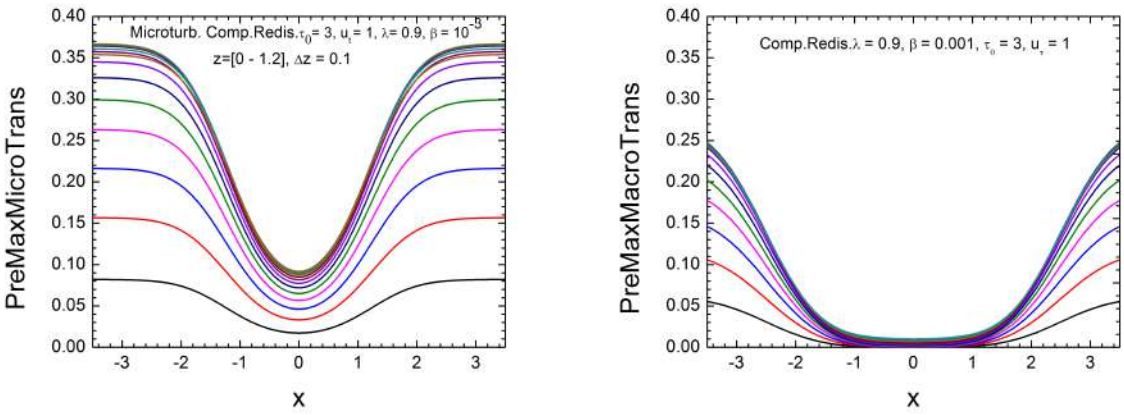

Figure 12. The same as in Fig.11 for micro- and macro-turbulence.

the medium. The time variable z grows in the figures with the increment $\Delta z = 0.1$ varying from bottom to top. When approaching maximum, changes in line profiles slow down, after which the lines slowly weaken, which is shown in Figs.13,14 and 15,16 where $\Delta z = 1$ and z grows from top to bottom. The figures show that the effect of gas-dynamic flows is strongest in the limit of macro-turbulence, which manifests itself in a sharp broadening of the spectral line and the appearance of large wings. In both extreme turbulent regimes, equality was assumed between the mean turbulent and thermal velocities was assumed in order to make the effect of turbulence more discernible.

It draws attention to the fact that many times after cessation of illumination of one of the boundaries of the medium some number of quanta continue to diffuse in it and leave the medium through both of its boundaries. The difference between these quantities gradually decreases, as a result of which weak, sometimes two-peaked emission lines are observed at both boundaries of the medium (Figs.13,14) so that they can appear also in the absorption spectrum (Figs.15,16).

4. Illumination by a stationary source. Evolution to the steady-state

In this section we will consider another problem, important for astrophysical applications, when the medium, starting from a certain moment of time, begins to be illuminated by external energy sources and remains under their influence for any length of time until the steady state field of radiation is established. It is assumed that the temporal action of the sources is described by the Heviside unit-step function. We are interested in the evolution of emission and absorption spectral lines formed

doi: https://doi.org/10.52526/25792776-24.71.2-215

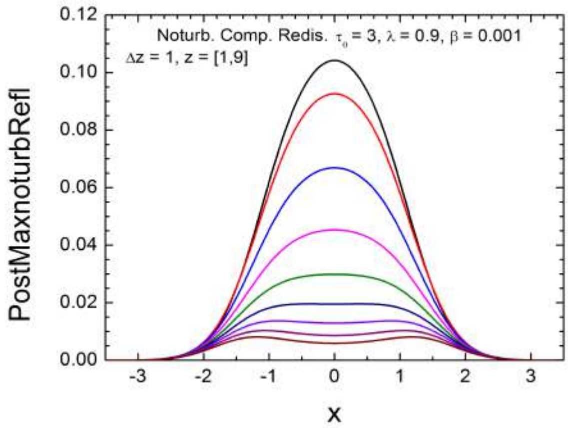

Figure 13. Evolution of the spectral line profiles formed as a result of radiation reflected from the medium after reaching the maximum of the PDF in the absence of turbulence.

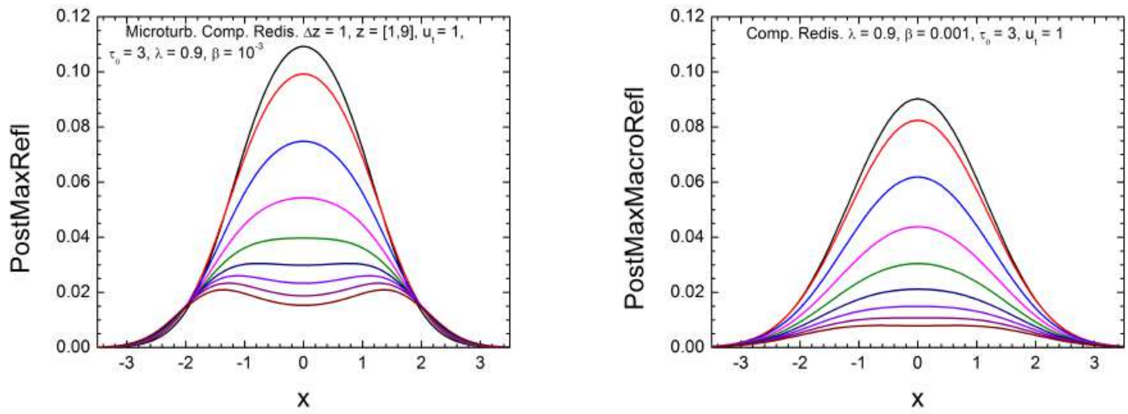

Figure 14. The same as in Fig.13 for micro- and macro-turbulence.

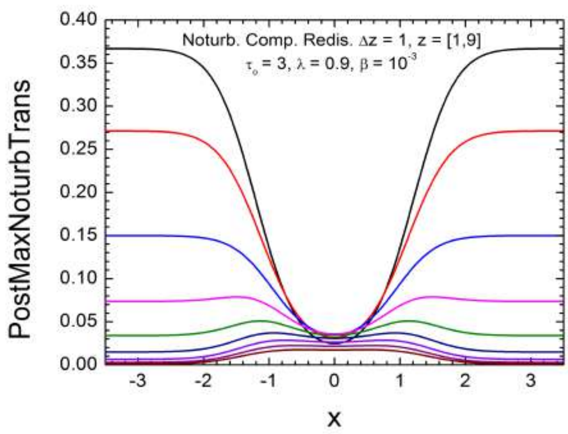

Figure 15. The transmitted spectra lines profiles evolution after PDF maximum in the absence of turbulence.

doi: https://doi.org/10.52526/25792776-24.71.2-215

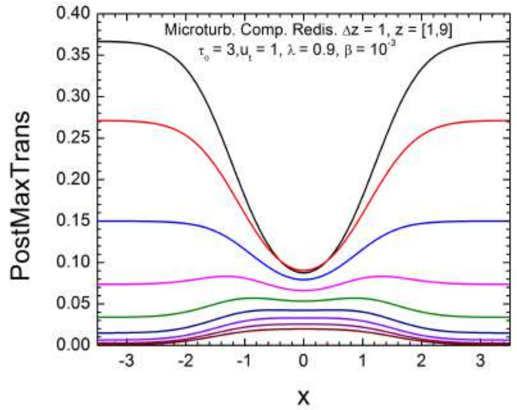

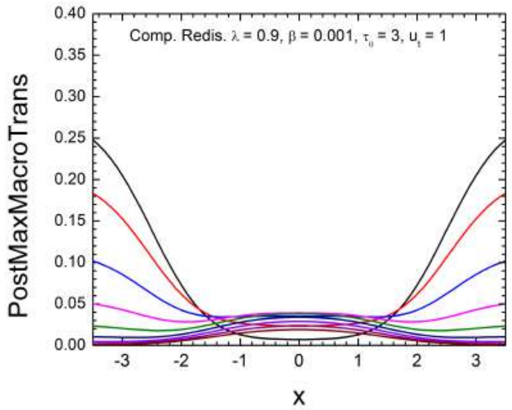

Figure 16. The same as in Fig.15 for micro- and macro-turbulence.

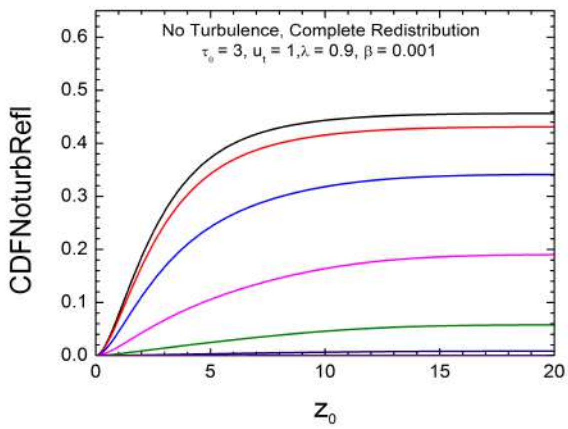

Figure 17. The cumulative distribution functions for the lines formed as a result of reflection from the medium in the absence of turbulence.

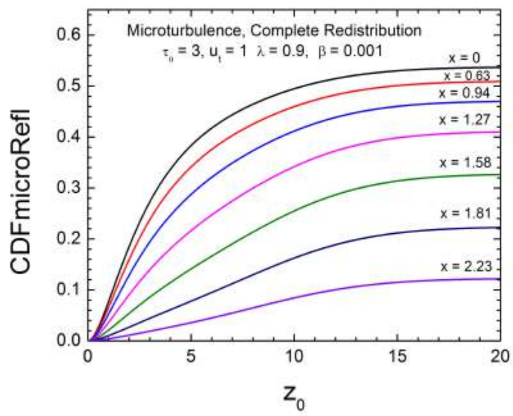

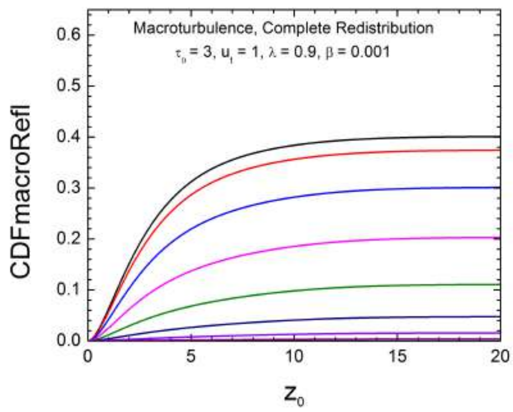

Figure 18. The same as in Fig.17 for the micro- and macro-turbulence.

doi: https://doi.org/10.52526/25792776-24.71.2-215

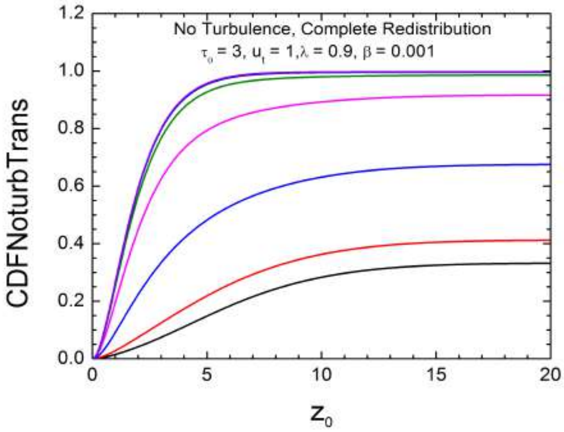

Figure 19. The cumulative distribution functions for the lines formed as a result of transmission through the medium in the absence of turbulence.

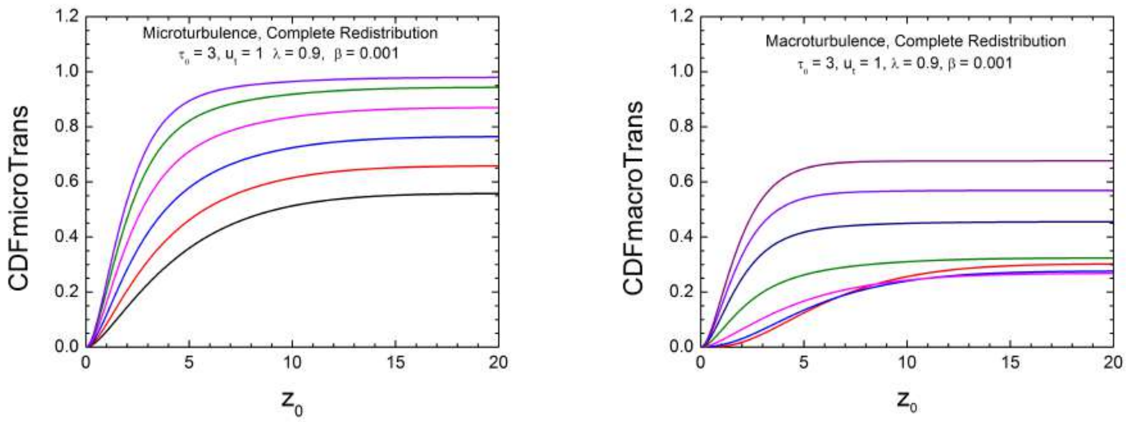

Figure 20. The same as in Fig.19 for the micro- and macro-turbulence.

as a result of reflection and transmission on the boundaries of the medium. The time dependence of the line profiles are described by cumulative distribution functions (CDF) given by Eqs.(12),(15) and (17).

Here, in addition to the initial phase of the appearance of the line spectra, we will be interested in their evolution and the rate at which the steady state is established, which depends both on the thickness of the medium and on the value of the scattering coefficient. Typical curves showing the variation of the spectral line profiles before reaching the stationary regime are shown in Figs.17-20. They are characterised by a plateau due to an asymptotic tendency of the line radiation towards their limiting values. As should be expected, the rate of the tendency towards stationary regime in the optically thin media we consider is sufficiently high. In fact, the curves achieve their limit values within the time interval $[5 \leq z_0 \leq 10]$. The illustrations above clearly show that the absorption lines formed as a result of transmission through the medium are established faster than the emission lines in the reflected spectrum. Another feature of the processes under study is their longer duration when the role of multiple scattering in the medium increases, i.e. at larger values of λ.

The absorption spectrum, as can also be seen in Figs.9-11, provides rich material for estimating both the optical characteristics of the line and the intensity of falling continuum radiation. The central residual line intensities together with equivalent widths provide important time-dependent information about these quantities and, as a consequence, provide an opportunity to study the physics of the observed phenomenon.

After reaching a plateau, the profiles of the observed spectral lines can be analysed using solutions

doi: https://doi.org/10.52526/25792776-24.71.2-215

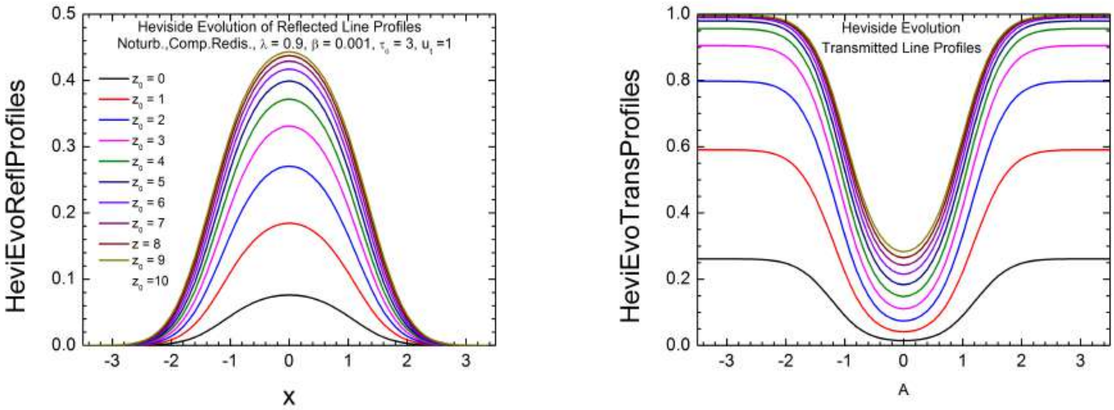

Figure 21. Evolution of the reflection and transmission lines arising under prolonged illumination by the energy sources in the absence of turbulence.

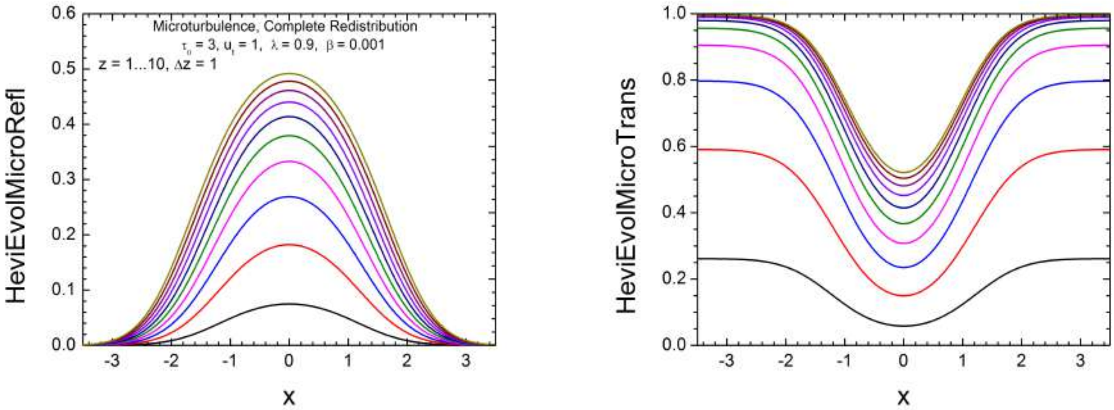

Figure 22. The same as in Fig.21 for micro-turbulence.

of classical stationary problems of the theory of radiation transfer on the line spectra formation. This will make it possible to draw conclusions about the lines themselves and the chemical content of elements, as well as about the characteristics of energy sources.

The identification of the spectral line and its assignment to a certain chemical element together with the dynamics of change and saturation rate reveal the physical picture of the dynamic process under study.

At the same time, as it is evident from Figs.17-20, the shape of the CDF distributions depends to a large extent on the nature and degree of turbulence development in the medium. This is also demonstrated in Figs.21-23, which show the evolution of spectral lines with the increment $\Delta z = 1$ before reaching a plateau. Particularly striking are the differences in central residual intensities and line widths depending on the nature and degree of turbulence in the medium.

5. Concluding remarks

The paper continues our study on the evolution of line spectra under the influence of non-stationary energy sources. One of the important factors acting on the observed pattern of changes in the line spectra are gas-dynamic flows, which almost always arise at the time-varying energy sources of the forms we consider. To identify them, we treated the problem of spectral line formation in a finite scattering and absorbing medium under two limiting regimes of micro- and macro-turbulence. The values of the optical parameters of the medium, such as the optical thickness of the medium, the scattering coefficient, and the parameter β, are chosen in such a way in order to describe a sufficiently

doi: https://doi.org/10.52526/25792776-24.71.2-215

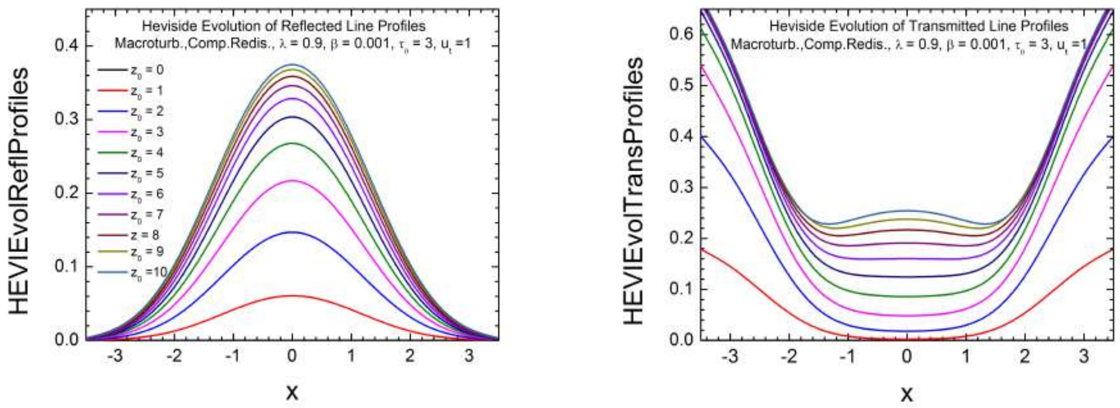

Figure 23. The same as in Figs.21,22 for macro-turbulence.

wide range of cases studied in practice. The results obtained concerning the evolutionary pattern of spectral lines arising both as a result of reflection from the medium and its passage in the two limiting regimes, as might be expected, are quite distinct, as well as differ from the case when turbulence is absent. These differences are of a general nature and are not limited to the Gaussian probability distribution of turbulent velocities considered in the paper. Note also that the value of the mean turbulent velocity $u_t = 1$ chosen in the paper seems to be rather high to be applicable in practice to macro-turbulent flows in view of the extreme broadening of spectral lines.

It should also be noted that the assumption of approximate equality of the two possible causes of time wasting adopted in this paper may be rather crude in many situations. A more general problem with an arbitrary ratio of these two quantities will be the subject of a future paper by the author.

References

Bellman R., Wing J. M., 1973, An Introduction to Invariant Imbedding, New York, Wiley and Sons

Casti J., Kalaba R., 1976, Imbedding Methods in Applied Mathematics (Russian transl.), M., Mir

Ganapol B. D., 1979, J. Quant. Spectrosc. Radiat. Transfer. , 22, 135

Gorbatskii V. G., Minin I. N., 1963, Nestatsionarnye zvezdy.

Gray D. F., 1978, , 59, 193

Matsumoto M., 1967, Publ. Astron. Soc. Jpn. , 19, 163

Matsumoto M., 1974, Publ. Astron. Soc. Jpn. , 26, 241

Nikoghossian A. G., 1984, Astrofizika, 21, 595

Nikoghossian A. G., 2007, Astrophysics, 50, 175

Nikoghossian A. G., 2017, Astrophysics, 60, 408

Nikoghossian A. G., 2021a, Astrophysics, 64, 490

Nikoghossian A., 2021b, Communications of the Byurakan Astrophysical Observatory, 68, 32

Nikoghossian A., 2022a, Communications of the Byurakan Astrophysical Observatory, 69, 140

Nikoghossian A., 2022b, Communications of the Byurakan Astrophysical Observatory, 69, 25

Nikoghossian A. G., 2023, Communications of the Byurakan Astrophysical Observatory, 70, 131

Sobolev V. V., 1985, Course in theoretical astrophysics (3rd revised and enlarged edition)

doi: https://doi.org/10.52526/25792776-24.71.2-215

The Master-Space Supergravity: Particle mechanics

G.Ter-Kazarian*

Byurakan Astrophysical Observatory, Byurakan, Aragatsotn Province, Armenia

Abstract

This report aims to expose further the assertions made in a recent theory of *global Master space* (MS_p)-SUSY (Ter-Kazarian, 2023a, 2024a) by developing its local extension. The global MS_p-SUSY reviews the physical processes underlying the standard Lorenz code of motion and its deformation tested in experiments for ultra-high energy cosmic ray and TeV-γ photons observed. The local extension of MS_p-SUSY yields the gauge theory of *translations*. This as a corollary makes room for the theory of $\widetilde{MS}_p$-Supergravity, subject to certain rules. The superspace is a direct sum of background semi-Riemannian 4D-space and curved Master space $\widetilde{MS}_p \equiv \underline{V}_2$ (2D semi-Riemannian space), $V_4 \oplus \underline{V}_2$, with an inclusion of additional fermionic coordinates $\Theta(\underline{\theta}, \underline{\bar{\theta}})$ and $\bar{\Theta}(\underline{\theta}, \underline{\bar{\theta}})$, which are induced by the spinors $\underline{\theta}$ and $\underline{\bar{\theta}}$ referred to $\widetilde{MS}_p$. Being embedded in V_4, the $\widetilde{MS}_p$ is the *unmanifested* indispensable individual companion of a particle of interest devoid of any matter influence. While all the particles are living on V_4, their superpartners can be viewed as living on $\widetilde{MS}_p$. In this framework supersymmetry and general coordinate transformations are described in a unified way as certain diffeomorphisms. The action of simple $\widetilde{MS}_p$-SG includes the Hilbert term for a *fictitious* graviton (with spin 2) coexisting with a *fictitious* fermionic field of, so-called, gravitino (sparticle with spin 3/2) described by the Rarita-Scwinger kinetic term. They are the bosonic and fermionic states of a gauge particle in V_4 and $\widetilde{MS}_p$, respectively, or vice versa. A curvature of $\widetilde{MS}_p$ arises entirely due to the inertial properties of the Lorentz-rotated frame of interest. This refers to the particle of interest itself, without relation to other matter fields, so that this can be globally removed by appropriate coordinate transformations. The supervielbein, being an alogue of Cartan's local frame, is the dynamical variable of superspace formulation, which identifies the tetrad field and the Rarita-Schwinger fields. The spin connection is the second dynamical variable in this theory. The tetrad field plays the role of a gauge field (graviton) associated with local transformations. The gravitino is a gauge field associated with local supersymmetry. Within that context, we consider particle mechanics.

Keywords: *Supersymmetry–Supergravity–Particle mechanics*

1. Introduction

The question about the very nature of the *uniform motion* of a particle in free space, which is one of the cornerstones put into physics by hand, at first glance classified as an empirical term rather than as a notion of pure reason and, thus, it may not seem like a subject of perception. While in recent years, the violation of CPT and Lorentz invariance at high energies has become a major concern for physicists. The discovery of the possibility of spontaneously breaking of Lorentz symmetry in bosonic string field theory (Kostelecky & Potting, 1991, 1996), there has been vital interest in its spontaneously breaking in the framework of quantum field theory as introduction of a preferred frame, or its explicit breaking in non-commutative geometries, as well as in certain supersymmetric theories. Spontaneous Lorentz break was discussed in several early papers, e.g. (Bialynicki-Birula, 1963, Bjorken, 1963, Cho & Freund, 1975, Eguchi, 1976, Guralnik, 1964, Nambu, 1968). Although precursors go back at least to early work by Dirac (Dirac, 1951) and Heisenberg (Heisenberg, 1957) in an effort to interpret the photon as a Nambu-Goldstone boson. An important aspect of spontaneous breaking is that both the fundamental theory and the effective low energy theory remain invariant under observer Lorentz transformations (Colladay & Kostelecky, 1997, 1998).

Quantum gravity (QG) has now gradually become a physical theory. Indeed, astrophysical experiments performed at the ultra-high energies (at ultra-short distances) should measure effects due to a QG regime. This QG search attempts to assess the state of our present knowledge and understanding of the laws of

*gago_50@yahoo.com

doi: https://doi.org/10.52526/25792776-24.71.2-230

physics on the Planck scale. Most ideas in QG about the violation of the standard Lorentz code (SLC) of motion have been tested in recent decades in ultra-high energy cosmic ray (UHECR) and astrophysical TeV-γ photons experiments. The UHECR- and TeV-γ threshold anomalies found in these experiments provide a wealth of invaluable modern tests of the origin of LIV and has a strong potential in providing competitive constraints on suggested scenarios. They reflect the expectation that the solutions to this mystery seemed to require new physics (see e.g. (Batista & et al., 2019, 2023, Mattingly, 2005) and references therein). It is a well-established fact that due to fundamental quantum uncertainties, the microstructure of spacetime should be viewed as a dynamical entity fluctuating within a two or three orders of magnitude of Planck length $\ell_P \approx 1.62 \times 10^{-33}$cm and Planck time t_P/c, at which the structure of space-time and quantum effects would become inextricably intertwined. This means that if such fluctuations are large enough to cause non-trivial deformations of classical smooth spacetime, the latter will develop a `foamy´ structure at the ultra-microscopic level and all sorts of geometric changes and topologically non-trivial structures will be formed (e.g. via quantum tunnelling (Garfinkle & Strominger, 1991)), evolving, interacting and lasting only a few Planck times. In phenomenological minimal-length models, foamy effects come from the presence of a minimal accessible length, which modifies the Heisenberg or Poincar´e algebra to accommodate a minimal uncertainty in position measurements at the Planck energy, $E_P = M_P c^2$ ($\sim 1.22 \times 10^{19}$ GeV). The minimal length appears as a kinematic feature, while the shape itself of the Hamiltonian may be deformed from the combined action of a modified position-momentum algebra and the choice of a relativity principle.

However, even thanks to the fruitful interplay between phenomenological analysis and high energy astronomical experiments, the scientific situation remains, in fact, more inconsistent to day. A systematic analysis of these properties happens to be surprisingly difficult by conventional theoretical methods. Up to now, there has been no conclusive evidence of violation of the laws of conventional physics, with the results instead yielding ever more stringent upper bounds on this task, thus confirming the related aspects with concomitant precision. This may be due to the fact that present instruments do not yet have the necessary sensitivity to detect Planck scale effects, or that some effects have not been taken into account in the available data. Of course, failure to find a violation of these laws in any one experiment or class of experiments does not give us a final proof, and even as the experimental limits move more closely towards the fundamental bounds of measurement uncertainty, new conceptual approaches to the task continue to appear. The tremendous importance of the question and the lure of what might be revealed by attaining the next decimal place of obtained experimental results are as strong a draw on this question as they are in any other aspect of precise tests of physical laws.

Our primary interest in the subject is to understand the underlying reality, in which the *uniform motion* would have well defined. In a recent paper Ter-Kazarian (2024a) we developed a microscopic theory of deformed Lorentz symmetry and deformed geometry induced by `foamy´ effects near the Planck scale and tested in ultra-high energy experiments. To this aim, we proposed a theory of MS$_p$-SUSY and derive SLC in a new perspective of global double MS$_p$-SUSY transformations. To the best of our knowledge no one has ever studied the very nature of the *uniform motion* and the physical processes underlying it. We just like to mention its key points as an example of the lines on which one should seek to make advances and that other people, we hope, will follow along those lines. A notable conceptual element is the concept of 2D MS$_p$($\equiv \underline{M}_2$), which is a physical structure with *intrinsic geometrical properties of its own* (see Appendix A). The MS$_p$ embedded in background 4D Minkowski space, M_4, is the *unmanifested* indispensable individual companion to the particle of interest as the intrinsic property devoid of any external influence. A comprehensive principle underlying the global MS$_p$-SUSY theory hinges on the following:

the particle perseveres in its permanent state of superoscillations between the spaces M_4 and $\underline{M}_2$, unless acted upon by some external force, i.e. the particle undergoes the SUSY - transformations at sequential transitions from M_4 to $\underline{M}_2$ and back ($M_4 \rightleftharpoons \underline{M}_2$).

We consider the spaces M_4 and $\underline{M}_2$ formally and, therefore, mathematical devoid of any sense of *physical space-time*. To derive the most important *relative inertial uniform motion*, it is necessary to impose specific conditions on the spinor transformation matrix M in $\underline{M}_2$. We are of course not limited within MS$_p$-SUSY to consider particular constant spinor $\underline{\theta}$ referred to $\underline{M}_2$, which yields the constant velocity $\vec{v}(\underline{\theta})$ (Appendix A), but can choose at will any other constant spinors $\underline{\theta}'$, $\underline{\theta}''$, ... yielding respectively the constant velocities $\vec{v'}(\underline{\theta}')$, $\vec{v}''(\underline{\theta}'')$, ... of inertial observers that move uniformly forever on rectilinear timelike worldlines, whose transformational law on the original spinor $\underline{\theta}$ is known (first condition):

$$\underline{\theta}'_\alpha = M_\alpha^{\ \beta}\underline{\theta}_\beta, \quad \bar{\underline{\theta}}_{\dot\alpha} = (M^*)_{\dot\alpha}^{\ \dot\beta}\,\bar{\underline{\theta}}_{\dot\beta}, \quad \dot\alpha, \dot\beta = 1, 2, \tag{1}$$

where $M \in SL(2, C)$ is the hermitian unimodular two-by-two matrix, the matrix M^* is related by a similarity

doi: https://doi.org/10.52526/25792776-24.71.2-230

transformation to $(M^{-1})^{\dagger}$, i.e. $(M^{\dagger})^{\beta}{}_{\alpha} = (M^{*})_{\alpha}{}^{\beta}$. The (1) gives the second founding property of SR that the bilinear combinations are $c := \underline{\theta}\,\bar{\underline{\theta}} = \underline{\theta}'\,\bar{\underline{\theta}}' = \cdots = const$, which yields a second postulate of SR (Einstein's postulate) (Appendix A). Therewith a quantity $\underline{e}_{\underline{m}}\,(\underline{\theta}\,\sigma^{\underline{m}}\,\bar{\underline{\xi}})$ (where $\underline{e}_{\underline{m}}$ is a basis vector, $\underline{\theta}$, $\underline{\xi}$ are Weyl spinors) is a Lorentz scalar if and only if the second condition holds too:

$$\tfrac{1}{2}\,Tr\left(\sigma^{\underline{m}}\,M\sigma^{\underline{n}}\,M^{\dagger}\right)\sigma^{\underline{n}}_{\alpha\dot{\alpha}} = (M^{-1})_{\alpha}{}^{\beta}\sigma^{\underline{m}}_{\beta\dot{\beta}}(M^{-1})^{\dagger\dot{\beta}}{}_{\dot{\alpha}}, \tag{2}$$

where the map from $SL(2,C)$ to the Lorentz group is established through the $\underline{\sigma}$-matrices (Appendix A). The latter, according to the embedding map, can be written in terms of $\vec{\sigma}$-Pauli spin matrices. The (2) combined with (103) give the first founding property (106) of SR.

The `superspace´ is a direct sum extension of background double spaces $M_4 \oplus \underline{M}_2$, with an inclusion of additional fermionic coordinates induced by the spinors $(\underline{\theta}, \bar{\underline{\theta}})$ referred to $\underline{M}_2$. Thanks to the embedding of $\underline{M}_2$ in M_4, the spinors $(\underline{\theta}, \bar{\underline{\theta}})$, in turn, induce the spinors $\theta(\underline{\theta}, \bar{\underline{\theta}})$ and $\bar{\theta}(\underline{\theta}, \bar{\underline{\theta}})$ (see (73)), as to M_4. Then the net result of sequential atomic double transitions induce the inhomogeneous Lorentz group, or Poincaré group, and that the unitary linear transformation $|x, t> \to U(L, a)|x, t>$ on vectors in the physical Hilbert space. Thus, we achieve the desired goal to derive the SLC in terms of spinors $(\underline{\theta}, \bar{\underline{\theta}})$ and period (τ) of superoscillations referred to the master space $\underline{M}_2$ (Appendix A). This calls for a complete reconsideration of our standard ideas of Lorentz motion code, to be now referred to as the *individual code of a particle*, defined as its intrinsic property. This reveals the nature of the most important concept of *physical space-time*, which *turns out to be a direct consequence of the processes of particle motion*. That is, we derive the relative *temporal* ($x^0 = ct$) and *spatial* ($|\vec{x}|$) coordinates of *physical space-time* as a function of constant spinors $(\underline{\theta}, \bar{\underline{\theta}})$ and a period τ of superoscillations as follows:

$$\begin{aligned} & x^0 = ct = (\underline{\theta}\,\bar{\underline{\theta}})\,k\tau/\sqrt{2}, \quad k = 1, 2, 3, ... \\ & |\vec{x}| = (\underline{\theta}_1\,\bar{\underline{\theta}}_1 - \underline{\theta}_2\,\bar{\underline{\theta}}_2)\,k\tau/\sqrt{2}. \end{aligned} \tag{3}$$

While all the particles are living on M_4, their superpartners can be viewed as living on MS_p. Particular emphasis is given that the ground state of MS_p-SUSY model has a vanishing energy value and is nondegenerate (SUSY unbroken). The particles in M_4 themselves can be considered as excited states above the underlying quantum vacuum of background double spaces $M_4 \oplus \underline{M}_2$, where the zero point cancellation occurs at ground-state energy, provided that the natural frequencies are set equal ($q_0^2 \equiv \nu_b = \nu_f$), because the fermion field has a negative zero point energy while the boson field has a positive zero point energy.

This theory, among other things, actually explores the first part of the phenomenon of inertia, which refers to *inertial uniform motion along rectilinear timelike world lines*. This developments are in many ways exciting, yet mysteries remain, and some of deeper issues are still unresolved, such as those which relate the inertial effects, which comprises a second half of phenomenon of inertia. Perhaps the most striking phenomenon of inertia is a deep mystery in physics, representing the most incomprehensible problem in need of resolution. Governing the motions of planets both fundamental phenomena of nature the gravity and inertia reside at the very beginning of physics, so that understanding in depth mystery of the origin of the whole phenomenon of inertia consisting of two parts represents a tremendous opportunity for present-day theoretical physics. General Relativity (GR) was a great success in explaining the gravity, and it showed how, by departing from ideas suggested by classical mechanics, you could make an advance in a new direction. Despite the advocated success of GR, which was a significant landmark in the development of the field, the phenomenon of inertia stood one of the major unattained goals since the time traced back to the works developed by Galileo (Drake, 1978) and Newton (Newton, 1687). More than four centuries passed since the famous far-reaching discovery by Galileo (in 1602-1604) of Weak Principle of Equivalence (WPE) that all bodies fall at the same rate Drake (1978), which establishes the independence of free-fall trajectories of the internal composition and structure of bodies. This led to an early empirical version of the suggestion that gravitation and inertia may somehow result from a single mechanism. Besides describing these early gravitational experiments, Newton in *Principia Mathematica* Newton (1687) has proposed a comprehensive approach to studying the relation between the gravitational and inertial masses of a body. The *principle of inertia* they developed is one of the fundamental principles of classical mechanics. This governs the *uniform motion* of a body and describes how it is affected by applied forces. Ever since, there is an ongoing quest to understand the reason for the universality of the inertia, attributing to the WPE. In other words, WPE states that all bodies at the same spacetime point in a given gravitational field will undergo the same acceleration. However, the nature of the relationship of gravity and inertia continues to

doi: https://doi.org/10.52526/25792776-24.71.2-230

elude us and, beyond the WPE, there has been little progress in discovering their true relation. Today there is no known feasible way to account for credible explanation of this problem.

With this perspective in sight, the necessity of *local* theory of MS$_p$-SUSY is twofold. First, the general idea behind the success of any global theory was the need to promote the symmetries to local symmetries. Second, these features deserve careful study, because the theory of global MS$_p$-SUSY provides valuable theoretical clue for a complete revision of our standard ideas about the Lorentz code of motion to be now referred to as the *intrinsic* property of a particle. This is a result of the first importance for a really comprehensive theory of inertia. In this respect, it is important to recall once more that GR was designed to incorporate Mach's principle of *relativity of inertia*, i.e. this is the gravitational influence of the entire Universe which creates inertia. Of course, GR enters with its own multifacets, and pretty well it over about many years has been on these lines, and physicists have gone a long way in its development. Viewed from the perspective of GR theory, the fictitious forces (i.e. pseudo-forces) - the forces that result from the acceleration of the reference frame itself and not from any physical force acting on the body, are attributed to geodesic motion in spacetime. But nothing is reliable and such efforts do not make sense. The fact that the theory conforms GR does not prove that it is correct. Indeed, as Einstein emphasized later Bondi (1952), Sciama (1953), GR is failed to account for the inertial properties of matter, so that an adequate theory of inertia is still lacking.

A local extension of the MS$_p$-SUSY algebra leads to the gauge theory of *translations*. The overall purpose of the present article, therefore, is to conceive a local MS$_p$-SUSY as the theory of $\widetilde{MS}_p$-SG, an early version of which is given in (Ter-Kazarian, 2023b). As this solution is in use throughout the subsequent papers, much more will be done to make the early results and formulations complete, clear and rigorous. The action of simple $\widetilde{MS}_p$-SG includes the Hilbert term for a *fictitious* graviton coexisting with a *fictitious* fermionic field of gravitino described by the Rarita-Scwinger kinetic term. Whereas a coupling of supergravity with matter superfields no longer holds. Instead, a deformation of MS$_p$ is the origin of these fields. Finally, we consider a particle mechanics.

We proceed according to the following structure. To start with, in Section 2 we discuss the idea of what is a local $\widetilde{MS}_p$-SUSY. Section 3 is devoted to the non-trivial linear representation of the $\widetilde{MS}_p$-SUSY algebra. In Section 4 we turn to a simple $(N = 1)$ $\widetilde{MS}_p$ - SG without auxiliary fields. On these premises, in Section 5 we derive particle mechanics and discuss the velocity and acceleration in M_4. The ideas underlying our theoretical framework and concluding remarks are described in section 6. Whereas we highlight a few points and discuss issues to be studied further. Such approach is more transparent at any step but needs some technical details, definitions and algebraic operations. In Appendix A, therefore, we briefly revisit the global `double space´- or MS$_p$-SUSY without going into the subtleties as a guiding principle to make the rest of paper understandable. For brevity, whenever possible undotted and dotted spinor indices often can be ruthlessly suppressed without ambiguity. Unless indicated otherwise, the natural units, $h = c = 1$ are used throughout.

2. The local $\widetilde{MS}_p$-SUSY

One might guess that the condition for the parameter $\partial_{\hat{\mu}}\epsilon = 0$ of a global MS$_p$-SUSY theory (Ter-Kazarian, 2024a) should be relaxed for the accelerated particle motion, so that a global SUSY will be promoted to a local SUSY in which the parameter $\epsilon = \epsilon(X^{\hat{\mu}})$ depends explicitly on $X^{\hat{\mu}} = (\widetilde{x}^{\mu}, \underline{\widetilde{x}}^{\underline{\mu}}) \in V_4 \oplus \underline{V}_2$, where $\widetilde{x}^{\mu} \in V_4$ and $\underline{\widetilde{x}}^{\underline{\mu}} \in \underline{V}_2$, with V_4 and $\underline{V}_2$ are the 4D and 2D semi-Riemannian spaces. This extension will address the *accelerated motion* and *inertia effects*. To trace a maximal resemblance in outward appearance to the theory of MS$_p$-SUSY, we here accept all its conventions and notations unless otherwise noted. A smooth embedding map, generalized for curved spaces, becomes $\widetilde{f}: \ \underline{V}_2 \longrightarrow V_4$ defined to be an immersion (the embedding which is a function that is a homeomorphism onto its image):

$$\underline{\widetilde{e}}_{\underline{0}} = \widetilde{e}_0, \quad \underline{\widetilde{x}}^{\underline{0}} = \widetilde{x}^0, \quad \underline{\widetilde{e}}_{\underline{1}} = \vec{\widetilde{n}}, \quad \underline{\widetilde{x}}^{\underline{1}} = |\vec{\widetilde{x}}|, \tag{4}$$

where $\vec{\widetilde{x}} = \widetilde{e}_i \widetilde{x}^i = \vec{\widetilde{n}}|\vec{\widetilde{x}}|$ $(i = 1, 2, 3)$ (the middle letters of the Latin alphabet $(i, j, ...)$ will be reserved for space indices). On the premises of (Ter-Kazarian, 2024a), we review the accelerated motion of a particle in a new perspective of local $\widetilde{MS}_p$-SUSY transformations (see Fig. 1) that a *creation* of a particle in $\underline{V}_2$ means its transition from initial state defined on V_4 into intermediate state defined on $\underline{V}_2$, while an *annihilation* of a particle in $\underline{V}_2$ means vice versa. The same interpretation holds for the *creation* and *annihilation* processes

doi: https://doi.org/10.52526/25792776-24.71.2-230

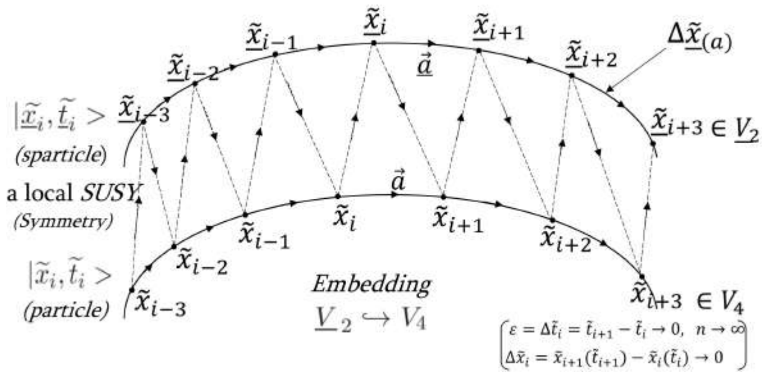

Figure 1. The extended Schwinger transformation function geometry. The net result of each atomic double transition of a particle $V_4 \rightleftharpoons V_2$ is as if we had operated with *a local space-time translation* with acceleration, $\vec{a}$, on the original space V_4. In the same way the acceleration, $\vec{\underline{a}}$, refers to $\underline{V}_2$ at $\underline{V}_2 \rightleftharpoons V_4$. The *atomic displacement*, $\Delta\underline{\tilde{x}}_{(a)}$, is caused in V_2 by double transition of a particle, $V_2 \rightleftharpoons V_4$. All the particles are living on V_4, while their superpartners can be viewed as living on *unmanifested* Master space, V_2.

in V_4. The net result of each atomic double transition of a particle $V_4 \rightleftharpoons \underline{V}_2$ to $\underline{V}_2$ and back is as if we had operated with *a local space-time translation* with acceleration, $\vec{a}$, on the original space V_4. Accordingly, the acceleration, $\vec{\underline{a}}$, holds in $\underline{V}_2$ at $\underline{V}_2 \rightleftharpoons V_4$. So, the accelerated motion of boson $A(\tilde{x})$ in V_4 is a chain of its sequential transformations to the Weyl fermion $\underline{\chi}(\underline{\tilde{x}})$ defined on $\underline{V}_2$ (accompanied with the auxiliary fields $\underline{\tilde{F}}$) and back,

$$\to A(\tilde{x}) \to \underline{\chi}^{(F)}(\underline{\tilde{x}}) \to A(\tilde{x}) \to \underline{\chi}^{(F)}(\underline{\tilde{x}}) \to, \tag{5}$$

and the same interpretation holds for fermion $\chi(\tilde{x})$. A useful guide in the construction of local superspace is that it should admit rigid superspace as a limit. The reverse is also expected, since if one starts with a constant parameter ϵ and performs a local Lorentz transformation, then this parameter will in general become space-time dependent as a result of this Lorentz transformation.

The mathematical structure of a local theory of $\widetilde{MS}_p$-SUSY has much in common with those used in the geometrical framework of standard supergravity theories. Such a local SUSY can already be read off from the algebra of a global MS$_p$-SUSY (Ter-Kazarian, 2024a) in the form

$$[\epsilon(X)Q,\, \bar{Q}\bar{\epsilon}(X)] = 2\epsilon(X)\sigma^{\hat{\mu}}\bar{\epsilon}(X)\tilde{p}_{\hat{\mu}}, \tag{6}$$

which says that the product of two supersymmetry transformations corresponds to a translation in 6D X-space of which the momentum

$$\tilde{p}_{\hat{\mu}} = i\tilde{\partial}_{\hat{\mu}} = \frac{\partial}{\partial X^{\hat{\mu}}} = (\frac{\partial}{\partial \tilde{x}^{\mu}}, \frac{\partial}{\partial \underline{\tilde{x}}^{\underline{\mu}}})$$

is the generator. We expect the notion of a general coordinate transformation should be

$$[\delta_{\epsilon_1(X)},\, \delta_{\epsilon_2(X)}]V = \tfrac{1}{2}\bar{\epsilon}_2(X)\sigma^{\hat{\mu}}\epsilon_1(X)\,\tilde{\partial}_{\hat{\mu}}V. \tag{7}$$

Then for the local $\widetilde{MS}_p$-SUSY to exist it requires the background spaces $(V_4,\, \underline{V}_2)$ to be curved. In this case, in order to become on the same footing with $\underline{V}_2$, the V_4 refers to the accelerated proper reference frame of a particle without relation to other matter fields. This leads us to extend the concept of differential forms to superspace. Points in curved superspace are then identified by the generalized coordinates

$$\begin{aligned} z^M &= (X^{\hat{\mu}},\, \Theta^{\hat{\alpha}},\, \bar{\Theta}_{\hat{\dot{\alpha}}}) = z^{(V_4)} \oplus z^{(\underline{V}_2)} \\ &= (\tilde{x}^{\mu},\, \theta^{\alpha},\, \bar{\theta}_{\dot{\alpha}}) \oplus (\underline{\tilde{x}}^{\underline{\mu}},\, \underline{\theta}^{\alpha},\, \bar{\underline{\theta}}_{\dot{\alpha}}), \end{aligned} \tag{8}$$

and differential elements

$$\begin{aligned} dz^M &= (dX^{\hat{\mu}},\, d\Theta^{\hat{\alpha}},\, d\bar{\Theta}_{\hat{\dot{\alpha}}}) = dz^{(V_4)} \oplus dz^{(\underline{V}_2)} \\ &= (d\tilde{x}^{\mu},\, d\theta^{\alpha},\, d\bar{\theta}_{\dot{\alpha}}) \oplus (d\underline{\tilde{x}}^{\underline{\mu}},\, d\underline{\theta}^{\alpha},\, d\bar{\underline{\theta}}_{\dot{\alpha}}), \end{aligned} \tag{9}$$

where $M \equiv (\hat{\mu}, \alpha, \dot{\alpha})$. Throughout we will use the 'two-in-one' notation of a theory MS$_p$-SUSY ((Appendix A), implying that any tensor (W) or spinor (Θ) with indices marked by 'hat' denote

$$\begin{aligned} W^{\hat{\mu}_1\cdots\hat{\mu}_m}_{\hat{\nu}_1\cdots\hat{\nu}_n} &:= W^{\mu_1\cdots\mu_m}_{\nu_1\cdots\nu_n} \oplus W^{\underline{\mu}_1\cdots\underline{\mu}_m}_{\underline{\nu}_1\cdots\underline{\nu}_n}, \\ \Theta^{\hat{\alpha}} &:= \theta^{\alpha} \oplus \underline{\theta}^{\alpha}, \quad \bar{\Theta}_{\hat{\dot{\alpha}}} := \bar{\theta}_{\dot{\alpha}} \oplus \bar{\underline{\theta}}_{\dot{\alpha}}. \end{aligned} \tag{10}$$

doi: https://doi.org/10.52526/25792776-24.71.2-230

This corresponds to the action of supercharge operators $Q \equiv$ (either q or $\underline{q}$) (see (88), (89)), which is due to the fact that the framework of $\widetilde{MS}_p$-SG combines bosonic and fermionic states in V_4 and $\underline{V}_2$ on the same base rotating them into each other under the action of operators $(q, \underline{q})$. The α are all upper indices, while $\dot{\alpha}$ is a lower index. Elements of superspace obey the following multiplication law: $z^M z^N = (-1)^{i(N)j(M)} z^N z^M$. Here $i(N)$ is a function of N and $j(M)$ is a function of M. These functions take the values zero or one, depending on whether N and M are vector or spinor indices. Exterior products in superspace are defined in complete analogy to ordinary space:

$$\begin{aligned} &dz^M \wedge dz^N = -(-1)^{i(N)j(M)} dz^N \wedge dz^M, \\ &dz^M z^N = (-1)^{i(N)j(M)} z^N \wedge dz^M. \end{aligned} \tag{11}$$

With this definition, differential forms have a standard extension to superspace. We shall drop the symbol $\wedge$ for exterior multiplication (unless indicated otherwise) and forbear to write the details out of a standard theory. They can be seen in, e.g. (Wess & Bagger, 1983, West, 1987, van Nieuwenhuizen, 1981). The multiplication of two local sequential supersymmetric transformations induces the motion

$$\begin{aligned} &g(0,\, \epsilon(X),\, \bar{\epsilon}(X))\, \Omega(X^{\hat{\mu}},\, \Theta^{\hat{\alpha}},\, \bar{\Theta}_{\hat{\dot{\alpha}}} \longrightarrow \\ &(X^{\hat{\mu}} + i\, \Theta^{\hat{\alpha}}\, \sigma^{\hat{\mu}}\, \bar{\epsilon}(X) - i\, \epsilon(X)\, \sigma^{\hat{\mu}}\, \bar{\Theta}_{\hat{\dot{\alpha}}},\, \Theta + \epsilon(X), \bar{\Theta} + \bar{\epsilon}(X)), \end{aligned} \tag{12}$$

which gives

$$\begin{aligned} &g_q(0,\, \xi(\widetilde{x}),\, \bar{\xi}(\widetilde{x}))\, \Omega_q(\widetilde{x},\, \theta,\, \bar{\theta}) \;\to \\ &(\widetilde{x}^m + i\, \theta\, \sigma^m\, \bar{\xi}(\widetilde{x}) - i\, \xi(\widetilde{x})\, \sigma^m\, \bar{\theta},\;\; \theta + \xi(\widetilde{x}),\, \bar{\theta} + \bar{\xi}(\widetilde{x})), \\ &g_{\underline{q}}(0,\, \underline{\xi}(\underline{\widetilde{x}}),\, \underline{\bar{\xi}}(\underline{\widetilde{x}}))\, \Omega_{\underline{q}}(\underline{\widetilde{x}},\, \underline{\theta},\, \underline{\bar{\theta}}) \;\to \\ &(\underline{\widetilde{x}^m} + i\, \underline{\theta}\, \sigma^{\underline{m}}\, \underline{\bar{\xi}}(\underline{\widetilde{x}}) - i\, \underline{\xi}(\underline{\widetilde{x}})\, \sigma^{\underline{m}}\, \underline{\bar{\theta}},\;\; \underline{\theta} + \underline{\xi}(\underline{\widetilde{x}}),\, \underline{\bar{\theta}} + \underline{\bar{\xi}}(\underline{\widetilde{x}})). \end{aligned} \tag{13}$$

In its simplest version, supergravity was conceived as a quantum field theory whose action included the gravitation field term, where the graviton coexists with a fermionic field called gravitino, described by the Rarita-Scwinger kinetic term. The two fields differ in their spin: 2 for the graviton, 3/2 for the gravitino. The different 4D $N = 1$ supergravity multiplets all contain the graviton and the gravitino, but differ by their systems of auxiliary fields. These fields would transform into each other under local supersymmetry. In this framework supersymmetry and general coordinate transformations are described in a unified way as certain diffeomorphisms. The motion (12) generates certain coordinate transformations:

$$z^M \;\longrightarrow\; z'^M = z^M - \zeta^M(z), \tag{14}$$

where $\zeta^M(z)$ arbitrary functions of z. The dynamical variables of superspace formulation are the frame field $E^A(z)$ and connection Ω. Using the analogue of Cartan's local frame, the superspace $(z^M,\, \Theta,\, \bar{\Theta})$ has at each point a tangent superspace spanned by the frame field defined as a 1-form over superspace

$$E^A(z) = dz^M E_M^{\;A}(z), \tag{15}$$

with coefficient superfields, generalizing the usual frame, namely supervierbien $E_M^{\;A}(z)$. Here, we use the first half of capital Latin alphabet $A, B, \ldots$ to denote the anholonomic indices related to the tangent superspace structure group, which is taken to be just the Lorentz group. The inverse vielbein $E_A^{\;M}(z)$ is defined by the relations

$$E_M^{\;A}(z)E_A^{\;N}(z) = \delta_M^{\;N}, \quad E_A^{\;M}(z)E_M^{\;B}(z) = \delta_A^{\;B}, \tag{16}$$

where

$$\delta_M^{\;N} = \begin{pmatrix} \delta_{\hat{m}}^{\;\hat{n}} & 0 & 0 \\ 0 & \delta_{\hat{\mu}}^{\;\hat{\nu}} & 0 \\ 0 & 0 & \delta_{\hat{\dot{\mu}}}^{\;\hat{\dot{\nu}}} \end{pmatrix}, \tag{17}$$

The formulation of supergravity in superspace provides a unified description of the vierbein and the Rarita-Schwinger fields, which are identified in a common geometric object, the local frame $E^A(z)$ of superspace. They are manifestly coordinate independent. The upper index A is reserved for the structure group, for which we take the Lorentz group. This is because we would like to recover supersymmetric flat space as a solution to our dynamical theory. With this choice, the reference frame defined by the vielbein is locally Lorentz covariant.

$$\delta E^A = E^B L_B^{\;A}(z), \quad \delta E_M^{\;A} = E_M^{\;B} L_B^{\;A}(z). \tag{18}$$

doi: https://doi.org/10.52526/25792776-24.71.2-230

The indices transforming under the structure group will be called Lorentz indices. The Lorentz generators $L_B^{\ A}(z)$ have three irreducible components: $L_{\hat{b}}^{\ \hat{a}}, L_{\beta}^{\ \alpha}$ and $L^{\dot{\hat{\beta}}}_{\ \dot{\alpha}}$. The vielbein forms $E^{\hat{a}} = dz^M E_M^{\hat{a}}$, $E^{\hat{\alpha}} = dz^M E_M^{\hat{\alpha}}$, and $E_{\hat{\dot{\alpha}}} = dz^M E_{M\hat{\dot{\alpha}}}$ are coordinate-independent irreducible Lorentz tensors.

To formulate covariant derivatives one must introduce a connection form

$$\phi = dz^M \phi_M, \quad \phi_M = \phi_{MA}^{\ \ \ B}, \tag{19}$$

transforming as follows under the structure group:

$$\delta\phi = \phi L - L\phi - dL. \tag{20}$$

Connections are Lie algebra valued one-forms

$$\phi = dz^M \phi_M^r(z) i T^r, \tag{21}$$

with the following transformation law:

$$\phi' = X^{-1}\phi X - X^{-1} dX, \tag{22}$$

where r runs over the dimension of the algebra. The connection is the second dynamical variable in this theory. The $\phi_{MA}^{\ \ \ B}$ is Lie algebra valued in its two Lorentz indices:

$$\phi_{MAB} = -(-1)^{ab}\phi_{MBA}. \tag{23}$$

Covariant derivatives with respect to local Lorentz transformations are constructed by means of the spin connection (or Lorentz connection), which is 1-form assuming values in the Lie algebra of the Lorentz group:

$$\omega_M(z) = \tfrac{1}{2}\omega^{AB}_{\ \ \ M}(z) S_{AB}, \tag{24}$$

with Lorentz generators S_{AB} of a given representation Y. The covariant derivative of the vielbein is called torsion:

$$T^A = dE^A + E^B \phi_B^{\ A}. \tag{25}$$

In flat space it is possible to transform the vielbein into the global reference frame: $E^A = e^A$. It is defined up to rigid Lorentz transformations. In this frame the connection vanishes: $\phi = 0$. The torsion, however, is non-zero because of the following non-zero components:

$$T_{\hat{\alpha}\dot{\hat{\beta}}}^{\ \ \ \hat{c}} = T_{\dot{\hat{\beta}}\hat{\alpha}}^{\ \ \ \hat{c}} = 2i\sigma_{\hat{\alpha}\dot{\hat{\beta}}}^{\ \ \ \hat{c}}. \tag{26}$$

The curvature tensor is defined in terms of the connection:

$$R = d\phi + \phi\phi. \tag{27}$$

It is a Lie algebra valued two-form:

$$R_A^{\ B} = \tfrac{1}{2} dz^M dz^N R_{NMA}^{\ \ \ \ \ B}. \tag{28}$$

Covariant derivatives with respect to local Lorentz transformations are constructed by means of the spin connection Ω, which is a 1-form in superspace. Supergauge transformations are constructed from the general coordinate and structure group transformations of superspace:

$$L_B^{\ A} = -\zeta^C \phi_{CB}^{\ \ \ A}. \tag{29}$$

They amount to a convenient reparametrization of these transformations. Supergauge transformations map Lorentz tensors into Lorentz tensors and reduce to supersymmetry transformations in the limit of flat space. The parameter ζ characterizes infinitesimal changes in coordinates. Whereas, either ζ^A or ζ^M may be chosen as the field-independent transformation parameter. Its companion then depends on the fields through the vielbein. Since we would like Lorentz tensors to transform into Lorentz tensors, we shall choose ζ^A to be field-independent. Supergauge transformations consist of a general coordinate transformation with field-independent parameter ζ^A followed by a structure group Lorentz transformation with field-dependent parameter (39). It is among this restricted class of transformations that we shall find the gauged supersymmetry transformations.

doi: https://doi.org/10.52526/25792776-24.71.2-230

The super-vielbein $E_M{}^A$ and spin-connection Ω contain many degrees of freedom. Although some of these are removed by the tangent space and supergeneral coordinate transformations, there still remain many degrees of freedom. There is no general prescription for deducing necessary covariant constraints which if imposed upon the superfields of super-vielbein and spin-connection will eliminate the component fields. However, some usual constraints can be found using tangent space and supergeneral coordinate transformations of the torsion and curvature covariant tensors, given in appropriate super-gauge. The transformation parameters ζ^A and $L_{\hat{a}\hat{b}}$ are functions of superspace. Their lowest components characterize general coordinate transformations in six-dimensional X-space $[\zeta^{\hat{a}}(X^{\hat{m}})]$, gauged supersymmetry transformations $[\zeta^{\hat{\alpha}}(X)], \zeta_{\hat{\dot\alpha}}(X)]$, and local Lorentz transformations $L_{\hat{a}\hat{b}}(X)$. We will use their higher components to transform away certain $\Theta=\bar{\Theta}=0$ components of the vielbein and the connection.

Let us consider the vielbein. Its transformation law may be written as a super-gauge transformation together with an additional Lorentz transformation $L_B{}^A$:

$$\delta_\zeta E_M{}^A = -\mathcal{D}_M\zeta^A - \zeta^B T_{BM}{}^A + E_M{}^B L_B{}^A. \tag{30}$$

The lowest component of this equation gives the transformation property of $E_M{}^A|_{\Theta=\bar{\Theta}=0}$. The $\Theta=\bar{\Theta}=0$ components of ζ^α and $\bar{\zeta}_{\dot\alpha}$ parametrize gauged supersymmetry transformations:

$$\begin{aligned} &\zeta^{\hat{a}}(z)|_{\Theta=\bar{\Theta}=0}=0, \quad \zeta^\alpha(z)|_{\Theta=\bar{\Theta}=0}=\zeta^\alpha(X), \\ &\bar{\zeta}_{\dot\alpha}(z)|_{\Theta=\bar{\Theta}=0}=\bar{\zeta}_{\dot\alpha}(X), \quad L_{AB}(z)=|_{\Theta=\bar{\Theta}=0}=0. \end{aligned} \tag{31}$$

Higher components of ζ^A enter $\delta E_M{}^A|$ through the covariant derivatives $\mathcal{D}_\alpha\zeta^A$ and $\bar{\mathcal{D}}^{\dot\alpha}\zeta^A$. One may use these higher components to transform super-vielbein to the final form, where the minimum number of independent component fields are the graviton, $e_{\hat\mu}{}^{\hat a}(X)$, and the gravitino, $\Psi_{\hat\mu}{}^\alpha(X), \bar{\Psi}_{\hat\mu\dot\alpha}(X)$. Since, by virtue of (10),

$$E_A{}^M(z)\big|_{\Theta=\bar{\Theta}=0} = E_a{}^\mu(z^{(V_4)})\big|_{\theta=\bar{\theta}=0}, \oplus\, E_{\underline{a}}{}^{\underline{\mu}}(z^{\underline{V}_2})\Big|_{\underline{\theta}=\underline{\bar{\theta}}=0} \tag{32}$$

accordingly, we find

$$E_a{}^\mu(z^{(V_4)})\big|_{\theta=\bar{\theta}=0} = \begin{pmatrix} e_\mu{}^a(x) & \frac12\psi_\mu{}^\alpha(x) & \frac12\bar{\psi}_{\mu\dot\alpha}(x) \\ 0 & \delta^\alpha_\gamma & 0 \\ 0 & 0 & \delta^{\dot\gamma}_{\dot\alpha} \end{pmatrix}, \tag{33}$$

and

$$E_{\underline{a}}{}^{\underline{\mu}}(z^{\underline{V}_2})\Big|_{\underline{\theta}=\underline{\bar{\theta}}=0} = \begin{pmatrix} e_{\underline{\mu}}{}^{\underline{a}}(\underline{\widetilde{x}}) & \frac12\psi_{\underline{\mu}}{}^\alpha(\underline{\widetilde{x}}) & \frac12\bar{\psi}_{\underline{\mu}\dot\alpha}(\underline{\widetilde{x}}) \\ 0 & \delta^\alpha_\gamma & 0 \\ 0 & 0 & \delta^{\dot\gamma}_{\dot\alpha} \end{pmatrix}. \tag{34}$$

The fields of graviton and gravitino cannot be gauged away. Provided, we have

$$\begin{aligned} &e_{\hat a}{}^{\hat\mu} e_{\hat\mu}{}^{\hat b} = \delta^{\hat b}_{\hat a}, \quad \Psi_{\hat a}{}^\gamma = e_{\hat a}{}^{\hat\mu}\Psi_{\hat\mu}{}^\alpha\delta^\gamma_\alpha, \\ &\bar{\Psi}_{\hat a\dot\gamma} = e_{\hat a}{}^{\hat\mu}\bar{\Psi}_{\hat\mu\dot\alpha}\delta_{\dot\gamma\dot\alpha}. \end{aligned} \tag{35}$$

The tetrad field $e_{\hat\mu}{}^{\hat a}(X)$ $(= e_\mu{}^a(x)\oplus e_{\underline{\mu}}{}^{\underline{a}}(\underline{\widetilde{x}}))$ plays the role of a gauge field associated with local transformations. The Majorana type field $\Psi_{\hat\mu}{}^\alpha(X)$ $(= \psi_\mu{}^\alpha(x)\oplus\psi_{\underline{\mu}}{}^\alpha(\underline{\widetilde{x}}))$ is the gauge field related to local supersymmetry. These two fields belong to the same supergravity multiplet which also accommodates auxiliary fields so that the local supersymmetry algebra closes. Under infinitesimal transformations of local supersymmetry, they transformed as

$$\begin{aligned} &\delta e_{\hat\mu}{}^{\hat a} = i(\Psi_{\hat\mu}\sigma^{\hat a}\zeta - \zeta\sigma^{\hat a}\bar{\Psi}_{\hat\mu}), \\ &\delta\Psi_{\hat\mu} = -2\mathcal{D}_{\hat\mu}\zeta^\alpha + ie_{\hat\mu}{}^{\hat c}\{\tfrac13 M(\varepsilon\sigma_{\hat c}\bar{\zeta})^\alpha + b_{\hat c}\zeta^\alpha + \tfrac13 b^{\hat d}(\zeta\sigma_{\hat d}\bar{\sigma}_{\hat c})\}, \end{aligned} \tag{36}$$

etc., where $M(X) = -6R(z)|_{\Theta=\bar{\Theta}=0}$ and $b_{\hat a}(X) = -3G(z)|_{\Theta=\bar{\Theta}=0}$ are the auxiliary fields, and

$$\begin{aligned} &\zeta^\alpha(z) = \zeta^\alpha(X), \quad \bar{\zeta}^\alpha(z) = \bar{\zeta}^\alpha(X), \\ &\zeta^{\bar a}(z) = 2i[\Theta\sigma^{\hat a}\bar{\zeta}(X) - \zeta(X)\sigma^{\hat a}\bar{\Theta}]. \end{aligned} \tag{37}$$

These auxiliary fields are not restricted by any differential equations in X-space. We cut short further description of the unitary supersymmetry representations that give rise to the concept of supermultiplets, since they are so well known.

doi: https://doi.org/10.52526/25792776-24.71.2-230

3. Non-trivial linear representation of the $\widetilde{MS}_p$-SUSY algebra

With these guidelines to follow, we start by considering a simplest example of a supersymmetric theory in six dimensional background curved spaces $V_4 \oplus \underline{V}_2$ as a $\widetilde{MS}_p$-generalization of flat space MS$_p$-SUSY model. We consider the chiral superfield, which is instructive because it contains the essential elements of the $\widetilde{MS}_p$-SUSY. The chiral superfields are defined as $\bar{\mathcal{D}}_{\hat{\dot{\alpha}}}\Phi = 0$, which reduces to $\bar{D}_{\hat{\dot{\alpha}}}\Phi = 0$ in flat space. To obtain a feeling for this model we may consider first example of non-trivial linear representation $(\widehat{\chi}, \mathcal{A}, \mathcal{F})$, of the $\widetilde{MS}_p$-SUSY algebra. This has $N = 1$ and $s_0 = 0$, and contains two Weyl spinor states $\widehat{\chi}(\chi,\, \underline{\chi})$, two complex scalar fields $\mathcal{A}(A,\, \underline{A})$, and two more real scalar degrees of freedom in the complex auxiliary fields $\mathcal{F}(F,\, \underline{F})$, which provide in a supersymmetry theory the fermionic and bosonic degrees of freedom to be equal off-shell as well as on-shell, and are eliminated when one goes on-shell. The component multiplets, $(\widehat{\chi}, \mathcal{A}, \mathcal{F})$, are called the chiral or scalar multiplets. We could define the component fields as the coefficient functions of a power series expansion in Θ and $\bar{\Theta}$. This decomposition, however, is coordinate-dependent. It is, therefore, more convenient to define them as

$$\mathcal{A} = \Phi|_{\Theta=\bar{\Theta}=0}\,, \quad \widehat{\chi}_\alpha = \tfrac{1}{\sqrt{2}}\mathcal{D}_\alpha\, \Phi|_{\Theta=\bar{\Theta}=0}\,, \quad \mathcal{F} = -\tfrac{1}{4}\mathcal{D}^\alpha\mathcal{D}_\alpha\, \Phi|_{\Theta=\bar{\Theta}=0}\,, \tag{38}$$

which carry Lorentz indices. They are related to the Θ and $\bar{\Theta}$ expansion coefficients through a transformation which depends on the supergravity multiplet. The transformation laws of the component fields are found from the transformation law of the superfield Φ: $\delta\Phi = -\zeta^A\mathcal{D}_A\Phi$, provided, the parameters ζ^A are specified as (37). Under infinitesimal transformations of local supersymmetry, the transformation law of the chiral multiplet, incorporating with embedding map $\underline{V}_2 \hookrightarrow V_4$ (4), and the transformation law $\underline{A}(\underline{\widetilde{x}}) = A(\widetilde{x})$ for spin-zero scalar field, give

$$\begin{aligned}
&\delta\underline{A} = -\sqrt{2}\zeta^\alpha\chi_\alpha,\\
&\delta\chi_\alpha = -\sqrt{2}\zeta_\alpha F - i\sqrt{2}\sigma_{\alpha\dot{\beta}}{}^{a}\bar{\zeta}^{\dot{\beta}}\widehat{D}_a\underline{A},\\
&\delta F = -\tfrac{\sqrt{2}}{3}M^*\zeta^\alpha\chi_\alpha + \bar{\zeta}^{\dot{\alpha}}\left(\tfrac{1}{6}\sqrt{2}b_{\alpha\dot{\alpha}}\chi^\alpha - i\sqrt{2}\widehat{D}_{\alpha\dot{\alpha}}\chi^\alpha\right),
\end{aligned} \tag{39}$$

where

$$\begin{aligned}
&\widehat{D}_a\underline{A} \equiv e_a{}^\mu\left[\left(\tfrac{\partial\widetilde{x}^0}{\partial\widetilde{x}^\mu}\right)\underline{\widetilde{\partial}_0}\,\underline{A} + \left(\tfrac{\partial|\underline{\widetilde{x}}|}{\partial\widetilde{x}^\mu}\right)\underline{\widetilde{\partial}_1}\,\underline{A} - \tfrac{1}{\sqrt{2}}\Psi_\mu{}^\beta\chi_\beta\right],\\
&\widehat{D}_a\chi_\alpha = e_a{}^\mu\left(\mathcal{D}_\mu\chi_\alpha - \tfrac{1}{\sqrt{2}}\Psi_{\mu\alpha}F - \tfrac{i}{\sqrt{2}}\bar{\Psi}_\mu{}^{\dot{\beta}}\widehat{D}_{\alpha\dot{\beta}}\underline{A}\right).
\end{aligned} \tag{40}$$

In the same way, we should define the spinor $\underline{\chi}$ as the field into which $A(x)$ transforms. In this case, the infinitesimal supersymmetry transformations for $Q = \underline{q}$ read

$$\begin{aligned}
&\delta A = -\sqrt{2}\underline{\zeta}^\alpha\underline{\chi}_\alpha,\\
&\delta\underline{\chi}_\alpha = -\sqrt{2}\underline{\zeta}_\alpha\underline{F} - i\sqrt{2}\sigma_{\alpha\,\dot{\beta}}{}^{\underline{a}}\bar{\underline{\zeta}}^{\dot{\beta}}\widehat{D}_{\underline{a}}A,\\
&\delta\underline{F} = -\tfrac{\sqrt{2}}{3}\underline{M}^*\underline{\zeta}^\alpha\underline{\chi}_\alpha + \bar{\underline{\zeta}}^{\dot{\alpha}}\left(\tfrac{1}{6}\sqrt{2}\underline{b}_{\alpha\,\dot{\alpha}}\underline{\chi}^\alpha - i\sqrt{2}\widehat{D}_{\alpha\,\dot{\alpha}}\underline{\chi}^\alpha\right),
\end{aligned} \tag{41}$$

where

$$\begin{aligned}
&\widehat{D}_{\underline{a}}A \equiv \underline{e}_{\underline{a}}{}^{\underline{\mu}}\left[\left(\tfrac{\partial\widetilde{x}^0}{\partial\underline{\widetilde{x}}^{\underline{\mu}}}\right)\widetilde{\partial}_0\, A + \left(\tfrac{\partial\widetilde{x}^i}{\partial\underline{\widetilde{x}}^{\underline{\mu}}}\right)\widetilde{\partial}_i\, A - \tfrac{1}{\sqrt{2}}\underline{\Psi}_{\underline{\mu}}{}^\beta\underline{\chi}_\beta\right],\\
&\widehat{D}_{\underline{a}}\chi_\alpha = \underline{e}_{\underline{a}}{}^{\underline{\mu}}\left(\mathcal{D}_{\underline{\mu}}\underline{\chi}_\alpha - \tfrac{1}{\sqrt{2}}\underline{\Psi}_{\underline{\mu}\,\alpha}\underline{F} - \tfrac{i}{\sqrt{2}}\bar{\underline{\Psi}}_{\underline{\mu}}{}^{\dot{\beta}}\widehat{D}_{\alpha\,\dot{\beta}}A\right).
\end{aligned} \tag{42}$$

The graviton and the gravitino form thus the basic multiplet of local $\widetilde{MS}_p$-SUSY, and one expects the simplest locally supersymmetric model to contain just this multiplet.

4. The simple $(N = 1)$ $\widetilde{MS}_p$ - SG without auxiliary fields

An essential difference arisen between the standard supergravity theories and some rather unusual properties of a $\widetilde{MS}_p$-SG theory is as follows. In the framework of the standard supergravity theories, as in GR, a curvature of the space-time acts on all the matter fields. The source of graviton is the energy-momentum tensor of matter fields, while the source of gravitino is the spin-vector current of supergravity. The gauge action of simple $\widetilde{MS}_p$-SG is the sum of the Hilbert action for the tetrad field - *fictitious* graviton, and the Rarita-Schwinger action for the *fictitious* gravitino field. Instead we argue that they refer to the particle of

doi: https://doi.org/10.52526/25792776-24.71.2-230

interest itself, without relation to other matter fields, so that these fields can be globally removed by appropriate coordinate transformations. The $\widetilde{MS}_p$-SG theory is so constructed as to make these two particles just as being the two bosonic and fermionic states in the curved background spaces V_4 and $\underline{V}_2$, respectively, or vice versa. Whereas, in order to become on the same footing with $\underline{V}_2$, the V_4 refers only to the accelerated proper reference frame of a particle. With these physical requirements, a standard coupling of supergravity with matter superfields evidently no longer holds. We are now looking for an alternative way of implications of $\widetilde{MS}_p$-SG for the model of accelerated motion and inertial effects.

We will use the techniques of (van Nieuwenhuizen, 1981) extended in a plausible fashion to the $\widetilde{MS}_p$-SG. The generalized Poincaré superalgebra for the simple $(N=1)$ $\widetilde{MS}_p$-SG reads:

$$\begin{array}{l} [P_{\hat{a}}, P_{\hat{b}}] = 0, \quad [S_{\hat{a}\hat{b}}, P_{\hat{c}}] = (\eta_{\hat{a}\hat{c}}P_{\hat{b}} - \eta_{\hat{b}\hat{c}}P_{\hat{a}}), \\ [S_{\hat{a}\hat{b}}, S_{\hat{c}\hat{d}}] = i(\eta_{\hat{a}\hat{c}}S_{\hat{b}\hat{d}} - \eta_{\hat{b}\hat{c}}S_{\hat{a}\hat{d}} + \eta_{\hat{b}\hat{d}}S_{\hat{a}\hat{c}} - \eta_{\hat{a}\hat{d}}S_{\hat{b}\hat{c}}), \\ [S_{\hat{a}\hat{b}}, Q^{\alpha}] = \frac{1}{2}(\gamma_{\hat{a}\hat{b}})^{\alpha}_{\beta}Q^{\beta}, \\ [P_{\hat{a}}, Q^{\beta}] = 0, \quad [Q_{\alpha}, \bar{Q}_{\dot{\beta}}] = \frac{1}{2}(\gamma^{\hat{a}})_{\alpha\dot{\beta}}P_{\hat{a}}. \end{array} \tag{43}$$

with $(S_{\hat{a}\hat{b}})^{\hat{c}}_{\hat{d}} = i(\delta^{\hat{c}}_{\hat{a}}\eta_{\hat{b}\hat{d}} - \delta^{\hat{c}}_{\hat{b}}\eta_{\hat{a}\hat{d}})$ (24) a given representation of the Lorentz generators. Using (43) and a general form for gauge transformations on B^A,

$$\delta B = \mathcal{D}\lambda = d\lambda + [B, \lambda], \tag{44}$$

with

$$\lambda = \rho^{\hat{a}}P_{\hat{a}} + \frac{1}{2}\kappa^{\hat{a}\hat{b}}S_{\hat{a}\hat{b}} + \bar{Q}\varepsilon, \tag{45}$$

we obtain that the $(e^{\hat{a}}, \omega^{\hat{a}\hat{b}}, \Psi)$ transform under Poincaré translations as

$$\delta e^{\hat{a}} = \mathcal{D}\rho^{\hat{a}}, \quad \delta\omega^{\hat{a}\hat{b}} = 0, \quad \delta\Psi = 0; \tag{46}$$

under Lorentz rotations as

$$\delta e^{\hat{a}} = \kappa^{\hat{a}}_{\hat{b}}\delta e^{\hat{b}}, \quad \delta\omega^{\hat{a}\hat{b}} = -\mathcal{D}\kappa^{\hat{a}\hat{b}}, \quad \delta\Psi = \frac{1}{4}\kappa^{\hat{a}\hat{b}}\gamma_{\hat{a}\hat{b}}\Psi; \tag{47}$$

and under supersymmetry transformation as

$$\delta e^{\hat{a}} = \frac{1}{2}\bar{\varepsilon}\gamma^{\hat{a}}\Psi, \quad \delta\omega^{\hat{a}\hat{b}} = 0, \quad \delta\Psi = \mathcal{D}\varepsilon. \tag{48}$$

In first-order formalism, the gauge fields $(e^{\hat{a}}, \omega^{\hat{a}\hat{b}}, \Psi)$, (with $\Psi = (\psi, \underline{\psi})$ a two-component Majorana spinor) are considered as an independent members of multiplet in the adjoint representation of the Poincaré supergroup of $D = 6$ $((3+1), (1+1))$ simple $(N = 1)$ $\widetilde{MS}_p$-SG with the generators $(P_{\hat{a}}, S_{\hat{a}\hat{b}}, Q^{\alpha})$. Unless indicated otherwise, henceforth the world indices are kept implicit without ambiguity. The operators carry Lorentz indices not related to coordinate transformations. The Yang-Mills connection for the Poincare´ supergroup is given by

$$B = B^A T_A = e^{\hat{a}}P_{\hat{a}} + \frac{1}{2}i\omega^{\hat{a}\hat{b}}S_{\hat{a}\hat{b}} + \Psi\bar{Q}. \tag{49}$$

The field strength associated with connection B is defined as the Poincaré Lie superalgebra-valued curvature two-form R^A. Splitting the index A, and taking the $\Theta = \bar{\Theta} = 0$ component of R^A, we obtain

$$\begin{array}{l} R^{\ \hat{a}\hat{b}}(\omega) = d\omega^{\hat{a}\hat{b}} - \omega^{\hat{a}}{}_{\hat{c}}\omega^{\hat{c}\hat{d}}, \\ \tilde{T}^{\hat{a}} = T^{\hat{a}} - \frac{1}{2}\bar{\Psi}\gamma^{\hat{a}}\Psi, \quad \rho = \mathcal{D}\Psi, \end{array} \tag{50}$$

where $\gamma^{\hat{a}} = (\gamma^a, \sigma^{\underline{a}})$, $R^{\ \hat{a}\hat{b}}(\omega)$ is the Riemann curvature in terms of the spin connection $\omega^{\hat{a}\hat{b}}$, and the generalized Weyl lemma (see App./(4)) requires that the, so-called, supertorsion $\tilde{T}^{\hat{a}}$ be inserted. The solution $\omega(e)$ satisfies the tetrad postulate that the completely covariant derivative of the tetrad field vanishes, therefore $R^{\hat{a}\hat{b}}(\omega) = R(\omega)e^{\hat{a}}e^{\hat{b}}$.

For the bosonic part of the gauge action (graviton of spin 2) of simple $\widetilde{MS}_p$-SG it then seems appropriate to take the generalized Hilbert action with $e = det\, e^{\hat{a}}{}_{\mu}(X)$. While the fermionic part of the standard gauge action (garvitino of spin 3/2), which has positive energy, is the Rarita-Schwinger action. The full nonlinear gravitino action in curved space then should be its extension to curved space, which can be achieved by inserting the Lorentz covariant derivative $\mathcal{D}\Psi = d\Psi + \frac{1}{2}\omega^{\ \hat{a}\hat{b}}\gamma_{\hat{a}\hat{b}}\Psi$. In both parts, the spin connection is

doi: https://doi.org/10.52526/25792776-24.71.2-230

considered a dependent field, otherwise in the case of an independent spin connection ω, the action will be invariant under diffeomorphism, and under local Lorentz rotations, but it will be not invariant under the neither the Poincaré translations nor the supersymmetry. In the case if spin connection is independent, we should have under the local Poincaré translations

$$\delta\hat{\mathcal{L}}_{pt} = \delta\left(\varepsilon_{\hat{a}\hat{b}\hat{c}\hat{d}}e^{\hat{a}}e^{\hat{b}}R^{\hat{c}\hat{d}} + 4\bar{\Psi}\gamma_{\hat{5}}e^{\hat{a}}\gamma_{\hat{a}}\mathcal{D}\Psi\right) = 2\varepsilon_{\hat{a}\hat{b}\hat{c}\hat{d}}R^{\hat{a}\hat{b}}\tilde{T}^{\hat{c}}\rho^{\hat{d}} + \text{surf. term}, \tag{51}$$

and under local supersymmetry transformations

$$\delta\hat{\mathcal{L}}_{SUSY} = -4\bar{\varepsilon}\gamma_{\hat{5}}\gamma_{\hat{a}}\mathcal{D}\Psi\tilde{T}^{\hat{a}} + \text{surf. term}. \tag{52}$$

The invariance of the action then requires the vanishing of the supertorsion $\tilde{T}^{\hat{a}} = 0$, which means that the connection is no longer an independent variable. So that the starting point of our approach is the action of a simple $\widetilde{MS}_p$-SG theory written in 'two in one'-notation (10), which is invariant under the local supersymmetry transformation (48), where the Poincaré superalgebra closes off shell without the need for any auxiliary fields:

$$\mathcal{L}_{MS-SG} = \varepsilon_{\hat{a}\hat{b}\hat{c}\hat{d}}e^{\hat{a}}e^{\hat{b}}R^{\hat{c}\hat{d}}(\omega) + 4\bar{\Psi}\gamma_{\hat{5}}e^{\hat{a}}\gamma_{\hat{a}}\mathcal{D}\Psi. \tag{53}$$

This is the sum of bosonic and fermionic parts with the same spin connection, where $\gamma_{\hat{a}} = (\gamma_a \oplus \sigma_{\underline{a}})$, $\gamma_{\hat{5}} = (\gamma_5 \oplus \gamma_{\underline{5}})$, $\gamma_{\underline{5}} = \begin{pmatrix} 1 & 0 \\ 0 & -1 \end{pmatrix}$ is given in the chiral or Weyl representations, i.e. in the irreducible 2-dimensional spinor representations $(\frac{1}{2}, 0)$ and $(0, \frac{1}{2})$, since two-component formalism works for a Weyl fermion. This is indispensable in order to solve algebraical constraints in superspace because they can be used as building blocks of any fermion field (van Nieuwenhuizen, 1981). In this representation, action of projection matrices $L = (1/2)(1+\gamma_{\underline{5}})$ and $R = (1/2)(1-\gamma_{\underline{5}})$ on a Dirac fermion leads to zero two lower components of the left-handed spinor and zero two upper components of the right-handed spinor, respectively. The two-component notation described above essentially does away with the vanishing components explicitly and deals only with the non-trivial ones. Taking into account that $g_{\hat{\mu}\hat{\nu}} = \eta_{\hat{a}\hat{b}}e_{\hat{\mu}}{}^{\hat{a}}e_{\hat{\nu}}{}^{\hat{b}}$ and $\gamma_{\hat{\mu}} = e_{\hat{\mu}}{}^{\hat{a}}\gamma_{\hat{a}}$, with $\eta_{\hat{a}\hat{b}} = (\eta_{ab} \oplus \eta_{\underline{ab}})$ related to the tangent space, where $\eta_{ab} = diag(+1,-1,-1,-1)$ and $\eta_{\underline{ab}} = diag(+1,-1)$, we can recast the generalized bosonic and fermionic actions given in (53), respectively, in the forms

$$\mathcal{L}^{(2)} = -\tfrac{1}{4}\sqrt{g}R(g,\Gamma) = -\tfrac{1}{4}eR(e,\omega), \tag{54}$$

and

$$\mathcal{L}^{(3/2)} = 4\varepsilon^{\hat{\mu}\hat{\nu}\hat{\rho}\hat{\sigma}}\bar{\Psi}_{\hat{\mu}}\gamma_{\hat{5}}\gamma_{\hat{\nu}}\mathcal{D}_{\hat{\rho}}\Psi_{\hat{\sigma}}. \tag{55}$$

Here we taken into account that $\mathcal{D}_{\hat{\rho}}\Psi_{\hat{\sigma}}$ is the curl due to the ε-symbol, and as far as $\varepsilon^{\hat{\mu}\hat{\nu}\hat{\rho}\hat{\sigma}}$ is the density (which always equals $0, \pm 1$), so there is no need to put the density e in front of fermionic part. The variation of action (53) with respect to $(e^{\hat{a}}, \omega^{\hat{a}\hat{b}}, \bar{\Psi})$ leads to the following equations for $\widetilde{MS}_p$ - SG:

$$\begin{aligned} &\varepsilon_{\hat{a}\hat{b}\hat{c}\hat{d}}e^{\hat{b}}R^{\hat{c}\hat{d}} + 2\bar{\Psi}\gamma_{\hat{5}}\gamma_{\hat{a}}\mathcal{D}\Psi = 0; \\ &\varepsilon_{\hat{a}\hat{b}\hat{c}\hat{d}}e^{\hat{c}}\tilde{T}^{\hat{d}} = 0; \;\; \gamma_{\hat{5}}e^{\hat{a}}\gamma_{\hat{a}}\mathcal{D}\Psi = 0, \end{aligned} \tag{56}$$

which can be rewritten as well in the form

$$\begin{aligned} &R^{\hat{\tau}\hat{\mu}} - \tfrac{1}{2}g^{\hat{\tau}\hat{\mu}}R + 2\varepsilon^{\hat{\lambda}\hat{\mu}\hat{\nu}\hat{\rho}}\bar{\Psi}_{\hat{\lambda}}\gamma_{\hat{5}}\gamma^{\hat{\tau}}\mathcal{D}_{\hat{\nu}}\Psi_{\hat{\rho}} = 0; \\ &\tilde{T}^{\hat{\lambda}}{}_{\hat{\mu}\hat{\nu}} = T^{\hat{\lambda}}{}_{\hat{\mu}\hat{\nu}} - \tfrac{1}{2}\bar{\Psi}_{\hat{\mu}}\gamma^{\hat{\lambda}}\Psi_{\hat{\nu}}; \\ &\varepsilon^{\hat{\mu}\hat{\nu}\hat{\rho}\hat{\sigma}}\gamma_{\hat{5}}\gamma_{\hat{\nu}}\mathcal{D}_{\hat{\rho}}\Psi_{\hat{\sigma}} = 0. \end{aligned} \tag{57}$$

This, according to (10), gives the following equations for the Rarita-Schwinger fields $\psi(x)$ and $\underline{\psi}(\underline{x})$ defined, respectively, on the $x \in V_4$ and $\underline{x} \in \underline{V}_2$:

$$\varepsilon^{\mu\nu\rho\sigma}\gamma_5\gamma_\nu\mathcal{D}_\rho\psi_\sigma = 0, \quad \varepsilon^{\underline{\mu}\underline{\nu}\underline{\rho}\underline{\sigma}}\gamma_{\underline{5}}\sigma_{\underline{\nu}}\underline{\mathcal{D}}_{\underline{\rho}}\underline{\psi}_{\underline{\sigma}} = 0. \tag{58}$$

doi: https://doi.org/10.52526/25792776-24.71.2-230

5. Particle mechanics in the 4D Minkowski space-time: Velocity and acceleration

From embedding map (4), we obtain the components of velocity of a particle

$$\begin{aligned} &\underline{\widetilde{v}}^{(\pm)} = \frac{d\underline{x}^{(\pm)}}{d\underline{\widetilde{x}}^{\underline{0}}} = \frac{1}{\sqrt{2}}(\underline{\widetilde{v}}^{\underline{0}} \pm \underline{\widetilde{v}}^{\underline{1}}), \\ &\underline{\widetilde{v}}^{\underline{1}} = \frac{d\underline{\widetilde{x}}^{\underline{1}}}{d\underline{\widetilde{x}}^{\underline{0}}} = |\vec{\widetilde{v}}| = |\frac{d\vec{\widetilde{x}}}{d\widetilde{x}^{0}}|, \end{aligned} \tag{59}$$

so that

$$\begin{aligned} &\underline{\widetilde{u}} = \underline{\widetilde{e}}_{\underline{m}} \underline{\widetilde{v}}^{\underline{m}} = (\underline{\vec{\widetilde{v}}}_{\underline{0}}, \underline{\vec{\widetilde{v}}}_{\underline{1}}), \\ &\underline{\vec{\widetilde{v}}}_{\underline{0}} = \underline{\widetilde{e}}_{0} \underline{\widetilde{v}}^{\underline{0}}, \quad \underline{\vec{\widetilde{v}}}_{\underline{1}} = \underline{\vec{\widetilde{e}}}_{\underline{1}} \underline{\widetilde{v}}^{\underline{1}} = \vec{n}|\vec{\widetilde{v}}| = \vec{\widetilde{v}}, \end{aligned} \tag{60}$$

therefore, $\underline{\widetilde{u}} = (\underline{\vec{\widetilde{v}}}_{\underline{0}}, \underline{\vec{\widetilde{v}}}_{\underline{1}}) = \widetilde{u} = (\widetilde{e}_0, \vec{\widetilde{v}})$. Thence, the components of the acceleration vector, $\dot{a}^{\hat{\rho}} = (a^{\rho}, \underline{a}^{\underline{\rho}})$, satisfy the following embedding relations

$$\underline{a}^{\underline{0}} = a^{0}, \quad \underline{a}^{\underline{1}} = |\vec{a}|. \tag{61}$$

The accelerated motion of a particle is described by the parameter $\epsilon = \epsilon(X^{\hat{\mu}})$ in (12) of local SUSY, which depends explicitly on $X^{\hat{\mu}} = (\widetilde{x}^{\mu}, \underline{\widetilde{x}}^{\underline{\mu}})$, where $\widetilde{x}^{\mu} \in V_4$ and $\underline{\widetilde{x}}^{\underline{\mu}} \in \underline{V}_2$. To be specific, let us focus for the motion (37) on the simple case of a peculiar anticommuting spinors $(\underline{\xi}(\underline{\widetilde{x}}), \underline{\bar{\xi}}(\underline{\widetilde{x}}))$ and $(\xi(\widetilde{x}), \bar{\xi}(\widetilde{x}))$ defined as

$$\begin{aligned} &\underline{\xi}^{\alpha}(\underline{\widetilde{x}}) = i\,\frac{\underline{\tau}(\underline{\widetilde{x}})}{2}\,\underline{\theta}^{\alpha}, \quad \underline{\bar{\xi}}_{\dot{\alpha}}(\underline{\widetilde{x}}) = -i\,\frac{\underline{\tau}^{*}(\underline{\widetilde{x}})}{2}\,\underline{\bar{\theta}}_{\dot{\alpha}}, \\ &\xi^{\alpha}(\widetilde{x}) = i\frac{\tau(\widetilde{x})}{2}\theta^{\alpha}, \quad \bar{\xi}_{\dot{\alpha}}(\widetilde{x}) = -i\frac{\tau^{*}(\widetilde{x})}{2}\bar{\theta}_{\dot{\alpha}}. \end{aligned} \tag{62}$$

Here the real parameter $\tau(\widetilde{x}) = \tau^{*}(\widetilde{x}) = \underline{\tau}(\underline{\widetilde{x}}) = \underline{\tau}^{*}(\underline{\widetilde{x}})$ can physically be interpreted as the *atomic duration time* of double transition of a particle $V_4 \rightleftharpoons \underline{V}_2$ (Fig. 1), i.e. the period of superoscillations. In this case, the *atomic displacement* caused by double transition, according to (60), reads

$$\Delta\underline{\widetilde{x}}_{(a)} = \underline{\widetilde{e}}_{\underline{m}} \Delta\underline{\widetilde{x}}^{\underline{m}}_{(a)} = \underline{\widetilde{u}}\tau(\underline{\widetilde{x}}), \tag{63}$$

where, according to the motion (100), the components $\Delta\underline{\widetilde{x}}^{\underline{m}}_{(a)}$ are written

$$\Delta\underline{\widetilde{x}}^{\underline{m}}_{(a)} = \underline{\widetilde{v}}^{\underline{m}}\,\tau(\underline{\widetilde{x}}) = i\underline{\theta}\,\sigma^{\underline{m}}\,\underline{\bar{\xi}}(\underline{\widetilde{x}}) - i\underline{\xi}(\underline{\widetilde{x}})\,\sigma^{\underline{m}}\,\underline{\bar{\theta}}. \tag{64}$$

The corresponding acceleration reads

$$a^{(\pm)} = i\underline{\theta}\,\sigma^{(\pm)}\,\frac{d^2\underline{\bar{\xi}}}{d\underline{\widetilde{s}}^2} - i\frac{d^2\underline{\xi}}{d\underline{\widetilde{s}}^2}\,\sigma^{(\pm)}\,\underline{\bar{\theta}}, \tag{65}$$

where $\sigma^{(\pm)} = \frac{1}{\sqrt{2}}(\sigma^{\underline{0}} \pm \sigma^{\underline{1}}) = \frac{1}{\sqrt{2}}(\sigma^{0} \pm \sigma^{3})$ and $d\underline{\widetilde{s}}^2 = d\underline{\widetilde{x}}^{(+)} d\underline{\widetilde{x}}^{(-)}$. By virtue of (62), the (65) is reduced to

$$a^{(\pm)} = v_c^{(\pm)}\,\frac{d^2\tau}{d\underline{\widetilde{s}}^2}, \tag{66}$$

where $v_c^{(\pm)} \equiv (\underline{\theta}\,\sigma^{(\pm)}\underline{\bar{\theta}})$.

In Van der Warden notations for the Weyl two-component formalism $(\underline{\bar{\theta}}_{\dot{\alpha}})^{*} = \underline{\theta}_{\alpha}$ and $\underline{\bar{\theta}}_{\dot{\alpha}} = (\underline{\theta}_{\alpha})^{*}$, the (66) gives

$$\begin{aligned} &\underline{\widetilde{a}} = \sqrt{2}(a^{(+)}a^{(-)})^{1/2} = \sqrt{2}\underline{v}_c\,\frac{d^2\tau}{d\underline{\widetilde{s}}^2}, \\ &\underline{v}_c = (v_c^{(+)}v_c^{(-)})^{1/2} = \sqrt{2}(\underline{\theta}_1\,\underline{\bar{\theta}}_1\underline{\theta}_2\,\underline{\bar{\theta}}_2)^{1/2}, \end{aligned} \tag{67}$$

with $v_c^{(+)} = \sqrt{2}(\underline{\theta}_1\,\underline{\bar{\theta}}_1)$ and $v_c^{(-)} = \sqrt{2}(\underline{\theta}_2\,\underline{\bar{\theta}}_2)$. The acceleration will generally remain a measure of the velocity variation over proper time $(\underline{\widetilde{s}})$. The (66) and (67) yield

$$\begin{aligned} &v^{(\pm)} = v_c^{(\pm)}\left(\frac{d\tau}{d\underline{\widetilde{s}}} + 1\right), \\ &\underline{\widetilde{v}} = \sqrt{2}(v^{(+)}v^{(-)})^{1/2} = \sqrt{2}\underline{v}_c\left(\frac{d\tau}{d\underline{\widetilde{s}}} + 1\right). \end{aligned} \tag{68}$$

The spinors $\theta(\underline{\theta}, \underline{\bar{\theta}})$ and $\bar{\theta}(\underline{\theta}, \underline{\bar{\theta}})$ satisfy the embedding map (4), namely $\Delta\underline{\widetilde{x}}^{\underline{0}} = \Delta\widetilde{x}^{0}$ and $(\Delta\underline{\widetilde{x}}^{\underline{1}})^2 = (\Delta\vec{\widetilde{x}})^2$, so from (100) we obtain

$$\begin{aligned} &\underline{\theta}\,\sigma^{0}\,\underline{\bar{\xi}} - \underline{\xi}\,\sigma^{0}\,\underline{\bar{\theta}} = \theta\,\sigma^{0}\,\bar{\xi} - \xi\,\sigma^{0}\,\bar{\theta}, \\ &(\underline{\theta}\,\sigma^{3}\,\underline{\bar{\xi}} - \underline{\xi}\,\sigma^{3}\,\underline{\bar{\theta}})^2 = (\theta\,\vec{\sigma}\,\bar{\xi} - \xi\,\vec{\sigma}\,\bar{\theta})^2. \end{aligned} \tag{69}$$

doi: https://doi.org/10.52526/25792776-24.71.2-230

Denote

$$\begin{aligned} \underline{v}^0_{(c)} &= \tfrac{1}{\sqrt{2}}\left(v_c^{(+)} + v_c^{(-)}\right) = (\underline{\theta}\,\bar{\underline{\theta}}), \\ \underline{v}^1_{(c)} &= \tfrac{1}{\sqrt{2}}\left(v_c^{(+)} - v_c^{(-)}\right) = (\underline{\theta}_1\,\bar{\underline{\theta}}_1 - \underline{\theta}_2\,\bar{\underline{\theta}}_2), \end{aligned} \tag{70}$$

then both relations in map (69) are reduced to

$$\theta\bar{\theta} = \underline{v}^0_{(c)}, \quad \theta\theta\bar{\theta}\bar{\theta} = -\tfrac{2}{3}(\underline{v}^1_{(c)})^2. \tag{71}$$

Here we have used the following spinor algebra relations (Wess & Bagger, 1983):

$$(\theta\sigma^m\,\bar{\theta})(\theta\sigma^n\,\bar{\theta}) = \tfrac{1}{2}\,\theta\theta\bar{\theta}\bar{\theta}\,g^{mn}. \tag{72}$$

By virtue of relations $\theta_\alpha\theta_\beta = \frac{1}{2}\varepsilon_{\alpha\beta}\theta\theta$ and $\bar{\theta}_{\dot{\alpha}}\bar{\theta}_{\dot{\beta}} = -\frac{1}{2}\varepsilon_{\dot{\alpha}\dot{\beta}}\bar{\theta}\bar{\theta}$, where the antisymmetric tensors $\varepsilon_{\alpha\beta}$ and $\varepsilon^{\alpha\beta}$ ($\varepsilon_{21} = \varepsilon^{12} = 1, \varepsilon_{12} = \varepsilon^{21} = -1, \varepsilon_{11} = \varepsilon_{22} = 0$), and that of the inner product of two spinors $\theta\theta = \theta^\alpha\theta_\alpha$ and $\bar{\theta}\bar{\theta} = \bar{\theta}_{\dot{\alpha}}\bar{\theta}^{\dot{\alpha}}$, are invariant under Lorentz transformations because of unimodular matrix M (Lahanas & Nanopoulos, 1987, Wess & Bagger, 1983), we obtain from (71): $\theta_1^2 + \theta_2^2 = \underline{v}^0_{(c)}$, and $\theta_1\theta_2 = \frac{1}{\sqrt{6}}\underline{v}^1_{(c)}$, which yield

$$\begin{aligned} \theta_1(\underline{\theta},\,\bar{\underline{\theta}}) &= \tfrac{1}{2}\left[\left(\underline{v}^0_{(c)} + \sqrt{\tfrac{2}{3}}\underline{v}^1_{(c)}\right)^{1/2} + \left(\underline{v}^0_{(c)} - \sqrt{\tfrac{2}{3}}\underline{v}^1_{(c)}\right)^{1/2}\right], \\ \theta_2(\underline{\theta},\,\bar{\underline{\theta}}) &= \tfrac{1}{2}\left[\left(\underline{v}^0_{(c)} + \sqrt{\tfrac{2}{3}}\underline{v}^1_{(c)}\right)^{1/2} - \left(\underline{v}^0_{(c)} - \sqrt{\tfrac{2}{3}}\underline{v}^1_{(c)}\right)^{1/2}\right]. \end{aligned} \tag{73}$$

The dynamical aspects of particle mechanics involve derivatives with respect to proper time along the particle worldline. A worldline C of a particle, parametrized by proper time as $C(s) = X^{\hat{\mu}}(s)$, will have as six-velocity the vector of components $u^{\hat{\mu}} = dX^{\hat{\mu}}/ds$ and $u^{\hat{a}} = \dot{e}^{\hat{a}}_{\hat{\mu}}u^{\hat{\mu}}$, which are the particle velocity along this curve respectively in the holonomic and anholonomic bases in the X-space.

6. Concluding remarks

In this section we highlight a few points and discuss issues to be studied further. To innovate the solution to the problems involved, in this paper we develop on the theory of $\widetilde{MS}_p$-SG, which is a *local* extension of a global MS$_p$-SUSY theory (Ter-Kazarian, 2024a).

(I) We emphasize that the MS$_p$-SUSY (which is about the *inertial motion*, first part of inertia), together with the $\widetilde{MS}_p$-SG (which is about the *acceleration and inertia effects*, second part of inertia), provide valuable theoretical clue for a complete revision of our ideas about the Lorentz code of motion, as well as the acceleration and inertia effects, to be now referred to as the *intrinsic* property of a particle of interest devoid of any matter influence. This is a result of the first importance for a really comprehensive entire theory of inertia, which radically contradicts Mach's principle of *relativity of inertia*.

(II) We consider the accelerated motion of a particle in a new perspective of local $\widetilde{MS}_p$-SUSY transformations, whereas a *creation* of a particle in $\underline{V}_2$ means its transition from initial state defined on V_4 into intermediate state defined on $\underline{V}_2$, while an *annihilation* of a particle in $\underline{V}_2$ means vice versa (Fig. 1). The same interpretation holds for the *creation* and *annihilation* processes in V_4.

(III) The local-SUSY is conceived as a theory of $\widetilde{MS}_p$-SG, which can only be implemented if $\underline{V}_2$ and V_4 are curved (deformed). The $\widetilde{MS}_p$, being embedded in the V_4, is the *unmanifested* indispensable individual companion of a particle of interest devoid of any matter influence. The superspace $(z^M,\,\Theta,\,\bar{\Theta})$ is a direct sum extension of background double spaces $V_4 \oplus \underline{V}_2$, with an inclusion of additional fermionic coordinates $(\Theta(\underline{\theta},\theta),\,\bar{\Theta}(\bar{\underline{\theta}},\bar{\theta}))$ induced by the spinors $(\underline{\theta},\bar{\underline{\theta}})$, which refer to $\underline{V}_2$. Thanks to the embedding $\underline{V}_2 \hookrightarrow V_4$, the spinors $(\underline{\theta},\bar{\underline{\theta}})$, in turn, induce the spinors $\theta(\underline{\theta},\bar{\underline{\theta}})$ and $\bar{\theta}(\underline{\theta},\bar{\underline{\theta}})$, as to V_4. While all the particles are living on V_4, their superpartners can be viewed as living on $\widetilde{MS}_p$. In this framework supersymmetry and general coordinate transformations are described in a unified way as certain diffeomorphisms. The action of simple $\widetilde{MS}_p$-SG includes the Hilbert term for a *fictitious* graviton coexisting with a *fictitious* fermionic field of gravitino described by the Rarita-Scwinger kinetic term. A coupling of supergravity with matter superfields no longer holds. The different 4D $N = 1$ supergravity multiplets all contain the graviton and the gravitino, but differ by their systems of auxiliary fields.

(IV) The accelerated motion of a particle is described by the parameter $\epsilon = \epsilon(X^{\hat{\mu}})$ of local SUSY, which depends explicitly on $X^{\hat{\mu}} = (\tilde{x}^\mu,\,\underline{\tilde{x}}^\mu)$, where $\tilde{x}^\mu \in V_4$ and $\underline{\tilde{x}}^\mu \in \underline{V}_2$. Here the real parameter $\tau(x) = \underline{\tau}(\underline{x})$ is

doi: https://doi.org/10.52526/25792776-24.71.2-230

interpreted as the *atomic duration time*, i.e. period of superoscillations, of double transition of a particle $V_4 \rightleftharpoons \underline{V}_2$.

(VI) Further studies on the $\widetilde{MS}_p$-SG are warranted with special emphasis on Palatini's formalism, the flat $\widetilde{MS}_p$-SG theory with Weitzenböck torsion as a $\widetilde{MS}_p$-Teleparallel SG theory, a general deformation of MS_p induced by external force exerted on a particle and inertial effects, the hypothesis of locality, which will essentially improve the framework of present paper. Actually,

a) using Palatini's formalism extended in a plausible fashion to the $\widetilde{MS}_p$ - SG, one will reinterpret a flat $\widetilde{MS}_p$-SG theory with Weitzenböck torsion as a $\widetilde{MS}_p$-Teleparallel SG theory, having the gauge *translation* group in tangent bundle. Whereas the Hilbert action vanishes and the gravitino action loses its spin connections, so one finds torsion induced by gravitinos. The accelerated reference frame has Weitzenböck torsion. The spin connection represents only *inertial effects*, but not gravitation at all. The action of a $\widetilde{MS}_p$-TSG theory will be invariant under the Poincaré supergroup and under diffeomorphisms.

b) The Weitzenböck connection ($\dot{\Gamma}$), which defines the Fock-Ivanenko derivative ($\dot{\mathcal{D}}_{\hat{\mu}}$) written in terms of covariant derivative ($\dot{\nabla}_{\hat{\mu}}$), defines the acceleration too. By means of it, one will derive a force equation, with torsion (or contortion) playing the role of force. The connection ($\dot{\Gamma}$) will be considered a kind of dual of the Levi-Civita connection (Γ), which is a connection with vanishing torsion (T), and non-vanishing *fictitious* curvature (R).

c) This allows one to complement a theory of $\widetilde{MS}_p$-TSG with implications for special cases. In particular, one will discuss the Newtonian limit, and describe the homogeneous acceleration field.

d) As we emphasized already essential difference arisen between the standard supergravity theories and some rather unusual properties of a $\widetilde{MS}_p$-SG theory is as follows. In the framework of the standard supergravity theories, as in GR, a curvature of the space-time acts on all the matter fields. The source of graviton is the energy-momentum tensor of matter fields, while the source of gravitino is the spin-vector current of supergravity. The gauge action of simple $\widetilde{MS}_p$-SG is the sum of the Hilbert action for the tetrad field - *fictitious* graviton, and the Rarita-Schwinger action for the *fictitious* gravitino field. Instead we argue that a deformation of MS_p is the origin of these fields. They refer to the particle of interest itself, without relation to other matter fields, so that these fields can be globally removed by appropriate coordinate transformations. With these physical requirements, a standard coupling of supergravity with matter superfields evidently no longer holds. We, therefore, would work out the theory of a general deformation of MS_p induced by external force exerted on a particle, in order to show that in the $\widetilde{MS}_p$-TSG theory the occurrence of the *absolute* and *inertial* accelerations, and the *inertial* force are obviously caused by this. In the same time, the *relative* acceleration (in Newton's terminology) (both magnitude and direction), to the contrary, has nothing to do with a deformation of $\underline{M}_2$ and, thus, it cannot produce the inertia effects. One will determine the most important period of superoscillations as a function of proper time for given deformed MS_p.

e) In standard framework of the construction of reference frame of an accelerated observer, the hypothesis of locality holds for huge proper acceleration lengths and that represents strict restrictions, because it approximately replaces a noninertial frame of reference $\widetilde{S}_{(2)}$, which is held stationary in the deformed space $\mathcal{M}_2 \equiv \underline{V}_2^{(\varrho)}$ ($\varrho \neq 0$), where $\underline{V}_2$ is the 2D semi-Riemannian space, with a continuous infinity set of the inertial frames $\{S_{(2)}, S'_{(2)}, S''_{(2)}, ...\}$ given in the flat $\underline{M}_2$ ($\varrho = 0$). In this situation the use of the hypothesis of locality is physically unjustifiable. In this study, therefore, it is worthwhile to take into account a deformation $\underline{M}_2 \longrightarrow \underline{V}_2^{(\varrho)}$, which will essentially improve the standard framework.

All the above mentioned problems (d,e) will become separate topics for research in subsequent papers (Ter-Kazarian, 2024c,b).

References

Batista R., et al. 2019, Frontiers in Astronomy and Space Sciences, 6, 1, Article 23

Batista R., et al. 2023, arxiv:2312.00409[gr-qc]

Bialynicki-Birula I., 1963, Phys. Rev., 130, 465

Bjorken J., 1963, Ann. Phys., 24, 174

Bondi H., 1952, Cosmology. Cambridge

Cho Y., Freund P., 1975, Phys. Rev. D, 12, 1711

Colladay D., Kostelecky V., 1997, Phys. Rev. D, 55, 6760

doi: https://doi.org/10.52526/25792776-24.71.2-230

Colladay D., Kostelecky V., 1998, Phys. Rev. D, 58, 116002

Dirac P., 1951, Proc. R. Soc. London, B209, 291

Drake S., 1978, Galileo at work. Chicago, University of Chicago Press

Eguchi T., 1976, Phys. Rev. D, 14, 2755

Garfinkle D., Strominger A., 1991, Phys. Lett. B, 256, 146

Guralnik G., 1964, Phys. Rev., 136, B1404

Heisenberg W., 1957, Rev. Mod. Phys., 29, 269

Kostelecky V., Potting R., 1991, Nucl. Phys. B, 359, 545

Kostelecky V., Potting R., 1996, Phys. Lett. B, 381, 89

Lahanas A., Nanopoulos D., 1987, Physics Reports, 145, 1

Mattingly D., 2005, Living Rev. Relativity, 8, 5

Nambu Y., 1968, Prog. Theor. Phys. Suppl., 68, 190

Newton I., 1687, Philosophiae Naturalis Principia Mathematica. http://plato.stanford.edu/entries/newton-principia

Sciama D., 1953, MNRAS, 113, Issue 1, 34

Ter-Kazarian G., 2023a, Communications of BAO, 70, 170

Ter-Kazarian G., 2023b, Communications of BAO, 70, Issue 2, 212

Ter-Kazarian G., 2024a, Gravitation and Cosmology, 30, No. 1, p. 8

Ter-Kazarian G., 2024c, Communications of BAO, 71, Issue 2,

Ter-Kazarian G., 2024b, Communications of BAO, 71, Issue 2,

Wess J., Bagger J., 1983, Supersymmetry and Supergravity. Princeton University Press, Princeton, New Jersey

West P., 1987, Introduction to Supersymmetry and Supergravity. World Scientific, Singapure

van Nieuwenhuizen P., 1981, Physics Reports, 68, 189

Appendices

Appendix A A glimpse on the global MS$_p$-SUSY

For a benefit of the reader, as a guiding principle to make the rest of paper understandable, in this section we necessarily recount some of the highlights behind of *global* MS$_p$-SUSY (Ter-Kazarian, 2023a, 2024a), on which the *local* $\widetilde{MS}_p$-SUSY is based.

The flat MS$_p$ is the 2D composite space

$$MS_p \equiv \underline{M}_2 = \underline{R}^1_{(+)} \oplus \underline{R}^1_{(-)}, \tag{74}$$

with Lorentz metric. The ingredient 1D-space $\underline{R}^1_{\underline{m}}$ is spanned by the coordinates $\eta^{\underline{m}}$. The following notational conventions are used throughout this paper: all quantities related to the space $\underline{M}_2$ will be underlined. In particular, the underlined lower case Latin letters $\underline{m}, \underline{n}, ... = (\pm)$ denote the world indices related to $\underline{M}_2$.

Suppose the position of the particle is specified by the coordinates $x^m(s)$ $(x^0 = t)$ in the basis e_m (m=0,1,2,3) at given point in the background M_4 space. Consider a smooth (injective and continuous) embedding $\underline{M}_2 \hookrightarrow M_4$. That is, a smooth map $f: \ \underline{M}_2 \longrightarrow M_4$ is defined to be an immersion (the embedding which is a function that is a homeomorphism onto its image):

$$\underline{e}_{\underline{0}} = e_0, \quad \underline{x}^{\underline{0}} = x^0, \quad \underline{e}_{\underline{1}} = \vec{n}, \quad \underline{x}^{\underline{1}} = |\vec{x}|, \tag{75}$$

where $\vec{x} = e_i x^i = \vec{n}|\vec{x}|$ $(i = 1, 2, 3)$. Given the inertial frames $S_{(4)}, S'_{(4)}, S''_{(4)}, ...$ in unaccelerated uniform motion in M_4, we may define the corresponding inertial frames $\underline{S}_{(2)}$, $\underline{S}'_{(2)}$, $\underline{S}''_{(2)}$,... in $\underline{M}_2$, which are used by the non-accelerated observers for the positions $\underline{x}^{\underline{r}}, \underline{x}'^{\underline{r}}, \underline{x}''^{\underline{r}}, ...$ of a free particle in flat $\underline{M}_2$. According to (75), the time axes of the two systems $\underline{S}_{(2)}$ and $S_{(4)}$ coincide in direction, and the time coordinates are taken the same. For the case at hand,

$$\underline{v}^{(\pm)} = \frac{d\eta^{(\pm)}}{d\underline{x}^{\underline{0}}} = \frac{1}{\sqrt{2}}(\underline{v}^{\underline{0}} \pm \underline{v}^{\underline{1}}), \quad \underline{v}^{\underline{1}} = \frac{d\underline{x}^{\underline{1}}}{d\underline{x}^{\underline{0}}} = |\vec{v}| = |\frac{d\vec{x}}{dx^0}|, \tag{76}$$

and that

$$\underline{u} = \underline{e}_{\underline{m}} \underline{v}^{\underline{m}} = (\underline{\vec{v}}_{\underline{0}}, \underline{\vec{v}}_{\underline{1}}), \quad \underline{\vec{v}}_{\underline{0}} = \underline{e}_{\underline{0}} \underline{v}^{\underline{0}}, \quad \underline{\vec{v}}_{\underline{1}} = \underline{e}_{\underline{1}} \underline{v}^{\underline{1}} = \vec{n}|\vec{v}| = \vec{v}, \tag{77}$$

therefore, $\underline{u} = u = (e_0, \vec{v})$. To explain why MS$_p$ is two dimensional, we note that only 2D real *null vectors* are allowed as the basis at given point in MS$_p$, which is embedded in M_4. Literally speaking, the $\underline{M}_2$ can be viewed as 2D space living on the 4D world sheet.

The elementary act of particle motion at each time step (t_i) through the infinitely small spatial interval $\triangle x_i = (x_{i+1} - x_i)$ in M_4 during the time interval $\triangle t_i = (t_{i+1} - t_i) = \varepsilon$ is probably the most fascinating challenge for physical research. Since this is beyond our perception, it appears legitimate to consider extension to the infinitesimal Schwinger transformation function, $F_{ext}(x_{i+1}, t_{i+1}; x_i, t_i)$, in fundamentally different aspect. We hypothesize that

in the limit $n \to \infty (\varepsilon \to 0)$, the elementary act of motion consists of an `annihilation´ of a particle at point $(x_i, t_i) \in M_4$, which can be thought of as the transition from initial state $|x_i, t_i>$ into unmanifested intermediate state, so-called, `motion´ state, $|\underline{x}_i, \underline{t}_i>$, and of subsequent `creation´ of a particle at infinitely close final point $(x_{i+1}, t_{i+1}) \in M_4$, which means the transition from `motion´ state, $|\underline{x}_i, \underline{t}_i>$, into final state, $|x_{i+1}, t_{i+1}>$. The motion state, $|\underline{x}_i, \underline{t}_i)>$, should be defined on unmanifested `master´ space, $\underline{M}_2$, which includes the points of all the atomic elements, $(\underline{x}_i, \underline{t}_i) \in \underline{M}_2$ $(i = 1, 2, ...)$.

This furnishes justification for an introduction of *unmanifested master space*, $\underline{M}_2$.

The fields of spin-zero $(\vec{S} = \vec{K} = 0)$ scalar field $A(x)$ and spin-one $A^n(x)$, corresponding to the $(1/2, 1/2)$ representation, transform under a general Lorentz transformation as follows:

$$\begin{array}{ll} \underline{A}(\underline{\eta}) \equiv A(x), & \text{(spin} \quad 0); \\ \underline{A}^{\underline{m}}(\underline{\eta}) = \Lambda^{\underline{m}}_{\ n} A^n(x), & \text{(spin} \quad 1). \end{array} \tag{78}$$

The map from $SL(2, C)$ to the Lorentz group is established through the $\vec{\sigma}$-Pauli spin matrices, $\sigma^m = (\sigma^0, \sigma^1, \sigma^2, \sigma^3) \equiv (I_2, \vec{\sigma})$, $\bar{\sigma}^m \equiv (I_2, -\vec{\sigma})$, where I_2 is the identity two-by-two matrix.

According to embedding map (75), the $\underline{\sigma}$-matrices are

$$\sigma^{\underline{m}} = \sigma^{(\pm)} = \frac{1}{\sqrt{2}}(\sigma^{\underline{0}} \pm \sigma^{\underline{1}}) = \frac{1}{\sqrt{2}}(\sigma^0 \pm \sigma^3). \tag{79}$$

doi: https://doi.org/10.52526/25792776-24.71.2-230

The matrices $\sigma^{\underline{m}}$ form a basis for two-by-two complex matrices $\underline{P}$:

$$\underline{P} = (p_{\underline{m}}\sigma^{\underline{m}}) = (p_{(\pm)}\sigma^{(\pm)}) = (p_{\underline{0}}\sigma^{\underline{0}} + p_{\underline{1}}\sigma^{\underline{1}}), \tag{80}$$

provided $p_{(\pm)} = i\partial_{\underline{\eta}^{(\pm)}}$, $p_{\underline{0}} = i\partial_{\underline{x}^{0}}$ and $p_{\underline{1}} = i\partial_{\underline{x}^{1}}$. The real coefficients $p'_{\underline{m}}$ and $p_{\underline{m}}$, like p'_m and p_m, are related by a Lorentz transformation $p'_{\underline{m}} = \Lambda^{\underline{n}}_{\underline{m}}\, p_{\underline{n}}$, because the relations $det(\sigma^{\underline{m}} p_{\underline{m}}) = p_{\underline{0}}^2 - p_{\underline{1}}^2$ and $det\, M = 1$ yield ${p'_{\underline{0}}}^2 - {p'_{\underline{1}}}^2 = p_{\underline{0}}^2 - p_{\underline{1}}^2$. Correspondence of $p_{\underline{m}}$ and $\underline{P}$ is uniquely: $p_{\underline{m}} = \frac{1}{2}Tr(\sigma^{\underline{m}}\,\underline{P})$, which combined with (82) yields

$$\Lambda^{\underline{m}}_{\ \underline{n}}(M) = \tfrac{1}{2}\, Tr\left(\sigma^{\underline{m}}\, M\sigma^{\underline{n}}\, M^{\dagger}\right). \tag{81}$$

Thus, both hermitian matrices P and P' or $\underline{P}$ and $\underline{P}'$ have expansions, respectively, in σ or $\underline{\sigma}$:

$$(\sigma^m\, p'_m) = M(\sigma^m\, p_m)M^{\dagger}, \quad (\sigma^{\underline{m}}\, p'_{\underline{m}}) = M(\sigma^{\underline{m}}\, p_{\underline{m}})M^{\dagger}, \tag{82}$$

where $M(M \in SL(2, C))$ is unimodular two-by-two matrix.

A two-component $(1/2, 0)$ Weyl fermion, $\chi_\beta(x)$, therefore, transforms under Lorentz transformation to yield $\underline{\chi}_{\alpha}(\underline{\eta})$:

$$\chi_\beta(x) \longrightarrow \underline{\chi}_{\alpha}(\underline{\eta}) = (M_R)_{\alpha}^{\ \beta}\, \chi_\beta(x), \quad \alpha, \beta = 1, 2, \tag{83}$$

where the orthochronous Lorentz transformation, corresponding to a rotation by the angles ϑ_3 and ϑ_2 about, respectively, the axes n_3 and n_2, is given by rotation matrix

$$M_R = e^{i\frac{1}{2}\sigma_2\vartheta_2} e^{i\frac{1}{2}\sigma_3\vartheta_3}. \tag{84}$$

There with the rotation of an hermitian matrix P is

$$p_{\underline{m}}\sigma^{\underline{m}} = M_R\, p_m \sigma^m\, M_R^{\dagger}, \tag{85}$$

where p_m and $p_{\underline{m}}$ denote the momenta $p_m \equiv m(ch\beta,\ sh\beta \sin\vartheta_2 \cos\vartheta_3,\ sh\beta \sin\vartheta_2 \sin\vartheta_3,$
$sh\beta \cos\vartheta_2)$, and $p_{\underline{m}} \equiv m(ch\underline{\beta},\ 0,\ 0,\ sh\underline{\beta})$.

A two-component $(0, 1/2)$ Weyl spinor field is denoted by $\bar{\chi}^{\dot{\beta}}(x)$, and transforms as

$$\bar{\chi}^{\dot{\beta}}(x) \longrightarrow \underline{\bar{\chi}}^{\dot{\alpha}}(\underline{\eta}) = (M_R^{-1})^{\dagger\dot{\alpha}}_{\ \ \ \dot{\beta}}\, \bar{\chi}^{\dot{\beta}}(x), \quad \dot{\alpha}, \dot{\beta} = 1, 2. \tag{86}$$

The so-called `dotted´ indices have been introduced to distinguish the $(0, 1/2)$ representation from the $(1/2, 0)$ representation. The `bar´ over the spinor is a convention that this is the $(0, 1/2)$-representation. We used the Van der Waerden notations for the Weyl two-component formalism: $(\underline{\bar{\chi}}_{\dot{\alpha}})^* = \underline{\chi}_{\alpha}$ and $\underline{\bar{\chi}}_{\dot{\alpha}} = (\underline{\chi}_{\alpha})^*$.

The odd part of the supersymmetry algebra is composed entirely of the spin-1/2 operators $Q_{\alpha}^{\ i},\ Q_{\beta}^{\ j}$. In order to trace a maximal resemblance in outward appearance to the standard SUSY theories, here we set one notation $\hat{m} = (m \quad \text{if} \quad Q = q,\ \text{or}\ \underline{m} \quad \text{if} \quad Q = \underline{q})$, and as before the indices α and $\dot{\alpha}$ run over 1 and 2.

If that is the case as above, a *creation* of a particle in $\underline{M}_2$ means its transition from initial state defined on M_4 into intermediate state defined on $\underline{M}_2$, while an *annihilation* of a particle in $\underline{M}_2$ means vice versa. The same interpretation holds for the *creation* and *annihilation* processes in M_4. All the fermionic and bosonic states taken together form a basis in the Hilbert space. The basis vectors in the Hilbert space composed of $H_B \otimes H_F$ is given by

$$\{|\underline{n}_b > \otimes|0>_f,\ |\underline{n}_b > \otimes f^{\dagger}\,|0>_f\},$$

or

$$\{|n_b > \otimes|\underline{0}>_f,\ |n_b > \otimes \underline{f}^{\dagger}\,|\underline{0}>_f\},$$

where we consider two pairs of creation and annihilation operators $(b^{\dagger},\ b)$ and $(f^{\dagger},\ f)$ for bosons and fermions, respectively, referred to the background space V_4, as well as $(\underline{b}^{\dagger},\ \underline{b})$ and $(\underline{f}^{\dagger},\ \underline{f})$ for bosons and fermions, respectively, as to background master space $\underline{V}_2$. The boson and fermion number operators are $N_b = b^{\dagger}b$ or $\underline{N}_b = \underline{b}^{\dagger}\underline{b}$, where $N_b|n_b >= n_b|n_b >$ and $\underline{N}_b|\underline{n}_b >= \underline{n}_b|\underline{n}_b >\ (= 0, 1, ..., \infty)$, and $N_f = f^{\dagger}f$ or $\underline{N}_f = \underline{f}^{\dagger}\underline{f}$, provided $N_f|n_f >= n_f|n_f >$ and $\underline{N}_f|\underline{n}_f >= \underline{n}_f|\underline{n}_f >\ (= 0, 1)$. Taking into account the action of $(b, b^{\dagger})$ or $(\underline{b}, \underline{b}^{\dagger})$ upon the eigenstates $|n_b >$ or $|\underline{n}_b >$, we may construct the quantum operators, $(q^{\dagger},\ \underline{q}^{\dagger})$ and $(q,\ \underline{q})$ as

$$\begin{aligned} q &= q_0, \underline{b}\, f^{\dagger}, \quad q^{\dagger} = q_0\, \underline{b}^{\dagger}\, f, \\ \underline{q} &= q_0\, b\underline{f}^{\dagger}, \quad \underline{q}^{\dagger} = q_0\, b^{\dagger}\, \underline{f}. \end{aligned} \tag{87}$$

doi: https://doi.org/10.52526/25792776-24.71.2-230

which replace bosons by fermions and vice versa:

$$\begin{array}{l} q\,|\underline{n}_b,\, n_f >= q_0\sqrt{\underline{n}_b}\,|\underline{n}_b-1,\, n_f+1>, \\ q^\dagger\,|\underline{n}_b,\, n_f >= q_0\sqrt{\underline{n}_b+1}\,|\underline{n}_b+1,\, n_f-1>, \end{array} \tag{88}$$

and that

$$\begin{array}{l} \underline{q}\,|n_b,\, \underline{n}_f >= q_0\sqrt{n_b}\,|n_b-1,\, \underline{n}_f+1>, \\ \underline{q}^\dagger\,|n_b,\, \underline{n}_f > q_0\sqrt{n_b+1}\,|n_b+1,\, \underline{n}_f-1>. \end{array} \tag{89}$$

This framework combines bosonic and fermionic states on the same footing, rotating them into each other under the action of operators q and $\underline{q}$. So, we may refer the action of the supercharge operators q and $q^\dagger$ to the background space M_4, having applied in the chain transformations of fermion χ (accompanied with the auxiliary field F as it will be seen later on) to boson $\underline{A}$, defined on $\underline{M}_2$:

$$\longrightarrow \chi^{(F)} \longrightarrow \underline{A} \longrightarrow \chi^{(F)} \longrightarrow \underline{A} \longrightarrow \chi^{(F)} \longrightarrow . \tag{90}$$

Respectively, we may refer the action of the supercharge operators $\underline{q}$ and $\underline{q}^\dagger$ to the $\underline{M}_2$, having applied in the chain transformations of fermion $\underline{\chi}$ (accompanied with the auxiliary field $\underline{F}$) to boson A, defined on the background space M_4:

$$\longrightarrow \underline{\chi}^{(\underline{F})} \longrightarrow A \longrightarrow \underline{\chi}^{(\underline{F})} \longrightarrow A \longrightarrow \underline{\chi}^{(\underline{F})} \longrightarrow . \tag{91}$$

The successive atomic double transitions of a particle $M_4 \rightleftharpoons \underline{M}_2$ is investigated within MS$_p$-SUSY, wherein all the particles are living on M_4, their superpartners can be viewed as living on MS$_p$. The underlying algebraic structure of MS$_p$-SUSY generators closes with the algebra of *translations* on the original space M_4 in a way that it can then be summarized as a non-trivial extension of the Poincaré group algebra those of the commutation relations of the bosonic generators of four momenta and six Lorentz generators referred to M_4. Moreover, if there are several spinor generators $Q_\alpha^{\ i}$ with $i = 1, ..., N$ - theory with $N-$extended supersymmetry, can be written as a graded Lie algebra of SUSY field theories, with commuting and anticommuting generators:

$$\begin{array}{l} \{Q_\alpha^{\ i},\, \bar{Q}^j_{\ \dot{\alpha}}\} = 2\delta^{ij}\,\sigma^{\hat{m}}_{\alpha\dot{\alpha}}\,p_{\hat{m}}; \\ \{Q_\alpha^{\ i},\, Q_\beta^{\ j}\} = \{\bar{Q}^i_{\ \dot{\alpha}},\, \bar{Q}^j_{\ \dot{\beta}}\} = 0; \quad [p_{\hat{m}},\, Q_\alpha^{\ i}] = [p_{\hat{m}},\, \bar{Q}^j_{\ \dot{\alpha}}] = 0, \quad [p_{\hat{m}},\, p_{\hat{n}}] = 0. \end{array} \tag{92}$$

The anticommuting (Grassmann) parameters $\epsilon^\alpha(\xi^\alpha,\, \underline{\xi}^\alpha)$ and $\bar{\epsilon}^\alpha(\bar{\xi}^\alpha,\, \underline{\bar{\xi}}^\alpha)$:

$$\{\epsilon^\alpha,\, \epsilon^\beta\} = \{\bar{\epsilon}^\alpha,\, \bar{\epsilon}^\beta\} = \{\epsilon^\alpha,\, \bar{\epsilon}^\beta\} = 0, \quad \{\epsilon^\alpha,\, Q_\beta\} = \cdots = [p_{\hat{m}},\, \epsilon^\alpha] = 0, \tag{93}$$

allow us to write the algebra (92) for $(N = 1)$ entirely in terms of commutators:

$$[\epsilon Q,\, \bar{Q}\bar{\epsilon}] = 2\epsilon\sigma^{\hat{m}}\bar{\epsilon}p_{\hat{m}}, \quad [\epsilon Q,\, \epsilon Q] = [\bar{Q}\bar{\epsilon},\, \bar{Q}\bar{\epsilon}] = [p^{\hat{m}},\, \epsilon Q] = [p^{\hat{m}},\, \bar{Q}\bar{\epsilon}] = 0. \tag{94}$$

For brevity, here the indices $\epsilon Q = \epsilon^\alpha Q_\alpha$ and $\bar{\epsilon}\bar{Q} = \bar{\epsilon}_{\dot{\alpha}}\bar{Q}^{\dot{\alpha}}$ will be suppressed unless indicated otherwise. This supersymmetry transformation maps tensor fields $\mathcal{A}(A,\, \underline{A})$ into spinor fields $\psi(\chi,\, \underline{\chi})$ and vice versa. From the algebra (94) we see that Q has mass dimension $1/2$. Therefore, as usual, fields of dimension ℓ transform into fields of dimension $\ell + 1/2$ or into derivatives of fields of lower dimension. It can be checked that the supersymmetry transformations close supersymmetry algebra:

$$(\delta_{\xi_1}\delta_{\xi_2} - \delta_{\xi_2}\delta_{\xi_1})\underline{A} = -2i(\xi_1\sigma^m\bar{\xi}_2 - \xi_2\sigma^m\bar{\xi}_1)(\delta^0_m\underline{\partial}_0 + \tfrac{1}{|\vec{x}|}x^i\delta_{im}\underline{\partial}_1)\underline{A}. \tag{95}$$

The guiding principle of MS$_p$-SUSY resides in constructing the superspace which is a 14D-extension of a direct sum of background spaces $M_4 \oplus \underline{M}_2$ (spanned by the 6D-coordinates $X^{\hat{m}} = (x^m,\, \underline{\eta}^{\underline{m}})$ by the inclusion of additional 8D-fermionic coordinates $\Theta^\alpha = (\theta^\alpha,\, \underline{\theta}^\alpha)$ and $\bar{\Theta}_{\dot{\alpha}} = (\bar{\theta}_{\dot{\alpha}},\, \underline{\bar{\theta}}_{\dot{\alpha}})$, as to $(q,\, \underline{q})$, respectively. Therewith thanks to the embedding $\underline{M}_2 \hookrightarrow M_4$, the spinors $(\underline{\theta}, \underline{\bar{\theta}})$, in turn, induce the spinors $\theta(\underline{\theta}, \underline{\bar{\theta}})$ and $\bar{\theta}(\underline{\theta}, \underline{\bar{\theta}})$, as to M_4. These spinors satisfy the following relations:

$$\begin{array}{l} \{\Theta^\alpha,\, \Theta^\beta\} = \{\bar{\Theta}_{\dot{\alpha}},\, \bar{\Theta}_{\dot{\beta}}\} = \{\Theta^\alpha,\, \bar{\Theta}_{\dot{\beta}}\} = 0, \\ [x^m,\, \theta^\alpha] = [x^m,\, \bar{\theta}_{\dot{\alpha}}] = 0, \quad [\underline{\eta}^{\underline{m}},\, \underline{\theta}^\alpha] = [\underline{\eta}^{\underline{m}},\, \underline{\bar{\theta}}_{\dot{\alpha}}] = 0. \end{array} \tag{96}$$

and $\Theta^{\alpha *} = \bar{\Theta}^{\dot{\alpha}}$. Points in superspace are identified by the generalized coordinates

$$z^{(M)} = (X^{\hat{m}},\, \Theta^\alpha,\, \bar{\Theta}_{\dot{\alpha}}) = (x^m,\, \theta^\alpha,\, \bar{\theta}_{\dot{\alpha}}) \oplus (\underline{\eta}^{\underline{m}}, \underline{\theta}^\alpha,\, \underline{\bar{\theta}}_{\dot{\alpha}}).$$

doi: https://doi.org/10.52526/25792776-24.71.2-230

We have then the one most commonly used `real´ or `symmetric´ superspace parametrized by

$$\Omega(X,\,\Theta,\,\bar\Theta)=e^{i(-X^{\hat m}p_{\hat m}+\Theta^\alpha Q_\alpha+\bar\Theta_{\dot\alpha}\bar Q^{\dot\alpha})}=\Omega_q(x,\,\theta,\,\bar\theta)\times\Omega_{\underline{q}}(\underline{\eta},\,\underline{\theta},\,\underline{\bar\theta}),\tag{97}$$

where we now imply a summation over $\hat m=(m,\underline{m})$. To study the effect of supersymmetry transformations, we consider

$$g(0,\,\epsilon,\,\bar\epsilon)\,\Omega(X,\,\Theta,\,\bar\Theta)=e^{i(\epsilon^\alpha Q_\alpha+\bar\epsilon_{\dot\alpha}\bar Q^{\dot\alpha})}\,e^{i(-X^{\hat m}p_{\hat m}+\Theta^\alpha Q_\alpha+\bar\Theta_{\dot\alpha}\bar Q^{\dot\alpha})}.\tag{98}$$

the transformation (98) induces the motion:

$$g(0,\,\epsilon,\,\bar\epsilon)\,\Omega(X^{\hat m},\,\Theta,\,\bar\Theta)\;\to(X^{\hat m}+i\,\Theta\,\sigma^{\hat m}\,\bar\epsilon-i\,\epsilon\,\sigma^{\hat m}\,\bar\Theta,\;\Theta+\epsilon,\,\bar\Theta+\bar\epsilon),\tag{99}$$

namely,

$$\begin{array}{l} g_q(0,\,\xi,\,\bar\xi)\,\Omega_q(x,\,\theta,\,\bar\theta)\;\to(x^m+i\,\theta\,\sigma^m\,\bar\xi-i\,\xi\,\sigma^m\,\bar\theta,\;\theta+\xi,\,\bar\theta+\bar\xi),\\ g_{\underline{q}}(0,\,\underline{\xi},\,\underline{\bar\xi})\,\Omega_{\underline{q}}(\underline{\eta},\,\underline{\theta},\,\underline{\bar\theta})\;\to(\underline{\eta}^{\underline{m}}+i\,\underline{\theta}\,\sigma^{\underline{m}}\,\underline{\bar\xi}-i\,\underline{\xi}\,\sigma^{\underline{m}}\underline{\bar\theta},\;\underline{\theta}+\underline{\xi},\,\underline{\bar\theta}+\underline{\bar\xi}).\end{array}\tag{100}$$

The spinors $\theta(\underline{\theta},\underline{\bar\theta})$ and $\bar\theta(\underline{\theta},\underline{\bar\theta})$ satisfy the embedding relations $\Delta\underline{x}^0=\Delta x^0$ and $\Delta\underline{x}^2=(\Delta\vec x)^2$, so from (100) we obtain

$$\underline{\theta}\,\sigma^0\,\underline{\bar\xi}-\underline{\xi}\,\sigma^0\,\underline{\bar\theta}=\theta\,\sigma^0\,\bar\xi-\xi\,\sigma^0\,\bar\theta,\quad(\underline{\theta}\,\sigma^3\,\underline{\bar\xi}-\underline{\xi}\,\sigma^3\,\underline{\bar\theta})^2=(\theta\,\vec\sigma\,\bar\xi-\xi\,\vec\sigma\,\bar\theta)^2,\tag{101}$$

which gives (73). The *atomic displacement* caused by double transition of a particle $M_4\rightleftharpoons\underline{M}_2$ reads

$$\Delta\underline{\eta}_{(a)}=\underline{e}_{\underline{m}}\Delta\underline{\eta}^{\underline{m}}_{(a)}=\underline{u}\tau,\tag{102}$$

where the components $\Delta\underline{\eta}^{\underline{m}}_{(a)}$ are written

$$\Delta\underline{\eta}^{\underline{m}}_{(a)}=(\underline{\theta}\,\sigma^{\underline{m}}\,\underline{\bar\theta})\tau.\tag{103}$$

In Van der Warden notations for the Weyl two-component formalism $\underline{\bar\theta}_{\dot\alpha}=(\underline{\theta}_\alpha)^*$, the (102) can be recast into the form

$$\Delta\underline{\eta}^2_{(a)}=\tfrac12\left[(\Delta\underline{x}^{\underline{0}}_{(a)}q)^2-(\Delta\underline{x}^{\underline{1}}_{(a)})^2\right],\tag{104}$$

where $\Delta\underline{x}^{\underline{0}}_{(a)}=\underline{v}^{\underline{0}}\tau$, $\Delta\underline{x}^{\underline{1}}_{(a)}=\underline{v}^{\underline{1}}\tau$, and $\underline{v}^{(\pm)}=\frac{1}{\sqrt2}(\underline{v}^{\underline{0}}\pm\underline{v}^{\underline{1}})$. Hence the velocities of light in vacuum, $\underline{v}^{\underline{0}}=c$, and of a particle ,$\underline{\vec v}_1=\underline{e}_1\underline{v}^{\underline{1}}=\vec n|\vec v|=\vec v$ $(|\vec v|\le c)$, are

$$\begin{array}{l}\underline{v}^{\underline{0}}=\underline{\theta}\,\sigma^{\underline{0}}\,\underline{\bar\theta}=(\underline{\theta}_1\,\underline{\bar\theta}_1+\underline{\theta}_2\,\underline{\bar\theta}_2)=\underline{\theta}\,\underline{\bar\theta},\\ \underline{v}^{\underline{1}}=\underline{\theta}\,\sigma^{\underline{1}}\,\underline{\bar\theta}=(\underline{\theta}_1\,\underline{\bar\theta}_1-\underline{\theta}_2\,\underline{\bar\theta}_2).\end{array}\tag{105}$$

Thus we derive the first founding property (i) that *the atomic displacement* $\Delta\underline{\eta}_{(a)}$, caused by double transition of a particle $M_4\rightleftharpoons\underline{M}_2$, is an invariant:

$$\text{(i)}\quad\Delta\underline{\eta}_{(a)}=\Delta\underline{\eta}'_{(a)}=\cdots=inv.\tag{106}$$

The (105) gives the second (ii) founding property that the bilinear combination $\underline{\theta}\,\underline{\bar\theta}$ is a constant:

$$\text{(ii)}\quad c=\underline{\theta}\,\underline{\bar\theta}=\underline{\theta}'\,\underline{\bar\theta}'=\cdots=const.\tag{107}$$

The latter yields a second postulate of SR (Einstein's postulate) - *the velocity of light, c, in free space appears the same to all observers regardless the relative motion of the source of light and the observer*. The c is the maximum attainable velocity (105) for uniform motion of a particle in Minkowski background space, M_4. Equally noteworthy is the fact that (106) and (107) combined yield *invariance of the element of interval between two events* $\Delta x=k\Delta\underline{\eta}_{(a)}$ *(for given integer number k) with respect to the Lorentz transformation*:

$$\begin{array}{l}k^2\Delta\underline{\eta}^2_{(a)}=(c^2-\underline{v}_1^2)\Delta t^2=(c^2-\vec v^{\,2})\Delta t^2=(\Delta x^0)^2-(\Delta\vec x)^2\equiv(\Delta s)^2=(\Delta x'^0)^2-\\(\Delta\vec x)'^2\equiv(\Delta s')^2=\cdots=inv.,\end{array}\tag{108}$$

where $x^0=ct,\quad x^{0'}=ct',\ldots.$ We have here introduced a notion of physical relative finite *time intervals* between two events $\Delta t=k\tau/\sqrt2$, $\Delta t'=k\tau'/\sqrt2,\ldots.$

doi: https://doi.org/10.52526/25792776-24.71.2-230

Communications of BAO, Vol. 71, Issue 2, 2024, pp. 249-267

The Master-Space Teleparallel Supergravity: Accelerated frames

G.Ter-Kazarian*

Byurakan Astrophysical Observatory, Byurakan, Aragatsotn Province, Armenia

Abstract

Using Palatini's formalism extended in a plausible fashion to the recent $\widetilde{MS}_p$-Supergravity (Ter-Kazarian, 2023c, 2024b), subject to certain rules, we reinterpret a flat $\widetilde{MS}_p$-SG theory with Weitzenböck torsion as the quantum field theory of Master-Space Teleparallel Supergravity ($\widetilde{MS}_p$-TSG), having the gauge *translation* group in tangent bundle. Here the spin connection represents only *inertial effects*, but not gravitation at all. In order to recover the covariance, we introduce a 1-form of the Yang–Mills connection assuming values in the Lie algebra of the translation group. The Hilbert action vanishes and the gravitino action loses its spin connections, so that the accelerated reference frame has Weitzenböck torsion induced by gravitinos. Due to the soldered character of the tangent bundle, torsion presents also the anholonomy of the translational covariant derivative. The gauge invariance of the tetrad provides torsion invariance under gauge transformations. The role of the Cartan-Killing metric usually comes, when it exists, from its being invariant under the group action. Here it does not exist, but we use the invariant Lorentz metric of Minkowski spacetime in its stead. The action of $\widetilde{MS}_p$-TSG is invariant under local translations, under local super symmetry transformations and by construction is invariant under local Lorentz rotations and under diffeomorphisms. So that this action is invariant under the Poincaré supergroup and under diffeomorphisms. We show the equivalence of the Teleparallel Gravity action with Hilbert action, which proves that the immediate cause of the *fictitious* Riemann curvature for the Levi-Civita connection arises entirely due to the inertial properties of the Lorentz-rotated frame of interest. The curvature of Weitzenböck connection vanishes identically, but for a tetrad involving a non-trivial translational gauge potential, the torsion is non-vanishing. We consider Weitzenböck connection a kind of dual of the Levi-Civita connection, which is a connection with vanishing torsion, and non-vanishing *fictitious* curvature. The Weitzenböck connection defines the acceleration through force equation, with torsion (or contortion) playing the role of force.

Keywords: *Supergravity–Teleparallel Supergravity–Accelerated frames*

1. Introduction

In a recent papers (Ter-Kazarian, 2023c, 2024b) we developed a quantum field theory of $\widetilde{MS}_p$-Supergravity as a *local* extension of the theory of *global Master space* (MS_p)-SUSY (Ter-Kazarian, 2023a, 2024a). The letter is the microscopic theory of deformed Lorentz symmetry and deformed geometry induced by foamy effects at the Planck scale, which tested in recent ultra-high energy experiments of cosmic rays (UHECRs) and astrophysical TeV-γ photons. They reflect the expectation that the solutions to this mystery appear to require new physics (see e.g. Batista & et al. (2019, 2023), Mattingly (2005) and references therein). These astrophysical experiments measure quantum gravity (QG) effects within a two or three orders of magnitude of Planck length $\ell_P \approx 1.62\times10^{-33}$cm and Planck time t_P/c. One of the most important efforts of this type has historically been the search for a violation of the standard Lorenz code (SLC) of motion in ultra-high energy experiments. To this aim, as a guiding principle to make the rest of paper understandable, in the appendices we necessarily recount succinctly some of the highlights behind of *global* MS_p-SUSY (Ter-Kazarian, 2023a, 2024a) and *local* $\widetilde{MS}_p$-SUSY (Ter-Kazarian, 2023c, 2024b) theories, which are in use throughout the present article.

In (Ter-Kazarian, 2023a, 2024a) (see Appendix A for brief outline), we developed a microscopic theory of deformed Lorentz symmetry and deformed geometry induced by foamy effects at the Planck scale, and

*gago_50@yahoo.com

doi: https://doi.org/10.52526/25792776-24.71.2-249

tested in ultra-high energy experiments. This theory, among other things, actually explores the first part of the phenomenon of inertia, which refers to *inertial uniform motion along rectilinear timelike world lines*. The phenomenon of inertia may be the most profound mystery in physics, and it is still the most important incomprehensive problem that needs to be solved. Today there is no known feasible way to account for credible explanation of this problem. With this perspective in sight, the *local* extension of MS_p-SUSY is the next necessary step.

In (Ter-Kazarian, 2023c, 2024b) (see Appendix B for brief outline), we conceived local $\widetilde{MS}_p$-SUSY as a quantum field theory of $\widetilde{MS}_p$-Supergravity (SG), in which we review the accelerated motion of a particle in a new perspective of local $\widetilde{MS}_p$-SUSY transformations. That is, a *creation* of a particle in curved Master space $\widetilde{MS}_p \equiv \underline{V}_2$ (2D semi-Riemannian space) means its transition from initial state defined on the background semi-Riemannian 4D-space V_4 into intermediate state defined on $\underline{V}_2$, while an *annihilation* of a particle in $\underline{V}_2$ means vice versa. The same interpretation holds for the *creation* and *annihilation* processes in V_4. The net result of each atomic double transition of a particle $V_4 \rightleftharpoons \underline{V}_2$ to $\underline{V}_2$ and back is as if we had operated with *a local space-time translation* with acceleration, $\vec{a}$, on the original space V_4. Accordingly, the acceleration, $\underline{\vec{a}}$, holds in $\underline{V}_2$ at $\underline{V}_2 \rightleftharpoons V_4$. So, the accelerated motion of boson $A(\widetilde{x})$ in V_4 is a chain of its sequential transformations to the Weyl fermion $\underline{\chi}(\underline{\widetilde{x}})$ defined on $\underline{V}_2$ (accompanied with the auxiliary fields $\underline{\widetilde{F}}$) and back, and the same interpretation holds for fermion $\chi(\widetilde{x})$. A curvature of $\widetilde{MS}_p$ within $\widetilde{MS}_p$-SG theory arises entirely due to the inertial properties of the Lorentz-rotated frame of interest.

Using Palatini's formalism generalized for the $\widetilde{MS}_p$-SG, in present article we reinterpret a flat $\widetilde{MS}_p$-SG theory with Weitzenböck torsion as a theory of $\widetilde{MS}_p$-TSG having the gauge *translation* group in tangent bundle. An important property of Teleparallel Gravity is that its spin connection is related only to the inertial properties of the frame, not to gravitation. Whereas the Hilbert action vanishes and the gravitino action loses its spin connections, so we find that the accelerated reference frame has Weitzenböck torsion induced by gravitinos.

We proceed according to the following structure. To start with, in Section 2 we discuss the Palatini's formalism and flat $\widetilde{MS}_p$-SG with torsion. Section 3 is devoted to the $\widetilde{MS}_p$-TSG with the translation group. In Section 4 we turn to the simple Newtonian gravitational field and 'absolute' acceleration. In Section 5 we derive the homogeneous acceleration field. As concluding remarks, we list in section 6 of what we think is the most important that distinguish a theory of $\widetilde{MS}_p$-TSG. In appendices A and B, we briefly revisit the global MS_p-SUSY and $\widetilde{MS}_p$-SG without going into the subtleties, respectively, as a guiding principle to make the paper understandable. We revisit the simple ($N = 1$) $\widetilde{MS}_p$ - SG without auxiliary fields in B.1. On these premises, we discuss the velocity and acceleration in M_4. Throughout we will use the 'two-in-one' notation of a theory MS_p-SUSY (Appendix A), implying that any tensor (W) or spinor (Θ) with indices marked by 'hat' denote

$$\begin{array}{l} W^{\hat{\mu}_1\cdots\hat{\mu}_m}_{\hat{\nu}_1\cdots\hat{\nu}_n} := W^{\mu_1\cdots\mu_m}_{\nu_1\cdots\nu_n} \oplus W^{\underline{\mu}_1\cdots\underline{\mu}_m}_{\underline{\nu}_1\cdots\underline{\nu}_n}, \\ \Theta^{\hat{\alpha}} := \theta^{\alpha} \oplus \underline{\theta}^{\alpha}, \quad \bar{\Theta}_{\hat{\dot{\alpha}}} := \bar{\theta}_{\dot{\alpha}} \oplus \bar{\underline{\theta}}_{\dot{\alpha}}. \end{array} \tag{1}$$

This corresponds to the action of supercharge operators $Q \equiv (\text{either}\, q\, \text{or}\, \underline{q})$ (see (86), (87)), which is due to the fact that the framework of $\widetilde{MS}_p$-SG combines bosonic and fermionic states in V_4 and $\underline{V}_2$ on the same base rotating them into each other under the action of operators $(q, \underline{q})$. The α are all upper indices, while $\dot{\alpha}$ is a lower index. For brevity, whenever possible undotted and dotted spinor indices often can be ruthlessly suppressed without ambiguity. Unless indicated otherwise, the natural units, $h = c = 1$ are used throughout.

2. Palatini's formalism and Flat $\widetilde{MS}_p$-SG with torsion

The method of finding the dependence of spin connection ω on other fields by first treating it as an independent field in the action and then solving its (always nonpropagating) field equation is known in standard supergravity as the Palatini's formalism. This leads to the simplest description of supergravity. So, solving from (114) (thus without matter) the field equation for ω, one finds $\omega = \omega(e)$. We will use the techniques of (van Nieuwenhuizen, 1981) but extended in a plausible fashion to the $\widetilde{MS}_p$-SG. We will find the spin connection as a function of tetrad and gravitino. Whereas the Hilbert action vanishes and the gravitino action loses its spin connections, and thus we will find torsion induced by gravitinos.

Palatini's formalism can be implemented as follows. Varying the spin connection in Hilbert action (118),

doi: https://doi.org/10.52526/25792776-24.71.2-249

which can conveniently be rewritten in the form

$$\mathcal{L}^{(2)} = -\tfrac{1}{16}\varepsilon^{\hat\mu\hat\nu\hat\rho\hat\sigma}\varepsilon_{\hat a\hat b\hat c\hat d}e^{\hat a}_{\hat\mu}e^{\hat b}_{\hat\nu}R_{\hat\rho\hat\sigma}{}^{\hat c\hat d}(\omega), \tag{2}$$

we obtain

$$\delta\mathcal{L}^{(2)} = -\tfrac{1}{4}\varepsilon^{\hat\mu\hat\nu\hat\rho\hat\sigma}\varepsilon_{\hat a\hat b\hat c\hat d}(\mathcal{D}_{\hat\sigma}e^{\hat a}_{\hat\mu})e^{\hat b}_{\hat\nu}\delta\omega^{\hat c\hat d}_{\hat\rho}, \tag{3}$$

where $\mathcal{D}e^{\hat a} = de^{\hat a} + \omega^{\hat a\hat b}e_{\hat b}$. Varying then the spin connection in the Rarita-Schwinger action (119), it yields

$$\delta\mathcal{L}^{(3/2)} = 2\varepsilon^{\hat\mu\hat\nu\hat\rho\hat\sigma}(\bar\Psi_{\hat\mu}\gamma_{\hat 5}\gamma_{\hat\nu}\sigma_{\hat c\hat d}\Psi_{\hat\sigma})(\delta\omega^{\hat c\hat d}_{\hat\rho}), \tag{4}$$

which can be recast in the form

$$\delta\mathcal{L}^{(3/2)} = \varepsilon^{\hat\mu\hat\nu\hat\rho\hat\sigma}\varepsilon_{\hat b\hat c\hat d\hat a}(\bar\Psi_{\hat\mu}\gamma^{\hat a}\Psi_{\hat\sigma})e^{\hat b}{}_{\hat\nu}\delta\omega^{\hat c\hat d}_{\hat\rho}. \tag{5}$$

For the field equation of the spin connection, comparison of (2) and (5) gives

$$\mathcal{D}_{\hat\mu}e^{\hat a}{}_{\hat\nu} - \mathcal{D}_{\hat\nu}e^{\hat a}{}_{\hat\mu} = \tfrac{1}{2}\bar\Psi_{\hat\mu}\gamma^{\hat a}\Psi_{\hat\nu}. \tag{6}$$

Solving this equation, we as usual introduce the contorsion tensor $K^{\hat a\hat b}$ (Aldrovandi & Pereira, 1995),

$$\omega^{\hat a\hat b} = \omega^{\hat a\hat b}(e) + K^{\hat a\hat b}. \tag{7}$$

By virtue of the first tetrad postulate (which is a definition of $\omega(e)$), we obtain

$$\begin{aligned}&\partial_{\hat\mu}e^{\hat a}{}_{\hat\nu} + \omega_{\hat\mu}{}^{\hat a}{}_{\hat\nu} - (\mu \leftrightarrow \nu) = 0,\\ &K_{\hat\mu\hat a\hat\nu} - K_{\hat\nu\hat a\hat\mu} = -\bar\Psi_{\hat\mu}\gamma_{\hat a}\Psi_{\hat\nu}.\end{aligned} \tag{8}$$

By substituting the second equation of (8) into the identity

$$(K_{\hat\mu\hat a\hat\nu} - K_{\hat\nu\hat a\hat\mu}) + (K_{\hat a\hat\mu\hat\nu} - K_{\hat\nu\hat\mu\hat a}) + (K_{\hat a\hat\nu\hat\mu} - K_{\hat\mu\hat\nu\hat a}) = 2K_{\hat\mu\hat a\hat\nu}, \tag{9}$$

and using the second tetrad postulate,

$$\partial_{\hat\mu}e^{\hat a}{}_{\hat\nu} + \omega_{\hat\mu}{}^{\hat a}{}_{\hat\nu} - \Gamma\,{}^{\hat a'}_{\hat\nu\hat\mu}e^{\hat a}{}_{\hat a'} = 0, \tag{10}$$

one obtains an expression for antisymmetric part $\Gamma^{\hat a}{}_{[\hat\mu\hat\nu]}$,

$$2T^{\hat a}_{\hat\mu\hat\nu} = \Gamma^{\hat a}{}_{[\hat\mu\hat\nu]} = -K_{[\hat\mu}{}^{\hat a}{}_{\hat\nu]}, \tag{11}$$

with the torsion tensor $T^{\hat a}$,

$$T^{\hat a} = \tfrac{1}{2}\bar\Psi\gamma^{\hat a}\Psi. \tag{12}$$

Thus, the invariance of the total action (117) under local supersymmetry transformation requires the vanishing of the supertorsion $\tilde T^{\hat a} = 0$, which means that the connection is no longer an independent variable. The same supertorsion-free condition is necessary for the invariance of the action under local Poincaré translations, because of the variation (115) in case of an independent ω. An effect of the supertorsion-free condition on the local Poincaré superalgebra is that all commutators on $\delta e^{\hat a}$ and $\delta\Psi$ close except the commutator of two local supersymmetry transformations on the gravitino. For this commutator on the vierbein one finds

$$\begin{aligned}&[\delta_{\epsilon_1(X)}, \delta_{\epsilon_2(X)}]e^{\hat a}(X) = \delta e^{\hat a}(X) = \mathcal{D}\rho^{\hat a}(X)\\ &= \tfrac{1}{2}\bar\epsilon_2(X)\gamma^{\hat a}\mathcal{D}\epsilon_1(X) - \tfrac{1}{2}\bar\epsilon_1(X)\gamma^{\hat a}\mathcal{D}\epsilon_2(X) = \tfrac{1}{2}\mathcal{D}(\bar\epsilon_2(X)\gamma^{\hat a}\epsilon_1(X)),\end{aligned} \tag{13}$$

so that $\rho^{\hat a}(X) = \frac{1}{2}\bar\epsilon_2(X)\gamma^{\hat a}\epsilon_1(X)$ in accord with (104). The dependence of $\omega^{\hat a\hat b}$ on the tetrad field then reads

$$\begin{aligned}&\omega_{\hat\mu\hat a\hat b}(e,\Psi) = \tfrac{1}{2}(R_{\hat\mu\hat b,\hat a} - R_{\hat\mu\hat a,\hat b} + R_{\hat a\hat b,\hat\mu}),\\ &R_{\hat\mu\hat\nu,\hat a} = -\partial_{\hat\mu}e_{\hat a\hat\nu} + \partial_{\hat\nu}e_{\hat a\hat\mu} - (\bar\Psi_{\hat\mu}\gamma_{\hat a}\Psi_{\hat\nu}),\end{aligned} \tag{14}$$

doi: https://doi.org/10.52526/25792776-24.71.2-249

provided, $R_{\hat{\mu}\hat{b},\hat{a}} = e^{\hat{\nu}}_{\hat{b}} R_{\hat{\mu}\hat{\nu},\hat{a}}$. Since $\omega(e,\Psi)$ is an extremum of the action, then according to the *Theorem (I)* in (?), under transformation $\omega^{\hat{a}\hat{b}} \to \omega^{\hat{a}\hat{b}} + \tau^{\hat{a}\hat{b}}$, for arbitrary $\tau^{\hat{a}\hat{b}} = -\tau^{\hat{b}\hat{a}}$, the symmetry

$$\begin{array}{l}\mathcal{L}^{(2)}(e,\omega(e,\Psi)+\tau) + \mathcal{L}^{(3/2)}(e,\Psi,\omega(e,\Psi)+\tau))\\ = \mathcal{L}^{(2)}(e,\omega(e,\Psi)) + \mathcal{L}^{(3/2)}(e,\Psi,\omega(e,\Psi))\\ -\frac{1}{4}(\tau_{\hat{\mu}\hat{\nu}\hat{\rho}}\tau^{\hat{\rho}\hat{\nu}\hat{\mu}} - (\tau^{\hat{\lambda}}_{\ \hat{\lambda}\hat{\mu}})^2) + \text{total derivative},\end{array} \tag{15}$$

holds because terms linear in τ cancel out. In particular case if $\tau^{\hat{a}\hat{b}} = -\omega^{\hat{a}\hat{b}}$, the Hilbert action with the Weitzenböck curvature vanishes, and the gravitino action loses its spin connections. So we may henceforth reinterpret flat $\widetilde{MS}_p$-SG with Weitzenböck torsion as a teleparallelism theory - a theory that involves only torsion, where a parallel transport is defined over finite distances and not only in an infinitesimal neighborhood. This theory represented an alternative way of including torsion to the scheme previously provided by a Einstein-Cartan theory. Using then the result for $\omega^{\hat{a}\hat{b}}$ in terms of the curls

$$\partial_{\hat{\mu}} e^{\hat{a}}_{\ \hat{\nu}} - \partial_{\hat{\nu}} e^{\hat{a}}_{\ \hat{\mu}} + \bar{\Psi}_{\hat{\mu}}\gamma^{\hat{a}}\Psi_{\hat{\nu}}, \tag{16}$$

in (14), we may rewrite the action of a $\widetilde{MS}_p$-TSG theory:

$$\begin{array}{l}\mathcal{L}_{MS-TSG} = 4\varepsilon^{\hat{\mu}\hat{\nu}\hat{\rho}\hat{\sigma}}\bar{\Psi}_{\hat{\mu}}\gamma_{\hat{5}}\gamma_{\hat{\nu}}\partial_{\hat{\rho}}\Psi_{\hat{\sigma}}\\ -R^2_{\hat{\mu}\hat{\nu}\hat{a}} - R_{\hat{\mu}\hat{\nu}\hat{a}}R^{\hat{a}\hat{\nu}\hat{\mu}} + \frac{1}{2}R^2_{\hat{\nu}\hat{\lambda}\hat{\lambda}},\end{array} \tag{17}$$

where the objects $R_{\hat{\mu}\hat{\nu}\hat{a}}$ is interpreted as the supercovariantized torsion tensor

$$-\mathcal{D}_{\hat{\mu}} e_{\hat{a}\hat{\nu}} + \mathcal{D}_{\hat{\nu}} e_{\hat{a}\hat{\mu}} - (\bar{\Psi}_{\hat{\mu}}\gamma_{\hat{a}}\Psi_{\hat{\nu}}). \tag{18}$$

3. The $\widetilde{MS}_p$-TSG with the translation group

In Teleparallel Gravity, the spin connection represents only *inertial effects*, but not gravitation at all. All quantities related to Teleparallel Gravity will be denoted with an over 'dot'. The spin connection reads

$$\dot{\omega}^{\hat{a}}_{\ \hat{b}\hat{\mu}} = L^{\hat{a}}_{\ \hat{d}}\partial_{\hat{\mu}} L_{\hat{b}}^{\ \hat{d}}, \tag{19}$$

and the energy-momentum density of the *inertial* or *fictitious* forces is

$$\dot{i}_{\hat{a}}^{\ \hat{\rho}} = \frac{1}{k}\dot{\omega}^{\hat{c}}_{\ \hat{a}\hat{\sigma}}\dot{S}_{\hat{c}}^{\ \hat{\rho}\hat{\sigma}}, \tag{20}$$

where $\dot{S}_{\hat{c}}^{\ \hat{\rho}\hat{\sigma}}$ is the so called superpotential (see (38)). Teleparallel Gravity is a gauge theory for the *translation* group (?). The $\widetilde{MS}_p$-TSG theory, therefore, has the gauge *translation* group in tangent bundle. Namely, at each point p of coordinates X of the base space $(V_4 \oplus \underline{V}_2)$, there is attached a Minkowski tangent-space (the fiber) $T_p(V_4 \oplus \underline{V}_2) = T_{X^{\hat{\mu}}}(V_4 \oplus \underline{V}_2)$, on which the point dependent gauge transformations,

$$X'^{\hat{a}} = X^{\hat{a}} + \varepsilon^{\hat{a}}(X), \tag{21}$$

take place. Under an infinitesimal tangent space translation, it transforms according to

$$\delta\Phi(X^{\hat{a}}(X^{\hat{\mu}})) = -\varepsilon^{\hat{a}}\partial_{\hat{a}}\Phi(X^{\hat{a}}(X^{\hat{\mu}})). \tag{22}$$

The generators of this group satisfy the Lie algebra $[P_{\hat{a}}, P_{\hat{b}}] = 0$. In order to recover the covariance, it is necessary to introduce a 1-form of the Yang–Mills connection assuming values in the Lie algebra of the translation group:

$$B = e^{\hat{a}} P_{\hat{a}}, \tag{23}$$

with gauge field $e^{\hat{a}}$. Introducing the covariant derivative

$$\dot{\mathcal{D}}_{\hat{\mu}} X^{\hat{a}} = \partial_{\hat{\mu}} X^{\hat{a}} + \dot{\omega}^{\hat{a}}_{\ \hat{b}\hat{\mu}} X^{\hat{b}}, \tag{24}$$

the tetrad, which is invariant under translations, becomes

$$\dot{e}^{\hat{a}}_{\ \hat{\mu}} = \dot{\mathcal{D}}_{\hat{\mu}} X^{\hat{a}} + \dot{\omega}^{\hat{a}}_{\ \hat{b}\hat{\mu}}. \tag{25}$$

doi: https://doi.org/10.52526/25792776-24.71.2-249

In this new class of frames, the gauge field transforms according to $\delta e^{\hat{a}}{}_{\hat{\mu}} = -\dot{\mathcal{D}}_{\hat{\mu}}\varepsilon^{\hat{a}}$. Thus the covariant derivative, $\dot{\mathcal{D}} = d + B$, with Yang–Mills connection reads

$$\dot{\mathcal{D}}_{\hat{\mu}} = (\delta^{\hat{a}}_{\hat{\mu}} + e_{\hat{\mu}}{}^{\hat{a}})\partial_{\hat{a}} = (\partial_{\hat{\mu}}X^{\hat{a}} + e_{\hat{\mu}}{}^{\hat{a}})\partial_{\hat{a}} = \dot{e}_{\hat{\mu}}{}^{\hat{a}}\partial_{\hat{a}}. \tag{26}$$

The curvature of the Weitzenböck connection

$$\dot{\Gamma}^{\hat{\rho}}{}_{\hat{\nu}\hat{\mu}} = \dot{e}_{\hat{a}}{}^{\hat{\rho}}\dot{\mathcal{D}}_{\hat{\mu}}\dot{e}^{\hat{a}}{}_{\hat{\nu}}, \tag{27}$$

vanishes identically, while for a tetrad $\dot{e}^{\hat{a}}$ with $e^{\hat{a}}{}_{\hat{\mu}} \neq \dot{\mathcal{D}}_{\hat{\mu}}\varepsilon^{\hat{a}}$, the torsion 2-form - the field strength (here we re-instate the factor $\wedge$),

$$\dot{T}^{\hat{a}} = d\dot{e}^{\hat{a}} = \tfrac{1}{2}\dot{T}^{\hat{a}}{}_{\hat{b}\hat{c}}\dot{e}^{\hat{b}} \wedge \dot{e}^{\hat{c}} = \dot{K}_{\hat{c}}{}^{\hat{a}} \wedge \dot{e}^{\hat{c}}, \tag{28}$$

is non-vanishing:

$$\dot{T}^{\hat{a}}{}_{\hat{\mu}\hat{\nu}} = \dot{\mathcal{D}}_{\hat{\mu}}\dot{e}^{\hat{a}}{}_{\hat{\nu}} - \dot{\mathcal{D}}_{\hat{\nu}}\dot{e}^{\hat{a}}{}_{\hat{\mu}} = \dot{\Gamma}^{\hat{a}}{}_{[\hat{\mu}\hat{\nu}]} = \dot{\mathcal{D}}_{\hat{\mu}}e^{\hat{a}}{}_{\hat{\nu}} - \dot{\mathcal{D}}_{\hat{\nu}}e^{\hat{a}}{}_{\hat{\mu}} \neq 0. \tag{29}$$

Here $\dot{K}^{\hat{a}\hat{b}}$ is the contorsion tensor, and we also taken into account the vanishing torsion, $[\dot{\mathcal{D}}_{\hat{\mu}}, \dot{\mathcal{D}}_{\hat{\nu}}]X^{\hat{a}} = 0$, of *inertial* tetrad, $\dot{e}^{\hat{a}}{}_{\hat{\mu}} = \dot{\mathcal{D}}_{\hat{\mu}}X^{\hat{a}}$. Hence

$$[\dot{e}_{\hat{\mu}}, \dot{e}_{\hat{\nu}}] = \dot{T}_{\hat{\mu}\hat{\nu}} = \dot{T}^{\hat{a}}{}_{\hat{\mu}\hat{\nu}}P_{\hat{a}}. \tag{30}$$

Due to the soldered character of the tangent bundle, torsion presents also the anholonomy of the translational covariant derivative:

$$[\dot{e}_{\hat{\mu}}, \dot{e}_{\hat{\nu}}] = \dot{T}_{\hat{\mu}\hat{\nu}} = \dot{T}^{\hat{\rho}}{}_{\hat{\mu}\hat{\nu}}P_{\hat{\rho}}. \tag{31}$$

The gauge invariance of the tetrad provides torsion invariance under gauge transformations. As a gauge theory for the translation group, the action (17) of the $\widetilde{MS}_p$-TSG theory can be recast in the form (see also Salgado et al. (2005))

$$\begin{aligned} \dot{\mathcal{L}}_{MS-TSG} &= \tfrac{1}{4}tr\left(\hat{\dot{T}} \wedge \star\hat{\dot{T}}\right) - 4\bar{\Psi}\gamma_{\hat{5}}\gamma_{\hat{d}}\mathcal{D}\Psi\dot{e}^{\hat{d}} \\ &= \tfrac{1}{4}\eta_{\hat{a}\hat{b}}\dot{T}^{\hat{a}} \wedge \star\dot{T}^{\hat{b}} - 4\bar{\Psi}\gamma_{\hat{5}}\gamma_{\hat{d}}\mathcal{D}\Psi\dot{e}^{\hat{d}}, \end{aligned} \tag{32}$$

where (we re-instate the factor $\wedge$) the torsion 2-form reads

$$\hat{\dot{T}} = \tfrac{1}{2}\dot{T}^{\hat{a}}{}_{\hat{\mu}\hat{\nu}}P_{\hat{a}}dX^{\hat{\mu}} \wedge dX^{\hat{\nu}}, \tag{33}$$

and

$$\star\hat{\dot{T}} = \tfrac{1}{2}\left(\star\dot{T}^{\hat{a}}{}_{\hat{\rho}\hat{\sigma}}\right)P_{\hat{a}}dX^{\hat{\rho}} \wedge dX^{\hat{\sigma}}. \tag{34}$$

Here $\star$ denotes the Hodge dual. That is, let Ω^p be the space of p-forms on an n-dimensional manifold $\mathbf{R}$ with metric. Since vector spaces Ω^p and Ω^{n-p} have the same finite dimension, they are isomorphic. The presence of a metric renders it possible to single out an unique isomorphism, called Hodge dual. Using a coordinate basis, the Hodge dual map $\star : \Omega^p \to \Omega^{n-p}$ is the C^∞-linear map $\star : \Omega^p \to \Omega^{n-p}$, which acts on the wedge product monomials of the basis 1-forms as

$$\star(\vartheta^{a_1\cdots a_p}) = \varepsilon^{a_1\cdots a_n}e_{a_{p+1}\cdots a_n}, \tag{35}$$

where e_{a_i} $(i = p+1, ..., n)$ are understood as the down indexed 1-forms $e_{a_i} = o_{a_i b}\,\vartheta^b$ and $\epsilon^{a_1...a_n}$ is the total antisymmetric pseudo-tensor. The operator $\star$ satisfies the property

$$\star\star(\vartheta^{a_1\cdots a_p}) = (-1)^{p(n-p)+(n-s)/2}\star(\vartheta^{a_1\cdots a_p}) \tag{36}$$

where s is the metric signature. Its inverse is

$$\star_{-1} = (-1)^{p(n-p)+(n-s)/2}\star. \tag{37}$$

A further relation involving Hodge duality reads ${}^\star(\alpha \wedge e_a) = (e_a \rfloor {}^\star\alpha)$, while for differential forms α, β of the same degree p, equation ${}^\star(\alpha \wedge \beta = {}^\star(\beta \wedge \alpha)$ holds.

In (32) we taken into account that the translation group is abelian, therefore its Cartan-Killing bilinear form is degenerate and cannot be used as a metric. Recall that the group manifold of translations is just the Minkowski spacetime $\mathcal{M}$, the quotient space between the Poincaré, $\mathcal{P}$, and the Lorentz, $\mathcal{L}$, groups:

doi: https://doi.org/10.52526/25792776-24.71.2-249

$\mathcal{M} = \mathcal{P}/\mathcal{L}$. Namely, $\mathcal{M}$ is homogeneous or transitive under X-space translations, which means that there is only one group element that moves a point of the $\mathcal{M}$ space into another given point of the $\mathcal{M}$ space. The role of the Cartan-Killing metric comes, when it exists, from its being invariant under the group action. Here it does not exist, but we can use the invariant Lorentz metric $\eta_{\hat{a}\hat{b}}$ of $\mathcal{M}$ in its stead. Defining the tensor of superpotential

$$\dot{S}_{\hat{a}}{}^{\hat{\rho}\hat{\sigma}} = -\dot{S}_{\hat{a}}{}^{\hat{\sigma}\hat{\rho}} := \dot{K}^{\hat{\rho}\hat{\sigma}}{}_{\hat{a}} - \dot{e}_{\hat{a}}{}^{\hat{\sigma}}\dot{T}^{\hat{c}\hat{\rho}}{}_{\hat{c}} + \dot{e}_{\hat{a}}{}^{\hat{\rho}}\dot{T}^{\hat{c}\hat{\sigma}}{}_{\hat{c}}, \tag{38}$$

the dual torsion can be rewritten in the form

$$\star\dot{T}^{\hat{\rho}}{}_{\hat{\mu}\hat{\nu}} = \tfrac{\dot{e}}{2}\varepsilon_{\hat{\mu}\hat{\nu}\hat{\lambda}\hat{\sigma}}\dot{S}^{\hat{\rho}\hat{\lambda}\hat{\sigma}}, \tag{39}$$

with $\dot{e} = det\,\dot{e}^{\hat{a}}{}_{\mu}(X) = \sqrt{-g}$, and hence

$$\dot{\mathcal{L}}_{MS-TSG} = \tfrac{\dot{e}}{8}\dot{T}_{\hat{\rho}\hat{\mu}\hat{\nu}}\dot{S}^{\hat{\rho}\hat{\mu}\hat{\nu}} - 4\bar{\Psi}\gamma_{\hat{5}}\gamma_{\hat{d}}\mathcal{D}\Psi\dot{e}^{\hat{d}}. \tag{40}$$

An entire torsion tensor can be written through the components of 'vector torsion' ($\dot{\mathcal{V}}_{\hat{\mu}} = \dot{T}^{\hat{\nu}}{}_{\hat{\mu}\hat{\nu}}$), 'axial torsion' ($\dot{\mathcal{A}}^{\hat{\mu}} = \frac{1}{6}\varepsilon^{\hat{\mu}\hat{\nu}\hat{\rho}\hat{\lambda}}\dot{T}_{\hat{\nu}\hat{\rho}\hat{\lambda}}$), and 'pure tensor torsion' ($\dot{\mathcal{T}}_{\hat{\rho}\hat{\mu}\hat{\nu}}$) (a tensor with vanishing vector and axial parts) as

$$\dot{T}_{\hat{\rho}\hat{\mu}\hat{\nu}} = \tfrac{2}{3}(\dot{\mathcal{T}}_{\hat{\rho}\hat{\mu}\hat{\nu}} - \dot{\mathcal{T}}_{\hat{\rho}\hat{\nu}\hat{\mu}}) + \tfrac{1}{3}(g_{\hat{\rho}\hat{\mu}}\dot{\mathcal{V}}_{\hat{\nu}} - g_{\hat{\rho}\hat{\nu}}\dot{\mathcal{V}}_{\hat{\mu}}) + \varepsilon_{\hat{\rho}\hat{\mu}\hat{\nu}\hat{\lambda}}\dot{\mathcal{A}}^{\hat{\lambda}}. \tag{41}$$

Making use of the identity $\dot{T}^{\hat{\mu}}{}_{\hat{\mu}\hat{\rho}} = \dot{K}^{\hat{\mu}}{}_{\hat{\rho}\hat{\mu}}$, the action (32) becomes

$$\dot{\mathcal{L}}_{MS-TSG} = \tfrac{\dot{e}}{4}\left(\tfrac{1}{4}\dot{T}^{\hat{\rho}}{}_{\hat{\mu}\hat{\nu}}\dot{T}_{\hat{\rho}}{}^{\hat{\mu}\hat{\nu}} + \tfrac{1}{2}\dot{T}^{\hat{\rho}}{}_{\hat{\mu}\hat{\nu}}\dot{T}^{\hat{\nu}\hat{\mu}}{}_{\hat{\rho}} - \dot{T}^{\hat{\rho}}{}_{\hat{\mu}\hat{\rho}}\dot{T}^{\hat{\nu}\hat{\mu}}{}_{\hat{\rho}}\right) - 4\bar{\Psi}\gamma_{\hat{5}}\gamma_{\hat{d}}\mathcal{D}\Psi\dot{e}^{\hat{d}}, \tag{42}$$

which consequently can be recast in the form

$$\dot{\mathcal{L}}_{MS-TSG} = -\varepsilon_{\hat{a}\hat{b}\hat{c}\hat{d}}\dot{K}^{\hat{a}}{}_{\hat{e}}\dot{K}^{\hat{e}\hat{b}}\dot{e}^{\hat{c}}\dot{e}^{\hat{d}} - 4\bar{\Psi}\gamma_{\hat{5}}\gamma_{\hat{d}}\mathcal{D}\Psi\dot{e}^{\hat{d}}, \tag{43}$$

or

$$\dot{\mathcal{L}}_{MS-TSG} = -\varepsilon_{\hat{a}\hat{b}\hat{c}\hat{d}}\dot{K}^{\hat{a}\hat{b}}\dot{T}^{\hat{c}}\dot{e}^{\hat{d}} - 4\bar{\Psi}\gamma_{\hat{5}}\gamma_{\hat{d}}\mathcal{D}\Psi\dot{e}^{\hat{d}} + \text{surface term}. \tag{44}$$

This action is invariant under local translations, under local super symmetry transformations and by construction is invariant under local Lorentz rotations and under diffeomorphisms (see Salgado et al. (2003, 2005), Stelle & West (1980)). In other words, the action (42) is invariant under the Poincaré supergroup and under diffeomorphisms.

It remains to see the equivalence of the Teleparallel Gravity action $\dot{\mathcal{L}}^{(2)}$ in (42) with Hilbert action $\mathcal{L}^{(2)}$ in (118), which will prove that the immediate cause of the *fictitious* Riemann curvature (R) for the Levi-Civita connection (Γ) is the acceleration. The curvature ($\dot{R}$) of Weitzenböck connection ($\dot{\Gamma}$) vanishes identically, but for a tetrad involving a non-trivial translational gauge potential ($\dot{e}_{\hat{\mu}}{}^{\hat{a}} \neq \dot{\mathcal{D}}_{\hat{\mu}}\varepsilon^{\hat{a}}$), the torsion ($\dot{T}$) is non-vanishing. The connection ($\dot{\Gamma}$) can be considered a kind of dual of the Levi-Civita connection (Γ), which is a connection with vanishing torsion (T), and non-vanishing *fictitious* curvature (R). Provided, the following relations hold:

$$\begin{aligned} \dot{\Gamma}^{\hat{\rho}}{}_{\hat{\mu}\hat{\nu}} &= \Gamma^{\hat{\rho}}{}_{\hat{\mu}\hat{\nu}} + \dot{K}^{\hat{\rho}}{}_{\hat{\mu}\hat{\nu}}, \\ \dot{R}^{\hat{\rho}}{}_{\hat{\lambda}\hat{\mu}\hat{\nu}} &= R^{\hat{\rho}}{}_{\hat{\lambda}\hat{\mu}\hat{\nu}} + \dot{Q}^{\hat{\rho}}{}_{\hat{\lambda}\hat{\mu}\hat{\nu}} \equiv 0, \end{aligned} \tag{45}$$

where $\dot{Q}$ is a 2-form assuming values in the Lie algebra of the Lorentz group,

$$\dot{Q} = \tfrac{1}{2}S_{\hat{a}}{}^{\hat{b}}\dot{Q}^{\hat{a}}{}_{\hat{b}\hat{\mu}\hat{\nu}}dX^{\hat{\mu}} \wedge dX^{\hat{\nu}}, \tag{46}$$

with the components

$$\dot{Q}^{\hat{a}}{}_{\hat{b}\hat{\mu}\hat{\nu}} = \mathcal{D}_{\hat{\mu}}\dot{K}^{\hat{a}}{}_{\hat{b}\hat{\nu}} - \mathcal{D}_{\hat{\nu}}\dot{K}^{\hat{a}}{}_{\hat{b}\hat{\mu}} + \dot{K}^{\hat{a}}{}_{\hat{c}\hat{\nu}}\dot{K}^{\hat{c}}{}_{\hat{b}\hat{\mu}} - \dot{K}^{\hat{a}}{}_{\hat{c}\hat{\mu}}\dot{K}^{\hat{c}}{}_{\hat{b}\hat{\nu}}. \tag{47}$$

The scalar version of second relation in (45) is

$$-\dot{R} = \dot{Q} \equiv \left(\dot{K}^{\hat{\mu}\hat{\nu}\hat{\rho}}\dot{K}_{\hat{\nu}\hat{\mu}\hat{\rho}} - \dot{K}^{\hat{\mu}\hat{\rho}}{}_{\hat{\mu}}\dot{K}^{\hat{\nu}}{}_{\hat{\rho}\hat{\nu}}\right) + \tfrac{2}{\dot{e}}\partial_{\hat{\mu}}\left(\dot{e}\dot{T}^{\hat{\nu}\hat{\mu}}{}_{\hat{\nu}}\right), \tag{48}$$

which proves that the immediate cause of the *fictitious* Riemann curvature (R) is the acceleration. Comparing with (42), this actually proves the equivalence of the Teleparallel Gravity action $\dot{\mathcal{L}}^{(2)}$ in (42) with Hilbert action $\mathcal{L}^{(2)}$ in (118):

$$\dot{\mathcal{L}}^{(2)} = \mathcal{L}^{(2)} + \text{surface term}. \tag{49}$$

doi: https://doi.org/10.52526/25792776-24.71.2-249

The dynamical aspects of particle mechanics involve derivatives with respect to proper time along the particle worldline, which is the line element written in frame (25):

$$ds^2 = \eta_{\hat{a}\hat{b}}\dot{e}^{\hat{a}}\dot{e}^{\hat{b}} = \eta_{\hat{a}\hat{b}}\dot{e}^{\hat{a}}{}_{\hat{\mu}}\dot{e}^{\hat{b}}{}_{\hat{\mu}}dX^{\hat{\mu}}dX^{\hat{\nu}} \equiv \eta_{\hat{\mu}\hat{\nu}}dX^{\hat{\mu}}dX^{\hat{\nu}}. \tag{50}$$

A worldline C of a particle, parametrized by proper time as $C(s) = X^{\hat{\mu}}(s)$, will have as six-velocity the vector of components $u^{\hat{\mu}} = dX^{\hat{\mu}}/ds$ and $u^{\hat{a}} = \dot{e}^{\hat{a}}_{\hat{\mu}}u^{\hat{\mu}}$, which are the particle velocity along this curve respectively in the holonomic and anholonomic bases in the X-space. The proper time can be written in the form $ds = u_{\hat{\mu}}dX^{\hat{\mu}} = u_{\hat{a}}\dot{e}^{\hat{a}}$. The equation of motion in the X-space is written as

$$\tfrac{du^{\hat{a}}}{ds} = \left(\dot{K}^{\hat{a}}{}_{\hat{b}\hat{\rho}} - \dot{\omega}^{\hat{a}}{}_{\hat{b}\hat{\rho}}\right)u^{\hat{b}}u^{\hat{\rho}}. \tag{51}$$

This equation can be rewritten in a purely spacetime form

$$\tfrac{du^{\hat{\rho}}}{ds} = \left(\dot{K}^{\hat{\rho}}{}_{\hat{\mu}\hat{\nu}} - \dot{\Gamma}^{\hat{\rho}}{}_{\hat{\mu}\hat{\nu}}\right)u^{\hat{\mu}}u^{\hat{\nu}}. \tag{52}$$

The corresponding acceleration cannot be given a covariant meaning without a connection, while each different connection $\Gamma^{\hat{\rho}}{}_{\hat{\mu}\hat{\nu}}$ will deffne a different acceleration. The Weitzenböck connection, which defines the Fock-Ivanenko derivative $\dot{\mathcal{D}}_{\hat{\mu}}$ written in terms of covariant derivative $\dot{\nabla}_{\hat{\mu}}$:

$$\dot{\mathcal{D}}_{\hat{\mu}}\Phi^{\hat{a}} = \dot{e}^{\hat{a}}{}_{\hat{\rho}}\dot{\nabla}_{\hat{\mu}}\Phi^{\hat{\rho}}, \tag{53}$$

will define the acceleration too

$$\begin{aligned}\dot{a}^{\hat{\rho}} &= \tfrac{\dot{\nabla}u^{\hat{\rho}}}{\dot{\nabla}s} = u^{\hat{\nu}}\dot{\nabla}_{\hat{\nu}}u^{\hat{\rho}} = \tfrac{du^{\hat{\rho}}}{ds} + \dot{\Gamma}^{\hat{\rho}}{}_{\hat{\mu}\hat{\nu}}u^{\hat{\mu}}u^{\hat{\nu}} \\ &= \dot{K}^{\hat{\rho}}{}_{\hat{\mu}\hat{\nu}}u^{\hat{\mu}}u^{\hat{\nu}} = \dot{T}^{\hat{\rho}}{}_{\hat{\nu}\hat{\mu}}u^{\hat{\mu}}u^{\hat{\nu}}.\end{aligned} \tag{54}$$

This is a force equation, with torsion (or contortion) playing the role of force. To transform the tetrad field into a reference frame in X-space with an observer attached to it, we may "attach" $\dot{e}_{\hat{0}}$ to the observer by identifying $u = \dot{e}_{\hat{0}} = \frac{d}{ds}$ with components $u^{\hat{\mu}} = \dot{e}_{\hat{0}}{}^{\hat{\mu}}$, such that $\dot{e}_{\hat{0}}$ will be the observer velocity. The Weitzenböck connection, $\dot{\Gamma}$, will attribute to the observer an acceleration

$$\dot{a}^{\hat{a}}_{(f,\dot{\Gamma})} = \dot{\omega}^{\hat{a}}{}_{\hat{0}\hat{0}} + \dot{K}^{\hat{a}}{}_{\hat{0}\hat{0}}, \tag{55}$$

seen by that very observer. Whereas,

$$\dot{\omega}^{\hat{a}}{}_{\hat{b}\hat{c}} = \dot{e}^{\hat{a}}{}_{\hat{\mu}}\dot{\nabla}_{\dot{e}_{\hat{c}}}, \dot{e}_{\hat{b}}{}^{\hat{\mu}}, \tag{56}$$

which literarily means the covariant derivative of $\dot{e}_{\hat{b}}$ along $\dot{e}_{\hat{c}}$, projected along $\dot{e}_{\hat{a}}$. As $\dot{a}^{\hat{\rho}}$ (54) is orthogonal to $u^{\hat{\rho}}$, its vanishing means that the $u^{\hat{\rho}}$ keeps parallel to itself along the worldline.

Another transport, distinct from parallel transport, is the Fermi-Walker transport, which absorbs the acceleration. Fermi-Walker transport for a vector $\mathbf{V}$ along a worldline with unit tangent $\mathbf{U}$ is characterized by a boost that compensates the acceleration $\dot{\mathbf{U}} \equiv \mathbf{U}/Ds$. The temporal-part of $\mathbf{V}$ remains unchanged, while the spatial-part becomes subject to a rotation preserving the length of the spatial-part of the vector $\mathbf{V}$ and, thus, its four-dimensional length. In particular,

$$\dot{\nabla}^{(FW)}_{\dot{e}_{\hat{0}}}\dot{e}_{\hat{0}}{}^{\hat{\rho}} = \dot{\nabla}_{\dot{e}_{\hat{0}}}\dot{e}_{\hat{0}}{}^{\hat{\rho}} - \dot{a}^{\hat{\rho}}, \tag{57}$$

implies that $\dot{e}_{\hat{0}}$, by this transport, is kept tangent along its own integral curve. Along the radial geodesics, however, Fermi-Walker transport becomes Levi-Civita's parallel transport.

4. A Newtonian gravitational field: 'absolute' acceleration

A Newtonian limit is obtained by assuming that the translational gauge field is stationary and weak. This means respectively that the time derivative of $e^a{}_\mu$ in M_4 vanishes, and that$|e^a{}_\mu| \ll 1$ (Aldrovandi & Pereira, 2013). In accord, all the particles are supposed to move in M_4 with a sufficient small velocity so that $u^i \ll u^0$. The equation of motion (52) rewritten purely in the terms of M_4 spacetime is then reduced to

$$\tfrac{du^\rho}{ds} + \dot{\Gamma}^\rho{}_{00}u^0u^0 = \dot{T}_0{}^\rho{}_0u^0u^0. \tag{58}$$

doi: https://doi.org/10.52526/25792776-24.71.2-249

In the class of frames in which the teleparallel spin connection $\dot{\omega}^{\hat{a}}{}_{\hat{b}\hat{\rho}}$ vanishes, and choosing a translational gauge in which $\partial_\mu x^a = \delta^a_\mu$, the tetrad has the form

$$\widetilde{e}^a{}_\mu = \delta^a{}_\mu + e^a{}_\mu.$$

Up to first order in the field $e^a{}_\mu$, we obtain

$$\dot{\Gamma}^\rho{}_{\mu\nu} \equiv \partial_\nu e^\rho{}_\mu,$$

where

$$e^\rho{}_\mu = \delta^\rho_a e^a{}_\mu.$$

The (58) becomes

$$\frac{d^2x^\rho}{ds^2} = \partial^\rho e_{00} u^0 u^0.$$

Substituting $u^0 = cdt/ds$, we obtain

$$\frac{d^2x^\rho}{ds^2} = \partial^\rho e_{00} c^2 (\frac{dt}{ds})^2.$$

For the temporal component this gives

$$\frac{d^2x^0}{ds^2} \equiv c^2 \frac{d^2t}{ds^2} = 0,$$

the solution of which is the constant dt/ds. Then the spatial components of d^2x^ρ/ds^2 reads

$$\frac{dv^i}{dt} = c^2 \partial^i e_{00},$$

where v^i is the particle three-velocity. If we identify $c^2 e_{00} = \Phi$, with the potential of the *fictitious* gravitational force (the inertial force):

$$F = -\nabla\Phi,$$

we obtain

$$\vec{a} = -\vec{F}.$$

Here we have taken into account that the components of $\vec{x}$ are given by $x^i = -x_i$, so that $\partial^i = -\partial_i$. As expected, due to the equivalence with the geodesic equation, the force equation (54) also can be approximated to the limit of a Newtonian gravitational field.

Now consider the Newtonian field with acceleration $-\underline{a}_{(c)}$, in $\underline{M}_2$, in the $\underline{x}^1$-direction of zero velocity and at $\underline{x}^0 = 0$. Let the parallel worldlines $\underline{x} = const$ be the geodesics. For $\underline{x}^0 = 0$ and $\underline{x}^1 = 1/v^0\underline{a}_{(c)}$, the parallel to the $\underline{x}^0$-axis through this point is touched by the worldline of an observer with constant intrinsic acceleration

$$\underline{a}_{(c)} = \sqrt{2}(a^{(+)}_{(c)} a^{(-)}_{(c)})^{1/2} = 2(\underline{\theta}_1\,\bar{\underline{\theta}}_1\underline{\theta}_2\,\bar{\underline{\theta}}_2)^{1/2}\, \frac{d^2\tau}{d\underline{s}^2}\Big|_{const}, \tag{59}$$

which is the hyperbola (see next subsect.) parameterized with proper time $\underline{s}$,

$$\underline{x}^0 = \underline{\rho}\sinh\frac{\underline{s}}{\underline{\rho}}, \quad \underline{x}^1 = \underline{\rho}\cosh\frac{\underline{s}}{\underline{\rho}}, \quad \underline{\rho} = \frac{1}{v^0\underline{a}_{(c)}}. \tag{60}$$

Let this observer measure the distance $\underline{\eta}(\underline{s})$ to the straight line $\underline{x} = \underline{\rho}$ orthogonal to his worldline:

$$\underline{\eta}(\underline{s}) = \underline{\rho} - \frac{\underline{\rho}}{\cosh\frac{\underline{s}}{\underline{\rho}}} = \frac{1}{2\underline{\rho}}\underline{s}^2 + \mathcal{O}(\underline{s}^4). \tag{61}$$

The acceleration then reads

$$\underline{a} = \frac{d^2\underline{\rho}}{\underline{s}^2} = \frac{1}{2\underline{\rho}} = v^0\underline{a}_{(c)}. \tag{62}$$

Since the velocity $\underline{\eta}/\underline{s}$ increases, the acceleration points into the negative $\underline{x}^1$-direction. Further, according to (126), the *absolute* acceleration in M_4 becomes

$$\vec{a}_{abs.} = -\underline{a} = -v^0\underline{a}_{(c)} = -4(\underline{\theta}_1\,\bar{\underline{\theta}}_1\underline{\theta}_2\,\bar{\underline{\theta}}_2)\frac{d\tau}{d\underline{s}}\,\frac{d^2\tau}{d\underline{s}^2}\Big|_{const}, \tag{63}$$

pointing into the negative $\vec{n} = \vec{x}/|\vec{x}|$-direction. It is for this special case: against *absolute* space, in the same event, and at the same velocity, an inertial observer and the *absolutely accelerated* observer can interpret gravity as acceleration and vice versa. Acceleration against Newton's absolute space now is no longer so implausible as it appeared a century ago. The vacuum of spacetime is filled with the fluctuations of all fields and a metric too. Absolute space is realized by a local inertial system.

doi: https://doi.org/10.52526/25792776-24.71.2-249

5. The homogeneous acceleration field

The torsion in affine connected master space $\underline{M}_2$ is described by the vector-valued 2-form $\underline{T}$ as

$$\underline{T} = d(e_{\underline{\mu}} e^{\underline{\mu}}), \tag{64}$$

where d denotes the operator of exterior covariant derivation. Let us now to study the accelerated frame of reference described by the constant torsion (written with re-instated factor $\wedge$) - the *fictitious* gravitational field strength,

$$T^{\underline{\mu}} = de^{\underline{\mu}} = \frac{1}{2} T^{\underline{\mu}}_{\underline{\lambda}\underline{\nu}} e^{\underline{\lambda}} \wedge e^{\underline{\nu}}, \tag{65}$$

in the $\underline{M}_2$. The metric of a *homogeneous* manifold is invariant under a *transitive* group of motions, i.e. if its action maps any point of the manifold into any other point (Schucking & Surowitz, 2007). For gravitational fields, the group of motions has to be *simply transitive*, i.e. there is only one group element that moves a point of the manifold into another given point of the manifold. The *homogeneity* group in the master space $\underline{M}_2$ is characterized by the *invariant differential* 1-*forms* $e^{\underline{\mu}}$ that determine the coframes. Namely, $\underline{M}_2$ is homogeneous if the metric is given in terms of *invariant differential* 1-*forms* $e^{\underline{\mu}} = e^{\underline{\mu}}{}_{\underline{\nu}} d\underline{x}^{\underline{\nu}}$ for a *simply transitive group*. Therefore the $e'^{\underline{\mu}}{}_{\underline{\nu}}$ and the $e^{\underline{m}}{}_{\underline{\nu}}$ are the same functions of their arguments $e'^{\underline{\mu}}{}_{\underline{\nu}}(\underline{x}'^{\underline{\lambda}}) = e^{\underline{\mu}}{}_{\underline{\nu}}(\underline{x}^{\underline{\lambda}})$, provided, $det[e'^{\underline{\mu}}{}_{\underline{\nu}}] \neq 0$ and $det[e^{\underline{\mu}}{}_{\underline{\nu}}] \neq 0$. In this case, the specific coframe vectors ($e^{\underline{\mu}}$),

$$\begin{aligned} &e^{(+)} = \frac{d\underline{x}^{(+)}}{\underline{a}_{(c)}\underline{x}^{(+)}}, \quad e^{(-)} = \underline{a}_{(c)}\underline{x}^{(+)} d\underline{x}^{(-)}, \\ &d\underline{s}^2 = 2e^{(+)}e^{(-)}, \end{aligned} \tag{66}$$

with constant acceleration $\underline{a}_{(c)}$ (59), are independent and yield the components of constant and thus homogeneous torsion (65):

$$T^{(+)}_{(+)\,(-)} = 0, \quad T^{(-)}_{(+)\,(-)} = \underline{a}_{(c)}. \tag{67}$$

The embedding map (100) gives

$$e^{(\pm)} = \frac{1}{\sqrt{2}}(d\underline{x}^{\underline{0}} \pm d\underline{x}^{\underline{1}}) = \frac{1}{\sqrt{2}}(dx^0 \pm d|\vec{x}|),$$

so that $d\underline{s}^2 = ds^2$. Using the relation $e^{\underline{\mu}} \rfloor e_{\underline{\lambda}} = \delta^{\underline{\mu}}_{\underline{\lambda}}$, the frame vectors $e_{(\pm)}$ read

$$e_{(+)} = \underline{a}_{(c)} x^{(+)} \partial_{(+)}, \quad e_{(-)} = (\underline{a}_{(c)} x^{(+)})^{-1} \partial_{(-)}. \tag{68}$$

The covariant components $a_{\underline{j}}$ of the constant acceleration vector, from the (54), can be written

$$a_j = T_{jkl} v^k v^l, \tag{69}$$

which is the geodesic acceleration adapted to frame (68), with

$$\begin{aligned} a_{(+)} &= T_{(+)\,(-)\,(+)} v^{(-)} v^{(+)} = \underline{a}_{(c)} v^{(-)} v^{(+)}, \\ a_{(-)} &= T_{(-)\,(+)\,(+)} v^{(+)} v^{(+)} = -\underline{a}_{(c)} \left(v^{(+)}\right)^2, \end{aligned} \tag{70}$$

where $v^{(\pm)} = \frac{1}{\sqrt{2}}(v^0 \pm |\vec{v}|)$. The contravariant components then are

$$a^{(+)} = -\underline{a}_{(c)} \left(v^{(+)}\right)^2, \quad a^{(-)} = \underline{a}_{(c)} v^{(-)} v^{(+)}. \tag{71}$$

Thus the acceleration four-vector reads

$$\mathbf{a} = a^{\underline{\mu}} e_{\underline{\mu}} = -\left(\underline{a}_{(c)} v^{(+)}\right)^2 x^{(+)} \partial_{(+)} + \frac{v^{(-)} v^{(+)}}{x^{(+)}} \partial_{(-)}. \tag{72}$$

This vector is orthogonal to the four-velocity
$a_j v^j = 0$, and tangent to the curves

$$\begin{aligned} \frac{dx^{(+)}}{d\sigma} &= -\left(\underline{a}_{(c)} v^{(+)}\right)^2 x^{(+)}, \\ \frac{dx^{(-)}}{d\sigma} &= \frac{v^{(-)} v^{(+)}}{x^{(+)}}, \end{aligned} \tag{73}$$

doi: https://doi.org/10.52526/25792776-24.71.2-249

described by the parameter σ. Integration gives

$$\begin{aligned} x^{(+)} &= C_1^{(+)} e^{-\left(\underline{a}_{(c)} v^{(+)}\right)^2 \sigma}, \\ x^{(-)} - C_1^{(-)} &= \frac{v^{(-)} v^{(+)} e^{\left(\underline{a}_{(c)} v^{(+)}\right)^2 \sigma}}{\left(\underline{a}_{(c)} v^{(+)}\right)^2 C_1^{(+)}}, \end{aligned} \tag{74}$$

with constants $C_1^{(\pm)}$. By eliminating these constants and using the relation

$$2v^{(+)}v^{(-)} = \left(v^0\right)^2 - |\vec{v}|^2 = 1, \tag{75}$$

we obtain

$$x^{(-)} - C_1^{(-)} = \frac{1}{2x^{(+)}\left(\underline{a}_{(c)} v^{(+)}\right)^2} \tag{76}$$

These curves can be obtained from the hyperbola

$$x^{(+)} x^{(-)} = (x^{(0)})^2 - |\vec{x}|^2 = \frac{1}{2(v^{(+)}\underline{a}_{(c)})^2}, \tag{77}$$

by translation in the $x^{(-)}$-direction. If we choose the velocity as a constant, say, $v^{(+)} = const > 0$, it follows from (75) that $v^{(-)}$ is also constant and the velocity vector field

$$\mathbf{v} = v^{\underline{\mu}} e_{\underline{\mu}} = v^{(+)}\, \underline{a}_{(c)} x^{(+)} \partial_{(+)} + v^{(-)} \frac{1}{\underline{a}_{(c)} x^{(+)}} \partial_{(-)}, \tag{78}$$

is invariant in the M_4. Since $v^{(+)}$ is constant, the vectors are parallel in the usual affine sense along lines $x^{(+)} = const$. In the same manner as above, we write

$$\frac{dx^{(+)}}{ds} = v^{(+)}\, \underline{a}_{(c)} x^{(+)}, \quad \frac{dx^{(-)}}{ds} = \frac{1}{2v^{(+)}\, \underline{a}_{(c)} x^{(+)}}, \tag{79}$$

so that integration gives

$$\begin{aligned} x^{(+)} &= C_2^{(+)}\, e^{v^{(+)}\, \underline{a}_{(c)} s}, \\ x^{(-)} - C_2^{(-)} &= -\frac{e^{v^{(+)}\, \underline{a}_{(c)} s}}{2C_2^{(+)} (v^{(+)}\underline{a}_{(c)})^2}, \end{aligned} \tag{80}$$

with constants $C_2^{(\pm)}$. By eliminating $C_2^{(+)}$ and proper time s, we obtain a set of identical hyperbolae

$$x^{(-)} - C_2^{(-)} = -\frac{1}{2x^{(+)}(v^{(+)}\underline{a}_{(c)})^2}, \tag{81}$$

that are obtained from the hyperbola

$$x^{(+)} x^{(-)} + \frac{1}{2(v^{(+)}\underline{a}_{(c)})^2} = 0, \tag{82}$$

or

$$(x^{(0)})^2 - |\vec{x}|^2 + \frac{1}{2(v^{(+)}\underline{a}_{(c)})^2} = 0, \tag{83}$$

by translation in the $x^{(-)}$-direction. The question is whether two events in M_4 are connected by a straight timelike line or by a hyperbolic path can easily be solved because the hyperbolic path has a smaller proper time. Thus, the results obtained clearly show that the accelerated frame of reference should be described as a frame with torsion. Whereas the frames expressing linear and rotational acceleration can be interpreted—via torsion—as an invariant property of spacetime.

6. Concluding remarks

In this section we highlight a few points of the $\widetilde{MS}_p$-TSG theory and discuss issues to be studied in subsequent paper.

(I) Using Palatini's formalism extended in a plausible fashion to the $\widetilde{MS}_p$ - SG, we reinterpret a flat $\widetilde{MS}_p$-SG theory with Weitzenböck torsion as a $\widetilde{MS}_p$-TSG theory, having the gauge *translation* group in tangent bundle. Whereas the Hilbert action vanishes and the gravitino action loses its spin connections, so we find torsion induced by gravitinos. The accelerated reference frame has Weitzenböck torsion.

doi: https://doi.org/10.52526/25792776-24.71.2-249

(II) The spin connection represents only *inertial effects*, but not gravitation at all. The action of a $\widetilde{MS}_p$-TSG theory is invariant under the Poincaré supergroup and under diffeomorphisms.

(III) The translation group is abelian, therefore its Cartan-Killing bilinear form is degenerate and cannot be used as a metric. Recall that the group manifold of translations is just the Minkowski spacetime $\mathcal{M}$, the quotient space between the Poincaré, $\mathcal{P}$, and the Lorentz, $\mathcal{L}$, groups: $\mathcal{M} = \mathcal{P}/\mathcal{L}$. Namely, $\mathcal{M}$ is homogeneous or transitive under X-space translations, which means that there is only one group element that moves a point of the $\mathcal{M}$ space into another given point of the $\mathcal{M}$ space. The role of the Cartan-Killing metric comes, when it exists, from its being invariant under the group action. Here it does not exist, but we can use the invariant Lorentz metric $\eta_{\hat{a}\hat{b}}$ of $\mathcal{M}$ in its stead.

(IV) The action of $\widetilde{MS}_p$-TSG is invariant under local translations, under local super symmetry transformations and by construction is invariant under local Lorentz rotations and under diffeomorphisms. So that this action is invariant under the Poincaré supergroup and under diffeomorphisms.

(V) We show the equivalence of the Teleparallel Gravity action with Hilbert action, which will prove that the immediate cause of the *fictitious* Riemann curvature for the Levi-Civita connection is the acceleration. The curvature of Weitzenböck connection vanishes identically, but for a tetrad involving a non-trivial translational gauge potential, the torsion is non-vanishing. We consider Weitzenböck connection a kind of dual of the Levi-Civita connection, which is a connection with vanishing torsion, and non-vanishing *fictitious* curvature. The Weitzenböck connection, which defines the Fock-Ivanenko derivative written in terms of covariant derivative, will define the acceleration through force equation, with torsion (or contortion) playing the role of force.

(VI) The Weitzenböck connection ($\dot{\Gamma}$), which defines the Fock-Ivanenko derivative ($\dot{\mathcal{D}}_{\hat{\mu}}$) written in terms of covariant derivative ($\dot{\nabla}_{\hat{\mu}}$), defines the acceleration too. By means of it, we derive a force equation, with torsion (or contortion) playing the role of force. The connection ($\dot{\Gamma}$) can be considered a kind of dual of the Levi-Civita connection (Γ), which is a connection with vanishing torsion (T), and non-vanishing *fictitious* curvature (R). Using this, we prove the equivalence of the Teleparallel Gravity action ($\dot{\mathcal{L}}^{(2)}$) in (42) with Hilbert action ($\mathcal{L}^{(2)}$) in (118).

(VII) We complement a theory of $\widetilde{MS}_p$-TSG with implications for special cases. In particular, we discuss the Newtonian limit, and describe the homogeneous acceleration field.

(VIII) Further studies on the $\widetilde{MS}_p$-TSG are warranted with special emphasis on the general deformation of MS_p induced by external force exerted on a particle and inertial effects, the hypothesis of locality, which will essentially improve the framework of present paper. Actually,

a) As we emphasized already essential difference arisen between the standard supergravity theories and some rather unusual properties of a $\widetilde{MS}_p$-SG theory is as follows. In the framework of the standard supergravity theories, as in GR, a curvature of the space-time acts on all the matter fields. The source of graviton is the energy-momentum tensor of matter fields, while the source of gravitino is the spin-vector current of supergravity. The gauge action of simple $\widetilde{MS}_p$-SG is the sum of the Hilbert action for the tetrad field - *fictitious* graviton, and the Rarita-Schwinger action for the *fictitious* gravitino field. Instead we argue that a deformation of MS_p is the origin of these fields. They refer to the particle of interest itself, without relation to other matter fields, so that these fields can be globally removed by appropriate coordinate transformations. With these physical requirements, a standard coupling of supergravity with matter superfields evidently no longer holds. Instead we should look for an alternative way of implications of $\widetilde{MS}_p$-SG for the model of accelerated motion and inertial effects. We, therefore, would work out the theory of a general deformation of MS_p induced by external force exerted on a particle, in order to show that in the $\widetilde{MS}_p$-TSG theory the occurrence of the *absolute* and *inertial* accelerations, and the *inertial* force are obviously caused by this. In the same time, the *relative* acceleration (in Newton's terminology) (both magnitude and direction), to the contrary, has nothing to do with a deformation of $\underline{M}_2$ and, thus, it cannot produce the inertia effects.

b) In standard framework of the construction of reference frame of an accelerated observer, the hypothesis of locality holds for huge proper acceleration lengths and that represents strict restrictions, because it approximately replaces a noninertial frame of reference $\widetilde{S}_{(2)}$, which is held stationary in the deformed space $\mathcal{M}_2 \equiv \underline{V}_2^{(\varrho)}$ ($\varrho \neq 0$), where $\underline{V}_2$ is the 2D semi-Riemannian space, with a continuous infinity set of the inertial frames $\{S_{(2)}, S'_{(2)}, S''_{(2)}, ...\}$ given in the flat $\underline{M}_2$ ($\varrho = 0$). In this situation the use of the hypothesis of locality is physically unjustifiable. In this study, therefore, it is worthwhile to take into account a deformation $\underline{M}_2 \longrightarrow \underline{V}_2^{(\varrho)}$, which will essentially improve the standard framework. The above mentioned problems (a,b) will be topic for research in subsequent paper (Ter-Kazarian, 2024c).

doi: https://doi.org/10.52526/25792776-24.71.2-249

References

Aldrovandi R., Pereira J., 1995, An introduction to geometrical physics. World Scientific, Singapore

Aldrovandi R., Pereira J., 2013, Teleparallel Gravity/An Introduction. Part of the book series: Fundamental Theories of Physics (FTPH, volume 173) Electronic ISSN 2365-6425

Batista R., et al. 2019, Frontiers in Astronomy and Space Sciences, 6, 1, Article 23

Batista R., et al. 2023, arxiv:2312.00409[gr-qc]

Mattingly D., 2005, Living Rev. Relativity, 8, 5

Salgado P., Rubilar G., Crisóstomo J., del Campo S., 2003, Phys. Rev. D, 68, 024021

Salgado P., del Campo S., Cataldo M., 2005, Eur. Phys. J. C, 44, 587

Schucking E., Surowitz E., 2007, arxiv:[gr-qc/0703149]

Stelle K., West P., 1980, Phys. Rev. D, 21, 1466

Ter-Kazarian G., 2023a, Communications of BAO, 70, Issue 2, 170

Ter-Kazarian G., 2023b, Communications of BAO, 70, Issue 2, 188

Ter-Kazarian G., 2023c, Communications of BAO, 70, Issue 2, 212

Ter-Kazarian G., 2024a, Gravitation and Cosmology, 30, No. 1, p. 8

Ter-Kazarian G., 2024c, Communications of BAO, 71, Issue 2,

Ter-Kazarian G., 2024b, Communications of BAO, 71, Issue 2,

van Nieuwenhuizen P., 1981, Physics Reports, 68, 189

doi: https://doi.org/10.52526/25792776-24.71.2-249

Appendices

Appendix A A global MS$_p$-SUSY

As a guiding principle to make the present paper understandable, in the next two sections we necessarily recount succinctly some of the highlights behind of *global* MS$_p$-SUSY (Ter-Kazarian, 2023a, 2024a) and *local* $\widetilde{MS}_p$-SUSY theories.

The flat MS$_p$ is the 2D composite space

$$MS_p \equiv \underline{M}_2 = \underline{R}^1_{(+)} \oplus \underline{R}^1_{(-)}, \tag{84}$$

with Lorentz metric. The ingredient 1D-space $\underline{R}^1_{\underline{m}}$ is spanned by the coordinates $\underline{\eta}^{\underline{m}}$. The following notational conventions are used throughout this paper: all quantities related to the space $\underline{M}_2$ will be underlined. In particular, the underlined lower case Latin letters $\underline{m}, \underline{n}, ... = (\pm)$ denote the world indices related to $\underline{M}_2$.

Suppose the position of the particle is specified by the coordinates $x^m(s)$ ($x^0 = t$) in the basis e_m (m=0,1,2,3) at given point in the background M_4 space. A smooth map $f:\ \underline{M}_2 \longrightarrow M_4$ is defined to be an immersion (the embedding which is a function that is a homeomorphism onto its image):

$$\underline{e}_{\underline{0}} = e_0, \quad \underline{x}^{\underline{0}} = x^0, \quad \underline{e}_{\underline{1}} = \vec{n}, \quad \underline{x}^{\underline{1}} = |\vec{x}|, \tag{85}$$

where $\vec{x} = e_i x^i = \vec{n}|\vec{x}|$ ($i = 1, 2, 3$). Given the inertial frames $S_{(4)}, S'_{(4)}, S''_{(4)}, ...$ in unaccelerated uniform motion in M_4, we may define the corresponding inertial frames $\underline{S}_{(2)}$, $\underline{S}'_{(2)}$, $\underline{S}''_{(2)}$,... in $\underline{M}_2$, which are used by the non-accelerated observers for the positions $\underline{x}^{\underline{r}}, \underline{x}'^{\underline{r}}, \underline{x}''^{\underline{r}}, ...$ of a free particle in flat $\underline{M}_2$. According to (85), the time axes of the two systems $\underline{S}_{(2)}$ and $S_{(4)}$ coincide in direction, and the time coordinates are taken the same. All the fermionic and bosonic states taken together form a basis in the Hilbert space. The basis vectors in the Hilbert space composed of $H_B \otimes H_F$ is given by

$$\{|\underline{n}_b > \otimes|0>_f,\ |\underline{n}_b > \otimes f^\dagger\,|0>_f\},$$

or

$$\{|n_b > \otimes|\underline{0}>_f,\ |n_b > \otimes \underline{f}^\dagger\,|\underline{0}>_f\},$$

where we consider two pairs of creation and annihilation operators ($b^\dagger$, b) and ($f^\dagger$, f) for bosons and fermions, respectively, referred to the background space M_4, as well as ($\underline{b}^\dagger$, $\underline{b}$) and ($\underline{f}^\dagger$, $\underline{f}$) for bosons and fermions, respectively, as to background master space $\underline{M}_2$. Accordingly, we construct the quantum operators, ($q^\dagger$, $\underline{q}^\dagger$) and (q, $\underline{q}$), which replace bosons by fermions and vice versa:

$$\begin{array}{l} q\,|\underline{n}_b,\, n_f >= q_0\sqrt{\underline{n}_b}\,|\underline{n}_b - 1,\, n_f + 1>, \\ q^\dagger\,|\underline{n}_b,\, n_f >= q_0\sqrt{\underline{n}_b + 1}\,|\underline{n}_b + 1,\, n_f - 1>, \end{array} \tag{86}$$

and that

$$\begin{array}{l} \underline{q}\,|n_b,\, \underline{n}_f >= q_0\sqrt{n_b}\,|n_b - 1,\, \underline{n}_f + 1>, \\ \underline{q}^\dagger\,|n_b,\, \underline{n}_f > q_0\sqrt{n_b + 1}\,|n_b + 1,\, \underline{n}_f - 1> . \end{array} \tag{87}$$

This framework combines bosonic and fermionic states on the same footing, rotating them into each other under the action of operators q and $\underline{q}$. So, we may refer the action of the supercharge operators q and $q^\dagger$ to the background space M_4, having applied in the chain transformations of fermion χ (accompanied with the auxiliary field F as it will be seen later on) to boson $\underline{A}$, defined on $\underline{M}_2$. Respectively, we may refer the action of the supercharge operators $\underline{q}$ and $\underline{q}^\dagger$ to the $\underline{M}_2$, having applied in the chain transformations of fermion $\underline{\chi}$ (accompanied with the auxiliary field $\underline{F}$) to boson A, defined on the background space M_4. While all the particles are living on M_4, their superpartners can be viewed as living on MS$_p$. In MS$_p$-SUSY theory, obviously as in standard unbroken SUSY theory, the vacuum zero point energy problem, standing before any quantum field theory in M_4, is solved. The particles in M_4 themselves can be considered as excited states above the underlying quantum vacuum of background double spaces $M_4\oplus$ MS$_p$, where the zero point cancellation occurs at ground-state energy, provided that the natural frequencies are set equal ($q_0^2 \equiv \nu_b = \nu_f$), because the fermion field has a negative zero point energy while the boson field has a positive zero point energy.

The odd part of the supersymmetry algebra is composed entirely of the spin-1/2 operators $Q_\alpha{}^i$, $Q_\beta{}^j$. In order to trace a maximal resemblance in outward appearance to the standard SUSY theories, here we set

doi: https://doi.org/10.52526/25792776-24.71.2-249

one notation $\hat{m} = (m \quad \text{if} \quad Q = q, \text{ or } \underline{m} \quad \text{if} \quad Q = \underline{q})$, and as before the indices α and $\dot{\alpha}$ run over 1 and 2. The underlying algebraic structure of MS_p-SUSY generators closes with the algebra of *translations* on the original space M_4 in a way that it can then be summarized as a non-trivial extension of the Poincaré group algebra those of the commutation relations of the bosonic generators of four momenta and six Lorentz generators referred to M_4. Moreover, if there are several spinor generators $Q_\alpha{}^i$ with $i = 1, ..., N$ - theory with $N-$extended supersymmetry, can be written as a graded Lie algebra of SUSY field theories, with commuting and anticommuting generators. The anticommuting (Grassmann) parameters $\epsilon^\alpha(\xi^\alpha, \underline{\xi}^\alpha)$ and $\bar{\epsilon}^\alpha(\bar{\xi}^\alpha, \underline{\bar{\xi}}^\alpha)$:

$$\{\epsilon^\alpha, \epsilon^\beta\} = \{\bar{\epsilon}^\alpha, \bar{\epsilon}^\beta\} = \{\epsilon^\alpha, \bar{\epsilon}^\beta\} = 0, \quad \{\epsilon^\alpha, Q_\beta\} = \cdots = [p_{\hat{m}}, \epsilon^\alpha] = 0, \tag{88}$$

allow us to write the algebra (**??**) for $(N = 1)$ entirely in terms of commutators:

$$[\epsilon Q, \bar{Q}\bar{\epsilon}] = 2\epsilon\sigma^{\hat{m}}\bar{\epsilon}p_{\hat{m}}, \quad [\epsilon Q, \epsilon Q] = [\bar{Q}\bar{\epsilon}, \bar{Q}\bar{\epsilon}] = [p^{\hat{m}}, \epsilon Q] = [p^{\hat{m}}, \bar{Q}\bar{\epsilon}] = 0. \tag{89}$$

For brevity, here the indices $\epsilon Q = \epsilon^\alpha Q_\alpha$ and $\bar{\epsilon}\bar{Q} = \bar{\epsilon}_{\dot{\alpha}}\bar{Q}^{\dot{\alpha}}$ will be suppressed unless indicated otherwise. This supersymmetry transformation maps tensor fields $\mathcal{A}(A, \underline{A})$ into spinor fields $\psi(\chi, \underline{\chi})$ and vice versa. From the algebra (89) we see that Q has mass dimension $1/2$. Therefore, as usual, fields of dimension ℓ transform into fields of dimension $\ell + 1/2$ or into derivatives of fields of lower dimension.

In the framework of standard generalization of the coset construction, we will take $G = G_q \times G_{\underline{q}}$ to be the supergroup generated by the MS_p-SUSY algebra (**??**). Let the stability group $H = H_q \times H_{\underline{q}}$ be the Lorentz group (referred to M_4 and $\underline{M}_2$), and we choose to keep all of G unbroken. Given G and H, we can construct the coset, G/H, by an equivalence relation on the elements of G: $\quad \Omega \sim \Omega h$, where $\Omega = \Omega_q \times \Omega_{\underline{q}} \in G$ and $h = h_q \times h_{\underline{q}} \in H$, so that the coset can be pictured as a section of a fiber bundle with total space, G, and fiber, H. So, the Maurer-Cartan form, $\Omega^{-1}d\Omega$, is valued in the Lie algebra of G, and transforms as follows under a global G transformation,

$$\begin{array}{l} \Omega \longrightarrow g\Omega h^{-1}, \\ \Omega^{-1}d\Omega \longrightarrow h(\Omega^{-1}d\Omega)h^{-1} - dh\, h^{-1}, \end{array} \tag{90}$$

with $g \in G$.

The \`superspace´ is a 14D-extension of a direct sum of background spaces $M_4 \oplus \underline{M}_2$ (spanned by the 6D-coordinates $X^{\hat{m}} = (x^m, \underline{\eta}^{\underline{m}})$ by the inclusion of additional 8D-fermionic coordinates $\Theta^\alpha = (\theta^\alpha, \underline{\theta}^\alpha)$ and $\bar{\Theta}_{\dot{\alpha}} = (\bar{\theta}_{\dot{\alpha}}, \underline{\bar{\theta}}_{\dot{\alpha}})$. Then the net result of sequential atomic double transitions induce the inhomogeneous Lorentz group, or Poincaré group, and that the unitary linear transformation $|x, t> \rightarrow U(L, a)|x, t>$ on vectors in the physical Hilbert space.

To study the effect of supersymmetry transformations, we consider

$$g(0, \epsilon, \bar{\epsilon})\, \Omega(X, \Theta, \bar{\Theta}) = e^{i(\epsilon^\alpha Q_\alpha + \bar{\epsilon}_{\dot{\alpha}}\bar{Q}^{\dot{\alpha}})}\, e^{i(-X^{\hat{m}}p_{\hat{m}} + \Theta^\alpha Q_\alpha + \bar{\Theta}_{\dot{\alpha}}\bar{Q}^{\dot{\alpha}})}. \tag{91}$$

the transformation (91) induces the motion:

$$g(0, \epsilon, \bar{\epsilon})\, \Omega(X^{\hat{m}}, \Theta, \bar{\Theta}) \rightarrow (X^{\hat{m}} + i\, \Theta\, \sigma^{\hat{m}}\, \bar{\epsilon} - i\, \epsilon\, \sigma^{\hat{m}}\, \bar{\Theta},\ \Theta + \epsilon,\ \bar{\Theta} + \bar{\epsilon}), \tag{92}$$

namely,

$$\begin{array}{l} g_q(0, \xi, \bar{\xi})\, \Omega_q(x, \theta, \bar{\theta}) \rightarrow (x^m + i\, \theta\, \sigma^m\, \bar{\xi} - i\, \xi\, \sigma^m\, \bar{\theta},\ \theta + \xi,\ \bar{\theta} + \bar{\xi}), \\ g_{\underline{q}}(0, \underline{\xi}, \underline{\bar{\xi}})\, \Omega_{\underline{q}}(\underline{\eta}, \underline{\theta}, \underline{\bar{\theta}}) \rightarrow (\underline{\eta}^{\underline{m}} + i\, \underline{\theta}\, \sigma^{\underline{m}}\, \underline{\bar{\xi}} - i\, \underline{\xi}\, \sigma^{\underline{m}}\, \underline{\bar{\theta}},\ \underline{\theta} + \underline{\xi},\ \underline{\bar{\theta}} + \underline{\bar{\xi}}). \end{array} \tag{93}$$

The spinors $\theta(\underline{\theta}, \underline{\bar{\theta}})$ and $\bar{\theta}(\underline{\theta}, \underline{\bar{\theta}})$ satisfy the embedding relations $\Delta\underline{x}^0 = \Delta x^0$ and $\Delta\underline{x}^2 = (\Delta\vec{x})^2$, so from (93) we obtain

$$\underline{\theta}\, \sigma^0\, \underline{\bar{\xi}} - \underline{\xi}\, \sigma^0\, \underline{\bar{\theta}} = \theta\, \sigma^0\, \bar{\xi} - \xi\, \sigma^0\, \bar{\theta}, \quad (\underline{\theta}\, \sigma^3\, \underline{\bar{\xi}} - \underline{\xi}\, \sigma^3\, \underline{\bar{\theta}})^2 = (\theta\, \vec{\sigma}\, \bar{\xi} - \xi\, \vec{\sigma}\, \bar{\theta})^2. \tag{94}$$

The *atomic displacement* caused by double transition of a particle $M_4 \rightleftharpoons \underline{M}_2$ reads

$$\Delta\underline{x}_{(a)} = \underline{e}_{\underline{m}}\Delta\underline{x}^{\underline{m}}_{(a)} = \underline{u}\tau, \tag{95}$$

where the components $\Delta\underline{x}^{\underline{m}}_{(a)}$ are written

$$\Delta\underline{x}^{\underline{m}}_{(a)} = (\underline{\theta}\, \sigma^{\underline{m}}\, \underline{\bar{\theta}})\tau. \tag{96}$$

doi: https://doi.org/10.52526/25792776-24.71.2-249

Hence the velocities of light in vacuum, $\underline{v}^{\underline{0}} = c$, and of a particle ,$\vec{\underline{v}}_{\underline{1}} = \underline{e}_{\underline{1}}\underline{v}^{\underline{1}} = \vec{n}|\vec{v}| = \vec{v}$ $(|\vec{v}| \leq c)$, are

$$\begin{aligned} \underline{v}^{\underline{0}} &= \underline{\theta}\,\sigma^{\underline{0}}\,\bar{\underline{\theta}} = (\underline{\theta}_1\,\bar{\underline{\theta}}_1 + \underline{\theta}_2\,\bar{\underline{\theta}}_2) = \underline{\theta}\,\bar{\underline{\theta}}, \\ \underline{v}^{\underline{1}} &= \underline{\theta}\,\sigma^{\underline{1}}\,\bar{\underline{\theta}} = (\underline{\theta}_1\,\bar{\underline{\theta}}_1 - \underline{\theta}_2\,\bar{\underline{\theta}}_2). \end{aligned} \tag{97}$$

Thus, we achieve the desired goal to derive the SLC in terms of spinors $(\underline{\theta}, \bar{\underline{\theta}})$ and period (τ) of superoscillations referred to the master space $\underline{M}_2$. This allows to introduce the physical finite *relative time* interval between two events as integer number of the *own atomic duration time* of double transition of a particle from M_4 to MS_p and back.

Thereby we consider the spaces M_4 and $\underline{M}_2$ as mathematical prior the *motion*, devoid of any sense of *physical space-time*, until we have to impose two specific conditions on the spinor transformation matrix M acting in $\underline{M}_2$ to derive the most important *inertial uniform motion* in M_4 with *physical properties of Special Relativity*. Actually, to derive the most important *relative inertial uniform motion* in mathematical Minkowski space M_4 devoid of any sense of *physical space-time*, it is necessary to impose specific conditions on the spinor transformation matrix M in $\underline{M}_2$. We are of course not limited within MS_p-SUSY to consider particular constant spinor $\underline{\theta}$ referred to $\underline{M}_2$, which yields the constant velocity $\vec{v}(\underline{\theta})$, but can choose at will any other constant spinors $\underline{\theta}'$, $\underline{\theta}''$, ... yielding respectively the constant velocities $\vec{v}'(\underline{\theta}')$, $\vec{v}''(\underline{\theta}'')$, ... of inertial observers that move uniformly forever on rectilinear timelike worldlines, whose transformational law on the original spinor $\underline{\theta}$ is known (first condition):

$$\underline{\theta}'_\alpha = M_\alpha{}^\beta \underline{\theta}_\beta, \quad \bar{\underline{\theta}}_{\dot\alpha} = (M^*)_{\dot\alpha}{}^{\dot\beta}\,\bar{\underline{\theta}}_{\dot\beta}, \quad \dot\alpha, \dot\beta = 1, 2, \tag{98}$$

where $M \in SL(2, C)$ is the hermitian unimodular two-by-two matrix, the matrix M^* is related by a similarity transformation to $(M^{-1})^\dagger$, i.e. $(M^\dagger)^\beta{}_\alpha = (M^*)_\alpha{}^\beta$. The (98) gives the second founding property of SR that the bilinear combinations are $c := \underline{\theta}\,\bar{\underline{\theta}} = \underline{\theta}'\,\bar{\underline{\theta}}' = \cdots = const$, which yields a second postulate of SR (Einstein's postulate). Therewith a quantity $\underline{e}_{\underline{m}}\,(\underline{\theta}\,\sigma^{\underline{m}}\,\bar{\underline{\xi}})$ (where $\underline{e}_{\underline{m}}$ is a basis vector, $\underline{\theta}$, $\underline{\xi}$ are Weyl spinors) is a Lorentz scalar if and only if the second condition holds:

$$\tfrac{1}{2}\,Tr\left(\sigma^{\underline{m}}\,M\sigma^{\underline{n}}\,M^\dagger\right)\sigma^{\underline{n}}_{\alpha\dot\alpha} = (M^{-1})_\alpha{}^\beta \sigma^{\underline{m}}_{\beta\dot\beta}(M^{-1})^{\dagger\dot\beta}{}_{\dot\alpha}, \tag{99}$$

where the map from $SL(2, C)$ to the Lorentz group is established through the $\underline{\sigma}$-matrices. The latter, according to embedding map, can be written in terms of $\vec\sigma$-Pauli spin matrices. The (99) combined with (96) give the first founding property $\Delta\underline{x}_{(a)} = \Delta\underline{x}'_{(a)} = \cdots = inv$ of SR. This calls for a complete reconsideration of our standard ideas of Lorentz motion code, to be now referred to as the *individual code of a particle*, defined as its intrinsic property. On these premises, we derive the two postulates on which the theory of SR is based. In the sequel, we turn to the deformation of these spinors (Ter-Kazarian, 2023b, 2024a): $\underline{\theta} \to \tilde{\underline{\theta}} = \lambda^{1/2}\,\underline{\theta}$, etc., where λ appears as a deformation scalar function of the Lorentz invariance (LIDF). This yields both the DLE and DMAV, respectively, in the form $\tilde{ds} = \lambda ds$ and $\tilde{c} = \lambda c$, provided, the invariance of DLE, and the same value of DMAV in free space hold for all inertial systems. Thus the Lorentz invariance deformation (LID)-generalization of global MS_p-SUSY theory formulates the generalized relativity postulates in a way that preserve the relativity of inertial frames, in spite of the appearance of modified terms in the LID dispersion relations. We complement this conceptual investigation with testing of various LIDFs in the UHECR- and TeV-γ threshold anomalies by implications for several scenarios: the Coleman and Glashow-type perturbative extension of SLC, the LID extension of standard model, the LID in quantum gravity motivated space-time models, the LID in loop quantum gravity models, and the LIDF for the models preserving the relativity of inertial frames.

Appendix B The $\widetilde{MS}_p$-Supergravity

A local extension of the MS_p-SUSY algebra leads to the gauge theory of *translations*. One might guess that the condition for the parameter $\partial_{\hat\mu}\epsilon = 0$ of a global MS_p-SUSY theory (Ter-Kazarian, 2023b, 2024a) should be relaxed for the accelerated particle motion, so that a global SUSY will be promoted to a local SUSY in which the parameter $\epsilon = \epsilon(X^{\hat\mu})$ depends explicitly on $X^{\hat\mu} = (\widetilde{x}^\mu, \widetilde{\underline{x}}^{\underline{\mu}}) \in V_4 \oplus \underline{V}_2$, where $\widetilde{x}^\mu \in V_4$ and $\widetilde{\underline{x}}^{\underline{\mu}} \in \widetilde{MS}_p(\equiv \underline{V}_2)$, with V_4 and $\underline{V}_2$ are the 4D and 2D semi-Riemannian spaces. This extension will address the *accelerated motion* and *inertia effects*.

doi: https://doi.org/10.52526/25792776-24.71.2-249

A smooth embedding map, generalized for curved spaces, becomes $\widetilde{f}: \underline{V}_2 \longrightarrow V_4$ defined to be an immersion (the embedding which is a function that is a homeomorphism onto its image):

$$\widetilde{\underline{e}}_{\underline{0}} = \widetilde{e}_0, \quad \widetilde{\underline{x}}^{\underline{0}} = \widetilde{x}^0, \quad \widetilde{\underline{e}}_{\underline{1}} = \vec{\widetilde{n}}, \quad \widetilde{\underline{x}}^{\underline{1}} = |\vec{\widetilde{x}}|, \tag{100}$$

where $\vec{\widetilde{x}} = \widetilde{e}_i\widetilde{x}^i = \vec{\widetilde{n}}|\vec{\widetilde{x}}|$ $(i = 1,2,3)$ (the middle letters of the Latin alphabet $(i,j,...)$ will be reserved for space indices). We expect the notion of a general coordinate transformation should be

$$[\delta_{\epsilon_1(X)},\, \delta_{\epsilon_2(X)}]V = \tfrac{1}{2}\bar{\epsilon}_2(X)\sigma^{\hat{\mu}}\epsilon_1(X)\,\widetilde{\partial}_{\hat{\mu}}V. \tag{101}$$

On the premises of (?), we review the accelerated motion of a particle in a new perspective of local $\widetilde{MS}_p$-SUSY transformations that a *creation* of a particle in $\underline{V}_2$ means its transition from initial state defined on V_4 into intermediate state defined on $\underline{V}_2$, while an *annihilation* of a particle in $\underline{V}_2$ means vice versa. The same interpretation holds for the *creation* and *annihilation* processes in V_4. The net result of each atomic double transition of a particle $V_4 \rightleftharpoons \underline{V}_2$ to $\underline{V}_2$ and back is as if we had operated with *a local space-time translation* with acceleration, $\vec{a}$, on the original space V_4. Accordingly, the acceleration, $\vec{\underline{a}}$, holds in $\underline{V}_2$ at $\underline{V}_2 \rightleftharpoons V_4$. So, the accelerated motion of boson $A(\widetilde{x})$ in V_4 is a chain of its sequential transformations to the Weyl fermion $\underline{\chi}(\widetilde{\underline{x}})$ defined on $\underline{V}_2$ (accompanied with the auxiliary fields $\widetilde{\underline{F}}$) and back,

$$\rightarrow A(\widetilde{x}) \rightarrow \underline{\chi}^{(\underline{F})}(\widetilde{\underline{x}}) \rightarrow A(\widetilde{x}) \rightarrow \underline{\chi}^{(\underline{F})}(\widetilde{\underline{x}}) \rightarrow, \tag{102}$$

and the same interpretation holds for fermion $\chi(\widetilde{x})$.

The mathematical structure of a local theory of $\widetilde{MS}_p$-SUSY has much in common with those used in the geometrical framework of standard supergravity theories. Such a local SUSY can already be read off from the algebra of a global MS_p-SUSY (?) in the form

$$[\epsilon(X)Q,\, \bar{Q}\bar{\epsilon}(X)] = 2\epsilon(X)\sigma^{\hat{\mu}}\bar{\epsilon}(X)\widetilde{p}_{\hat{\mu}}, \tag{103}$$

which says that the product of two supersymmetry transformations corresponds to a translation in 6D X-space of which the momentum $\widetilde{p}_{\hat{\mu}} = i\widetilde{\partial}_{\hat{\mu}}$ is the generator. We expect the notion of a general coordinate transformation should be

$$[\delta_{\epsilon_1(X)},\, \delta_{\epsilon_2(X)}]V = \tfrac{1}{2}\bar{\epsilon}_2(X)\sigma^{\hat{\mu}}\epsilon_1(X)\,\widetilde{\partial}_{\hat{\mu}}V. \tag{104}$$

Then for the local $\widetilde{MS}_p$-SUSY to exist it requires the background spaces $(V_4,\, \underline{V}_2)$ to be curved. In order to become on the same footing with $\underline{V}_2$, the V_4 refers to the accelerated proper reference frame of a particle without relation to other matter fields. This leads us to extend the concept of differential forms to superspace. A useful guide in the construction of local superspace is that it should admit rigid superspace as a limit. The superspace is a direct sum of background semi-Riemannian 4D-space and curved Master space $V_4 \oplus \widetilde{MS}_p$, with an inclusion of additional fermionic coordinates $\Theta(\underline{\theta}, \underline{\bar{\theta}})$ and $\bar{\Theta}(\underline{\theta}, \underline{\bar{\theta}})$, which are induced by the spinors $\underline{\theta}$ and $\underline{\bar{\theta}}$ referred to $\widetilde{MS}_p$.

The multiplication of two local sequential supersymmetric transformations induces the motion (a generalization of the motion (93))

$$\begin{aligned} &g(0,\, \epsilon(X),\, \bar{\epsilon}(X))\,\Omega(X^{\hat{\mu}},\, \Theta^{\hat{\alpha}},\, \bar{\Theta}_{\hat{\dot{\alpha}}} \longrightarrow \\ &(X^{\hat{\mu}} + i\,\Theta^{\hat{\alpha}}\,\sigma^{\hat{\mu}}\,\bar{\epsilon}(X) - i\,\epsilon(X)\,\sigma^{\hat{\mu}}\,\bar{\Theta}_{\hat{\dot{\alpha}}},\, \Theta + \epsilon(X), \bar{\Theta} + \bar{\epsilon}(X)), \end{aligned} \tag{105}$$

which gives

$$\begin{aligned} &g_q(0,\, \xi(\widetilde{x}),\, \bar{\xi}(\widetilde{x}))\,\Omega_q(\widetilde{x},\, \theta,\, \bar{\theta}) \rightarrow \\ &(\widetilde{x}^m + i\,\theta\,\sigma^m\,\bar{\xi}(\widetilde{x}) - i\,\xi(\widetilde{x})\,\sigma^m\,\bar{\theta},\; \theta + \xi(\widetilde{x}),\, \bar{\theta} + \bar{\xi}(\widetilde{x})), \\ &\underline{g}_q(0,\, \underline{\xi}(\widetilde{\underline{x}}),\, \underline{\bar{\xi}}(\widetilde{\underline{x}}))\,\Omega_{\underline{q}}(\widetilde{\underline{x}},\, \underline{\theta},\, \underline{\bar{\theta}}) \rightarrow \\ &(\widetilde{\underline{x}}^{\underline{m}} + i\,\underline{\theta}\,\sigma^{\underline{m}}\,\underline{\bar{\xi}}(\widetilde{\underline{x}}) - i\,\underline{\xi}(\widetilde{\underline{x}})\,\sigma^{\underline{m}}\,\underline{\bar{\theta}},\; \underline{\theta} + \underline{\xi}(\widetilde{\underline{x}}),\, \underline{\bar{\theta}} + \underline{\bar{\xi}}(\widetilde{\underline{x}})). \end{aligned} \tag{106}$$

Being embedded in V_4, the $\widetilde{MS}_p$ is the *unmanifested* indispensable individual companion of a particle of interest devoid of any matter influence. While all the particles are living on V_4, their superpartners can be viewed as living on $\widetilde{MS}_p$. In this framework supersymmetry and general coordinate transformations are described in a unified way as certain diffeomorphisms. The action of simple $\widetilde{MS}_p$-SG includes the Hilbert term for a *fictitious* graviton coexisting with a *fictitious* fermionic field of, so-called, gravitino (sparticle) described by the Rarita-Scwinger kinetic term. These two particles differ in their spin: 2 for the graviton, 3/2 for the gravitino. They are the bosonic and fermionic states of a gauge particle in V_4 and $\widetilde{MS}_p$, respectively, or vice versa.

doi: https://doi.org/10.52526/25792776-24.71.2-249

B.1 The simple $(N=1)$ $\widetilde{MS}_p$ - SG without auxiliary fields, revisited

The generalized Poincaré superalgebra for the simple $(N=1)$ $\widetilde{MS}_p$-SG reads:

$$\begin{array}{l} [P_{\hat a},P_{\hat b}]=0, \quad [S_{\hat a\hat b},P_{\hat c}]=(\eta_{\hat a\hat c}P_{\hat b}-\eta_{\hat b\hat c}P_{\hat a}), \\ [S_{\hat a\hat b},S_{\hat c\hat d}]=i(\eta_{\hat a\hat c}S_{\hat b\hat d}-\eta_{\hat b\hat c}S_{\hat a\hat d}+\eta_{\hat b\hat d}S_{\hat a\hat c}-\eta_{\hat a\hat d}S_{\hat b\hat c}), \\ [S_{\hat a\hat b},Q^{\alpha}]=\frac{1}{2}(\gamma_{\hat a\hat b})^{\alpha}_{\beta}Q^{\beta}, \\ [P_{\hat a},Q^{\beta}]=0, \quad [Q_{\alpha},\bar Q_{\dot\beta}]=\frac{1}{2}(\gamma^{\hat a})_{\alpha\dot\beta}P_{\hat a}. \end{array} \tag{107}$$

with $(S_{\hat a\hat b})^{\hat c}_{\hat d}=i(\delta^{\hat c}_{\hat a}\eta_{\hat b\hat d}-\delta^{\hat c}_{\hat b}\eta_{\hat a\hat d})$ (**??**) a given representation of the Lorentz generators. Using (107) and a general form for gauge transformations on B^A,

$$\delta B=\mathcal{D}\lambda=d\lambda+[B,\lambda], \tag{108}$$

with

$$\lambda=\rho^{\hat a}P_{\hat a}+\frac{1}{2}\kappa^{\hat a\hat b}S_{\hat a\hat b}+\bar Q\varepsilon, \tag{109}$$

we obtain that the $(e^{\hat a},\omega^{\hat a\hat b},\Psi)$ transform under Poincaré translations as

$$\delta e^{\hat a}=\mathcal{D}\rho^{\hat a}, \quad \delta\omega^{\hat a\hat b}=0, \quad \delta\Psi=0; \tag{110}$$

under Lorentz rotations as

$$\delta e^{\hat a}=\kappa^{\hat a}_{\hat b}\delta e^{\hat b}, \quad \delta\omega^{\hat a\hat b}=-\mathcal{D}\kappa^{\hat a\hat b}, \quad \delta\Psi=\frac{1}{4}\kappa^{\hat a\hat b}\gamma_{\hat a\hat b}\Psi; \tag{111}$$

and under supersymmetry transformation as

$$\delta e^{\hat a}=\frac{1}{2}\bar\varepsilon\gamma^{\hat a}\Psi, \quad \delta\omega^{\hat a\hat b}=0, \quad \delta\Psi=\mathcal{D}\varepsilon. \tag{112}$$

In first-order formalism, the gauge fields $(e^{\hat a},\omega^{\hat a\hat b},\,\Psi)$, (with $\Psi=(\psi,\underline{\psi})$ a two-component Majorana spinor) are considered as an independent members of multiplet in the adjoint representation of the Poincaré supergroup of $D=6$ $((3+1),(1+1))$ simple $(N=1)$ $\widetilde{MS}_p$-SG with the generators $(P_{\hat a},S_{\hat a\hat b},Q^{\alpha})$. Unless indicated otherwise, henceforth the world indices are kept implicit without ambiguity. The operators carry Lorentz indices not related to coordinate transformations. The Yang-Mills connection for the Poincare´ supergroup is given by

$$B=B^AT_A=e^{\hat a}P_{\hat a}+\frac{1}{2}i\omega^{\hat a\hat b}S_{\hat a\hat b}+\Psi\bar Q. \tag{113}$$

The field strength associated with connection B is defined as the Poincaré Lie superalgebra-valued curvature two-form R^A. Splitting the index A, and taking the $\Theta=\bar\Theta=0$ component of R^A, we obtain

$$\begin{array}{l} R^{\ \hat a\hat b}(\omega)=d\omega^{\hat a\hat b}-\omega^{\hat a}{}_{\hat c}\omega^{\hat c\hat d}, \\ \tilde T^{\hat a}=T^{\hat a}-\frac{1}{2}\bar\Psi\gamma^{\hat a}\Psi, \quad \rho=\mathcal{D}\Psi, \end{array} \tag{114}$$

where $\gamma^{\hat a}=(\gamma^a,\sigma^{\underline{a}})$, $R^{\ \hat a\hat b}(\omega)$ is the Riemann curvature in terms of the spin connection $\omega^{\hat a\hat b}$, and the generalized Weyl lemma (see App./(4)) requires that the, so-called, supertorsion $\tilde T^{\hat a}$ be inserted. The solution $\omega(e)$ satisfies the tetrad postulate that the completely covariant derivative of the tetrad field vanishes, therefore $R^{\hat a\hat b}(\omega)=R(\omega)e^{\hat a}e^{\hat b}$.

For the bosonic part of the gauge action (graviton of spin 2) of simple $\widetilde{MS}_p$-SG it then seems appropriate to take the generalized Hilbert action with $e=det\,e^{\hat a}{}_{\mu}(X)$. While the fermionic part of the standard gauge action (garvitino of spin 3/2), which has positive energy, is the Rarita-Schwinger action. The full nonlinear gravitino action in curved space then should be its extension to curved space, which can be achieved by inserting the Lorentz covariant derivative $\mathcal{D}\Psi=d\Psi+\frac{1}{2}\omega^{\ \hat a\hat b}\gamma_{\hat a\hat b}\Psi$. In both parts, the spin connection is considered a dependent field, otherwise in the case of an independent spin connection ω, the action will be invariant under diffeomorphism, and under local Lorentz rotations, but it will be not invariant under the neither the Poincaré translations nor the supersymmetry. In the case if spin connection is independent, we should have under the local Poincaré translations

$$\begin{array}{l} \delta\hat{\mathcal{L}}_{pt}=\delta\left(\varepsilon_{\hat a\hat b\hat c\hat d}e^{\hat a}e^{\hat b}R^{\hat c\hat d}+4\bar\Psi\gamma_{\hat 5}e^{\hat a}\gamma_{\hat a}\mathcal{D}\Psi\right) \\ =2\varepsilon_{\hat a\hat b\hat c\hat d}R^{\hat a\hat b}\tilde T^{\hat c}\rho^{\hat d}+\text{surf. term}, \end{array} \tag{115}$$

doi: https://doi.org/10.52526/25792776-24.71.2-249

and under local supersymmetry transformations

$$\delta\hat{\mathcal{L}}_{SUSY} = -4\bar{\varepsilon}\gamma_{\hat{5}}\gamma_{\hat{a}}\mathcal{D}\Psi\tilde{T}^{\hat{a}} + \text{surf. term.} \tag{116}$$

The invariance of the action then requires the vanishing of the supertorsion $\tilde{T}^{\hat{a}} = 0$, which means that the connection is no longer an independent variable. So that the starting point of our approach is the action of a simple $\widetilde{MS}_p$-SG theory written in 'two in one'-notation (1), which is invariant under the local supersymmetry transformation (112), where the Poincaré superalgebra closes off shell without the need for any auxiliary fields:

$$\mathcal{L}_{MS-SG} = \varepsilon_{\hat{a}\hat{b}\hat{c}\hat{d}}e^{\hat{a}}e^{\hat{b}}R^{\hat{c}\hat{d}}(\omega) + 4\bar{\Psi}\gamma_{\hat{5}}e^{\hat{a}}\gamma_{\hat{a}}\mathcal{D}\Psi. \tag{117}$$

This is the sum of bosonic and fermionic parts with the same spin connection, where $\gamma_{\hat{a}} = (\gamma_a \oplus \sigma_{\underline{a}})$, $\gamma_{\hat{5}} = (\gamma_5 \oplus \gamma_{\underline{5}})$, $\gamma_{\underline{5}} = \begin{pmatrix} 1 & 0 \\ 0 & -1 \end{pmatrix}$ is given in the chiral or Weyl representations, i.e. in the irreducible 2-dimensional spinor representations $(\frac{1}{2}, 0)$ and $(0, \frac{1}{2})$, since two-component formalism works for a Weyl fermion. This is indispensable in order to solve algebraical constraints in superspace because they can be used as building blocks of any fermion field (van Nieuwenhuizen, 1981). In this representation, action of projection matrices $L = (1/2)(1 + \gamma_{\underline{5}})$ and $R = (1/2)(1 - \gamma_{\underline{5}})$ on a Dirac fermion leads to zero two lower components of the left-handed spinor and zero two upper components of the right-handed spinor, respectively. The two-component notation described above essentially does away with the vanishing components explicitly and deals only with the non-trivial ones. Taking into account that $g_{\hat{\mu}\hat{\nu}} = \eta_{\hat{a}\hat{b}}e_{\hat{\mu}}{}^{\hat{a}}e_{\hat{\nu}}{}^{\hat{b}}$ and $\gamma_{\hat{\mu}} = e_{\hat{\mu}}{}^{\hat{a}}\gamma_{\hat{a}}$, with $\eta_{\hat{a}\hat{b}} = (\eta_{ab} \oplus \eta_{\underline{ab}})$ related to the tangent space, where $\eta_{ab} = diag(+1, -1, -1, -1)$ and $\eta_{\underline{ab}} = diag(+1, -1)$, we can recast the generalized bosonic and fermionic actions given in (117), respectively, in the forms

$$\mathcal{L}^{(2)} = -\tfrac{1}{4}\sqrt{g}R(g, \Gamma) = -\tfrac{1}{4}eR(e, \omega), \tag{118}$$

and

$$\mathcal{L}^{(3/2)} = 4\varepsilon^{\hat{\mu}\hat{\nu}\hat{\rho}\hat{\sigma}}\bar{\Psi}_{\hat{\mu}}\gamma_{\hat{5}}\gamma_{\hat{\nu}}\mathcal{D}_{\hat{\rho}}\Psi_{\hat{\sigma}}. \tag{119}$$

Here we taken into account that $\mathcal{D}_{\hat{\rho}}\Psi_{\hat{\sigma}}$ is the curl due to the ε-symbol, and as far as $\varepsilon^{\hat{\mu}\hat{\nu}\hat{\rho}\hat{\sigma}}$ is the density (which always equals $0, \pm 1$), so there is no need to put the density e in front of fermionic part.

The accelerated motion of a particle is described by the parameter $\epsilon = \epsilon(X^{\hat{\mu}})$ in (105) of local SUSY, which depends explicitly on $X^{\hat{\mu}} = (\widetilde{x}^{\mu}, \underline{\widetilde{x}}^{\underline{\mu}})$, where $\widetilde{x}^{\mu} \in V_4$ and $\underline{\widetilde{x}}^{\underline{\mu}} \in \underline{V}_2$. To be specific, let us focus for the motion on the simple case of a peculiar anticommuting spinors $(\underline{\xi}(\underline{\widetilde{x}}), \underline{\bar{\xi}}(\underline{\widetilde{x}}))$ and $(\xi(\widetilde{x}), \bar{\xi}(\widetilde{x}))$ defined as

$$\begin{aligned} \underline{\xi}^{\alpha}(\underline{\widetilde{x}}) = i\,\frac{\underline{\tau}(\underline{\widetilde{x}})}{2}\,\underline{\theta}^{\alpha}, \quad \underline{\bar{\xi}}_{\dot{\alpha}}(\underline{\widetilde{x}}) = -i\,\frac{\underline{\tau}^{*}(\underline{\widetilde{x}})}{2}\,\underline{\bar{\theta}}_{\dot{\alpha}}, \\ \xi^{\alpha}(\widetilde{x}) = i\frac{\tau(\widetilde{x})}{2}\theta^{\alpha}, \quad \bar{\xi}_{\dot{\alpha}}(\widetilde{x}) = -i\frac{\tau^{*}(\widetilde{x})}{2}\bar{\theta}_{\dot{\alpha}}. \end{aligned} \tag{120}$$

Here the real parameter $\tau(\widetilde{x}) = \tau^{*}(\widetilde{x}) = \underline{\tau}(\underline{\widetilde{x}}) = \underline{\tau}^{*}(\underline{\widetilde{x}})$ can physically be interpreted as the *atomic duration time* of double transition of a particle $V_4 \rightleftharpoons \underline{V}_2$, i.e. the period of superoscillations. In this case, the *atomic displacement* caused by double transition reads

$$\Delta\underline{\widetilde{x}}_{(a)} = \underline{\widetilde{e}}_{\underline{m}}\Delta\underline{\widetilde{x}}^{\underline{m}}_{(a)} = \underline{\widetilde{u}}\tau(\underline{\widetilde{x}}), \tag{121}$$

where, according to the motion (93), the components $\Delta\underline{\widetilde{x}}^{\underline{m}}_{(a)}$ are written

$$\Delta\underline{\widetilde{x}}^{\underline{m}}_{(a)} = \underline{\widetilde{v}}^{\underline{m}}\,\tau(\underline{\widetilde{x}}) = i\underline{\theta}\,\sigma^{\underline{m}}\,\underline{\bar{\xi}}(\underline{\widetilde{x}}) - i\underline{\xi}(\underline{\widetilde{x}})\,\sigma^{\underline{m}}\,\underline{\bar{\theta}}. \tag{122}$$

The corresponding acceleration reads

$$a^{(\pm)} = i\underline{\theta}\,\sigma^{(\pm)}\,\frac{d^2\underline{\bar{\xi}}}{d\underline{\widetilde{s}}^2} - i\frac{d^2\underline{\xi}}{d\underline{\widetilde{s}}^2}\,\sigma^{(\pm)}\,\underline{\bar{\theta}}, \tag{123}$$

where $\sigma^{(\pm)} = \frac{1}{\sqrt{2}}(\sigma^{\underline{0}} \pm \sigma^{\underline{1}}) = \frac{1}{\sqrt{2}}(\sigma^{0} \pm \sigma^{3})$ and $d\underline{\widetilde{s}}^2 = d\underline{\widetilde{x}}^{(+)}d\underline{\widetilde{x}}^{(-)}$. By virtue of (120), the (123) is reduced to

$$a^{(\pm)} = v_c^{(\pm)}\,\frac{d^2\tau}{d\underline{\widetilde{s}}^2}, \tag{124}$$

where $v_c^{(\pm)} \equiv (\underline{\theta}\,\sigma^{(\pm)}\underline{\bar{\theta}})$.

doi: https://doi.org/10.52526/25792776-24.71.2-249

In Van der Warden notations for the Weyl two-component formalism $(\underline{\bar{\theta}}_{\dot{\alpha}})^* = \underline{\theta}_\alpha$ and $\underline{\bar{\theta}}_{\dot{\alpha}} = (\underline{\theta}_\alpha)^*$, the (124) gives

$$\begin{aligned} \underset{\sim}{\widetilde{a}} &= \sqrt{2}(a^{(+)}a^{(-)})^{1/2} = \sqrt{2}\underline{v}_c \tfrac{d^2\tau}{d\underset{\sim}{\widetilde{s}}^2}, \\ \underline{v}_c &= (v_c^{(+)}v_c^{(-)})^{1/2} = \sqrt{2}(\underline{\theta}_1\,\underline{\bar{\theta}}_1\underline{\theta}_2\,\underline{\bar{\theta}}_2)^{1/2}, \end{aligned} \tag{125}$$

with $v_c^{(+)} = \sqrt{2}(\underline{\theta}_1\,\underline{\bar{\theta}}_1)$ and $v_c^{(-)} = \sqrt{2}(\underline{\theta}_2\,\underline{\bar{\theta}}_2)$. The acceleration will generally remain a measure of the velocity variation over proper time $(\underset{\sim}{\widetilde{s}})$. The (124) and (125) yield

$$\begin{aligned} v^{(\pm)} &= v_c^{(\pm)}\left(\tfrac{d\tau}{d\underset{\sim}{\widetilde{s}}} + 1\right), \\ \underset{\sim}{\widetilde{v}} &= \sqrt{2}(v^{(+)}v^{(-)})^{1/2} = \sqrt{2}\underline{v}_c\left(\tfrac{d\tau}{d\underset{\sim}{\widetilde{s}}} + 1\right). \end{aligned} \tag{126}$$

The spinors $\theta(\underline{\theta},\underline{\bar{\theta}})$ and $\bar{\theta}(\underline{\theta},\underline{\bar{\theta}})$ satisfy the embedding map (100), namely $\Delta\underset{\sim}{\widetilde{\underline{x}}}^{\underline{0}} = \Delta\widetilde{x}^0$ and $(\Delta\underset{\sim}{\widetilde{\underline{x}}}^{\underline{1}})^2 = (\Delta\vec{\widetilde{x}})^2$, so from (93) we obtain

$$\begin{aligned} &\underline{\theta}\,\sigma^0\,\underline{\bar{\xi}} - \underline{\xi}\,\sigma^0\,\underline{\bar{\theta}} = \theta\,\sigma^0\,\bar{\xi} - \xi\,\sigma^0\,\bar{\theta}, \\ &(\underline{\theta}\,\sigma^3\,\underline{\bar{\xi}} - \underline{\xi}\,\sigma^3\,\underline{\bar{\theta}})^2 = (\theta\,\vec{\sigma}\,\bar{\xi} - \xi\,\vec{\sigma}\,\bar{\theta})^2. \end{aligned} \tag{127}$$

Denote

$$\begin{aligned} \underline{v}^{\underline{0}}_{(c)} &= \tfrac{1}{\sqrt{2}}\left(v_c^{(+)} + v_c^{(-)}\right) = (\underline{\theta}\,\underline{\bar{\theta}}), \\ \underline{v}^{\underline{1}}_{(c)} &= \tfrac{1}{\sqrt{2}}\left(v_c^{(+)} - v_c^{(-)}\right) = (\underline{\theta}_1\,\underline{\bar{\theta}}_1 - \underline{\theta}_2\,\underline{\bar{\theta}}_2), \end{aligned} \tag{128}$$

then

$$\begin{aligned} \theta_1(\underline{\theta},\,\underline{\bar{\theta}}) &= \tfrac{1}{2}\left[\left(\underline{v}^{\underline{0}}_{(c)} + \sqrt{\tfrac{2}{3}}\underline{v}^{\underline{1}}_{(c)}\right)^{1/2} + \left(\underline{v}^{\underline{0}}_{(c)} - \sqrt{\tfrac{2}{3}}\underline{v}^{\underline{1}}_{(c)}\right)^{1/2}\right], \\ \theta_2(\underline{\theta},\,\underline{\bar{\theta}}) &= \tfrac{1}{2}\left[\left(\underline{v}^{\underline{0}}_{(c)} + \sqrt{\tfrac{2}{3}}\underline{v}^{\underline{1}}_{(c)}\right)^{1/2} - \left(\underline{v}^{\underline{0}}_{(c)} - \sqrt{\tfrac{2}{3}}\underline{v}^{\underline{1}}_{(c)}\right)^{1/2}\right]. \end{aligned} \tag{129}$$

The dynamical aspects of particle mechanics involve derivatives with respect to proper time along the particle worldline, which is the line element written in frame (25):

$$ds^2 = \eta_{\hat{a}\hat{b}}\dot{e}^{\hat{a}}\dot{e}^{\hat{b}} = \eta_{\hat{a}\hat{b}}\dot{e}^{\hat{a}}{}_{\hat{\mu}}\dot{e}^{\hat{b}}{}_{\hat{\mu}}dX^{\hat{\mu}}dX^{\hat{\nu}} \equiv \eta_{\hat{\mu}\hat{\nu}}dX^{\hat{\mu}}dX^{\hat{\nu}}. \tag{130}$$

A worldline C of a particle, parametrized by proper time as $C(s) = X^{\hat{\mu}}(s)$, will have as six-velocity the vector of components $u^{\hat{\mu}} = dX^{\hat{\mu}}/ds$ and $u^{\hat{a}} = \dot{e}^{\hat{a}}_{\hat{\mu}}u^{\hat{\mu}}$, which are the particle velocity along this curve respectively in the holonomic and anholonomic bases in the X-space.

doi: https://doi.org/10.52526/25792776-24.71.2-249

Communications of BAO, Vol. 71, Issue 2, 2024, pp.268-274

Spotedness of most active flare stars detected by TESS

A.A. Akopian*

Byurakan Astrophysical Observatory, Armenia

Abstract

A new method has been proposed to determine the coverage of starspots by using periodic functions related to flare frequency. The distribution of starspots on flare stars is modeled through a von Mises circular distribution, with parameters derived from the corresponding flare frequency function. Estimates of spot coverage for the stars studied have been obtained.

Keywords: *flare stars, starspots*

1. Introduction

The idea of spots existing on stars was proposed by the French astronomer Ismaël Bouillaud (latinized as Bullialdus) in 1667 (Bullialdi, 1667) . He suggested that the variability of the star Mira (o Cet), discovered by David Fabricius in 1596, could be explained by the presence of cold, dark spots on the star's surface. Although Bouillaud's logically sound hypothesis was later proven incorrect for Mira, it found application much later, after about 300 years. In 1947, Kron (1947) reported the possible detection of spots on the surface of the star AR Lacertae B. Subsequent studies by Kron and others laid the foundation for the introduction of a new type of variable star - rotating variable stars.

The study of flare stars and closely related rotating variable stars, such as BY Dra and RS CVn, has reached a new level thanks to observational data from space telescopes such as Kepler and TESS. Data from Kepler and TESS indicate that *i*) flare stars also exhibit rotational variability, which is due to their rotation and nonuniform spot distribution across their surfaces, and *ii*) the flare-productive active regions of stars are closely associated with stellar spots. Results from the author's previous works (Akopian, 2015, 2019, 2023) suggest that the axial rotation of a star, due to the uneven distribution of spots across its surface, modulates not only the observed radiation flux but also the frequency of observed flares. Therefore, it is expected that there is a close relationship between the qualitative and quantitative characteristics of stellar spots and the flare activity of stars.

In (Akopian, 2023) data from the orbital observatory TESS (Yang et al., 2022) have been utilized to study the most active 21 flare stars , which exhibited 100 or more flares each from July 2018 to October 2020. The axial rotation periods of them were calculated (for nine stars for the first time) using two complementary algorithms: the Lomb-Scargle and the BLS (Box Least Squares).

Using the BLS algorithm, the duration of the "plateau" during the deep minimum phase was determined for all the stars, providing information on the compactness of the starspot distribution along the stellar longitude. In particular, a relationship was identified between the parameter k of the periodic functions of flare frequency and the relative duration of the "plateau" during the stars' deep minimum phases.

The calculated axial rotation periods were then used to determine the parameters of the periodic or cyclical variability in the flare frequencies of the stars. Corresponding periodic functions of flare frequency were obtained, revealing that the periods of these flare frequency functions closely matched the axial rotation periods of the stars. The expected (theoretical) phase distributions of the flares were constructed and compared with the observed flare distributions for the same time frame. This comparison, conducted using the chi-squared criterion, confirmed the periodicity of the flare frequency for all stars, without exception. It has been pointed out that the similarity of the periodic flare frequency functions to the von Mises angular distribution function is likely not coincidental.

*aakopian57@gmail.com

doi: https://doi.org/10.52526/25792776-24.71.2-268

This paper aims to determine the spot coverage of flare stars and the rotating variable with flare activity through the periodic flare frequency function (PFFF) determined in (Akopian, 2023).

2. Problem Statement

This work is based on the following assumptions and premises:

1) Analysis of Kepler and TESS photometric data demonstrates the presence of rotational modulation in flare stars. The observed variability aligns with a model that includes stellar rotation and an uneven distribution of starspots.

2) The basic assumption is Ambartsumian's idea that the random and independent nature of flares allows us to represent the sequence of stellar flares as a random Poisson process (Ambartsumian, 1969). Since the flare frequency is modulated by the star's rotation, it is necessary to treat the flare sequence as a Poisson process with a cyclical/periodic parameter. In previous works (Akopian, 2015, 2019, 2023) , a function of the form

$$\lambda\left(t\right)=\frac{\lambda exp\left[ksin\left(\omega_0 t+\vartheta\right)\right]}{I_0\left(k\right)}\ \left(k\geq 0,\ \omega_0\geq 0,\ 0\leq\vartheta\leq 2\pi,\ \lambda>0\ \right), \tag{1}$$

where k, ω_0, ϑ, λ are constants and $I_0\left(k\right)=\int\limits_0^{2\pi} exp\left[ksin\left(u\right)\right]du$ where $I_0\left(k\right))$ is the modified Bessel function of the first kind of order 0, was successfully used to describe a Poisson process with a periodic parameter. This function, proposed by Kutoyants (1980) provides a variety of periodic functions depending on the value of parameter k.

3) According to (Yang et al., 2017), flare activity is positively correlated with the size of the spots ((see Figure 10 in Yang et al., 2017), which suggests a similar correlation between the spot size and the number of flares. Since the Poisson process parameter $\lambda\left(t\right)$ represents the average number of events (in this case, flares) per unit of time, it follows that the spot coverage parameter of a star can be determined by assessing the $\lambda\left(t\right)$ parameter.

4) Considering the known properties of trigonometric functions, we observe that the function $\lambda\left(t\right)$ is essentially identical to the von Mises distribution function:

$$M\left(x|\mu,\,k\right)=\frac{exp\left[kcos\left(x-\mu\right)\right]}{2I_0\left(k\right)} \tag{2}$$

where μ is the mean (simultaneously the mode and median) direction of the distribution, k is the concentration measure, $1/k$ is the variance, and $1-I_1\left(k\right)/I_0\left(k\right)$ is the circular variance. This was first pointed out in (Akopian, 2023). The von Mises distribution, also known as the circular normal distribution or Tikhonov distribution, is widely used for statistical analysis of angular (circular) data and serves as a good approximation for the wrapped normal distribution (the circular analogue of the normal distribution).

Thus, to determine the spot distribution on the hemisphere of the star facing the observer, it is necessary to first determine the PFFF of the star and represent it as a von Mises distribution function, which, due to the positive correlation between flare activity and spot size (Yang et al., 2017), will simultaneously serve as a distribution function for the effective area of spots on the star's hemisphere facing the observer, up to a constant factor.

Second, the obtained PFFF must be related to the observed light curves. This can be done by comparing the minima and maxima of the PFFF and the light curve. At the maximum of the light curve, the least spot-covered hemisphere (out of all possible) with minimal flaring activity is observed, and conversely, at the minimum of the light curve, the most spot-covered hemisphere with maximal flare activity is observed. Thus, the task is reduced to representing the ratio of fluxes at the maximum and minimum through the analogous ratio for $\lambda\left(t\right)$, which is equal

$$\frac{\lambda_{max}}{\lambda_{min}}=exp\left(2k\right).$$

doi: https://doi.org/10.52526/25792776-24.71.2-268

For large angular inclinations of the star's axis (60°–90°) relative to the line of sight, these hemispheres, due to the symmetry of the above functions, can be considered diametrically opposite, which allows for an estimate of the overall spot coverage of the star.

3. Determining the Spot Coverage Using PFFF and the von Mises Distribution

In this section, the three main steps for estimating the coverage of starspots (spottedness) are described. The first subsection presents a concise overview of the determination of the PFFF function. The second subsection presents how to transform PFFF functions into a circular von Mises distribution. This step seems too important because von Mises distribution is a well-known and well-studied distribution that provides many useful statistical tools.

3.1. Determining the PFFF

Let's consider the registration of n flares from a star in the time interval $(0, T)$ as a statistical event. The likelihood function of this event, given the chosen form of the PFFF (1), is represented as:

$$\exp\left(-\frac{\lambda T}{2\pi}\right)\left(\frac{\lambda}{I_0(k)}\right)^n exp\left[k\sum_{i=1}^{n} sin\left(\omega_0 t_i+\vartheta\right)\right] \tag{3}$$

where t_i are the flare moments of the star.

From the problem statement, it follows that the angular frequency ω_0 should be equal or close to the rotational frequency of the star, i.e. $\omega_0 \approx 2\pi/P_r$. To estimate the maximum likelihood for the other parameters, we have (Kutoyants, 1980):

$$\hat{\lambda}=\frac{2\pi n}{T} \tag{4}$$

$$\tan\left(\hat{\vartheta}\right)=\frac{\sum_{i=1}^{n} cos\left(\omega_0 t_i\right)}{\sum_{i=1}^{n} sin\left(\omega_0 t_i\right)} \tag{5}$$

$$\frac{dlog I_0\left(k\right)}{dk}\Big|_{k=\hat{k}}=\frac{\sqrt{\left(\sum_{i=1}^{n} sin\left(\omega_0 t_i\right)\right)^2+\left(\sum_{i=1}^{n} cos\left(\omega_0 t_i\right)\right)^2}}{n} \tag{6}$$

Here, the time interval T should be a multiple of the period $2\pi/\omega_0$, and $\hat{\vartheta}$ is selected from the roots of the second equation according to the following rule:

$$\hat{\vartheta}=\begin{cases}\hat{\vartheta},\ \ if\ sgn\left(\sum\limits_{i=1}^{n} sin\left(\omega_0 t_i\right)\right)=sgn\left(\sum\limits_{i=1}^{n} cos\left(\omega_0 t_i\right)\right)\\ \hat{\vartheta}+2\pi,\ \ if\ \hat{\vartheta}<0\ \ and\ sgn\left(\sum\limits_{i=1}^{n} sin\left(\omega_0 t_i\right)\right)=sgn\left(\sum\limits_{i=1}^{n} cos\left(\omega_0 t_i\right)\right)\\ \hat{\vartheta}+\pi,\ \ in\,other\,cases.\end{cases} \tag{7}$$

By setting ω_0 and determining the parameters $\hat{\lambda}$, $\hat{\vartheta}$, $\hat{k}$, the function λ(t) is fully determined. The likelihood measure for the hypothesis of periodicity in the frequency of flares is the logarithm of the likelihood ratio between two Poisson processes: one with a periodic parameter (hypothesis H_1) and the other with a stationary parameter (hypothesis H_0):

$$\ln L_{H_1/H_0}=k\sum_{i=1}^{n} sin\left(\omega_0 t_i+\vartheta\right)-nln\left(I_0\left(k\right)\right)$$

This implies, as noted in (Lewis, 1970), that the hypothesis of stationarity can be confidently rejected if the logarithm of the likelihood ratio:

$$\ln L_{H_1/H_0}>3 \tag{8}$$

doi: https://doi.org/10.52526/25792776-24.71.2-268

	TIC	P_f	k	ϑ	$\lambda_{max}/\lambda_{min}$	lnL_{H_1/H_0}	χ^2	μ	μ_0
1	25118964	1.008	0.489	2.075	2.661	5.901	3.155	1.444	1.955
2	141807839	0.813	0.324	1.619	1.912	3.142	1.533	3.968	4.016
3	141914082	2.700	0.321	4.786	1.902	3.017	1.890	5.857	2.876
4	141975926	1.155	0.508	5.579	2.764	7.578	1.131	5.482	3.207
5	150359500	1.057	0.398	0.342	2.215	8.870	0.952	0.739	5.793
6	167344043	2.662	0.393	2.330	2.191	6.167	4.385	0.655	1.415
7	220432563	1.134	0.540	5.396	2.925	7.788	2.834	5.865	3.407
8	277298771	1.156	0.434	5.988	2.382	4.776	4.720	4.338	2.473
9	358176584	0.921	0.326	2.487	1.920	3.207	2.475	4.513	6.233
10	359313701	1.765	0.428	1.244	2.351	5.301	1.985	1.705	1.378
11	364588501	2.252	0.274	0.131	1.729	3.548	2.641	4.492	3.052
12	373431012	0.510	0.332	4.579	1.941	3.016	2.185	4.504	1.229
13	382258517	3.295	0.363	2.238	2.066	3.916	2.470	1.785	2.452
14	441734910	1.359	0.461	1.376	2.513	5.665	1.014	4.395	4.511

Table 1. Parameters of PFFF and von Mises distribution for selected stars

Agreement with observational data is checked by comparing the expected (theoretical) distribution of flares with the corresponding observed distribution using the chi-squared test (Pearson's goodness-of-fit test). A more detailed description of the method is provided in works (Akopian, 2019, 2023). This article uses the previously determined PFFFs in work (Akopian, 2023) for the stars that meet the condition (8). The main parameters of PFFFs are presented in columns 3-9 of the Table 1.

3.2. Representation as a von Mises Circular Distribution

To represent the results in terms of a von Mises distribution, we need only (parameter of concentration k remains unchanged) to estimate the mean $\hat{\mu}$ of the distribution as follows:

$$\tan(\hat{\mu}) = \frac{\sum_{i=1}^{n} sin(\omega_0 t_i)}{\sum_{i=1}^{n} cos(\omega_0 t_i)} \tag{9}$$

Thus, considering equation (5) $\tan\left(\hat{\vartheta}\right) = 1/tan(\hat{\mu})$. From the roots of equation (9), $\hat{\mu}$ is chosen according to the following rule:

$$\hat{\mu} = \begin{cases} \hat{\mu}, \quad if \quad \left(\sum_{i=1}^{n} cos(\omega_0 t_i)\right) > 0 \\ \hat{\mu}+\pi, \quad if \quad \left(\sum_{i=1}^{n} sin(\omega_0 t_i)\right) \geq 0 \quad and \quad \left(\sum_{i=1}^{n} cos(\omega_0 t_i)\right) < 0 \\ \hat{\mu}-\pi, \quad if \quad \left(\sum_{i=1}^{n} sin(\omega_0 t_i)\right) < 0 \quad and \quad \left(\sum_{i=1}^{n} cos(\omega_0 t_i)\right) < 0 \end{cases} \tag{10}$$

Using the relationships in (5), (7), (9), and (10) , one can establish a connection between the parameters $\hat{\mu}$ and $\hat{\vartheta}$. The main parameters $\hat{\mu}, \hat{\mu_0}$ of von Mises circular distribution presented in 9th and 10th columns of Table 1 , where $\hat{\mu_0}$ is the first bin start angle (in radians).

In Fig. 1 an example of a representation of PFFF in terms of a von Mises circular distribution is presented. On the right panel of the figure expected (theoretical) phase distribution (black bars) of flares versus observed (black dots) are given for the star TIC 358176584. On the left panel observed distribution of flares (red bars) is presented as a von Mises distribution, where the red dots around the circle indicate flares, the blue stem is the mean direction of distribution $\hat{\mu}$, blue dot - the first bin start angle $\hat{\mu}_0$. The sequence of bars from left to right on the left panel matches the clockwise order of the right panel.

3.3. Determining Spot Coverage

As noted in Section 2, the ratio of the registered flux at the minimum to the maximum flux can be expressed through the PFFF parameters, and the spot coverage of the star can be determined in this way. The relationship is as follows:

doi: https://doi.org/10.52526/25792776-24.71.2-268

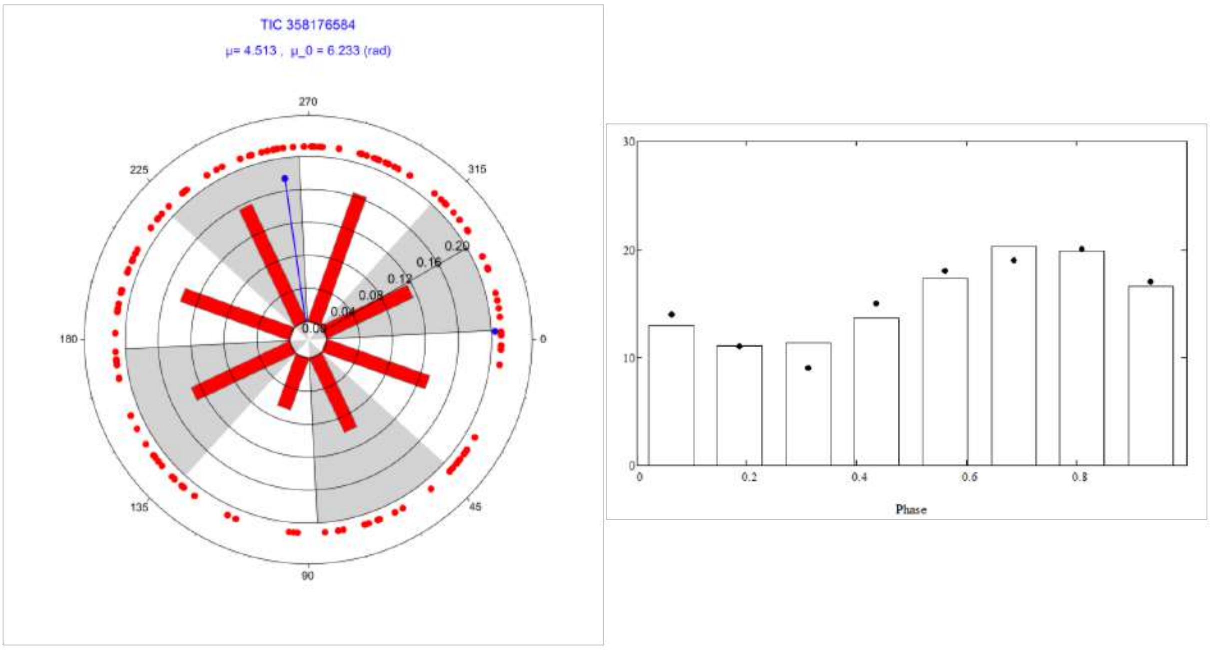

Figure 1. Phase distribution of flares/starspots

$$\frac{F_{min}}{F_{max}} = \frac{L_{st}S_{st} - S_{spmin}\,(L_{st} - L_{sp})}{L_{st}S_{st} - S_{spmax}\,(L_{st} - L_{sp})}] \tag{11}$$

where F_{min}, F_{max} are the registered fluxes, L_{st}, L_{sp} are the average surface brightnesses of the spotless star surface and the starspots, respectively, S_{st} is the area of the hemisphere of the star in projection, and S_{spmin}, S_{spmax} are the areas occupied by spots on this surface at the minimum and maximum fluxes.

The above-mentioned relationship between spot size and flare activity (Yang et al., 2017) can be written as:

$$\frac{S_{spmin}}{S_{spmax}} = \frac{\lambda_{max}}{\lambda_{min}} = e^{2k} \tag{12}$$

Introducing the notation $F_{min}/F_{max} \equiv F_r$, $S_{spmax/}S_{st} \equiv A$, $L_{sp}/L_{st} \equiv L_r$ after straightforward transformations, we can obtain the following expression for the spot coverage parameter A.

$$A = \frac{1 - F_r}{(e^{2k} - F_r)\,(1 - L_r)} \tag{13}$$

In the case where the radiation from the spots is neglected, $L_r = 0$, and thus:

$$A = \frac{1 - F_r}{e^{2k} - F_r} \tag{14}$$

In this case, the spot coverage parameter can only be estimated from below. In the approximation of spot radiation, analogous to the Sun, we can assume $L_r = 0.2 \div 0.3$, which leads to an increase in the estimate from 25% to 40%. A slight increase could also result from considering edge effects, such as the limb darkening of the stars. By definition, A is the ratio of the spot surface area to the surface area of the minimally spotted hemisphere of the star in projection. For the maximally spotted hemisphere, this ratio is increased by a factor of e^{2k}. The overall spot coverage of the star can only be estimated in cases where these hemispheres are opposite each other, which occurs when the star's rotation axis is tilted by approximately 90°. In this case, the total spot coverage parameter A_{total} is equal to:

$$A_{total} = \frac{A\left(1 + e^{2k}\right)}{2} \tag{15}$$

doi: https://doi.org/10.52526/25792776-24.71.2-268

-	TIC	F_r	A	Ae^{2k}	A_{total}	Sector
1	25118964	0.961	0.023	0.061	0.042	2
2	141807839	0.971	0.031	0.060	0.046	2
3	141914082	0.953	0.049	0.094	0.072	5
4	141975926	0.957	0.024	0.066	0.045	1
5	150359500	0.961	0.031	0.069	0.050	4
6	167344043	0.889	0.085	0.187	0.136	2
7	220432563	0.961	0.200	0.058	0.039	27
8	277298771	0.961	0.028	0.066	0.047	2
9	358176584	0.954	0.048	0.091	0.068	1
10	359313701	0.985	0.011	0.026	0.018	15
11	364588501	0.979	0.028	0.038	0.048	3
12	373431012	0.977	0.024	0.035	0.046	6
13	382258517	0.988	0.011	0.017	0.023	3
14	441734910	0.945	0.035	0.088	0.061	15

Table 2. Spottedness of stars

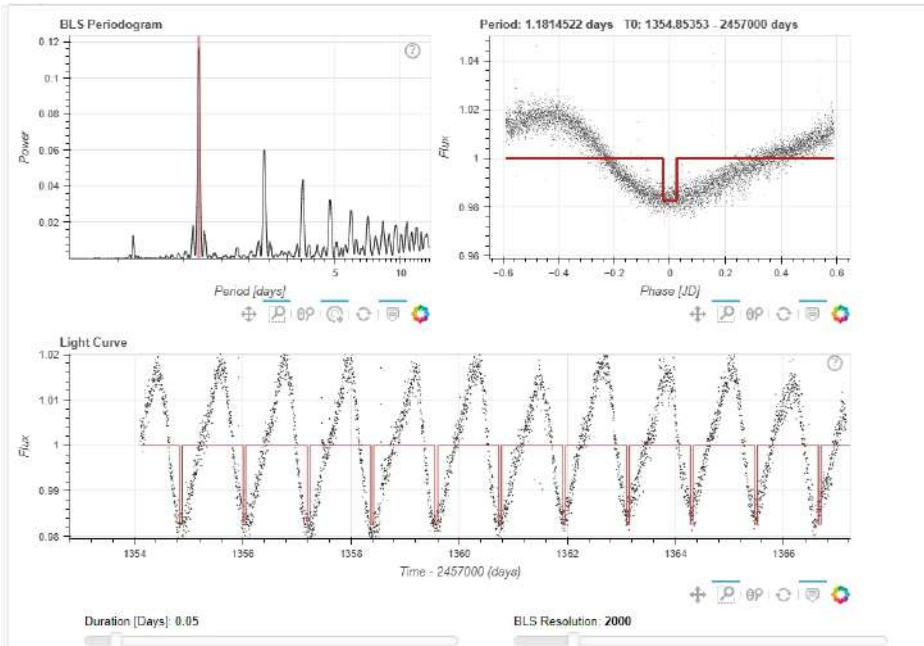

Figure 2. Illustration of the definition of the F_r ratio for the star TIC 27729877, TESS sector 2

Using the obtained expressions, the ratio F_r and the spottedness of the studied stars were determined (Table 2). The most regular light curves were selected to determine the ratio F_r. For this analysis, data from the Science Processing Operations Center (SPOC) with two-minute exposures were utilized. Column 7 ('Sector') indicates the TESS observation sector from which these light curves were obtained. An illustration is given in Fig. 2.

4. Conclusions

A novel approach has been introduced to evaluate the coverage of starspots by using periodic functions that are linked to flare frequency. The spatial distribution of starspots on flare-active stars is modeled using a von Mises circular distribution, with parameters obtained from the related flare frequency function. As a result, the selected stars' spot coverage estimates have been calculated.

doi: https://doi.org/10.52526/25792776-24.71.2-268

References

Akopian A. A., 2015, Astrophysics, 58, 62

Akopian A. A., 2019, Astrophysics, 62, 518

Akopian A. A., 2023, Astrophysics, 66, 516

Ambartsumian V. A., 1969, Stars, Nebulae, and Galaxies. Izd-vo. Akad Nauk Arm. SSR

Bullialdi I., 1667, Ad astronomos monita duo

Kron G. E., 1947, Publications of the Astronomical Society of the Pacific, 59, 261

Kutoyants Y. A., 1980, Evaluation of the Parameters of Random Processes. Izd-vo AN Armyanskoi SSR

Lewis P., 1970, Journal of Sound and Vibration, 12, 353

Yang H., Liu J., 2019, The Astrophysical Journal Supplement Series, 241, 29

Yang H., et al., 2017, The Astrophysical Journal, 849, 36

Yang Z., Zhang L., Meng G., Han X. L., Misra P., Yang J., Pi Q., 2022, Astronomy & Astrophysics, 669, A15

doi: https://doi.org/10.52526/25792776-24.71.2-268

Communications of BAO, Vol.1, Issue 2, 2024, pp. 275-288

Complete simplification of the solution of the diffuse reflection problem by the method of "decomposition of resultant field" (DRF)

H. V. Pikichyan *

Byurakan Astrophysical Observatory NAS RA, 378433, Aragatsotn region, Armenia

Abstract

The classical diffuse reflection problem (DRP) of radiation from a plane-parallel semi-infinite medium under isotropic scattering in the case of the general law $r(x, x')$ of radiation redistribution by frequencies in the elementary act of scattering is considered. It is shown that the solution of the DRP $\rho\left(x, \mu; x^{'}, \mu^{'}\right)$, which depends on four independent variables, with the help of author's recently developed method of "decomposition of the resultant field-DRF" it is possible to express explicitly through auxiliary functions $G_i(z)$, $Q_i(x)$ that depend on only one independent variable. A significant difference between this DRF method and the widely used traditional approach of "decomposition of a single act - DSA" of scattering is that it no longer requires any decomposition or a special representation of the characteristics of a single act of scattering (in the case under consideration, the function of redistribution of radiation by frequencies - $r(x, x')$) . In DRF, the resulting field of multiply scattered radiation itself is searched directly in the decomposed form. It is obvious that after each successive single act of scattering, the resulting radiation field in the medium becomes more and more smoother, so that with the same required accuracy, its decomposition will contain fewer terms than the decomposition of the characteristic of a single act of scattering. This circumstance makes the DRF method especially effective in relation to the DSA approach in cases where the latter requires taking into account a large number of terms of the decomposition of the frequency redistribution function $r(x, x')$. Explicit analytical expressions of the two-way relationship are also obtained between the desired values of the traditional and the methods proposed by the author.

Keywords: *radiative transfer, diffuse reflection problem, redistribution of radiation by frequencies, Ambartsumian's nonlinear functional equation, eigenfunctions in radiative transfer, decomposition of the resulting field*

1. Introduction and purpose of the work

The classical diffuse reflection problem (DRP) of radiation from a scattering-absorbing semi-infinite plane-parallel medium in astrophysics has a key importance in the analysis and interpretation of stellar and planetary spectra, as well as in the problems of radiative energy transfer in media where the processes of multiple interactions of radiation with matter take place. The solution of DRP depends on many independent variables, so in theoretical astrophysics, precise and approximate methods have traditionally been developed, to reduce it to the definition of auxiliary functions that depend on a smaller number of variables (Chandrasekhar, 1950, Sobolev, 1956, 1972). In the well-known methods of solving the DRP, the achievement of the separation of variables of the resulting field of multiply scattered radiation is still traditionally achieved with the help of preliminary application of variable separation procedures in the description of the single scattering act itself (below, we will combine such methods, under the conditional name of the approach "decomposition of a single act (DSA)" of scattering). As a result, the variables are also automatically separated in the desired solution of the DRP, i.e. in the resulting field of multiply scattered radiation (see, for example, Ambartsumian's pioneering work in the case of anisotropic scattering (Ambartsumian, 1943, 1944) . However, in those applications where the solution DRP requires taking into account a large number of terms (for example, in (Smokity & Anikonov, 2008) it is about 150 and more) in the decomposition of

*hovpik@gmail.com

doi: https://doi.org/10.52526/25792776-24.71.2-275

the characteristics of a single act of scattering (for example, scattering indicatrix in anisotropic scattering or frequency redistribution functions in noncoherent scattering), this approach obviously becomes less effective. Indeed: a) for the characteristics of the elementary act of scattering, the construction of an optimal decomposition with the required accuracy is already a separate difficult task, and b) in the case of a large number of terms in the single act expansion, the number of nonlinear integral equations in the final system of solving the DRP also increases, which significantly complicates the calculation of the resulting field of multiply scattered radiation. Therefore, there is a need to search for a new, simpler, and more effective way to solve the DRP, free from these difficulties.

In the author's latest works (Pikichyan, 2023a,b,c, 2024), a method of so-called decomposition of the resulting field (DRF) of radiation was developed to solve the DRP. The DRF approach compares favorably with the hitherto widely used traditional REA method in that the separation of independent variables in the solution of the problem is achieved without any decomposition or special representation of the characteristic of the elementary act of scattering. Here the description of the final field of multiple scattering is looking for in a decomposed form and there is no need for any preliminary decomposition or a special representation of the characteristics of a single act of scattering. The effectiveness of the DRF method is based on the obvious fact that with each successive act of scattering, the resulting field of diffuse radiation becomes more and more smoother. As a result, the representation, with a certain accuracy, of this field of multiply scattered radiation in the form of a bilinear series should naturally include a smaller number of terms of decomposition than the representation, with the same accuracy, of the characteristics of a single act of scattering. With this approach: a) there is no need to preliminarily consider the non-simple problem of decomposition of characteristics of the single act of scattering and b) the number of equations and auxiliary functions in the final system of nonlinear integral equations in the DRF approach should be significantly less than in the traditional DSA method. In (Pikichyan, 2023a) , using the DRF method, the case of anisotropic scattering was considered, where each azimuthal harmonic of the DRP solution dependent on two angular variables was explicitly expressed in terms of specially constructed eigenfunctions depending on only one angular variable. In the same work (Pikichyan, 2023a), in a similar way the separation of frequency variables x, and x' was achieved in the case of one-dimensional isotropic scattering medium with redistribution of radiation over frequencies under the general law $r\left(x,x'\right)$. Further, in (Pikichyan, 2023b), a three-dimensional case of DRP in the case of noncoherent isotropic scattering with the same redistribution function $r\left(x,x'\right)$ was considered, as a result, the solution $\rho\left(x,\mu;x^{'},\mu^{'}\right)$ which depended on four variables: two frequency variables $\left(x,x^{'}\right)$ and two angular variables $\left(\mu,\mu^{'}\right)$, using DRF were explicitly expressed in terms of eigenfunctions $\beta_i\left(x,\mu\right)$ dependent on only two independent variables. A more general case of DRP, when in a single act of scattering take place redistribution of radiation both: as in frequencies as of directions, was considered in (Pikichyan, 2023c). Here the solution of DRP $\rho\left(x,\mu;x^{'},\mu^{'};\varphi{-}\varphi^{'}\right)$ was expressed through the specially introduced eigenfunctions $\beta_i\left(x,\mu,\varphi\right)$. And finally, in the report (Pikichyan, 2024), the main results of the work (Pikichyan, 2023b) were presented in a slightly more compact form without mathematical calculations. In the works (Pikichyan, 2023a,b, 2024), explicit analytical relations of the two-way relationship between the auxiliary functions of the DRF and DSA methods were also given, and possible general schemes for the organization of numerical calculations were described.

In this paper, the analysis of the DRP, studied in the works (Pikichyan, 2023b, 2024), is continued with the aim of further, even greater simplification of its solution. In these works (Pikichyan, 2023b, 2024) it has already been shown that the desired value $\rho\left(x,\mu:x'.\mu'\right)$ depends on four independent variables is expressed in terms of some specially constructed eigenfunctions $\beta_i\left(x,\mu\right)$ that depend on only two independent variables. No decomposition procedure or special representation of the frequency redistribution function was used. It is shown below that the solution of the DRP in the case of incoherent isotropic scattering under an arbitrary redistribution law of radiation by frequencies can be simplified even further. Eigenfunctions $\beta_i\left(x,\mu\right)$ that depend on two independent variables can be reduced to the construction of two functions $G_i\left(z\right)$ and $Q_i\left(x\right)$, which have only one independent variable each. Here, $z=\frac{\mu}{\alpha(x)}$ is the combined variable, and the value of $\alpha\left(x\right)$, as usual, represents the absorption coefficient profile in the elementary act of scattering. The solution of the DRP is the density of the conditional probability $\rho\left(x,\mu:x',\mu'\right)$ of the diffuse reflection of a quantum from a semiinfinite medium: at a dimensionless frequency x, in the direction of μ (cosine of the angle of incidence of the quantum in relation to the normal to the boundary of the medium) in a solid angle of $2\pi d\mu$, provided that it enters the medium at a frequency x' , from the direction μ'.

doi: https://doi.org/10.52526/25792776-24.71.2-275

2. Initial ratios

In the case of isotropic scattering, the solution of the DRP is given by the expression (Pikichian, 1978, 1980)

$$\rho\left(x,\mu;x',\mu'\right)=\frac{\lambda}{2\mu'}\frac{\int_{-\infty}^{+\infty}\int_{-\infty}^{+\infty}\varphi\left(x'';x,\mu\right)r\left(x'',x'''\right)\varphi\left(x''';x',\mu'\right)dx''dx'''}{\frac{\alpha(x)}{\mu}+\frac{\alpha(x')}{\mu'}} \tag{1}$$

where the auxiliary function is given by:

$$\varphi\left(x',x;\mu\right)=\delta\left(x'-x\right)+\int_0^1\rho\left(x,\mu;x',\mu'\right)d\mu' \tag{2}$$

$$\varphi\left(x',x;\mu\right)=\delta\left(x'-x\right)+\frac{\lambda}{2}\int_{-\infty}^{+\infty}\varphi\left(x'';x,\mu\right)dx''\int_{-\infty}^{+\infty}r\left(x'',x'''\right)dx'''\int_0^1\frac{\varphi\left(x''';x',\mu'\right)}{\frac{\alpha(x)}{\mu}+\frac{\alpha(x')}{\mu'}}\frac{d\mu'}{\mu'} \tag{3}$$

In (1) the natural separation of angular variables takes place due to the isotropy of scattering, i.e. the desired function $\rho\left(x,\mu;x',\mu'\right)$ of the four independent variables is naturally expressed through the auxiliary function $\varphi\left(x',x;\mu\right)$ which has the smaller number, the three, of variables. In the works (Pikichyan, 2023b, 2024), a new function was introduced through the desired function $\rho\left(x,\mu;x',\mu'\right)$

$$K\left(x,\mu;x',\mu'\right)\equiv\mu'\left[\frac{\alpha\left(x\right)}{\mu}+\frac{\alpha\left(x'\right)}{\mu'}\right]\rho\left(x,\mu;x',\mu'\right) \tag{4}$$

for which, using the DRF method, a bilinear expansion was constructed through its eigenfunctions $\beta_j\left(x,\mu\right)$ in the n-th approximation,

$$K\left(x,\mu;x',\mu'\right)\sim K_n\left(x,\mu;x',\mu'\right)=\sum_{j=1}^{n}\nu_j\beta_j\left(x,\mu\right)\beta_j\left(x',\mu'\right)\ . \tag{5}$$

From expressions (2), (4) and (5) it follows

$$\varphi\left(x',x;\mu\right)=\delta\left(x'-x\right)+\sum_{j=1}^{n}\nu_j\beta_j\left(x,\mu\right)\int_0^1\frac{\beta_j\left(x',\mu'\right)}{\frac{\alpha(x)}{\mu}+\frac{\alpha(x')}{\mu'}}\frac{d\mu'}{\mu'} \tag{6}$$

where the eigenfunctions $\beta_j\left(x,\mu\right)$ satisfy a system of nonlinear integral equations

$$\frac{2}{\lambda}\nu_j\beta_j\left(x,\mu\right)=Z_j\left(x;[\beta]\right)+\sum_{k=1}^{n}\nu_kD_{kj}\left(x,\mu;[\beta^3]\right)+\sum_{k=1}^{n}\sum_{l=1}^{n}\nu_k\nu_lV_{klj}\left(x,\mu;[\beta^5]\right)\ . \tag{7}$$

Here the designations were introduced:

$$Z_j\left(x;[\beta]\right)\equiv\int_{-\infty}^{+\infty}r\left(x,x'\right)\overline{\beta}_j\left(x'\right)dx'\ ,\qquad \overline{\beta}_j\left(x'\right)\equiv\int_0^1\beta_j\left(x',\mu'\right)d\mu' \tag{8}$$

$$D_{kj}\left(x,\mu;[\beta^3]\right)\equiv\int_{-\infty}^{+\infty}r\left(x,x''\right)w_{kj}\left(x''\right)dx''+\int_{-\infty}^{+\infty}\int_{-\infty}^{+\infty}w_k\left(x'',x,\mu\right)r\left(x'',x'\right)\overline{\beta}_j\left(x'\right)dx'dx'', \tag{9}$$

$$V_{klj}\left(x,\mu;[\beta^5]\right)\equiv\int_{-\infty}^{+\infty}\int_{-\infty}^{+\infty}w_k\left(x'',x,\mu\right)r\left(x'',x'''\right)w_{lj}\left(x'''\right)dx''dx'''\ , \tag{10}$$

$$w_{kj}\left(x''\right)\equiv\int_{-\infty}^{+\infty}\int_0^1w_k\left(x'',x',\mu'\right)\beta_j\left(x',\mu'\right)d\mu'dx', \tag{11}$$

$$w_k\left(x'',x',\mu'\right)=\beta_k\left(x',\mu'\right)\int_0^1\frac{\beta_k\left(x'',\mu''\right)}{\frac{\alpha(x')}{\mu'}+\frac{\alpha(x'')}{\mu''}}\frac{d\mu''}{\mu''}\ . \tag{12}$$

The eigenvalues ν_i satisfy a nonlinear algebraic system

doi: https://doi.org/10.52526/25792776-24.71.2-275

$$\frac{2}{\lambda}\nu_i = b_i + \sum_{k=1}^{n} \nu_k c_{ki} + \sum_{k=1}^{n}\sum_{l=1}^{n} \nu_k \nu_l f_{kli} \ , \tag{13}$$

The designations are accepted here:

$$b_i = \int\limits_{-\infty}^{+\infty}\int\limits_{-\infty}^{+\infty} \overline{\beta}_i(x)\, r(x,x')\, \overline{\beta}_i(x')\, dx'dx \ , \quad c_{ki} = 2\int\limits_{-\infty}^{+\infty}\int\limits_{-\infty}^{+\infty} w_{ki}(x'')\, r(x'',x')\, \overline{\beta}_i(x')\, dx'dx'', \tag{14}$$

$$f_{kli} = \int_{-\infty}^{+\infty}\int_{-\infty}^{+\infty} w_{ki}(x'')\, r(x'',x''')\, w_{li}(x''')\, dx''dx''' \tag{15}$$

3. Separation of variables in the desired eigenfunctions $\beta_j(x,\mu)$

It is easy to see that the integral in (12) depends only on the variable x'' and the combination of $\frac{\alpha(x')}{\mu'}$, of parameters x', and μ' of the quantum entering the medium. This property makes it possible in formulas (7)-(12) to switch to a new variable $\frac{\alpha(x)}{\mu} = \frac{1}{z}$, denoting $\widetilde{\beta}_j(x,z) = \beta_j(x,\mu)$, instead of (7) we get

$$\frac{2}{\lambda}\nu_j \widetilde{\beta}_j(x,z) = Q_j(x) + \sum_{k=1}^{n} \nu_k \widetilde{\beta}_k(x,z)\, \widetilde{q}_{kj}(z) \ , \tag{16}$$

from which the ratios immediately follow:

$$\frac{2}{\lambda}\nu_j G_{ij}(z) = \delta_{ij} + \sum_{k=1}^{n} \nu_k G_{ik}(z)\, \widetilde{q}_{kj}(z) \ , \tag{17}$$

$$\widetilde{\beta}_j(x,z) = \sum_{i=1}^{n} Q_i(x)\, G_{ij}(z) \ . \tag{18}$$

Thus, the definition of eigenfunctions $\widetilde{\beta}_j(x,z)$, which depend on two independent variables, can be reduced to finding two auxiliary functions - $Q_i(x)$ and $G_{ij}(z)$, each of which depends on only one independent variable. From the ratios (1), (6) and (18) it follows that the solution of the initial DRP can be analytically simplified in three stages:

$$\rho(x,\mu;x',\mu') \longrightarrow \varphi(x',x;\mu) \longrightarrow \widetilde{\beta}_k(x,z) \longrightarrow Q_i(x) \ , \ G_{ij}(z)\,. \tag{19}$$

4. Orthonormalization conditions

An eigenfunctions of the kernel $K(x,\mu;x',\mu')$ appearing in (4) and (5) were introduced in (Pikichyan, 2023b, 2024) by means of equations

$$\nu_j \beta_j(x,\mu) = \int_{-\infty}^{+\infty}\int_0^1 K(x,\mu;x',\mu')\, \beta_j(x',\mu')\, d\mu' dx' \tag{20}$$

and meet the orthonormalization condition

$$\int_{-\infty}^{+\infty}\int_0^1 \beta_i(x,\mu)\, \beta_j(x,\mu)\, d\mu dx = \delta_{ij} \ . \tag{21}$$

It is not difficult to show (see Appendix A) that condition (21) for auxiliary functions $Q_m(x)$ and $G_{mj}(z)$ will be rewritten in two equivalent forms:

$$\sum_{m=1}^{n}\sum_{l=1}^{n}\int_{-\infty}^{+\infty} \alpha(x)\, Q_m(x)\, Q_l(x)\, \mathcal{G}_{mlij}(x)\, dx = \delta_{ij} \ , \tag{22}$$

$$\sum_{m=1}^{n}\sum_{l=1}^{n}\int_0^{\infty} G_{mi}(z)\, L_{ml}(z)\, G_{lj}(z)\, dz = \delta_{ij} \ , \tag{23}$$

doi: https://doi.org/10.52526/25792776-24.71.2-275

where the values $\mathcal{G}_{mlij}(x)$ and $L_{ml}(z)$ are introduced by means of notation:

$$\mathcal{G}_{mlij}(x) \equiv \int_0^{\frac{1}{\alpha(x)}} G_{mi}(z)\, G_{lj}(z)\, dz \ , \tag{24}$$

$$L_{mh}(z') \equiv 2\int_{E(z')} \alpha(x')\, Q_m(x')\, Q_h(x')\, dx' \ . \tag{25}$$

5. Finding auxiliary functions $Q_j(x)$ and $G_{ik}(z'')$ of a one variable

5.1. Functional equation for $Q_j(x)$

For the auxiliary function $Q_j(x)$ a functional equation is obtained (see Appendix B)

$$Q_j(x) = \sum_{i=1}^{n} \int_{-\infty}^{+\infty} r(x, x'')\, Q_i(x'')\, S_{ij}\left(x'', \left[Q^2\right]\right) dx'' \ , \tag{26}$$

in which the value of $S_{ij}\left(x'', \left[Q^2\right]\right)$ is given by the expression

$$S_{ij}\left(x'', \left[Q^2\right]\right) \equiv p_{ij}(x'')\, \alpha(x'') + \sum_{k=1}^{n} \nu_k \sum_{l=1}^{n} \sum_{m=1}^{n} \int_{-\infty}^{+\infty} H_{ijkml}(x'', x')\, Q_m(x')\, Q_l(x')\, \alpha(x')\, dx' \ . \tag{27}$$

Taking into account the condition of orthonormalization (22) gives expression (27) a form,

$$S_{ij}\left(x'', \left[Q^2\right]\right) = p_{ij}(x'')\left[\alpha(x'') + \nu_j\right] - \sum_{k=1}^{n} \nu_k \sum_{l=1}^{n} \sum_{m=1}^{n} \int_{-\infty}^{+\infty} \widetilde{H}_{ikmlj}(x'', x')\, Q_m(x')\, Q_l(x')\, \alpha(x')\, dx', \tag{28}$$

in which it is very important (see "b" of section 6.2), that j-th eigenvalue of ν_j is out of the sign of sum. In (27) - (28) the following designations are also adopted:

$$p_{ij}(x') \equiv \int_0^{\frac{1}{\alpha(x')}} G_{ij}(z')dz' \tag{29}$$

$$H_{ijkml}(x'', x') \equiv \int_0^{\frac{1}{\alpha(x'')}} G_{ik}(z'')\, dz'' \int_0^{\frac{1}{\alpha(x')}} \frac{G_{mk}(z')\, G_{lj}(z')}{z' + z''} z' dz' \ , \tag{30}$$

$$\widetilde{H}_{ijkml}(x'', x') \equiv \int_0^{\frac{1}{\alpha(x'')}} G_{ik}(z'')\, z'' dz'' \int_0^{\frac{1}{\alpha(x')}} \frac{G_{mk}(z')\, G_{lj}(z')}{z'' + z'} dz' \ . \tag{31}$$

From the comparison of (29) - (31) taking into account (23) follows the relationship

$$H_{ijkml}(x'', x') = p_{ij}(x'')\, \mathcal{G}_{mlkj}(x') - \widetilde{H}_{ijkml}(x'', x') \ . \tag{32}$$

5.2. Functional equation for $G_{ik}(z)$

It can be shown that the value $\tilde{q}_{kj}(z)$, which appears in (16)-(17), by means of the relation (7)-(12) (see Appendix C) takes the form

$$\begin{gathered} \tilde{q}_{kj}(z) \equiv \sum_{i=1}^{n} z \int_0^{\infty} \frac{G_{ik}(z'')}{z + z''} dz'' \cdot \\ \cdot \sum_{l=1}^{n} \left\{ \int_0^{\infty} M_{il}(z'', z')\, G_{lj}(z')\, dz' + \nu_l \sum_{s=1}^{n} \int_0^{\infty} F_{is}(z'', z''')\, G_{sl}(z''')\, \mathcal{L}_{lj}\left(z'''; \left[G^2\right]\right) dz''' \right\} \end{gathered} \tag{33}$$

where the permutation was used

doi: https://doi.org/10.52526/25792776-24.71.2-275

$$\int_{-\infty}^{+\infty} \dots dx \int_0^{\frac{1}{\alpha(x)}} \dots dz = 2\int_0^{\infty} \dots dz \int_{E(z)} \dots dx \ , \qquad E(z) = \left\{ x : \alpha(x) \le \frac{1}{z} \right\} \tag{34}$$

and following designations are adopted:

$$\mathcal{L}_{lj}\left(z'''; \left[G^2\right]\right) \equiv \int_0^{\infty} \frac{\sum_{m=1}^{n} \sum_{h=1}^{n} G_{ml}(z') L_{mh}(z') G_{hj}(z')}{z''' + z'} z' dz' \ , \tag{35}$$

$$M_{il}\left(z'', z'\right) \equiv 4 \int_{E(z'')} \int_{E(z')} Q_i\left(x''\right) r\left(x'', x'\right) Q_l\left(x'\right) \alpha\left(x'\right) dx' dx'' \ , \tag{36}$$

$$F_{is}\left(z'', z'''\right) \equiv 4 \int_{E(z'')} \int_{E(z''')} Q_i\left(x''\right) r\left(x'', x'''\right) Q_s\left(x'''\right) dx''' dx'' \ . \tag{37}$$

From the relations (33) and (17) the functional equation for the quantities $G_{ik}(z'')$ is obtained

$$\frac{2}{\lambda} \nu_j G_{pj}(z) = \delta_{pj} + z \sum_{k=1}^{n} \nu_k G_{pk}(z) \sum_{i=1}^{n} \int_0^{\infty} \frac{G_{ik}(z'')}{z + z''} W_{ij}\left(z'', \left[G^3\right]\right) dz'' \ , \tag{38}$$

where the designations are accepted

$$W_{ij}\left(z'', \left[G^3\right]\right) \equiv \sum_{l=1}^{n} \left[\int_0^{\infty} M_{il}\left(z'', z'\right) G_{lj}\left(z'\right) dz' + \nu_l \sum_{s=1}^{n} \int_0^{\infty} F_{is}\left(z'', z'''\right) G_{sl}\left(z'''\right) \mathcal{L}_{lj}\left(z'''; \left[G^2\right]\right) dz''' \right] . \tag{39}$$

The use of orthonormalization (23) gives expression (39) form

$$\begin{aligned} W_{ij}\left(z'', \left[G^3\right]\right) = & \sum_{s=1}^{n} \int_0^{\infty} M_{is}\left(z'', z'\right) G_{sj}\left(z'\right) dz' + \nu_j \sum_{k=1}^{n} \int_0^{\infty} F_{ik}\left(z'', z'''\right) G_{kj}\left(z'''\right) dz''' - \\ & - \sum_{l=1}^{n} \nu_l \sum_{s=1}^{n} \int_0^{\infty} F_{is}\left(z'', z'''\right) G_{sl}\left(z'''\right) \widetilde{\mathcal{L}_{lj}}\left(z'''; \left[G^2\right]\right) z''' dz''' \end{aligned} \tag{40}$$

where the value is entered

$$\widetilde{\mathcal{L}_{lj}}\left(z'''; \left[G^2\right]\right) \equiv \int_0^{\infty} \frac{\sum_{m=1}^{n} \sum_{h=1}^{n} G_{ml}(z') L_{mh}(z') G_{hj}(z')}{z''' + z'} dz' \ , \tag{41}$$

which satisfies of the expression

$$\mathcal{L}_{lj}\left(z'''; \left[G^2\right]\right) = \delta_{lj} - z''' \ \widetilde{\mathcal{L}_{lj}}\left(z'''; \left[G^2\right]\right) . \tag{42}$$

6. Algebraic systems for finding the eigenvalues

In the functional equations (26)-(27) and (38)-(39), the eigenvalues of problem (20) are still to be determined

6.1. A system of nonlinear algebraic equations

To determine these eigenvalues, there is already a system of nonlinear algebraic equations (13), and it remains only to express the quantities included in it through auxiliary functions of one variable $Q_i(x)$ and $G_{ij}(z)$. After simple but somewhat cumbersome calculations (see Appendix D). for the quantities b_i, c_{kj}, f_{kli} appear in the algebraic system, the following expressions are obtained:

$$b_i = \sum_{k=1}^{n} \sum_{j=1}^{n} \int_{-\infty}^{+\infty} \int_{-\infty}^{+\infty} \Omega_{ki}(x) r\left(x, x'\right) \Omega_{ji}\left(x'\right) dx' dx = \sum_{k=1}^{n} \sum_{j=1}^{n} \int_0^{\infty} \int_0^{\infty} G_{ki}(z) U_{kj}\left(z, z'\right) G_{ji}\left(z'\right) dz' dz \ , \tag{43}$$

doi: https://doi.org/10.52526/25792776-24.71.2-275

$$c_{kj} = 2\sum_{s=1}^{n}\sum_{l=1}^{n}\int_{-\infty}^{+\infty}\int_{-\infty}^{+\infty}\mathit{\Gamma}_{skj}\left(x''\right)Q_s\left(x''\right)r\left(x'',x'\right)\Omega_{lj}\left(x'\right)dx'dx'' \ , \tag{44}$$

$$f_{kli} = \sum_{s=1}^{n}\sum_{h=1}^{n}\int_{-\infty}^{+\infty}\int_{-\infty}^{+\infty}\mathit{\Gamma}_{ski}\left(x''\right)Q_s\left(x''\right)r\left(x'',x'''\right)Q_h\left(x'''\right)\mathit{\Gamma}_{hli}\left(x'''\right)dx'''dx'' \ , \tag{45}$$

where auxiliary quantities have the form:

$$\Omega_{ki}\left(x\right) \equiv Q_k\left(x\right)\alpha\left(x\right)p_{ki}\left(x\right) \ , \tag{46}$$

$$\mathit{\Gamma}_{skj}\left(x''\right) = \sum_{q=1}^{n}\sum_{m=1}^{n}\int_{-\infty}^{+\infty}H_{sjkqm}\left(x''x'\right)Q_q\left(x'\right)Q_m\left(x'\right)\alpha\left(x'\right)dx' = \int_{0}^{\frac{1}{\alpha(x'')}}G_{sk}\left(z''\right)\mathcal{L}_{kj}\left(z''';\left[G^2\right]\right)dz''. \tag{47}$$

6.2. A system of linear algebraic equations for determining eigenvalues

In addition to the system of **nonlinear** algebraic equations (13), a system of **linear** algebraic equations can also be obtained to determine the eigenvalues of ν_j (see Appendix E).

$$\nu_j = \mathcal{A}_j + \sum_{k=1}^{n}\nu_k\mathcal{B}_{ij} \ , \tag{48}$$

where the values $\mathcal{A}_j$ and $\mathcal{B}_{ij}$ are given by expressions:

$$\mathcal{A}_j \equiv \frac{\int_{-\infty}^{+\infty}Q_j\left(x\right)dx - \sum_{i=1}^{n}\int_{-\infty}^{+\infty}\alpha\left(x''\right)\Omega_{ij}\left(x''\right)dx''}{\sum_{i=1}^{n}\int_{-\infty}^{+\infty}\Omega_{ij}\left(x''\right)dx''} \ , \tag{49}$$

$$\mathcal{B}_{kj} \equiv \frac{\sum_{i=1}^{n}\sum_{l=1}^{n}\sum_{m=1}^{n}\int_{-\infty}^{+\infty}\int_{-\infty}^{+\infty}\alpha\left(x''\right)Q_i\left(x''\right)\widetilde{H}_{ikmlj}\left(x'',x'\right)Q_m\left(x'\right)Q_l\left(x'\right)\alpha\left(x'\right)dx'dx''}{\sum_{i=1}^{n}\int_{-\infty}^{+\infty}\Omega_{ij}\left(x''\right)dx''} \tag{50}$$

7. The final system of equations for solving the DRP

The above equations (26), (38), (13), (48) together define a final system consisting of nonlinear integral equations and two types of algebraic equations (nonlinear and linear) to find the auxiliary functions $Q_j\left(x\right)$, $G_{ji}\left(z\right)$ and the eigenvalues ν_j.

$$\left\{\begin{array}{l} \frac{2}{\lambda}\nu_j G_{pj}\left(z\right) = \delta_{pj} + z\sum_{k=1}^{n}\nu_k G_{pk}\left(z\right)\sum_{i=1}^{n}\int_0^{\infty}\frac{G_{ik}(z'')}{z+z''}W_{ij}\left(z'',\left[G^3\right]\right)dz'' \\ Q_j\left(x\right) = \sum_{i=1}^{n}\int_{-\infty}^{+\infty}r\left(x,x''\right)Q_i\left(x''\right)S_{ij}\left(x'',\left[Q^2\right]\right)dx'' \\ \frac{2}{\lambda}\nu_i = b_i + \sum_{k=1}^{n}\nu_k c_{ki} + \sum_{k=1}^{n}\sum_{l=1}^{n}\nu_k\nu_l f_{kli} \quad or \quad \nu_j = \mathcal{A}_j + \sum_{k=1}^{n}\nu_k\mathcal{B}_{ij} \end{array}\right. \tag{51}$$

8. The final forms of explicit solution of the DRP, which were obtained by two methods, DSA and DRF

Now it is not difficult to give an explicit form of the solution of the DRP obtained by both methods: the new DRF and the traditional DSA.

8.1. Explicit form of solution using the DRF method

In terms of the auxiliary functions of a single variable $Q_i\left(x\right)$ and $G_{ij}\left(z\right)$ taking into account the notation $\rho\left(x,\mu;x',\mu'\right) \equiv \widetilde{\rho}\left(x,z;x',z'\right)$ from (4), (5) and (18) we get the expression

$$\widetilde{\rho}\left(x,z;x',z'\right) = \frac{1}{\alpha\left(x'\right)}\sum_{i=1}^{n}\sum_{k=1}^{n}Q_i\left(x\right)R_{ik}\left(z,z'\right)Q_k\left(x'\right) \ , \tag{52}$$

doi: https://doi.org/10.52526/25792776-24.71.2-275

where the value of $R_{ik}(z,z')$ is given as

$$R_{ik}(z,z') = z\frac{\sum_{j=1}^{n}\nu_j G_{ij}(z)\,G_{kj}(z')}{z+z'}\ . \tag{53}$$

From (52) - (53) it can be seen that when solving the DRP using the DRF method, similar to the traditional DSA method, the classical structure of separation of independent variables is preserved (compare, below, with formula (58) - (59).

8.2. An explicit solution of DRP using the traditional DSA method

To compare the DRF and DSA methods, it is also appropriate to cite here the solution of DRP using the traditional DSA method (see and compare with the works (Engibaryan & Nikogosyan, 1972a,b). From the relation (1) by substituting the bilinear decomposition of the function of redistribution of radiation by frequencies in a single scattering act

$$r(x'',x''') = \sum_{i=1}^{N} A_i\alpha_i(x'')\,\alpha_i(x''')\ , \tag{54}$$

a well-known solution is easily obtained

$$\widetilde{\rho}(x,z;x',z') = \frac{\lambda}{2}\frac{z}{\alpha(x')}\frac{\sum_{i=1}^{N} A_i\widetilde{\varphi}_i(x,z)\,\widetilde{\varphi}_i(x',z')}{z+z'}\ , \tag{55}$$

where auxiliary function $\widetilde{\varphi}_i(x,z)$ satisfies the analogue of Ambartsumian's functional equation

$$\widetilde{\varphi}_i(x,z) = \alpha_i(x) + \frac{\lambda}{2}z\sum_{j=1}^{n} A_j\widetilde{\varphi}_j(x,z)\int_{-\infty}^{+\infty}\alpha_i(x')\,dx'\int_0^{\frac{1}{\alpha(x')}}\frac{\widetilde{\varphi}_j(x',z')}{z+z'}dz'\ . \tag{56}$$

It is also easy to show that the auxiliary function $\widetilde{\varphi}_i(x,z)$ is representable in the form (see Appendix F).

$$\widetilde{\varphi}_i(x,z) = \sum_{k=1}^{N}\alpha_k(x)\,g_{ki}(z)\ , \tag{57}$$

then the explicit DRP decision obtained by the DSA method will take the form of

$$\widetilde{\rho}(x,z;x',z') = \frac{1}{\alpha(x')}\sum_{k=1}^{N}\sum_{j=1}^{N}\alpha_k(x)\,\mathcal{R}_{kj}(z,z')\,\alpha_j(x')\ , \tag{58}$$

where the value of $\mathcal{R}_{kj}(z,z')$ is given as

$$\mathcal{R}_{kj}(z,z') \equiv \frac{\lambda}{2}z\frac{\sum_{i=1}^{N} A_i g_{ki}(z)\,g_{ji}(z')}{z+z'}\ . \tag{59}$$

The auxiliary function of one argument $g_{jk}(z)$, which appears in (59), satisfies the functional equation

$$g_{jk}(z) = \delta_{jk} + \frac{\lambda}{2}z\sum_{i=1}^{N} A_i g_{ji}(z)\int_0^{\infty}\frac{\sum_{h=1}^{N} u_{hk}(z')\,g_{hi}(z')}{z+z'}dz'\ , \tag{60}$$

where the value of $u_{jk}(z')$ is given by the expression

$$u_{jk}(z') \equiv 2\int_{E(z)}\alpha_j(x)\,\alpha_k(x)\,dx\ . \tag{61}$$

9. Two-way relationship between the auxiliary functions of the DRF and DSA techniques

For a practical assessment of the relative effectiveness of the DRF and DSA methods, it is very useful to provide a two-way analytical relationship between the functions that determine the solution of the DRP.

doi: https://doi.org/10.52526/25792776-24.71.2-275

9.1. The $\widetilde{\varphi}_k(x', z')$ are known, i.e. the values: A_i, $\alpha_s(x)$ and $g_{si}(z)$ it is necessary to find $\widetilde{\beta}_j(x,z)$ and ν_j.

Explicit expressions are obtained (see Appendix G):

$$\widetilde{\beta}_j(x,z) = \frac{\sum_{k=1}^{n} A_k q_{kj} \sum_{s=1}^{n} \alpha_s(x) g_{sk}(z)}{\sum_{k=1}^{N} A_k q_{kj}^2}, \qquad \nu_j = \frac{\lambda}{2} \sum_{i=1}^{n} A_i q_{ij}^2, \tag{62}$$

where the values q_{kj} are determined from the algebraic system

$$q_{ij} = \frac{\sum_{k=1}^{n} A_k a_{ik} q_{kj}}{\sum_{k=1}^{N} A_k q_{kj}^2}. \tag{63}$$

The a_{ik} coefficients in expression (63) are as follows

$$a_{ik} = \sum_{s=1}^{n}\sum_{l=1}^{n} \int_{-\infty}^{+\infty} \alpha(x)\alpha_s(x)\Theta_{sikl}(x)\alpha_l(x)\,dx = \sum_{s=1}^{n}\sum_{l=1}^{n}\int_0^{\infty} g_{si}(z)\Lambda_{sl}(z)g_{lk}(z)\,dz, \tag{64}$$

where the symbols are used:

$$\Theta_{sikl}(x) \equiv \int_0^{\frac{1}{\alpha(x)}} g_{si}(z) g_{lk}(z)\,dz, \qquad \Lambda_{sl}(z) \equiv 2\int_{E(z)} \alpha(x)\alpha_s(x)\alpha_l(x)\,dx. \tag{65}$$

9.2. Known $\widetilde{\beta}_j(x,z)$, i.e. the values $Q_i(x)$ and $G_{ij}(z)$, it is necessary to find $\widetilde{\varphi}_i(x,z)$

From the relation (57) it can be seen that the auxiliary function $\widetilde{\varphi}_i(x,z)$, which depends on two independent variables (x,z), is explicitly expressed in terms of two functions, $\alpha_s(x)$ and $g_{ki}(z)$, by only one variable. At the same time, the functions $\alpha_s(x)$ in advance are already known from the construction of the expansion (54), so in this DRP only the functions of $g_{si}(z)$ are sought. To define them, an explicit expression is obtained (see Appendix H).

$$g_{ki}(z) = \delta_{ki} + z\sum_{j=1}^{n} \nu_j \tilde{G}_{kj}(z) \sum_{h=1}^{n} \int_0^{\infty} \frac{G_{hj}(z')}{z+z'} \gamma_{hi}(z')\,dz', \tag{66}$$

where the designations are accepted:

$$\tilde{G}_{kj}(z) \equiv \sum_{m=1}^{n} \vartheta_{km} G_{mj}(z), \qquad \vartheta_{km} \equiv \int_{-\infty}^{+\infty} \vartheta(x)\alpha_k(x)Q_m(x)\,dx, \tag{67}$$

$$\gamma_{hi}(z') \equiv 2\int_{E(z')} Q_h(x')\alpha_i(x')\,dx', \tag{68}$$

the value $\vartheta(x)$ is a given weight function that appears in the orthonormalization condition

$$\int_{-\infty}^{+\infty} \vartheta(x)\alpha_k(x)\alpha_s(x)\,dx = \delta_{ks}.$$

.

10. Conclusion

It was shown above that the proposed DRF method, in contrast to the traditional DSA approach, makes it possible in the case of isotropic scattering under the general law of radiation redistribution by frequencies to achieve complete simplification of the solution of the DRP from a semi-infinite plane-parallel medium, without any decomposition or special representation of the characteristics of a single act of scattering, i.e., of the radiation redistribution function by frequencies $r(x'', x''')$. At the same time, the solution of the DRP, which depends on four independent variables, as in the traditional DSA method, can be reduced to the definition of auxiliary functions of only one independent variable. Explicit analytical expressions of the two-way relationship between the desired functions of the traditional and the methods proposed by the author are also obtained.

doi: https://doi.org/10.52526/25792776-24.71.2-275

References

Ambartsumian V. A., 1943, Zhour. Theor. Exp. Phys. (in Russian), (Engl. transl., V. A. Ambartsumian: Selected papers, Part I., Ed. Meylan, pp.187-208, CSP , 2010), 13, 313

Ambartsumian V. A., 1944, J. Phys., 8, 65

Chandrasekhar S., 1950, Radiative Transfer. Oxford University Press, London

Engibaryan N. B., Nikogosyan A. G., 1972a, Astrophysics, 8, 128

Engibaryan N. B., Nikogosyan A. G., 1972b, Akademiia Nauk Armianskoi SSR Doklady, 54, 91

Pikichian O. V., 1978, Akademiia Nauk Armianskoi SSR Doklady, 67, 151

Pikichian O. V., 1980, Soobshcheniya Byur. Observ. (in Russian), Communications of the Byurakan Astrophysical Observatory, 52, 148

Pikichyan H. V., 2023a, Communications of the Byurakan Astrophysical Observatory, 70, 143

Pikichyan H. V., 2023b, Communications of the Byurakan Astrophysical Observatory, 70, 204

Pikichyan H. V., 2023c, Communications of the Byurakan Astrophysical Observatory, 70, 235

Pikichyan H. V., 2024, Communications of the Byurakan Astrophysical Observatory, 71, 72

Smokity O. I., Anikonov A. S., 2008, Light scattering in media of high optical thickness. St. Petersburg, Nauka Publ, 440 p., (in Russian)

Sobolev V. V., 1956, Perenos Luchistoy Energii v Atmosferakh Zvyozd i Planet, Gostekhizdat, 391 p. (in Russian), Published in English as A Treatise on Radiative Transfer (D. Van Nostrand, 1963). Gostekhizdat

Sobolev V. V., 1972, Rasseyaniye sveta v atmosferakh planet, Izd. "Nauka", M., 336 p. (in Russian), (Eng. transl.: Sobolev V. V., 1975, Light scattering in planetary atmospheres (International Series of Monographs in Natural Philosophy vol.76),). Pergamon Press, Oxford, 256 p.)

doi: https://doi.org/10.52526/25792776-24.71.2-275

Appendices

Appendix A

In relation (21), we replace the variable $\frac{\alpha(x)}{\mu} = \frac{1}{z}$, taking into account the notation $\widetilde{\beta}_j(x,z) = \beta_j(x,\mu)$ we get

$$\int_{-\infty}^{+\infty} \alpha(x)\, dx \int_0^{\frac{1}{\alpha(x)}} \widetilde{\beta}_i(x,z)\, \widetilde{\beta}_j(x,z)\, dzdx = \delta_{ij} \ . \tag{A.1}$$

From (18) we have the expressions

$$\widetilde{\beta}_i(x,z) = \sum_{m=1}^{n} Q_m(x)\, G_{mi}(z) \ , \qquad \widetilde{\beta}_j(x,z) = \sum_{l=1}^{n} Q_l(x)\, G_{lj}(z) \ , \tag{A.2}$$

the substitution of which in (A.1) gives the relation

$$\sum_{m=1}^{n}\sum_{l=1}^{n} \int_{-\infty}^{+\infty} \alpha(x)\, Q_m(x)\, Q_l(x)\, dx \int_0^{\frac{1}{\alpha(x)}} G_{mi}(z)\, G_{lj}(z)\, dzdx = \delta_{ij} \ . \tag{A.3}$$

Let's change the order of integration in the expression (A.3) following the example

$$\int_{-\infty}^{+\infty} \ldots dx \int_0^{\frac{1}{\alpha(x)}} \ldots dz = 2\int_0^{\infty} \ldots dz \int_{E(z)} \ldots dx \ , \tag{A.4}$$

then the ratio (A.3) will take the form of

$$\sum_{m=1}^{n}\sum_{l=1}^{n} \int_0^{\infty} G_{mi}(z)\, G_{lj}(z)\, dz \cdot 2\int_{E(z)} \alpha(x)\, Q_m(x)\, Q_l(x)\, dx = \delta_{ij} \ . \tag{A.5}$$

Taking into account in expressions (A.3) and (A.5) the notations:

$$\mathcal{G}_{mlij}(x) \equiv \int_0^{\frac{1}{\alpha(x)}} G_{mi}(z)\, G_{lj}(z)\, dz, \qquad L_{mh}(z) \equiv 2\int_{E(z)} \alpha(x)\, Q_m(x)\, Q_h(x)\, dx \tag{A.6}$$

leads to two forms of orthonormalization conditions in the form of relations (22) and (23).

Appendix B

From formulas (7) - (12) it is not difficult to obtain

$$Q_j(x) = Z_j(x) + \sum_{k=1}^{n} \nu_k \int_{-\infty}^{+\infty} r(x,x'')\, dx'' \int_{-\infty}^{+\infty} \int_0^{\frac{1}{\alpha(x')}} \widetilde{\beta}_k(x',z')\, \tilde{B}_k(x'',z')\, \widetilde{\beta}_j(x',z')\, dz'dx', \tag{B.1}$$

where the ratio was used

$$\int_0^1 \frac{\beta_k(x'',\mu'')}{\frac{\alpha(x')}{\mu'} + \frac{\alpha(x'')}{\mu''}} \frac{d\mu''}{\mu''} \equiv B_k\left(x'', \frac{\alpha(x')}{\mu'}\right) \equiv \widetilde{B}_k(x'',z') = \sum_{i=1}^{n} Q_i(x'')z' \int_0^{\frac{1}{\alpha(x'')}} \frac{G_{ik}(z'')}{z'+z''} dz'', \tag{B.2}$$

In the last integral (B.2), the expression (18) is also taken into account. For the value $Z_j(x)$ appearing in (B.1) taking into account (18), we get:

$$Z_j(x) \equiv \int\limits_{-\infty}^{+\infty} r(x,x')\, dx' \int\limits_0^1 \beta_j(x',\mu')d\mu' = \int\limits_{-\infty}^{+\infty} r(x,x')\, \alpha(x')\, dx' \int\limits_0^{\frac{1}{\alpha(x')}} \widetilde{\beta}_j(x',z')dz' =$$

doi: https://doi.org/10.52526/25792776-24.71.2-275

$$= \int\limits_{-\infty}^{+\infty} r\left(x,x'\right)dx' \sum_{i=1}^{n} Q_i\left(x'\right)\alpha\left(x'\right) \int\limits_{0}^{\frac{1}{\alpha(x')}} G_{ij}\left(z'\right)dz'$$

$$Z_j\left(x\right) = \sum_{i=1}^{n} \int_{-\infty}^{+\infty} r\left(x,x''\right)Q_i\left(x''\right)p_{ij}\left(x''\right)\alpha\left(x''\right)dx'' \;, \tag{B.3}$$

where indicated

$$p_{ij}\left(x'\right) \equiv \int_0^{\frac{1}{\alpha(x')}} G_{ij}\left(z'\right)dz' \;. \tag{B.4}$$

Taking into account (B.2) and (B.3) from (B.1), we obtain the expression

$$Q_j\left(x\right) = \sum_{i=1}^{n} \int_{-\infty}^{+\infty} r\left(x,x''\right)Q_i\left(x''\right)p_{ij}\left(x''\right)\alpha\left(x''\right)dx'' +$$

$$+\sum_{i=1}^{n} \int_{-\infty}^{+\infty} r\left(x,x''\right)Q_i\left(x''\right)dx'' \sum_{k=1}^{n}\nu_k \sum_{m=1}^{n}\sum_{l=1}^{n} \int_{-\infty}^{+\infty} H_{ijkml}\left(x'',x'\right)Q_m\left(x'\right)Q_l\left(x'\right)\alpha\left(x'\right)dx' \;, \tag{B.5}$$

from which follow (26)-(31).

Appendix C

With the help of relations (7)-(12) it is not difficult to arrive at the expression

$$\frac{2}{\lambda}\nu_j\beta_j\left(x,\mu\right) = Q_j\left(x\right) + \sum_{k=1}^{n}\nu_k\beta_k\left(x,\mu\right)q_{kj}\left(\frac{\alpha\left(x\right)}{\mu}\right) \;, \tag{C.1}$$

where the value of $q_{kj}\left(\frac{\alpha(x)}{\mu}\right)$ has the form

$$q_{kj}\left(\frac{\alpha\left(x\right)}{\mu}\right) \equiv \int_{-\infty}^{+\infty} B_k\left(x'',\frac{\alpha\left(x\right)}{\mu}\right)dx'' \int_{-\infty}^{+\infty} r\left(x'',x'\right)\overline{\beta}_j\left(x'\right)dx' +$$

$$+\sum_{l=1}^{n}\nu_l \int_{-\infty}^{+\infty} B_k\left(x'',\frac{\alpha\left(x\right)}{\mu}\right)dx'' \int_{-\infty}^{+\infty} r\left(x'',x'''\right)w_{lj}\left(x'''\right)dx''' \;, \tag{C.2}$$

in this case, the value of $B_k\left(x'',\frac{\alpha(x)}{\mu}\right)$ is given by the expression (B.2). By switching to the variable z and taking into account $q_{kj}\left(\frac{\alpha(x)}{\mu}\right) \equiv \widetilde{q}_{kj}\left(z\right)$, we get

$$\widetilde{q}_{kj}\left(z\right) \equiv \int_{-\infty}^{+\infty} \widetilde{B}_k\left(x'',z\right)dx'' \int_{-\infty}^{+\infty} r\left(x'',x'\right)\alpha\left(x'\right)dx' \int_0^{\frac{1}{\alpha(x')}} \widetilde{\beta}_j\left(x',z'\right)dz' + \sum_{l=1}^{n}\nu_l \cdot$$

$$\cdot \int_{-\infty}^{+\infty} \widetilde{B}_k\left(x'',z\right)dx'' \int_{-\infty}^{+\infty} r\left(x'',x'''\right)dx''' \int_{-\infty}^{+\infty} \alpha\left(x'\right)dx' \int_0^{\frac{1}{\alpha(x')}} \widetilde{\beta}_l\left(x',z'\right)\widetilde{B}_l\left(x''',z'\right)\widetilde{\beta}_j\left(x',z'\right)dz'dx' \;. \tag{C.3}$$

Setting in (C.3) of the relation (18) taking into account (B.2) we come to the expression

$$\widetilde{q}_{kj}\left(z\right) = \sum_{i=1}^{n} \int_{-\infty}^{+\infty} Q_i\left(x''\right)dx'' z \int_0^{\frac{1}{\alpha(x'')}} \frac{G_{ik}\left(z''\right)}{z+z''}dz'' \sum_{l=1}^{n} \int_{-\infty}^{+\infty} r\left(x'',x'\right)Q_l\left(x'\right)\alpha\left(x'\right)dx' \int_0^{\frac{1}{\alpha(x')}} G_{lj}\left(z'\right)dz' +$$

$$+\sum_{l=1}^{n}\nu_l \sum_{i=1}^{n} \int_{-\infty}^{+\infty} Q_i\left(x''\right)dx'' z \int_0^{\frac{1}{\alpha(x'')}} \frac{G_{ik}\left(z''\right)}{z+z''}dz'' \sum_{s=1}^{n} \int_{-\infty}^{+\infty} r\left(x'',x'''\right)Q_s\left(x'''\right)dx''' \cdot$$

doi: https://doi.org/10.52526/25792776-24.71.2-275

$$\cdot \sum_{m=1}^{n} \sum_{h=1}^{n} \int_{-\infty}^{+\infty} \alpha\left(x'\right) Q_m\left(x'\right) Q_h\left(x'\right) dx' \int_0^{\frac{1}{\alpha(x')}} G_{ml}\left(z'\right) G_{hj}\left(z'\right) z' dz' \int_0^{\frac{1}{\alpha(x''')}} \frac{G_{sl}\left(z'''\right)}{z'+z'''} dz''', \tag{C.4}$$

from which it already follows (33).

Appendix D

For the output of expressions (43)-(47), the initial formulas are (13)-(15). From the latter, on the basis of expression (18), the left part of the expression (43) is first derived, then the substitution of places in the double integral is performed according to the sample (A.4) and the right part of the expression (43) is obtained. Forms (44) - (45) are also obtained in the same way, while the main quantities included in (14) - (15) are given by the expressions:

$$\overline{\beta}_i\left(x\right) = \sum_{k=1}^{n} Q_k\left(x\right) \alpha\left(x\right) p_{ki}\left(x\right), \quad w_{ki}\left(x''\right) = \sum_{s=1}^{n} Q_s\left(x''\right) \Gamma_{ski}\left(x''\right). \tag{D.1}$$

Appendix E

From the relations (26) and (28) by integration along x within (-∞,+∞), the relations (48)-(50) are obtained, taking into account the known relationship of the absorption profile with the frequencies redistribution function

$$\int_{-\infty}^{+\infty} r\left(x, x''\right) dx = \alpha\left(x''\right). \tag{E.1}$$

Appendix F

To make the transition from expression (56) to form (57), note that the double integral in the right-hand side of (56) depends only on the variable z and let's take into account the notation, then

$$h_j\left(x', z\right) \equiv \int_0^{\frac{1}{\alpha(x')}} \frac{\widetilde{\varphi}_j\left(x', z'\right)}{z+z'} dz', \quad \omega_{ji}\left(z\right) \equiv \int_{-\infty}^{+\infty} h_j\left(x', z\right) \alpha_i\left(x'\right) dx', \tag{F.1}$$

relation (56) will take the form of a linear algebraic system

$$\widetilde{\varphi}_i\left(x, z\right) = \alpha_i\left(x\right) + \frac{\lambda}{2} z \sum_{j=1}^{N} A_j \widetilde{\varphi}_j\left(x, z\right) \omega_{ji}\left(z\right). \tag{F.2}$$

If we now introduce the resolvent by means of the equation

$$g_{ki}\left(z\right) = \delta_{ki} + \frac{\lambda}{2} z \sum_{j=1}^{N} A_j g_{kj}\left(z\right) \omega_{ji}\left(z\right), \tag{F.3}$$

we arrive at the explicit expression (57). By substituting (57) in (55) we immediately get (58) - (59). If we substitute the second of the relations (F.1) into (F.3), then, taking into account (57) and replacing the integrals in the double integral (according to the example (A.4)), the relation (F.1) turns into the functional equation (60).

Appendix G

In the same approximation $N = n$, we equalize the values of the function $K\left(x, \mu; x', \mu'\right)$ obtained by two methods, DRF and DSA

$$\sum_{j=1}^{n} \nu_j \beta_j\left(x, \mu\right) \beta_j\left(x', \mu'\right) = \frac{\lambda}{2} \sum_{k=1}^{n} A_k \varphi_k\left(x, \mu\right) \varphi_k\left(x', \mu'\right). \tag{G.1}$$

doi: https://doi.org/10.52526/25792776-24.71.2-275

Taking into account the orthonormalization condition (21), the following expressions are obtained from (G.1):

$$\nu_j \beta_j (x, \mu) = \frac{\lambda}{2} \sum_{k=1}^{N} A_k \varphi_k (x, \mu) q_{kj} \ , \qquad q_{kj} \equiv \int_{-\infty}^{+\infty} \int_0^1 \varphi_k (x', \mu') \beta_j (x', \mu') \, d\mu' dx'. \tag{G.2}$$

If condition (21) is applied to the first relation of (G.2) and also applied the operator $\int\limits_{-\infty}^{+\infty} \int\limits_0^1 \varphi_k (x', \mu') \ldots d\mu' dx'$, then taking into account the second of the conditions (G.2) it is not difficult to come to the following expressions (see (Pikichyan, 2023b, 2024)):

$$\nu_j = \frac{\lambda}{2} \sum_{k=1}^{n} A_k q_{kj}^2 \ , \qquad \nu_j q_{ij} = \frac{\lambda}{2} \sum_{k=1}^{n} A_k a_{ik} q_{kj} \ , \qquad a_{ik} \equiv \int_{-\infty}^{+\infty} \int_0^1 \varphi_i (x', \mu') \varphi_k (x', \mu') \, d\mu' dx', \tag{G.3}$$

$$\beta_j (x, \mu) = \frac{\sum_{k=1}^{n} A_k \varphi_k (x, \mu) q_{kj}}{\sum_{k=1}^{n} A_k q_{kj}^2} \ , \qquad q_{ij} = \frac{\sum_{k=1}^{n} A_k a_{ik} q_{kj}}{\sum_{k=1}^{n} A_k q_{kj}^2} \ . \tag{G.4}$$

Relations (62), (64)-(65) are easily obtained from expressions (G.2)-(G.4) in the standard transition to the variable z, taking into account (57), as well as by replacing the integrals of the variables x and z in the double integral (G.3).

Appendix H

To obtain the relation (66), first substitute the expansion (54) into the expression (1), then it is not difficult to see that

$$\varphi_i (x, \mu) \equiv \int_{-\infty}^{+\infty} \varphi (x'; x, \mu) \, \alpha_i (x') \, dx'. \tag{H.1}$$

By substituting the expression

$$\varphi (x', x; \mu) = \delta (x' - x) + \int_0^1 \rho (x, \mu; x', \mu') \, d\mu' \ , \tag{H.2}$$

given in (2), we get

$$\varphi_i (x, \mu) = \alpha_i (x) + \int_{-\infty}^{+\infty} \int_0^1 \rho (x, \mu; x', \mu') \, \alpha_i (x') \, d\mu' dx' \ . \tag{H.3}$$

Taking into account expressions (4)-(5) turns (H.3) into a ratio (see Pikichyan (2023b, 2024))

$$\varphi_i (x, \mu) = \alpha_i (x) + \sum_{k=1}^{n} \nu_k \beta_k (x, \mu) \int_{-\infty}^{+\infty} \int_0^1 \frac{\beta_k (x', \mu') \, \alpha_i (x')}{\frac{\alpha(x)}{\mu} + \frac{\alpha(x')}{\mu'}} \frac{d\mu'}{\mu'} dx' \ . \tag{H.4}$$

Proceeding in a standard way here: moving from the variable μ to the z variable, then using explicit expressions (18) and (57) taking into account the orthonormalization condition $\int_{-\infty}^{+\infty} \vartheta (x) \, \alpha_k (x) \, \alpha_s (x) \, dx = \delta_{ks}$ of values $\alpha_i (x)$ with the weight $\vartheta (x)$, swapping the integrals, it is not difficult to obtain the relations (66)-(68).

doi: https://doi.org/10.52526/25792776-24.71.2-275

Communications of BAO, Vol. 71, Issue 2, 2024, pp. 289-306

A deformation of Master-Space and inertia effects within the theory of Master Space-Teleparallel Supergravity

G.Ter-Kazarian*

Byurakan Astrophysical Observatory, Byurakan, Aragatsotn Province, Armenia

Abstract

In the framework of the theory of *Master space*-Teleparallel Supergravity ($\widetilde{MS}_p$-TSG) (Ter-Kazarian, 2024b), having the gauge *translation* group in tangent bundle, in present article we address the theory of a general deformation of the flat MS_p induced by external force exerted on a particle, subject to certain rules. Our idea is that the *universality* of gravitation and inertia attribute to the single mechanism of origin from geometry but having a different nature. We have ascribed, therefore, the inertia effects to the geometry itself but as having a nature other than 4D Riemannian space. We consider a general smooth deformation map $\Omega(\varrho):\underline{M}_2\to\mathcal{M}_2$ in terms of the *world - deformation* tensor Ω, the flat MS_p, and a general smooth differential 2D-manifold, $\mathcal{M}_2$. The Ω is a function of *local rate*, $\varrho(\underline{x})$, of instantaneously change of the velocity of massive test particle under the unbalanced external net force. A general deformation is composed of the two subsequent deformations $\overset{\circ}{\Omega}$: $\underline{M}_2\to\underline{V}_2$ and $\breve{\Omega}:\underline{V}_2\to\mathcal{M}_2$, where $\underline{V}_2$ is the 2D semi-Riemannian space, $\overset{\circ}{\Omega}$ and $\breve{\Omega}$ are the corresponding world deformation tensors. In the simple case of $\Omega=\overset{\circ}{\Omega}$, $\breve{\Omega}^{\mu}{}_{\nu}\equiv\delta^{\mu}_{\nu}$, we have to write the rate, ϱ, in terms of the Lorentz spinors $(\underline{\theta},\underline{\bar{\theta}})$ referred to $\underline{M}_2$, and period of superoscillations (τ). The latter can be defined as a function of proper time ($\underline{s}$) induced by the *world-deformation* tensor $\Omega(\underline{s})$. In this way we show that the occurrence of the, so-called, *absolute* and *inertial* accelerations, and that the *inertial* force as well, are obviously caused by a general deformation of the flat MS_p. Therewith the *relative* acceleration in 4D Minkowski space, M_4, (both magnitude and direction, in Newton's terminology), to the contrary, has nothing to do with a deformation of $\underline{M}_2$ and, thus, it cannot produce the inertia effects. We calculate the relativistic inertial force in Minkowski, semi-Riemannian and post Riemannian spaces. This furnishes a justification for the introduction of the Weak Principle of Equivalence (WPE). We discuss the inertia effects beyond the hypothesis of locality with special emphasis on deformation $\underline{M}_2\longrightarrow\underline{V}_2^{(\varrho)}$, which essentially improves the standard framework. Whereas we derive the tetrad fields as a function of ϱ, describing corresponding *fictitious graviton.* The *fictitious gravitino* will be arisen under infinitesimal transformations of local supersymmetry.

Keywords: *Teleparallel Supergravity–Spacetime Deformation–Inertia Effects*

1. Introduction

Using Palatini's formalism extended in a plausible fashion to the $\widetilde{MS}_p$-Supergravity (Ter-Kazarian, 2023c, 2024c), in a recent papers (Ter-Kazarian, 2024b) we reinterpret a flat $\widetilde{MS}_p$-SG theory with Weitzenböck torsion as the quantum field theory of $\widetilde{MS}_p$-TSG, having the gauge *translation* group in tangent bundle. For a benefit of the reader as a guiding principle to make the rest of paper understandable, we necessarily recount succinctly some of the highlights behind of $\widetilde{MS}_p$-SG and $\widetilde{MS}_p$-TSG in the Appendix.

A quantum field theory of $\widetilde{MS}_p$-Supergravity is a *local* extension of the theory of *global Master space* (MS_p)-SUSY (Ter-Kazarian, 2023a, 2024a). The latter, in turn, is the microscopic theory of: 1) standard Lorentz code of motion (SLC), 2) deformed Lorentz symmetry and 3) deformed geometry induced by foamy effects at the Planck scale, and tested in ultra-high energy experiments. Therewith we derive the SLC in a new perspective of global double MS_p-SUSY transformations. The MS_p-SUSY provides valuable theoretical clue for a complete revision of our standard ideas about the Lorentz code of motion to be now referred to as the *intrinsic* property of a particle. This is a result of the first importance for a really comprehensive theory of inertia. The MS_p-SUSY theory, among other things, actually explores the first part of the phenomenon of

*gago_50@yahoo.com

doi: https://doi.org/10.52526/25792776-24.71.2-289

inertia, which refers to *inertial uniform motion along rectilinear timelike world lines.* This developments are in many ways exciting, yet mysteries remain, and some of deeper issues are still unresolved, such as those which relate the inertial effects. This comprises a second half of phenomenon of inertia, which stood one of the major unattained goals since the time traced back to the works developed by Galileo and Newton. The *principle of inertia* they developed is one of the fundamental principles of classical mechanics. This governs the *uniform motion* of a body and describes how it is affected by applied forces. Ever since, there is an ongoing quest to understand the reason for the universality of the gravitation and inertia, attributing to the WPE, which establishes the independence of free-fall trajectories of the internal composition and structure of bodies. However, the nature of the relationship of gravity and inertia continues to elude us and, beyond the WPE, there has been little progress in discovering their true relation. Viewed from the perspective of GR theory, the fictitious forces are attributed to geodesic motion in spacetime. Physicists have gone a long way in developing this theory. But nothing is reliable and such efforts do not make sense. Indeed, as Einstein emphasized later (Bondi, 1952, Sciama, 1953), GR is failed to account for the inertial properties of matter, so that an adequate theory of inertia is still lacking.

We reinterpret the flat $\widetilde{MS}_p$-SG theory with Weitzenböck torsion as the theory of $\widetilde{MS}_p$-TSG having the gauge *translation* group in tangent bundle. An important property of Teleparallel Gravity is that its spin connection is related only to the inertial properties of the frame, not to gravitation. Whereas the Hilbert action vanishes and the gravitino action loses its spin connections, so we find that the accelerated reference frame has Weitzenböck torsion induced by gravitinos. The action of $\widetilde{MS}_p$-TSG is invariant under local translations, under local super symmetry transformations and by construction is invariant under local Lorentz rotations and under diffeomorphisms. So that this action is invariant under the Poincaré supergroup and under diffeomorphisms. The Weitzenböck connection defines the acceleration through force equation, with torsion (or contortion) playing the role of force. Thus, the results obtained clearly show that the frames expressing linear and rotational acceleration can be interpreted via torsion as an invariant property of spacetime.

In the present article, our idea is that the *universality* of gravitation and inertia attribute to the single mechanism of origin from geometry but having a different nature. We have ascribed, therefore, the inertia effects to the geometry itself but as having a nature other than 4D Riemannian space (for earlier version see (Ter-Kazarian, 2012)). We show that in the $\widetilde{MS}_p$-TSG theory the occurrence of the *absolute* and *inertial* accelerations, and the *inertial* force are obviously caused by a general deformation of the flat MS_p. While the *relative* acceleration (both magnitude and direction, in Newton's terminology) in 4D Minkowski space, M_4 , to the contrary, has nothing to do with a deformation of $\underline{M}_2$ and, thus, it cannot produce the inertia effects. We calculate the relativistic inertial force in Minkowski, semi-Riemannian and post Riemannian spaces. Despite of totally different and independent sources of gravitation and inertia, this establishes the independence of free-fall trajectories of the mass, internal composition and structure of bodies. This furnishes a justification for the introduction of the Weak Principle of Equivalence (WPE). We discuss the inertia effects by going beyond the hypothesis of locality with special emphasis on deformation $\underline{M}_2 \longrightarrow \underline{V}_2^{(\varrho)}$, which essentially improves the standard framework.

With this perspective in sight, we will proceed according to the following structure. To start with, in Section 2 we briefly review a general deformation of the flat MS_p. Section 3 is devoted to the model building in background M_4. In Section 4 we discuss the inertia effects beyond the hypothesis of locality with special emphasis on deformation $\underline{M}_2 \longrightarrow \underline{V}_2^{(\varrho)}$, which essentially improves the standard framework. Whereas we derive the tetrad fields describing *fictitious graviton.* In Section 5 we calculate the inertial force in the semi-Riemannian space V_4. In Section 6 we discuss the inertial effects in the background post Riemannian geometry. We bring the concluding remarks in section 7. In Appendix, we will briefly review the theories of $\widetilde{MS}_p$-SG and $\widetilde{MS}_p$-TSG. For brevity, whenever possible undotted and dotted spinor indices often can be ruthlessly suppressed without ambiguity. Unless indicated otherwise, the natural units, $h = c = 1$ are used throughout.

2. A general deformation of the flat MS_p

In this section we will briefly discuss a general deformation of the flat MS_p induced by external force exerted on a particle, to show that in the $\widetilde{MS}_p$-SG theory the occurrence of the so-called *absolute* and *inertial* accelerations, as well as *inertial effects* (fictitious gravity) are obviously caused by this. For brevity reason, we shall forbear here to review the mathematical aspects of the spacetime deformation technique.

doi: https://doi.org/10.52526/25792776-24.71.2-289

We invite the interested reader to consult (Ter-Kazarian, 2011, 2012) for a more rigorous formulation with various applications. We now extend, for the self-contained arguments, just necessary geometrical ideas of this framework without going into the subtleties, as applied to the 2D deformation $\underline{M}_2 \to \mathcal{M}_2$. In the framework of spacetime deformation theory (Ter-Kazarian, 2011), we consider a smooth deformation map

$$\Omega(\varrho) : \underline{M}_2 \to \mathcal{M}_2, \tag{1}$$

written in terms of the *world - deformation* tensor Ω, the flat MS_p, and a general smooth differential 2D-manifold, $\mathcal{M}_2$. The *world-deformation* tensor, $\Omega(\varrho)$, is a function of *local rate*, $\varrho(\underline{x})$, of instantaneously change of the velocity ($\underline{v}^{(\pm)}$) of massive test particle under the unbalanced external net force. The tensor, $\Omega(\varrho)$, can be written in the form

$$\Omega(\varrho) = D(\varrho)\,\mathcal{Y}(\varrho) \quad (\Omega^{\underline{m}}_{\underline{n}}(\varrho) = D^{\underline{m}}_{\underline{\mu}}(\varrho)\mathcal{Y}^{\underline{\mu}}_{\underline{n}}(\varrho)), \tag{2}$$

provided with the invertible distortion matrix $D\,(D^{\underline{m}}_{\underline{\mu}})$ and the tensor $\mathcal{Y}\,(\mathcal{Y}^{\underline{\mu}}_{\underline{n}} = \partial\,\widetilde{x}^{\underline{\mu}}/\partial\,\underline{x}^{\underline{n}})$. The principle foundation of a world-deformation tensor comprises the following two steps. 1) The basis vectors $\underline{e}_{(m)}$, at any point $p \in \underline{M}_2$ is undergone the deformation transformations by means of the matrix $D(\varrho)$:

$$e_{\underline{\mu}}(\varrho) = D^{\underline{m}}_{\underline{\mu}}(\varrho) e_{\underline{m}}. \tag{3}$$

2) A diffeomorphism

$$\widetilde{\underline{x}}^{\underline{\mu}}(\underline{x}) : \underline{M}_2 \to \mathcal{M}_2 \tag{4}$$

is constructed by seeking a new holonomic coordinates $\widetilde{\underline{x}}^{\underline{\mu}}(\underline{x})$ as the solutions of the first-order partial differential equations:

$$e_{\underline{\mu}}\,\mathcal{Y}^{\underline{\mu}}_{\underline{m}} = \Omega_{\underline{m}}^{\ \underline{n}}\,\underline{e}_{\underline{n}}, \tag{5}$$

where the conditions of integrability,

$$\partial_{\underline{m}}\,\mathcal{Y}^{\underline{\mu}}_{\underline{n}} = \partial_{\underline{n}}\,\mathcal{Y}^{\underline{\mu}}_{\underline{m}}, \tag{6}$$

and non-degeneracy,

$$det|\mathcal{Y}^{\underline{\mu}}_{\underline{m}}| \neq 0, \tag{7}$$

necessarily hold (Pontryagin, 1984, et al., 1986). Therefore, the $\vartheta \equiv d\underline{x}^{\underline{m}}$ is undergone the following deformation transformations:

$$\vartheta^{\underline{\mu}} = \mathcal{Y}^{\underline{\mu}}_{\underline{m}}\,\underline{\vartheta}^{\underline{m}} = \Omega_{\underline{m}}^{\ \underline{n}}\, < e^{\underline{\mu}}, \underline{e}_{\underline{n}} > \underline{\vartheta}^{\underline{m}}. \tag{8}$$

The deformation (1) is composed of the two subsequent deformations

$$\overset{\circ}{\Omega}\!: \underline{M}_2 \to \underline{V}_2 \tag{9}$$

and

$$\breve{\Omega} : \underline{V}_2 \to \mathcal{M}_2, \tag{10}$$

where $\underline{V}_2$ is the 2D semi-Riemannian space, $\overset{\circ}{\Omega}$ and $\breve{\Omega}$ are the corresponding world deformation tensors. In what follows, we consider the simple spacetime deformation map,

$$\Omega(\varrho) : \underline{M}_2 \to \underline{V}_2 \quad (\Omega = \overset{\circ}{\Omega},\ \breve{\Omega}^{\mu}{}_{\nu} \equiv \delta^{\mu}_{\nu}). \tag{11}$$

The quantities denoted by wiggles here refer to $\underline{V}_2$, but the quantities referring to flat $\underline{M}_2$ space are left, as before, without wiggles. In this case the norm of the infinitesimal displacement on the general smooth differential 2D-manifold $\underline{V}_2$ can be written in terms of the anholonomic spacetime structures:

$$i\tilde{d}(\varrho) = \Omega_b{}^a(\varrho)\,\underline{e}_{\,a}\underline{e}^b \equiv \pi_b{}^{\tilde{c}}(\varrho)\,\pi_{\tilde{c}}{}^a(\varrho)\,\underline{e}_{\,a}\underline{e}^b\ \in\ \underline{V}_2. \tag{12}$$

The matrices, $\pi(\widetilde{\underline{x}})(\varrho) := (\pi_{\tilde{c}}{}^a)(\varrho)$, yield local tetrad deformations

$$e_{\tilde{c}}(\varrho) = \pi_{\tilde{c}}{}^a(\varrho)\,\underline{e}_a, and e^{\tilde{c}}(\varrho) = \pi^{\tilde{c}}{}_b(\varrho)\,\underline{e}^b. \tag{13}$$

They are referred to as the *first deformation matrices*, while the matrices

$$\gamma_{\tilde{c}\tilde{d}}(\widetilde{\underline{x}}) = {}^{*}o_{ab}\,\pi_{\tilde{c}}{}^a(\widetilde{\underline{x}})\,\pi_{\tilde{d}}{}^b(\widetilde{\underline{x}}), \tag{14}$$

doi: https://doi.org/10.52526/25792776-24.71.2-289

are *second deformation matrices.* The matrices,

$$\pi^{a}{}_{\tilde{c}}(\underset{\sim}{x}) \in GL(2,R)\,\forall\,\tilde{x}, \tag{15}$$

in general, give rise to right cosets of the Lorentz group, i.e. they are the elements of the quotient group

$$GL(2,R)/SO(1,1), \tag{16}$$

because the Lorentz matrices, L^r_s, $(r,s=1,0)$ leave the Minkowski metric invariant. A right-multiplication of $\pi_{\tilde{c}}{}^{a}(\underset{\sim}{x})$ by a Lorentz matrix gives an other deformation matrix.

The invertible distortion matrix $D(\varrho)$ is given by a constitutive ansätz:

$$D(\varrho) = \begin{pmatrix} 1 & -\varrho\underline{v}^{(-)} \\ \varrho\underline{v}^{(+)} & 1 \end{pmatrix}, \tag{17}$$

where $\underline{\mu} = (\tilde{\pm})$, $\underline{m} = (\pm)$. These transformations imply a violation $(e^2_{(\tilde{\pm})}(\varrho) \neq 0)$ of the condition $(\underline{e}^{\,2}_{(\pm)} = 0)$ of null vectors. The components of metric tensor in $\underline{V}_2$, by virtue of (17), read

$$\begin{array}{l} g_{\tilde{0}\tilde{0}} = (1+\frac{\varrho v^{\underline{1}}}{\sqrt{2}})^2 - \frac{\varrho^2}{2}, \quad g_{\tilde{1}\tilde{1}} = -(1-\frac{\varrho v^{\underline{1}}}{\sqrt{2}})^2 + \frac{\varrho^2}{2}, \\ g_{\tilde{1}\tilde{0}} = g_{\tilde{0}\tilde{1}} = -\sqrt{2}\varrho. \end{array} \tag{18}$$

In general, we parameterize the world-deformation tensor with parameters ν_1 and ν_2 as follows:

$$\begin{array}{l} \Omega^{\;(+)}_{(+)} = \Omega^{\;(-)}_{(-)} = \nu_1(1+\nu_2\,\overline{\varrho}^2), \\ \Omega^{\;(-)}_{(+)} = -\nu_1(1-\nu_2)\varrho\underline{v}^{(-)}, \\ \Omega^{\;(+)}_{(-)} = \nu_1(1-\nu_2)\varrho\underline{v}^{(+)}, \end{array} \tag{19}$$

where $\overline{\varrho}^2 = \underline{v}^2\varrho^2$, $\underline{v}^2 = \underline{v}^{(+)}\underline{v}^{(-)} = 1/2\gamma^2_{\underline{1}}$, and $\gamma_{\underline{1}} = (1-(v^{\underline{1}})^2)^{-1/2}$. The relation (8) can then be recast in an alternative form

$$\vartheta = \nu_1 \begin{pmatrix} 1 & -\nu_2\varrho\,\underline{v}^{(+)} \\ \nu_2\varrho\,\underline{v}^{(-)} & 1 \end{pmatrix} \underline{\vartheta}. \tag{20}$$

The transformation equation for the coordinates, according to (20), becomes

$$\vartheta^{(\tilde{\pm})} = \nu_1\,(\underline{\vartheta}^{(\pm)} \mp \nu_2\,\varrho\underline{v}^{(\pm)}\underline{\vartheta}^{(\mp)}) = \nu_1\,(\underline{v}^{(\pm)} \mp \nu_2\,\varrho\underline{v}^2)d\underline{x}^{\underline{0}}, \tag{21}$$

which in turn yields the general transformation equations for spatial and temporal coordinates. The latter give a reasonable change at low velocities $\underline{v}^{\underline{1}} \simeq 0$, as

$$d\widetilde{\underline{x}^{\underline{0}}} = \nu_1\,d\underline{x}^{\underline{0}}, \quad d\underset{\sim}{\tilde{x}}^{\underline{1}} \simeq \nu_1\,(d\underline{x}^{\underline{1}} - \frac{\nu_2\varrho}{\sqrt{2}}d\underline{x}^{\underline{0}}). \tag{22}$$

In high velocity limit

$$\underline{v}^{\underline{1}} \simeq 1, \quad \overline{\varrho} \simeq 0, \quad d\underline{x}^{(-)} = \underline{v}^{(-)}d\underline{x}^{\underline{0}} \simeq 0,\; \underline{v}^{(+)} \simeq \underline{v} \simeq \sqrt{2}, \tag{23}$$

we have

$$d\widetilde{\underline{x}^{\underline{0}}} = \nu_1\,d\underline{x}^{\underline{0}} \simeq \nu_1\,d\underline{x}^{\underline{1}} \simeq d\underset{\sim}{\tilde{x}}^{\underline{1}}. \tag{24}$$

To this end, *the inertial effects become zero.*

Our idea here is this. Suppose a second observer, who makes measurements using a frame of reference $\widetilde{S}_{(2)}$ which is held stationary in $\underline{V}_2$, uses for the test particle the spacetime coordinates $\underset{\sim}{\tilde{x}}^{r}(\tilde{x}^{\underline{0}}, \tilde{x}^{\underline{1}})$. Then the norm of the infinitesimal displacement on $\underline{V}_2$ can be rewritten as

$$i\widetilde{d} \equiv d\underset{\sim}{\tilde{s}} = \tilde{e}_{\underline{0}}d\tilde{x}^{\underline{0}} + \tilde{e}_{\underline{1}}d\tilde{x}^{\underline{1}}, \tag{25}$$

where $\tilde{e}_{\underline{0}}$ and $\tilde{e}_{\underline{1}}$ are, respectively, the temporal and spatial basis vectors. The difference of the line elements $d\underline{s} \in \underline{M}_2$ and $d\underset{\sim}{\tilde{s}} \in \underline{V}_2$ can be interpreted in naive way by the second observer that he is subject to gravity, so that he thinks he is in the curved space which is due to the deformation of flat space $\underline{M}_2$. However, this difference with equal justice can be reinterpreted by him as a definite criterion for the character of his own state of being in the *absolute* accelerated local non-inertial frame in $\underline{M}_2$, rather than to any quality

doi: https://doi.org/10.52526/25792776-24.71.2-289

of a deformation of $\underline{M}_2$. That is, the (22) becomes conventional transformation equations to accelerated ($a_{net} \neq 0$) axes if we assume

$$\frac{d(\nu_2 \varrho)}{\sqrt{2} d\underline{x}^0} = a_{net} \quad \text{and} \quad \nu_1(\underline{v}_1 \simeq 0) = 1, \tag{26}$$

where a_{net} is the magnitude of proper net acceleration. We may calculate a magnitude a_{net} from the embedding relations (104), by considering a test particle accelerated in M_4, under an unbalanced net force other than gravitational. The $\vec{a}_{net}$ will be a local net 3-acceleration of an arbitrary observer with proper linear 3 - acceleration $\vec{a}$ and proper 3-angular velocity $\vec{\omega}$ in M_4 measured in the rest frame

$$\vec{a}_{net} = \frac{d\vec{u}}{ds} = \vec{a} \wedge \vec{u} + \vec{\omega} \times \vec{u}, \tag{27}$$

where $\mathbf{u}$ is the 4-velocity. A magnitude of $\vec{a}_{net}$ can be computed as the simple invariant of the absolute value $|\frac{d\mathbf{u}}{ds}|$ as measured in rest frame:

$$|\mathbf{a}| = |\frac{d\mathbf{u}}{ds}| = \left(\frac{du^l}{ds}, \frac{du_l}{ds}\right)^{1/2}. \tag{28}$$

The dynamical aspects of particle mechanics involve derivatives with respect to proper time along the particle worldline, which is the line element written in frame (139). Then the very concept of the local *absolute acceleration* (in Newton's terminology) can be introduced using the Fermi-Walker transported frames

$$\vec{a}_{abs} := \vec{e}_{\underline{1}} \frac{d\varrho}{\sqrt{2} d\underline{s}} = \vec{e}_{\underline{1}}\, \underline{a} = \vec{n}\, |\mathbf{a}|, \tag{29}$$

where the axis $\vec{e}_{\underline{1}}$ of the system $S_{(2)}$, according to embedding map (88), lies along the net 3-acceleration,

$$\vec{e}_{\underline{1}} = \vec{n} = \frac{\vec{a}_{net}}{|\vec{a}_{net}|}. \tag{30}$$

The (21), in general, gives

$$\frac{d^2 \underline{\widetilde{x}}^{(\pm)}}{d(\underline{x}^0)^2} = \mp \frac{1}{2\gamma_{\underline{1}}^2} \sqrt{2} d\underline{x}^0. \tag{31}$$

Then a magnitude of so-called an *inertial acceleration*

$$a_{in} := \frac{d^2 \underline{\widetilde{x}}^1}{d\underline{\widetilde{s}}^2} = \Gamma^{\underline{1}}_{\underline{\widetilde{\mu}}\underline{\widetilde{\nu}}}(\varrho) \frac{d\underline{\widetilde{x}}^{\widetilde{\mu}}}{d\underline{\widetilde{s}}} \frac{d\underline{\widetilde{x}}^{\widetilde{\nu}}}{d\underline{\widetilde{s}}}, \tag{32}$$

where $\Gamma^{\underline{1}}_{\underline{\widetilde{\mu}}\underline{\widetilde{\nu}}}(\varrho)$ are the Christoffel symbols constructed by the metric (18), reads

$$a_{in} = \frac{1}{\sqrt{2}} \left(\frac{d^2 \underline{\widetilde{x}}^{(+)}}{d\underline{\widetilde{s}}^2} - \frac{d^2 \underline{\widetilde{x}}^{(-)}}{d\underline{\widetilde{s}}^2} \right) = -\frac{1}{\Omega^2 \gamma_{\underline{1}}} \frac{d(\nu_2 \varrho)}{\sqrt{2} d\underline{s}}. \tag{33}$$

In particular case of $\nu_1 = \nu_2 = 1$, the world-deformation tensor is simplified to

$$\Omega_{\underline{m}}^{\underline{n}} = \Omega(\overline{\varrho}) \delta_{\underline{m}}^{\underline{n}}, \quad \Omega(\overline{\varrho}) = 1 + \overline{\varrho}^2. \tag{34}$$

In this case a deformed line element becomes $d\underline{\widetilde{s}}^2 = \Omega^2(\overline{\varrho})\, d\underline{s}^2$. These, combined with (33), yield a relationship of the magnitudes of *absolute* and *inertial* accelerations

$$\Omega^2(\overline{\varrho})\, \gamma_{\underline{1}}\, a_{in} = -\frac{d\varrho}{\sqrt{2} d\underline{s}} = -a_{abs}. \tag{35}$$

Thus we show that a general deformation of MS_p is the origin of the local *absolute* ($\vec{a}_{abs}$) and *inertial* ($\vec{a}_{in}$) accelerations, with the following key relation between them:

$$\Omega^2(\overline{\varrho})\, \gamma_{\underline{1}}\, \vec{a}_{in} = -\vec{a}_{abs}. \tag{36}$$

In Section 3, we will study the inertial effects stemming from (36). Now by means of (109) and (110), we have to write the rate, ϱ, in terms of the Lorentz spinors $(\underline{\theta}, \underline{\bar{\theta}})$, and period of superoscillations (τ):

$$\varrho(\underline{\theta}, \underline{\bar{\theta}}, \tau) = \sqrt{2}(\underline{\widetilde{v}} - \sqrt{2} v_c) = 2\sqrt{2}(\underline{\theta}_1\, \underline{\bar{\theta}}_1 \underline{\theta}_2\, \underline{\bar{\theta}}_2)^{1/2} \frac{d\tau}{d\underline{\widetilde{s}}}. \tag{37}$$

A period of superoscillations, $\tau(\underline{\widetilde{s}})$, can then be determined as a function of proper time $(\underline{\widetilde{s}})$ induced by the *world-deformation* tensor $\Omega(\underline{\widetilde{s}})$:

$$\tau(\underline{\widetilde{s}}) = 4^{-1} (\underline{\theta}_1\, \underline{\bar{\theta}}_1 \underline{\theta}_2\, \underline{\bar{\theta}}_2)^{-1} \int_0^{\underline{\widetilde{s}}} \sqrt{\Omega(\underline{\widetilde{s}}') - 1}\, d\underline{\widetilde{s}}'. \tag{38}$$

So that the magnitudes of the net and absolute accelerations induced by the $\Omega(\underline{\widetilde{s}})$ read

$$a_{net} = \sqrt{2} v_c\, a_{abs} = \frac{d}{d\underline{s}} \sqrt{\Omega(\underline{\widetilde{s}}) - 1}. \tag{39}$$

doi: https://doi.org/10.52526/25792776-24.71.2-289

3. Model building in background M_4

The (36) provides a quantitative means for the *inertial force* $\vec{f}_{(in)}$:

$$\vec{f}_{(in)} = m\vec{a}_{in} = -\frac{m\,\vec{a}_{abs}}{\Omega^2(\overline{\varrho})\,\gamma_{\underline{1}}} = -m\,\vec{a}_{abs}\frac{\sqrt{2}\underline{v}_c}{(1+\overline{\varrho}^2)^2}, \tag{40}$$

where $\overline{\varrho} = 2\underline{v}_c^2(d\tau/d\widetilde{\underline{s}}) = (1/\gamma_{\underline{1}}^2)(d\tau/d\widetilde{\underline{s}})$. In case of absence of rotation, we may write the local *absolute acceleration* (29) in terms of the relativistic force f^l acting on a particle with coordinates $x^l(s)$:

$$f^l(f^0,\,\vec{f}) = m\frac{d^2x^l}{ds^2} = L^l_k(\vec{v})F^k. \tag{41}$$

Here $F^k(0,\,\vec{F})$ is the force defined in the rest frame of the test particle, $L^l_k(\vec{v})$ is the Lorentz transformation matrix $(i,j=1,2,3)$:

$$L^i_j = \delta_{ij} - (\gamma-1)\frac{v_iv_j}{|\vec{v}|^2}, \quad L^0_i = \gamma v_i, \tag{42}$$

where $\gamma = (1-\vec{v}^2)^{-1/2} = \gamma_{\underline{1}}$. So

$$|\mathbf{a}| = \frac{1}{m}|f^l| = \frac{1}{m}(f^lf_l)^{1/2} = \frac{1}{m\gamma}|\vec{f}|, \tag{43}$$

and hence the (40) and (43) give

$$\vec{f}_{(in)} = -\frac{\sqrt{2}v_c}{\gamma(1+\overline{\varrho}^2)^2}[\vec{F} + (\gamma-1)\vec{n}(\vec{n}\cdot\vec{F})]. \tag{44}$$

At low velocities $|\vec{v}| \simeq 0$ and tiny accelerations $\frac{d\tau}{d\underline{s}} \to 0$ we usually experience, one has $\underline{v}_c(\underline{\theta},\bar{\underline{\theta}},\tau \simeq const) \simeq 0$, and that $\Omega(\overline{\varrho}) \simeq 1$, the (44) is reduced to the conventional non-relativistic law of inertia

$$\vec{f}_{(in)} = -m\vec{a}_{abs} = -\vec{F}. \tag{45}$$

At high velocities $|\vec{v}| \simeq 1$, if $(\vec{n}\cdot\vec{F}) \neq 0$, the inertial force (44) becomes

$$\vec{f}_{(in)} \simeq -\frac{1}{(1+\overline{\varrho}^2)^2\,\gamma}\vec{n}(\vec{n}\cdot\vec{F}), \tag{46}$$

and it vanishes in the limit of the photon ($|\vec{v}| = 1$, $\overline{\varrho}^2 = \gamma^{-4}(d\tau/d\widetilde{\underline{s}}) \to 0$, $m = 0$). Thus, a deformation of $\underline{M}_2$ is the cause of arising the *absolute* and *inertial* accelerations, and the *inertial* force. Whereas the *relative* acceleration in 4D Minkowski space, M_4, (both magnitude and direction, in Newton's terminology), to the contrary, has nothing to do with a deformation of $\underline{M}_2$ and, thus, it cannot produce the inertia effects.

4. Beyond the hypothesis of locality

In standard framework of SR, an assumption is required for the construction of reference frame of an accelerated observer to relate the ideal inertial observers to actual observers that are all noninertial, i.e., accelerated. Therefore, it is a long-established practice in physics to use the hypothesis of locality, see e.g. (Maluf & Faria, 2008, Maluf et al., 2007, Marzlin, 1996, Mashhoon, 2002, 2011, Misner et al., 1973) and references therein, for extension of the Lorentz invariance to accelerated observers in Minkowski space-time. The geometrical structures, referred to a noninertial coordinate frame of accelerating and rotating observer in Minkowski space-time, were computed on the base of the assumption that an accelerated observer is pointwise inertial, which in effect replaces an accelerated observer at each instant with a momentarily comoving inertial observer along its wordline. This assumption is known to be an approximation limited to motions with sufficiently low accelerations, which works out because all relevant length scales in feasible experiments are very small in relation to the huge acceleration lengths of the tiny accelerations we usually experience, therefore, the curvature of the wordline could be ignored and that the differences between observations by accelerated and comoving inertial observers will also be very small. However, it seems quite clear that such an approach is a work in progress, which reminds us of a puzzling underlying reality of inertia, and that it will have to be extended to describe physics for arbitrary accelerated observers. Ever since this question has become a major preoccupation of physicists. The hypothesis of locality represents strict restrictions, because it approximately replaces a noninertial frame of reference $\widetilde{S}_{(2)}$, which is held stationary in the deformed space $\mathcal{M}_2 \equiv \underline{V}_2^{(\varrho)}$ $(\varrho \neq 0)$, where $\underline{V}_2$ is the 2D semi-Riemannian space, with

doi: https://doi.org/10.52526/25792776-24.71.2-289

a continuous infinity set of the inertial frames $\{S_{(2)}, S'_{(2)}, S''_{(2)}, ...\}$ given in the flat $\underline{M}_2\,(\varrho = 0)$. In this situation the use of the hypothesis of locality is physically unjustifiable. Therefore, it is worthwhile to go beyond the hypothesis of locality with special emphasis on deformation $\underline{M}_2 \longrightarrow \underline{V}_2^{(\varrho)}$, which we might expect will essentially improve the standard framework.

Following (Mashhoon, 2002, Misner et al., 1973), let us to introduce a geodesic coordinate system - the coordinates relative to the accelerated observer (the laboratory coordinates), in the neighborhood of the accelerated path. We choose the zeroth leg of the frame, $e_{\tilde{0}}$, as before, to be the unit vector $\mathbf{u}$ that is tangent to the worldline at a given event $x^\mu(s)$, where (s) is a proper time measured along the accelerated path by the standard (static inertial) observers in the underlying global inertial frame. In analogy with the Faraday tensor (Maluf & Faria, 2008, Maluf et al., 2007, Marzlin, 1996, Mashhoon, 2002, 2011), one can identify the antisymmetric acceleration tensor

$$\Phi_{ab} \longrightarrow (-\mathbf{a},\, \omega), \tag{47}$$

with $\mathbf{a}(s)$ as the translational acceleration

$$\Phi_{0i} = -a_i, \tag{48}$$

and $\omega(s)$ as the frequency of rotation of the local spatial frame with respect to a nonrotating (Fermi- Walker transported) frame

$$\Phi_{ij} = -\varepsilon_{ijk}\,\omega^k. \tag{49}$$

The invariants constructed out of Φ_{ab} establish the acceleration scales and lengths. The hypothesis of locality holds for huge proper acceleration lengths. Suppose the displacement vector $z^\mu(s)$ represents the position of the accelerated observer. According to the hypothesis of locality, at any time (s) along the accelerated worldline the hypersurface orthogonal to the worldline is Euclidean space and we usually describe some event on this hypersurface ("local coordinate system") at x^μ to be at $\widetilde{x}^\mu$, where x^μ and $\widetilde{x}^\mu$ are connected via $\widetilde{x}^{\,0} = s$ and

$$x^\mu = z^\mu(s) + \widetilde{x}^{\,i}\,\bar{e}^{\,\mu}_{\,\hat{i}}(s). \tag{50}$$

The standard metric of semi-Riemannian 4D background space $V_4^{(0)}$ in noninertial system of the accelerating and rotating observer, computed on this base.

Then the hypothesis of locality leads to the 2D semi-Riemannian space, $V_{\underline{2}}^{(0)}$, with the incomplete metric $\widetilde{g}(\varrho = 0)$:

$$\widetilde{g} = \left[(1 + \widetilde{x}^{\,\underline{1}}\widetilde{\varphi}_0)^2 - (\widetilde{x}^{\,\underline{1}}\widetilde{\varphi}_1)^2\right] d\widetilde{x}^{\,\underline{0}} \otimes d\widetilde{x}^{\,\underline{0}} - 2\,(\widetilde{x}^{\,\underline{1}}\widetilde{\varphi}_1)\, d\widetilde{x}^{\,\underline{1}} \otimes d\widetilde{x}^{\,\underline{0}} - d\widetilde{x}^{\,\underline{1}} \otimes d\widetilde{x}^{\,\underline{1}}, \tag{51}$$

provided,

$$\widetilde{x}^{\,\underline{1}}\widetilde{\varphi}_0 = \widetilde{x}^{\,i}\,\Phi^0_i, \quad \widetilde{x}^{\,\underline{1}}\widetilde{\varphi}_1 = \widetilde{x}^{\,i}\,\Phi^j_i\,\widetilde{e}^{\,-1}_j. \tag{52}$$

Therefore, our strategy now is to deform the metric (51) by carrying out an additional deformation of semi-Riemannian 4D background space

$$V_4^{(0)} \longrightarrow V_4^{(\varrho)}, \tag{53}$$

in order it becomes on the same footing with the complete metric $\widetilde{g}\quad(\varrho \neq 0)$ (18) of the distorted space $\underline{V}_2^{(\varrho)}$. Let the Latin letters $\hat{r}, \hat{s}, ... = 0, 1$ be the anholonomic indices referred to the anholonomic frame $e_{\hat{r}} = e^{\tilde{s}}{}_{\hat{r}}\,\partial_{\tilde{s}}$, defined on the $\underline{V}_2^{(\varrho)}$, with $\partial_{\tilde{s}} = \partial/\partial\,\widetilde{x}^{\underline{s}}$ as the vectors tangent to the coordinate lines. So, a smooth differential 2D-manifold $\underline{V}_2^{(\varrho)}$ has at each point $\widetilde{x}^{\underline{s}}$ a tangent space $\widetilde{T}_{\widetilde{\underline{x}}}\underline{V}_2^{(\varrho)}$, spanned by the frame, $\{e_{\hat{r}}\}$, and the coframe members $\vartheta^{\hat{r}} = e_{\underline{s}}{}^{\hat{r}}\, d\widetilde{x}^{\underline{s}}$, which constitute a basis of the covector space $\widetilde{T}^{\star}_{\widetilde{\underline{x}}}\underline{V}_2^{(\varrho)}$. All this nomenclature can be given for $\underline{V}_2^{(0)}$ too. Then, we may compute corresponding vierbein fields $\widetilde{e}_r{}^{\hat{s}}$ and $e_r{}^{\hat{s}}$ from the equations

$$g_{\tilde{r}\tilde{s}} = \widetilde{e}_{\tilde{r}}{}^{\hat{r}'}\,\widetilde{e}_{\tilde{s}}{}^{\hat{s}'}\,o_{\hat{r}'\hat{s}'}, \quad g_{\tilde{r}\tilde{s}}(\varrho) = e_{\tilde{r}}{}^{\hat{r}'}(\varrho)\,e_{\tilde{s}}{}^{\hat{s}'}(\varrho)\,o_{\hat{r}'\hat{s}'}, \tag{54}$$

with $\widetilde{g}_{rs}$ (51) and $g_{\tilde{r}\tilde{s}}(\varrho)$ (18). Hence

$$\begin{aligned} &\widetilde{e}_{\tilde{0}}{}^{\hat{0}} = 1 + \vec{a}\cdot\vec{\widetilde{x}}, \quad \widetilde{e}_{\tilde{0}}{}^{\hat{1}} = \vec{\omega}\wedge\vec{\widetilde{x}}, \quad \widetilde{e}_{\tilde{1}}{}^{\hat{0}} = 0, \quad \widetilde{e}_{\tilde{1}}{}^{\hat{1}} = 1, \\ &e_{\tilde{0}}{}^{\hat{0}}(\varrho) = 1 + \tfrac{\varrho v_1}{\sqrt{2}}, \quad e_{\tilde{0}}{}^{\hat{1}}(\varrho) = \tfrac{\varrho}{\sqrt{2}}, \quad e_{\tilde{1}}{}^{\hat{0}}(\varrho) = -\tfrac{\varrho}{\sqrt{2}}, \quad e_{\tilde{1}}{}^{\hat{1}}(\varrho) = 1 - \tfrac{\varrho v_1}{\sqrt{2}}. \end{aligned} \tag{55}$$

A deformation (53) is equivalent to a straightforward generalization of (50) as

$$x^\mu \longrightarrow x^\mu_{(\varrho)} = z^\mu_{(\varrho)}(s) + \widetilde{x}^{\,i}\,e^{\mu}{}_{\hat{i}}(s), \tag{56}$$

doi: https://doi.org/10.52526/25792776-24.71.2-289

provided, as before, $\widetilde{x}^{\mu}$ denotes the coordinates relative to the accelerated observer in 4D background space $V_4^{(\varrho)}$. A displacement vector from the origin is then

$$dz^{\mu}_{\varrho}(s) = e^{\mu}{}_{\hat{0}}(\varrho)\, d\widetilde{x}^{0}. \tag{57}$$

Inverting $e_r{}^{\hat{s}}(\varrho)$ (55), we obtain

$$e^{\mu}{}_{\hat{a}}(\varrho) = \pi_{\hat{a}}{}^{\hat{b}}(\varrho)\, \overline{e}^{\mu}{}_{\hat{b}}, \tag{58}$$

where

$$\begin{array}{l} \pi^{\hat{0}}_{\hat{0}}(\varrho) \equiv (1+\frac{\varrho^2}{2\gamma^2_{\underline{1}}})^{-1}(1-\frac{\varrho v_{\underline{1}}}{\sqrt{2}})\,(1+\vec{a}\cdot\vec{\widetilde{x}}), \quad \pi^{\hat{i}}_{\hat{0}}(\varrho) \equiv -(1+\frac{\varrho^2}{2\gamma^2_{\underline{1}}})^{-1}\frac{\varrho}{\sqrt{2}}\,\widetilde{e}^{i}\,(1+\vec{a}\cdot\vec{\widetilde{x}}), \\ \pi^{\hat{0}}_{\hat{i}}(\varrho) \equiv (1+\frac{\varrho^2}{2\gamma^2_{\underline{1}}})^{-1}\left[(\vec{\omega}\wedge\vec{\widetilde{x}})(1-\frac{\varrho v_{\underline{1}}}{\sqrt{2}})-\frac{\varrho}{\sqrt{2}}\right]\widetilde{e}_i^{-1}, \quad \pi^{\hat{j}}_{\hat{i}}(\varrho) = \delta^{j}_{i}\,\pi(\varrho), \\ \pi(\varrho) \equiv (1+\frac{\varrho^2}{2\gamma^2_{\underline{1}}})^{-1}\left[(\vec{\omega}\wedge\vec{\widetilde{x}})\,\frac{\varrho}{\sqrt{2}}+1+\frac{\varrho v_{\underline{1}}}{\sqrt{2}}\right]. \end{array} \tag{59}$$

Thus,

$$dx^{\mu}_{\varrho} = dz^{\mu}_{\varrho}(s) + d\widetilde{x}^{i}\, e^{\mu}_{\hat{i}} + \widetilde{x}^{i}\, de^{\mu}{}_{\hat{i}}(s) = (\tau^{\hat{b}}\, d\widetilde{x}^{0} + \pi^{\hat{b}}_{\hat{i}}\, d\widetilde{x}^{i})\, \overline{e}^{\mu}{}_{\hat{b}}, \tag{60}$$

where

$$\tau^{\hat{b}} \equiv \pi^{\hat{b}}_{\hat{0}} + \widetilde{x}^{i}\left(\pi^{\hat{a}}_{\hat{i}}\Phi^{b}_{a} + \frac{d\pi^{\hat{b}}_{\hat{i}}}{ds}\right). \tag{61}$$

Hence, in general, the metric in noninertial frame of arbitrary accelerating and rotating observer in Minkowski space-time is

$$\widetilde{g}(\varrho) = \eta_{\mu\nu}\, dx^{\mu}_{\varrho}\otimes dx^{\nu}_{\varrho} = W_{\mu\nu}(\varrho)\, d\widetilde{x}^{\mu}\otimes d\widetilde{x}^{\nu}, \tag{62}$$

which can be conveniently decomposed according to

$$\begin{array}{l} W_{00}(\varrho) = \pi^2\left[(1+\vec{a}\cdot\vec{\widetilde{x}})^2 + (\vec{\omega}\cdot\vec{\widetilde{x}})^2 - (\vec{\omega}\cdot\vec{\omega})(\vec{\widetilde{x}}\cdot\vec{\widetilde{x}})\right] + \gamma_{00}(\varrho), \\ W_{0i}(\varrho) = -\pi^2\,(\vec{\omega}\wedge\vec{\widetilde{x}})^{i} + \gamma_{0i}(\varrho), \quad W_{ij}(\varrho) = -\pi^2\,\delta_{ij} + \gamma_{ij}(\varrho), \end{array} \tag{63}$$

provided,

$$\begin{array}{l} \gamma_{00}(\varrho) = \pi\left[(1+\vec{a}\cdot\vec{\widetilde{x}})\zeta^{0} - (\vec{\omega}\wedge\vec{\widetilde{x}})\cdot\vec{\zeta}\right] + (\zeta^{0})^2 - (\vec{\zeta})^2, \quad \gamma_{0i}(\varrho) = -\pi\,\zeta^{i} + \tau^{\hat{0}}\,\pi^{\hat{0}}_{\hat{i}}, \\ \gamma_{ij}(\varrho) = \pi^{\hat{0}}_{\hat{i}}\,\pi^{\hat{0}}_{\hat{j}}, \quad \zeta^{0} = \pi\left(\tau^{\hat{0}} - 1 - \vec{a}\cdot\vec{\widetilde{x}}\right), \quad \vec{\zeta} = \pi\left(\vec{\tau} - \vec{\omega}\wedge\vec{\widetilde{x}}\right). \end{array} \tag{64}$$

As we expected, according to (62)- (64), the matric $\widetilde{g}(\varrho)$ is decomposed in the following form:

$$g(\varrho) = \pi^2(\varrho)\,\widetilde{g} + \gamma(\varrho), \tag{65}$$

where

$$\gamma(\varrho) = \gamma_{\mu\nu}(\varrho)\, d\widetilde{x}^{\mu}\otimes d\widetilde{x}^{\nu}, \quad \text{and} \quad \Upsilon(\varrho) = \pi^{\hat{a}}_{\hat{a}}(\varrho) = \pi(\varrho). \tag{66}$$

In general, the geodesic coordinates are admissible as long as

$$\left(1+\vec{a}\cdot\vec{\widetilde{x}}+\frac{\zeta^{0}}{\pi}\right)^2 > \left(\vec{\omega}\wedge\vec{\widetilde{x}}+\frac{\vec{\zeta}}{\pi}\right)^2. \tag{67}$$

The equations (51) and (62) say that the vierbein fields, with entries

$$\eta_{\mu\nu}\,\overline{e}^{\mu}{}_{\hat{a}}\,\overline{e}^{\nu}{}_{\hat{b}} = o_{\hat{a}\hat{b}} \quad \text{and} \quad \eta_{\mu\nu}\,e^{\mu}{}_{\hat{a}}\,e^{\nu}{}_{\hat{b}} = \gamma_{\hat{a}\hat{b}}, \tag{68}$$

lead to the relations

$$\widetilde{g} = o_{\hat{a}\hat{b}}\,\widetilde{\vartheta}^{\hat{a}}\otimes\widetilde{\vartheta}^{\hat{b}}, \quad \text{and} \quad g = o_{\hat{a}\hat{b}}\,\vartheta^{\hat{a}}\otimes\vartheta^{\hat{b}} = \gamma_{\hat{a}\hat{b}}\,\widetilde{\vartheta}^{\hat{a}}\otimes\widetilde{\vartheta}^{\hat{b}}, \tag{69}$$

which readily leads to the coframe fields:

$$\begin{array}{l} \widetilde{\vartheta}^{\hat{b}} = \overline{e}_{\mu}{}^{\hat{b}}\,dx^{\mu} = \widetilde{e}^{\hat{b}}{}_{\mu}\,d\widetilde{x}^{\mu}, \quad \widetilde{e}^{\hat{b}}{}_{0} = N^{b}_{0}, \quad \widetilde{e}^{\hat{b}}{}_{i} = N^{b}_{i}, \\ \vartheta^{\hat{b}} = \overline{e}_{\mu}{}^{\hat{b}}\,dx^{\mu}_{\varrho} = e^{\hat{b}}{}_{\mu}\,d\widetilde{x}^{\mu} = \pi^{\hat{b}}{}_{\hat{a}}\,\widetilde{\vartheta}^{\hat{a}}, \quad e^{\hat{b}}{}_{0} = \tau^{\hat{b}}, \quad e^{\hat{b}}{}_{i} = \pi^{\hat{b}}{}_{\hat{i}}. \end{array} \tag{70}$$

Here

$$N^{0}_{0} = N \equiv \left(1+\vec{a}\cdot\vec{\widetilde{x}}\right), \quad N^{0}_{i} = 0, \quad N^{i}_{0} = N^{i} \equiv \left(\vec{\omega}\cdot\vec{\widetilde{x}}\right)^{i}, \quad N^{j}_{i} = \delta^{j}_{i}. \tag{71}$$

doi: https://doi.org/10.52526/25792776-24.71.2-289

In the standard $(3+1)$-decomposition of space-time, N and N^i are known as *lapse function* and *shift vector*, respectively (Gronwald & Hehl, 1996). Hence, we may easily recover the frame field

$$e_{\hat{a}} = e^{\mu}{}_{\hat{a}}\, \widetilde{e}_{\mu} = \pi_{\hat{a}}{}^{\hat{b}}\, \widetilde{e}_{\hat{b}}, \tag{72}$$

by inverting (70):

$$\begin{aligned} e_{\hat{0}}(\varrho) &= \frac{\pi(\varrho)}{\pi(\varrho)\,\tau^{\hat{0}}(\varrho) - \pi^{\hat{0}}_{\hat{k}}(\varrho)\,\tau^{\hat{k}}(\varrho)}\, \widetilde{e}_0 - \frac{\tau^{\hat{i}}(\varrho)}{\pi(\varrho)\,\tau^{\hat{0}}(\varrho) - \pi^{\hat{0}}_{\hat{k}}(\varrho)\,\tau^{\hat{k}}(\varrho)}\, \widetilde{e}_i, \\ e_{\hat{i}}(\varrho) &= -\frac{\pi^{\hat{0}}_{\hat{i}}(\varrho)}{\pi(\varrho)\,\tau^{\hat{0}}(\varrho) - \pi^{\hat{0}}_{\hat{k}}(\varrho)\,\tau^{\hat{k}}(\varrho)}\, \widetilde{e}_0 + \pi^{-1}(\varrho) \left[\delta^j_i + \frac{\tau^j(\varrho)\,\pi^{\hat{0}}_{\hat{i}}(\varrho)}{\pi(\varrho)\,\tau^{\hat{0}}(\varrho) - \pi^{\hat{0}}_{\hat{k}}(\varrho)\,\tau^{\hat{k}}(\varrho)} \right] \widetilde{e}_j. \end{aligned} \tag{73}$$

A *generalized transport* for deformed frame $e_{\hat{a}}$, which includes both the Fermi-Walker transport and deformation of $\underline{M}_2$, can be written in the form

$$\frac{de^{\mu}{}_{\hat{a}}}{ds} = \widetilde{\Phi}_a{}^b\, e^{\mu}{}_{\hat{b}}, \tag{74}$$

where a *deformed acceleration tensor* $\widetilde{\Phi}_a{}^b$ concisely is given by

$$\widetilde{\Phi} = \frac{d\ln\pi}{ds} + \pi\,\Phi\,\pi^{-1}. \tag{75}$$

Thus, we derive the tetrad fields $e_r{}^{\hat{s}}(\varrho)$ (55) and $e^{\mu}{}_{\hat{a}}(\varrho)$ (73) as a function of *local rate* ϱ of instantaneously change of a constant velocity (both magnitude and direction) of a massive particle in M_4 under the unbalanced net force, describing corresponding *fictitious graviton.* Therewith the *fictitious gravitino*, $\psi_{\hat{m}}{}^{\alpha}(\varrho)$, will be arisen under infinitesimal transformations of local supersymmetry.

5. The inertial force in the semi-Riemannian space V_4

We can always choose *natural coordinates* $X^{\alpha}(T, X, Y, Z) = (T, \vec{X})$ with respect to the axes of the local free-fall coordinate frame $S_4^{(l)}$ in an immediate neighbourhood of any space-time point $(\widetilde{x}_p) \in V_4$ in question of the background semi-Riemannian space, V_4, over a differential region taken small enough so that we can neglect the spatial and temporal variations of gravity for the range involved. The values of the metric tensor $\widetilde{g}_{\mu\nu}$ and the affine connection $\widetilde{\Gamma}^{\lambda}_{\mu\nu}$ at the point $(\widetilde{x}_p)$ are necessarily sufficient information for determination of the natural coordinates $X^{\alpha}(\widetilde{x}^{\mu})$ in the small region of the neighbourhood of the selected point. Then the whole scheme outlined above will be held in the frame $S_4^{(l)}$. The general *inertial force* then reads

$$\widetilde{\vec{f}}_{(in)} = -\frac{\sqrt{2}\underline{v}_c \vec{e}_f}{(1+\overline{\varrho}^2)^2}\, |f^{\alpha}_{(l)} - m\frac{\partial X^{\alpha}}{\partial \widetilde{x}^{\sigma}}\Gamma^{\sigma}_{\mu\nu}\frac{d\widetilde{x}^{\mu}}{ds}\frac{d\widetilde{x}^{\nu}}{ds}|. \tag{76}$$

As before, the two systems S_2 and $S_4^{(l)}$ can be chosen in such a way as the axis $e_{\underline{1}}$ of $S_{(2)}$ lies $(e_{\underline{1}} = \vec{e}_f)$ along the acting net force

$$\vec{f} = \vec{f}_{(l)} + \vec{f}_{g(l)}, \tag{77}$$

while the time coordinates in the two systems are taken the same

$$\underline{x}^{\underline{0}} = x^0 = X^0 = T. \tag{78}$$

Here $\vec{f}_{(l)}$ is the SR value of the unbalanced relativistic force other than gravitational and $\vec{f}_{g(l)}$ is the gravitational force given in the frame $S_4^{(l)}$. Despite of totally different and independent sources of gravitation and inertia, at $f^{\alpha}_{(l)} = 0$, the (76) establishes the independence of free-fall trajectories of the mass, internal composition and structure of bodies. This furnishes a justification for the introduction of the WPE.

6. The inertial effects in the background post Riemannian geometry

If the nonmetricity tensor

$$N_{\lambda\mu\nu} = -\mathcal{D}_{\lambda}\, g_{\mu\nu} \equiv -g_{\mu\nu\,;\lambda}$$

doi: https://doi.org/10.52526/25792776-24.71.2-289

does not vanish, the general formula for the affine connection written in the space-time components is (Poplawski, 2009)

$$\Gamma^{\rho}{}_{\mu\,\nu} = \overset{\circ}{\Gamma}{}^{\rho}{}_{\mu\,\nu} + K^{\rho}{}_{\mu\nu} - N^{\rho}{}_{\mu\nu} + \tfrac{1}{2} N_{(\mu\ \nu)}{}^{\rho}, \tag{79}$$

where the metric alone determines the torsion-free Levi-Civita connection $\overset{\circ}{\Gamma}{}^{\rho}{}_{\mu\nu}$,

$$K^{\rho}{}_{\mu\nu} : \quad = 2Q_{(\mu\nu)}{}^{\rho} + Q^{\rho}{}_{\mu\nu}$$

is the non-Riemann part - the affine *contortion tensor*. The torsion,

$$Q^{\rho}{}_{\mu\nu} = \frac{1}{2} T^{\rho}{}_{\mu\nu} = \Gamma^{\rho}{}_{[\mu\,\nu]},$$

given with respect to a holonomic frame, $d\,\vartheta^{\rho} = 0$, is a third-rank tensor, antisymmetric in the first two indices, with 24 independent components. We now compute the relativistic inertial force for the motion of the matter, which is distributed over a small region in the U_4 space and consists of points with the coordinates x^{μ}, forming an extended body whose motion in the space, U_4, is represented by a world tube in space-time. Suppose the motion of the body as a whole is represented by an arbitrary timelike world line γ inside the world tube, which consists of points with the coordinates $\tilde{X}^{\mu}(\tau)$, where τ is the proper time on γ. Define

$$\delta x^{\mu} = x^{\mu} - \tilde{X}^{\mu}, \quad \delta x^{0} = 0, \quad u^{\mu} = \tfrac{d\,\tilde{X}^{\mu}}{d\,s}. \tag{80}$$

The *Papapetrou equation of motion for the modified momentum* (Bergmann & Thompson, 1953, Møller, 1958, Papapetrou, 1974, Poplawski, 2009) is

$$\tfrac{\overset{\circ}{\mathcal{D}}\,\Theta^{\nu}}{\mathcal{D}\,s} = -\tfrac{1}{2}\ \overset{\circ}{R}{}^{\nu}{}_{\mu\sigma\rho}\, u^{\mu}\, J^{\sigma\rho} - \tfrac{1}{2}\, N_{\mu\rho\lambda}\, K^{\mu\rho\lambda :\, \nu}, \tag{81}$$

where $K^{\mu}_{\nu\lambda}$ is the contortion tensor,

$$\Theta^{\nu} = P^{\nu} + \tfrac{1}{u^0}\ \overset{\circ}{\Gamma}{}^{\nu}_{\mu\,\rho}\,(u^{\mu}\, J^{\rho 0} + N^{0\mu\rho}) - \tfrac{1}{2u^0}\, K_{\mu\rho}{}^{\nu}\, N^{\mu\rho 0} \tag{82}$$

is referred to as the *modified 4-momentum*,

$$P^{\lambda} = \int \tau^{\lambda 0}\, d\,\Omega,$$

is the ordinary 4-momentum, $d\,\Omega := d\,x^4$, and the following integrals are defined:

$$\begin{array}{l} M^{\mu\rho} = u^0 \int \tau^{\mu\rho}\, d\,\Omega, \quad M^{\mu\nu\rho} = -u^0 \int \delta x^{\mu}\, \tau^{\nu\rho}\, d\,\Omega, \quad N^{\mu\nu\rho} = u^0 \int s^{\mu\nu\rho}\, d\,\Omega, \\ J^{\mu\rho} = \int (\delta x^{\mu}\, \tau^{\rho 0} - \delta x^{\rho}\, \tau^{\mu 0} + s^{\mu\rho 0})\, d\,\Omega = \frac{1}{u^0}(-M^{\mu\rho 0} + M^{\rho\mu 0} + N^{\mu\rho 0}), \end{array} \tag{83}$$

where $\tau^{\mu\rho}$ is the energy-momentum tensor for particles, $s^{\mu\nu\rho}$ is the spin density. The quantity $J^{\mu\rho}$ is equal to

$$\int (\delta x^{\mu}\, \tau^{kl} - \delta x^{\rho}\, \tau^{\mu\lambda} + s^{\mu\rho\lambda})\, d\,S_{\lambda},$$

taken for the volume hypersurface, is a tensor called the *total spin tensor*. The quantity $N^{\mu\nu\rho}$ is also a tensor. The relation $\delta x^0 = 0$ gives $M^{0\nu\rho} = 0$. It was assumed that the dimensions of the body are small, so integrals with two or more factors δx^{μ} multiplying $\tau^{\nu\rho}$ and integrals with one or more factors δx^{μ} multiplying $s^{\nu\rho\lambda}$ can be neglected. The *Papapetrou equations of motion for the spin* (Bergmann & Thompson, 1953, Møller, 1958, Papapetrou, 1974, Poplawski, 2009) is

$$\tfrac{\overset{\circ}{\mathcal{D}}}{\mathcal{D}s}\, J^{\lambda\nu} = u^{\nu}\, \Theta^{\lambda} - u^{\lambda}\, \Theta^{\nu} + K^{\lambda}{}_{\mu\rho}\, N^{\nu\mu\rho} + \tfrac{1}{2}\, K_{\mu\rho}{}^{\lambda}\, N^{\mu\nu\rho} - K^{\nu}{}_{\mu\rho}\, N^{\lambda\mu\rho} - \tfrac{1}{2}\, K_{\mu\rho}{}^{\nu}\, N^{\mu\rho\lambda}. \tag{84}$$

Computing from (81), in general, the relativistic inertial force, exerted on the extended spinning body moving in the RC space U_4, can be found to be

$$\begin{array}{l} \vec{f}_{(in)}(x) = -\frac{m\vec{a}_{abs}(x)}{\Omega^2(\tilde{\varrho})\,\gamma_q} = -m\,\frac{\vec{e}_f}{\Omega^2(\tilde{\varrho})\,\gamma_q}\,\Big|\frac{1}{m}\, f^{\alpha}_{(l)} - \frac{\partial X^{\alpha}}{\partial x^{\mu}}\,\Big[\overset{\circ}{\Gamma}{}^{\mu}_{\nu\lambda}\, u^{\nu}\, u^{\lambda} + \\ \frac{1}{u^0}\ \overset{\circ}{\Gamma}{}^{\mu}_{\nu\rho}\,(u^{\nu}\, J^{\rho 0} + N^{0\nu\rho}) - \frac{1}{2u^0}\, K_{\nu\rho}{}^{\mu}\, N^{\nu\rho 0} + \frac{1}{2}\ \overset{\circ}{R}{}^{\mu}{}_{\nu\sigma\rho}\, u^{\nu}\, J^{\sigma\rho} + \frac{1}{2}\, N_{\nu\rho\lambda}\, K^{\nu\rho\lambda :\, \mu}\Big]\Big|. \end{array} \tag{85}$$

doi: https://doi.org/10.52526/25792776-24.71.2-289

7. Concluding remarks

In this section we briefly highlight a few key points. In the framework of $\widetilde{MS}_p$-TSG, we address the theory of a general deformation of MS_p induced by external force exerted on a particle. A coupling of supergravity with matter superfields no longer holds. Instead, the source of these fields is the deformation of the flat MS_p. Considering the simple spacetime deformation map, $\Omega(\varrho) : \underline{M}_2 \to \underline{V}_2$ ($\Omega = \overset{\circ}{\Omega}$, $\breve{\Omega}^{\mu}{}_{\nu} \equiv \delta^{\mu}_{\nu}$), we have to write the rate, ϱ, in terms of the Lorentz spinors $(\underline{\theta}, \underline{\bar{\theta}})$, and period of superoscillations (τ). A period of superoscillations, $\tau(\underline{s})$, can be defined as a function of proper time $(\underline{s})$ induced by the *world-deformation* tensor $\Omega(\underline{s})$. In this way we show that the occurrence of the *absolute* and *inertial* accelerations, and the *inertial* force, in turn, are obviously caused by a general deformation of flat MS_p. Whereas, the *relative* acceleration in 4D Minkowski space, M_4, (in Newton's terminology) (both magnitude and direction), to the contrary, has nothing to do with a deformation of $\underline{M}_2$ and, thus, it cannot produce the inertia effects. We calculate the relativistic inertial force in Minkowski, semi-Riemannian and post Riemannian spaces. Despite of totally different and independent sources of gravitation and inertia, the general inertial force establishes the independence of free-fall trajectories of the mass, internal composition and structure of bodies. This furnishes a justification for the introduction of the WPE. We discuss the inertia effects beyond the hypothesis of locality with special emphasis on deformation $\underline{M}_2 \longrightarrow \underline{V}_2^{(\varrho)}$, which essentially improves the standard framework. we derive the tetrad fields as a function of ϱ, describing corresponding *fictitious graviton*. Therewith the *fictitious gravitino*, $\psi_{\hat{m}}{}^{\alpha}(\varrho)$, will be arisen under infinitesimal transformations of local supersymmetry.

References

Bergmann P., Thompson R., 1953, Phys. Rev., 89, 400

Bondi H., 1952, Cosmology. Cambridge

Gronwald F., Hehl F., 1996, On the Gauge Aspects of Gravity. Proc. of the 14th Course of the School of Cosmology and Gravitation on Quantum Gravity, held at Erice, Italy. Eds. Bergmann P G, de Sabbata V, and Treder H.-J., World Scientific, Singapore

Maluf J., Faria F., 2008, Ann. der Physik, 520, 326

Maluf J., Faria F., Ulhoa S., 2007, Class. Quantum Grav., 24, 2743

Marzlin K.-P., 1996, Phys. Lett. A, 215, 1

Mashhoon B., 2002, Ann. der Physik, 514, 532

Mashhoon B., 2011, Ann. der Physik, 523, 226

Misner C., Thorne K., Wheeler J., 1973, Gravitation. Freeman, San Francisco

Møller C., 1958, Ann. Phys. (NY), 4, 347

Papapetrou A., 1974, Lectures on general relativity. (Reidel D)(ISBN 9027705402)

Pontryagin L., 1984, Continous Groups. Nauka, Moscow

Poplawski N., 2009, Spacetime and fields. arXiv[gr-qc/0911.0334]

Salgado P., Rubilar G., Crisóstomo J., del Campo S., 2003, Phys. Rev. D, 68, 024021

Salgado P., del Campo S., Cataldo M., 2005, Eur. Phys. J. C, 44, 587

Sciama D., 1953, MNRAS, 113, Issue 1, 34

Stelle K., West P., 1980, Phys. Rev. D, 21, 1466

Ter-Kazarian G., 2011, Class. Quantum Grav., 28, 055003

Ter-Kazarian G., 2012, Advances in Mathematical Physics, 2012, Article ID 692030, 41 pages,doi:10.1155/2012/692030

Ter-Kazarian G., 2023a, Communications of BAO, 70, Issue 2, 170

Ter-Kazarian G., 2023b, Communications of BAO, 70, Issue 2, 188

Ter-Kazarian G., 2023c, Communications of BAO, 70, Issue 2, 212

Ter-Kazarian G., 2024a, Gravitation and Cosmology, 30, No. 1, p. 8

Ter-Kazarian G., 2024c, Communications of BAO, 71, Issue 2,

doi: https://doi.org/10.52526/25792776-24.71.2-289

Ter-Kazarian G., 2024b, Communications of BAO, 71, Issue 2,

de Andrade V., Pereira J., 1997, Phys. Rev. D, 56, 4689

et al. B. D., 1986, Contemporary Geometry. Nauka, Moscow

van Nieuwenhuizen P., 1981, Physics Reports, 68, 189

doi: https://doi.org/10.52526/25792776-24.71.2-289

Appendices

Appendix A The $\widetilde{MS}_p$-SG and $\widetilde{MS}_p$-TSG

Throughout we will use the 'two-in-one' notation of a theory MS$_p$-SUSY, implying that any tensor (W) or spinor (Θ) with indices marked by 'hat' denote

$$\begin{array}{l} W^{\hat{\mu}_1\cdots\hat{\mu}_m}_{\hat{\nu}_1\cdots\hat{\nu}_n} := W^{\mu_1\cdots\mu_m}_{\nu_1\cdots\nu_n} \oplus W^{\underline{\mu}_1\cdots\underline{\mu}_m}_{\underline{\nu}_1\cdots\underline{\nu}_n}, \\ \Theta^{\hat{\alpha}} := \theta^{\alpha} \oplus \underline{\theta}^{\alpha}, \quad \bar{\Theta}_{\hat{\dot{\alpha}}} := \bar{\theta}_{\dot{\alpha}} \oplus \underline{\bar{\theta}}_{\dot{\alpha}}. \end{array} \tag{86}$$

This corresponds to the action of supercharge operators $Q \equiv (\text{either}\, q \,\text{or}\, \underline{q})$, which is due to the fact that the framework of $\widetilde{MS}_p$-SG combines bosonic and fermionic states in V_4 and $\underline{V}_2$ on the same base rotating them into each other under the action of operators $(q, \underline{q})$. The α are all upper indices, while $\dot{\alpha}$ is a lower index.

A.1 The $\widetilde{MS}_p$-SG

A local extension of the MS$_p$-SUSY algebra leads to the gauge theory of *translations*. One might guess that the condition for the parameter $\partial_{\hat{\mu}}\epsilon = 0$ of a global MS$_p$-SUSY theory (Ter-Kazarian, 2023b, 2024a) should be relaxed for the accelerated particle motion, so that a global SUSY will be promoted to a local SUSY in which the parameter $\epsilon = \epsilon(X^{\hat{\mu}})$ depends explicitly on $X^{\hat{\mu}} = (\widetilde{x}^{\mu}, \underline{\widetilde{x}}^{\underline{\mu}}) \in V_4 \oplus \underline{V}_2$, where $\widetilde{x}^{\mu} \in V_4$ and $\underline{\widetilde{x}}^{\underline{\mu}} \in \widetilde{MS}_p (\equiv \underline{V}_2)$, with V_4 and $\underline{V}_2$ are the 4D and 2D semi-Riemannian spaces. This extension will address the *accelerated motion* and *inertia effects*.

A smooth embedding map, generalized for curved spaces, becomes

$$\widetilde{f}: \ \underline{V}_2 \longrightarrow V_4, \tag{87}$$

defined to be an immersion (the embedding which is a function that is a homeomorphism onto its image):

$$\underline{\widetilde{e}}_{\underline{0}} = \widetilde{e}_0, \quad \underline{\widetilde{x}}^{\underline{0}} = \widetilde{x}^0, \quad \underline{\widetilde{e}}_{\underline{1}} = \vec{\widetilde{n}}, \quad \underline{\widetilde{x}}^{\underline{1}} = |\vec{\widetilde{x}}|, \tag{88}$$

where $\vec{\widetilde{x}} = \widetilde{e}_i \widetilde{x}^i = \vec{\widetilde{n}}|\vec{\widetilde{x}}|$ $(i = 1, 2, 3)$ (the middle letters of the Latin alphabet $(i, j, ...)$ will be reserved for space indices). On the premises of (Ter-Kazarian, 2024a), we review the accelerated motion of a particle in a new perspective of local $\widetilde{MS}_p$-SUSY transformations that a *creation* of a particle in $\underline{V}_2$ means its transition from initial state defined on V_4 into intermediate state defined on $\underline{V}_2$, while an *annihilation* of a particle in $\underline{V}_2$ means vice versa. The same interpretation holds for the *creation* and *annihilation* processes in V_4. The net result of each atomic double transition of a particle $V_4 \rightleftharpoons \underline{V}_2$ to $\underline{V}_2$ and back is as if we had operated with *a local space-time translation* with acceleration, $\vec{a}$, on the original space V_4. Accordingly, the acceleration, $\underline{\vec{a}}$, holds in $\underline{V}_2$ at $\underline{V}_2 \rightleftharpoons V_4$. So, the accelerated motion of boson $A(\widetilde{x})$ in V_4 is a chain of its sequential transformations to the Weyl fermion $\underline{\chi}(\underline{\widetilde{x}})$ defined on $\underline{V}_2$ (accompanied with the auxiliary fields $\underline{\widetilde{F}}$) and back,

$$\rightarrow A(\widetilde{x}) \rightarrow \underline{\chi}^{(\underline{F})}(\underline{\widetilde{x}}) \rightarrow A(\widetilde{x}) \rightarrow \underline{\chi}^{(\underline{F})}(\underline{\widetilde{x}}) \rightarrow, \tag{89}$$

and the same interpretation holds for fermion $\chi(\widetilde{x})$.

The mathematical structure of a local theory of $\widetilde{MS}_p$-SUSY has much in common with those used in the geometrical framework of standard supergravity theories. Such a local SUSY can already be read off from the algebra of a global MS$_p$-SUSY (Ter-Kazarian, 2024a) in the form

$$[\epsilon(X)Q, \, \bar{Q}\bar{\epsilon}(X)] = 2\epsilon(X)\sigma^{\hat{\mu}}\bar{\epsilon}(X)\widetilde{p}_{\hat{\mu}}, \tag{90}$$

which says that the product of two supersymmetry transformations corresponds to a translation in 6D X-space of which the momentum $\widetilde{p}_{\hat{\mu}} = i\widetilde{\partial}_{\hat{\mu}}$ is the generator. In order to become on the same footing with $\underline{V}_2$, the V_4 refers to the accelerated proper reference frame of a particle without relation to other matter fields. This leads us to extend the concept of differential forms to superspace. Being embedded in V_4, the $\widetilde{MS}_p$ is the *unmanifested* indispensable individual companion of a particle of interest devoid of any matter influence. While all the particles are living on V_4, their superpartners can be viewed as living on $\widetilde{MS}_p$. In this framework supersymmetry and general coordinate transformations are described in a unified way as certain diffeomorphisms. The action of simple $\widetilde{MS}_p$-SG includes the Hilbert term for a *fictitious* graviton coexisting with a *fictitious* fermionic field of, so-called, gravitino (sparticle) described by the Rarita-Scwinger kinetic term. These two particles differ in their spin: 2 for the graviton, 3/2 for the gravitino. They are the bosonic and fermionic states of a gauge particle in V_4 and $\widetilde{MS}_p$, respectively, or vice versa.

doi: https://doi.org/10.52526/25792776-24.71.2-289

A.2 The simple $(N=1)$ $\widetilde{MS}_p$ - SG without auxiliary fields, revisited

The generalized Poincaré superalgebra for the simple $(N=1)$ $\widetilde{MS}_p$-SG reads:

$$\begin{array}{l}[P_{\hat a},P_{\hat b}]=0,\quad [S_{\hat a\hat b},P_{\hat c}]=(\eta_{\hat a\hat c}P_{\hat b}-\eta_{\hat b\hat c}P_{\hat a}),\\ [S_{\hat a\hat b},S_{\hat c\hat d}]=i(\eta_{\hat a\hat c}S_{\hat b\hat d}-\eta_{\hat b\hat c}S_{\hat a\hat d}+\eta_{\hat b\hat d}S_{\hat a\hat c}qq-\eta_{\hat a\hat d}S_{\hat b\hat c}),\\ [S_{\hat a\hat b},Q^{\alpha}]=\frac{1}{2}(\gamma_{\hat a\hat b})^{\alpha}_{\beta}Q^{\beta},\\ [P_{\hat a},Q^{\beta}]=0,\quad [Q_{\alpha},\bar Q_{\dot\beta}]=\frac{1}{2}(\gamma^{\hat a})_{\alpha\dot\beta}P_{\hat a}.\end{array} \tag{91}$$

with $(S_{\hat a\hat b})^{\hat c}_{\hat d}=i(\delta^{\hat c}_{\hat a}\eta_{\hat b\hat d}-\delta^{\hat c}_{\hat b}\eta_{\hat a\hat d})$ a given representation of the Lorentz generators. Using (91) and a general form for gauge transformations on B^A,

$$\delta B=\mathcal{D}\lambda=d\lambda+[B,\lambda], \tag{92}$$

with

$$\lambda=\rho^{\hat a}P_{\hat a}+\frac{1}{2}\kappa^{\hat a\hat b}S_{\hat a\hat b}+\bar Q\varepsilon, \tag{93}$$

we obtain that the $(e^{\hat a},\omega^{\hat a\hat b},\Psi)$ transform under Poincaré translations as

$$\delta e^{\hat a}=\mathcal{D}\rho^{\hat a},\quad \delta\omega^{\hat a\hat b}=0,\quad \delta\Psi=0; \tag{94}$$

under Lorentz rotations as

$$\delta e^{\hat a}=\kappa^{\hat a}_{\hat b}\delta e^{\hat b},\quad \delta\omega^{\hat a\hat b}=-\mathcal{D}\kappa^{\hat a\hat b},\quad \delta\Psi=\frac{1}{4}\kappa^{\hat a\hat b}\gamma_{\hat a\hat b}\Psi; \tag{95}$$

and under supersymmetry transformation as

$$\delta e^{\hat a}=\frac{1}{2}\bar\varepsilon\gamma^{\hat a}\Psi,\quad \delta\omega^{\hat a\hat b}=0,\quad \delta\Psi=\mathcal{D}\varepsilon. \tag{96}$$

In first-order formalism, the gauge fields $(e^{\hat a},\omega^{\hat a\hat b},\,\Psi)$, (with $\Psi=(\psi,\underline{\psi})$ a two-component Majorana spinor) are considered as an independent members of multiplet in the adjoint representation of the Poincaré supergroup of $D=6$ $((3+1),(1+1))$ simple $(N=1)$ $\widetilde{MS}_p$-SG with the generators $(P_{\hat a},S_{\hat a\hat b},Q^{\alpha})$. Unless indicated otherwise, henceforth the world indices are kept implicit without ambiguity. The operators carry Lorentz indices not related to coordinate transformations. The Yang-Mills connection for the Poincare´ supergroup is given by

$$B=B^AT_A=e^{\hat a}P_{\hat a}+\frac{1}{2}i\omega^{\hat a\hat b}S_{\hat a\hat b}+\Psi\bar Q. \tag{97}$$

The field strength associated with connection B is defined as the Poincaré Lie superalgebra-valued curvature two-form R^A. Splitting the index A, and taking the $\Theta=\bar\Theta=0$ component of R^A, we obtain

$$\begin{array}{l}R^{\ \hat a\hat b}(\omega)=d\omega^{\hat a\hat b}-\omega^{\hat a}{}_{\hat c}\omega^{\hat c\hat d},\\ \tilde T^{\hat a}=T^{\hat a}-\frac{1}{2}\bar\Psi\gamma^{\hat a}\Psi,\quad \rho=\mathcal{D}\Psi,\end{array} \tag{98}$$

where $\gamma^{\hat a}=(\gamma^a,\sigma^{\underline{a}})$, $R^{\ \hat a\hat b}(\omega)$ is the Riemann curvature in terms of the spin connection $\omega^{\hat a\hat b}$, and the generalized Weyl lemma requires that the, so-called, supertorsion $\tilde T^{\hat a}$ be inserted. The solution $\omega(e)$ satisfies the tetrad postulate that the completely covariant derivative of the tetrad field vanishes, therefore $R^{\hat a\hat b}(\omega)=R(\omega)e^{\hat a}e^{\hat b}$.

For the bosonic part of the gauge action (graviton of spin 2) of simple $\widetilde{MS}_p$-SG it then seems appropriate to take the generalized Hilbert action with $e=det\,e^{\hat a}{}_{\mu}(X)$. While the fermionic part of the standard gauge action (garvitino of spin 3/2), which has positive energy, is the Rarita-Schwinger action. The full nonlinear gravitino action in curved space then should be its extension to curved space, which can be achieved by inserting the Lorentz covariant derivative $\mathcal{D}\Psi=d\Psi+\frac{1}{2}\omega^{\ \hat a\hat b}\gamma_{\hat a\hat b}\Psi$. In both parts, the spin connection is considered a dependent field, otherwise in the case of an independent spin connection ω, the action will be invariant under diffeomorphism, and under local Lorentz rotations, but it will be not invariant under the neither the Poincaré translations nor the supersymmetry. In the case if spin connection is independent, we should have under the local Poincaré translations

$$\begin{array}{l}\delta\hat{\mathcal{L}}_{pt}=\delta\left(\varepsilon_{\hat a\hat b\hat c\hat d}e^{\hat a}e^{\hat b}R^{\hat c\hat d}+4\bar\Psi\gamma_{\hat 5}e^{\hat a}\gamma_{\hat a}\mathcal{D}\Psi\right)\\ =2\varepsilon_{\hat a\hat b\hat c\hat d}R^{\hat a\hat b}\tilde T^{\hat c}\rho^{\hat d}+\text{surf. term},\end{array} \tag{99}$$

doi: https://doi.org/10.52526/25792776-24.71.2-289

and under local supersymmetry transformations

$$\delta\hat{\mathcal{L}}_{SUSY} = -4\bar{\varepsilon}\gamma_{\hat{5}}\gamma_{\hat{a}}\mathcal{D}\Psi\tilde{T}^{\hat{a}} + \text{surf. term.} \tag{100}$$

The invariance of the action then requires the vanishing of the supertorsion $\tilde{T}^{\hat{a}} = 0$, which means that the connection is no longer an independent variable. So that the starting point of our approach is the action of a simple $\widetilde{MS}_p$-SG theory written in 'two in one'-notation (86), which is invariant under the local supersymmetry transformation (96), where the Poincaré superalgebra closes off shell without the need for any auxiliary fields:

$$\mathcal{L}_{MS-SG} = \varepsilon_{\hat{a}\hat{b}\hat{c}\hat{d}}e^{\hat{a}}e^{\hat{b}}R^{\hat{c}\hat{d}}(\omega) + 4\bar{\Psi}\gamma_{\hat{5}}e^{\hat{a}}\gamma_{\hat{a}}\mathcal{D}\Psi. \tag{101}$$

This is the sum of bosonic and fermionic parts with the same spin connection, where $\gamma_{\hat{a}} = (\gamma_a \oplus \sigma_{\underline{a}})$, $\gamma_{\hat{5}} = (\gamma_5 \oplus \gamma_{\underline{5}})$, $\gamma_{\underline{5}} = \begin{pmatrix} 1 & 0 \\ 0 & -1 \end{pmatrix}$ is given in the chiral or Weyl representations, i.e. in the irreducible 2-dimensional spinor representations $(\frac{1}{2}, 0)$ and $(0, \frac{1}{2})$, since two-component formalism works for a Weyl fermion. This is indispensable in order to solve algebraical constraints in superspace because they can be used as building blocks of any fermion field (van Nieuwenhuizen, 1981). Taking into account that $g_{\hat{\mu}\hat{\nu}} = \eta_{\hat{a}\hat{b}}e_{\hat{\mu}}{}^{\hat{a}}e_{\hat{\nu}}{}^{\hat{b}}$ and $\gamma_{\hat{\mu}} = e_{\hat{\mu}}{}^{\hat{a}}\gamma_{\hat{a}}$, with $\eta_{\hat{a}\hat{b}} = (\eta_{ab} \oplus \eta_{\underline{ab}})$ related to the tangent space, where $\eta_{ab} = diag(+1, -1, -1, -1)$ and $\eta_{\underline{ab}} = diag(+1, -1)$, we can recast the generalized bosonic and fermionic actions given in (101), respectively, in the forms

$$\mathcal{L}^{(2)} = -\tfrac{1}{4}\sqrt{g}R(g, \Gamma) = -\tfrac{1}{4}eR(e, \omega), \tag{102}$$

and

$$\mathcal{L}^{(3/2)} = 4\varepsilon^{\hat{\mu}\hat{\nu}\hat{\rho}\hat{\sigma}}\bar{\Psi}_{\hat{\mu}}\gamma_{\hat{5}}\gamma_{\hat{\nu}}\mathcal{D}_{\hat{\rho}}\Psi_{\hat{\sigma}}. \tag{103}$$

The components of the acceleration vector, $\dot{a}^{\hat{\rho}} = (a^{\rho}, \underline{a}^{\underline{\rho}})$, satisfy the following embedding relations

$$\underline{a}^{\underline{0}} = a^0, \quad \underline{a}^{\underline{1}} = |\vec{a}|. \tag{104}$$

The accelerated motion of a particle is described by the parameter $\epsilon = \epsilon(X^{\hat{\mu}})$ of local SUSY, which depends explicitly on $X^{\hat{\mu}} = (\tilde{x}^{\mu}, \underline{\tilde{x}}^{\underline{\mu}})$, where $\tilde{x}^{\mu} \in V_4$ and $\underline{\tilde{x}}^{\underline{\mu}} \in \underline{V}_2$. To be specific, let us focus for the motion on the simple case of a peculiar anticommuting spinors $(\underline{\xi}(\underline{x}), \bar{\underline{\xi}}(\underline{x}))$ and $(\xi(x), \bar{\xi}(x))$ defined as

$$\begin{aligned} \underline{\xi}^{\alpha}(\underline{x}) &= i\,\frac{\underline{\tau}(\underline{x})}{2}\,\underline{\theta}^{\alpha}, \quad \bar{\underline{\xi}}_{\dot{\alpha}}(\underline{x}) = -i\,\frac{\underline{\tau}^{*}(\underline{x})}{2}\,\bar{\underline{\theta}}_{\dot{\alpha}}, \\ \xi^{\alpha}(x) &= i\frac{\tau(x)}{2}\theta^{\alpha}, \quad \bar{\xi}_{\dot{\alpha}}(x) = -i\frac{\tau^{*}(x)}{2}\bar{\theta}_{\dot{\alpha}}. \end{aligned} \tag{105}$$

Here the real parameter $\tau(x) = \tau^{*}(x) = \underline{\tau}(\underline{x}) = \underline{\tau}^{*}(\underline{x})$ can physically be interpreted as the *atomic duration time* of double transition of a particle $V_4 \rightleftharpoons \underline{V}_2$, i.e. the period of superoscillations. In this case, the *atomic displacement* caused by double transition reads

$$\Delta\underline{\tilde{x}}_{(a)} = \underline{\tilde{e}}_{\underline{m}}\Delta\underline{\tilde{x}}^{\underline{m}}_{(a)} = \underline{\tilde{u}}\tau(\underline{\tilde{x}}), \tag{106}$$

where the components $\Delta\underline{\tilde{x}}^{\underline{m}}_{(a)}$ are written

$$\Delta\underline{\tilde{x}}^{\underline{m}}_{(a)} = \underline{\tilde{v}}^{\underline{m}}\,\tau(\underline{\tilde{x}}) = i\underline{\theta}\,\sigma^{\underline{m}}\,\bar{\underline{\xi}}(\underline{\tilde{x}}) - i\underline{\xi}(\underline{\tilde{x}})\,\sigma^{\underline{m}}\,\bar{\underline{\theta}}. \tag{107}$$

In Van der Warden notations for the Weyl two-component formalism, we have

$$\underline{v}^2 = 2v^{(+)}v^{(-)} = (\underline{v}^{\underline{0}})^2 - (\underline{v}^{\underline{1}})^2 = 4(\underline{\theta}_1\,\bar{\underline{\theta}}_1\underline{\theta}_2\,\bar{\underline{\theta}}_2)\frac{d\tau}{d\underline{x}^{(+)}}\,\frac{d\tau}{d\underline{x}^{(-)}} = 1, \tag{108}$$

provided,

$$\begin{aligned} a^{(+)} &= \sqrt{2}v_c^{(+)}\,\frac{d^2\tau}{d\underline{x}^{(+)2}}, \\ a^{(-)} &= \sqrt{2}v_c^{(-)}\,\frac{d^2\tau}{d\underline{x}^{(-)2}}, \\ \underline{a} &= \sqrt{2}(a^{(+)}a^{(-)})^{1/2} = 2(\underline{\theta}_1\,\bar{\underline{\theta}}_1\underline{\theta}_2\,\bar{\underline{\theta}}_2)^{1/2}\frac{d^2\tau}{d\underline{s}^2}, \end{aligned} \tag{109}$$

with $v_c^{(+)} = \sqrt{2}(\underline{\theta}_1\,\bar{\underline{\theta}}_1)$ and $v_c^{(-)} = \sqrt{2}(\underline{\theta}_2\,\bar{\underline{\theta}}_2)$. The acceleration will generally remain a measure of the velocity variation over proper time $(\underline{s})$. The (109) gives

$$\begin{aligned} v^{(+)} &= v_c^{(+)}\left(\frac{d\tau}{d\underline{x}^{(+)}} + 1\right), \\ v^{(-)} &= v_c^{(-)}\left(\frac{d\tau}{d\underline{x}^{(-)}} + 1\right), \\ \underline{v} &= \sqrt{2}(v^{(+)}v^{(-)})^{1/2} = 2(\underline{\theta}_1\,\bar{\underline{\theta}}_1\underline{\theta}_2\,\bar{\underline{\theta}}_2)^{1/2}\left(\frac{d\tau}{d\underline{s}} + 1\right), \end{aligned} \tag{110}$$

doi: https://doi.org/10.52526/25792776-24.71.2-289

where $d\underline{s}^2 = d\underline{x}^{(+)}d\underline{x}^{(-)}$. The spinors $\theta(\underline{\theta}, \bar{\underline{\theta}})$ and $\bar{\theta}(\underline{\theta}, \bar{\underline{\theta}})$ satisfy the embedding map (88), namely $\Delta\underline{\widetilde{x}}^{\underline{0}} = \Delta\widetilde{x}^0$ and $(\Delta\underline{\widetilde{x}}^{\underline{1}})^2 = (\Delta\vec{\widetilde{x}})^2$, so we obtain

$$\begin{aligned} &\underline{\theta}\,\sigma^0\,\underline{\bar{\xi}} - \underline{\xi}\,\sigma^0\,\underline{\bar{\theta}} = \theta\,\sigma^0\,\bar{\xi} - \xi\,\sigma^0\,\bar{\theta}, \\ &(\underline{\theta}\,\sigma^3\,\underline{\bar{\xi}} - \underline{\xi}\,\sigma^3\,\underline{\bar{\theta}})^2 = (\theta\,\vec{\sigma}\,\bar{\xi} - \xi\,\vec{\sigma}\,\bar{\theta})^2. \end{aligned} \tag{111}$$

Denote

$$\begin{aligned} \underline{v}^{\underline{0}}_{(c)} &= \tfrac{1}{\sqrt{2}}\left(v_c^{(+)} + v_c^{(-)}\right) = (\underline{\theta}\,\underline{\bar{\theta}}), \\ \underline{v}^{\underline{1}}_{(c)} &= \tfrac{1}{\sqrt{2}}\left(v_c^{(+)} - v_c^{(-)}\right) = (\underline{\theta}_1\,\underline{\bar{\theta}}_1 - \underline{\theta}_2\,\underline{\bar{\theta}}_2), \end{aligned} \tag{112}$$

then

$$\begin{aligned} \theta_1(\underline{\theta}, \underline{\bar{\theta}}) &= \tfrac{1}{2}\left[\left(\underline{v}^{\underline{0}}_{(c)} + \sqrt{\tfrac{2}{3}}\underline{v}^{\underline{1}}_{(c)}\right)^{1/2} + \left(\underline{v}^{\underline{0}}_{(c)} - \sqrt{\tfrac{2}{3}}\underline{v}^{\underline{1}}_{(c)}\right)^{1/2}\right], \\ \theta_2(\underline{\theta}, \underline{\bar{\theta}}) &= \tfrac{1}{2}\left[\left(\underline{v}^{\underline{0}}_{(c)} + \sqrt{\tfrac{2}{3}}\underline{v}^{\underline{1}}_{(c)}\right)^{1/2} - \left(\underline{v}^{\underline{0}}_{(c)} - \sqrt{\tfrac{2}{3}}\underline{v}^{\underline{1}}_{(c)}\right)^{1/2}\right]. \end{aligned} \tag{113}$$

A.3 The $\widetilde{MS}_p$-TSG with the translation group

In Teleparallel Gravity, the spin connection represents only *inertial effects*, but not gravitation at all. All quantities related to Teleparallel Gravity will be denoted with an over 'dot'. The spin connection reads

$$\dot{\omega}^{\hat{a}}{}_{\hat{b}\hat{\mu}} = L^{\hat{a}}{}_{\hat{d}}\partial_{\hat{\mu}}L_{\hat{b}}{}^{\hat{d}}, \tag{114}$$

and the energy-momentum density of the *inertial* or *fictitious* forces is

$$\dot{i}_{\hat{a}}{}^{\hat{\rho}} = \tfrac{1}{k}\dot{\omega}^{\hat{c}}{}_{\hat{a}\hat{\sigma}}\dot{S}_{\hat{c}}{}^{\hat{\rho}\hat{\sigma}}, \tag{115}$$

where $\dot{S}_{\hat{c}}{}^{\hat{\rho}\hat{\sigma}}$ is the so called superpotential (see (130)). Teleparallel Gravity is a gauge theory for the *translation* group (de Andrade & Pereira, 1997). The $\widetilde{MS}_p$-TSG theory, therefore, has the gauge *translation* group in tangent bundle. Namely, at each point p of coordinates X of the base space $(V_4 \oplus \underline{V}_2)$, there is attached a Minkowski tangent-space (the fiber) $T_p(V_4 \oplus \underline{V}_2) = T_{X^{\hat{\mu}}}(V_4 \oplus \underline{V}_2)$, on which the point dependent gauge transformations,

$$X'^{\hat{a}} = X^{\hat{a}} + \varepsilon^{\hat{a}}(X), \tag{116}$$

take place. Under an infinitesimal tangent space translation, it transforms according to

$$\delta\Phi(X^{\hat{a}}(X^{\hat{\mu}})) = -\varepsilon^{\hat{a}}\partial_{\hat{a}}\Phi(X^{\hat{a}}(X^{\hat{\mu}})). \tag{117}$$

The generators of this group satisfy the Lie algebra $[P_{\hat{a}}, P_{\hat{b}}] = 0$. In order to recover the covariance, it is necessary to introduce a 1-form of the Yang–Mills connection assuming values in the Lie algebra of the translation group:

$$B = e^{\hat{a}}P_{\hat{a}}, \tag{118}$$

with gauge field $e^{\hat{a}}$. Introducing the covariant derivative

$$\dot{\mathcal{D}}_{\hat{\mu}}X^{\hat{a}} = \partial_{\hat{\mu}}X^{\hat{a}} + \dot{\omega}^{\hat{a}}{}_{\hat{b}\hat{\mu}}X^{\hat{b}}, \tag{119}$$

the tetrad, which is invariant under translations, becomes

$$\dot{e}^{\hat{a}}{}_{\hat{\mu}} = \dot{\mathcal{D}}_{\hat{\mu}}X^{\hat{a}} + \dot{\omega}^{\hat{a}}{}_{\hat{b}\hat{\mu}}. \tag{120}$$

In this new class of frames, the gauge field transforms according to $\delta e^{\hat{a}}{}_{\hat{\mu}} = -\dot{\mathcal{D}}_{\hat{\mu}}\varepsilon^{\hat{a}}$. Thus the covariant derivative, $\dot{\mathcal{D}} = d + B$, with Yang–Mills connection reads

$$\dot{\mathcal{D}}_{\hat{\mu}} = (\delta^{\hat{a}}_{\hat{\mu}} + e_{\hat{\mu}}{}^{\hat{a}})\partial_{\hat{a}} = (\partial_{\hat{\mu}}X^{\hat{a}} + e_{\hat{\mu}}{}^{\hat{a}})\partial_{\hat{a}} = \dot{e}_{\hat{\mu}}{}^{\hat{a}}\partial_{\hat{a}}. \tag{121}$$

The curvature of the Weitzenböck connection

$$\dot{\Gamma}^{\hat{\rho}}{}_{\hat{\nu}\hat{\mu}} = \dot{e}_{\hat{a}}{}^{\hat{\rho}}\dot{\mathcal{D}}_{\hat{\mu}}\dot{e}^{\hat{a}}{}_{\hat{\nu}}, \tag{122}$$

doi: https://doi.org/10.52526/25792776-24.71.2-289

vanishes identically, while for a tetrad $\dot{e}^{\hat{a}}$ with $e^{\hat{a}}{}_{\hat{\mu}} \neq \dot{\mathcal{D}}_{\hat{\mu}}\varepsilon^{\hat{a}}$, the torsion 2-form - the field strength (here we re-instate the factor $\wedge$),

$$\dot{T}^{\hat{a}} = d\dot{e}^{\hat{a}} = \tfrac{1}{2}\dot{T}^{\hat{a}}{}_{\hat{b}\hat{c}}\dot{e}^{\hat{b}} \wedge \dot{e}^{\hat{c}} = \dot{K}_{\hat{c}}{}^{\hat{a}} \wedge \dot{e}^{\hat{c}}, \tag{123}$$

is non-vanishing:

$$\dot{T}^{\hat{a}}{}_{\hat{\mu}\hat{\nu}} = \dot{\mathcal{D}}_{\hat{\mu}}\dot{e}^{\hat{a}}{}_{\hat{\nu}} - \dot{\mathcal{D}}_{\hat{\nu}}\dot{e}^{\hat{a}}{}_{\hat{\mu}} = \dot{\Gamma}^{\hat{a}}{}_{[\hat{\mu}\hat{\nu}]} = \dot{\mathcal{D}}_{\hat{\mu}}e^{\hat{a}}{}_{\hat{\nu}} - \dot{\mathcal{D}}_{\hat{\nu}}e^{\hat{a}}{}_{\hat{\mu}} \neq 0. \tag{124}$$

Here $\dot{K}^{\hat{a}\hat{b}}$ is the contorsion tensor, and we also taken into account the vanishing torsion, $[\dot{\mathcal{D}}_{\hat{\mu}}, \dot{\mathcal{D}}_{\hat{\nu}}]X^{\hat{a}} = 0$, of *inertial* tetrad, $\dot{e}^{\hat{a}}{}_{\hat{\mu}} = \dot{\mathcal{D}}_{\hat{\mu}}X^{\hat{a}}$. Hence

$$[\dot{e}_{\hat{\mu}}, \dot{e}_{\hat{\nu}}] = \dot{T}_{\hat{\mu}\hat{\nu}} = \dot{T}^{\hat{a}}{}_{\hat{\mu}\hat{\nu}}P_{\hat{a}}. \tag{125}$$

Due to the soldered character of the tangent bundle, torsion presents also the anholonomy of the translational covariant derivative:

$$[\dot{e}_{\hat{\mu}}, \dot{e}_{\hat{\nu}}] = \dot{T}_{\hat{\mu}\hat{\nu}} = \dot{T}^{\hat{\rho}}{}_{\hat{\mu}\hat{\nu}}P_{\hat{\rho}}. \tag{126}$$

The gauge invariance of the tetrad provides torsion invariance under gauge transformations. As a gauge theory for the translation group, the action of the $\widetilde{MS}_p$-TSG theory can be recast in the form (see also (Salgado et al., 2005))

$$\begin{aligned}\dot{\mathcal{L}}_{MS-TSG} &= \tfrac{1}{4}tr\left(\dot{\hat{T}} \wedge \star\dot{\hat{T}}\right) - 4\bar{\Psi}\gamma_{\hat{5}}\gamma_{\hat{d}}\mathcal{D}\Psi\dot{e}^{\hat{d}} \\ &= \tfrac{1}{4}\eta_{\hat{a}\hat{b}}\dot{T}^{\hat{a}} \wedge \star\dot{T}^{\hat{b}} - 4\bar{\Psi}\gamma_{\hat{5}}\gamma_{\hat{d}}\mathcal{D}\Psi\dot{e}^{\hat{d}},\end{aligned} \tag{127}$$

where (we re-instate the factor $\wedge$) the torsion 2-form reads

$$\dot{\hat{T}} = \tfrac{1}{2}\dot{T}^{\hat{a}}{}_{\hat{\mu}\hat{\nu}}P_{\hat{a}}dX^{\hat{\mu}} \wedge dX^{\hat{\nu}}, \tag{128}$$

and

$$\star\dot{\hat{T}} = \tfrac{1}{2}\left(\star\dot{T}^{\hat{a}}{}_{\hat{\rho}\hat{\sigma}}\right)P_{\hat{a}}dX^{\hat{\rho}} \wedge dX^{\hat{\sigma}}. \tag{129}$$

Here $\star$ denotes the Hodge dual. That is, let Ω^p be the space of p-forms on an n-dimensional manifold $\mathbf{R}$ with metric. Since vector spaces Ω^p and Ω^{n-p} have the same finite dimension, they are isomorphic. The presence of a metric renders it possible to single out an unique isomorphism, called Hodge dual.

Defining the tensor of superpotential

$$\dot{S}_{\hat{a}}{}^{\hat{\rho}\hat{\sigma}} = -\dot{S}_{\hat{a}}{}^{\hat{\sigma}\hat{\rho}} := \dot{K}^{\hat{\rho}\hat{\sigma}}{}_{\hat{a}} - \dot{e}_{\hat{a}}{}^{\hat{\sigma}}\dot{T}^{\hat{c}\hat{\rho}}{}_{\hat{c}} + \dot{e}_{\hat{a}}{}^{\hat{\rho}}\dot{T}^{\hat{c}\hat{\sigma}}{}_{\hat{c}}, \tag{130}$$

the dual torsion can be rewritten in the form

$$\star\dot{T}^{\hat{\rho}}{}_{\hat{\mu}\hat{\nu}} = \tfrac{\dot{e}}{2}\varepsilon_{\hat{\mu}\hat{\nu}\hat{\lambda}\hat{\sigma}}\dot{S}^{\hat{\rho}\hat{\lambda}\hat{\sigma}}, \tag{131}$$

with $\dot{e} = det\,\dot{e}^{\hat{a}}{}_{\mu}(X) = \sqrt{-g}$, and hence

$$\dot{\mathcal{L}}_{MS-TSG} = \tfrac{\dot{e}}{8}\dot{T}_{\hat{\rho}\hat{\mu}\hat{\nu}}\dot{S}^{\hat{\rho}\hat{\mu}\hat{\nu}} - 4\bar{\Psi}\gamma_{\hat{5}}\gamma_{\hat{d}}\mathcal{D}\Psi\dot{e}^{\hat{d}}. \tag{132}$$

Making use of the identity $\dot{T}^{\hat{\mu}}{}_{\hat{\mu}\hat{\rho}} = \dot{K}^{\hat{\mu}}{}_{\hat{\rho}\hat{\mu}}$, the action (127) becomes

$$\dot{\mathcal{L}}_{MS-TSG} = -\varepsilon_{\hat{a}\hat{b}\hat{c}\hat{d}}\dot{K}^{\hat{a}\hat{b}}\dot{T}^{\hat{c}}\dot{e}^{\hat{d}} - 4\bar{\Psi}\gamma_{\hat{5}}\gamma_{\hat{d}}\mathcal{D}\Psi\dot{e}^{\hat{d}} + \text{surface term}. \tag{133}$$

This action is invariant under local translations, under local super symmetry transformations and by construction is invariant under local Lorentz rotations and under diffeomorphisms (see Salgado et al. (2003, 2005), Stelle & West (1980)). In other words, this action is invariant under the Poincaré supergroup and under diffeomorphisms.

It remains to see the equivalence of the Teleparallel Gravity action $\dot{\mathcal{L}}^{(2)}$ with Hilbert action $\mathcal{L}^{(2)}$ in (102), which will prove that the immediate cause of the *fictitious* Riemann curvature (R) for the Levi-Civita connection (Γ) is the acceleration. The curvature ($\dot{R}$) of Weitzenböck connection ($\dot{\Gamma}$) vanishes identically, but for a tetrad involving a non-trivial translational gauge potential ($\dot{e}_{\hat{\mu}}{}^{\hat{a}} \neq \dot{\mathcal{D}}_{\hat{\mu}}\varepsilon^{\hat{a}}$), the torsion ($\dot{T}$) is non-vanishing. The connection ($\dot{\Gamma}$) can be considered a kind of dual of the Levi-Civita connection (Γ), which is a connection with vanishing torsion (T), and non-vanishing *fictitious* curvature (R). The immediate cause of

doi: https://doi.org/10.52526/25792776-24.71.2-289

the *fictitious* Riemann curvature (R) is the acceleration. Consequently this actually proves the equivalence of the Teleparallel Gravity action $\dot{\mathcal{L}}^{(2)}$ with Hilbert action $\mathcal{L}^{(2)}$:

$$\dot{\mathcal{L}}^{(2)} = \mathcal{L}^{(2)} + \text{surface term}. \tag{134}$$

The equation of motion in the X-space is written as

$$\frac{du^{\hat{a}}}{ds} = \left(\dot{K}^{\hat{a}}{}_{\hat{b}\hat{\rho}} - \dot{\omega}^{\hat{a}}{}_{\hat{b}\hat{\rho}}\right) u^{\hat{b}} u^{\hat{\rho}}. \tag{135}$$

This equation can be rewritten in a purely spacetime form

$$\frac{du^{\hat{\rho}}}{ds} = \left(\dot{K}^{\hat{\rho}}{}_{\hat{\mu}\hat{\nu}} - \dot{\Gamma}^{\hat{\rho}}{}_{\hat{\mu}\hat{\nu}}\right) u^{\hat{\mu}} u^{\hat{\nu}}. \tag{136}$$

The corresponding acceleration cannot be given a covariant meaning without a connection, while each different connection $\Gamma^{\hat{\rho}}{}_{\hat{\mu}\hat{\nu}}$ will deffne a different acceleration. The Weitzenböck connection, which defines the Fock-Ivanenko derivative $\dot{\mathcal{D}}_{\hat{\mu}}$ written in terms of covariant derivative $\dot{\nabla}_{\hat{\mu}}$:

$$\dot{\mathcal{D}}_{\hat{\mu}} \Phi^{\hat{a}} = \dot{e}^{\hat{a}}{}_{\hat{\rho}} \dot{\nabla}_{\hat{\mu}} \Phi^{\hat{\rho}}, \tag{137}$$

will define the acceleration too

$$\begin{aligned} \dot{a}^{\hat{\rho}} &= \frac{\dot{\nabla} u^{\hat{\rho}}}{\dot{\nabla} s} = u^{\hat{\nu}} \dot{\nabla}_{\hat{\nu}} u^{\hat{\rho}} = \frac{du^{\hat{\rho}}}{ds} + \dot{\Gamma}^{\hat{\rho}}{}_{\hat{\mu}\hat{\nu}} u^{\hat{\mu}} u^{\hat{\nu}} \\ &= \dot{K}^{\hat{\rho}}{}_{\hat{\mu}\hat{\nu}} u^{\hat{\mu}} u^{\hat{\nu}} = \dot{T}^{\hat{\rho}}{}_{\hat{\nu}\hat{\mu}} u^{\hat{\mu}} u^{\hat{\nu}}. \end{aligned} \tag{138}$$

This is a force equation, with torsion (or contortion) playing the role of force. The dynamical aspects of particle mechanics involve derivatives with respect to proper time along the particle worldline, which is the line element written in frame:

$$ds^2 = \eta_{\hat{a}\hat{b}} \dot{e}^{\hat{a}} \dot{e}^{\hat{b}} = \eta_{\hat{a}\hat{b}} \dot{e}^{\hat{a}}{}_{\hat{\mu}} \dot{e}^{\hat{b}}{}_{\hat{\mu}} dX^{\hat{\mu}} dX^{\hat{\nu}} \equiv \eta_{\hat{\mu}\hat{\nu}} dX^{\hat{\mu}} dX^{\hat{\nu}}. \tag{139}$$

A worldline C of a particle, parametrized by proper time as $C(s) = X^{\hat{\mu}}(s)$, will have as six-velocity the vector of components $u^{\hat{\mu}} = dX^{\hat{\mu}}/ds$ and $u^{\hat{a}} = \dot{e}^{\hat{a}}_{\hat{\mu}} u^{\hat{\mu}}$, which are the particle velocity along this curve respectively in the holonomic and anholonomic bases in the X-space. The proper time can be written in the form $ds = u_{\hat{\mu}} dX^{\hat{\mu}} = u_{\hat{a}} \dot{e}^{\hat{a}}$. To transform the tetrad field into a reference frame in X-space with an observer attached to it, we may "attach" $\dot{e}_{\hat{0}}$ to the observer by identifying $u = \dot{e}_{\hat{0}} = \frac{d}{ds}$ with components $u^{\hat{\mu}} = \dot{e}_{\hat{0}}{}^{\hat{\mu}}$, such that $\dot{e}_{\hat{0}}$ will be the observer velocity. The Weitzenböck connection, $\dot{\Gamma}$, will attribute to the observer an acceleration

$$\dot{a}^{\hat{a}}_{(f,\dot{\Gamma})} = \dot{\omega}^{\hat{a}}{}_{\hat{0}\hat{0}} + \dot{K}^{\hat{a}}{}_{\hat{0}\hat{0}}, \tag{140}$$

seen by that very observer. Whereas,

$$\dot{\omega}^{\hat{a}}{}_{\hat{b}\hat{c}} = \dot{e}^{\hat{a}}{}_{\hat{\mu}} \dot{\nabla}_{\dot{e}_{\hat{c}}}, \dot{e}_{\hat{b}}{}^{\hat{\mu}}, \tag{141}$$

which literarily means the covariant derivative of $\dot{e}_{\hat{b}}$ along $\dot{e}_{\hat{c}}$, projected along $\dot{e}_{\hat{a}}$. As $\dot{a}^{\hat{\rho}}$ (138) is orthogonal to $u^{\hat{\rho}}$, its vanishing means that the $u^{\hat{\rho}}$ keeps parallel to itself along the worldline.

doi: https://doi.org/10.52526/25792776-24.71.2-289

Radiation and Scattering of Massive Photons

G.A.Saiyan *[1,2]

[1]Kelly Serrvices Incorporation,USA, Kansas 66210, USA
[2]Byurakan Astrophysical Observatory, Republic of Armenia

Abstract

With the aid of a modified Planck's law for massive photons, it is shown that the ratio of the mean value of the photon mass equivalent to its rest (invariant) mass tends to be one with a decrease in temperature. A modified Stefan - Boltzmann law is obtained at different temperature regimes, as well as the Wien's displacement law. At high temperatures the modified Planck' s law approaches the standard Planck' s law. It is also shown that the cross-section of the Thomson scattering slightly increases opacity of the scattering medium. The Compton shift in frequency for a massive photon appears to be frequency-dependent and slightly less than its value for a massless photon, except in the case of forward scattering when no change in frequency takes place. Astrophysical aspects of the massive photon hypothesis are discussed with regard to standard stellar models, early stages of the Universe, and the Breit-Weeler process, as well as active galactic nuclei. Estimates of the spreading time of the wave packet of the massive photon show that for frequencies $\nu \geq 4.052 \times 10^9 Hz(\lambda \leq 7.4)$ it exceeds the age of the Universe.

Keywords: *masive photon, optical dispersion in vacuum; modified Planck's law, Thomson scattering, Compton scattering, spreading time of the wave packet*

1. Introduction

The hypothesis that the photon has a nonzero rest mass has been the matter of numerous discussions over the past decades. Though this topic falls out of the traditional field of physical studies, it is of interest because of its fundamental impact on many aspects of physics and astrophysics. The mathematical basis for discussing the idea of photons with nonzero mass is the Proca equation (Poenaru, 2006, Tu et al., 2004) for massive vector bosons with spin 1. In the covariant form, it is a generalization of Maxwell's equations in the case of a massive electromagnetic field. The presence of a term with the mass of the photon in the Proca equation violates the condition of gauge invariance in electrodynamics and leads to a series of consequences, of which we note the effect of optical dispersion in vacuum - the hypothesis of an intrinsic dispersion of light, associated with the presumable dependence of its speed on the frequency of radiation. The effect of dispersion in vacuum is typical for de Broglie waves, which formally makes them akin to a massive electromagnetic field. Unlike the latter, de Broglie waves do not carry any physical interaction but are only a form of describing the behavior of particles within the framework of wave-particle duality. However, de Broglie wavelength of a photon coincides with the wavelength of an electromagnetic radiation associated with the photon (Blokhintsev, 1976). This gives a reason to at least formally consider it as a concentrated electromagnetic wave packet consisting of quasi-monochromatic waves. Bass & Schredinger (1955), who brought attention to the possibility of existence of "weighted" photons, noted that the presence of the non-zero mass of the photon leads to the third, longitudinal, polarization of radiation instead of two transverse polarizations in the normal, massless one. De Brogle & Vigier (1972) pointed out to a physical experiment with laser beams, resulted in the assumption on the possibility of existence of massive photons with the rest mass not exceeding $10^{-48})g$. Measurements of the relative variation in the speed of light$\delta c/c$ (the ratio of the velocity variation (δc) to its invariant value $c = 2.99792458 \times 10^8 m/s$, which used in the Lorentz transformations), produced by different authors at different radio frequencies under terrestrial conditions (see Tu et al., 2004, and references therein), confirmed the constancy of the speed of light with an accuracy of $\sim 10^{-7} - 10^{-4}$. Studies of active processes in distant astrophysical objects Shaefer (1999) show

*grigori_saiyan@hotmail.com

doi: https://doi.org/10.52526/25792776-24.71.2-307

a relative variation in the speed of light, starting from orders of magnitude $\sim\ 10^{-21} - 10^{-12}$, resulting from the estimate of the difference in the time of arrival of signals at different frequencies (time dispersion effect). The existence of the nonzero rest mass of the photon is assumed in some models of quantum gravity Biller & et al. (1999). Obviously, in this case we are dealing with a very weak physical effect, the direct detection of which is currently still below the experimental threshold as decades ago (Goldhaber & Nieto, 1976). This circumstance, which has no effect on physics in everyday reality, may be more significant in extreme astrophysical conditions. If the hypothesis about nonzero mass of the photon has a right to exist, then one of the questions that naturally arises from it is how it may affect the nature of blackbody radiation. This problem was first considered by Torres-Hernandez (1985)by making use of a partition function Feynman (2018). He referred to the remark in the work of Bass & Schredinger (1955) that the contribution of longitudinally polarized photons in achieving of thermodynamic equilibrium in the black-body cavity can be neglected (the probability of the transition of "transverse" photons into "longitudinal" photons is extremely small, as shown by Kobzarev & Okun (1968). In this paper we are going to uncover some mathematical details just briefly mentioned by Torres-Hernandez (1985), but seem to be important for completeness of theoretical consideration of the topic. We show that at low temperatures the rest mass of the photon approaches the mean mass equivalent (Saiyan, 2023)of the Planck' photons.In addition to this we derive Stefan-Boltzmann law for high and low temperatures in connection with the radiation pressure. We derive Wien's displacement law regarding massive photons and discuss the effect of nonzero mass of the photons on Thomson and Compton scattering. Some astrophysical aspects, related to the results presented here, are discussed in Section 3 alongside with spreading time of wave packets of photons of different frequencies.

2. Modified Planck's law (MPL)

The formula, obtained by Torres-Hernandez (1985) for the spectral energy density of radiation, can be written in the form

$$\rho(\nu, m_\gamma, T) = \rho(\nu, T)\sqrt{1 - (\frac{m_\gamma c^2}{h\nu})^2} \tag{1}$$

which we call here and thereafter the modified Planck's law (MPL). Here ν is the radiation frequency, m_γ -the rest mass of the photon, T is the temperature of the blackbody radiation and

$$\rho(\nu, T) = \frac{8\pi h\nu^3}{c^3}\frac{1}{e^{(\frac{h\nu}{kT})} - 1} \tag{2}$$

is the standard Planck spectral density of radiation, $h = 6.626 \times 10^{-34} Js$ is the Planck constant and $k = 1.38 \times 10^{-23} \frac{J}{K}$ is the Boltzmann constant. This topic was also discussed by Pardy (2018) and Nyambuya (2017), but without reference to the work of Torres-Hernandez (1985), which seems to us physically more consistent. From expression (1) it follows that at $m_\gamma = \frac{h\nu}{c^2} = 7.362 \times 10^{-51}\nu(kg)$ Planck's law turns to zero. This allows us to introduce a purely formal definition of the "rest frequency" of the photon

$$\nu_0 = \frac{m_\gamma c^2}{h} = 1.358 \times 10^{50} m_\gamma \quad (Hz) \tag{3}$$

if the mass is determined independently. The estimates of the rest mass are related to the measurement methodology and the frequency range used for this Butto & Tikva (2022) and Saiyan (2023), although the value of m_γ must be constant by its very meaning. Entering a dimensionless variable in (1) $x = \frac{h\nu}{kT}$, we write:

$$\frac{m_\gamma c^2}{h\nu} = \frac{\beta}{x}, \quad \beta = \frac{m_\gamma c^2}{kT} = 6.522 \times 10^{39}\frac{m_\gamma}{T}. \tag{4}$$

At high temperatures $m_\gamma c^2 \ll kT(\beta \ll 1)$, the MPL tends to be the standard Planck's law. As can be seen in (2), in this case

$$m_\gamma \ll 1.533 \times 10^{-40} T(kg). \tag{5}$$

At low temperatures $\beta \gg 1, x \gg 1$, both functions asymptotically tend to zero.

doi: https://doi.org/10.52526/25792776-24.71.2-307

2.1. Derivation of MPL

Here we will give a derivation of MPL that is somewhat different from the one given by **??** but having more details and leading to the same result. We start with the dispersion equation which can be obtained from the Proca equation (Tu et al., 2004):

$$k^2 = \frac{\omega^2}{c^2} - (\frac{m_\gamma c}{\hbar})^2 = 4\frac{\pi^2}{c^2}(\nu^2 - \nu_0^2), \quad \hbar = \frac{h}{2\pi}, \tag{6}$$

where k is the modulus of the wave vector ω is the cyclic frequency $\omega = 2\pi\nu$ and which we will rewrite in the form

$$k = 2\frac{\pi}{c}\sqrt{\nu^2 - \nu_0^2}. \tag{7}$$

Then the density of the number of oscillatory modes in the interval of wave numbers $(k, k+dk)$ in volume V of a black-body radiating cavity within which thermodynamic equilibrium has been achieved is equal to $dN(k) = \frac{k^2}{2\pi^2}Vdk$, or, in terms of frequencies, after differentiating equation (6), and taking into account two states of polarization of the photon,

$$dN(\nu) = 8\frac{\pi V}{c^3}\nu^2\sqrt{1 - (\frac{m_\gamma c^2}{h\nu})^2} \tag{8}$$

For the density of the number of states with radiation energy in the frequency interval $(\nu, \nu + d\nu)$, we have:

$$h\nu\frac{dN(\nu)}{\nu} = \frac{8\pi h\nu^3}{c^3}\sqrt{1 - (\frac{m_\gamma c^2}{h\nu})^2}\,d\nu \tag{9}$$

Because the mean occupation number of each energy state is given by the Planck distribution $\langle n\rangle = \frac{1}{e^{(\frac{h\nu}{kT})}-1}$ (Feynman, 2018) for MPL we find

$$\rho(\nu, m_\gamma, T) = (\frac{8\pi h\nu^3}{c^3})\sqrt{1 - (\frac{m\gamma c^2}{h\nu})^2}\,\frac{1}{e^{(\frac{h\nu}{kT})} - 1}, \tag{10}$$

which coincides with (1). In fact, MPL differs from the standard Planck's law only in the presence of a radical expression. The average energy of a Planck photon will then be determined by the ratio of the total energy density in the radiation spectrum to the density of the number of photons, i.e., the expression

$$\langle\epsilon\rangle = kT\frac{\int_{h\nu_0}^{\infty}\rho(\nu, m_\gamma, T)d\nu}{\int_{h\nu_0}^{\infty}\frac{\rho(\nu,m_\gamma,T)\nu}{d}\nu} \quad \epsilon = h\nu. \tag{11}$$

Consequently, the average mass of the Planck photon (the average mass equivalent) is $\langle m\rangle = \frac{\langle\epsilon\rangle}{c^2}$. As follows from (10), for the standard Planck's law with $(\nu_0 = 0)$ $\langle\epsilon\rangle = 2.701kT$. Using expression (8), it is possible to obtain the temperature-dependent ratio of the average mass of the photon to its rest mass. To do this, let us rewrite MPL (9) in the form:

$$\rho(x, m_\gamma, T) = (\frac{8\pi}{(hc)^3}(kT)^4\frac{x^3}{e^x - 1}\sqrt{1 - (\frac{\beta}{x})^2}, \quad x \geq \beta. \tag{12}$$

The graph of the function (normalized on the constant factor) is shown on the Fig 1. below for different values of the parameter β. The graph with $\beta 0$ corresponds to the standard Planck's law and depends only on temperature. The graphs with $\beta > 0$ are dependent on temperature and the rest mass of the photon. Unlike the standard Planck's law, which turns into zero for $x0$, MPL turns into zero for $x = \beta$. Increase in β is equivalent to decrease in temperature. For $x \ll 1$ we get an analogue of the Rayleigh-Jeans law

$$\rho(x, m_\gamma, T) = \frac{8\pi}{(hc)^3}(kT)^4x^2\sqrt{1 - (\frac{\beta}{x})^2} \tag{13}$$

The condition $x \gg 1$ leads to Wien's radiation law:

doi: https://doi.org/10.52526/25792776-24.71.2-307

$$\rho(x, m_\gamma, T) = \frac{8\pi}{(hc)^3}(kT)^4 x^2 \sqrt{1 - (\frac{\beta}{x})^2}. \tag{14}$$

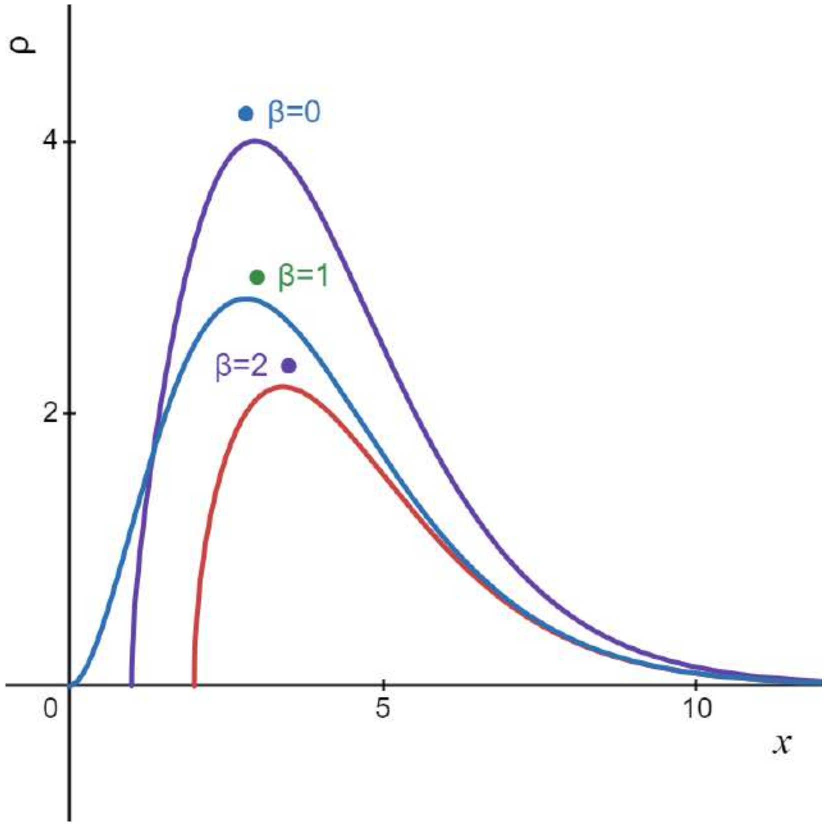

Figure 1. Modified Planck's laws (MPL)

The ratio of the average equivalent mass of a photon to its rest mass $\frac{\langle m \rangle}{m_\gamma}$ can be written simply as $\frac{\langle \epsilon \rangle}{\beta kT}$, from which it can be seen that for $\beta \ll 1$ (in the case of high temperatures) it tends to infinity (and the law of blackbody radiation tends to the standard Planck's law), which can formally be interpreted as a decrease in the photon's rest mass or an increase in the average mass equivalent of the photon while maintaining the rest mass. More detailed behavior of this function at small and large values of the parameter β is discussed in the Appendix. Correspondingly, it also determines the difference between the modified Stefan-Boltzmann law in these extreme cases and its standard analogue. At small values of the parameter $\beta \ll 1$, the average mass of the photon is defined by formula (A.6) of the Appendix, which gives:

$$\langle m \rangle = \frac{6.493939 - 0.822407\beta^2}{2.404112 - 0.5\beta^2(1 + \beta - ln\beta)} \frac{kT}{c^2}, \tag{15}$$

where the expression dependent on β is simply the ratio of integrals in (8), for which we use the notation $\alpha(\beta)$ in Appendix. For large values of β, the mass ratio is given by the last formula (A.16)

$$\frac{\langle m \rangle}{m_\gamma} = \frac{\alpha(\beta)}{\beta} \approx 1. \tag{16}$$

Hence it follows that the average photon mass equivalent is the upper bound for the photon's rest mass (which is to be expected), and their values approach each other at low temperatures. In Table 1 we present the results of numerical integration of the mass ratio $r =< m > /m_\gamma$ for different values of β.

Table 1. Mass ratio vs. parameter β

β	0.005	0.05	0.5	5	50
r	540.2	54.12	5.622	1.361	1.039

We see how steeply the mean mass equivalent approaches the rest mass of the photon with an increase in β. Even for intermediate temperatures ($m_\gamma c^2 \sim kT$) these two masses are close enough to each other

doi: https://doi.org/10.52526/25792776-24.71.2-307

within the same order of magnitude. As we said above (and it also can be seen from equation (10)), for the standard Planck spectrum:

$$\langle m \rangle = 2.701 \frac{kT}{c^2} = 4.141 \times 10^{-40} T kg. \tag{17}$$

It is interesting to evaluate the mean mass equivalent of the photon for some temperatures that are of physical interest. The best approximation to absolute zero, achieved experimentally, is estimated to be equal to $T = 3.8 \times 10^(- 11 \circ K$ (Depner & et al., 2021). Then for the hypothetic radiation with such a low effective temperature

$$\langle m \rangle = 1.574 \times 10^{-50} kg. \tag{18}$$

For the CMB photon with the temperature of $T = 2.725 \circ K$ (Fixsen, 2009, Peebles, 2020), we have

$$\langle m \rangle = 1.128 \times 10^{-39} kg. \tag{19}$$

This number is expectedly different (as it follows from the equations shown above) from estimates of m, obtained by investigation of CMB dipole anisotropy (De Bernardis et al., 1984) with a confidence level of $68\% : m_\gamma \sim (2.9 \pm 0.1) \times 10^{-54} kg$. In the meantime, based on radio-wave interferometriv measurements of the free-space velocity of electromagnetic waves on 72 GHz (almost twice less than the frequency of CMB radiation, peaked at $160.2 GHz$),with the accuracy $\sim 10^{-7}$ (Froome, 1958). One can estimate the upper limit of $m_\gamma < 4.3 \times 10^{-43} kg$ (see Tu et al., 2004). These results simply point to the low value of β ($\beta \ll 1$) and show that CMB radiation is blackbody radiation by its nature, not noticeably affected by the massive photon if the temperature is high. It follows from (12) that the mass equivalent of the photon tends to infinity with unlimited increase in temperature. This is a purely formal outcome that cannot be satisfied because of the reasons explained below in the text.

The mass equivalent of the photon, used in this paper and earlier in Saiyan (2023), is defined in free space and does not have to be confused with the effective mass of the photon defined in quantum electrodynamics instead of the term relativistic mass. It comes into play due to the interaction of photons with a medium (such as plasma triggered by a strong laser pulse in the gas) (Emelyanov, 2017, Mendonca, 2001, Yee, 1984) and is determined through the frequency of plasma oscillations. These two concepts are the same only if the rest mass of the photon equals zero. The only similarity is that the effective mass at high temperatures (if the energy of radiation is much greater than the rest energy of an electron) is proportional to the temperature Emelyanov (2017), as we have stated above for the mass equivalent and the rest mass in formulas (14) and (15) for high and low temperatures. As we can conclude from (15), our calculations show that the massiveness of the photon seems to be more significant factor at low temperatures ($kT \ll m_\gamma c^2$) and is negligible for high temperatures when the MPL approaches the standard Planck law (low and high temperatures are linked to the independently estimated rest mass of the photon). This conclusion agrees with the statement of Primak & Sher (1980) according to which the photon would acquire a non-zero mass mγ below some low temperature ". This idea is in tune with the physical model of Resca (2023) for dark energy as a Bose-Einstein condensate of cosmologically massive photons. The process which is taking place for bosons under some critical temperature, but impossible for massless photons in free space. The Bose-Einstein condensate was achieved in 2010 in a microscopic optical cavity for photons with effective mass (Klaers et al., 2010).

2.2. Modified Stefan-Boltzmann Law

The modified Stefan - Boltzmann law can be obtained by defining the upper integral in (10) after substituting expression (9) into it and integrating over all frequencies. This gives the total radiation energy density across the spectrum:

$$u(T) = \frac{8\pi}{(hc)^3} (kT)^4 \int_\beta^\infty \frac{x^3}{e^x - 1} \sqrt{1 - (\frac{\beta}{x})^2} dx. \tag{20}$$

Following the integration method for $\beta \ll 1$, presented in the Appendix, it is possible to write the modified Stefan-Boltzmann law, which, unlike the standard one, contains a temperature-dependent correction factor (see also Nyambuya, 2017, Pardy, 2018, Torres-Hernandez, 1985).

doi: https://doi.org/10.52526/25792776-24.71.2-307

$$u(T) = \sigma T^4[1 - \frac{5}{4(\pi)^2}(\frac{m_\gamma c^2}{kT})^2], \tag{21}$$

in which the Stefan-Boltzmann constant is given by the expression $\sigma = \frac{8}{15}\frac{(\pi)^5}{(hc)^3}k^4$. At high β values (that is, at low temperatures $kT \ll m_\gamma c^2$) the dependence of the total radiation density on temperature already changes. Returning to the first formula in (A.16) in Appendix we find:

$$u(T) = \frac{8\pi}{(hc)^3}\sqrt{\frac{\pi}{2}}(m_\gamma c^2)^4(\beta)^{\frac{5}{2}}e^{-\beta}. \tag{22}$$

That is, the radiation density at low temperatures is characterized by the presence of a rapidly decreasing exponential term and with a decrease in temperature tends to zero much faster than in the case of the standard Stefan-Boltzmann law. This is due to the fact that the condition $\beta \gg 1$ automatically entails $x \gg 1$, which means a transition to the Wien's radiation law. In the case of the Raleigh-Jeans law, the condition $x \ll 1$ automatically entails the condition $\beta ll 1$, but the converse is no longer true: $x \ll 1$ does not follow $\beta \ll 1$. As we can see, a massive photon gas has a more complex temperature behavior than a massless one. This circumstance also affects the behavior of radiation pressure in different temperature regimes.

2.3. Modified Wien's Displacement Law

This aspect of the theory of massive photon radiation has not been discussed in the literature, as far as we know, but it is an important component of the theory of blackbody radiation. If we take the derivative of function (11) with respect to the dimensionless variable x, we arrive at the equation $(3x^2 - \beta^2)(e^x - 1) = x(e^x)(x^2 - \beta^2)$, which can be conveniently transformed to the form:

$$e^x[x^2(3 - x) + \beta^2(x - 2)] = 3x^2 - 2\beta^2. \tag{23}$$

This coincides with the standard equation for finding the maximum frequency of the standard Planck's law for $\$beta = 0$

$$e^x(3 - x) = 3, \tag{24}$$

that has two solutions: the trivial $x = 0$, which defines the minimum of radiation at $\nu = 0$ and $x_m = 2.821$, which defines the maximum. The frequency of radiation maximum for $\beta > 0$ can be found from the following relation:

$$\nu_m = x_m \times \frac{kT}{h} = 2.08366 \times 10^{10} T \frac{Hz}{K} x_m, \tag{25}$$

where values of x_m can be computed numerically for arbitrary β. Some examples are shown in Table 2.

Table 2. Parameters of MPL

0	2.82144	5.87892
1	2.96720	6.18264
2	3.40845	7.10205
3	4.09228	8.52692
4	4.91805	10.22670
5	5.81583	12.09740
6	6.75108	14.06700
10	10.63470	22.15760
15	15.58460	32.46840
20	20.56150	42.84320
25	25.54840	53.23420
30	30.53980	63.63460
50	50.52330	105.2730

Hence it follows that the maximum of the radiation of massive photons with decreasing temperature (increasing β) has a greater shift to the high-frequency part of the spectrum compared to the standard

doi: https://doi.org/10.52526/25792776-24.71.2-307

Planck's law. One can easily see that for large values of β (low temperatures) $x_m \approx \beta$ (more precisely $x_m \approx \beta + 0.5$), which gives us the equation

$$x_m = 4.8 \times 10^{-11} \frac{\nu_m}{T} \frac{K}{Hz} \approx \beta = \frac{m_\nu c^2}{kT}. \tag{26}$$

From the last relation, we have

$$m_\gamma \approx 4.8 \times 10^(-11) \frac{k}{c^2} \nu_m = 8.668 \times 10^{-51} \nu_m \frac{kg}{Hz} \tag{27}$$

This relation shows that the ratio $\frac{m_\gamma}{\nu_m}$ remains constant at low temperatures and equal to $8.668 \times 10^{-51} \frac{kg}{Hz}$. The lowest frequencies of electromagnetic radiation, discussed in publications, are around $10^{-3} Hz$ (estimated for the Earth's magnetic field) and known as micro-pulsations (Troitskaya & Gul'elmi, 1967). Bass & Schredinger (1955)consider the micro-pulsations as Gaussian fluctuations of the permanent magnetic field. If we substitute this number into the last relation instead of ν_m we obtain m_γ $8.668 \times 10^{-54} kg$, which is almost the same number as the one accepted by Physical Data Group (PDG) (Navas & and Particle Data Group, 2024) and considered to be the most reliable upper experimental limit for the rest mass of the photon.

2.4. Radiation pressure of amassive photon gas

The radiation pressure is determined by the formula p=u/3. In the explicit form

$$p = \frac{1}{3} \sigma T^4 [1 - \frac{5}{4\pi^2} \frac{m_\gamma c^2}{(kT)^2}], \tag{28}$$

if the high temperature condition is satisfied ($m_\gamma c^2 \ll kT$). At low temperatures

$$p = \frac{1}{3} \frac{8\pi}{(hc)^3} \sqrt{\frac{\pi}{2}} (m_\gamma c^2)^4 \beta)^{\frac{5}{2}} e^{-\beta}. \tag{29}$$

For high temperatures we have the following inequality:

$$T \gg 6.523 \times 10^{39} m_\gamma \frac{K}{kg}. \tag{30}$$

The rest mass estimates, obtained from observations of different astrophysical sources in different wavelength ranges and under different conditions of the space environment vary within $(10^(-63) - 10^(-31))kg$ (Navas & and Particle Data Group, 2024, Shaefer, 1999, Tu et al., 2004). If we accept the upper limit for the rest mass of the photon suggested by PDG, then the temperature can be considered high if

$$T \gg 1.163 \times 10^{-14} \circ K. \tag{31}$$

This condition is met in the Universe with great excess. That is, virtually MPL does not differ noticeably from the standard Planck law as we stated above. But if the estimate of the photon rest mass is refined to a higher order of magnitude, then this conclusion must be revised. For example, if we accept $m_\gamma \approx 10^{-31} kg$ (based on studies of Mark 421 galaxy (see Shaefer, 1999, and references therein) as the upper limit of all estimates of the rest mass, then we must infer that the temperature is high if the following condition holds:

$$T \gg (10^8 - 10^9) \circ K \tag{32}$$

From the perspective of application of MPL it may affect some conclusions regarding stellar models. But is this upper limit of m_γ acceptable from a physical point of view?

3. Applications in astrophysics

3.1. Stellar models

As we know, the internal structure of stars is described by polytropic models, the stability of which is defined by the balance of gravitational forces and the net force of gas and radiant pressure, which depends on temperature. For stars such as the Sun, the Eddington model with a polytropic index of n=3 is considered

doi: https://doi.org/10.52526/25792776-24.71.2-307

the most acceptable (Eddington, 1926). In the model, the ratio of gas pressure to net gas and radiation pressure is assumed to be constant throughout the volume. It is obvious that due to properties of the massive photon gas set above, that criterion no longer holds. Estimates of the temperature in the nuclear region of the Sun lead to the values at which thermonuclear reactions begin, and the condition of high temperatures is excessively fulfilled even for values of m_γ of higher orders of magnitude. This allows to neglect the correction term in the expressions for the Stefan-Boltzmann law and radiant pressure. Therefore, in general, it can be assumed that conclusions, derived within the framework of conventional stellar models, remain valid and the massiveness of photons, by and large, does not play a significant role here. Note that the radiation pressure is much more significant in massive stars, where temperatures in nuclear regions can reach $T \sim 1.5 \times (10^8 - 10^9) \circ K$, and the main source of opacity of the medium is the Thomson scattering (Maeder et al., 2012). If the upper limit of m_γ, discussed above is accepted, then for temperatures just mentioned, $\beta \approx 1$, and correction factor to the Stefan-Boltzmann law and radiant pressure should be taken into consideration.

3.2. Radiation scattering

We will briefly discuss the effect of the "massiveness" of radiation on two types of scattering Thomson and Compton. Massive radiation is a solution of the Proca equation, in which the wave vector is represented in the form (5) or (6), reflecting the effect of optical dispersion in vacuum. We will limit ourselves to considering the classical case of the Thomson scattering at the qualitative level. Despite quantum theories are also available in publications (Crowley & Gregori, 2014), the massiveness of the photon is not considered there. Describing the scattering of a monochromatic electromagnetic wave on a non-relativistic electron, we consider the dependence of its phase velocity on the frequency, using it instead of the standard speed of light. As a rule, the dependence of the electric field strength on coordinates and the influence of the magnetic field strength vector on the expression for the Lorentz force are neglected due to the smallness of the electron's velocity compared to the speed of light. Taking into consideration the radiation reaction, the total cross section of Thomson scattering (in terms of the cyclic frequency of the electromagnetic wave ω takes the form Terletsky & Ribakov (1980):

$$\sigma_T(\omega) = \frac{\sigma_0}{1 + \frac{4(r_0)^2(\omega^2)}{9c^2}}, \tag{33}$$

where σ_0 is the cross-section of the classic Thomson scattering. In the absence of radiation reaction, it is independent of frequency ω: $\sigma_0 = \frac{8\pi}{3} r_0^2$. The phase velocity can be found from (5):

$$\sigma v_p h = \frac{\omega}{k} = c\frac{\omega}{\sqrt{\omega^2 - (\omega_0)^2}}. \tag{34}$$

Substituting this formula in the expression instead of the usual speed of light, we get:

$$\sigma_T(\omega) = \frac{\sigma_0}{1 + (\frac{4(r_0)^2}{9c^2})(\omega^2 - (\omega_0)^2)}. \tag{35}$$

It follows that the cross-section of the Thomson scattering of a massive electromagnetic wave on an electron is greater than the same cross-section in scattering of a massless wave. The cross-section increases with increase of the rest mass and energy of the photon. This increases the optical thickness of the medium, making it less permeable to massive radiation. In this case, the standard Thomson cross-section is reached not at $\omega = 0$, but at $\omega = \omega_0$. It is natural to expect that the same conclusion about the cross-section is true for Compton scattering as well, which transforms into Thomson scattering at low photon energy. It is well known that Compton scattering is incoherent, unlike Thomson scattering, and is characterized by a shift in the frequency of the scattered photon depending on the scattering angle towards lower values compared to its frequency before scattering due to the transfer of energy to the electron. This (Compton) shift is usually written in terms of wavelengths in the form:

$$\Delta\lambda = \lambda\prime - \lambda = \frac{h}{m_e c}(1 - \cos\theta), \tag{36}$$

where $\lambda_e, \lambda\prime$ are the wavelengths of the photon before and after scattering respectively, θ is the scattering angle, and $\lambda_e = \frac{h}{m_e c} h)$ is the electron's Compton wavelength. It can be shown that in the case of massive photons, this shift is slightly less than the one expected for zero-mass photons. This can be verified by

doi: https://doi.org/10.52526/25792776-24.71.2-307

writing down the laws of conservation of energy and linear momentum for this case of Compton scattering in the electron's rest system:

$$E_\gamma + E_e = E\prime_\gamma + E\prime_{=} E\prime_\gamma + \sqrt{(p\prime_e c)^2 + (m_e c)^2}), \tag{37}$$

$$p_\gamma + p_e = p\prime_\gamma + p\prime_e, \tag{38}$$

In the equations shown above E_γ, p_γ are the energy and linear momentum of the photon before scattering, E_e - electron rest energy. Energies and momenta of the photon and electron after scattering are provided with an apostrophe sign. Now we can find the difference in wavelengths of the incident and scattered photon (from the system of equations (36, 37) by substituting into it the expressions for specified quantities in the form:

$$\Delta\lambda = \lambda\prime - \lambda, \lambda = \frac{c}{\nu}, \lambda\prime = \frac{c}{\nu\prime}, \tag{39}$$

$$E_\gamma = h\nu, E_e = m_e c^2, E\prime'_\gamma = h\nu\prime, \tag{40}$$

$$p_e = 0, p_\gamma = \hbar k, p\prime_\gamma = \hbar k\prime \tag{41}$$

The magnitudes of wave vectors of incident k and scattered k'photon in (40) are defined by formula (5) for the optical dispersion in vacuum.

$$\Delta\lambda = \lambda\prime - \lambda = \lambda_e[1 - \sqrt{(1 - \frac{\lambda\prime^2}{\lambda_0^2})(1 - \frac{\lambda^2}{\lambda_0^2})} \cos\theta - \frac{\lambda\lambda\prime}{\lambda_0^2}]. \tag{42}$$

Here, $\lambda_0 = \frac{h}{m_\gamma c}$ is the photon ' s Compton wavelength. λ_0 is the limiting value of the photon wavelength, infinite if $m_\gamma = 0$. Obviously, in this case (41) follows the ordinary Compton formula. By substituting, $\lambda\prime = \lambda + \Delta\lambda$,(41) can be reduced to a form that determines the irreducible dependence of the Compton shift on the wavelength of the incoming photon, an effect that is missing from the ordinary Compton effect. The expression on the right side of 41) can be simplified considering that $\lambda\prime, \lambda \ll \lambda_0$. Neglecting terms of order of smallness higher than two, we obtain:

$$\Delta\lambda = \lambda_e 1 - [1 - \frac{1}{2\lambda_0^2}(\lambda\prime^2 + \lambda^2)\cos\theta - \frac{\lambda\lambda\prime}{\lambda_0{}^2}. \tag{43}$$

For $\theta = 0$ the equation (42) in terms of $\Delta\lambda$ takes the form of a quadratic equation

$$\Delta\lambda[1 - \frac{\lambda_e}{2\lambda_0^2}\Delta\lambda] = 0, \tag{44}$$

which has one physically acceptable solution $\Delta\lambda = 0$, the same as in the case of the ordinary Compton effect, which means that there is no change in the frequency of the photon as it is scattered forward. Further, in vertical scattering $\theta = \frac{\pi}{2}$ we have a linear equation the solution of which is

$$\Delta\lambda = \lambda_e \frac{1 - \frac{\lambda^2}{\lambda_0^2}}{1 + \frac{\lambda_e\lambda}{\lambda_0^2}}. \tag{45}$$

That is, the Compton shift is less than in the case of massless photons when it simply equals λ_e. At $\theta = \pi$ (backscattering) (42) is reduced to a quadratic equation with one physically acceptable solution:

$$\Delta\lambda \approx \lambda_e(1 - \frac{\lambda^2}{\lambda_0^2}) \leq 2\lambda_e. \tag{46}$$

This leads to the same conclusion as for vertical scattering: the Compton shift for massive photons is smaller than for massless photons. The solution (45) slightly differs from backscattering case in the standard Compton-effect when $\Delta\lambda = 2\lambda_e$.

doi: https://doi.org/10.52526/25792776-24.71.2-307

3.3. Early stages of the Universe

We have already mentioned above that as the radiation temperature increases, the average mass equivalent of the Planck photon grows boundlessly. This result is formal for two reasons. The first one is that with an increase in temperature and, correspondingly, radiation density, the probability of two-photon and multiphoton collisions increases, leading to the production of electron-positron pairs at energies above 1.022 MeV, which limits the further growth of the photon's mass equivalent. The reaction of particle-antiparticle pair production, resulting from massless photons collision, is known as the Breit-Weeler process (Breit & Wheeler, 1934) (hereafter the BW-process) and is the opposite of the annihilation process. Experiments show very low probability of the phenomenon ($\sim (10^{-7} - 10^{-5})$ (Ribeyre & et al., 2016), depending on the energies of the photons), which has not been confirmed over almost eight more decades (Adam & et al., Adam & et al.). Collisions between photons lead to the "viscosity" of the photon gas and deviation from the condition of ideality. Speaking in general, the radiation of colliding photons cannot be described by Planck's standard law. The cross-section of BW-process is $\sim {r_0}^2$ (where $r_0 \approx 2.8179 \times 10^{-15} m$ is the classical electron radius) with an accuracy of up to a coefficient of the order of unity (Ribeyre & et al., 2016). At these distances, quantum electrodynamic effects become significant. The Compton wavelength of a massive photon reaches the value of r_0 at energies with the equivalent temperature $T \sim 10^12 \circ K$, which is typical for the transition from the quark epoch to the hadron epoch in the early universe.

The second reason is that it makes sense to talk about photons as independent particles and carriers of electromagnetic interaction up to temperatures not higher than $\sim 10^15 \circ K$. In this case, a spontaneous violation of the symmetry of electroweak interaction, associated with a drop in temperature as the Universe expands, takes place, after which the electromagnetic interaction separates from the weak one, and becomes a distinct physical force. This happens at the times of $\sim 10^{-12}$ seconds after the Big Bang and is interpreted as an electroweak phase transition due to the Higgs mechanism (Higgs 1964). In the case of photons with non-zero mass, as in Thomson scattering, it is natural to expect an increase in the scattering cross-section for the BW-process compared to massless photons, and, therefore, an increase in its probability. As a result, it will increase the production of electron-positron pairs. The last circumstance as it said above limits growth of the photon mass equivalent and contributes to an increase in the opacity of the cosmic medium for high-frequency radiation in the range of energy values that exceeds the excitation threshold of the BW process. It results in limitation of the spectral range of high energy photons in cosmological medium. But we must make the following remarks as well. With the exponentially growing volume of the Universe in the early inflation epoch (Guth, 1981, Linde, 1984, Tsujikawa, 2003) and the rapid increase in the rate of cooling because of the expansion, the annihilation process won't be able to compensate for the loss of photons due to BW-process which cannot be long lasting. Collisions between massive photons seem to have more chances to produce particle - antiparticle pairs compared with massless photons. This production will increase the role of Thomson scattering in the formation of opacity of the cosmological medium. In the meantime, the existence of more electrons caused by more frequent collisions of the photons increases the probability of the formation of neutral atoms and decreases the opacity. It is difficult to say to what extent this process in the presence of a massive photon field affects the estimate of duration of the pre-recombination period in the evolution of the Universe. We do not know any estimates regarding this matter. However, from the above said, one can assume that the onset of the post-recombination epoch could have occurred somewhat earlier than is generally believed.

It is interesting to notice that because always $m_\gamma \leq \langle m > \rangle$ (regardless the value of parameter β and the upper limit of the mass equivalent of the photon is defined by (16), for $T = 10^{15} \circ K$ we have $m_\gamma \leq 4.141 \times 10^{-25} kg$ - the mass nearly equal to the mass of the Higgs boson ($125.35 GeV = 2.231 \times 10^{-25} kg$, (ATLAS Collaboration, 2023) (125.11 GeV). The conclusion is that photons cannot have the rest mass greater than this. None of the existing measurements of this quantity are close to this limit.

3.4. Active galactic nuclei

The BW-process, described in the previous section, can also be implemented using the inverse Compton effect in the near-nuclear regions of active galaxies, such as Markarian 421 and 501, which demonstrate a high degree of activity across the spectrum, from radio to gamma rays (Acciari et al., 2020, Aharonyaan & et al., 1997, Carnerero et al., 2017). The activation of the BW - process in these sources is possible because of synchro-Compton scattering, when photons of synchrotron radiation sharply increase their energy during inverse Compton scattering on the relativistic electrons that generated them proportionally toγ^2, where

doi: https://doi.org/10.52526/25792776-24.71.2-307

γ 1000 is the Lorentz factor (Beckmann, 2006, Sunyaev, 1986). For example, radio frequencies can "migrate" to the ultraviolet region, and optical photons can "migrate" to the gamma range. The role of massive photons in these processes can be manifested not only in the existence of time dispersion and variations in the speed of light. These high energy photons will contribute to EBL (Extragalactic Background light, which is another component of the total diffuse cosmic radiation in addition to CMB), and that way, to the pair-production cutoff (Franceschini et al., 1994, Stecker & de Jager, 1997)which is comprehensively explained and discussed by (Franceschini, 2021) who also has mentioned that the number of such energetic photons is decreasing very sharply with energy $\propto \gamma^{-2,-3}$ at least).

4. Spreading time of the photon wave packet

The wave packet of a massive photon can be formally represented as a very concentrated superposition of quasi-monochromatic waves with very close frequencies. Since (as can be seen from (5)) the dependence of frequency on the wave vector is nonlinear, purely theoretically, there must be some spreading of the wave packet of a massive photon in free space. For the massless photon the wave packet in vacuum is infinite, that is, the photon does not spread out in free space. As is known (Zemtsov & Bychkov, 2005), the spreading time of the wave packet is

$$\tau = \frac{(\Delta x)^2}{d^2\omega/dk^2} \tag{47}$$

where Δx is its width. If $\Delta x \sim \lambda = \frac{c}{\nu} = \frac{2\pi c}{\omega}$, one can estimate τ by finding ω from the equation (4):

$$\omega = \sqrt{(kc)^2 + \omega_0^2}\omega_0 = 2\pi\nu_0. \tag{48}$$

Performing differentiation, we obtain

$$\frac{d^2\omega}{dk^2} = \frac{2\pi\nu^3}{\nu_0^2}, \quad \tau \sim \frac{2\pi\nu}{\nu_0^2} = \frac{2\pi\nu h^2}{m_\gamma{}^2c^4} \tag{49}$$

Taking as above $m_\gamma < 10^{-18}eV = 1.783 \times 10^{-54}kg$, we obtain

$$\tau > 1.074 \times 10^8\nu(s) \tag{50}$$

If the left-hand side of the inequality is taken to be equal to the age of the Universe in seconds,

$$t_u \ \sim 4.352 \times 10^17(s), \tag{51}$$

then all photons with the frequency $\nu \geq 4.052 \times 10^9 Hz(\lambda \leq 7.4cm)$ have wave packets with a spreading time greater than the age of the Universe. For CMB radiation $\nu = 1.602 \times 10^11Hz$ we have $\tau \sim 1.721 \times 10^19s$ which exceeds this age by almost 40 times. Virtually, in a very wide range of frequencies, which are of interest to astrophysics, the wave packet of a massive photon does not spread.

5. Conclusions and discussion

The paper derives Planck's law of radiation for massive photons. The dependence of the ratio of the mean mass equivalent of the photon to its rest (invariant) mass on different temperature regimes is studied. It tends to infinity at high temperatures and approaches unity at low temperatures. In the first case MPL approaches the standard Planck's law, and the massiveness of the photon becomes a nonsignificant factor in the radiation process. At intermediate and low temperatures, deviation of MPL from Planck's law increases, and the massiveness of the photon should be considered with the lowering intensity of the radiation. Stefan-Boltzmann and Wien's displacement laws for massive photons are derived, as well as an expression for radiation pressure, which takes different forms at high and low temperatures. The estimate of the Thomson cross-section of the scattering of massive photons on a free electron turned out to be slightly greater than its value in the usual case, which increases the optical thickness of the scattering medium. In the case of Compton scattering, the wavelength shift is less than its value in the process of massless photons, except in the case of scattering forward, where the wavelength remains unaltered. Apparently, the existence of the rest mass of the photon ($m_\gamma < 10^{-54}kg$) is not a significant factor for the wide range of astrophysical events.

doi: https://doi.org/10.52526/25792776-24.71.2-307

However, this conclusion may change with mass estimates of a higher order of magnitude. Estimates of the spreading time of the massive photon show that they remain stable in free space at time intervals exceeding the age of the Universe. Slight deviations of the Thomson and Compton scattering cross-sections (as well as Compton shift) from their standard values could serve as indirect evidence in favor of the hypothesis that the photon has a rest mass. As we know, these deviations have not been discovered so far.

References

ATLAS Collaboration 2023, Phys. Lett. B, 843, 137880

Acciari V. A., Ansaldo S., et al. 2020, Astron.&Astrophys, A86, 86

Adam J., et al., Phys. Rev. Lett., p. 052302

Aharonyaan F. L., et al. 1997, Astron. & Astrophys., 327, L5

Bass L., Schredinger E., 1955, Proc.Royal.Soc A, 232, 6

Batman G., Erdelyi A., 1974, Vischie Transcendentnie Funktsii Higher Transcendental Functions. Nauka, Moscow, Russia

Beckmann L., 2006, Inverse Compton Scattering. University of Maryland, USA

Biller S. D., et al. 1999, Limits to Qiantum Gravity Effects from Observations of TeV Flares in Active Galaxies. AIP Conf.Proc. 516 (2000),New York

Blokhintsev D. I., 1976, Osnovi Kvantovoi Meckhaniki Foundations of Quantum Mechanics. Nauka

Breit G., Wheeler G. A., 1934, Phys.Rev., 46, 1087

Butto N., Tikva R., 2022, Journal of High Energy Physics, Gravitation and Cosmology, 8, 76

CMS Collaboration 2020, Phys. Let. B, 805, 135425

Carnerero M. I., Raiteri C. M., et al. 2017, Mon.Not.R.Astron.Soc, 472, 3789

Crowley B. J. B., Gregori G., 2014, High Energy Density Phys., 13, 55

De Bernardis P., Masi S., Melchiori F., Molet A., 1984, Astrophys.J., 284, L21

De Brogle L., Vigier J. P., 1972, Phys. Rev. Let., 28, 1001

Depner C., et al. 2021, Phys. Rev. Let., 127 (10), 100401

Dombey N., 1980, Nature, 288, 643

Eddington A. S., 1926, he Internal Constitution of the Star. Cambridge University Press

Emelyanov S., 2017, Nuc. Phys. B, 919, 110

Feynman R. P., 2018, Statistical Mechanics. CRC Press Taylor and Francis Group, Boca Rayton, Florida,USA

Fixsen D. J., 2009, Astrophys.J., 707, 916

Franceschini A., 2021, Universe, 7, 146

Franceschini A., Mazzei P., de Zotti G., Danese L., 1994, Astrophys.J, 427, 140

Froome K. D., 1958, Proc. Phys. Soc. Lond. Sect. A, 247, 109

Goldhaber A. S., Nieto M. M., 1976, Scientific Ammerican, 235, 86

Goldhaber A. S., Nieto M. M., 2010, Rev. Mod. Phys., 82, 939

Guth A. H., 1981, Phys. Rev. D., 23, 347

Higgs P. M., 1964, Phys. Rev. Let., 13, 508

Klaers J., Schmidt J., Vewinger F., Weitz M., 2010, Nature, 468, 545

Kobzarev Y. I., Okun L. B., 1968, Sov. Phys. Usp, 11, 338

Linde A. D., 1984, Rep. Prog. Phys., 47, 925

Maeder A., Georgy C., et al 2012, Astron. & Astrophys., 539, A110

Mendonca J. T., 2001, The Theory of Photon Acceleration. Institute of Physics Publishing

Navas S., and Particle Data Group 2024, Phys. Rev. D, 110, 030001

Nyambuya G. G., 2017, Prespacetime Journal, 8, 663

doi: https://doi.org/10.52526/25792776-24.71.2-307

Pardy M., 2018, arXiv:hep - ph/ 0308190v1

Peebles P. J. E., 2020, Cosmology's century. An inside history of our modern understanding of the Universe. Princeton University Press

Poenaru D. N., 2006, Proca equation of a massive vector boson field

Primak J. R., Sher M. A., 1980, Nature, 288, 680

Resca L. G., 2023, Indian J. Phys., 97, 605

Ribeyre X., et al. 2016),, Phys. Rev, E93, 013201

Saiyan G. A., 2023, ComBAO, 70, 348

Shaefer B. E., 1999, Phys.Rev.Lett., 82, 4964

Stecker F. W., de Jager O. C., 1997, Astrophys.J., 476, 712

Sunyaev R. A., 1986, Compton scattering

Terletsky Y. P., Ribakov Y. P., 1980, Electrodinamika. Visshaya Shkola

Torres-Hernandez J., 1985, Phys. Rev. A, 32, 623

Troitskaya V. A., Gul'elmi A. V., 1967, Sp. Sci. Rev., 7, 689

Tsujikawa S., 2003, arXiv.hep-ph/0304257

Tu L.-C., Luo J., Gillis G., 2004, Rep.Prog. Phys., 68, 77

Yee J. H., 1984, Journal of the Korean Physical Society, 17, 100

Zemtsov Y. K., Bychkov K. V., 2005, Textbook on Atomic Physics po Atomnoi Fizike. Moscow State University

doi: https://doi.org/10.52526/25792776-24.71.2-307

Appendices

Appendix A Analytical study of integrals

Integrals in (10) can analytically be evaluated in two extreme cases, low and high temperatures (i.e., at very large and small β). Torres-Hernandez (1985) discussed these extreme physical cases just in a few words not presenting any detailed calculations. Although it is obvious that at $\beta \ll 1$ MPL approaches the standard Planck's law, it is nevertheless interesting to clarify the expression for the mean mass equivalent of the photon at non-zero values of this parameter. It makes theoretical analysis of the problems considered here more complete. Omitting the constant factors in the upper and lower integrals in (10) and introducing notations $I_1(\beta), I_2(\beta)$ for them, we write it down in terms of the variable x and parameter β, introduced earlier in the text:

$$I_1(\beta) = \int_{\beta}^{\infty} \frac{x^3}{e^x - 1}\sqrt{1 - (\frac{\beta}{x})^2} dx \tag{52}$$

$$I_(2)(\beta) = \int_{\beta}^{\infty} \frac{x^2}{e^x - 1}\sqrt{1 - \frac{\beta}{x}^2} dx \tag{53}$$

Decomposing the first integral into the Taylor series by powers of β and applying Leibniz's formula, we get, limiting ourselves to the first two terms,

$$I_(1)(\beta) \approx \zeta(4)\Gamma(4) - 1/2\zeta(2)\beta^2, \tag{54}$$

where $\zeta(s)$ is the Riemann zeta function, and $\Gamma(x)$ is the gamma function (Batman & Erdelyi, 1974):

$$\zeta(s) = \frac{1}{\Gamma(s)} \int_0^{\infty} \frac{x^{s-1}}{e^x - 1} dx \tag{55}$$

$$\Gamma(x) = \int_0^{\infty} e^{-t} t^{x-1} dt. \tag{56}$$

To estimate the second integral in (52), it is convenient to decompose the square root in the Tylor series by powers of *beta* in the vicinity of the point $\beta = 0$, which leads to the difference between the two integrals:

$$I_2(\beta) \approx \int_{\beta}^{\infty} \frac{x^2}{e^x - 1} dx - \frac{1}{2}\beta^2 \int_{\beta}^{\infty} \frac{dx}{e^x - 1}, \tag{57}$$

if we confine ourselves, as before, to the first two terms. The first integral in (A.6) can be written as

$$\int_{\beta}^{\infty} \frac{x^2}{e^x - 1} dx = \int_0^{\infty} \frac{x^2}{e^x - 1} dx - \int_0^{\beta} \frac{x^2}{e^x - 1} dx \approx \zeta(3)\Gamma(3) - \frac{1}{2}\beta^2, \tag{58}$$

using the fact that with small β in the last integral in (A.7) $e^x - 1 \approx x$. In the last integral in (A.6) one can make a substitution $t = e^x - 1$, and making β -$ln(\beta)$. Thus

$$I_2(\beta) \approx \zeta(3)\Gamma(3) - \frac{1}{2}\beta^2(1 + \beta - ln\beta). \tag{59}$$

Hence it follows that at high temperatures

$$\langle m \rangle = \frac{\zeta(4)\Gamma(4) - \frac{1}{2}\zeta(2)\beta^2}{\zeta(3)\Gamma(3) - \frac{1}{2}\beta^2(1 + \beta - ln(\beta))} \frac{kT}{c^2}. \tag{60}$$

This expression leads to (14) after substituting numerical values of the zeta and gamma functions. The expression for $I_1(\beta)$ leads to (20) and (27), because

$$I_(1)(\beta) = \frac{\pi^4}{15}(1 - \frac{5\beta^2}{4\pi^2}). \tag{61}$$

To analyze integrals $I_1(\beta)$, $I_2(\beta)$ at low temperatures, note that if $\beta \gg 1$, then $x \gg 1$ as well. Therefore, $e^x \gg 1$, and $e^x - 1 \approx e^x$. Then, if we set $t = \frac{x}{\beta}$, the integral $I_1(\beta)$ can be rewritten in the form:

doi: https://doi.org/10.52526/25792776-24.71.2-307

$$I_1\beta) = \beta^4 \int_1^\infty t^2 e^(- \beta t)\sqrt{t^2-1})dt, \tag{62}$$

which can be expressed in terms of the Macdonald function $K_\nu(\beta)$ using the following representation Batman & Erdelyi (1974):

$$\Gamma(\nu+\frac{1}{2})K_\nu(z) = \sqrt{\pi}\frac{z}{2}^\nu \int_1^\infty e^{-\beta t}(t^2-1)^{\nu-\frac{1}{2}}dt, \nu > -\frac{1}{2}, Rez > 0, \tag{63}$$

where ν is the order of the Macdonald function. In our case $\nu = 1, Rez = \beta \gg 1$. It gives

$$\frac{K_1(\beta)}{\beta} = \int_1^\infty e^{-\beta t}\sqrt{t^2-1}dt. \tag{64}$$

Since $t^2 = (t^2-1)+1$, for (64) we have:

$$I_1(\beta) = \beta^2[K_2(\beta) + \beta K_1(\beta)]. \tag{65}$$

With the aim of (64) the integral (62) can be expressed in the following way:

$$I_2(\beta) = \beta^3 \int_1^\infty t e^{-\beta t}\sqrt{t^2-1}dt = -\beta^3 \frac{K_1(\beta)}{\beta}\beta. \tag{66}$$

For $\beta \gg 1$ $K_n u(\beta) \sim \sqrt{\frac{\pi}{2\beta}}e^{-\beta}$ and then

$$I_1(\beta) \approx \sqrt{\pi}2\beta^{\frac{5}{2}}e^(- \beta), \quad I_2(\beta) \approx \sqrt{\pi}2\beta^{\frac{3}{2}}e^{-\beta}, \quad \alpha(\beta) = \frac{I_1(\beta)}{I_2(\beta)} \approx \beta. \tag{67}$$

Hence it follows the formula (15) in the text.

doi: https://doi.org/10.52526/25792776-24.71.2-307

Communications of BAO, Vol. 71, Issue 2, 2024, pp. 322-329

An Astronomical Interpretation of a Small Example from Armenian Folklore*

H.A. Malkhasyan †

NAS RA V. Ambartsumian Byurakan Astrophysical Observatory (BAO), Armenia

Abstract

This article examines an individual fragment of Armenian folklore about the Aratsani (Euphrates) River from an astronomical perspective, focusing on the central characters - the dragon-fish and the bear. Through this analysis, a wealth of "astronomical knowledge" rooted in ancient mythological perceptions is revealed. Specifically, the mentioned figures in the sky correspond respectively to the modern constellations of the Southern Fish (Piscis Austrinus) and the Great Bear (Ursa Major).The described scenes are correlated with the heliacal rising and setting of the main star of Southern Fish constellations. Furthermore, all defining characteristics of the figures are given precise astronomical and mythological interpretations. The legend also highlights expressions related to the unfolding time, which are thoroughly explained based on celestial phenomena and ancient Armenian calendrical concepts. It is demonstrated that the described celestial events are associated with a 65–70-day period, referred to in the Protohaykian calendar structure as the "extra-annual period." Additionally, the legend reveals close calendrical and ritualistic connections with the astronomical context of Fish-shaped Dragon Stones (Vishapakars). The comprehensive astronomical analysis enables the dating of the legend described to 18800 BC.

This serves as a small but striking example of how folklore can act as a unique source of rich astronomical information.

Keywords: *Armenian Folklore, Dragon-fish, Vishapakar, Piscis Austrinus, Ursa Major, Ethnoastronomy, Armenian Calendar History, Cultural Astronomy.*

1. Introduction

In recent decades, numerous examples of astronomical analyses of Armenian folklore have been published. Some of these studies focus on the calendrical content included in Armenian fairy tales (Broutian, 2008, 2009, 2010, 2011), others provide astronomical interpretations of specific small episodes or characters from the Armenian epic "Sasnay Tsrer" (The Daredevils of Sassoun) (Broutian, 2020b, 2021a,b,c). However, folklore is often used as a supplementary source of information in the study of astronomical heritage monuments, such as the "Zorats Qarer" megalithic complex (Malkhasyan, 2021, 2022, 2023a, 2024), the Dragon Stones stelae (Vishapakars) (Broutian, 2020a), and other material artifacts with calendrical significance (Broutian, 2007). These studies primarily reveal close connections between Armenian folklore and the fundamental structure of the so-called Protohaykian calendar (Broutian, 2011, 2016). In the references above, a variety of approaches to astronomical interpretation have been employed. However, these approaches are far from forming a standardized methodology. Nevertheless, in all cases, ancient Armenian mythological and calendrical concepts are used as key "tools" for the analysis. This article presents an example of such an analysis. **The challenge posed is to extract the possible maximum astronomical information from a highly concise narrative**. To achieve this, the subject of analysis is a brief traditional legend recorded in the historical Mush province (Bulanykh, Western Armenia) (Bense (1972), p. 48).

*A brief report on the results of this work was presented at the international conference "Armenology in the Context of Languages and Cultures", held on April 18–19, 2023, in Moscow.

†malkhasyan.hayk84@gmail.com

2. Material and Methods

Before proceeding with the analysis, it is essential to provide the full text[1] of the legend in question. The following is told about the Aratsani (Euphrates) River:

"Hunters were pursuing[2] a bear, which, while escaping, fell into the river. A few minutes later, the bear suddenly resurfaced and its fur plucked. The river becomes bloody, and shortly after that, a dragonfish with a split belly spreads out on the surface of the water. It is placed on a wagon, transported to the city (Manazkert), and distributed part by part among the townspeople." (Bense (1972), p. 48)

2.1. Identification of Main Characters

For the purposes of astronomical interpretation, the main characters and objects of the legend have been isolated and aligned with the corresponding astronomical concepts (Table 1). The following enumerated list corresponds to the justifications for these associations:

1) In the present case, the celestial parallel for the bear should be considered as the modern constellation of Great Bear. This equivalence has been discussed in more detail in another context (Malkhasyan, 2021), so there is no need to repeat the justification here.

2) Although the role of hunters is not highly emphasized in the legend, their presence clearly points to an ancient scene of hunting. The bear was explicitly identified, reflecting hunting practices from ancient times. The hunters actively pursue 'the bear', which implies a star or constellation that rises and sets after the stars of the Great Bear. In particular, hunters are described as present when the bear falls into the river, but are not mentioned when the bear emerges. This is logical, as the constellations that 'follow' the Great Bear are below the horizon during its rise and are not visible, unlike at the time of their setting. It is also worth noting that in the "Hamatarats Ashkharhacoyc" (Extensive World Map) by Ghukas Vanandeci (1695), the constellation of Boötes (Eznarats), which "follows" Great Bear, is named "Arjapan" (Guard of the Bear). On the other hand, Vanandeci (1695) illustrates another constellation in this region as a man with a club. With some reservation, It is possible to propose that the legend refers to these very constellations, with a higher probability for Boötes (Eznarats).

3) The earliest known Mesopotamian cuneiform sources reference a constellation called "Fish" written as ^{mul}KU$_6$. This star name corresponds to the Southern Fish constellation (Piscis Austrinus), particularly its brightest star, Fomalhaut (α Piscis Austrini) (Hunger & Pingree, 1999, Van der Waerden, 1974). In Mesopotamia, this constellation had significant mythological value, strongly associated with the primary God, Haya. From his shoulders sacred rivers are said to flow, one of which is the Aratsani (Euphrates) River.

4) The fall of the bear into the river should be interpreted as its setting below the horizon. In other words, the river here must be understood as the actual visible horizon.

5) Similarly, both in Mesopotamian (Van der Waerden (1974) p. 82) and Armenian (Tumanyan (1968) p. 97) sources, the modern constellation of the Great Bear is attested as "The Wagon". Numerous functional associations between the bear and the wagon are noted in Armenian folklore (Malkhasyan, 2021). Thus, in this particular legend, the celestial parallel for the wagon should again be viewed as the constellation of Great Bear.

Thus, in the legend there were identified several main characters and objects, which have been aligned with the corresponding astronomical concepts (Table 1). Now, let us examine the contexts in which these characters are depicted and correlate the astronomical phenomena associated with these situations.

[1] Translated from Armenian and annotated by **Mariam Kurazyan.**

[2] The following describes the actions of hunters chasing the bear, not just passively following it but actively trying to catch or drive it. Violent measures are being applied to suppress and destroy it.

Table 1. Main characters from the legend and corresponding astronomical concepts.

No.	Characters	Corresponding Astronomical Concepts
1	Bear	Great Bear (Ursa Major) constellation
2	Hunters	Constellations of the Boötes and/or Hercules?
3	River	Actual (visible) Horizon
4	Dragon-fish	Southern Fish (Piscis Austrinus) constellation
5	Wagon	Great Bear (Ursa Major) constellation

2.2. The Actions of the Bear

The bear is described in two situations, each of which corresponds to different positions of the Great Bear (Ursa Major) constellation in the sky. These are as follows:

A. **Falling into the river:** This corresponds to the descent of the bright stars of the constellation (the position after which the stars set below the horizon and are no longer visible).

B. **Emerging from the river with plucked fur:** This aligns with the moments when the stars of the same constellation rise above the horizon. The bear's condition—emerging from the river with its fur plucked—likely corresponds to a position in which not all of the constellation's stars are visible above the horizon, meaning part of the constellation has yet to rise (see subtitle 3.3). It is notable that, today, for an observer at the geographical latitude of the Armenian Highlands, six of the seven brightest stars of the Great Bear constellation do not set due to their proximity to the North Pole (Figure 1a). However, in the legend, the bear completely submerged underwater, suggesting that, historically, the settings of the constellation's seven brightest stars could all have been observed.

Taking into account only this fact, one can estimate the time period when a person would have been able to witness the setting of all seven bright stars in the Great Bear (Ursa Major) constellation. For the geographical latitude of the Mush region (38°44′ North), the time interval would be approximately 22000–10000 BC (Figure 1b). This is the period in which it would have been possible to observe the setting of all bright stars of the Great Bear (Stellarium contributors, 2024). Thus, **this legend could have originated only during the following specified time frame.**

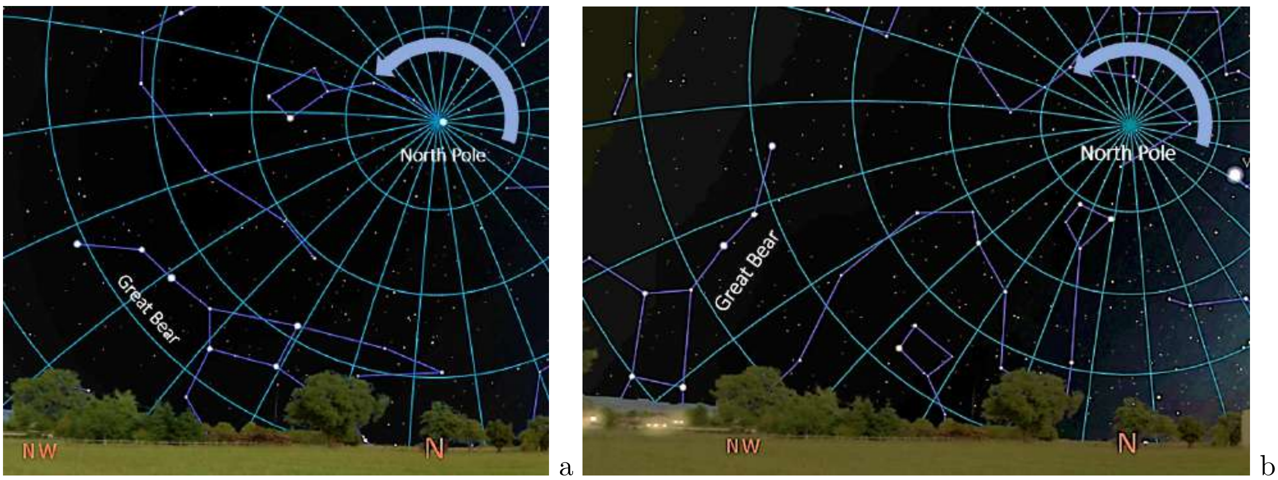

Figure 1. a - The northern sky in 2024 CE, when 6 out of 7 bright stars of the Great Bear constellation do not set; b - The night sky in 10000 BC, from the same latitude (38°44′ North), when the settings of all 7 stars could be observed. (Stellarium contributors, 2024)

2.3. Descriptions of the Dragon-Fish

The dragon-fish is described in three distinct situations. Let us now explore how these situations are linked to the positions of the Southern Fish constellation in the sky and to mythological concepts.

a. **With a split belly:** It is evident that the fish is either dead or severely damaged. In such a condition, fish typically surface belly-up[3], an orientation opposite to their natural swimming posture. It should be noted that the constellation of Southern Fish is described by Aratus as *"on his back the Fish"* (Allen (1963) pp. 344-347). Additionally, the Southern Fish is depicted on its back in other astronomical maps (Hoffmann (2021) pp. 98-99). Therefore, this depiction of the mythological dragon-fish reinforces its connection to the Southern Fish constellation.

b. **Spreading out on the surface of the water:** When the river is considered as the horizon, the dragon fish that appear on the surface can be interpreted as the Southern Fish constellation (more specifically, its brightest star, Fomalhaut (Malkhasyan, 2023b)) on the horizon. This suggests either the rising of the star over the eastern or its setting on the western horizon.

c. **On a wagon:** The fish is divided into parts and distributed to the townspeople on the wagon, while the wagon-Great Bear constellation, as demonstrated on another occasion, at one point also held the meaning of a spread, a funeral wagon and a shroud (Malkhasyan, 2021). This fully explains the depiction of the fish on the wagon (for more details, see subtitle 3.2).

Thus, all the main characters of the legend and their descriptions have been examined and explained through astronomical concepts and established mythological understandings.

3. Analysis of Information on Calendrical Significance

As we have observed, through detailed analyses, certain time-indicating data also emerge (the rising and setting of stars are inherently linked to specific times). In this regard, certain details from the legend are particularly noteworthy, namely:

- **The dragon-fish is divided into parts and distributed among the people.**
- **The river is stained with blood.** The reddening of the river can have two possible meanings: the horizon may take on this hue right before the sunrise or right after the sunset.
- **The time between the bear's immersion and its emergence is described as very short (only a few minutes).** Here, we observe the following apparent contradiction: there is almost no mention of time between these scenes in the legend, which means that these scenes follow each other almost immediately. However, the time gap between the setting and rising of the bright stars of the Great Bear constellation is quite long - approximately two months. To provide a well-founded interpretation of the mentioned information, we must turn our attention to the structure of the ancient Protohaykian calendar that is known to us.

3.1. The Basic Structure of the Protohaykian Calendar

The Protohaykian calendar consists of two main periods: a 295-300-day primary year (10 lunar synodic months) and a 70-65-day extra-annual period (similar to a Lent period) (Broutian, 1997). The extra-annual period, in this sense, was not perceived as time (Broutian, 2011). In other words, its beginning was considered the end of the year, and its end marked the beginning of the new year. Between these two points, "time is absent," much like how contemporary people perceive a brief moment of transition between the old year and the new year at midnight on New Year's Eve. In ancient times, this brief interval was considered to last 65-70 days (Broutian, 2007).

The beginning of the main year was marked close to the summer solstice by observing the heliacal rising of the calendar's main star. It was demonstrated that this calendar was used in parallel with the development of cereal agriculture, beginning around 9000 BC, when the main star of the calendar was α Virginis (Spica) (Broutian, 2016).

[3] If "the narrator sees the fish with a split belly," then it is indeed on the visible surface of the water, with its belly facing upward.

At the same time, astronomical studies of the Fish-shaped Dragon Stones revealed that they represented the cultic manifestations of the Southern Fish constellation and were associated with the heliacal rising of the constellation's main star, Fomalhaut (Malkhasyan, 2023b). According to calculations, this event occurred around 18800 BC, four days before the summer solstice, and was related to the key event of the calendar at that time—the transition to the new year (Malkhasyan, 2023b). Furthermore, the heliacal setting of the same star occurred approximately 70 days before the summer solstice, and this period appears to have also been regarded as "out of the year," similar to the structure of the Protohaykian calendar (Malkhasyan, 2023b).

3.2. Religious and Ritualistic Interpretation of the Legend

As mentioned above, the ancient Protohaykian calendar (c. 9000 BC) was an agrarian calendar, with its main star, Spica of the Virgo constellation, symbolizing the grain ear (see Subsection 3.1 above). The central event of this calendar revolved around offering the primary "concept" of bread (Broutian, 2016). This brings to mind the Christian story of feeding 5000 people with bread and fish (Matthew 15:32-39; Mark 8:1-10). It is also worth recalling the Last Supper, which features the ritual of breaking bread and the words of Jesus (Matthew 26:26-28; Mark 14:22-24; Luke 22:19-20). Jesus offers his body symbolically as bread, breaking it into pieces, and shares wine as a symbol of his blood. In the legend of the dragon-fish, the river becomes bloodied when its belly is split open, signifying the fish's blood. Indeed, this dragon-fish, which in ancient times was associated with God Haya, the principal deity of the Mesopotamian pantheon (Hoffmann (2021) pp. 93-95; Davtyan (2004) pp. 109-110), is similarly offered "ceremonially" in a wagon (funeral wagon, spread, shroud) (Malkhasyan, 2021), aligning with the above-mentioned religious perceptions. Two notable examples highlight the parallels between Christian imagery and the dragon-fish. First, there exists an icon of Christ's baptism engraved on the skull of a Loko fish (dragon-fish) (Sargsyan (2023) p. 223) (Figure 2a). Second, the lintel of the Armenian early medieval Church of the Holy Mother of God (Katoghike, Tsiranavor) is a Fish-shaped Dragon Stone (Figure 2b). The church door is perceived as a boundary between two worlds (Broutian, 2018), and the stone dragon-fish placed upon it symbolizes the boundary between these realms. Thus, **the offering of the fish's body in the legend should be interpreted as a profoundly significant religious and ritualistic practice of the era, likely tied to the most important annual event of the Protohaykian calendar.**

a b

Figure 2. a - Icon depicting the baptism of Jesus Christ on the skull of a Loko fish. Displayed at the Matenadaran Institute of Ancient Manuscripts, Armenia; b - Fish-shaped Dragon Stone on the door of the Church of the Holy Mother of God (Katoghike, Tsiranavor) (6^{th} century CE). Located in Avan administrative district, Yerevan.

3.3. The Relative Positions of the Southern Fish and Great Bear Constellations

Taking into account the aforementioned connections (subtitles 3.1 and 3.2), it is entirely logical to examine the period around 18800 BC in order to clarify the interpretations of the "river blooded" episode and the described chronological contradiction in the narrative. Let us observe the positions of the constellation Great Bear in the sky during the heliacal rising and setting of the main star of the Southern Fish.

As shown in Figure 3a, during the heliacal rising of Fomalhaut in 18800 BC, from the geographic latitude of Mush province (38°44' North), the position of Great Bear in the sky appears as if it is descending headfirst—creating the impression of plunging into the river. Since the legend describes the fish on the verge of death, it is essential to examine the sky during the heliacal setting (or "death") of Fomalhaut (Figure 3b).

As depicted in Figure 3b, at the moment of Fomalhaut's heliacal setting, six of Great Bear's seven bright stars remain visible above the horizon, while one (η Ursae Majoris) is still below the horizon and is not visible (Figure 3b). This celestial configuration aligns perfectly with the legend's imagery of a bear with "plucked fur" emerging from the river.

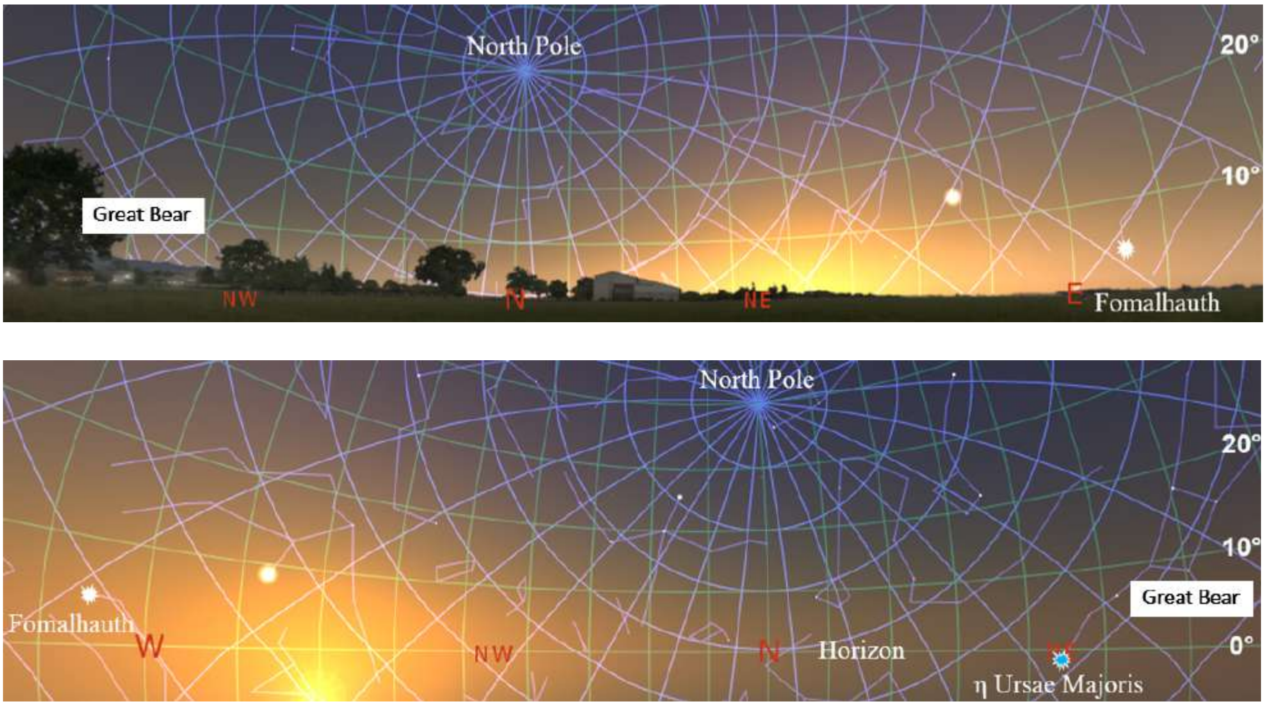

a

b

Figure 3. a - The morning sky on the day of Fomalhaut's heliacal rising, four days before the summer solstice in 18800 BC; b - The evening sky as it appeared 20 days after the vernal equinox in 18800 BC, at the moment of Fomalhaut's heliacal setting. (Stellarium contributors, 2024)

Let us return to the previously mentioned temporal "contradiction" (Title 3). The legend describes only a few minutes passing between the bear submerging into the water and emerging, while the settings and risings of the Great Bear constellation occur over much longer intervals. A similar contradiction arises with the dragon-fish. It surfaces (heliacal rising) in a lifeless state (heliacal setting). This apparent contradiction is fully resolved when considered within the framework of the Protohaykian calendar's extra-annual period.

The 65–70-day extra-annual interval was perceived as a single unified event, its beginning and end being understood to occur simultaneously (Broutian, 2011). It is notable that this understanding has also been preserved in the Christian Liturgical Calendar (2024). Specifically, it is reflected in the more than 40-day period between the Crucifixion, the Resurrection, and the Ascension of Christ, which, by the way, aligns quite well with the position of the extra-annual period in the Protohaykian calendar. Furthermore, the extra-annual period represents a calendrical manifestation of the Underworld, with its beginning and end defined by the thresholds of entry and exit (Broutian, 2011, 2018). As discussed earlier, the Dragon-fish serves as such a threshold marker (Figure 2a). Similarly, the Great Bear constellation had a symbolic role in guiding transitions to and from the Underworld (Malkhasyan, 2021). The bear's actions in raising the dragon-fish to the water's surface metaphorically represent a passage from one world to another.

Thus, this legend appears to recount the extra-annual period of a calendar likely in use around 18800 BC. The interval begins with the heliacal setting of Fomalhaut and the acronical[4] rising of Great Bear's brightest stars and concludes at summer solstice with Fomalhaut's heliacal rising and the cosmic[5] setting (disappearance) of Great Bear's brightest stars.

Concluding Remarks

As we can see, the legend in question, in addition to its condensed astronomical content, also contains clear information about highly structured calendrical and ritualistic concepts passed down from ancient times. The analysis of this information reveals a remarkable parallel between the Fish-shaped Dragon Stones, their period of worship (Malkhasyan, 2023b), and the primary calendrical characteristic of that era—the extra-annual period.

It is important to emphasize that during the estimated time frame of 18800 BC (Upper Paleolithic), fishing was one of the primary activities supporting human livelihood (Sardaryan (1967) pp. 86-87), playing a crucial role in subsistence. The core concept of the extra-annual period is fasting (Broutian, 2016). Interestingly, this time of year corresponds to the spawning and reproductive cycles of the region's major fish species. Hence, it is entirely reasonable that fishing might have been "prohibited" during this period of 18800 BC, perhaps to ensure bountiful harvests in the future.

This legend of the dragon-fish is, of course, not the only Armenian tale with calendrical significance. Similar themes are found in many Armenian folk tales ("AFT" (1959a) p. 407; "AFT" (1959b) p. 39; ("AFT", 1968) p. 501), where the main character is often the Fish-Boy. However, a detailed astronomical analysis of the following must be reserved for another occasion, as it requires an extensive examination of a significant body of material.

References

Allen, R.H. 1963. *Star Names Their Lore and Meaning.* New York: Dover Edition.

Bense. 1972. *Armenian Ethnography and Folklore, (Collected by Sahak Movsisyan (Bense), compiled by his son Soghomon Taronetsi).* Yerevan: NAS ASSR Institute of Archeology and Ethnography, 3.

Broutian, Gr. 1997. *The Armenian Calendar.* Mother See of Holy Etchmiadzin.

Broutian, Gr. 2007. The Oldest Armenian Calendar Concept According to the Analyze of the Ornaments of a Vessel from 28-27th c. B.C. *Bazmavep*, **1-4**, 149–163.

Broutian, Gr. 2008. Some calendar realities in Armenian fairy tales. *Etchmiadzin*, **2**, 49–66.

Broutian, Gr. 2009. Calendar realities in Armenian fairy tales. *Etchmiadzin*, **12**, 62–83.

Broutian, Gr. 2010. Some calendar realities in Armenian fairy tales. *Etchmiadzin*, **6**, 22–44.

Broutian, Gr. 2011. The Understanding of Time and Space According to Armenian Fairy Tales. *Bazmavep*, **3-4**, 459–484.

Broutian, Gr. 2016. The Beginning of the Protohaykian Calendar. *Bazmavep*, **3-4**, 11–63.

Broutian, Gr. 2018. Armenian Ram-shaped and Hores-shaped Tombstones and Old Armenian Cosmic and Calendrical Conceptions. *Etchmiadzin*, **2**, 71–86.

[4]The rising that occurs immediately after sunset is called acronical rising.
[5]The setting of a star just before sunrise is called cosmic setting.

Broutian, Gr. 2020a. An Astronomical Attempt to Determine the Armenian "Vishap" stone stelae. *Etchmiadzin*, **4**, 44–69.

Broutian, Gr. 2020b. An Astronomical Attempt to Determine the Temporal Origin of an Episode of the Armenian Epic "Sasnay Tsrer". *Etchmiadzin*, **7**, 39–53.

Broutian, Gr. 2021a. An Astronomical Attempt to Determine the Temporal Origin of an Episode of the Armenian Epic "Sasnay Tsrer". *Communications of BAO*, **68(1)**, 105–113.

Broutian, Gr. 2021b. An Attempt to Determine the Temporal Origin of an Episode of the Armenian Epic "Sasna Tsrer". *Etchmiadzin*, **12**, 72–85.

Broutian, Gr. 2021c. An Attempt to Determine the Temporal Origin of an Episode of the Armenian Epic "Sasna Tsrer". *Etchmiadzin*, **10**, 63–79.

Davtyan, A. 2004. *Armenian Stellar Mithology.* Yerevan: "Tigran Metz".

Hoffmann, S.M. 2021. *Wie Der Löwe An Den Himmel Kam (Auf Den Spuren Der Sternbilder).* Stuttgart, Germany: Kosmos.

Hunger, H., & Pingree, D. 1999. *Astral Sciences in Mesopotamia.* Leiden, Boston, Köln: Brill.

Liturgical Calendar. 2024. *"Yekeghetsakan Oracuyc," Ordered by His Holiness Karekin II.* Mother See of Holy Etchmiadzin.

Malkhasyan, H.A. 2021. Some New Results of the Study of "Zorats Qarer" Megalithic Monument (Platform 2). *Bazmavep*, **3-4**, 149–199.

Malkhasyan, H.A. 2022. On "Observational Instruments" composed of Stones No. 12, 13 and 14 of "Zorats Qarer" Monument. *Communications of BAO*, **69(1)**, 100–121.

Malkhasyan, H.A. 2023a. On Comprehensive Examination Results of The Observational "Instruments" No. 12, 13 and 14 of "Zorats Qarer" Megalithic Monument. *Bazmavep*, **1-2**, 125–182.

Malkhasyan, H.A. 2023b. On The Astronomical Context of Fish-shaped Vishap Stone Stelae. *Communications of BAO*, **70(2)**, 249–259.

Malkhasyan, H.A. 2024. Some New Results of the Study of "Zorats Qarer" Megalithic Monument (Platform 3). *Bazmavep*, **1-2**, 87–128.

Sardaryan, S. 1967. *Primitive Society in Armenia.* Yerevan: YSU,"Mitk" publ.

Sargsyan, Y. 2023. *Aratta, Origins of the Legacy.* "Lusakn".

Stellarium contributors. 2024. *Stellarium v24.3 Astronomy Software.*

Tumanyan, B.E. 1968. *"The History of Armenian Astronomy".* Yerevan: Yerevan State University.

Van der Waerden, B.L. 1974. *Science Awakening II: The Birth of Astronomy.* First Edition: Oxford University Press.

Vanandeci, Gh. 1695. *Hamatarats Ashkharhacoyc.* Amsterdam: (map).

"AFT". 1959a. *Armenian folk tales.* NAS ASSR, Vol. 1.

"AFT". 1959b. *Armenian folk tales.* NAS ASSR, Vol. 2.

"AFT". 1968. *Armenian folk tales.* NAS ASSR, Vol. 9.

IAU South-West and Central Asian Regional Office of Astronomy for Development

Mickaelian A. M.*, Farmanyan S. V., and Mikayelyan G. A.

NAS RA V. Ambartsumian Byurakan Astrophysical Observatory (BAO),
Byurakan 0213, Aragatzotn Province, Armenia

Abstract

The International Astronomical Union (IAU) announced its Strategic Plan on Astronomy for Development in 2009, during the International Year of Astronomy (IYA) (for 2011-2020, extended to 2021-2030). One of its main components was the creation of the Office of Astronomy for Development (OAD) and corresponding Regional Offices (ROADs) for implementation and coordination of its aims. The OAD was created in Cape Town, South Africa and later on ROADs were created in 11 regions. Since 2015, Armenia has hosted one of them, IAU South West Asian (SWA) IAU ROAD, later renamed South West and Central Asian (SWCA) ROAD. At present, already six countries have officially joined (Armenia, Georgia, Iran, Kazakhstan, Tajikistan, and Turkey), but the Office serves for a rather broad region, from Eastern Europe to Central Asia. Armenia's geographical location and its historical role in astronomy (both for well-known archaeoastronomical heritage and the presence of the famous Byurakan Astrophysical Observatory (BAO) founded by Viktor Ambartsumian in 1946) serve as a link between Europe and Eastern Partnership countries, Middle East and Asia in general. We run activities in 3 directions, Task Forces (TF): TF1 Universities and Research, TF2 Children and Schools and TF3 Public Outreach. In addition, we participate in the OAD Flagship Projects; Flagship 1: *Astrotourism*, Flagship 2: *Astro for Mental Health*, Flagship 3: *Hack4Dev*. We present our projects and all other accomplishments and discuss the role of our ROAD in maintaining contacts and development of astronomy in the region, as well as contacts between Europe and the Eastern Partnership countries. The most up-to-date information about the IAU SWCA ROAD is available on its webpage at http://iau-swa-road.aras.am/eng/index.php.

Keywords: *IAU – OAD – ROAD – astronomical research – astronomical education – public outreach – astronomy for development – European Eastern Partnership.*

1. Introduction

The International Astronomical Union (IAU) developed and adopted in 2009 a decadal Strategic Plan (SP) now entitled *"Astronomy for Development"* (IAU, 2009). The SP significantly increases the role of astronomy for other sciences, technology, culture, and society, as it is tightly linked to all this (Figure 1). This plan has been resulted from an extensive process of consultation beginning with a meeting of stakeholders in Paris in January 2008 and including feedback from key stakeholders during the various drafts of the SP. It was endorsed by the General Assembly of the IAU in Rio de Janeiro in August 2009, and builds on the momentum of the very successful International Year of Astronomy 2009 (IYA). The objective of this SP is to use Astronomy to stimulate development in all regions of the world. Crucial for the implementation of the SP was the creation of a global *"Office of Astronomy for Development"* (OAD). The OAD is tasked with establishing and strategically coordinating Regional Offices (ROADs) and Language Expertise Centres (LOADs) across the world, as well as three Task Forces, namely

- **TF1: Astronomy for Universities & Research** (Professional Astronomy; scientific networks, including developing professional astronomy in all regional countries; stimulating interdisciplinary research)
- **TF2: Astronomy for Children & Schools** (Astronomical Education at all levels: children (UNAWE, etc.), pupils, students, etc.; working tightly with the IAU OAE and IAU OYA; working with teachers, educators, etc.)

*aregmick@yahoo.com, Corresponding author

doi: https://doi.org/10.52526/25792776-24.71.2-331

- **TF3: Astronomy for the Public** (Public Outreach, Communicating Astronomy with the Public (CAP), Amateur Astronomy, Astronomical Heritage, Archaeoastronomy & Astronomy in Culture (AAC), etc.; working tightly with the **IAU OAO**; working with communicators, amateurs, journalists).

In addition, there are 3 Flagship Projects:

- **Flagship 1: Astrotourism** (an intersection of Astronomy and Tourism; it is a niche travel industry that focuses on celestial events, dark sky destinations, and space-related activities)
- **Flagship 2: Astronomy for Mental Health** (focused on harnessing the inspirational potential of Astronomy, and using it as a tool for improving people's mental health and wellbeing)
- **Flagship 3: Hackathons for Development** (using Hackathons to accelerate global development and insights)

Through a strong partnership with the South African government, the OAD is hosted at the South African Astronomical Observatory (www.astro4dev.org), a facility of the National Research Foundation. In addition, eight regional offices were created, one of them in Armenia.

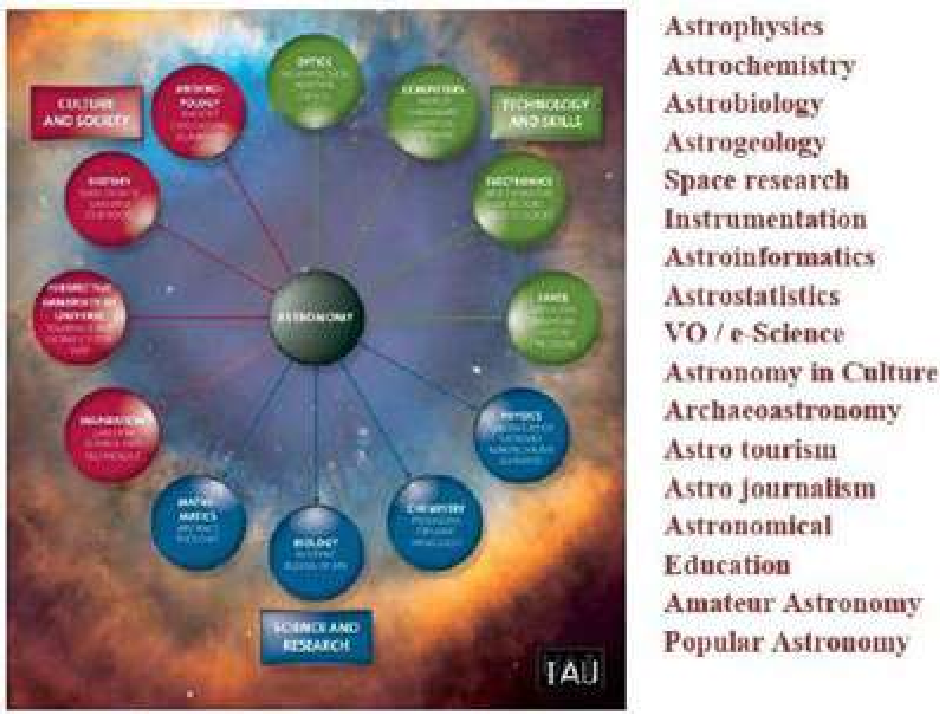

Figure 1. The relation of Astronomy with other sciences, technology, culture and society. A number of inter- and multi- disciplinary sciences and other fields are listed having tight relation to astronomy.

2. The Establishment of the IAU SWA ROAD

Armenia showed interest and activities in the establishment of one of the regional IAU offices since the beginning of the initiative (2009-2011). Armenia's proposal to host a ROAD was rather strong both from the point of view of the available facilities and ongoing activities. The proposal was finally approved on 10 June, 2015 and an agreement was signed between the IAU and the Byurakan Astrophysical Observatory (BAO) on 6 August 2015. The office was formally established on 1 September 2015 and was called **IAU South West Asian (SWA) ROAD**. Dr. Areg Mickaelian became its Director. SWA Regional Steering Committee was created in September 2015, as well as SWA webpage was opened also in September 2015 (http://iau-swa-road.aras.am, Figure 2). The staff members joined on 1 October 2015. Finally, the Inauguration Ceremony was held on 13 October 2015. IAU OAD / SWA ROAD Workshop was also attached to this event. Representatives from the IAU (General Secretary Piero Benvenuti, former Vice-President George Miley, OAD Director Kevin Govender) and representatives of regional and some other countries (Georgia, Iran, Turkey, Russia, Israel, Jordan) were present.

doi: https://doi.org/10.52526/25792776-24.71.2-331

Like our long tradition to organize joint Armenian-Georgian (Byurakan-Abastumani) workshops (colloquia) since 1974, we conducted a new series of Armenian-Iranian Astronomical Workshops (AIAW). The first one was organized on 13-16 October, 2015 in Byurakan, so that all Iranian guests were able to participate in the IAU SWA ROAD Inauguration Ceremony.

Georgia and Iran were the first countries along with Armenia to officially join the SWA ROAD. During many years and centuries, these countries have had numerous relations in all areas, including science and Astronomy.

Figure 2. IAU South West and Central Asian ROAD webpage and logo showing also the geographical location of the SWCA region and 6 countries.

Astronomy in Georgia is generally represented in Abastumani Astrophysical Observatory (AbAO) founded in 1932. It is one of the leading scientific institutes in the country. Main fields of research are Solar System bodies (including near-Earth asteroids), various aspects of Solar physics, stellar astronomy (including binary stars and open clusters), extragalactic objects (AGNs), theoretical astrophysics, cosmology, atmospheric and Solar-terrestrial physics. Although research in these fields are carried out in other institutions in Georgia as well: Institute of Theoretical Physics at Ilia State Univ., Javakhishvili Tbilisi State Univ., School of Physics at Free Univ. of Tbilisi. In AbAO, several telescopes are operational today: 70cm Maksutov meniscus telescope, 53cm azimuthal reflector, 22cm reflector ORI, 40cm double astrograph, 53cm large and 11.5cm small solar coronagraphs. Spectroscopic and photometric observations are carried out. In 2007 the Observatory was integrated with Ilia State Univ., merging scientific research and education which facilitated the growth of a new generation of researchers.

Astronomy in Iran routes back to many thousand years ago. When Cyrus the Great, the founder of the Persian Empire, captured Babylon in 539 B.C., Magi who migrated there transformed Babylonian astronomy. In 13th century, Maragheh Observatory with a unique place in the history of Medieval Astronomy, was established. At present, research in Astronomy and Astrophysics has been conducted in a number of universities in Iran. There are two dedicated research institutes in Iran, IPM School of Astronomy in Tehran and Research Institute for Astronomy and Astrophysics in Maragheh (RIAAM). Among the most active universities in Astronomy are IASBS in Zanjan, Ferdowsi Univ. of Mashhad (FUM), Univ. of Tabriz, Shiraz, Birjand, Kerman and Zanjan universities, and Amirkabir Univ. of Technology and Sharif Univ. of Technology, both in Tehran. With nearly 400 members, the Astronomical Society of Iran (ASI) is an NGO that represents the Iranian community of astronomy. It also publishes the *International Journal of Astronomy and Astrophysics* (IJAA). The Iranian National Observatory (INO) is under construction at an altitude of 3600m at Gargash summit 300km southern Tehran. One of the major observing facilities of the observatory is a 3.4m alt-azimuthal Ritchey-Chretien optical telescope which is currently under design.

doi: https://doi.org/10.52526/25792776-24.71.2-331

Since the beginning, IAU SWA ROAD developed activities in all three Task Forces. A number of meetings and schools were organized and a number of other projects were accomplished. Especially, successful were the activities related to Scientific Tourism (and later more specific Astronomical Tourism or Astro Tourism) in Armenia and in the region. We were awarded two grants in 2016: OAD grant for the development of Astro Tourism in the South West Asia and Swiss SDC grant for the development of Scientific Tourism in Armenia.

SWCA ROAD representatives, the Director Areg Mickaelian and BAO Director Haik Harutyunian took part in the **IAU Arab World ROAD opening** in December 2015. In February-March 2016, Areg Mickaelian and Sona Farmanyan took part in the **OAD/ROADs meeting in Cape Town, South Africa**. The whole SWA team (Areg Mickaelian, Susanna Hakopian, the new TF1 coordinator, Sona Farmanyan, and Gor Mikayelyan) visited Georgia in March-April 2016 for tightening the collaboration and exchange of scientific knowledge. In August 2016, Areg Mickaelian and Sona Farmanyan were invited to RIAAM, Maragheh, Iran to participate in a workshop and gave talks. In 2020, Areg Mickaelian and Gor Mikayelyan participated in the next **OAD/ROADs meeting in Cape Town, South Africa**.

We hold regular telecons both with OAD/ROADs and with the SWA ROAD Steering Committee to give short reports on the accomplished affairs, and to discuss all current and future matters.

3. Expansion to IAU SWCA ROAD

In May 2016, Areg Mickaelian and the Scientific Secretary of BAO Elena Nikoghosyan visited three Central Asian countries, Uzbekistan, Kazakhstan and Tajikistan to recover our former contacts and collaboration. As a result, during June 2016, Kazakhstan and Tajikistan with official letters also joined our ROAD. This significantly strengthens our centre and expands its sphere of activities to Central Asia.

In **Kazakhstan**, Fesenkov Astrophysical Institute (APhI), Almaty (founded in 1941) is the main astronomical centre. At present *Dr.* Chingiz Omarov is the Director, and *Dr.* Assylkhan Bibossinov (also member of the SWCA Steering Committee) is the Deputy Chairman of the National Centre of Space Research and Technology, to which APhI is affiliated. One of the outstanding scientists, *Prof.* Eduard Denissyuk, was one of the first astronomers to spectroscopically observe Markarian galaxies and has long-year collaboration with BAO astronomers. There are three attached observatories to APHI: Kamenskoe Plateau Observatory (altitude 1450m, AZT-8 70cm, Zeiss-600 60cm, Hertz telescope-reflector 50cm, Wide aperture Maksutov meniscus telescope 50cm), Tian-Shan Observatory (TShAO, altitude 2735m, two 1m telescopes) and Assy-Turgen Observatory (altitude 2750m, 1m tele- scope). The research subjects are: *physics of stars and nebulae; physics of the Moon and planets; cosmology, stellar dynamics & computational astrophysics; nuclear astrophysics; artificial Earth satellites; advanced astrophysical research.* Kazakh National University (KazNU) (with 16,000 students) is the main university preparing professional astronomers/astrophysicists.

In **Tajikistan**, Institute of Astrophysics of Academy of Science of the Republic of Tajikistan, in Dushanbe (founded in 1932) is the main astronomical centre. At present, *Dr.* Gulchehra Kokhirova is the Director. *Profs.* Pulat Babadjanov and Khursand Ibadinov, former directors and most eminent Tajik astronomers, are still active and strongly supported collaboration in frame of IAU ROAD as well. There are three attached observatories: Hissar Observatory (HisAO, altitude 730m, AZT-8, 40cm astrograph), the observatory "Sanglokh" (altitude 2300m) in Dangara area (1m telescope, 60cm Carl Zeiss) and its branch, the observatory "Pamir" (altitude 4350m) in Murghab district of Badakhshan (70cm telescope). Sanglokh Observatory was recently re-operated and the President of Tajikistan was present at the opening ceremony. The Institute's research subjects include: *comets and asteroids, experimental astrophysics, meteor astronomy, ionospheric, astrometry, variable stars, structure and dynamics of stellar systems.*

Due to the involvement of Kazakhstan and Tajikistan, our regional centre was renamed to **IAU South West and Central Asian (SWCA) ROAD**. Corresponding changes and additions were done at our webpage.

On November 17, 2017, **Turkey** officially joined the South West and Central Asian ROAD office and expressed its desire to carry out its activities for the development of Astronomy by adopting Armenia's coordinating role. It is important to state that we also made a political big step. Armenia recognized as an astronomical centre by Turkey. Although it was set up by the IAU, however at present Turkey also accepts it and joins. Now our cooperation will be closer, visits and exchange of scientific experience more active.

doi: https://doi.org/10.52526/25792776-24.71.2-331

We hope to work on various astronomical topics to develop astronomy, to organize conferences, to carry out all the activities that this cooperation assumes. There is a number of observatories, astronomical institutes, and universities with astronomy/astrophysics departments in Turkey (the first institute of astronomy was established in 1933 in Istanbul University). At present the main observatory is TUBITAK National Observatory (TUG, founded in 1995). Currently TUG is the most modern observatory of Turkey consisting of 1.5m Russian-Turkish Telescope (RTT150), 1.0m telescope and several smaller size robotic telescopes. In 2014 Ataturk University (Erzurum) opened the latest astronomy department. At present, the two largest telescopes in Turkey are 4m and 2.5m.

4. Other Collaborations

Beside activities for the regional countries, IAU SWCA ROAD also encourages and strengthens collaboration with other regions and countries. Especially, promising are contacts with three neighbouring ROADs: **East Asian** (based in Beijing, China), **Arab World** (based in Amman, Jordan) and **European** (Leiden, Netherlands). The first one is coordinating a huge region (China, Mongolia, North Korea) and is especially interested in the development of Silk Road projects that also relate Armenia. Arab World ROAD is in fact in the same big region (Middle East) and is our closest neighbour (an official agreement was signed between SWCA and Arab World ROADs, as well as between BAO and Sharjah University). The more recently established European ROAD (E-ROAD) in fact involves also Armenia and Turkey, as the astronomical societies of these countries are among EAS Affiliated Societies unified by E-ROAD. We have discussed possibilities to tighter collaborate in all areas (TFs) and establish new programs. Particularly, EU Erasmus+ program on International Credit Mobility (ICM) was successful in 2023-2024; 7 Armenian researchers and ROAD members visited Leiden University for joint work.

In addition, we have discussed with Indian astronomers the possibilities to collaborate, as India is not a member of any ROAD and the closest one is SWCA. In 2024, Areg Mickaelian and Gayane Baleyan visited ARIES, Nainital, India for delivering seminars and discussion of possible collaboration.

5. Projects, Events and Other Activities

It is a rule that both senior and young scientists from regional countries (especially Georgia and Iran) most often participate in our meetings, schools and other events. We also have many missions to the regional countries, again most often Georgia and Iran.

Armenia is rather active in organizing astronomical meetings, schools and other events. Among the most important meetings and schools held in Armenia, we would like to mention the **IAU Symposia and Colloquia**: IAU S029: *Non-Stable Phenomena in Galaxies* (1966), IAU S129: *Observational Evidence of Activity in Galaxies* (1986), IAU S137: *Flare stars in Star Clusters, Associations and Solar Vicinity* (1989), IAU S194: *Activity in Galaxies and Related Phenomena* (1998), IAU C184: *AGN Surveys* (2001), IAU S304: *Multiwavelength AGN Surveys and Studies* (2013) and IAU S365: *Dynamics of Solar and Stellar Convection Zones and Atmospheres* (2023). Another large event was the all-European annual astronomical meeting in 2007, **JENAM-2007** (Joint European and National Astronomical Meeting), held in Yerevan, Armenia. It was the biggest ever scientific event in Armenia. Out of other meetings, one may mention joint meetings with a given country, namely Byurakan-Abastumani (Armenian-Georgian) Colloquia in 1974–2024, Armenian-French Workshops in 1995 and 2009, and the Armenian-Iranian Astronomical Workshop in 2015, as well as many meetings dedicated to the anniversaries of BAO, Viktor Ambartsumian, Anania Shirakatsi, Beniamin Markarian, Ludwik Mirzoyan, Marat Arakelian and others. Especially many guests from the regional countries were present at BAO-70 anniversary meeting in 2016 and Viktor Ambartsumian 110th anniversary meeting in 2018. Our office has been awarded OAD grants for organization of **Regional Astronomical Workshops** in 2018 and 2019, and many regional guests were present as well.

Among the summer schools, **Byurakan International Summer Schools (BISS)** are already very famous. We have started this initiative in 2006 and so far, have organized 9 such events: 1BISS in 2006, 2BISS in 2008, 3BISS combined with the IAU International School for Young Scientists (ISYA) in 2010, 4BISS in 2012, 5BISS in 2016, 6BISS in 2018, 7BISS in 2020, 8BISS in 2022 and 9BISS in 2024. A **Regional Summer School on Space Sciences and Technologies** was organized in 2019 and this was the first step to establish the above-mentioned subjects in Armenia. In addition, it became the beginning of the series

doi: https://doi.org/10.52526/25792776-24.71.2-331

of **SWCA Regional Astronomical Summer Schools (RASS)**; 1RASS in 2019, 2RASS in 2021 and 3RASS combined with the Inter-Regional Astronomical Summer School (IRASS) in 2023 between SWCA and Arab World ROADs. This was the 1st such event among all Regional Offices. **Byurakan Summer Schools for YSU students (BSS)** are our local schools. They have been organized in 1995, 2005, 2009, 2013 and 2023. For the school students, on the initiative of Sona Farmanyan, we organize **BAO Science Camps (BSC)**; 10 such events were held in 2014-2024. **ArAS School Astronomical Lectures** program was started in 2012 on the initiative of Yervant Terzian and Areg Mickaelian. During 2012-2024, we have organized 11 such programs. In addition, since 2016, we have had *"My Universe"* contest and the winners visited BAO.

Our ROAD representatives are rather active in participating in many international and regional meetings and have given numerous talks at such events related to our activities: scientific, educational, public, and in general about our SWCA ROAD.

In frame of the collaboration between Armenia and Iran, on 15-18 August 2016, Areg Mickaelian (IAU SWCA ROAD Director) and Sona Farmanyan (IAU SWCA ROAD TF3 Programme Coordinator) were invited to the **Research Institute for Astronomy and Astrophysics of Maragha (RIAAM)**. During these days, the 8th Advanced Astrophysics Workshop of Maragheh was organized. Areg Mickaelian delivered two lectures on *"Astronomical Surveys, Catalogues, Databases, Archives, and Virtual Observatories"* and *"Multi-Wavelength Studies of Active Galaxies"*. Sona Farmanyan delivered two talks on *"Archaeoastronomy and Cultural Astronomy in South West and Central Asia"* and *"Ancient Mythology and Cosmology"*. Sona also presented the IAU SWCA ROAD activities during 2015-2016. A number of discussions were held with Iranian astronomers, including *Prof.* Hossein Ebadie (RIAAM Director) and *Prof.* Pantea Davoudifar, with whom there was a collaboration in co-supervising of two Iranian MSc students.

The fourth **Middle East and African IAU Regional meeting (MEARIM IV)** was jointly hosted by Entoto Observatory & Research Center (EORC) and East African Regional Office of Astronomy for Development (ROAD-IAU) and was conducted from 22-25 May 2017 in Addis Ababa, Ethiopia with the theme of *"Exploring our Universe for the benefit of Humankind"*. During the symposium there were activities such as scientific paper presentations, Plenary Guest and Invited speaker sessions, meetings and discussion on the general progress and Assessments of Astronomy and Astrophysics development in the Middle East and Africa Region. From Armenia, Areg Mickaelian (Director of BAO and SWCA ROAD) and Sona Farmanyan (Public Outreach Coordinator of SWCA ROAD) participated to the meeting and presented 5 talks on various subjects, including the one about SWCA ROAD.

The seventh **Middle East and African IAU Regional meeting (MEARIM VII)** took place in 2023 in Cairo, Egypt. From Armenia, Areg Mickaelian (Director of BAO and SWCA ROAD) and Gayane Baleyan (Public Manager of BAO) participated to the meeting and presented 2 talks.

A number of visits have been conducted to **Georgia, both Tbilisi and Abastumani**. Areg Mickaelian has been invited to deliver lectures in frame of the European Eastern Partnership (EaP) program in Tbilisi, particularly at EaPEC conferences and in frame of European GEANT project. In July 2019, our team visited Abastumani Astrophysical Observatory (AbAO) and delivered two invited seminars (by Areg Mickaelian and Arus Harutyunyan), as well as discussions were held on the collaboration in frame of the SWCA ROAD and Astro Tourism project. In 2024, Georgian colleagues hosted the 16th Byurakan-Abastumani Astronomical Colloquium in AbAO with participation of 13 Armenian scientists.

Visits to Iran have been conducted in 2015, 2016 and 2018 (the next one is planned for 2025). In November 2018, our team visited Tehran (Institute for Fundamental Research, IPM, Iranian National Observatory, INO and Tehran University) and gave two invited seminars (by Areg Mickaelian and Grigor Broutian). Discussions were held on future collaboration both on research and education and outreach.

The International Conference *"Astronomical Heritage of the Middle East"* approved by UNESCO Director General within UNESCO Participation Program for 2016-2017 was devoted to the role of Astronomy in Culture and other fields of human activities was held on 13-17 November, 2017 in Armenia. The conference brought together over 70 participants from 20 countries. A discussion of the problems of astronomy-related interdisciplinary sciences and further possible collaborations was organized. The Proceedings of the Meeting will be published by the Astronomical Society of the Pacific Conference Series (ASP CS), which is a world-wide known publication and the papers will appear in all libraries and electronic

doi: https://doi.org/10.52526/25792776-24.71.2-331

databases (including ADS). Another such meeting, ***"Astronomical Heritage of the Middle East 2"*** has been approved by UNESCO and will be held on 6-10 October 2025.

We have given many **presentations on our ROAD** and its activities at a number of international meetings: NKAS (Belgrade, Serbia, 2015), IAU GA XXIX (Honolulu, Hawaii, USA, 2015), Arabic ROAD Inauguration Ceremony (Amman, Jordan, 2015), Conferences on *Astronomical Silk Road* (Beijing and Urumqi, China, 2015), OAD/ROADs meetings (Cape Town, South Africa, 2016 and 2020), EWASS-2016 (Athens, Greece), 8th Advanced Astrophysics Workshop of Maragheh (Iran, 2016), MEARIM-IV (Addis Ababa, Ethiopia, 2017), EWASS-2017 (Prague, Czech Rep.), Armenia-Brandenburg Workshop (Nor Amberd, Armenia, 2017), The 12th Arab Conference on Astronomy and Science Space (Amman, Jordan, 2018), EWASS-2018 (Liverpool, UK), IAU GA XXX (Vienna, Austria, 2018), EWASS-2019 (Lyon, France), EWASS-2020 (online), EASS-2021 (online), EWASS-2022 (Valencia, Spain), IAU GA XXXI (Busan, South Korea, 2022), EAS Annual Meetings 2023 (Krakow, Poland) and 2024 (Padova, Italy) and IAU GA XXXII (Cape Town, South Africa, 2024).

We maintain a tight relation between the **IAU SWCA ROAD and Eastern Europe**. This includes collaboration with European countries, collaboration (and partial involvement) with the IAU European ROAD, ArAS affiliation to the European Astronomical Society (EAS), ArAS collaboration with the Euro-Asian Astronomical Society (EAAS), Armenia's participation in South-East Regional European Astronomical Committee (SREAC), H2020 program (since 2016 Armenia is an associate member), collaboration between the Armenian Virtual Observatory (ArVO) and EuroVO, VO-France (also VO-Paris), GAVO, and VObs.it. We also have contacts with other European organizations; Euroscience, SEAC, etc.

6. Astrotourism Projects

Several projects on Scientific or Astro Tourism have been accomplished, the most important, Astro Tourism in SWCA region. Being the pioneer of Scientific (and Astronomical) tourism, IAU SWCA ROAD has initiated the creation of an astronomical tourism webpage for the region. The IAU South West and Central Asian Regional Office of Astronomy for Development implements international astronomical project focused on the region. Within the framework of the above-mentioned project "Astro Tourism" webpage has been created, which aims to introduce places of certain astronomical value that present interest for the astronomical tourism. Here you can learn about the history of astronomy and its development not only in Armenia but also in other countries of the region. The webpage also provides information on modern and ancient observatories, sundials, planetariums, space related museums and many more.

Figure 3. IAU South West and Central Asian ROAD project on Astrotourism in SWCA region.

doi: https://doi.org/10.52526/25792776-24.71.2-331

7. Regional Workshops and Schools

We give here the summary table (1) of our Regional Astronomical Workshops (RAW) and Regional Astronomical Summer Schools (RASS), as well as joint meetings between two countries during 2013-2024. Events planned for 2025 are also given.

Table 1:

Year	Place	Events	Short
2013	Byurakan, Armenia	14^{th} Armenian-Georgian Astronomical Colloquium	
2015	Byurakan, Armenia	1^{st} Regional Astronomical Workshop	1RAW
2015	Byurakan, Armenia	Armenian-Iranian Astronomical Workshop	AIAW
2017	Yerevan, Armenia	UNESCO Regional Astronomical Conference *"Astronomical Heritage of the Middle East"*	AHME
2018	Byurakan, Armenia	2^{nd} Regional Astronomical Workshop	2RAW
2019	Byurakan, Armenia	1^{st} Regional Astronomical Summer School	1RASS
2019	Byurakan, Armenia	3^{rd} Regional Astronomical Workshop	3RAW
2021	Byurakan, Armenia	2^{nd} Regional Astronomical Summer School	2RASS
2023	Byurakan, Armenia	15^{th} Armenian-Georgian Astronomical Colloquium	
2023	Byurakan, Armenia	3^{rd} Regional Astronomical Summer School / 1^{st} Inter-regional Astronomical Summer School	3RASS/1IRASS
2023	Byurakan, Armenia	Armenian-Russian Joint Workshop on Space	
2024	Byurakan, Armenia	4^{th} Regional Astronomical Workshop	4RAW
2024	Abastumani, Georgia	16^{th} Armenian-Georgian Astronomical Colloquium	
2025	Byurakan, Armenia	17^{th} Armenian-Georgian Astronomical Colloquium	
2025	Byurakan, Armenia	4^{th} Regional Astronomical Summer School	4RASS
2025	Yerevan, Armenia	UNESCO Regional Astronomical Conference *"Astronomical Heritage of the Middle East – 2"*	AHME-2

doi: https://doi.org/10.52526/25792776-24.71.2-331

8. Summary and Future Plans

The status of the regional astronomical centre supports the regional and international contacts and collaboration both for Armenia and the neighboring countries; this way Armenia, by holding such a centre, strongly contributes to collaborations at all levels: professional, educational and popular. Astronomy in fact plays an important political role in establishing and strengthening friendship and cooperation of the regional nations, which is especially important in our complicated area.

Among our future plans, we envisage to enlarge the number of participating countries (involving more Central Asian and maybe some other ones), work harder for fundraising for implementation of various projects (in all three task forces), organize regional meetings, workshops, conferences on Astronomical Heritage and Astro Tourism, schools and camps.

Among the future plans and activities, we will organize the following:

- Inviting new countries to join (Uzbekistan, etc.)
- Establishing Regional telescopes collaborative network
- Developing Regional Astro Tourism project
- 2nd UNESCO Regional Astronomical Conference "Astronomical Heritage of the Middle East – 2"
- Future Regional Astronomical Workshops 2025 (5RAW), 2026, 2027, ...
- Future Byurakan International Summer Schools (BISS) 2026 (10BISS), 2028 (11BISS), ...
- Future Regional Astronomical Summer Schools (RASS) 2025 4RASS, 2027 5RASS, etc.
- Future Joint Meetings: Arm-Georgian 2025, Arm-Iranian, etc.
- Byurakan Science Camps (BSC), Space Camps, ArAS/BAO School Lectures

Acknowledgements

IAU SWCA ROAD team would like to thank IAU OAD, BAO and NAS RA Presidium for supporting the office and its activities and E-ROAD for collaboration in *Project Management* during 2023-2024.

References

Doran R., Chaparro G., Farmanyan S. V., et al. 2020, in Proc. IAU General Assembly XXX FM 15, Vienna, Austria. Astronomy in Focus XXX, p. 555–557

Farmanyan, S. V.; Mickaelian, A. M. 2018, ComBAO 65, p. 155-159

IAU 2009. https://iau.org/static/education/strategicplan_2010-2020.pdf

Mickaelian, A. 2015, *Armenia as a Regional Centre for Astronomy for Development activities*, Highlights in Astronomy (HiA) 16, 565

Mickaelian A. M., 2017, Publ. Astron. Observ. of Belgrade (PAOB), 96, p. 343

Mickaelian A. M., Khosroshahi H. G., Harutyunian H. A., 2016a, Proceedings of the Armenian-Iranian Astronomical Workshop, held on 13-16 October 2015 in Byurakan, Armenia. Yerevan, NAS RA "Gitutyun" Publishing House, p. 1-256

Mickaelian A., Azatyan N., Farmanyan S., Mikayelyan G., 2016b, in Proc. IAU General Assembly XXIX FM20, Honolulu, Hawaii, USA. Astronomy in Focus, Vol. 29A, Cambridge Univ. Press (CUP), pp. 422–423

Mickaelian A. M., Hakopian S. A., Farmanyan S. V., Mikayelyan G. A., 2017, ComBAO, 64, 1, p. 136-148

Mickaelian A. M., Farmanyan S. V., Mikayelyan G. A., 2019, in Proc. Conf. *"Astronomical Heritage of the Middle East"*, held on 13-17 November 2017 in Yerevan, Armenia. ASP CS Vol. 520, pp. 267–277

Mickaelian, A. M.; Farmanyan, S. V.; Mikayelyan, G. A. 2019, *IAU Regional Office of Astronomy for Development: Coordination in Southwest and Central Asia*, ASP Conference Series (CS) 520, p. 267-

Mickaelian A. M., Farmanyan S. V., Mikayelyan G. A., 2020, ComBAO, 67, 1, p. 68-74

Astronomy in Georgia

B.B. Chargeishvili *

Evgeni Kharadze Georgian National Astrophysical Observatory, Abastumani, Georgia

Abstract

We provide a brief history of Georgian astronomy and discuss its current state. The discussion also covers the scientific facilities of Georgia's leading astrophysical institute, the Evgeni Kharadze Georgian National Astrophysical Observatory, as well as current scientific projects and specialists involved in them. It also includes educational activities on astronomy in Georgia.

Keywords: *History, Telescopes, Scientists, Projects, Outreach*

1. History

Here we consider the state of astronomy in Georgia. To summarize the history, note that while comprehensive knowledge of contemporary astronomy can be found in old Georgian texts and literary monuments, there is no documented evidence of any professional astronomical activity in ancient Georgia. This must be due to the historical fact that in our history there was no more or less prolonged period of peace. The beginning of professional scientific activity in Georgia in the field of astronomy is associated with the establishment in 1932 of the first astronomical research institution, the Abastumani Astrophysical Observatory (AbAO), which is attributed to the unbelievable efforts of the renowned scientist and esteemed individual, Evgeni Kharadze. As the AbAO is Georgia's foremost institution for professional astrophysical study, we shall focus on its history and present art of state. Following the most recent reorganization in 2019, the observatory's official name has changed to Evgeni Kharadze Georgian National Astrophysical Observatory. Step by step, AbAO gained new facilities, telescopes, and other scientific instruments. The field of research interest grew and became wider. And almost fifteen years ago, we had about 10 telescopes on the mountain Kanobili, where the observatory is located, and the research field included almost all branches of contemporary astrophysics, say variable stars, nova and supernova stars, galaxies, nebulae, the study of the sun, the solar system, and the upper atmosphere, theoretical astrophysics, and cosmology. In many branches, the observatory held a leading position, such as spectral classification, polarimetric study of solar planets and the moon, and plasma astrophysics. Researchers in Abastumani created valuable stellar 2D classification catalogs (Chargeishvili et al., 2013, Kharadze et al., 2014) and lunar polarimetric atlases (Dzhapiashvili & Korol', 1982).

International scientific relations have been the concern of all generations of scientists in our observatory. Scientists from our observatory were members of the IAU and participated in the work of different commissions and divisions. Scientists from foreign countries such as Germany, Bulgaria, Hungary, Ukraine, and Russia visited AbAO to get acquainted with and master the advanced results of Georgian scientists in various fields of astrophysics such as spectral classification, plasma astrophysics, and others. Our scientists have developed very productive relationships with such foreign research institutions as Space Research Institute, Moscow, Russia (Zeleny & Taktakishvili, 1987); The Special Astrophysical Observatory, Karachay-Cherkessia, Russia (Bartaya et al., 1994); Pushkov Institute of Terrestrial Magnetism, Ionosphere and Radio Wave Propagation, Moscow, Russia (Kulidzhanishvili et al., 1985); Keldysh Institute of Applied Mathematics, Moscow, Russia (Molotov et al., 2008); Space Research Institute, Sofia, Bulgaria (Chagelishvili et al., 1991); Toyama University, Toyama, Japan (Chargeishvili et al., 1993, Zaqarashvili et al., 1996, Zhao et al., 1993a,b); Katholic University of Leuven, Leuven, Belgium (Bagashvili et al., 2017, Mdzinarishvili et al., 2020, Shergelashvili & Poedts, 2005, Shergelashvili et al., 2005); Space Research Institute, Graz, Austria (Srivastava et al., 2010, Zaqarashvili et al., 2010); Astrophysical Observatory of Turin, Torin, Italy (Bodo

*bidzina@aidio.net

doi: https://doi.org/10.52526/25792776-24.71.2-340

et al., 2005, 2007, Tevzadze et al., 2010); Kepler Astronomical Center, Pedagogical University, Zielona Góra, Poland (Gil et al., 2002, Melikidze et al., 2000); Carnegie Mellon University, Pittsburgh, Pennsylvania, USA (Kahniashvili et al., 2009, 2010). Our observatory scientists have participated in many international scientific conferences and workshops. In 1986, AbAO was the initiator of such an important workshop as the Joint Varena-Abastumani Workshop on Plasma Astrophysics, which later found its continuation as the Varena-Abastumani-ESA-Nagoya Workshop on Plasma Astrophysics. In 2014, the observatory hosted an international symposium on the topic "our mysterious sun: magnetic coupling between solar interior and atmosphere" with participation from world-renowned scientists. The annual Georgian-Armenian, Burakan-Abastumani astronomy colloquiums, created in 1974 by close friends and observatory founders Evgeny Khaaradze and Viktor Ambartsumyan, are a great example of deep scientific ties and human international friendship.

The transition from photographic plates to CCD matrices in astronomy came at a difficult political and economic time for Georgia, and the observatory could not keep up with technological developments and equip its instruments with advanced technologies. It led to the cancellation of some scientific projects because several instruments became inoperative. Unfortunately, for the past 50 years, we have had no possibility of adding any serious scientific instruments. The last time, only several telescopes were operating. Among them are the Meniscus 70-cm telescope, the AZT 14 telescope, the double astrograph, and the Big Coronagraph. Although practical astronomy had such difficulties, many of our astronomers became involved in projects analyzing abundant satellite data, and the branch of data analysis became leading mostly in solar physics. Today, our theoretical astrophysicists have come closer to data analysis. This should increase the potential for future observational projects. And it was very timely that the observatory got an opportunity from the government to replace our old, non-functioning 1.25-meter AZT 11 with a new, Austrian-made robotic 1.5-meter telescope equipped with a modern spectrographic interface. The installation of this telescope and the new dome has just been completed and is currently undergoing testing and debugging.

To conclude the history of the Observatory, it is important to honor the memory of the deceased scientists who set the standards of the Observatory both in the field of science and human relations, including E. Kharadze, Sh. Vashakidze, R. Bartaia, V. Dzapiashvili, J. Lominadze, A. Pataraia, R. Kiladze, E. Tsikarishvili and many others.

2. Present state

The population of Georgia is 3.7 million. Accordingly, there are few organizations involved in astrophysical research. The largest organization is our 'Evgenii Kharadze Georgian National Observatory' (Abastumani Astrophysical Observatory). There is the 'Center for Theoretical Astrophysics of the Institute of Theoretical Physics' at Ilia State University (with 7 scientists), which is engaged in research in the field of astrophysics, and a person at Ivane Javakhishvili Tbilisi University, who also works in this field. The majority of specialists working in the field of astrophysics in Georgia come from AbAO. Our scientific staff counts 54 people, and their annual scientific productivity expressed in publications is about 80 publications. Among them, articles are 60, and refereed articles in highly ranked international journals are 40.

2.1. Scientific projects

Here we briefly outline the state-funded scientific projects conducted at the AbAO. Our scientific stuff is organized in three scientific departments. They are 'Galaxies and Stars', 'Sun and Solar System', and 'Theoretical Physics and Cosmology'. The field of study which ongoing state-founded scientific projects cover is traditionally wide and includes galaxies, stars, asteroids, the sun, pulsars, shear flows in astrophysical plasma, and cosmology. The projects are distributed among the departments as follows:
'Galaxies and stars'
1. A study of variable stars and other transients
2. Study of active hearts of galaxies at high energies
3. Search for GW optical matches within the GRANDMA collaboration.
4. Study of selected active galaxies through monitoring
5. Study of the physical characteristics of galaxies at different stages of evolution
6. A study of structure growth with the three-point function of galaxies
7. Search and study of periodic processes and transit events in stars of different spectral groups by photometric and spectroscopic methods

doi: https://doi.org/10.52526/25792776-24.71.2-340

'Sun and the solar system'
8. Study of dangerous asteroids approaching Earth in the Abastumani observatory
9. Solar Atmosphere/Magnetoseismology of the Solar Interior and Space Weather
10. Modeling and observations of solar and space weather processes
11. Study of physical processes in the chromosphere.
12. Magnetospheric heating and pair formation caused by magnetocentrifugal effects in pulsars and other compact objects.
'Theoretical Physics and Cosmology'
13. Testing non-standard cosmological models by studying the physics of gravitational waves, primordial magnetic fields, hidden energy, and neutrinos.
14. Formation of turbulence and coherent structures/flows in astrophysical flat and disk shear flows.
15. Dynamics of astrophysical flat and disk shear flows - non-ideal magnetohydrodynamic effects.

As one can see, our scientific projects count 15. Among them, the projects using actual observations of our telescopes are only 5. We hope that the new telescope will increase interest in our projects in native observational data from Abastumani. Even more new projects will appear concerning the ASA 15 telescope abilities.

In addition to state-founded scientific projects, the observatory hosts research projects funded by the National Science Foundation.

2.2. Scientific facilities

Abastumani Astrophysical Observatory is located in two different places. The main staff of our observatory works at the Tbilisi Office in the center of Tbilisi. The observatory is 250 km from Tbilisi and is built on the nice mountain Kanobili. On the mountain, we have about 10 astronomers and about 40 supporting personnel.

The most busy is the Meniscus 70 cm diameter telescope. The Maksutov System Meniscus Telescope was installed in 1955. This wide-field telescope is designed to observe the various objects in the night sky and to perform a lot of photometric or spectroscopy measurements. The telescope is equipped with Different Refractive Index Prisms (1, 2, 4, 8, degrees) located in front of the objective, which allows, if necessary, to perform the spectral classification of stars and the detection of the objects in special class.

Another operating telescope is AZT-14, Reflector with Parabolic Mirror. AZT-14, was installed in 1968. Cassegrain system. Objective diameter: 48 cm. The telescope is used for photometric study of variable stars.

One more telescope that is operable but is not loaded with many projects is 40-cm Wide Field Double Astrograph. It was installed in 1978. It consists of two identical refractors. Objective diameter: 40 cm. This telescope was used successfully for many years to perform astronomy observations of the solar system, observations of various types of stars in our galaxy, and extragalactic purposes.

The next science-used solar telescope that is only left among others that became non-actual and inoperable is the Solar Coronagraph. The Solar, Large Non-Eclipse Coronagraph, was installed in 1977. Objective diameter: 53 cm. The telescope is used for high-dispersion observations of the physical and dynamic characteristics of the Sun's outer atmosphere and for studying the "fine" structure of the chromosphere and the Corona.

The Schmidt-Cassegrain System telescope with automatic control was installed in 2018. The correction plate's diameter is 36 cm. It is mainly used for the polarimetric and photometric study of celestial bodies.

The chromospheric and photospheric telescopes were installed in 1957. Both of these telescopes (two tubes) were mounted on the same Parallax Unit, and therefore they have a common remote control and the clock mechanism. The chromospheric telescope is a refractor with an objective diameter of 6 cm. The telescope—narrow spectral band interference—polarizing filter, allows to get the 1.7-cm-diameter image of the sun (in the center of H alpha line) with the chromatic features such as prominences, filaments, and eruptions. The Photospheric Telescope is a refractor with an objective diameter of 13 cm. The telescope provides a 7.8-cm-diameter image of the sun (in the white band) with photosphere features such as granules, sunspots, and solar flares. Observational data collected by this telescope are valuable even today because of their long-term, more than three activity cycles, and uniformity. Today, observations made with this telescope are not scientifically valid, but we want to use it for educational purposes.

The final but most important one is our flagman, the Telescope ASA AZ1500 f6.

doi: https://doi.org/10.52526/25792776-24.71.2-340

- Optical design: Ritchey-Chrétien RC
- Main mirror aperture: 1,500 mm
- Dome internal diameter: 12.0 m
- Dome outer diameter: 12.5 m
- Shutter width: 3.0 meters

Telescope equipped with CCD Camera Andor iKon-XL 230 BV. Pixel number: 4096 x 4108. Pixel size: 15 microns. CCD type: Monochrome

Telescope equipped with Shelyak Whoppshel Spectrograph Spectrograph type: Echelle

- Spectral resolution: R = 30,000 and 15,000 (average at spectral range)
- Spectral range: 400 – 750 nm

2.3. Digitization of the glass and film library

Several attempts were made in previous years to digitize the vast observational data collected at our observatory over the course of more than 50 years. These initiatives were made by small groups of our astronomers with financial assistance from various grants. They helped answer specific local scientific challenges but did little to help with the larger task of digitizing the entire collection. After the reorganization of the observatory, we established the "Department of Technical Support and Development of Scientific Infrastructure," which includes a special team of six personnel concerned with systemizing and digitizing the observatory's glass and film collections. The glass library of the Abastumni Astrophysical Observatory contains around 70,000 photographic plates and films. Materials are mainly collected using the following instruments:

The 40-cm reflector has been making observations since 1937. Direct images of the moon, planets, asteroids, comets, and spectra of "trapezium"-type systems and clusters were obtained. In total, there are around 6500 images. Until 1963, two 20-cm cameras were utilized with the 40-cm telescope. Later, polarimetric and photometric measurements were made using this telescope. The 44 cm Schmidt camera was built in 1940. Before 1985, 25,000 photographic plates had been received. This telescope was used to observe supernovae, comets, galaxies, and other celestial objects. The 70-cm meniscus telescope has been in operation since 1955. We have received 20,500 photographic plates. Several sky review program observations have been made. Direct images of galaxies, binary stars, supernovae, and other objects are obtained. The telescope operated with preobjective prisms. The telescope's unique spectral material was used to perform two-dimensional spectral classification in certain parts of the sky. The 40-cm double astrograph has been operational since 1979. Astrometric measurements are made. Three thousand negatives were taken. For many years, several instruments have been observing the sun. There is also a rich, unique observational material of solar eclipses from the 1936 expeditions. Since 1957, atmospheric physicists have observed ozone and nighttime high-level lighting. There is an abundance of content to digitize.

So far, the digitization team has digitized astronomical logbooks from all stellar telescopes. 1600 spectroheliograph tapes and over 16,000 Schmidt's anaberration camera films have been scanned. The scanning of the spectral material on the 70-cm meniscus telescope has begun. The scanned materials are currently saved as ".tif" files. In the near future, it will be integrated into ".fits" files with suitable headers that preserve logbook details. A search engine program has been developed. Finally, we will publish it on our website for public consumption, as most observatories do.

2.4. Popularization of science in Georgia

From the very beginning of our observatory, all young astronomers were involved in guiding visitors on Mount Kanobili. At that time, we received visitors free of charge, and the guides did not receive a salary for this. Nowadays, we have a department of "Science Outreach". Now visitors have to pay for the visit, but in many cases, when we have special requests from schools or universities, our astronomers organize free lectures and excursions. I must say that popularization of astronomy is even more important now, since there is no astronomy subject in state schools and undergraduate programs at universities. Three state universities have only master's courses in astrophysics, without providing classical basic knowledge

doi: https://doi.org/10.52526/25792776-24.71.2-340

of astronomy. In order to increase the interest of schoolchildren in astronomy, we decided to combine the educational function, and for the third year now, free interactive lectures and seminars for schoolchildren have been held weekly in the Tbilisi office. In these classes, in addition to theoretical knowledge, students learn to assemble simple telescopes from scrap materials. These materials are purchased at the expense of the observatory, and after assembly, they are given to children as gifts. Two months ago, we organized the first "Astrophysical Conference of Young Scientists," where our young scientists and schoolchildren presented their reports. Our astronomers give popular lectures in various public schools. We intend to expand the scope and cover rural areas. After the repair of the accommodation infrastructure on Mount Kanobili is completed, we are going to organize annual summer schools for schoolchildren there. It would be great if this took on an international character.

Acknowledgements

The author would like to thank the organizers of the Southwest and Central Asian 4th Regional Astronomy Workshop, in particular Dr. Areg Mikaelian, Director of the Burakan Astrophysical Observatory.

References

Bagashvili S. R., et al., 2017, Astron. Astrophys. , 603, A134

Bartaya R. A., Chargeishvili K. B., Chentsov E. L., Shkhagosheva Z. U., 1994, Bulletin of the Special Astrophysics Observatory, 38, 103

Bodo G., Chagelishvili G., Murante G., Tevzadze A., Rossi P., Ferrari A., 2005, Astron. Astrophys. , 437, 9

Bodo G., Tevzadze A., Chagelishvili G., Mignone A., Rossi P., Ferrari A., 2007, Astron. Astrophys. , 475, 51

Chagelishvili G. D., Chanishvili R. G., Lominadze D. G., Filipov L. G., Khristov T. S., 1991, Advances in Space Research, 11, 61

Chargeishvili B., Zhao J., Sakai J.-I., 1993, , 145, 297

Chargeishvili K. B., Bartaya R. A., Kharadze E. K., 2013, VizieR Online Data Catalog: Spectral Classes in Kapteyn areas 68-91 (Chargeishvili+, 2000), VizieR On-line Data Catalog: III/271. Originally published in: 2000AbaOB..75...93C; 2013yCat.3271....0C

Dzhapiashvili V. P., Korol' A. N., 1982, Polarimetric atlas of the moon.. Tbilisi Metsniereba

Gil J. A., Melikidze G. I., Mitra D., 2002, Astron. Astrophys. , 388, 235

Kahniashvili T., Maravin Y., Kosowsky A., 2009, Phys. Rev. D. , 80, 023009

Kahniashvili T., Kisslinger L., Stevens T., 2010, Phys. Rev. D. , 81, 023004

Kharadze E. K., Bartaya R. A., Chargeishvili K. B., 2014, VizieR Online Data Catalog: Spectral Classes in Kapteyn areas 92-115 (Kharadze+, 2003), VizieR On-line Data Catalog: III/275. Originally published in: 2003AbaOB..76....3K

Kulidzhanishvili V. I., Stepanov A. I., Nikolskii G. M., 1985, Abastumanskaia Astrofizicheskaia Observatoriia Byulleten, 60, 109

Mdzinarishvili T. G., Shergelashvili B. M., Japaridze D. R., Chargeishvili B. B., Kosovichev A. G., Poedts S., 2020, Advances in Space Research, 65, 1843

Melikidze G. I., Gil J. A., Pataraya A. D., 2000, Astrophys. J. , 544, 1081

Molotov I., et al., 2008, Advances in Space Research, 41, 1022

Shergelashvili B. M., Poedts S., 2005, Astron. Astrophys. , 438, 1083

Shergelashvili B. M., Zaqarashvili T. V., Poedts S., Roberts B., 2005, Astron. Astrophys. , 429, 767

Srivastava A. K., Zaqarashvili T. V., Kumar P., Khodachenko M. L., 2010, Astrophys. J. , 715, 292

Tevzadze A. G., Chagelishvili G. D., Bodo G., Rossi P., 2010, Mon. Not. R. Astron. Soc. , 401, 901

Zaqarashvili T., Chargeishvili B., Sakai J., 1996, Astrophys. Space. Sci. , 246, 107

Zaqarashvili T. V., Díaz A. J., Oliver R., Ballester J. L., 2010, Astron. Astrophys. , 516, A84

Zeleny L. M., Taktakishvili A. L., 1987, Astrophys. Space. Sci. , 134, 185

Zhao J., Chargeishvili B., Sakai J.-I., 1993a, , 146, 331

Zhao J., Chargeishvili B., Sakai J.-I., 1993b, , 147, 131

doi: https://doi.org/10.52526/25792776-24.71.2-340

Communications of BAO, Vol. 71, Issue 2, 2024, pp. 345-350

Deciphering Galactic Halos: A Detailed Review of Star Formation in NGC 5128 (Cen A)

M. Abdollahi *[1], S. T. Aghdam[1], A. Javadi †[1], S. A. Hashemi[2,3], J. Th. van Loon[4], H. Khosroshahi[1], R. Hamedani Golshan[5], E. Saremi[1,6,7], and M. Saberi[8]

[1]School of Astronomy, Institute for Research in Fundamental Sciences (IPM), Tehran, 19568-36613, Iran
[2]Department of Physics, Sharif University of Technology, Tehran, 11155-9161, Iran
[3]Department of Physics and Astronomy, University of California Riverside, CA 92521, The USA
[4]Lennard-Jones Laboratories, Keele University, ST5 5BG, UK
[5]I. Physikalisches Institut, Universität zu Köln, Zülpicher Straße 77, 50937 Cologne, Germany
[6]Instituto de Astrofisica de Canarias, C/ Vìa Làctea s/n, 38205 La Laguna, Tenerife, Spain
[7]Departamento de Astrofisica, Universidad de La Laguna, 38205 La Laguna, Tenerife, Spain
[8]Rosseland Centre for Solar Physics, University of Oslo, P.O. Box 1029, Blindern, NO-0315, Oslo, Norway

Abstract

NGC 5128 (Centaurus A), the closest giant elliptical galaxy outside the Local Group to the Milky Way, is one of the brightest extragalactic radio sources. It is distinguished by a prominent dust lane and powerful jets, driven by a supermassive black hole at its core. Using previously identified long-period variable (LPV) stars from the literature, this study aims to reconstruct the star formation history (SFH) of two distinct regions in the halo of NGC 5128. These regions reveal remarkably similar SFHs, despite being located about 28 kpc apart on opposite sides of the galaxy's center. In Field 1, star formation rates (SFRs) show notable increases at approximately 800 Myr and 3.8 Gyr ago. Field 2 exhibits similar peaks at these times, along with an additional rise around 6.3 Gyr ago. The increase in SFR around 800 Myr ago is consistent with earlier research suggesting a merger event. Since no LPV catalog exists for the central region of NGC 5128, we focused our investigation on its outer regions, which has provided new insights into the complex evolutionary history of this cornerstone galaxy. The SFH traced by LPVs supports a scenario in which multiple events of nuclear activity have triggered episodic, jet-induced star formation.

Keywords: *stars: AGB and LPV – stars: formation – galaxies: halos – galaxies: evolution – galaxies: star formation – galaxies: individual: NGC 5128*

1. Introduction

Our position within the Local Group (LG) provides an excellent opportunity to study the resolved stellar populations of spiral galaxies, enhancing our understanding of their formation and evolution. However, because the LG lacks a giant elliptical (GE) galaxy, our knowledge of such systems relies on observations of the nearest elliptical galaxies in neighboring groups. NGC 5128 (Centaurus A), situated 3.8 Mpc away ($\mu = 27.87 \pm 0.16$ mag; Rejkuba et al., 2004, and $E(B-V) = 0.15 \pm 0.05$ mag; Rejkuba, M., 2004a), presents a rare opportunity to study a nearby GE galaxy in details (Harris et al., 1999; Charmandaris et al., 2000; Rejkuba, M., 2004a, 2005), as it resides within the Centaurus galaxy group (Karachentsev, 2005).

NGC 5128 is considered a post-merger galaxy (Peng et al., 2002) and is one of the few halos that has been resolved into individual stars (Rejkuba et al., 2011). The stellar populations in NGC 5128's halo serve as crucial indicators of its star formation history, revealing evidence of past interactions and mergers.

The active galactic nucleus (AGN) at the center of NGC 5128 drives powerful radio jets, providing the closest example of this galactic outflows (Crockett et al., 2012). How AGN activity influences star formation and the evolution of its host galaxy remains a crucial but unresolved question in galaxy formation and evolution theory (Ciotti & Ostriker, 1997; Silk & Rees, 1998, 2005; Binney, 2004; Springel et al., 2005; Sijacki et al., 2007; Schawinski et al., 2007).

*m.abdollahi@ipm.ir, Corresponding author
†atefeh@ipm.ir

doi: https://doi.org/10.52526/25792776-24.71.2-345

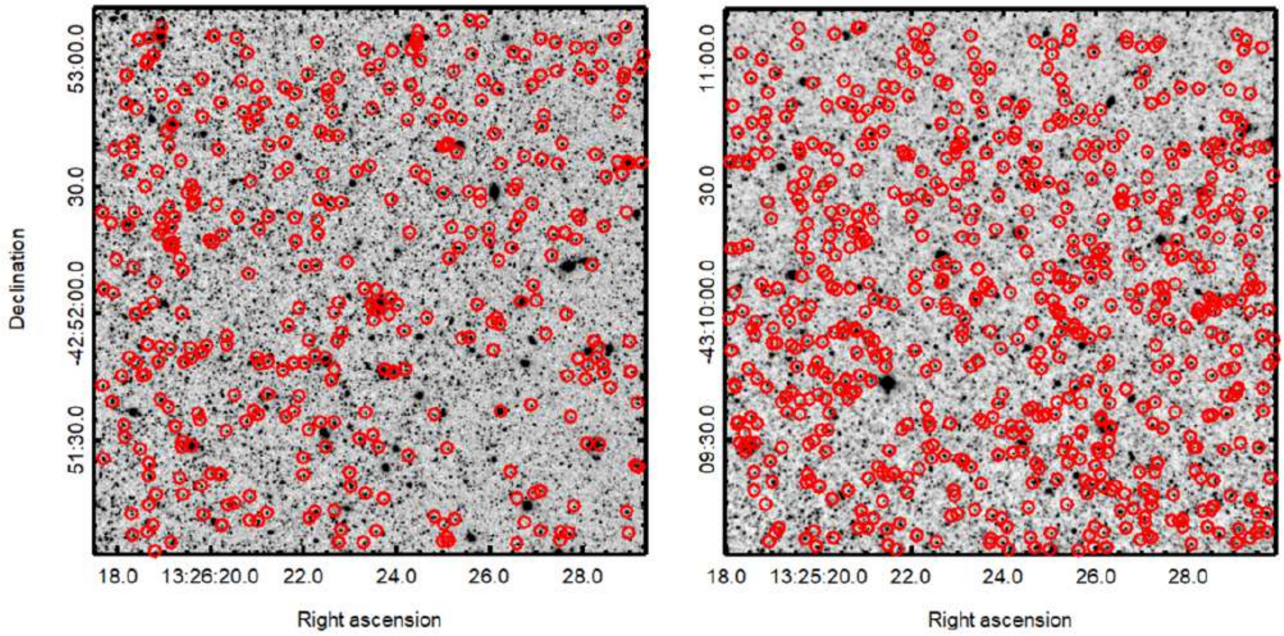

Figure 1. The images of the fields studied here (each approximately 2.3×2.3 arcminutes) are shown. Red circles indicate the locations of the selected LPV stars. (Left panel) The northwestern field is centered at $\alpha = 13^h\ 26^m\ 23^s.5$, $\delta = -42^\circ\ 52'\ 0''$, on the eminent northeastern part of the halo, at a distance of $\sim 17'$ (~ 18.8 kpc) from the center of the galaxy presented by Ma et al., 1998, with dimensions of $2'.28 \times 2'.30$ (5.7 kpc^2). (Right panel) The southern field is centered at $\alpha = 13^h\ 25^m\ 26^s$, $\delta = -43^\circ\ 10'\ 0''$, at a distance of $\sim 9'$ (~ 9.9 kpc) from the center, with dimensions of $2'.25 \times 2'.31$ (5.7 kpc^2).

The star formation history is essential for understanding galaxy formation and evolution. In resolved galaxies, SFH is usually derived from color–magnitude diagrams (CMDs) of individual stars, revealing signatures of various stellar populations (e.g., Tolstoy & Saha, 1996; Holtzman et al., 1999; Olsen, 1999; Dolphin, 2002,Javadi et al., 2011b). However, this analysis is typically limited to a few dozen galaxies, mostly within our Local Group, due to observational constraint.

This work aims to determine the SFH of two small fields in the halo of NGC 5128 by using long-period variable stars as tracers, to explore the connection between the halo's SFH and its merger history.

2. Data

We utilized near-infrared data published by Rejkuba, M., 2004b and analyzed by Rejkuba et al., 2003. This catalog was obtained using the ISAAC instrument on the ESO Paranal UT1 Antu 8.2 m Very Large Telescope, covering two distinct fields in the northwestern and southern regions of the halo of NGC 5128 (referred to as Field 1 and Field 2, respectively), as shown in Figure 1.

Rejkuba, M. (2004a) identified 15,574 and 18,098 stars in Fields 1 and 2, respectively. However, our focus is on long-period variable stars with periods exceeding 70 days, which form the basis for a method for constructing the star formation history as developed by Javadi et al. (2011a).

Rejkuba et al. (2003) identified LPV stars using multi-epoch photometry in the Ks band, along with single-epoch photometry in the Js and H bands, in two mentioned fields. However, based on the specified criteria, we selected 395 LPV stars in Field 1 and 671 in Field 2. The distribution of these selected LPV stars, marked by red circles, is displayed in Figure 1.

3. Method

As mentioned in the previous section, Javadi et al. (2011a) developed a method to calculate star formation histories based on long-period variable stars. During the LPV phase, stars reach their peak luminosity, providing a valuable opportunity to establish a strong correlation between birth mass and this peak. Based

doi: https://doi.org/10.52526/25792776-24.71.2-345

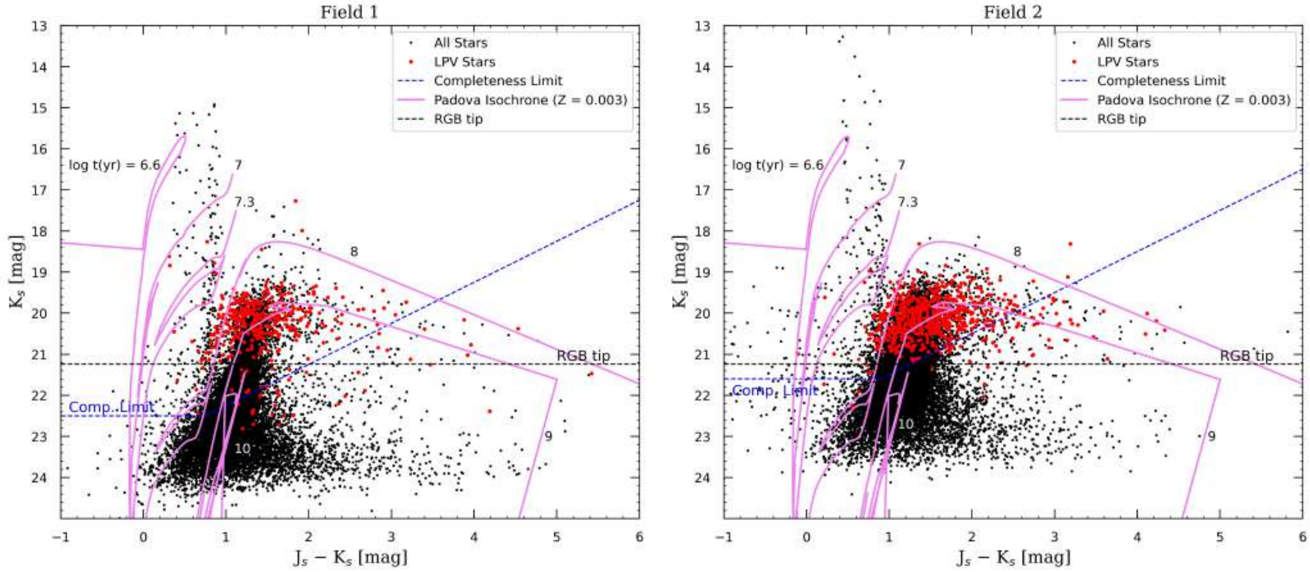

Figure 2. The K_s vs. $J_s - K_s$ color-magnitude diagram (CMD) shows stars with at least three K_s-band detections (black dots) and long-period variable (LPV) stars (red dots) in Field 1 (left) and Field 2 (right). The black and blue dotted lines represent the tip of the red giant branch (RGB) and the completeness limit magnitudes, respectively, for each field (Rejkuba et al., 2003). The purple lines indicate theoretical stellar isochrones for a metallicity of $Z = 0.003$ across six different ages (Marigo et al., 2017).

Table 1. The age-metallicity relation investigated by Woodley et al. (2009) and Yi et al. (2004) assuming $Z_\odot = 0.0198$ (Rejkuba et al., 2011).

Woodley et al., 2009		Yi et al., 2004	
Age range (Gyr)	Z	Age range (Gyr)	Z
age $\geq$ 12	0.001	age $\geq$ 10	0.0003
8 $\leq$ age <12	0.003	6 $\leq$ age <10	0.001
6.5 $\leq$ age <8	0.006	4 $\leq$ age <6	0.003
5.5 $\leq$ age <6.5	0.008	3 $\leq$ age <4	0.010
3 $\leq$ age <5.5	0.010	2 $\leq$ age <3	0.020
2 $\leq$ age <3	0.020	age <2	0.039
age <2	0.030		

on this correlation, relations—including the birth mass-luminosity, age-mass, and pulsation duration relations—can be derived for each metallicity from the Padova stellar evolutionary models (Marigo et al., 2017). By inputting the stars' magnitudes into these relations, we can determine the components of an equation that statistically reconstructs the star formation history of galaxies based on the initial mass function.

$$\xi(t) = \frac{dn'(t)}{\delta t} \; \frac{\int_{\min}^{\max} f_{\rm IMF}(m) m \; dm}{\int_{m(t)}^{m(t+dt)} f_{\rm IMF}(m) \; dm}, \tag{1}$$

where m is birth mass and $f_{\rm IMF}(m)$ is Kroupa initial mass function (IMF) (Kroupa, 2001).

As shown in Figure 2, we expect all LPV stars to be located near the peaks of the isochrones derived from the Padova stellar evolutionary models. However, some stars appear spread into redder regions due to surrounding dust. To correct for dust effects, these stars need to be shifted back to the isochrone peaks before their magnitudes are used in the mentioned statistical equations.

This method, which has since been applied in a variety of studies (Javadi et al., 2011a, 2011b, 2017; Rezaei kh. et al., 2014; Hamedani Golshan et al., 2017; Hashemi et al., 2018; Navabi et al., 2021; Saremi et al., 2020; Parto et al., 2023; Abdollahi et al., 2023;Aghdam et al., 2024; Khatamsaz et al., 2024), considers a range of metallicities to define the epochs of star formation for each case and enables comparisons among them.

However, we go a step further by incorporating the age-metallicity relation, which provides an opportunity to address uncertainties in the metallicity. To elaborate, this approach allows us to determine the

doi: https://doi.org/10.52526/25792776-24.71.2-345

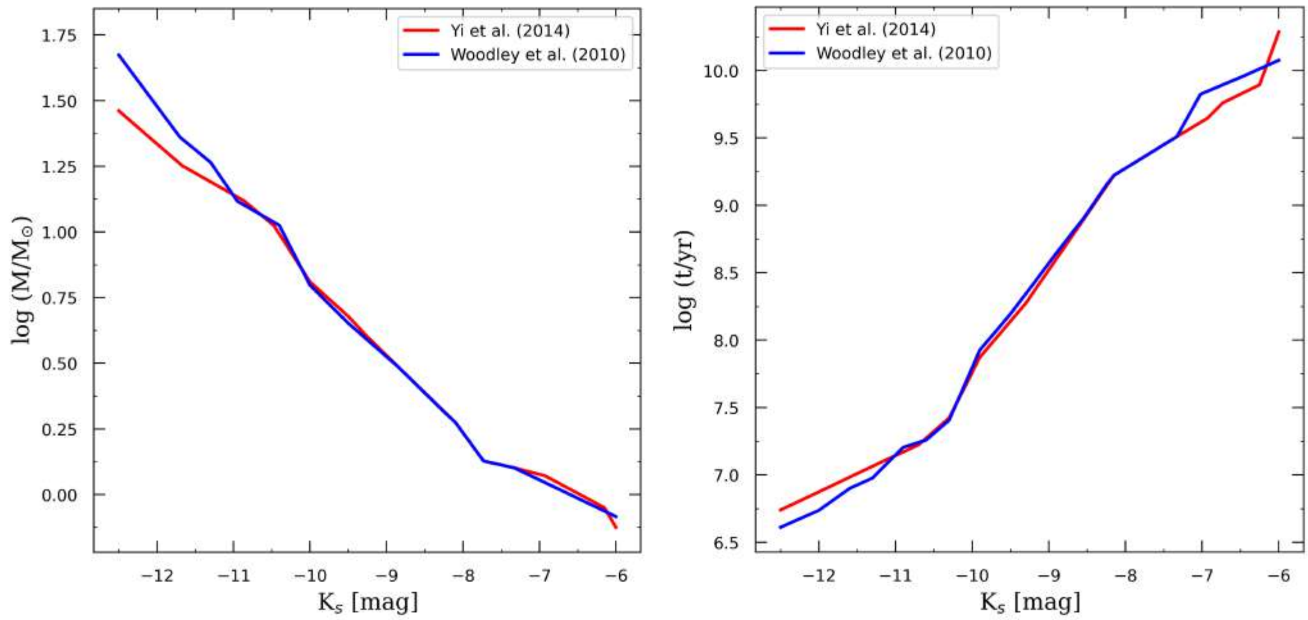

Figure 3. The mass–luminosity (left panel) and age–luminosity (right panel) relations, considering the AMRs determine by Yi et al. (2004) (red line) and Woodley et al. (2009) (blue line).

metallicity of the galaxy across each age range, as presented in Table 1.

We redefined the mass-luminosity and age-mass relations based on the age-metallicity relation (AMR), resulting in a single, unified relation that encompasses the full range of metallicities experienced by the galaxy. Figure 3 illustrates these relations for the models determined by Yi et al. (2004) and Woodley et al. (2009). As shown, the trends in these diagrams are similar, with only slight differences at the beginning and end of the intervals. Using the AMR approach, we can now overcome the metallicity degeneracy and establish Equation 1 to derive the SFH for the two separate fields.

4. Results and Discussion

In our analysis of the SFH of NGC 5128, illustrated in Figure 4, Field 1 exhibited two major star formation epochs: one approximately 3.6 billion years ago and another around 800 million years ago. Field 2, however, showed three significant epochs, occurring roughly 6.3 billion, 3.6 billion, and 800 million years ago. The latter two epochs align with those in Field 1, suggesting a connection between these distant regions, despite being separated by 28 kpc on opposite sides of the galaxy. This similarity in SFH across such large distances implies shared galactic-scale influences.

Comparing our results with previous studies reveals further insights into the history of NGC 5128. Evidences such as the galaxy's unusual structure (Graham, 1979), optical and neutral hydrogen shells (Malin et al., 1983; Peng et al., 2002; Schiminovich et al., 1994), and ongoing star formation suggest a history of mergers and interactions (Rejkuba, M., 2004b). Specifically, literature indicates a major merger with a smaller, gas-rich galaxy around 1 Gyr ago (Malin et al., 1983; Sparke, 1996), which aligns with our observed peak in star formation around the previous 800 Myr. Additionally, a possible minor merger could explain the secondary star formation peak, indicating this galaxy has undergone multiple interactions over time.

Furthermore, NGC 5128's central supermassive black hole has likely driven active galactic nucleus (AGN) activity, fueled by abundant cold gas. Such activity, as noted in studies by Saxton et al., 2001 and Hardcastle et al., 2009, has been linked to increased the star formation rate. The age estimates for the nuclear molecular layer (∼150 Myr) and inner lobes (∼30 Myr) suggest that the AGN was active well before these epochs, potentially contributing to the sustained rise in star formation observed up to around 800 Myr ago.

doi: https://doi.org/10.52526/25792776-24.71.2-345

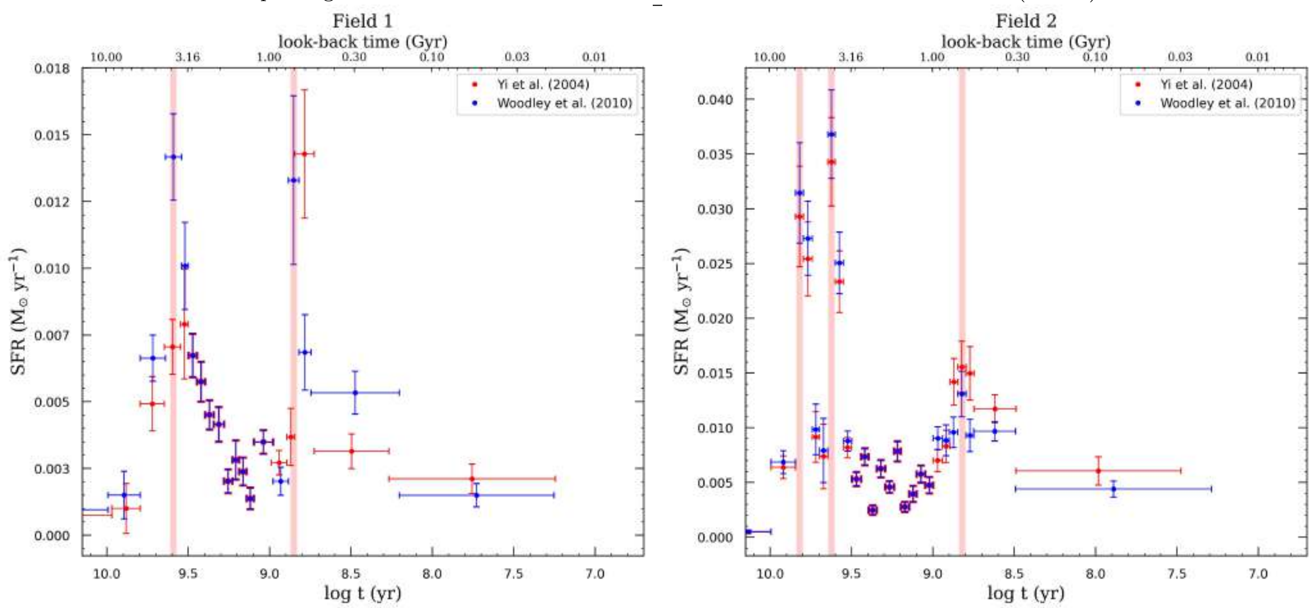

Figure 4. The SFH derived using the age-metallicity relations (AMRs) from Yi et al. (2004) (red markers) and Woodley et al. (2009) (blue markers) is shown for Field 1 (left panel) and Field 2 (right panel). Highlighted regions indicate the peaks of star formation during major epochs.

5. Conclusion

In this study, we investigated the star formation history (SFH) of NGC 5128, the nearest giant elliptical galaxy to the Local Group, by employing a statistical approach based on long-period variable (LPV) stars. Our analysis focused on two distinct regions within the halo of this galaxy, providing insights into the star formation activity in the outer regions of this unique system. Key findings include:

- A novel method based on the age-metallicity relation of LPV stars was introduced and employed to investigate the SFH of NGC 5128.
- Despite their significant separation, both studied regions exhibited a similar SFH, suggesting equivalent evolutionary influences across the galaxy.
- Evidence of peaks in star formation supports the occurrence of a past collision or merger in NGC 5128.
- Our findings indicate that active galactic nucleus (AGN) activity can enhance the star formation rate in galaxies.

References

Abdollahi H., et al., 2023, Astrophys. J. , 948, 63

Aghdam S. T., et al., 2024, Astrophys. J. , 972, 47

Binney J., 2004, MNRAS, 347, 1093

Charmandaris V., Combes F., van der Hulst J. M., 2000, Astron. Astrophys. , 356, L1

Ciotti L., Ostriker J. P., 1997, Astrophys. J. Lett. , 487, L105

Crockett R. M., et al., 2012, MNRAS, 421, 1603

Dolphin A. E., 2002, MNRAS, 332, 91

Graham J. A., 1979, Astrophys. J. , 232, 60

Hamedani Golshan R., Javadi A., van Loon J. T., Khosroshahi H., Saremi E., 2017, Mon. Not. R. Astron. Soc. , 466, 1764

Hardcastle M. J., Evans D. A., Croston J. H., 2009, Mon. Not. R. Astron. Soc. , 396, 1929

Harris G. L. H., Harris W. E., Poole G. B., 1999, Astron. J. , 117, 855

Hashemi S. A., Javadi A., van Loon J. T., 2018, MNRAS, 483, 4751

doi: https://doi.org/10.52526/25792776-24.71.2-345

Holtzman J. A., et al., 1999, The Astronomical Journal, 118, 2262

Javadi A., van Loon J. T., Mirtorabi M. T., 2011a, MNRAS, 411, 263

Javadi A., van Loon J. T., Mirtorabi M. T., 2011b, MNRAS, 414, 3394

Javadi A., van Loon J. T., Khosroshahi H. G., Tabatabaei F., Hamedani Golshan R., Rashidi M., 2017, Mon. Not. R. Astron. Soc. , 464, 2103

Karachentsev I. D., 2005, Astron. J. , 129, 178

Khatamsaz F., Abdollahi M., Abdollahi H., Javadi A., Van Loon J., 2024, in IAU General Assembly. p. 648

Kroupa P., 2001, Mon. Not. R. Astron. Soc. , 322, 231

Lamers, H. J. G. L. M. Kruijssen, J. M. D. Bastian, N. Rejkuba, M. Hilker, M. Kissler-Patig, M. 2017, A&A, 606, A85

Ma C., et al., 1998, The Astronomical Journal, 116, 516

Malin D., Quinn P., Graham J., 1983, Astrophys. J. , 272, L5

Marigo P., et al., 2017, Astrophys. J. , 835, 77

Morganti R., Killeen N. E. B., Ekers R. D., Oosterloo T. A., 1999, MNRAS, 307, 750

Navabi M., et al., 2021, Astrophys. J. , 910, 127

Olsen K. A., 1999, The Astronomical Journal, 117, 2244

Parto T., et al., 2023, Astrophys. J. , 942, 33

Peng E. W., Ford H. C., Freeman K. C., White R. L., 2002, Astron. J. , 124, 3144

Rejkuba, M. 2004a, A&A, 413, 903

Rejkuba, M. 2004b, A&A, 413, 903

Rejkuba M., Minniti D., Silva D. R., 2003, Astron. Astrophys. , 406, 75

Rejkuba M., Greggio L., Zoccali M., 2004, Astron. Astrophys. , 415, 915

Rejkuba M., Greggio L., Harris W. E., Harris G. L. H., Peng E. W., 2005, Astrophys. J. , 631, 262

Rejkuba M., Harris W. E., Greggio L., Harris G. L. H., 2011, Astron. Astrophys. , 526, A123

Rezaei kh. S., Javadi A., Khosroshahi H., van Loon J. T., 2014, MNRAS, 445, 2214

Saremi E., et al., 2020, Astrophys. J. , 894, 135

Saxton C. J., Sutherland R. S., Bicknell G. V., 2001, Astrophys. J. , 563, 103

Schawinski K., Thomas D., Sarzi M., Maraston C., Kaviraj S., Joo S.-J., Yi S. K., Silk J., 2007, MNRAS, 382, 1415

Schiminovich D., van Gorkom J. H., van der Hulst J. M., Kasow S., 1994, Astrophys. J. Lett. , 423, L101

Sijacki D., Springel V., Di Matteo T., Hernquist L., 2007, MNRAS, 380, 877

Silk J., 2005, MNRAS, 364, 1337

Silk J., Rees M. J., 1998, Astron. Astrophys. , 331, L1

Sparke L. S., 1996, Astrophys. J. , 473, 810

Springel V., Di Matteo T., Hernquist L., 2005, The Astrophysical Journal, 620, L79

Tolstoy E., Saha A., 1996, Astrophys. J. , 462, 672

Woodley K. A., Harris W. E., Puzia T. H., Gómez M., Harris G. L., Geisler D., 2009, The Astrophysical Journal, 708, 1335

Yi S., Peng E., Ford H., Kaviraj S., Yoon S.-J., 2004, MNRAS, 349, 1493

doi: https://doi.org/10.52526/25792776-24.71.2-345

Pulsars and Millisecond Pulsars I: Advancements, Open Questions and finding Gaps via statistical insights

Maria Rah[1,2]*, Areg Mickaelian [1], Francesco Flammini Dotti[3], Rainer Spurzem[2,3]

[1] NAS RA V.Ambartsumian Byurakan Astrophysical Observatory (BAO), Byurakan, Armenia

[2] The Silk Road Project at the National Astronomical Observatory, Chinese Academy of Sciences, China

[3] Astronomisches Rechen-Inst., ZAH, Univ. of Heidelberg, Germany

Abstract

Investigating the development of pulsars and millisecond pulsars (MSPs) highlights for us statistical insights, important research areas, and unresolved aspects to address. Through the following work, we provide a detailed demographical study of these astrophysical objects by combining data from several observational techniques (radio, X-ray, and gamma-ray) in different environments: Galactic Field (GF) and Globular Clusters (GC). Although observational studies provide direct insights into the emission properties, periodic timing (e.g. millisecond pulsars), and spatial distribution of pulsars, theoretical models are essential to interpret these findings and unravel the underlying physical processes driving their unique characteristics. We focus on the "magnetic field-spin" relationship, exploring spin-up—where accretion transfers angular momentum to the pulsar in binary systems—and spin-down, driven by magnetic dipole radiation or particle winds dissipating rotational energy. These mechanisms illuminate the intricate dynamics linking spin evolution to magnetic field decay. Building on these theoretical frameworks and the application of advanced numerical simulation tools such as NBODY6++GPU, CMC, and COMPASS, we provide a critical means to quantitatively test and refine our understanding of spin and magnetic field evolution in such compact objects. However, despite the advances offered by these tools, significant issues remain, particularly in interpreting the intricate dynamics of binary interactions involving pulsars and millisecond pulsars, as well as in accurately incorporating the physics of these compact objects into comprehensive numerical simulations. This analysis underscores the critical need for enhanced modeling frameworks and more refined observational studies to address unresolved questions regarding the formation processes, evolutionary pathways, and magnetic field degradation of pulsars and MSPs. These numerical integrations of compact objects into comprehensive models of objects with a large number of stars will highlight the necessity of advancing simulation techniques. By improving these simulations, we can more accurately model the intricate physics governing pulsar behavior and ultimately resolve these outstanding challenges in astrophysics.

Keywords: Pulsars, Millisecond Pulsars, Statistical Insights, Evolution, Simulations, and Gaps.

1. Introduction

A specific type of neutron star, known as a pulsar, is characterized by its emission of periodic electromagnetic radiation pulses, detectable across multiple wavelengths due to its intense magnetic fields and rapid rotation. Generally, pulsars typically exhibit spin periods ranging from about 0.1 to several seconds. With this unique property, normal pulsars represent a broader category of such neutron stars. However, within this category, millisecond pulsars (MSPs) stand out as a unique subclass distinguished by their extremely short spin periods, typically ranging from 1 to 10 milliseconds (Lorimer, 2008). As we mentioned, Pulsars and MSPs are unique because they are periodic, they work as accurate cosmic clocks, and they make it possible to study general relativity and dense matter physics with outstanding accuracy (Baker, 2023, Zhang et al., 2022). The stark difference in rotation speed arises from a transformative "recycling" process, where the pulsar gains angular momentum from a companion star in a binary system (Chattopadhyay, 2021). This process not

*mariarah.astro@gmail.com, Corresponding author

doi: https://doi.org/10.52526/25792776-24.71.2-351

only accelerates the spin of the pulsar, but also alters its magnetic field, behavior, and evolutionary pathway, differentiating MSPs from their slower-rotating counterparts. MSPs are commonly found in binary systems as neutron stars recycle material and angular momentum from their companion star (Demorest et al., 2010). The aforementioned recycling process happens quite frequently in low-mass X-ray binaries, where millisecond pulsars have periods as short as a few milliseconds (Freire et al., 2012, Lattimer & Prakash, 2007).

2. Historical Milestones and Future Directions for the current study

The historical evolution of pulsar research extends over nearly a century, starting with hypothesis put forward by V.Ambartsumian in 1929 concerning stars comprised of atomic nuclei (Han et al., 2021, Mickaelian, 2018), Following this claim, less than 2 years later, neutron stars were discovered by James Chadwick, and the first pulsar was identified by Jocelyn Bell Burnell and Antony Hewish in 1967 (Hewish & Burnell, 1970). Since then, advances in radio astronomy and the development of sophisticated instruments such as the Arecibo Telescope, the Parkes Multibeam Survey around 1998, and the construction of FAST, which became operational in 2017, and further accelerating discoveries have greatly expanded pulsar catalogs. See Figure 1 that shows that the rate of discovering regular pulsars surged after 2016, coinciding with advancements in survey technologies and contributions from CHIME starting in 2018 (Padmanabh et al., 2024, Sengar et al., 2023, Zhou et al., 2023).

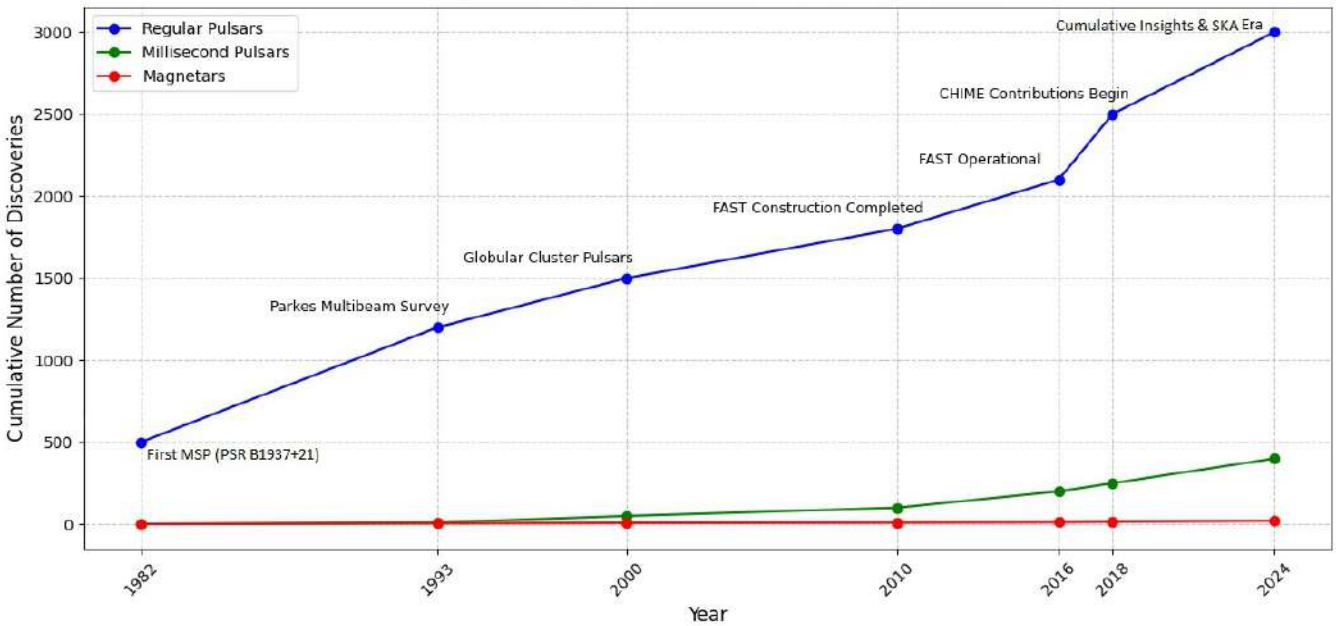

Figure 1. This figure depicts the cumulative discoveries of Regular Pulsars, Millisecond Pulsars, and Magnetars from 1982 to 2024. As is evident in the figure, the focus is on pulsars. We can find that with the growth and development of technology, which has increased the accuracy of discovery methods, the number of recorded normal pulsars is very large, and this in itself is evidence of the need to study them and their evolution pathway with greater precision and accuracy. Find more (Padmanabh et al., 2024, Sengar et al., 2023, Zhou et al., 2023)

.

Magnetars are a rare type of neutron star with extremely strong magnetic fields, billions of times stronger than typical pulsars, known for emitting intense bursts of X-rays and gamma rays (Kaspi & Beloborodov, 2017, Musolino et al., 2024) . Despite steady increases in millisecond pulsars and magnetars, their numbers remain significantly lower than regular pulses, underscoring the prevalence of the latter in astronomical research. This graph effectively illustrates the impact of technological progress on the field of pulsar discovery. We now have a better understanding of these things because of later discoveries like binary pulsars that verified the predictions of gravitational waves (Falxa et al., 2023, Hulse & Taylor, 1975).

The current study serves as the first installment in a series dedicated to an statistical investigation of

doi: https://doi.org/10.52526/25792776-24.71.2-351

pulsars and millisecond pulsars as an outstanding subject of interest in contemporary astrophysics. In the following papers, which will be published in the next two issues of the current journal, we will respectively study in depth the special evolutions of pulsars and millisecond pulsars, and then, examine their evolutions during the evolutions of globular clusters by numerical simulation using NBODY6++GPU (Kamlah et al., 2022, Spurzem et al., 2023). The code will be updated for a new model of neutron star and pulsar evolution (see Sect. 7 and Ye & Fragione, 2022, Ye et al., 2019).

3. Statistics and observational perspectives

Pulsars and MSPs are found in different environments, including globular clusters (GC) and galactic fields (GF), which each have their own population features (Han et al., 2021). For better understanding, we refer to the cumulative number of objects found in these environments in Figure 2.

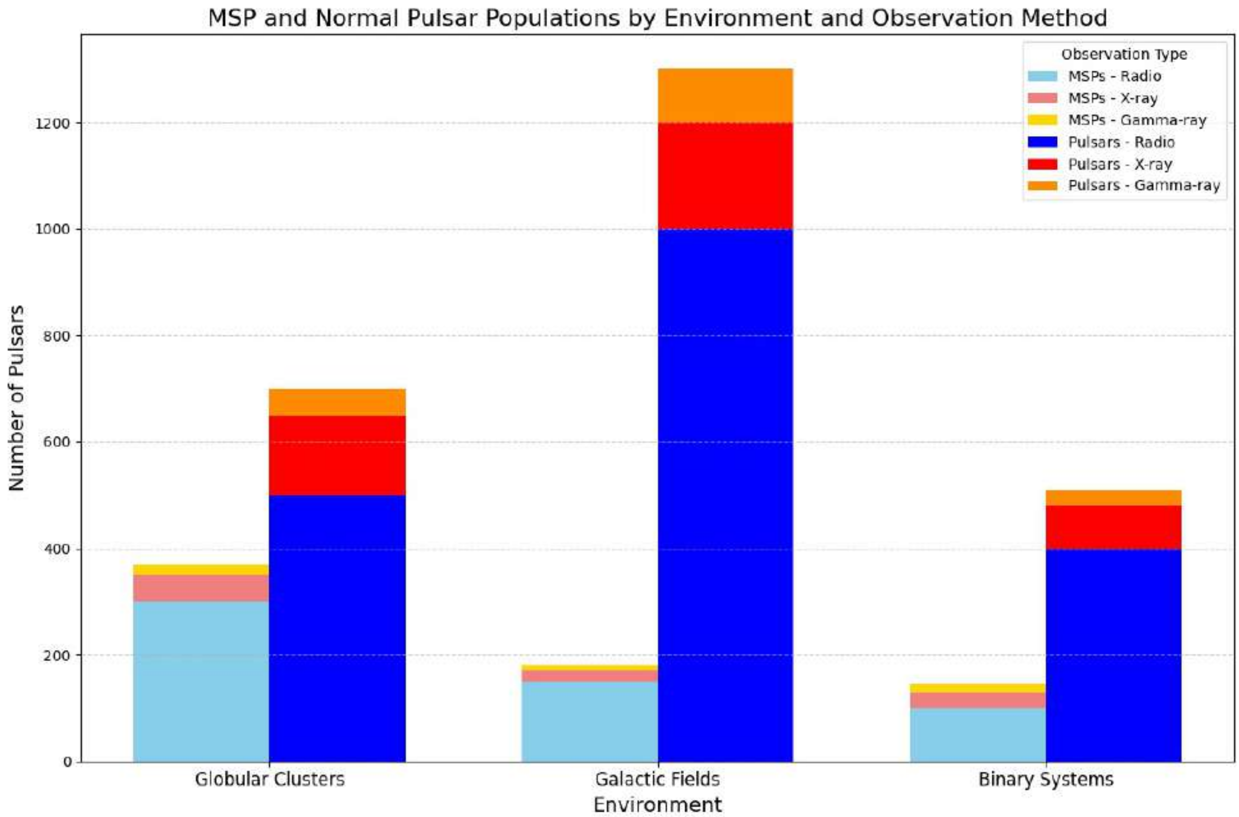

Figure 2. The chart shows the groups of millisecond pulsars (MSPs) and normal pulsars found through radio, X-ray, and gamma-ray research in three different types of astrophysical settings: globular clusters, galactic fields, and binary systems. See more in Abbott (2017), Abbott et al. (2016). The data provides a comparative analysis of how different observation approaches contribute to pulsar discovery in these specific astrophysical environments. We took the data in this figure from the ATNF Pulsar Catalog and other major pulsar research databases, with additional information from high-energy observational missions such as Fermi-LAT and Chandra.

Binary interactions that typically recycle the material of neutron stars in globular clusters often appear as MSPs, which rotate quickly and provide steady emissions that may be detected at various wavelengths. Observations such as X-ray studies from NICER and Chandra can be used to learn more about these groups. These studies show emission hotspots and accretion processes that are connected to the objects in question (Brightman et al., 2016, Deneva et al., 2019). Radio observations remain indispensable for discovering new pulsars and improving observational datasets through Pulsar Timing Arrays (PTAs) due to their unique capabilities. They excel at detecting faint pulsar signals, especially in distant globular clusters where other wavelengths fall short and enable precise timing measurements essential for gravitational wave detection via PTAs (Ferdman et al., 2010, Kramer & Champion, 2013). Similar gamma-ray observations from the Fermi

doi: https://doi.org/10.52526/25792776-24.71.2-351

Large Area Telescope (Fermi-LAT) have shown that MSPs are important high-energy sources (Abdo et al., 2013, Freire et al., 2012, Perera et al., 2019). Using more than one observational method has helped us to learn more about the populations of pulsars and how they change over time. This has shown how complex the relationship is between environmental factors and star formation (Abbott et al., 2016, Freire et al., 2017, Pan et al., 2021).

4. Theoretical framework

The magnetic field-spin relation (B-S) for pulsars and MSPs is influenced by their environment. Understanding these variations in the B-S relation is crucial to explaining the differences in pulsar and MSP populations in different astrophysical environments (Chen et al., 2021, Freire et al., 2012). See Figure 3 for a more detailed comparison. These diagrams are essential for understanding the effect of numerous parameters on pulsar behavior, specifically concerning "spin-up and spin-down" rates and stability.

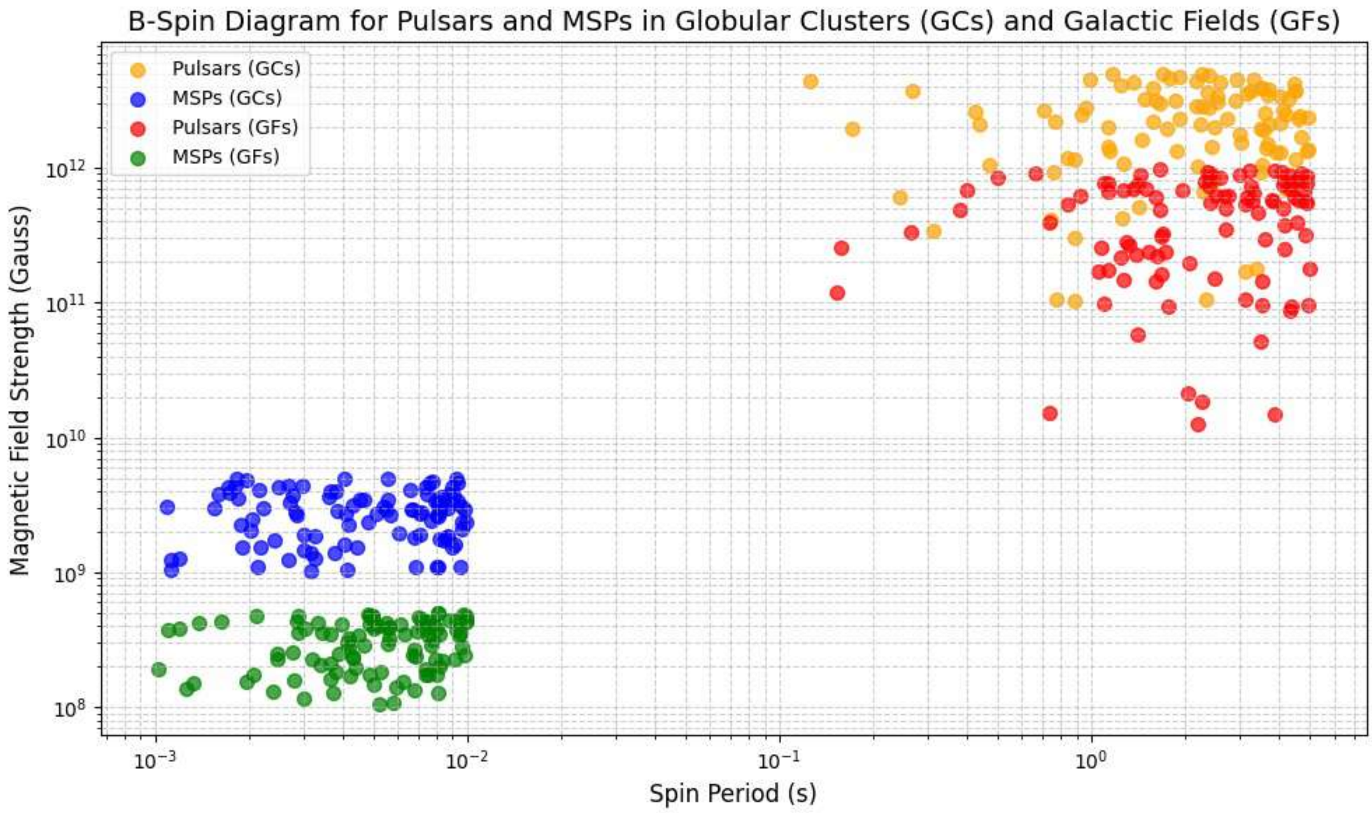

Figure 3. The B-S Diagram shows the spin periods and magnetic field of regular pulsars and millisecond pulsars (MSPs) in two different settings: Globular Clusters (GCs) and Galactic Fields (GFs). Normal pulsars are shown in orange (GCs) and red (GFs), whereas MSPs are denoted in blue (GCs) and green (GFs). The data points reflect simulated pulsar populations. See more: (Chattopadhyay, 2021, Lee et al., 2023, Ye & Fragione, 2022)

In the evolution of globular clusters, where interactions and transfer of mass in the binary are more common, the B-S relation for normal pulsars tends to show faster magnetic field decay with a quicker spin-down, while MSPs exhibit faster spin-up and weaker magnetic fields due to frequent recycling processes. In contrast, GF pulsars evolve more slowly, with a broader distribution of spin periods and magnetic field strengths, while MSPs in the GF show slower spin-up rates and weaker magnetic field decay compared to their counterparts in GCs (Lee et al., 2023). In globular clusters, millisecond pulsars (MSPs) exhibit rapid rotation rates primarily due to their interactions with companion stars, which facilitate the transfer of angular momentum during accretion events. These interactions typically occur in binary systems, where a pulsar can capture material from a nearby star, often a white dwarf or another neutron star. As the pulsar accretes this material, it gains angular momentum, leading to an increase in its rotation speed—a process known as

doi: https://doi.org/10.52526/25792776-24.71.2-351

"recycling" (Ferdman et al., 2010, Kramer & Champion, 2013). The high stellar density characteristic of globular clusters enhances the likelihood of binary interactions, allowing for frequent encounters that result in the formation of binaries. This environment significantly contributes to the rapid rotation periods observed in many MSPs, which can be less than 30 milliseconds, distinguishing them from normal pulsars (Abbott et al., 2021, Demorest et al., 2010, Freire et al., 2012). Thus, the dynamics of binary interactions within globular clusters play a crucial role in the evolution and characteristics of millisecond pulsars (Abbott et al., 2021, Kramer et al., 2021).

Besides, the magnetic field of a pulsar changes according to its environment, and thus also concerns the local stellar density and the dynamical evolution of the involved objects. This makes the evolution of these systems very complicated. The B-S diagram in Figure 3 shows how pulsars attain stable rotations via accretion processes, which in turn enhance the angular momentum transmission. The B-S relation has a feedback mechanism wherein the spin of the pulsar may affect the mass loss and development of the companion star (Chattopadhyay, 2021, Shi & Ng, 2024). Furthermore, pulsar magnetic fields may weaken with time, mainly due to accretion and interactions with the surrounding matter. This deterioration of the magnetic field can significantly affect the overall stability of the pulsar and influence its spin-down rates, as a weaker magnetic field is less effective at extracting rotational energy from the neutron star. As a result, the ability of pulsars to emit radiation efficiently is compromised, ultimately impacting their observational characteristics and lifecycle (Lattimer & Prakash, 2007, Zhang et al., 2022).

Recent models have included stellar dynamics in simulations, providing a more comprehensive understanding of MSP development in many contexts (Abbott et al., 2021, Chen et al., 2021). Researchers have found that clusters with a large number of stars, such as globular clusters, have a higher chance of having frequent stellar encounters. This means that there are more binary systems that are potential millisecond pulsars. Moreover, theoretical models indicate that binary interactions significantly influence MSP populations in both globular clusters and galactic fields(Belczynski et al., 2018, Freire et al., 2017, Perera et al., 2019).

5. Comparison of different numerical studies

Numerical simulations of star clusters provide a powerful tool for studying the evolution of pulsars within these environments: In these systems, the dynamics of stars is influenced solely by gravitational interactions. The use of advanced computational models, such as N-body codes, allows researchers to simulate the complex behaviors of stellar populations in a highly populated environment, including pulsars, over time. These models are particularly advantageous for studying open and globular clusters, where many pulsars can interact with each other and with other stars in the system. N-body simulations excel at handling large datasets, enabling the study of multiple pulsars simultaneously and observing their dynamical evolution, such as gravitational encounters or tidal disruptions, affect their spin evolution, magnetic field dynamics, and overall stability(Aarseth, 2003, Spurzem, 1999). However, these models also have limitations, as they may oversimplify the value of the parameters for certain physical processes or struggle with computational time when simulating extremely dense environments or large numbers of stars or struggle with computational time when simulating extremely dense environments or large numbers of stars. Despite these drawbacks, N-body codes are essential for exploring intricate scenarios that involve multiple pulsars, such as the formation of millisecond pulsars (MSPs) through binary interactions or the impact of pulsar wind interactions on the surrounding stellar population. As such, these simulations offer valuable insights into pulsar evolution in star clusters, but must be continuously updated to address the complexities of real astrophysical systems once the theoretical and observational framework offer new insights. According to our statistical investigation, the NBODY6++GPU code has one of the most practical and accurate results to model dynamical interactions in dense star settings, which makes it perfect for looking at pulsars in globular clusters(Spurzem et al., 2023, Wang et al., 2015). Although NBODY6++GPU has successfully modeled the production of neutron stars, the generation of pulsars within the code is in near complete development, with ongoing improvements by its users and original creators aiming to address this aspect (Giersz & Spurzem, 1994, Spurzem, 1999). Recent improvements in GPU technology have made NBODY6++GPU run much faster and better, allowing more complex simulations to run in much less time than CPU-based models (Spurzem et al., 2023).

When comparing the three astrophysical numerical codes: NBODY6++GPU, CMC, and COMPAS, we find distinct advantages and disadvantages for each. See more comparative details at the statistical chart

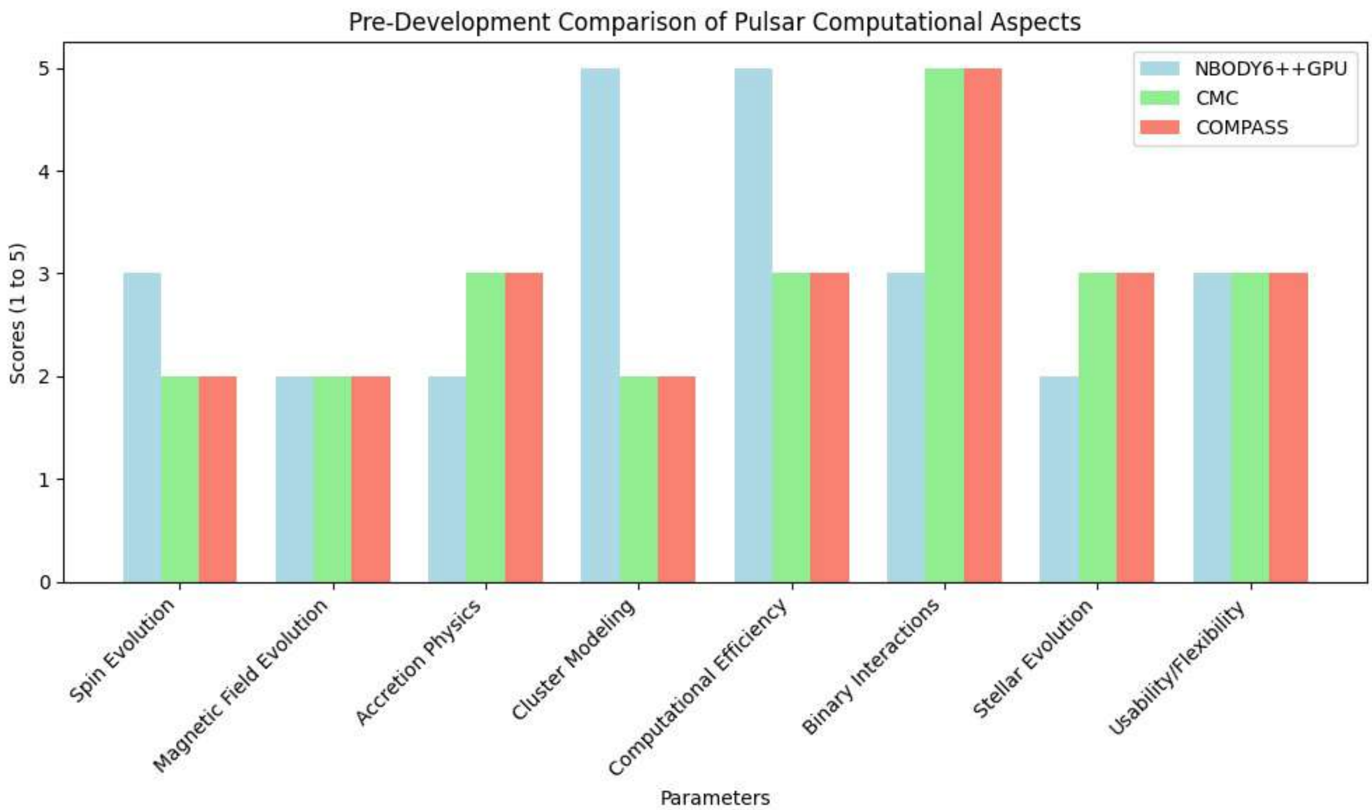

Figure 4. The graph compares three numerical studies, done through COMPAS, CMC, and NBODY6++GPU, which are derived from various development factors for pulsars such as spin evolution, magnetic field dynamics, and accretion physics. It shows that CMC and COMPAS perform similarly in most areas, especially when it comes to binary interactions and stellar evolution. However, NBODY6++GPU demonstrates notable strengths in cluster modeling and computational efficiency. See more: (Chattopadhyay et al., 2020, Wang et al., 2016, Ye et al., 2019).

in Figure 4.To briefly summarize, NBODY6++GPU is good in modeling large number of self-gravitating systems (i.e., star clusters) and also adding many subroutines that reflect stellar evolution, binary gravitational interactions and 3 body interactions. It significantly outperforms others in cluster modeling, making it ideal for researchers focusing on dynamics of star clusters. You can find more about the high accuracy of NBODY6++GPU through these references(Kamlah et al., 2022, Spurzem et al., 2023, Wang et al., 2015). On the other hand, CMC, as a Monte Carlo code, takes a probabilistic approach to modeling cluster dynamics, predicting the system's evolution rather than directly calculating each timestep as done by direct N-body codes like NBODY6++GPU. While it is less computationally precise for detailed dynamical interactions, its approach allows for the modeling of large-scale systems and long-term stellar evolution in a manner that is distinct from direct simulation methods. However, CMC offers a complementary approach to NBODY6++GPU, focusing on probabilistic modeling that provides insight into broader evolutionary trends, though it has potential for enhancement in cluster modeling and spin evolution accuracy (Ye & Fragione, 2022, Ye et al., 2019). Meanwhile, COMPAS stands out in stellar evolution and binary interactions, providing robust tools for studying binary star systems and their evolution. While it offers comprehensive features for these studies, COMPAS might not be the best choice for users who need strong capabilities in cluster modeling and magnetic field evolution, where it scores comparatively lower. Thus, each code has unique strengths and weaknesses, which makes it suitable for different aspects of astrophysical research depending on the specific needs of the study(Chattopadhyay et al., 2020).

NBODY6++GPU stands out among simulation software for its ability to incorporate real physical phenomena, such as tidal forces from gravitational interactions in binary systems and mass transfer between stellar companions. Its robust framework enables accurate modeling of key components of neutron star dynamics, including the spin evolution and other critical properties essential for characterizing these stars as pulsars and millisecond pulsars (MSPs). This capability makes NBODY6++GPU particularly suited for studying pulsars within the dynamic environments of star clusters, providing valuable insights into their formation and

doi: https://doi.org/10.52526/25792776-24.71.2-351

evolutionary pathways accuracly. By further enhancing the code to refine the calculation of special properties of pulsars, such as spin periods and magnetic field , NBODY6++GPU can serve as a powerful tool for advancing our understanding of pulsars and MSPs in astrophysical contexts. This feature is crucial for precisely predicting the interactions that result in the creation of pulsars and MSPs in globular clusters (Wang et al., 2015), cf. (Chattopadhyay et al., 2020, Ye et al., 2019). Moreover, the incorporation of observational data into simulation frameworks has gained significant importance. By comparing simulation results with observational data, like the Fermi Large Area Telescope (Fermi-LAT) and the Chandra X-ray Observatory, researchers can test their models and learn more about pulsar populations (Freire et al., 2017, Perera et al., 2019). The synergy between simulations and observations is vital for resolving outstanding problems about MSP creation processes and their evolutionary paths (Abbott(LIGO) et al., 2017).

6. Outstanding research questions

Future investigations will try to answer the following unanswered research questions:

1. Formation Mechanisms: What specific processes lead to the formation of MSPs within different environments like GCs and GFs? (Chattopadhyay, 2021, Chattopadhyay et al., 2020, Lee et al., 2023, Ye & Fragione, 2022, Ye et al., 2019).

2. Binary Interactions: How do various binary configurations—such as structural properties (e.g., spin and magnetic field of neutron stars) and orbital parameters (e.g., semi-major axis and eccentricity)—influence the spin-up processes of neutron stars (Arca Sedda et al., 2023, Galloway et al., 2024).

3.Magnetic Field Evolution: What mechanisms govern the decay or enhancement of magnetic fields in pulsars over timescales ranging from millions to billions of years, and how do these processes differ between pulsars in globular clusters, influenced by dense stellar interactions, and those in the relatively isolated environments of the Galactic field (Igoshev et al., 2021, Wang et al., 2016, Zhang et al., 2022).

4. Gravitational Wave Detection: Pulsar timing arrays (PTAs) have revolutionized astrophysics by enabling the detection of gravitational waves through the precise monitoring of millisecond pulsars. These arrays are particularly sensitive to low-frequency gravitational waves from cosmic phenomena such as supermassive black hole mergers. Building on this capability, how can we further optimize PTAs to enhance their sensitivity and detect gravitational waves from even more distant or subtle cosmic events?(Abbott(LIGO) et al., 2017, Lee et al., 2023).

5. Probing the Equation of State with Pulsars: How can pulsars, under the extreme conditions -ultra high densities, intense gravitational fields, and rapid rotation- provide critical insights into the equation of state for nuclear matter, particularly in the dense cores of neutron stars?(Lattimer, 2021, Zhang et al., 2022).

6. Role of Pulsars in Cosmic Evolution: How do pulsars contribute to cosmic evolution, and in what ways do their roles and influences on stellar dynamics differ between the dense, interaction-rich environments of globular clusters and the relatively isolated conditions of the Galactic field?(Chattopadhyay, 2021, Chattopadhyay et al., 2020, Ye et al., 2019).

These questions emphasize that modeling the evolutionary processes of pulsars and MSPs requires advancements in theoretical frameworks and simulations.

7. Discussion and future research

The relevance of observational missions using instruments like FAST, CHIME, and NICER is highlighted by recent developments in the detection and characterization of pulsars and millisecond pulsars (MSPs). Because of these efforts, pulsar catalogs have been greatly expanded, revealing exotic systems like transitional MSPs[1] and black widow pulsars[2]. Pulsar Timing Arrays (PTAs) have attained nanosecond accuracy, facilitating progress in gravitational wave astronomy (Pan et al., 2021, Perera et al., 2019). These statistical findings have improved our understanding of pulsar distributions and evolutionary pathways, particularly within the

[1] Millisecond pulsars that alternate between accretion-powered X-ray states and rotation-powered radio states, showcasing their evolving nature in binary systems.

[2] These are millisecond pulsars in binary systems that emit intense radiation, often ablating their low-mass companion stars over time.

doi: https://doi.org/10.52526/25792776-24.71.2-351

Galactic Field (GF) and contrasting globular clusters (GCs). Theoretical advancements in pulsar evolution, especially regarding spin and magnetic field dynamics, have been clarified using advanced numerical simulations. During the last years, it was possible to numerically simulate their mechanisms, like accretion, tidal spin-up, and gravitational interactions in dense settings using numerical tools such as NBODY6++GPU, CMC, and COMPAS. These codes have shown how stellar dynamics, pulsar recycling in globular clusters, and the galactic field interact with each other (Liu et al., 2021, Zhang et al., 2022). NBODY6++GPU has effectively simulated the formation of neutron stars, yet the inclusion of pulsar generation within the code represents a promising area for further exploration which is soon going to be explored. The Nbody6++GPU team is working to enhance its capabilities to address this exciting challenge. Expanding this system to incorporate features tailored to pulsars will be crucial for advancing our understanding of these fascinating objects and their diverse types. Very accurate modeling of pulsar populations may help researchers resolve inconsistencies between theoretical predictions and observed data. Our statistical review of the recent progress in pulsars and MSPs revealed that these developments are crucial for accurately analyzing pulsar dynamics and interactions within astrophysical contexts (Chattopadhyay, 2021, Chattopadhyay et al., 2020, Ye & Fragione, 2022, Ye et al., 2019). In conclusion, addressing these challenges through improved numerical models will deepen our understanding of pulsars and MSP formation and enable more rigorous testing of advanced astrophysical theories. The ongoing development of NBODY6++GPU presents an exciting opportunity to explore the complex mechanisms underlying pulsar evolution with greater precision.

Acknowledgments

FFD and RS acknowledge support by the German Science Foundation (DFG), priority program SPP 1992 ”Exploring the diversity of extrasolar planets” (project Sp 345/22-1 and central visitor program), and by DFG project Sp 345/24-1.

References

Aarseth S., 2003, Gravitational N-body simulations: tools and algorithms. Cambridge University Press

Abbott B. P., 2017, The Astrophysical Journal Letters, 848, 59pp

Abbott B. P., et al., 2016, Physical review letters, 116, 061102

Abbott R., et al., 2021, The Astrophysical Journal Letters, 913, L27

Abbott(LIGO) B. P., et al., 2017, The Astrophysical Journal, 839, 12

Abdo A., et al., 2013, The Astrophysical Journal Supplement Series, 208, 17

Arca Sedda M., Kamlah A. W., Spurzem R., Rizzuto F. P., Naab T., Giersz M., Berczik P., 2023, Monthly Notices of the Royal Astronomical Society, 526, 429

Baker D., 2023, PhD thesis, University of Toronto (Canada)

Belczynski K., et al., 2018, Astronomy & Astrophysics, 615, A91

Brightman M., et al., 2016, The Astrophysical Journal, 816, 60

Chattopadhyay D., 2021, PhD thesis, Swinburne

Chattopadhyay D., Stevenson S., Hurley J. R., Rossi L. J., Flynn C., 2020, Monthly Notices of the Royal Astronomical Society, 494, 1587

Chen S., et al., 2021, Monthly Notices of the Royal Astronomical Society, 508, 4970

Demorest P. B., Pennucci T., Ransom S., Roberts M., Hessels J., 2010, nature, 467, 1081

doi: https://doi.org/10.52526/25792776-24.71.2-351

Deneva J., et al., 2019, The Astrophysical Journal, 874, 160

Falxa M., et al., 2023, Monthly Notices of the Royal Astronomical Society, 521, 5077

Ferdman R. D., et al., 2010, Classical and Quantum Gravity, 27, 084014

Freire P. C., et al., 2012, Monthly Notices of the Royal Astronomical Society, 423, 3328

Freire P., et al., 2017, Monthly Notices of the Royal Astronomical Society, 471, 857

Galloway D., Goodwin A., Hilder et al. 2024, Monthly Notices of the Royal Astronomical Society, 535, 647

Giersz M., Spurzem R., 1994, Monthly Notices of the Royal Astronomical Society, 269, 241

Han J., et al., 2021, Research in Astronomy and Astrophysics, 21, 107

Hewish A., Burnell S., 1970, Monthly Notices of the Royal Astronomical Society, 150, 141

Hulse R. A., Taylor J. H., 1975, Astrophysical Journal, vol. 195, Jan. 15, 1975, pt. 2, p. L51-L53., 195, L51

Igoshev A. P., Popov S. B., Hollerbach R., 2021, Universe, 7, 351

Kamlah A. W. H., et al., 2022, , 511, 4060

Kaspi V. M., Beloborodov A. M., 2017, Annual Review of Astronomy and Astrophysics, 55, 261

Kramer M., Champion D. J., 2013, Classical and Quantum Gravity, 30, 224009

Kramer M., et al., 2021, Physical Review X, 11, 041050

Lattimer J., 2021, Annual Review of Nuclear and Particle Science, 71, 433

Lattimer J. M., Prakash M., 2007, Physics reports, 442, 109

Lee J., Hui C., Takata J., Kong A., Tam P.-H. T., Li K.-L., Cheng K., 2023, The Astrophysical Journal, 944

Liu P., Yang Y.-Y., Zhang J.-W., Rah M., 2021, Research in Astronomy and Astrophysics, 21, 104

Lorimer D. R., 2008, Living reviews in relativity, 11, 1

Mickaelian A., 2018, Communications of BAO,, Vol.2 (LXV), pp.162

Musolino C., Rezzolla L., Most E. R., 2024, arXiv preprint arXiv:2410.06253

Padmanabh P., et al., 2024, Astronomy & Astrophysics, 686, A166

Pan Z., et al., 2021, The Astrophysical Journal Letters, 915, L28

Perera B., et al., 2019, Monthly Notices of the Royal Astronomical Society, 490, 4666

Sengar R., et al., 2023, Monthly Notices of the Royal Astronomical Society, 522, 1071

Shi Z., Ng C.-Y., 2024, The Astrophysical Journal, 972, 78

Spurzem R., 1999, Journal of Computational and Applied Mathematics, 109, 407

Spurzem R., Rizzuto F., Sedda M. A., Kamlah A., Berczik P., et. al 2023, NIC symposium 2022, arXiv preprint arXiv:2307.08068

Wang L., Spurzem R., Aarseth S., Nitadori K., Berczik P., Kouwenhoven M., Naab T., 2015, Monthly Notices of the Royal Astronomical Society, 450, 4070

Wang L., et al., 2016, Monthly Notices of the Royal Astronomical Society, 458, 1450

Ye S. Y., Fragione G., 2022, The Astrophysical Journal, 940, 162

Ye S. Y., Kremer K., Chatterjee S., Rodriguez C. L., Rasio F. A., 2019, The Astrophysical Journal, 877

Zhang J., et al., 2022, Publications of the Astronomical Society of the Pacific, 134, 114201

Zhou D., et al., 2023, Monthly Notices of the Royal Astronomical Society, 526, 2657

doi: https://doi.org/10.52526/25792776-24.71.2-351

Communications of BAO, Vol. 71, Issue 2, 2024, pp. 360-366

Active galaxies in the field and in Galaxy Clusters

R. R. Andreasyan [*], S. A. Hakopian[†], A. P. Mahtessian[‡], and A. G. Sukiasyan[§]

NAS RA Byurakan Astrophysical Observatory after V. A. Ambarsumian

Abstract

We review the current activities of the Department of Active Galaxies of Byurakan Astrophysical Observatory. The studies include broad areas, ranging from manifestations of activity in our galaxy, other galaxies and clusters of galaxies to the study of magnetic fields, the formation of these fields, and cosmological questions.

Keywords: *active galaxies, magnetic field, clusters of galaxies*

1. Introduction

The study of active galaxies is one of the traditional directions of Byurakan observatory. Here are presented some of recent works carried out in the department of active galaxies of BAO. There are

- The spectrophotometric observations of SBS galaxies,
- The study of formation and morphology of magnetic fields of galaxies and particularly in our Galaxy,
- The investigation of properties of the neighborhood of giant extragalactic radio sources,
- The study of galactic clusters et.c.t.

2. The spectrophotometric observations of SBS galaxies.

- Detailed studies of the individual galaxies, which we performing, are based on the data from panoramic/ wide-field spectroscopy, provided from observations with multipupil spectrographs. The one another object we investigate is SBS 1001+555, one of the nearest SBS galaxies with redshift z=0.0037 (fig.1a). Observations of the main region of star formation in it we carried out with the 6-m telescope using the multipupil fiber spectrograph MPFS. The observed region includes the brightest in the optical range condensation, contritely standing out from the diffuse background, which is composing the elongated shape of the galaxy. An analysis of the surface distribution of the parameters of the emission in the most intense in the obtained spectrum (fig.1b) the Ballmer H_α line (fig.1c) revealed, in particular, the presence besides the main HII-region of three faint secondary HII-regions; this is indicative of the ongoing star-formation processes in the galaxy. The results obtained on the kinematics of the gases in the velocity field, on the spectral features of the HII-regions along with other available multiwavelength data, including data from IRAC mission, revealed new interesting details, connected to activity processes that undergoing in SfG galaxies (Hakopian, et all. 2022).
- One of important directions in the work of our department is the spectrophotometric observations of galaxies of the Second Byurakan Survey (SBS) as a base for complex investigations of activity processes. The observations were carried out with the 2.6m telescope of the Byurakan observatory and the 6m telescope of the SAO of the Russian Federation. Here are some of the last works that are part of the large program, began with completion of the follow-up spectroscopy for about 500 objects

[*]randrasy@bao.sci.am, Corresponding author
[†]susanaha@bao.sci.am
[‡]amahtes@bao.sci.am
[§]andranik.sukiasyan094@gmail.com

doi: https://doi.org/10.52526/25792776-24.71.2-360

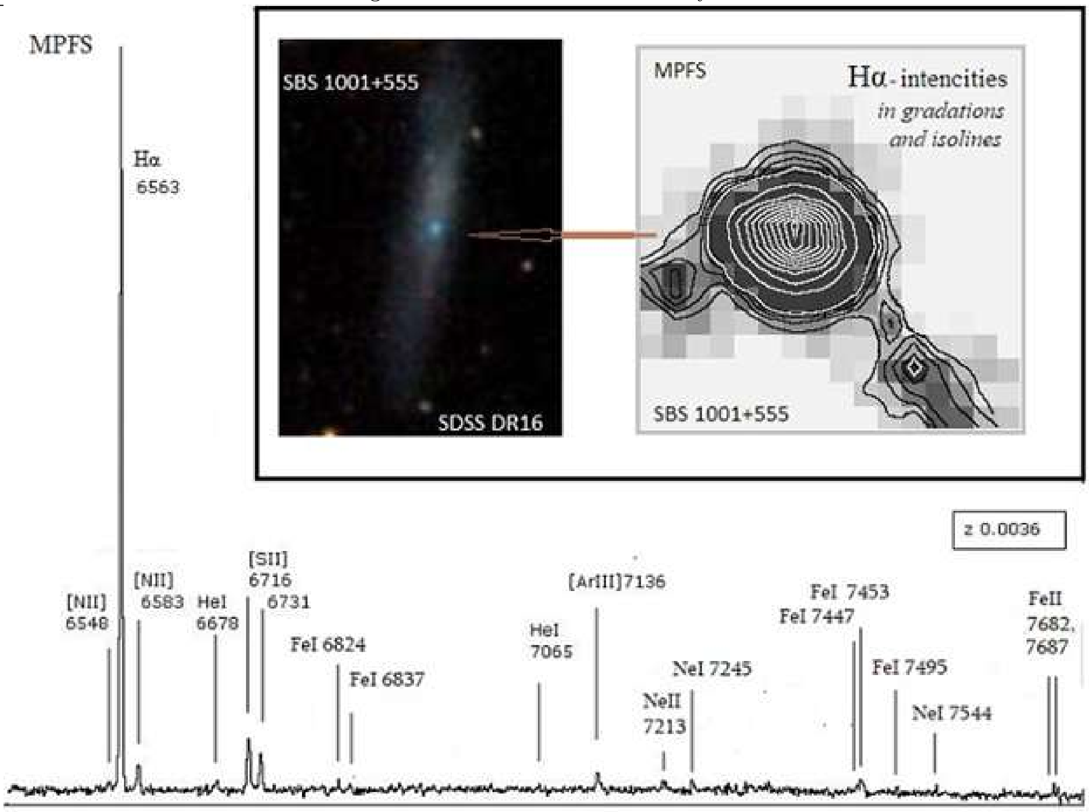

Figure 1. An optical and H_α images (a; b), and optical spectra (c) of SBS galaxy 1001+555.

composed the samples in the seven 16sq.deg selected fields of the survey (fig 2).
The study provided for the two adjacent fields, 4th and 5th, got name "100sbs". About hundred nearby galaxies (0.01<z<0.12), composing approximately 80 % of these two samples, are galaxies with active star formation, being classified as SfG (star-forming galaxy) in our "adapted scheme".

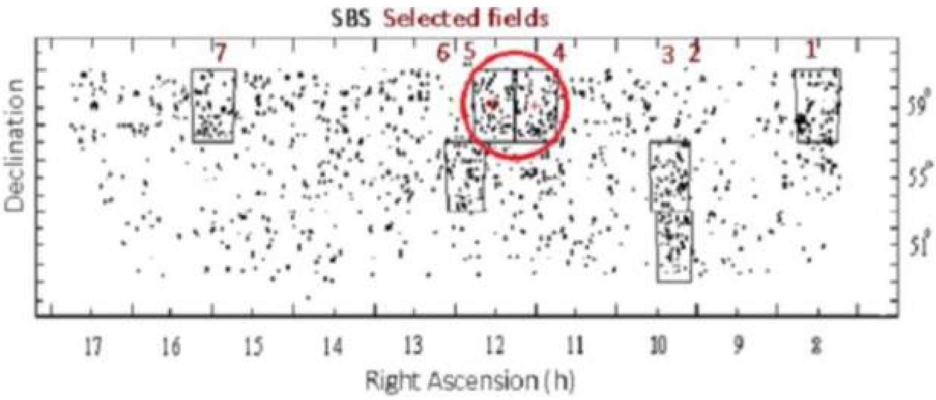

Figure 2. 7 selected fields of the survey.

In its frames we consider two SfG-classes - SfGcont, i.e. star-forming in continual phase and SfGneb, i.e. star-forming in nebular phase. The usage and comparative analysis of spectral data available from SDSS (Sloan Digital Sky Survey) for all "100sbs" and those we obtained earlier allowed, in particular, improving classification. Each of Sfgcont and SfGneb classes was divided into 5 subclasses according to spectral data, primarily, the intensities and equivalent widths of the Ballmer H_α line. For SfGcont 1, the equivalent widths start from EW(H_α)=5^0A, and for SfGneb 1 from EW(H_α) = 100^0A. Below (fig.3) are examples of such galaxies and their spectra. (Hakopian 2021).

doi: https://doi.org/10.52526/25792776-24.71.2-360

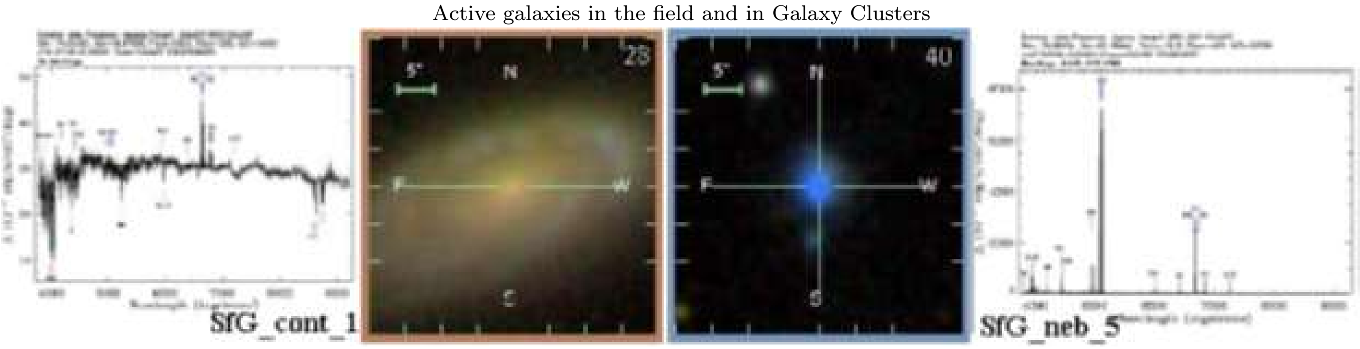

Figure 3. Examples of SfGcont and SfGneb classes of galaxies.

3. The study of environment of radio galaxies of different FR classes

Studies of extended radio galaxies belonging to different morphological classes (FR classification) (Fanaroff, Riley 1974), and their surroundings are carried out (Fig.4). Powerful radio galaxies are mostly supergiant galaxies at the center of galaxy clusters

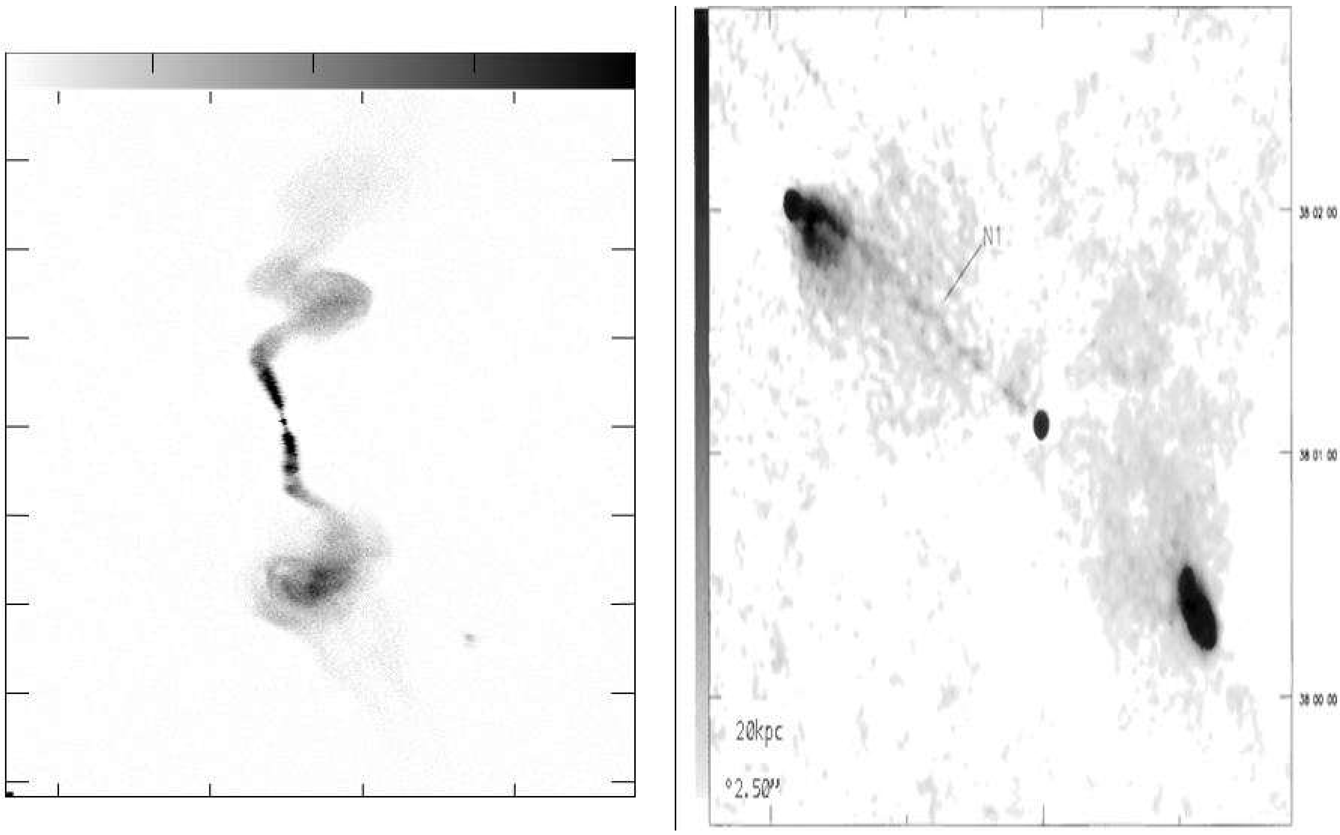

Figure 4. Extragalactic radio sources FRI 3C449 (left) and FRII 3C111(right).

The difference of morphology of FRI and FRII classes of radio galaxies is obvious. This difference may be due to the physical properties of the host optical galaxy or the state of the environment. Here we study the second possibility. We investigate regions with radius of 500 pc around of the central radio galaxies from our sample (Andreasyan; Abrahamyan 2021). For this study were chosen about 30 nearby 3C radio galaxies of different FR types. We bring the maps of optical galaxies that are overlaid on the radio map of 3C radio source. It was used also the maps of these regions in all available wavelength. The first investigated extragalactic radio sources are 3C31, 3C449, NGC315, NGC6251. Here we present more detail analyses and new results for the radio galaxy of FRI type 3C31. The 3C31 class FRI radio source has been identified with the NGC 383 galaxy, which is the central object of the group of galaxies, which in turn is a member of the Perseus-Pisces supercluster (Sakai et al. 1994) and has been studied quite well. Numerous results and useful data have now been obtained for these objects (Martel et al. 1999; Laing & Bridle 2002; Hardcastle et al. 2002). Of these, here we highlight some of the data of interest to us, which can be used in the present

doi: https://doi.org/10.52526/25792776-24.71.2-360

work. Figures 5 and 6 show optical images of the region in the center of which is the galaxy NGC 383. The optical image shows a map of the radio image of the FRI class 3C31 radio galaxy at different frequencies, 145, 360, 615, and 1400 MHz corresponding to LOFAR, VLA, GMRT and FIRST observations, respectively.

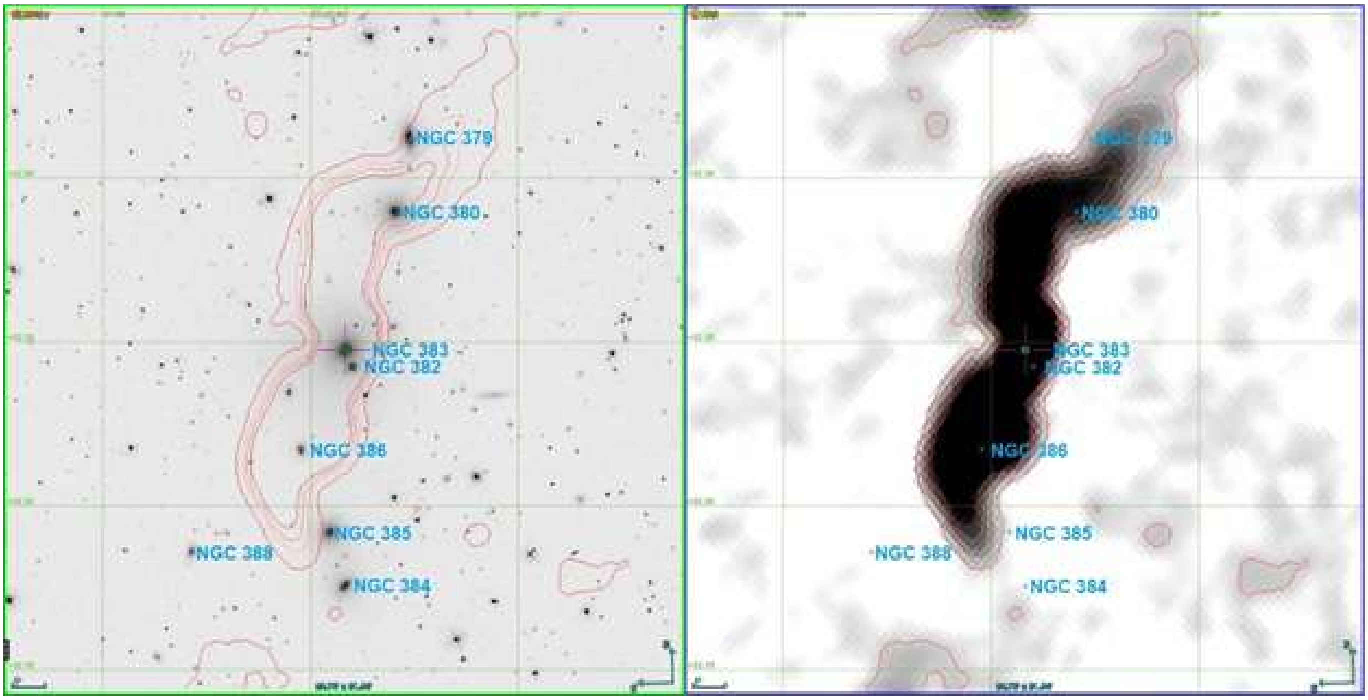

Figure 5. The region of a group of galaxies with the central object NGC 383 and radio source 3C31 of the FRI class at a frequency of 1400 MHz.

From the pictures it is clear that the galaxies NGC 380 and NGC 386 are located strictly on the same line but on different sides from the central galaxy NGC 383. The direction of this line coincides with the direction of the radio jets of 3C31. The difference of the red shift of the northern galaxy relative to the central galaxy is negative, and that of the southern galaxy is positive. Radio jet simulations (Laing & Bridle 2002) have shown that the direction of the jet is approximately 520 with the line of sight. Moreover, the northern part of the jet approaches the observer, while the southern part moves away. All this can be explained within the framework of the assumption that galaxies NGC 380 and NGC 386 move in the same direction as the radio jets. The calculations are presented in Table 1.

Table 1.

object	z	δz	δV km/s	D kpc	V_0 km/s	T Myr
NGC383	0.01700	0	0	0	0	-
NGC380	0.01476	-0.00224	-672	106.53	860.2	117
NGC386	0.01853	+0.00153	+459	78.12	587.5	126

The table shows that the galaxies NGC 380 and NGC 386 were near the galaxy NGC 383 about 120 million years ago. A very close passage of these three galaxies then probably occurred, after which the recession of the galaxies NGC 380 and NGC 386 from the more massive central galaxy NGC383 began. A natural question arises whether such a close passage can be the cause (trigger) of the beginning of radioactivity of the central galaxy. A reliable argument for such assumption can be considered that the modeling of the spectral characteristics of the radio emission of the central part of the radio galaxy 3C31 gives an estimate of the age of the central jet of about 100 million years (Heesen et al. 2018).

4. The study of galactic clusters.

Evolution of galaxies in groups of galaxies. Another direction of work of our department is finding and studying the physical properties of galactic groups (Magtesyan et al.2018). The accepted mechanism for the evolution of galaxies in groups is based on the process of merging of galaxies. However, there is another, opposite mechanism of group evolution corresponding to the concept of V. Ambartsumyan. Many

doi: https://doi.org/10.52526/25792776-24.71.2-360

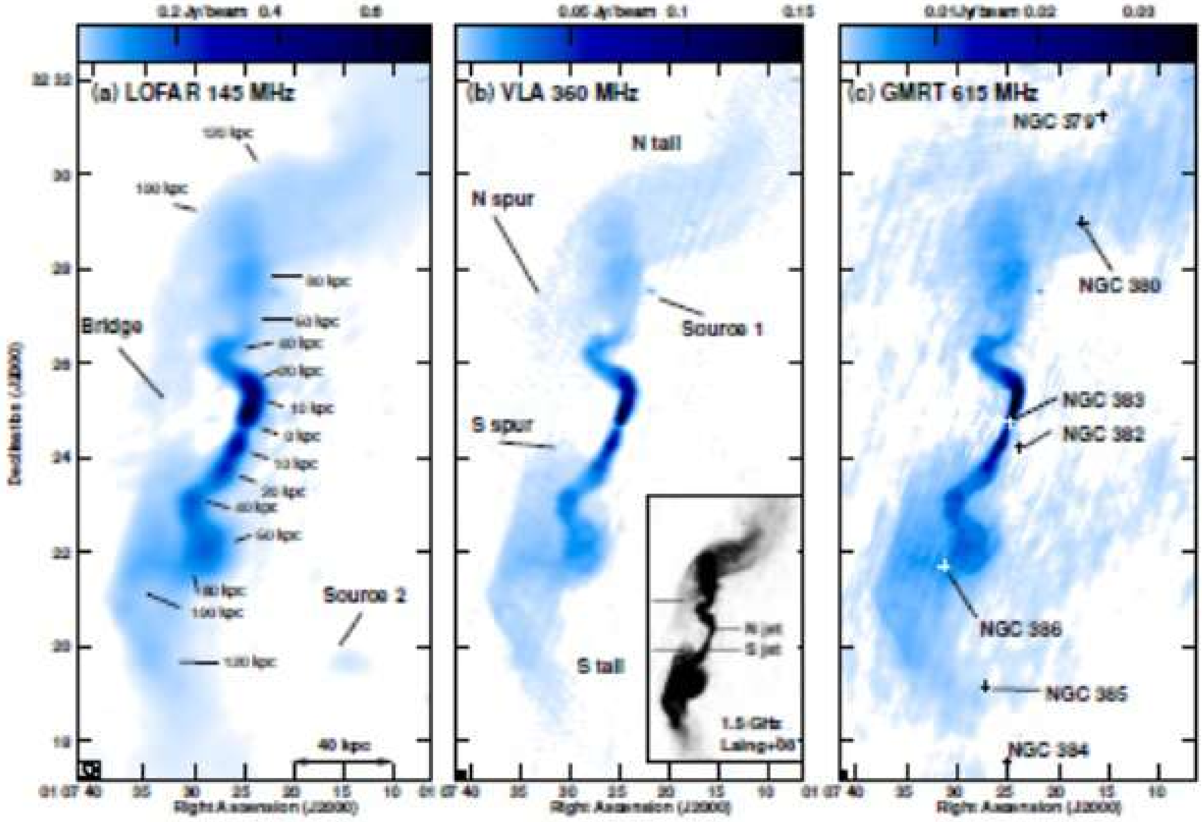

Figure 6. The region of a group of galaxies with the central object NGC 383 and radio source 3C31 of the FRI class at a frequency of 145, 360 and 615 MHz. (Heesen et al. 2018).

observational data can be successfully explained by both mechanisms, but some data are better suited to the second mechanism. According to the galaxy merger mechanism, the mass and luminosity of the central galaxy should increase with time, and the difference between the luminosities of the first and second most luminous galaxies should also increase. Moreover, the main galaxy of the group becomes elliptical. According to the second scenario, such an effect should not be observed. The above mentioned has been verified by statistical analysis of data from a large list of galaxy groups that is complete up to a magnitude of 15.5 m (Magtesyan and Movsesyan 1994). As a result of the analysis, the expectations corresponding to the merger mechanism were not confirmed, which shows in favor of the mechanism of the Byurakan concept.

5. Investigations in cosmology (about accelerating expansion of Universe).

It was shown that in the basis of the justification of the hypothesis of the expansion of the Universe with acceleration, and later in the confirmation of this hypothesis the same methodological error is present in the works. In all these works it is done standardization of luminosity of supernovae 1a type. It depends from the decay rate of the luminosity after the luminosity maximum of the supernova and from the color index of the star at its maximum brightness. These parameters according to the rule accepted by all authors should not depend on the redshift of the stars. Otherwise, we will artificially introduce the evolution of luminosity. However, our studies show that in estimated luminosities in all known samples of supernova type 1a stars the standardization parameters depend too strongly on redshift. It makes unacceptable such kind of standardization of supernovae luminosity. Such an approach removes the true evolution of supernova luminosity, having the effect of opposite direction. Therefore, the hypothesis of the accelerated expansion of the Universe is a consequence of the wrong estimate of the luminosity of supernovae. It means that the universe is expanding with deceleration. The dark energy theory is not applicable (Abraham Mahtesyanet all. 2022).

doi: https://doi.org/10.52526/25792776-24.71.2-360

6. Magnetic fields of galaxies.

6.1. A Biermann battery effect as a possible mechanism of formation of magnetic fields in active galaxies.

The essence of Birman's mechanism lies in the fact that the electrons and protons participating in the gas movement in radial directions, having a large difference in mass, interact with the particles of the rotating medium at different times and in different places. As a result, electrons and protons acquire different rotational speed components, a circular electric current and a dipole magnetic field is generated.

It was shown that in the active galaxies, whose central regions have strong outflow of ionized gas into the rotating medium, the Birman (battery mechanism) effect works, thanks to which a magnetic field is generated from scratch in the medium, which can later be strengthened by the so-called dynamo mechanisms (Mikhailov, E. A.; Andreasyan, R. R 2021).

This mechanism also works in case of accretion of matter on the nuclei of galaxies. In our recent work, the effectiveness of the Birman mechanism in accretion discs was studied. It is necessary to solve an integral equation of the second order, if the interaction of the generated magnetic fields on the movement of charged particles is considered. It has been shown that the generated fields are quite significant and can play an important role in the further evolution of magnetic fields in accretion disks (Andreasyan, R. R.; Marchevsky, I. K.; Mikhailov, E. A. 2024).

6.2. A study of the magnetic field of our Galaxy using the Faraday rotation data of pulsars and extragalactic radio sources.

When polarized radiation passes through a magneto-ionic medium, the plane of polarization rotates. In radio astronomy, this rotation is characterized by the so-called Rotation Measure (RM). Such data are known for about 40,000 extragalactic radio sources and more than 2,300 pulsars. For pulsars, data are also known on the Dispersion Measures, which are caused by the phenomenon of signal delay of a given pulse at different frequencies. These data are directly derived from observations of pulsars. Theoretically they are expressed by the electron density ne in the interstellar medium through which the polarized radio emission of the pulsar passes and the projection of the magnetic field B_L (in Gauss) in this medium, using the following formulas:

$$RM = d\Psi/d(\lambda^2) = \alpha \int n_e B_L dL, (\alpha = 8.1 * 10^5) \tag{1}$$

$$t_2 - t_1 = (2\pi e^2/m)(1/\omega_2^2 - 1/\omega_1^2)DM \tag{2}$$

$$DM = \int n_e dL \tag{3}$$

$d\Psi$ - is the difference of plane of polarization in different wavelength λ.

t -is the time of receiving the radio signal from pulsar.

ω - is the frequency of radio wave.

In these formulas, integration is carried out over the entire traversed path of radiation (L in parsecs) from the pulsar to the observer.

Formula 3 makes it possible to determine the distance of a pulsar with the known electron density distribution in the Galaxy, and formula 2 together with formula 1 makes possible to determine the average component of the interstellar magnetic field $[B_L]$ on the line of sight in microgauss (μG).

$$< B_L >= (1/\alpha)(RM)/(DM) = 1.23(RM)/(DM) \tag{4}$$

$$B_l(R)n_e(R, l) = (1/\alpha)d(RM)/d(R) \tag{5}$$

$$B_l(DM) = (1/\alpha)d(RM)/d(DM) \tag{6}$$

doi: https://doi.org/10.52526/25792776-24.71.2-360

Using formulas 4 and observational data, it is possible to study the direction and magnitude of the average magnetic field in the direction of the pulsar, and formulas 5 and 6, with sufficient data, make it possible to construct a map of the magnetic field of the Galaxy.

Faraday rotation data on 336 pulsars and more than 2000 extragalactic radio sources are used in a detailed study of the magnetic field in the direction of galactic longitude $40^o < l < 70^o$, including the Sagittarius spiral arm region. The highly regular magnetic field in the northern hemisphere of the galaxy is directed to the Sun, when the magnetic field of southern hemisphere is directed from the Sun. This is clear from the study of the distribution of rotation measures of pulsars as well as from these data of extragalactic radio sources. We propose that the Sagittarius spiral arm lies mainly to the north of the Galactic plane, while the magnetic field with opposite direction below this plane is the field of the halo of the southern hemisphere of the Galaxy.

This result is consistent with the model of a two-component magnetic field of the galaxy proposed in (Andreasyan and Makarov 1989)

References

Andreasyan R. R., Abrahamyan H. V., 2021, Communications of the Byurakan Astrophysical Observatory, 68, 75

Andreasyan R. R., Makarov A. N., 1989, Astrophysics, 30, 101

Andreasyan R. R., Mikhailov E. A., Andreasyan H. R., 2020, Astronomy Reports, 64, 189

Andreasyan R. R., Marchevsky I. K., Mikhailov E. A., 2024, Astronomy Reports, 68, 238

Fanaroff B. L., Riley J. M., 1974, Mon. Not. R. Astron. Soc. , 167, 31P

Hakopian S. A., 2021, Communications of the Byurakan Astrophysical Observatory, 68, 522

Hakopian S. A., Dodonov S. N., Moiseev A. V., Smirnova A. A., 2022, Astrophysics, 65, 297

Hardcastle M. J., Worrall D. M., Birkinshaw M., Laing R. A., Bridle A. H., 2002, Mon. Not. R. Astron. Soc. , 334, 182

Heesen V., et al., 2018, Mon. Not. R. Astron. Soc. , 476, 1756

Laing R. A., Bridle A. H., 2002, Mon. Not. R. Astron. Soc. , 336, 1161

Magtesyan A. P., Movsesyan V. G., 1994, Astrophysics, 37, 161

Mahtessian A. P., Movsisyan V. H., Mahtessian L. A., Karapetian G. S., 2018, Communications of the Byurakan Astrophysical Observatory, 65, 401

Mahtessian A. P., Karapetian G. S., Hovhannisyan M. A., Mahtessian L. A., 2022a, Communications of the Byurakan Astrophysical Observatory, 69, 280

Mahtessian L. A., Hovhannisyan M. A., Karapetyan R. A., Amiraghyan L. A., Grigoryan M. L., Mahtessian A. P., 2022b, Communications of the Byurakan Astrophysical Observatory, 69, 345

Martel A. R., et al., 1999, Astrophys. J. Suppl. Ser. , 122, 81

Mikhailov E. A., Andreasyan R. R., 2021, Open Astronomy, 30, 127

Sakai S., Giovanelli R., Wegner G., 1994, Astron. J. , 108, 33

doi: https://doi.org/10.52526/25792776-24.71.2-360

Communications of BAO, Vol. 71, Issue 2, 2024, pp. 367-376

Byurakan Astrophysical Observatory Research Department *"Astronomical Surveys"*: recent results

A. M. Mickaelian*[1], H. V. Abrahamyan†[1], G. M. Paronyan‡[1], G. A. Mikayelyan§[1], R. R. Andreasyan¶[1], A. G. Sukiasyan‖[1], L. A. Hambardzumyan**[1], V. K. Mkrtchyan††[1], A. A. Gasparyan‡‡[1], and M. Dennefeld[2]

[1]NAS RA V. Ambartsumian Byurakan Astrophysical Observatory (BAO) Byurakan 0213, Aragatzotn Province, Armenia
[2]Institut d'Astrophysique de Paris (IAP), 98bis Bd Arago, 75014 Paris, France

Abstract

We review the field of active galaxies (both AGN and Starbursts) focusing on their multiwavelength search and studies at the Byurakan Astrophysical Observatory (BAO). Many famous historical surveys carried out in Byurakan are known and many more are active and ongoing. We give examples of studies in optical wavelengths, IR, radio and X-ray, as well as multiwavelength studies. The studies are characterized by a multiwavelength approach to statistical analysis of a large amount of data obtained in different wavelengths. Results on HRC/BHRC sample objects (optical identifications of ROSAT X-ray sources), studies of Markarian galaxies in UV and multiwavelength SEDs, abundance and star formation determinations in Mrk galaxies from SDSS spectra, revised optical classification of "LINERs", study and classification of SDSS spectra for Byurakan-IRAS Galaxies, summary of observations and study of Byurakan-IRAS Galaxies (BIG objects), discovery of new bright ULIRGs from the IRAS PSC/FSC Combined Catalogue and their spectral classification, radio variable sources at 1400 MHz and their optical variability, classification of BZCAT objects having uncertain types (BZU objects), and optical variability of blazars are presented. At the end, we briefly present our new fine classification of active galaxies based on all our previous studies.

Keywords: *Astronomical Surveys – Astronomical Databases – Active Galaxies – Active Galactic Nuclei – QSO – Blazar – Seyfert galaxy – LINER – Starburst galaxy – Markarian galaxies.*

Introduction

The Byurakan Astrophysical Observatory (BAO) was always active in surveys, especially extragalactic ones. Astronomical surveys are rather important because they are related to the following:

- Discovery of **new cosmic objects**
- **Types of Cosmic objects**
- **Abundance** of Cosmic objects
- **Spatial distribution:** Stellar (Galactic) Astronomy and Cosmology, **kinematics and dynamics**
- The **geometry of Space**

*aregmick@yahoo.com, Corresponding author
†abrahamyanhayk@gmail.com
‡paronyan_gurgen@yahoo.com
§gormick@mail.ru
¶randreasyan@gmail.com
‖andranik.suqiasyan.1995@mail.ru
**hambardzumyanlian@gmail.com
††varduhi.mkrtchyan.99@bk.ru
‡‡gasparyananna1997@mail.ru
dennefel@iap.fr

doi: https://doi.org/10.52526/25792776-24.71.2-367

- **Luminosity functions** of Cosmic objects, their **evolution**
- The development of**Multiwavelength Astronomy**
- **Statistics**
- Revelation of **astrophysical relations, laws, and regularities**

Here is the list of the most important surveys carried out by BAO astronomers (Table 1).

Table 1. Most important extragalactic surveys by BAO astronomers.

Years	Authors	Survey	Short	Type of objects	Number of objects
1965-1980	B. Markarian, V. Lipovetsky,J. Stepanian	First Byurakan Survey (Markarian Survey)	FBS	UV-excess galaxies	1544
1973-1979	R. Shahbazian	Shahbazian Survey	Shkh	Compact groups of compact galaxies	377
1976	M. Arakelian	Arakelian Survey	Akn	High surface brightness galaxies	621
1978-1991	B. Markarian, J. Stepanian, L. Erastova, V. Chavushyan	Second Byurakan Survey	SBS	UVX and Emission-line galaxies, QSOs	3600
1979-2005	M. Kazarian, et al.	Kazarian Survey	Kaz	UV-excess galaxies	706
1987-1996	H. Abrahamian, A. Mickaelian	First Byurakan Survey, 2nd Part	FBS BSOs	QSOs and Seyferts	1103
1995-2004	A. Mickaelian, et al.	Byurakan-IRAS Galaxies	BIG	IRAS galaxies	1278
2002-2006	A. Mickaelian, et al.	Byurakan-Hamburg-ROSAT Catalogue	BHRC	ROSAT sources	4253
2018	A. Mickaelian, H. Abrahamyan, et al.	Variable radio sources at 1400 MHz	NVSS/FIRST	Variable radio sources	6301

The importance of active galaxies is rather high as they play crucial role in many aspects, such as:

- **Formation and** of galaxies
- **Morphology**
- **Interacting and merging galaxies**
- **Star formation** in galaxies
- **The luminosity function** of galaxies
- **Radiation mechanisms**
- **Multiwavelength activity**
- The presence of **relativistic jets**
- The theory of **supermassive black holes (SMBH)**
- **Energy sources**
- **Cosmological role of Active Galaxies**

The recent results on active galaxies are related to their multiwavelength studies using large amount of data from X-ray, UV, optical, IR and radio ranges, namely large-area or all-sky surveys, with heavy use of cross-correlations, classifications on activity types using our observations and SDSS spectra, building diagnostic diagrams, Spectral Energy Distributions (SEDs), etc. For classification of SDSS spectra, we have used our new approach that is focused on detailed analysis of the most important emission lines and introducing fine details, like subtypes for the main broad-line Seyfert galaxies and narrow-line Seyfert ones. Results on HRC/BHRC sample objects (optical identifications of ROSAT X-ray sources), studies of Markarian galaxies in UV and multiwavelength SEDs, abundance and star formation determinations in Mrk galaxies from SDSS spectra (for spectra having higher signal-to noise ratio), revised optical classification of LINERs, study and classification of SDSS spectra for Byurakan-IRAS Galaxies (BIG objects), summary of observations and study of BIG objects, discovery of new bright ULIRGs from the IRAS PSC/FSC Combined Catalogue (complied earlier by our group) and their spectral classification using SDSS spectra, 6301 radio variable sources at 1400 MHz and their optical variability, classification of BZCAT objects having uncertain types (BZU objects), and optical variability of blazars are given in individual sections.

doi: https://doi.org/10.52526/25792776-24.71.2-367

BAO Research Department *"Astronomical Surveys"*

Currently, 10 researchers work at BAO Research Department (RD) "Astronomical Surveys". However, 3 of them are engaged in the stellar astrophysics, namely Dr. Kamo Gigoyan, Dr. Gayane Kostandyan and Karen Gigoyan (late-type stars, IR stars, variables, etc.). All others work on extragalactic subjects. They are:

- **Dr. Areg Mickaelian** – Head of the RD "Astronomical Surveys", Leading Researcher, BAO Director, PhD in Astrophysics in 1994, PI of RA HESC Advanced Research Grant 21AG-1C053 (2021-2026), main research topic "Multiwavelength search and studies of Active Galaxies"

- **Dr. Hayk Abrahamyan** – Researcher, BAO Deputy Director, PhD in Astrophysics in 2020, also teaching Physics and Astrophysics, involved in RA HESC Advanced Research Grant 21AG-1C053 (2021-2026), main research topic "Search and studies of extragalactic radio sources"

- **Gurgen Paronyan** – Researcher, PhD student, involved in RA HESC Advanced Research Grant 21AG-1C053 (2021-2026), main research topic "Search and studies of extragalactic X-ray sources"

- **Gor Mikayelyan** – Researcher, PhD student, Head of BAO Astroinformatics Infrastructural Department, involved in RA HESC Advanced Research Grant 21AG-1C053 (2021-2026), main research topic "Search and studies of IR galaxies"

- **Liana Hambardzumyan** – Researcher, also works at the Yerevan State University (YSU) Institute of Physics, main research topic "Study of jet structure of Blazars"

- **Varduhi Mkrtchyan** – Junior Researcher, also teaching Physics and Astrophysics, involved in RA HESC Advanced Research Grant 21AG-1C053 (2021-2026), main research topic "Morphology of Active Galaxies"

- **Anna Gasparyan** – Junior Researcher, also teaching Physics and Astrophysics

We tightly collaborate with the other BAO Research Department, "Active Galaxies" with the following researchers:

- **Dr. Ruben Andreasyan** – Head of the RD "Active Galaxies", Leading Researcher, PhD in Astrophysics in 198?, involved in RA HESC Advanced Research Grant 21AG-1C053 (2021-2026), main research topics "Studies of extragalactic radio sources" and *"Study of the Galactic distribution of pulsars"*

- **Andranik Sukiasyan** – Junior Researcher, involved in RA HESC Advanced Research Grant 21AG-1C053 (2021-2026), main research topic *"Study of QSOs UV wavelength range"*

We have three foreign scientific advisors:

- **Tigran Arshakian** (Köln, Germany)

- **Valeri Hambaryan** (Jena, Germany)

- **Michel Dennefeld** (IAP, France, Project Advisor)

Research Projects

Along with our regular research work, we have and had a number of projects / research grants, including:

- RA Science Committee **Advanced Research Grant** 21AG-1C053 (2021-2026): Revelation of Early Stages of Galaxies Evolution by Means of Multiwavelength Study of Active Galaxies, PI Areg Mickaelian

- **Armenian National Science and Education Fund (ANSEF) grant** 2022-2023: Search and studies of luminous X-ray galaxies, PI Areg Mickaelian

- **ANSEF grant** 2020: Optical Properties of Infrared Galaxies, PI Gor Mikayelyan

doi: https://doi.org/10.52526/25792776-24.71.2-367

- **V. Ambartsumian International Science Prize (VA Prize) grant** 2019-2020: Optical Classification of Variable Radio Sources, PI Hayk Abrahamyan
- **VA Prize grant** 2019-2020: Optical Properties of Infrared Galaxies, PI Gor Mikayelyan
- **ANSEF grant** PS-astroex-4193 (2016): Radio properties of active galaxies, PI Hayk Abrahamyan
- **ANSEF grant PS-astroex-4195** (2016): Multiwavelength Studies of Blazars, PI Areg Mickaelian
- RA Science Committee **Thematic Grant** 15T-1C257 (2015-2017): Spectral and Multiwavelength Study of Markarian Galaxies, PI Areg Mickaelian

Optical studies of active galaxies

Among the optical studies, most important are studies of Markarian (Mrk) galaxies and FBS Blue Stellar Objects (BSOs). We have carried out a homogeneous classification for activity types for Markarian galaxies by means of the SDSS spectra. 779 Mrk galaxies appeared to have SDSS spectroscopy (due to smaller sky area covered by SDSS compared to Markarian Survey). We give in Table 2 the distribution by activity types for these 779 Mrk objects.

Table 2. Most important extragalactic surveys by BAO astronomers.

Type	**Number**	%
HII	533	68.42
Composite	31	3.98
LINER	12	1.54
Sy 2.0	4	0.51
Sy 1.9	5	0.64
Sy 1.8	8	1.03
Sy 1.5	11	1.41
Sy 1.2	21	2.70
Sy 1.0	4	0.51
QSO	2	0.26
NLS1.5	5	0.64
NLS1.2	8	1.03
NLS1	4	0.51
AGN	11	1.41
Em	52	6.68
Abs	65	8.34
Star	3	0.39
TOTAL	**779**	**100.00**

Infrared Studies of Active Galaxies

IRAS Point Source Catalog (PSC) served as the main source for identification and study of IR galaxies, among which there are many Active Galaxies, as well as high-luminosity IR galaxies (ULIRGs, HLIRGs). In Figure 1 we give infrared and far-infrared luminosities of IRAS galaxies vs. redshift. The outliers are objects with especially high IR/FIR luminosity, so called IR-excess galaxies. This way we have introduced a new class of objects. The importance of IR galaxies is given as follows (their relation to the following topics):

- **Formation and evolution of galaxies**
- **Star formation and SFR** in galaxies
- **Morphology**

doi: https://doi.org/10.52526/25792776-24.71.2-367

- **Interacting and merging galaxies**
- Variety of **types of active galaxies** (many Seyferts, LINERs, Starbursts and Composites)
- The **luminosity function of galaxies** (higher redshifts)
- **Radiation mechanisms / Energy sources**
- **Cosmological role of Active Galaxies**
- Interrelationship between **Starburst, AGN and interaction/merging phenomena**

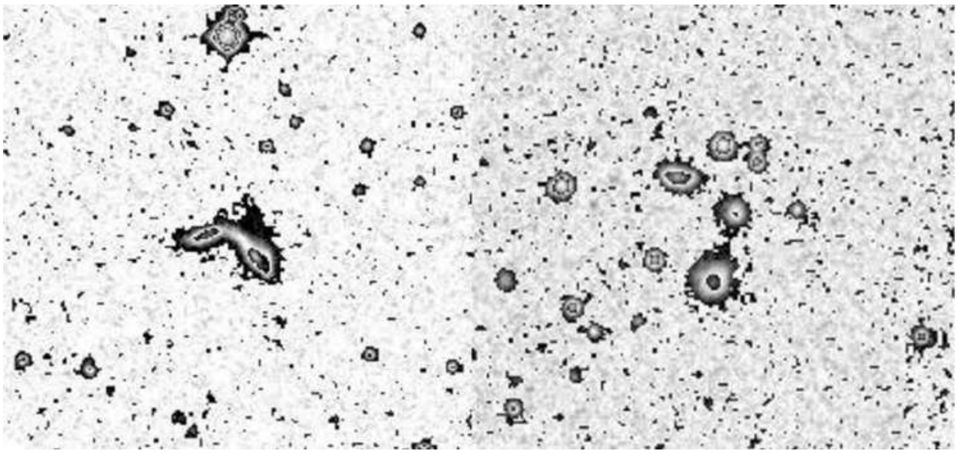

Figure 1. Examples of two systems of interacting IR galaxies; several components can be notices.

High-luminosity IR galaxies

High-luminosity IR galaxies (LIRGs, ULIRGs, and HLIRGs) are important for studies related to star-formation processes in the early Universe, as their luminosity allows to detect them at large distances. High IR indicates active star-formation and often starburst processes, which is typical to HII (starburst, SB) and/or existence of Active Galactic Nuclei (AGN). An interesting question is whether the starburst triggers AGN or vice versa or there is no direct impact. Considering that very often such objects manifest double and multiple structure, it is also interesting to investigate the interrelationship between the SB, nuclear activity and interactions or merging. We have analyzed the IRAS PSC/FSC Combined Catalogue for search for new bright ULIRGs. By means of the SDSS DR14 data, namely redshifts for those objects having spectroscopy, we have calculated the IR luminosities and have found 114 very high-luminosity IR galaxies; 107 ULIRGs and 7 HLIRGs. Among them, 48 new ULIRGs and 7 new HLIRGs have been discovered. These objects have been studied by SDSS color-color, luminosity-redshift and other diagrams. Further studies included the content of the sample for activity types and other available data. The classification for their activity types resulted in: 1 BLL, 2 Quasars, 29 Seyfert types 1.0-1.8, 5 Seyfert type 2, 14 LINERS, 36 HII regions, and 14 objects with Composite spectra (Composites). Among the type 1 Seyfert galaxies there are many objects with Narrow Lines (NLS1s).

IRAS PSC/FSC Combined Catalog

We have compiled an IRAS PSC/FSC Combined Catalog to increase the efficiency of using IRAS PSC and FSC (Abrahamyan et al. 2015). Special cross-correlation technique was applied developed by A. M. Mickaelian, which included flexible search radius (corresponding to 3σ of errors for each individual source) and evaluation/selection of the associations (categories by confidence: 1, 2 and 3). In total, we have resulted in 345,163 sources (73,770 associations between PSC/FSC) and all others are individual sources either in PSC or FSC. Thus, we have obtained an IRAS-based large all-sky homogeneous sample of IR sources: QSOs, AGN, SBs, late-type stars, planetary nebulae, variables, etc. Cross-correlations with AKARI-IRC, AKARI-FIS and WISE data were carried out; accurate positions were derived and estimation of star/galaxy type was done. Having all these data, in total 17 photometric measurements from 1.25μ to 160μ range are available allowing building Spectral Energy Distributions (SEDs), etc.

doi: https://doi.org/10.52526/25792776-24.71.2-367

Building an IRAS-based large all-sky homogeneous sample of IR-selected extragalactic sources

One of our subprojects is Building of an IRAS PSC/FSC Combined Catalog based large all-sky homogeneous sample of IR-selected extragalactic sources: galaxies and QSOs. For this purpose, we carry out the following actions:

- Cross-correlations with catalogs of known galaxies (RNGC, RC3, etc.)
- Cross-correlations with catalogs of known QSOs (Milliquas)
- Cross-correlations with catalogs of possible galaxies (PGC, APM, SDSS) and QSOs (SDSS, Gaia, etc.)
- Cross-correlations with other IR catalogs and databases
- Cross-correlations with multiwavelength catalogs and databases (gamma-ray, X-ray, UV, optical, sub-mm/mm and radio)
- Revelation of the morphological and activity types and IR-luminosities

Radio Studies of Active Galaxies

We have carried out several projects on studies of radio galaxies and radio properties of active and normal galaxies.

Radio variable sources at 1400 MHz and their optical variability

We have cross-correlated NVSS and FIRST radio catalogues having radio flux measurements at the same 1.4 GHz frequency. This way we benefit from repeated observations from both catalogues, as they give more accurate positions and fluxes and more important, reveal large differences between the two measured fluxes, thus allowing to establish radio variability. As a result, 79,382 radio variables have been revealed, including 6301 with flux differences at 1.4 GHz larger than 15 mJy, 1917 with flux differences ¿ 45 mJy and 260 with flux differences ¿ 200 mJy. By using a special technique, 2425 optically variable objects out of 6301 radio sources have been revealed. 2425 radio sources with both high radio and optical variability into four categories have been divided. 1206 (19%) out of 6301 radio sources have activity types from available catalogues and 619 (25.5%) out of 2425 radio sources with at the same time radio and optical variability have activity types from available catalogues. In addition, 279 radio sources out of 2425 have high variability in optical range. We have established their activity types when available. The IR fluxes and colors for the 6301 variable radio sources have been studied. Color-color diagrams show that most of the "unknown" sources are galaxies. The activity types for 110 (42%) out of 260 extremely high variable radio sources also have been retrieved.

Blazars

The definition of Blazars has several criteria, both historical and introduced by ourselves. We list here all related physical parameter that may define a Blazar:

- Selected radio sources
- X-ray and gamma-ray emission
- Radio spectral index is α = -0.154±0.01 (based on 1435 objects)
- Average flux ratio radio/opt = 17.996 (based on 1810 objects)
- Average flux ratio X/opt = 0.052 (based on 1101 objects)
- Average flux ratio radio/X = 86.197 (based on 1860 objects)
- Average optical variability: ΔR = 1.20±0.13, ΔB = 0.98±0.11
- Average radio variability: $|FIRST - NVSS|$-3σ = 38.01 mJy (based on 805 sources)
- Absolute magnitudes (SDSSr band): M_{BZB}= -22.19, M_{BZG}= -22.44, M_{BZQ}= -22.97, M_{BZU} = -22.42, M_{All}= -22.78.

doi: https://doi.org/10.52526/25792776-24.71.2-367

Classification of BZCAT objects for activity types

Having 3561 objects in the BZCAT catalogue v.5, it is important to clarify what physical type of objects are included. They are divided into 4 groups: BZB (BL Lac objects), BZQ (Flat Spectrum Radio Quasars, FSRQs), BZG (Blazar-like extended objects; galaxies) and BZU (Uncertain type). Altogether, 749 (54.95%) Blazars out of 1363 changed classification after our classification by activity types. Another paper of this volume is dedicated to these studies (Abrahamyan et al.), so we will not focus on this topic in details.

X-ray Studies of Active Galaxies

Optical identifications of ROSAT Faint Source Catalogue (FSC) led to revelation of many new interesting optical objects, including a big number of extragalactic ones. The Joint HRC/BHRC Catalogue is based on the combination of two major studies; optical identification projects of ROSAT BSC and ROSAT FSC, both based on Hamburg Quasar Survey (HQS) low-dispersion spectra. The 1st one was published by Zickgraf et al. (2003; A&A 406, 535) and resulted in 5341 identified BSC sources and the 2nd one was published by Mickaelian et al. (2006; A&A 449, 425) and resulted in 2791 identified FSC sources. While the 1st project used only HQS, in the 2nd one we used HQS, DSS1 and DSS2 to find faint objects and to achieve almost 100% result for studies X-ray sources.

A work was carried out to reveal all X-ray galaxies in HRC/BHRC Combined Catalogue (Paronyan et al. 2018) by cross-correlations with known catalogs of AGN and galaxies, their optical images (including DSS1/DSS2 and SDSS) and other parameters (radio, IR, X-ray properties, etc.). We have carried out classification of X-ray galaxies for their activity types using SDSS spectroscopic database and have revealed active galaxies (AGN and Starbursts). The classification has been carried out according to our new scheme and many narrow-line objects (Seyferts and Quasars) have been revealed.

Activity types of HRC/BHRC objects

In this study we carried out detailed spectral classification of 371 (173+198) AGN candidates from the Joint HRC/BHRC sample, which is a combination of HRC (Hamburg-ROSAT Catalogue) and BHRC (Byurakan-Hamburg-ROSAT Catalogue). These objects were revealed as optical counterparts for ROSAT X-ray sources; however, spectra for 371 of them were given in SDSS without definite spectral classification. We studied these 371 objects using the SDSS spectra and revealed the detailed activity types for them. Three diagnostic diagrams and direct examination of the spectra were used to obtain more confident classification. We also identified these sources in other wavelength ranges and calculated some of their parameters.

Database of Markarian galaxies

We have created a Database of Markarian galaxies with multiwavelength data (MW) including all possible information from gamma-ray, X-ray, UV, optical, IR, sub-mm/mm and radio domains (https://www.bao.am/activities/projects/21AG-1C053/mg/). In Figure 2 we give an example of such page for the famous Blazar Mrk 421 with its various images and numerical data.

Fine Classification of Active Galaxies

We have carried out a detailed Fine classification of the emission-line spectrum of active galaxies (https://www.bao.am/activities/projects/21AG-1C053/mickaelian/). One of the most important results is the introduction of subtypes for Narrow-Line Quasars (NLQ) similar to Narrow-Line Seyfert 1 galaxies (NLS1: NLS1.0, NLS1.2, NLS1.5, NLS1.8, NLS1.9, introduced by Osterbrock & Pogge 1985). These galaxies have soft X-ray detected by ROSAT surveys and have the same physical nature as X-ray QSOs, hence this classification scheme will extend their luminosity range to higher ones. We have introduced NLQ1.0, NLQ1.2, NLQ1.5, NLQ1.8 and NLQ1.9, though the last 2 subtypes are extremely rare and are rather difficult to reveal.

Our classification scheme may be given as the following:

- **Broad Line QSOs – BLQ (BLQSO)** – Q1.0, Q1.2, Q1.5, Q1.8, Q1.9
- **Narrow Line QSOs – NLQ (NLQSO)** – NLQ1.0, NLQ1.2, NLQ1.5, NLQ1.8, NLQ1.9

doi: https://doi.org/10.52526/25792776-24.71.2-367

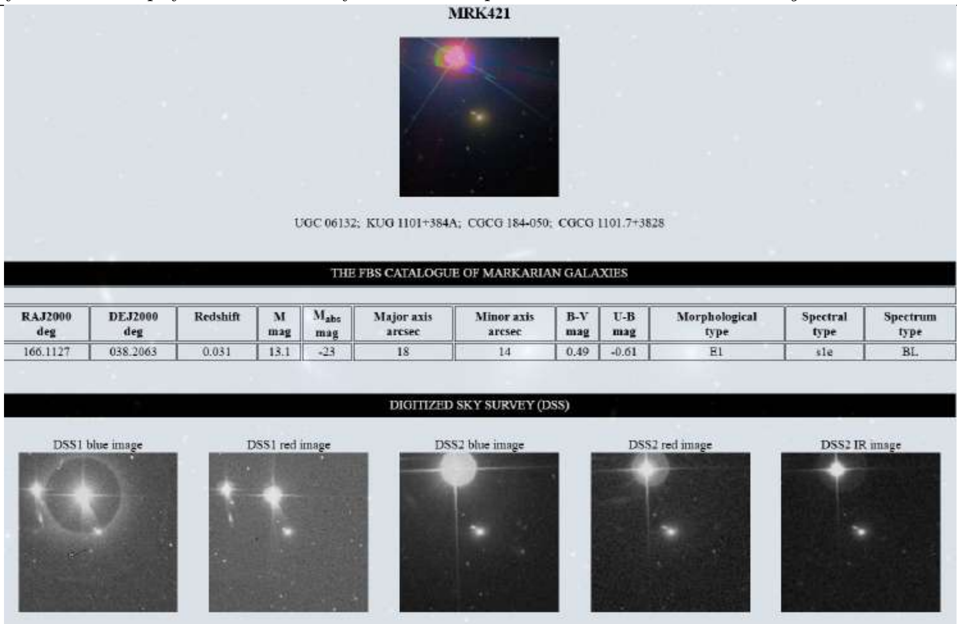

MRK421

UGC 06132; KUG 1101+384A; CGCG 184-050; CGCG 1101.7+3828

THE FBS CATALOGUE OF MARKARIAN GALAXIES

RAJ2000 deg	DEJ2000 deg	Redshift	M mag	M_{abs} mag	Major axis arcsec	Minor axis arcsec	B-V mag	U-B mag	Morphological type	Spectral type	Spectrum type
166.1127	038.2063	0.031	13.1	-23	18	14	0.49	-0.61	E1	s1e	BL

DIGITIZED SKY SURVEY (DSS)

DSS1 blue image DSS1 red image DSS2 blue image DSS2 red image DSS2 IR image

Figure 2. An example of individual page for the famous Blazar Mrk 421 with its various images and numerical data.

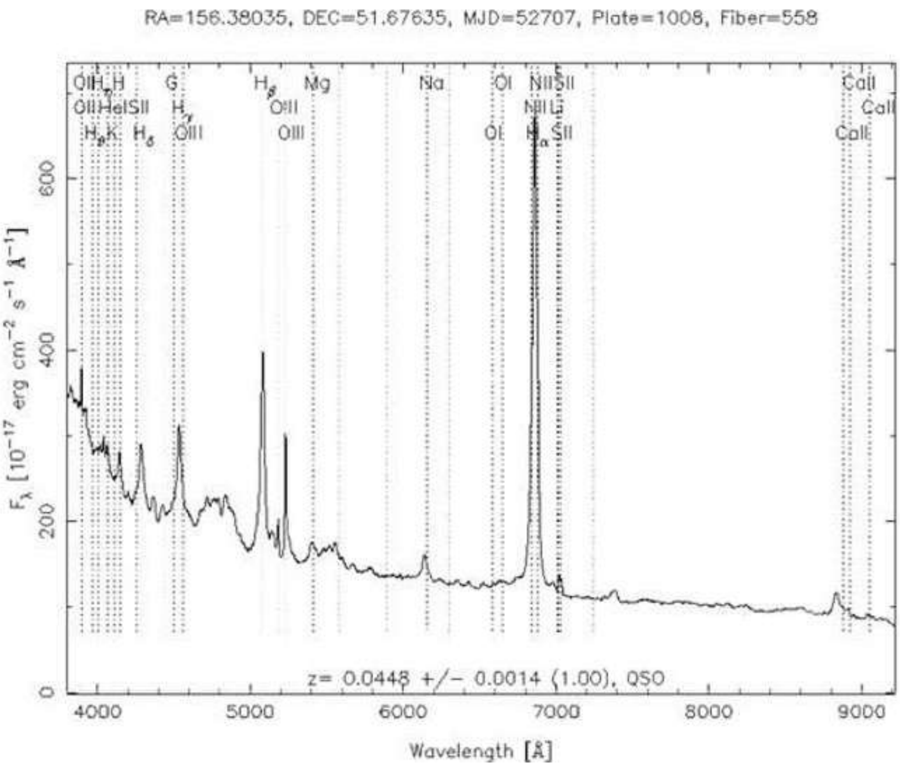

Figure 3. An example of **Narrow Line Seyfert Galaxy (NLS1)** having comparatively narrow broad lines (H-alpha, H-beta, etc.) and two bumps on both sides of H-beta, consisting of many FeII and some other lines. Such objects also have strong soft X-ray radiation.

- **Broad Line Seyfert 1s – BLS (S, Sy, Sey)** – S1.0, S1.2, S1.5, S1.8, S1.9 (Osterbrock 1981)
- **Narrow Line Seyfert 1s** – NLS (NLS1, Osterbrock & Pogge 1985) – NLS1.0, NLS1.2, NLS1.5, NLS1.8, NLS1.9
- **Narrow Line AGN – NLA (NLAGN)** – S2.0, LINER (Heckman 1980), HII (Sargent & Searle 1970)
- **Composite Spectrum objects** – Comp (Veron et al. 1997) – HII/LINER, HII/Sy, LINER/Sy, HII/LINER/Sy.

doi: https://doi.org/10.52526/25792776-24.71.2-367

In addition, in the future we will introduce two more novelties:

- **Diagnostic Diagrams for BLS** (based on decomposition of line profiles into broad and narrow lines for S1.2, S1.5, S1.8, S1.9 types and further classification of objects by diagnostic diagrams),
- Classifications based on the **shorter wavelength range of QSOs**; classification by L-alpha, CIV, CIII and MgII lines.

Summary of the Results

We have achieved many results in various wavelength ranges: X-ray, UV, optical, IR and radio, as well as in multiwavelength studies of active galaxies. In Table 3 we list all our accomplished or ongoing projects on multiwavelength search and studies of active galaxies. We give the years, authors, name of the survey, short designation, objective or types of objects discovered and studied, and the number of objects.

Table 3. Summary of the accomplished and ongoing projects on multiwavelength search and studies of active galaxies.

Years	Authors	Survey	Short	Objectives	Number of objects
1986-2001	H. Abrahamian, A. Mickaelian	First Byurakan Survey, 2nd Part	FBS BSOs	QSOs and Seyferts	1103
1994-2010	A. Mickaelian et al.	Byurakan-IRAS Galaxies	BIG	IRAS galaxies	1278
2001-pres.	A. Mickaelian	Bright AGN	AGN	Statistical studies of bright AGN	∼ 10 000
2001-2007	A. Mickaelian, et al.	Fine analysis of AGN spectra	Bright AGN	Physical properties of AGN	90
2002-pres.	A. Mickaelian, et al.	Search for new AGN in DFBS	DFBS AGN	New bright active galaxies	∼ 10 000
2002-2006	A. Mickaelian et al.	Byurakan-Hamburg-ROSAT Catalogue	BHRC	ROSAT sources	2791
2003-2010	L. Sargsyan, A. Mickaelian et al.	Spitzer ULIRGs	Spitzer	ULIRGs	32
2006-pres.	A. Mickaelian, et al.	Fine classification of active galaxies	Mickaelian classification	Accurate types and subtypes of active galaxies	∼ 10 000
2010-pres.	A. Mickaelian et al.	Studies of Markarian galaxies	Mrk	Markarian galaxies	1544
2010-pres.	G. Paronyan, A. Mickaelian, et al.	HRC/BHRC AGN content	X-ray AGN	X-ray AGN	4253
2013-pres.	A. Mickaelian, G. Paronyan et al.	Search for X-ray/radio AGN	ROSAT/NVSS	X-ray/radio AGN	9193
2013-2018	H. Abrahamyan, A. Mickaelian et al.	Variable radio sources at 1400 MHz	NVSS/FIRST	Variable radio sources	6301
2014-pres.	H. Abrahamyan, A. Mickaelian et al.	Activity types and MW study of Blazars	BZCAT	Blazars	3561
2015-pres.	G. Mikayelyan, A. Mickaelian et al.	IRAS PSC/FSC Combined Catalogue extragalactic sources	IRAS	IRAS galaxies	145 902
2018-pres.	G. Mikayelyan, A. Mickaelian et al.	IRAS PSC/FSC Combined Catalogue ULIRGs/HLIRGs	ULIRG/HLIRG	High luminosity IR galaxies	114
2021-pres.	A. Mickaelian, et al.	Markarian galaxies Electronic Database	Mrk	Building an Electronic Database with all available data	1515

Acknowledgements

This work was partially supported by the Republic of Armenia Ministry of Education and Science (RA MES) Higher Education and Science Committee (HESC), in the frames of the Advanced Research Project 21AG-1C053 (2021-2026). This work was made possible in part by research grant PS-astroex-2597 from the Armenian National Science and Education Fund (ANSEF) based in New York, USA (2022-2023).

References

Abrahamian H. V., Mickaelian A. M., 1995, Astrofizika, 38, 201

Abrahamyan H. V., Mickaelian A. M., Paronyan G. M., Mikayelyan G. A., Gyulzadyan M. V., 2018, Astronomy and Computing, 25, 176

Abrahamyan H. V., Mickaelian A. M., Paronyan G. M., Mikayelyan G. A., Gyulzadyan M. V., 2019a, Communications of the Byurakan Astrophysical Observatory, 66, 1

Abrahamyan H. V., Mickaelian A. M., Paronyan G. M., Mikayelyan G. A., 2019b, Astronomische Nachrichten, 340, 437

Abrahamyan H. V., Mickaelian A. M., Paronyan G. M., Mikayelyan G. A., Sukiasyan A. G., 2023a, Astrophysics, 66, 11

Abrahamyan H. V., Mickaelian A. M., Mikayelyan G. A., Paronyan G. M., Sukiasyan A. G., Mkrtchyan V. K., Hambardzumyan L. A., 2023b, Communications of the Byurakan Astrophysical Observatory, 70, 83

Heckman T. M., 1981, Astrophys. J. Lett. , 250, L59

Kazarian M. A., 1979, Astrofizika, 15, 193

Markarian B. E., Stepanian J. A., Lipovetsky V. A., 1989a, in QSO Physical Properties and Spectra. p. 88

Markarian B. E., Lipovetsky V. A., Stepanian J. A., Erastova L. K., Shapovalova A. I., 1989b, Soobshcheniya Spetsial'noj Astrofizicheskoj Observatorii, 62, 5

Mickaelian A. M., 2000a, Astronomical and Astrophysical Transactions, 18, 557

Mickaelian A. M., 2000b, Astrophysics, 43, 309

Mickaelian A. M., Gigoyan K. S., Russeil D., 1997, Astrophysics, 40, 379

Mickaelian A. M., Akopian S. A., Balaian S. K., Burenkov A. N., 1998, Astronomy Letters, 24, 635

doi: https://doi.org/10.52526/25792776-24.71.2-367

Mickaelian A. M., Gonçalves A. C., Véron-Cetty M. P., Véron P., 1999, Astrofizika, 42, 5

Mickaelian A. M., Gonçalves A. C., Véron-Cetty M. P., Véron P., 2001, Astrophysics, 44, 14

Mickaelian A. M., Balayan S. K., Hakopian S. A., 2002, in Green R. F., Khachikian E. Y., Sanders D. B., eds, Astronomical Society of the Pacific Conference Series Vol. 284, IAU Colloq. 184: AGN Surveys. p. 217

Mickaelian A. M., Abrahamyan H. V., Paronyan G. M., Mikayelyan G. A., 2021, Frontiers in Astronomy and Space Sciences, 7, 82

Mickaelian A. M., Abrahamyan H. V., Mikayelyan G. A., Paronyan G. M., 2022, Communications of the Byurakan Astrophysical Observatory, 69, 10

Mikayelyan G. A., Mickaelian A. M., Abrahamyan H. V., Paronyan G. M., 2018, Communications of the Byurakan Astrophysical Observatory, 65, 13

Osterbrock D. E., 1981, Astrophys. J. , 249, 462

Osterbrock D. E., Pogge R. W., 1985, Astrophys. J. , 297, 166

Paronyan G. M., Mickaelian A. M., Harutyunyan G. S., Abrahamyan H. V., Mikayelyan G. A., 2019, Astrophysics, 62, 147

Paronyan G. M., Mickaelian A. M., Abrahamyan H. V., Mikayelyan G. A., 2020, Astrophysics, 63, 166

Veron P., Goncalves A. C., Veron-Cetty M. P., 1997, Astron. Astrophys. , 319, 52

doi: https://doi.org/10.52526/25792776-24.71.2-367

Communications of BAO, Vol. 71, Issue 2, 2024, pp. 377-382

Machine Learning Classification of Young Stellar Objects and Evolved Stars in the Magellanic Clouds Using the Probabilistic Random Forest Classifier

Sepideh Ghaziasgar *[1], Mahdi Abdollahi †[1], Atefeh Javadi ‡[1], Jacco Th. van Loon §[2], Iain McDonald ¶[3], Joana Oliveira ‖[2], and Habib G. Khosroshahi **[1,5]

[1]School of Astronomy, Institute for Research in Fundamental Sciences (IPM), P.O. Box 19568-36613, Tehran, Iran
[2]Lennard-Jones Laboratories, Keele University, ST5 5BG, UK
[3]Jodrell Bank Centre for Astrophysics, Alan Turing Building, University of Manchester, M13 9PL, UK
[5]Iranian National Observatory, Institute for Research in Fundamental Sciences (IPM), Tehran, Iran

Abstract

The Magellanic Clouds (MCs) are excellent locations to study stellar dust emission and its contribution to galaxy evolution. Through spectral and photometric classification, MCs can serve as a unique environment for studying stellar evolution and galaxies enriched by dusty stellar point sources. We applied machine learning classifiers to spectroscopically labeled data from the Surveying the Agents of Galaxy Evolution (SAGE) project, which involved 12 multiwavelength filters and 618 stellar objects at the MCs. We classified stars into five categories: young stellar objects (YSOs), carbon-rich asymptotic giant branch (CAGB) stars, oxygen-rich AGB (OAGB) stars, red supergiants (RSG), and post-AGB (PAGB) stars. Following this, we augmented the distribution of imbalanced classes using the Synthetic Minority Oversampling Technique (SMOTE). Therefore, the Probabilistic Random Forest (PRF) classifier achieved the highest overall accuracy, reaching 89% based on the recall metric, in categorizing dusty stellar sources before and after data augmentation. In this study, SMOTE did not impact the classification accuracy for the CAGB, PAGB, and RSG categories but led to changes in the performance of the OAGB and YSO classes.

Keywords: *stars: classification - stars: AGB, RSG, and post-AGB - stars: YSOs - galaxies: spectral catalog - galaxies: Local Group - methods: machine learning*

1. Introduction

The Magellanic Clouds (MCs), as nearby dwarf galaxies with the distance of 50 kpc and 60 kpc (Pietrzyński et al., 2013, Subramanian & Subramaniam, 2009, 2011) and metallicities of 0.5 and $0.2Z_\odot$ (Russell & Dopita, 1992), offer an ideal environment to study stellar contributions to dust production (Ruffle et al., 2015).

The life cycle of stars is represented by different stellar classes, each with distinct physical characteristics and processes. Dusty stellar objects enriched chemically during evolution can be classified into young stellar objects (YSOs) and evolved stars (Boyer et al., 2011).

Young stellar objects (YSOs) are in the early phases of star formation. They are surrounded by gas and dust and offer a window into the physical processes driving star formation and galaxy evolution (Kokusho et al., 2023, Sewiło et al., 2013, Suh, 2016). Also, the luminosity of YSOs can vary from optical to IR depending on their mass and evolution stage (Miettinen, 2018, Oliveira et al., 2013).

*sepide.ghaziasgar@gmail.com, Corresponding author
†m.abdollahi@ipm.ir
‡atefeh@ipm.ir
§j.t.van.loon@keele.ac.uk
¶Iain.Mcdonald-2@manchester.ac.uk
‖j.oliveira@keele.ac.uk
**habib@ipm.ir

doi: https://doi.org/10.52526/25792776-24.71.2-377

Evolved stars, including asymptotic giant branch (AGB) stars with low– and intermediate mass (0.8-8 $M_\odot$) and red supergiants (RSGs) with high mass ($M \geq 8\ M_\odot$), are dust producers that enrich the ISM with heavy elements (Herwig, 2005, Höfner & Olofsson, 2018). The significant brightness of AGBs ($\sim 10^{3-4}\ L_\odot$), along with their radial pulsations, makes these stars detectable in the infrared (Goldman et al., 2017, McDonald & Zijlstra, 2016). Many evolved AGBs are long-period variables (LPVs) (Javadi & van Loon, 2019, 2022, Javadi et al., 2013, Marigo et al., 2017, Navabi et al., 2021, Saremi et al., 2021, Torki et al., 2023, Whitelock et al., 2003). AGB stars are classified into oxygen-rich (OAGB) and carbon-rich (CAGB) subcategories based on their chemical abundance, while RSGs represent massive stars in the final stages of their lives (Javadi et al., 2011, Levesque, 2010, Massey & Olsen, 2003, Yang et al., 2020), often culminating in supernovae or compact remnants. Post-AGB (PAGB) stars mark a transitional phase, shedding their outer layers before evolving into white dwarfs, revealing unique chemical signatures (Kamath, 2020, Kamath et al., 2014, 2015, van Winckel, 2003).

Machine learning algorithms are powerful tools for classifying stellar objects (Baron, 2019, Ghaziasgar et al., 2022, 2024, Kinson et al., 2021, 2022). The availability of more spectroscopically and photometrically labeled data enhances the ability of these algorithms to classify dusty stellar classes with greater accuracy, improving the overall reliability of stellar classification.

2. Data

The dataset used in this study is derived from the Surveying the Agents of Galaxy Evolution (SAGE) project for tracking dust and gas in Magellanic Clouds (Meixner et al., 2006). This dataset comprises multiwavelength spectroscopically labeled near-infrared and mid-infrared filters. From the SAGE spectral catalog, as shown in Table 1, we selected 12 multiwavelength filters for each spectral class (SpClass) and 618 dusty stellar objects in the MCs (Jones et al., 2017, Kemper et al., 2010, Ruffle et al., 2015, Woods et al., 2011). The features selected for training include UMmag, BMmag, VMmag, IMmag, J2mag, H2mag, Ks2mag, IRAC1, IRAC2, IRAC3, IRAC4 and [24].

We augmented our dataset using the SMOTE (Synthetic Minority Oversampling Technique) approach (Chawla et al., 2011) that addresses the class imbalance in datasets as presented in Table 1. Instead of simply duplicating instances from the minority class, SMOTE generates synthetic samples by interpolating between existing data points. This method selects a random data point from the minority class and creates new samples along the line segments connecting the sample to the nearest neighbor (Chawla et al., 2011). The SMOTE algorithm, applied to the training datasets, balances the population of minority classes with the majority class, potentially improving classifier performance. The Simple approach represents the original imbalanced dataset, while the SMOTE approach refers to the augmented dataset, where class imbalance has been addressed using SMOTE.

Table 1: This is a spectral classification of dusty stars in the Magellanic Clouds. Based on SMOTE methodology, the "Augmented Data" column represents the population after data augmentation.

Classes	LMC	SMC	Total	*Augmented Data
CAGB	136	38	174	200
OAGB	88	19	107	193
PAGB	33	4	37	183
RSG	72	22	94	190
YSO	157	49	206	206

3. Classification Models

We employed supervised learning algorithms to classify samples of YSOs and evolved stars (Ghaziasgar et al., 2022, 2024). The algorithms were trained on spectroscopically labeled data and evaluated on a test dataset to assess their accuracy. The models we used included Probabilistic Random Forest (PRF) (Baron, 2019, Kinson et al., 2021, 2022, Reis et al., 2019), Random Forest (RF) (Baron, 2019, Baron & Poznanski,

doi: https://doi.org/10.52526/25792776-24.71.2-377

2017, Breiman, 2001, Carliles et al., 2010), K-Nearest Neighbor (KNN) (Altman, 1992), C-Support Vector Classification (SVC) including SVC-poly and SVC-rbf (Baron, 2019, Vapnik, 1995), and Gaussian Naive Bayes (GNB) (Wilson et al., 2023). Among all the classifiers, the PRF model performed best before and after data augmentation with the SMOTE method, as detailed below.

The PRF classifier, the developed version of RF, is designed to handle noisy and uncertain datasets (Reis et al., 2019). The RF is a machine learning algorithm that builds an ensemble of decision trees, each trained on a randomly selected subset of features and data, to avoid overfitting and generalize well to new data. In RF, predictions are made through majority voting for classification studies (Baron, 2019, Breiman, 2001). However, RF assumes that data and labels are fixed and accurate, making it less effective when dealing with noisy or uncertain inputs. The PRF overcomes this limitation by introducing a probabilistic framework that treats both features and labels as probability distributions rather than fixed values. PRF routes data points probabilistically across tree branches, accounting for uncertainties in both features and labels. This probabilistic framework enhances its ability to handle noisy inputs effectively (Kinson et al., 2021, 2022, Reis et al., 2019).

4. Results and Ongoing works

We presented the classification results, as can be seen in Table 2, Fig. 1 and Fig. 2, using two approaches, Simple and SMOTE, named based on the distribution of each dataset. As shown, in comparison to other classifiers, SMOTE outperforms Simple in PRF and RF classification. Based on the recall metric, the PRF classifier demonstrated the highest total accuracy, achieving 89%. Using the SMOTE technique, the performance of the best model for the CAGB, PAGB, and RSG classes did not improve, with accuracy remaining at 100%, 100% and 88%, respectively. However, SMOTE led to some variations in the OAGB and YSO classes.

In the following, we can compare photometrically labeled data with spectroscopically labeled data with similar features. Additionally, incorporating multiwavelength data as model inputs could refine label determination for each object. More multiwavelength and spectroscopic observations are needed to improve dusty stellar classifications, especially for less populated classes like PAGBs and RSGs.

Table 2: Classification report; contains the model's precision, recall, and f1-score values for each class. The f1-score is calculated by averaging. The macro average f1-score represents an average of the f1-score over classes. The weighted average f1-score is calculated as the mean of all per-class f1-scores while considering each class's support.

(a). Classification report, Simple PRF.

Class	Precision	Recall	F1-score
CAGB	0.95	1.00	0.97
OAGB	0.80	0.73	0.76
PAGB	0.50	1.00	0.67
RSG	0.78	0.88	0.82
YSO	0.95	0.88	0.91
accuracy			0.89
macro avg	0.80	0.90	0.83
weighted avg	0.89	0.89	0.89

(b). Classification report, SMOTE PRF.

Class	Precision	Recall	F1-score
CAGB	0.86	1.00	0.92
OAGB	1.00	0.64	0.78
PAGB	0.50	1.00	0.67
RSG	0.70	0.88	0.78
YSO	1.00	0.92	0.96
accuracy			0.89
macro avg	0.81	0.89	0.82
weighted avg	0.91	0.89	0.89

doi: https://doi.org/10.52526/25792776-24.71.2-377

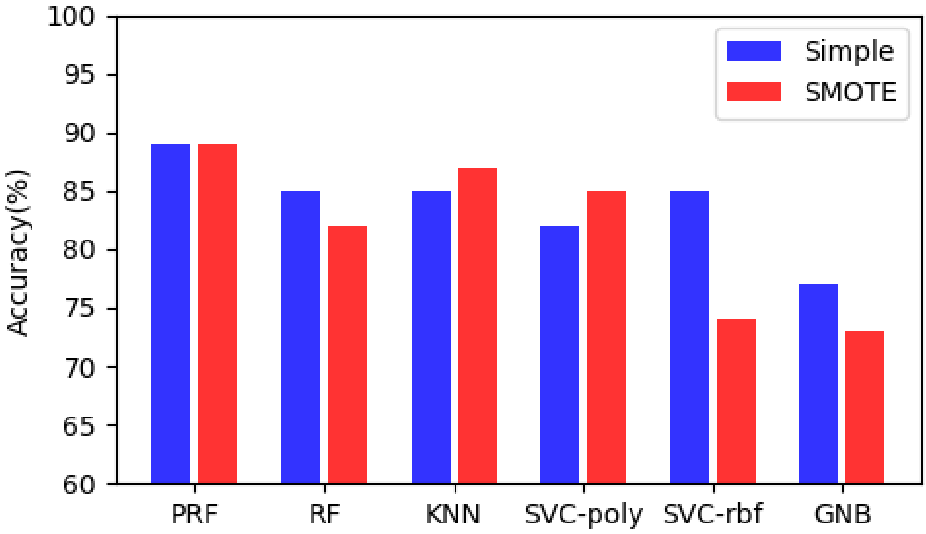

Figure 1: This plot presents the performance of Simple classifiers and SMOTE classifiers based on their accuracy scores.

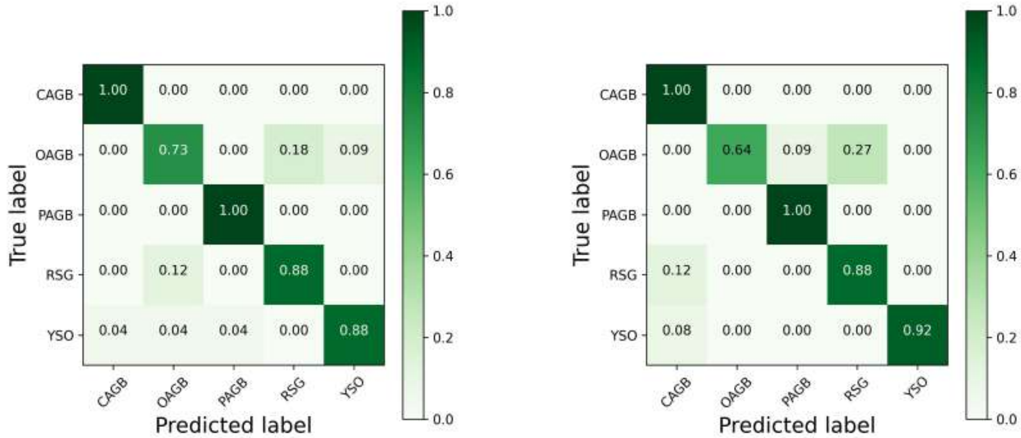

Figure 2: These are the confusion matrices for the Probabilistic Random Forest. The left panel presents the results before data augmentation, and the right panel displays the results after data augmentation with SMOTE. The matrix displays the number of objects predicted by the model in each class. The diagonal elements represent the predicted and actual labels for each class.

doi: https://doi.org/10.52526/25792776-24.71.2-377

Acknowledgements

The authors thank the School of Astronomy at the Institute for Research in Fundamental Sciences (IPM) and the Iranian National Observatory (INO) for supporting this research. S. Ghaziasgar is grateful for the support of the Byurakan Astrophysical Observatory (BAO).

References

Altman N. S., 1992, The American Statistician, 46, 175

Baron D., 2019, arXiv e-prints, p. arXiv:1904.07248

Baron D., Poznanski D., 2017, Mon. Not. R. Astron. Soc. , 465, 4530

Boyer M. L., et al., 2011, Astron. J. , 142, 103

Breiman L., 2001, Machine Learning, 45, 5

Carliles S., Budavári T., Heinis S., Priebe C., Szalay A. S., 2010, Astrophys. J. , 712, 511

Chawla N. V., Bowyer K. W., Hall L. O., Kegelmeyer W. P., 2011, arXiv e-prints, p. arXiv:1106.1813

Ghaziasgar S., Masoudnezhad A., Javadi A., van Loon J. T., Khosroshahi H. G., Khosravaninezhad N., 2022, arXiv e-prints, p. arXiv:2211.03403

Ghaziasgar S., et al., 2024, in EAS2024, European Astronomical Society Annual Meeting. p. 371

Goldman S. R., et al., 2017, Mon. Not. R. Astron. Soc. , 465, 403

Herwig F., 2005, Ann. Rev. Astron. Astrophys. , 43, 435

Höfner S., Olofsson H., 2018, Astron. Astrophys. Rev. , 26, 1

Javadi A., van Loon J. T., 2019, in Kerschbaum F., Groenewegen M., Olofsson H., eds, IAU Symposium Vol. 343, Why Galaxies Care About AGB Stars: A Continuing Challenge through Cosmic Time. pp 283–290 (arXiv:1811.12025), doi:10.1017/S1743921318006671

Javadi A., van Loon J. T., 2022, in Decin L., Zijlstra A., Gielen C., eds, IAU Symposium Vol. 366, The Origin of Outflows in Evolved Stars. pp 210–215 (arXiv:2204.08944), doi:10.1017/S1743921322001326

Javadi A., van Loon J. T., Mirtorabi M. T., 2011, Mon. Not. R. Astron. Soc. , 411, 263

Javadi A., van Loon J. T., Khosroshahi H., Mirtorabi M. T., 2013, Mon. Not. R. Astron. Soc. , 432, 2824

Jones O. C., et al., 2017, Mon. Not. R. Astron. Soc. , 470, 3250

Kamath D., 2020, Journal of Astrophysics and Astronomy, 41, 42

Kamath D., Wood P. R., Van Winckel H., 2014, Mon. Not. R. Astron. Soc. , 439, 2211

Kamath D., Wood P. R., Van Winckel H., 2015, Mon. Not. R. Astron. Soc. , 454, 1468

Kemper F., et al., 2010, Publ. Astron. Soc. Pac. , 122, 683

Kinson D. A., Oliveira J. M., van Loon J. T., 2021, Mon. Not. R. Astron. Soc. , 507, 5106

Kinson D. A., Oliveira J. M., van Loon J. T., 2022, Mon. Not. R. Astron. Soc. , 517, 140

Kokusho T., Torii H., Kaneda H., Fukui Y., Tachihara K., 2023, Astrophys. J. , 953, 104

Levesque E. M., 2010, in Leitherer C., Bennett P. D., Morris P. W., Van Loon J. T., eds, Astronomical Society of the Pacific Conference Series Vol. 425, Hot and Cool: Bridging Gaps in Massive Star Evolution. p. 103 (arXiv:0911.4720), doi:10.48550/arXiv.0911.4720

Marigo P., et al., 2017, Astrophys. J. , 835, 77

Massey P., Olsen K. A. G., 2003, Astron. J. , 126, 2867

McDonald I., Zijlstra A. A., 2016, Astrophys. J. Lett. , 823, L38

Meixner M., et al., 2006, Astron. J. , 132, 2268

Miettinen O., 2018, Astrophys. Space. Sci. , 363, 197

Navabi M., et al., 2021, Astrophys. J. , 910, 127

Oliveira J. M., et al., 2013, Mon. Not. R. Astron. Soc. , 428, 3001

Pietrzyński G., et al., 2013, Nature. , 495, 76

Reis I., Baron D., Shahaf S., 2019, Astron. J. , 157, 16

Ruffle P. M. E., et al., 2015, Mon. Not. R. Astron. Soc. , 451, 3504

doi: https://doi.org/10.52526/25792776-24.71.2-377

Russell S. C., Dopita M. A., 1992, Astrophys. J. , 384, 508

Saremi E., Javadi A., Navabi M., van Loon J. T., Khosroshahi H. G., Bojnordi Arbab B., McDonald I., 2021, Astrophys. J. , 923, 164

Sewiło M., et al., 2013, Astrophys. J. , 778, 15

Subramanian S., Subramaniam A., 2009, Astron. Astrophys. , 496, 399

Subramanian S., Subramaniam A., 2011, in Astronomical Society of India Conference Series. p. 144

Suh K.-W., 2016, Journal of Astronomy and Space Sciences, 33, 119

Torki M., Navabi M., Javadi A., Saremi E., van Loon J. T., Ghaziasgar S., 2023, in Bisikalo D., Wiebe D., Boily C., eds, IAU Symposium Vol. 362, The Predictive Power of Computational Astrophysics as a Discover Tool. pp 353–355 (arXiv:2204.11530), doi:10.1017/S1743921322001405

Vapnik V. N., 1995, The nature of statistical learning theory. Springer-Verlag New York, Inc.

Whitelock P. A., Feast M. W., van Loon J. T., Zijlstra A. A., 2003, Mon. Not. R. Astron. Soc. , 342, 86

Wilson A. J., Lakeland B. S., Wilson T. J., Naylor T., 2023, Mon. Not. R. Astron. Soc. , 521, 354

Woods P. M., et al., 2011, Mon. Not. R. Astron. Soc. , 411, 1597

Yang M., et al., 2020, Astron. Astrophys. , 639, A116

van Winckel H., 2003, Ann. Rev. Astron. Astrophys. , 41, 391

doi: https://doi.org/10.52526/25792776-24.71.2-377

Detection of the Long Period Variable Stars of And II Dwarf Satellite galaxy

Hedieh Abdollahi *[1, 2], Atefeh Javadi[1], Jacco Th. van Loon[3], Iain McDonald[4, 5], Mahdi Abdollahi[1], Elham Saremi[6, 7, 8], Habib G. Khosroshahi[1, 9], and Hamidreza Mahani[1]

[1]School of Astronomy, Institute for Research in Fundamental Sciences (IPM), P.O. Box 1956836613, Tehran, Iran
[2]Konkoly Observatory, HUN-REN Research Centre for Astronomy and Earth Sciences, MTA Centre of Excellence, Konkoly-Thege Miklós út 15-17, H-1121, Budapest, Hungary
[3]Lennard-Jones Laboratories, Keele University, ST5 5BG, UK
[4]Department of Physical Sciences, The Open University, Walton Hall, Milton Keynes, UK
[5]Jodrell Bank Centre for Astrophysics, Alan Turing Building, University of Manchester, M13 9PL, UK
[6]Instituto de Astrofísica de Canarias, Calle Vía L'actea s/n, E-38205 La Laguna, Spain
[7]Departamento de Astrofísica, Universidad de La Laguna, E-38205 La Laguna, Spain
[8]School of Physics & Astronomy, University of Southampton, Highfield Campus, Southampton SO17 1BJ, UK
[9]Iranian National Observatory, Institute for Research in Fundamental Sciences (IPM), Tehran, Iran

Abstract

We conducted an extensive study of the spheroidal dwarf satellite galaxies around the Andromeda galaxy to produce an extensive catalog of LPV stars. The optical monitoring project consists of 55 dwarf galaxies and four globular clusters that are members of the Local Group. We have made observations of these galaxies using the WFC mounted on the 2.5 m INT in nine different periods, both in the i-band filter Sloan and in the filter V-band Harris. We aim to select AGB stars with brightness variations larger than 0.2 mag to investigate the evolutionary processes in these dwarf galaxies. The resulting catalog of LPV stars in Andromeda's satellite galaxies offers updated information on features like half-light radii, TRGB magnitudes, and distance moduli. This manuscript will review the results obtained for And II galaxy. Using the Sobel filter, we have calculated the distance modulus for this satellite galaxy, which ranges from 23.90 to 24.11 mag.

Keywords: *stars: evolution – stars: AGB and LPV– stars: luminosity function, mass function – stars: mass-loss – stars: oscillations – galaxies: stellar content galaxies: Local Group*

1. Introduction

Dwarf galaxies are known to show a wide range of properties due to complications within the galactic environment-affecting star formation rates, gas composition, and interactions with other galaxies (Vollmer, 2013). Within the Local Group, they are noteworthy for their proximity, their variety,and the large range in metallicity and morphology. Their simpler star formation history compared to other galaxies makes them easier to study. The studies of dwarf galaxies have the potential to provide clues on galaxy formation scenarios, both the hierarchical and downsizing models. Dwarf galaxies are very crucial in attempts to understand dark matter since they are dominated by this form of matter, unlike globular star clusters. Their distribution in galaxy clusters may indicate the distribution of dark matter; hence, they may serve as better indicators of mass distribution within clusters than brighter galaxies.

Generally, dwarf galaxies have low stellar density and have undergone minimal dynamical evolution, preserving their initial mass function. Several questions remain about galaxy evolution, such as the differences between the evolutionary processes of dwarf satellites and isolated dwarfs, and the impact of gas removal mechanisms on star formation. Focusing on dwarf galaxies, particularly Andromeda satellites, the Isaac Newton telescope monitoring survey of dwarf galaxies in the Local Group (INT survey) was conducted to study their evolutionary history. Observations were made at three-month intervals from June 2015 to February 2018. To study galaxy evolution, asymptotic giant branch (AGB) stars were observed because they are key tracers of SFH (Hamedani Golshan et al., 2017, Hashemi et al., 2019, Javadi et al., 2011b, 2017,

*hediehabdollahi@ipm.ir, Corresponding author

doi: https://doi.org/10.52526/25792776-24.71.2-383

Table 1. Observational properties and half-light radius of targets.

Galaxy	R.A. [a] (J2000)	Dec [a] (J2000)	ϵ^b	[Fe/H][c] (dex)	r_h [b] (arcmin)	r_h *Exponential* (arcmin)	r_h *Plummer* (arcmin)	r_h *Sérsic* (arcmin)	N_{Total}	N_{LPV}
And I [d]	00 45 39.80	+38 02 28.00	0.28 ± 0.03	-1.45 ± 0.04	3.90 ± 0.10	3.20 ± 0.30	-	-	10243	470
And II	01 16 29.78	+33 25 08.75	0.16 ± 0.02	-1.64 ± 0.04	5.30 ± 0.10	$5.32^{+0.19}_{-0.02}$	$5.21^{+0.09}_{-0.12}$	$5.35^{+0.16}_{-0.05}$	10384	728
And III	00 35 33.78	+36 29 51.91	0.59 ± 0.04	-1.78 ± 0.04	2.20 ± 0.20	$2.33^{+0.07}_{-0.20}$	$2.21^{+0.19}_{-0.08}$	$2.15^{+0.25}_{-0.02}$	5409	573
And V	01 10 17.10	+47 37 41.00	$0.26^{+0.09}_{-0.07}$	-1.6 ± 0.3	$1.60^{+0.20}_{-0.10}$	$1.88^{+0.04}_{-0.17}$	$1.84^{+0.08}_{-0.14}$	$1.86^{+0.06}_{-0.16}$	7928	398
And VI	23 51 46.30	+24 34 57.00	0.41 ± 0.03	-1.3 ± 0.14	2.30 ± 0.20	$2.24^{+0.15}_{-0.03}$	$2.00^{+0.02}_{-0.16}$	$2.27^{+0.12}_{-0.07}$	6336	364
And VII [e]	23 26 31.74	+50 40 32.57	0.13 ± 0.04	-1.40 ± 0.30	3.50 ± 0.10	3.80 ± 0.30	-	-	?	55
And IX [f]	00 52 53.00	+43 11 45.00	$0.00^{+0.16}_{-0.00}$	-2.2 ± 0.2	$2.00^{+0.30}_{-0.20}$	2.50 ± 0.26	-	-	8653	77
And X	01 06 33.70	+44 48 15.80	$0.10^{+0.34}_{-0.10}$	-1.93 ± 0.11	$1.10^{+0.40}_{-0.20}$	$1.30^{+0.35}_{-0.20}$	$1.29^{+0.36}_{-0.19}$	$1.28^{+0.37}_{-0.18}$	4025	418
And XI	00 46 20.00	+33 48 05.00	$0.19^{+0.28}_{-0.19}$	-2.0 ± 0.2	0.60 ± 0.20	$0.54^{+0.18}_{-0.06}$	$0.53^{+0.19}_{-0.05}$	$0.53^{+0.19}_{-0.05}$	3999	495
And XII	00 47 27.00	+34 22 29.00	$0.61^{+0.16}_{-0.48}$	-2.1 ± 0.2	$1.80^{+1.20}_{-0.70}$	$1.72^{+0.33}_{-0.18}$	$1.72^{+0.33}_{-0.18}$	$1.73^{+0.33}_{-0.18}$	3555	237
And XIII	00 51 51.00	+33 00 16.00	$0.61^{+0.14}_{-20}$	-1.9 ± 0.2	$0.80^{+0.40}_{-0.30}$	$0.71^{+0.25}_{-0.07}$	$0.69^{+0.27}_{-0.05}$	$0.73^{+0.23}_{-0.09}$	3794	587
And XIV	00 51 35.00	+29 41 49.00	$0.17^{+0.16}_{-0.17}$	-2.26 ± 0.05	1.50 ± 0.20	$1.67^{+0.20}_{-0.17}$	$1.66^{+0.21}_{-0.16}$	$1.66^{+0.21}_{-0.16}$	7876	360
And XV	01 14 18.70	+38 07 03.00	0.24 ± 0.10	-1.8 ± 0.2	1.30 ± 0.10	$1.55^{+0.01}_{-0.25}$	$1.48^{+0.08}_{-0.18}$	$1.46^{+0.10}_{-0.16}$	7215	439
And XVI	00 59 29.80	+32 22 36.00	0.29 ± 0.08	-2.1 ± 0.2	1.00 ± 0.10	$1.19^{+0.01}_{-0.19}$	$1.14^{+0.06}_{-0.14}$	$1.13^{+0.07}_{-0.13}$	2972	183
And XVII	00 37 07.00	+44 19 20.00	0.50 ± 0.10	-1.9 ± 0.2	1.48 ± 0.30	$1.48^{+0.01}_{-0.17}$	$1.47^{+0.02}_{-0.17}$	$1.48^{+0.02}_{-0.17}$	10369	430
And XVIII	00 02 14.50	+45 05 20.00	$0.03^{+0.28}_{-0.03}$	-1.8 ± 0.1	0.80 ± 0.10	$0.97^{+0.15}_{-0.01}$	$0.95^{+0.01}_{-0.15}$	$0.93^{+0.03}_{-0.13}$	2638	266
And XIX	00 19 32.10	+35 02 37.10	$0.58^{+0.05}_{-0.10}$	-1.9 ± 0.1	$14.20^{+3.40}_{-1.90}$	$14.28^{+0.49}_{-0.08}$	$14.22^{+0.55}_{-0.02}$	$14.44^{+0.33}_{-0.24}$	7441	1676
And XX	00 07 30.70	+35 07 56.40	$0.11^{+0.41}_{-0.11}$	-1.5 ± 0.1	$0.40^{+0.20}_{-0.10}$	$0.50^{+0.04}_{-0.10}$	$0.49^{+0.05}_{-0.09}$	$0.46^{+0.07}_{-0.06}$	4050	654
And XXI	23 54 47.70	+42 28 15.00	$0.36^{+0.10}_{-0.13}$	-1.8 ± 0.2	$4.10^{+0.80}_{-0.40}$	$3.83^{+0.27}_{-0.55}$	$3.82^{+0.28}_{-0.54}$	$3.82^{+0.28}_{-0.54}$	2621	293
And XXII	01 27 40.00	+28 05 25.00	$0.61^{+0.10}_{-0.14}$	-1.8	$0.90^{+0.30}_{-0.20}$	0.90 ± 0.18	$0.87^{+0.21}_{-0.15}$	$0.85^{+0.23}_{-0.13}$	4645	295

[a] Coordinates inferred from the NASA/IPAC Extragalactic Database (NED) (2024) portal.
[b] All ellipticities are referred from Martin et al. (2016), except for And VI which is from McConnachie (2012).
[c] McConnachie (2012), [d] Saremi et al. (2020) , [e] Navabi et al. (2021), and [f] Abdollahi et al. (2023).
$\epsilon = 1 - b/a$, where b is the semi-minor axis and a is the semi-major axis.

Rezaeikh et al., 2014). AGB stars, which can become long-period variable (LPV) stars, provide insights into the dynamics and evolution of dwarf galaxies (Javadi et al., 2013, 2016). Stars with initial masses between 0.5 to 8 $M_\odot$ can reach the late stages of the AGB evolutionary path (Höfner & Olofsson, 2018). AGB stars reach their maximum luminosity during these stages, making them easier to observe in faint dwarf galaxies. The luminosity of LPVs is linked to their initial birth mass, providing clues about their mass, age, and pulsation duration. AGB stars are excellent indicators for reconstructing SFH as they age from 10 Myr to 10 Gyr (Javadi et al., 2011a).

Table 1 lists the M 31 satellites in this study, detailing the observational time, epoch, filter, exposure time, airmass, and seeing conditions for each galaxy. Of the 24 dwarf galaxies in the Andromeda system, four (M 110, M 32, Pisces I, and Pegasus) lacked sufficient observational epochs to detect long-period variable (LPV) stars, while three had already been studied previously (Abdollahi et al., 2023, Navabi et al., 2021, Saremi et al., 2021).

As illustrated in Figure 1, And II is significantly larger than the other Andromeda satellites, except for And XIX. And II was first identified through the analysis of images acquired with the 48-inch Schmidt telescope at Palomar Observatory, during observations conducted by Sidney Van den Bergh in 1970 and 1971 (van den Bergh, 1972). In this paper, we present the results of time-series observations of this galaxy, performed using the INT Telescope.

2. Observation and Data

The Wide Field Camera (WFC) on the 2.5 m INT telescope at the Observatorio del Roque de los Muchachos in La Palma is equipped with four 2048×4096 CCDs, each with a pixel scale of 0.33 arcseconds.

Long-period variable stars exhibit distinctive brightness fluctuations due to intrinsic mechanisms such as pulsations and eclipses. Time-series observations enable the quantification of periodicity, the detection of transient events, and the study of different evolutionary phases. This approach reveals detailed behaviors such as light-curves, amplitude modulation, and phase shifts. To investigate the magnitude variations of the LPV in And II, time series observations were performed using Sloan i, Harris V, and RGO I filters with the WFC to analyze photometric variability. The i-band filter enhances the contrast of spectral energy

doi: https://doi.org/10.52526/25792776-24.71.2-383

distributions (SEDs) for cool, evolved stars, particularly LPVs. The V filter, with a peak transmission around 528 nm, is used to determine stellar color, which is directly related to temperature.

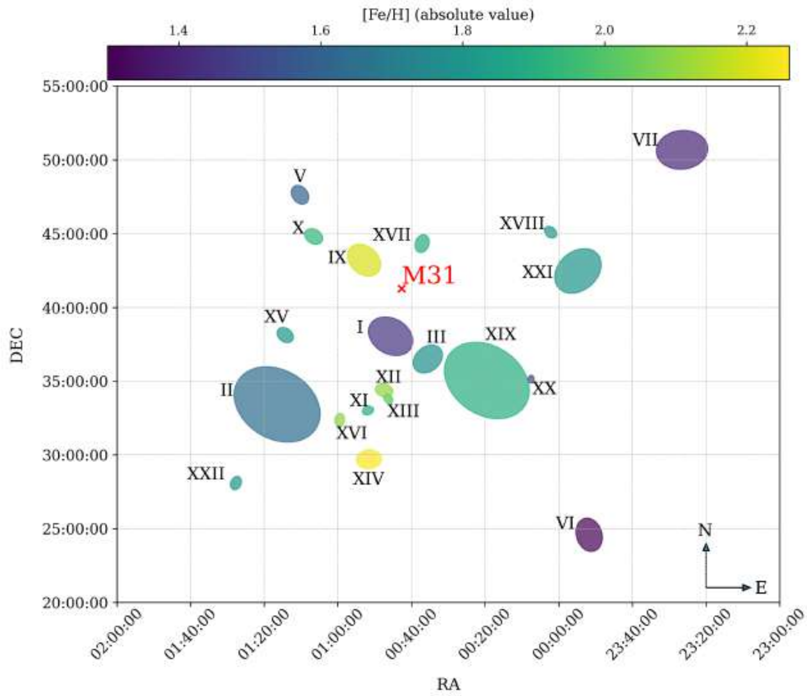

Figure 1. Satellite galaxies of Andromeda. The semi-major axis of the galaxies is represented proportionally to their actual sizes, based on data from Table 1.

3. Methodology

3.1. Data reduction and Photometry

To obtain the science images of And II from raw data, the images were processed using the 'THELI' pipeline, which is optimized for precise astrometry and multi-chip CCD cameras.

Photometry in both i and V filters was performed using the `DAOPHOT/ALLSTAR` package (Stetson, 1987). Initially, a selection of approximately 30-40 isolated stars located at various positions in the field was made using the `PSF` routine. The purpose was to construct a point-spread function (PSF) model for each image following the `FIND` and `PHOT` procedures. A master image was then created by combining individual images through the `DAOMATCH`, `DAOMASTER`, and `MONTAGE2` routines. This master image was used to generate a star list with the `ALLSTAR` routine. Subsequently, the `ALLFRAME` routine used the star list to estimate the instrumental magnitudes of stars by fitting the PSF models to the individual images (Stetson, 1994). The transformation of instrumental magnitudes into the standard system was accomplished using observations of standard stars (Landolt, 1992) and the `NEWTRIAL` routine (Stetson, 1996).

3.2. Calibration and photometry assessment

The photometric calibration process was conducted in three stages. First, aperture corrections were applied using the `DAOGROW` and `COLLECT` routines to calculate the differences in magnitude between the PSF-fitting and largest aperture photometry of about 40 isolated bright stars in each frame (Stetson, 1990). The `NEWTRIAL` routine then adjusted these aperture corrections for all stars in each frame.

Second, the transformation to the standard photometric system was carried out by constructing transformation equations for each frame, which accounted for zero-point and atmospheric extinction. The mean of other zero-points was used for frames lacking a standard-field observation. The `CCDAVE` routine applied these transformation equations to the program stars for each frame, and the `NEWTRIAL` routine subsequently calibrated all other stars using the program stars as local standards.

Finally, relative photometry between epochs was conducted to accurately distinguish variable from non-variable sources. Approximately 1000 common stars were selected across all frames within the magnitude

doi: https://doi.org/10.52526/25792776-24.71.2-383

interval 18 to 21 mag. Each star's deviation at each epoch was determined relative to the mean magnitude calculated from all epochs. These mean magnitudes were computed by weighting the individual measurements. The resulting corrections were then applied to the frames.

To evaluate the completeness of the survey, artificial stars were added using the `ADDSTAR` routine (Stetson, 1987) in both i- and V-band single frames, across discrete 0.5 mag bins ranging from 16 to 24.5 mag. The fraction of recovered artificial stars was estimated with the `ALLFRAME` routine. The results indicated that the survey is sufficiently complete up to 22 mag in the i and V bands, near the tip of the RGB, and up to 50% complete for stars with a magnitude of approximately 23 mag in both filters, confirming that nearly the entire AGB and RSG populations are detected for the primary research purpose.

3.3. Detection of long-period variables

The foreground stars were removed by cross-correlating the catalog with the Gaia DR3 catalog before LPV cognition (Gaia Collaboration et al., 2021). The method developed by Welch & Stetson (1993) and refined by Stetson (1996) involves calculating the Stetson variability index. This index quantifies a star's brightness variability based on time series observations, considering the measured magnitudes and their errors. The next step involves calculating the pairwise product of these standardized deviations. For variable stars, it is expected that the magnitudes in the i and V filters will either increase or decrease together across different observational nights within a time interval of less than half a minimum period (60 days for LPVs (McDonald & Zijlstra, 2016)). Although the magnitude of change could vary, for each observation pair, the direction of change should remain the same to yield a positive product that measures the coherence of the deviations: if the deviations from the mean are consistent and correlated across observations, it will be positive to indicate variability; otherwise, random noise cancels out due to uncorrelated deviations. The index of variability, L, normalizes and weights them based on the number of observations. A large value of L denotes that the large probability of a star being an LPV is hence very useful for selecting the variable stars out of an extensive dataset.

The accuracy of the variability indices method is confirmed through simulations, such as the `ADDSTAR` subroutine. This includes introducing artificial stars with known properties into the data and evaluating how effectively the method retrieves these inputs. This procedure aids in gauging the method's dependability and accuracy.

3.4. Amplitude of Variability for Candidate Stars

The variability amplitude was estimated by assuming a sinusoidal light-curve shape. By comparing the standard deviation in the magnitudes to the value expected for a completely random sampling of a sinusoidal variation (0.701), the amplitude can be determined using the equation that defines it as the difference between the minimum and maximum brightness.

In this study, we prioritize stars with amplitudes exceeding 0.2 mag due to our uncertainty regarding the nature of stars with lower amplitudes.

$$A = 2\sigma/0.701, \tag{1}$$

4. Results

The photometric analysis of the And II dwarf galaxy has not only led to the discovery of LPV stars but has also aided in the estimation of the tip of the red giant branch (TRGB). This estimation is crucial for calculating the distance modulus, which is fundamental for comprehending the spatial arrangement of galaxies. Moreover, the analysis offers a method for determining the half-light radius of these galaxies.

In Figure 2, the upper left subplot illustrates the distribution of LPV candidates in the studied areas. Red circles indicate LPV candidates, while solid and dashed black circles represent the half-light radius and twice the half-light radius of the dwarf galaxy, respectively. The black arrows point toward the center of the Andromeda galaxy. As illustrated in this subplot, photometric measurements required the utilization of CCD1, CCD3, and CCD4 of WFC due to the considerable size of this galaxy. As a result, the total number of stars identified (10, 384) and the detected LPV stars (825) are notably higher than those found in other target galaxies.

doi: https://doi.org/10.52526/25792776-24.71.2-383

In the upper right subplot, the left panel shows stellar sources within two half-light radii, the middle panel presents the histogram of the luminosity function, and the right panel displays the Sobel filter response for edge detection of the tip of the red giant branch (TRGB). These plots are specific to And II and resulted in TRGB = 20.40±0.10 mag (The TRGB is highlighted with red lines and arrows). The distance modulus computed for this galaxy stands at 23.81±0.10 mag (∼ 578 kpc). The results for the TRGB and distance modulus align with those reported in the study by McConnachie et al. (2004).

The lower left subplot shows the color-magnitude diagram (CMD) of the And II dwarf satellite galaxy. The gray points denote stars that were identified photometrically in the final images. The black dots represent stars situated within two times the half-light radius of the center of the target galaxy. Green points indicate potential long-period variable candidates throughout the entire studied field, while red points highlight LPV candidates within two times the half-light radius. The magenta lines illustrate the relevant isochrones.

Finally, the lower right subplot displays the light-curve of a sample variable star in And II galaxy.

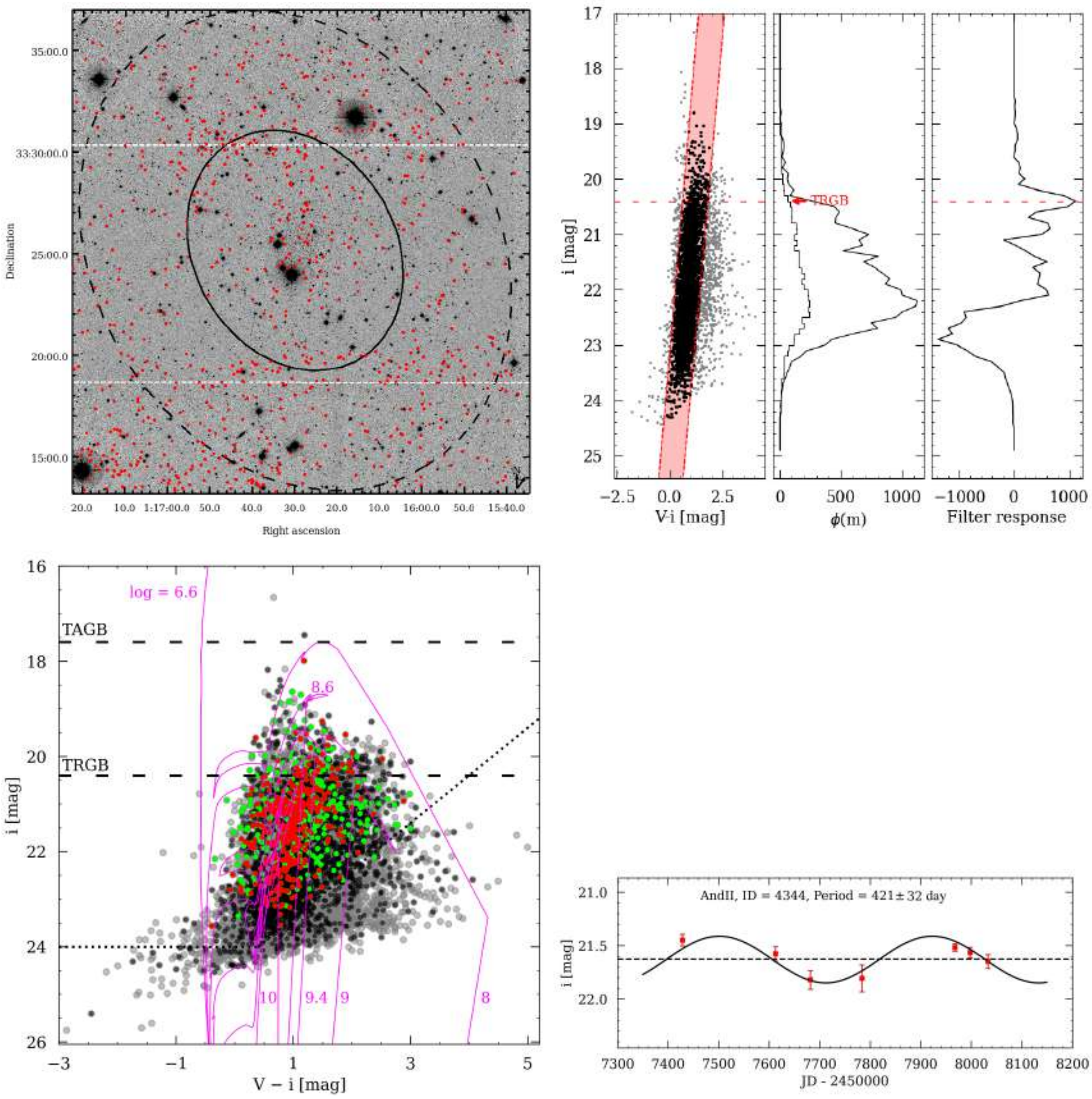

Figure 2. Distribution of the LPVs, detection of the TRGB, CMD, and light-curve in the And II galaxy.

.

5. Summary

We utilized the Wide Field Camera (WFC) on the Isaac Newton Telescope (INT) to conduct observations aimed at monitoring most of the dwarf galaxies observable from the northern hemisphere. Our observations primarily focused on the i-band filter, with additional V-band observations carried out over up to nine epochs. This study presents the initial findings for galaxy And II, showcasing our methodology and the potential scientific insights that this project can provide.

doi: https://doi.org/10.52526/25792776-24.71.2-383

For each of these galaxies, we developed photometric catalogs focused mainly on the area covered by CCD4 of the WFC, which spans $11.26'' \times 22.55''$. These catalogs are comprehensive, providing both extensive photometric data and the identification of potential long-period variable (LPV) stars, especially those exhibiting amplitude variations greater than 0.2 mag. We derived the distance modulus for these galaxies by analyzing the tip of the RGB in the photometric data. Additionally, we measured the half-light radii for these satellite galaxies.

In future papers in this series, we will utilize these catalogs to explore the star formation history and dust production of all identified LPV candidates across the monitored galaxies. Furthermore, we investigate how color, and consequently temperature, changes during variability phases. By analyzing these changes and luminosity data, we aim to determine the variations in stellar radius and their correlation with mid-infrared excess.

Acknowledgements

We sincerely thank BAO for their warm hospitality during the conference, which greatly enhanced our experience and contributed to our success. We also appreciate the support from the H.A. via the 'SeismoLab' KKP-137523 Élvonal grant from the Hungarian Research, Development and Innovation Office (NKFIH).

References

Abdollahi H., et al., 2023, Astrophys. J. , 948, 63

Gaia Collaboration et al., 2021, Astron. Astrophys. , 649, A1

Hamedani Golshan R., Javadi A., van Loon J. T., Khosroshahi H., Saremi E., 2017, Mon. Not. R. Astron. Soc. , 466, 1764

Hashemi S. A., Javadi A., van Loon J. T., 2019, Mon. Not. R. Astron. Soc. , 483, 4751

Höfner S., Olofsson H., 2018, Astron. Astrophys. Rev. , 26, 1

Javadi A., van Loon J. T., Mirtorabi M. T., 2011a, Mon. Not. R. Astron. Soc. , 414, 3394

Javadi A., van Loon J. T., Mirtorabi M. T., 2011b, in Kerschbaum F., Lebzelter T., Wing R. F., eds, Astronomical Society of the Pacific Conference Series Vol. 445, Why Galaxies Care about AGB Stars II: Shining Examples and Common Inhabitants. p. 497 (arXiv:1101.5271), doi:10.48550/arXiv.1101.5271

Javadi A., van Loon J. T., Khosroshahi H., Mirtorabi M. T., 2013, Mon. Not. R. Astron. Soc. , 432, 2824

Javadi A., van Loon J. T., Khosroshahi H., 2016, memsai, 87, 278

Javadi A., van Loon J. T., Khosroshahi H. G., Tabatabaei F., Hamedani Golshan R., Rashidi M., 2017, Mon. Not. R. Astron. Soc. , 464, 2103

Landolt A. U., 1992, Astron. J. , 104, 340

Martin N. F., et al., 2016, Astrophys. J. , 833, 167

McConnachie A. W., 2012, Astron. J. , 144, 4

McConnachie A. W., Irwin M. J., Ferguson A. M. N., Ibata R. A., Lewis G. F., Tanvir N., 2004, Mon. Not. R. Astron. Soc. , 350, 243

McDonald I., Zijlstra A. A., 2016, Astrophys. J. Lett. , 823, L38

NASA/IPAC Extragalactic Database (NED) 2024, NASA/IPAC Extragalactic Database, https://ned.ipac.caltech.edu/

Navabi M., et al., 2021, Astrophys. J. , 910, 127

Rezaeikh S., Javadi A., Khosroshahi H., van Loon J. T., 2014, Mon. Not. R. Astron. Soc. , 445, 2214

Saremi E., et al., 2020, Astrophys. J. , 894, 135

Saremi E., Javadi A., Navabi M., van Loon J. T., Khosroshahi H. G., Bojnordi Arbab B., McDonald I., 2021, Astrophys. J. , 923, 164

Stetson P. B., 1987, Publ. Astron. Soc. Pac. , 99, 191

Stetson P. B., 1990, Publ. Astron. Soc. Pac. , 102, 932

Stetson P. B., 1994, Publ. Astron. Soc. Pac. , 106, 250

Stetson P. B., 1996, Publ. Astron. Soc. Pac. , 108, 851

Vollmer B., 2013, in Oswalt T. D., Keel W. C., eds, , Vol. 6, Planets, Stars and Stellar Systems. Volume 6: Extragalactic Astronomy and Cosmology. p. 207, doi:10.1007/978-94-007-5609-0˙5

Welch D. L., Stetson P. B., 1993, Astron. J. , 105, 1813

van den Bergh S., 1972, Astrophys. J. Lett. , 171, L31

doi: https://doi.org/10.52526/25792776-24.71.2-383

A Deep Dive into Stellar Populations in M33's Central Region: Near-Infrared Observations and Analysis

Mina Alizadeh*[1,2], Atefeh Javadi[2], Jacco Th. van Loon[3], Yousefali Abedini[1,4], Hedieh Abdollahi[2,5], and Sarina Seifipour[6]

[1]Department of Physics, Faculty of Science, University of Zanjan, 38791-45371, Zanjan, Iran
[2]School of Astronomy, Institute for Research in Fundamental Sciences (IPM), Tehran, 19568-36613, Iran
[3]Lennard-Jones Laboratories, Keele University, ST5 5BG, UK
[4]Center for Research in Climate Change and Global Warming(CRCC), IASBS, Zanjan, Iran
[5]Konkoly Observatory, HUN-REN Research Centre for Astronomy and Earth Sciences, MTA Centre of Excellence, Konkoly-Thege Miklós út 15-17, H-1121, Budapest, Hungary
[6]Department of Physics, Sharif University of Technology, Tehran, 11155-9161, Iran

Abstract

Data collection was conducted using three cameras on the UK Infrared Telescope (UKIRT) from 2003 to 2007. Throughout three nights in August 2005, the UKIRT Fast-Track Imager (UFTI) made K-band observations. The J and H bands Wide Field Camera (WFCAM) data were gathered from 2005 to 2007. Furthermore, from 2003 to 2007, UIST data for the central region of M33 were collected in the K-band. Since luminosity is more closely correlated with birth mass in the latter stages of a star's evolution, we concentrated on these stars. We will combine all the PSF photometry catalogs of the UIST, the UFTI, and the WFCAM to present a novel master catalog of the central square kiloparsec to re-identify the LPV populations. By having more data points for each point source, the probability of detecting more LPVs goes up; also, a period might be derived for some. In addition to that, the SFH will be estimated more accurately by having a larger sample of variable stars.

Keywords: *stars: evolution – stars: long-period variables – stars: luminosity function – stars: mass-loss – galaxies: individual: M 33 – galaxies: central regions – photometry: near-infrared – telescopes: UKIRT*

1. Introduction

Spiral galaxies are among the universe's most significant and expansive structures. With their rotating, gaseous discs and spiral arms, these galaxies are the best targets to understand the galactic structure and stellar population dynamics. In the central region, they contain various stellar components, such as nuclear star clusters, bulges, and bars. However, the factors behind the presence and formation of these structures and spiral arms are not yet fully understood (Javadi et al., 2011a). M33 is one of the three spiral galaxies within the Local Group. Located in the Triangulum constellation, M33 spans approximately a degree across the sky. The inclination angle of 56 ° makes it an excellent candidate for examination of the intricate structure and stellar composition of a spiral galaxy similar to our own (Javadi et al., 2011b). However, compared to our own Milky Way, where the central regions are heavily obscured by the intervening dusty disc, M33 provides a unique opportunity to study a spiral galaxy up close and gain insight into the structure and evolutionary processes of the central regions (Benjamin et al., 2005, van Loon et al., 2003). Galactic evolution is heavily influenced by the final stages of stellar evolution. During these stages, evolved stars lose mass, in which they return enriched and sometimes dusty matter to the interstellar medium (ISM) in addition to energy and momentum (Javadi et al., 2013). These evolved stars, particularly in their later stages, are highly luminous and often among the coolest, which makes them prominently visible at infrared (IR) wavelengths (Javadi et al., 2017). Asymptotic giant branch (AGB) stars and red supergiants have main-sequence masses of up to 30 $M_{\odot}$. In their cooler atmospheres, they have strong radial pulsations. These pulsations make them

*minaalizadah@gmail.com, Corresponding author

doi: https://doi.org/10.52526/25792776-24.71.2-389

identifiable as long-period variables (LPVs) in photometric monitoring campaigns that span months to years (Ita et al., 2004a,b, Whitelock et al., 1991, Wood, 2000). Long-period variable (LPV) stars achieve their maximum luminosity during the final stages of their evolution. This peak luminosity has a direct relationship with their birth mass (Navabi et al., 2021). Consequently, LPV stars allow us to derive the star formation history (SFH) across a broad age range, spanning approximately 30 Myr to 10 Gyr (Marigo et al., 2008). Therefore, star formation history can be derived from the mass function of LPVs, for which, in this work, we check the SFH in the inner square kpc of M33. We can also correlate spatial distributions of LPVs of different masses with galactic structures (spheroid, disc, and spiral arm components) (Javadi et al., 2015, 2017).

Many variability surveys of M33 have been conducted, mostly at optical wavelengths. However, observation cadences have generally been too short to adequately identify LPVs (Javadi et al., 2010). However, in our M33 monitoring project, we attempted to solve this problem by using longer observation periods at different times. We used three cameras at the UK InfraRed Telescope (UKIRT) between 2003 and 2007 to look for LPVs in the central parts of M33. We know that the birth mass of a star is directly related to its brightness when it is nearing the end of its evolution. This region's observations were obtained in three different bands: J, H, and K. Data for the J, H and K bands were collected by the Wide Field Camera (WFCAM) between 2005 and 2007. Additionally, UIST data from 2003 to 2007 were gathered to reach K-band data for M33's central region (Alizadeh et al., 2024).

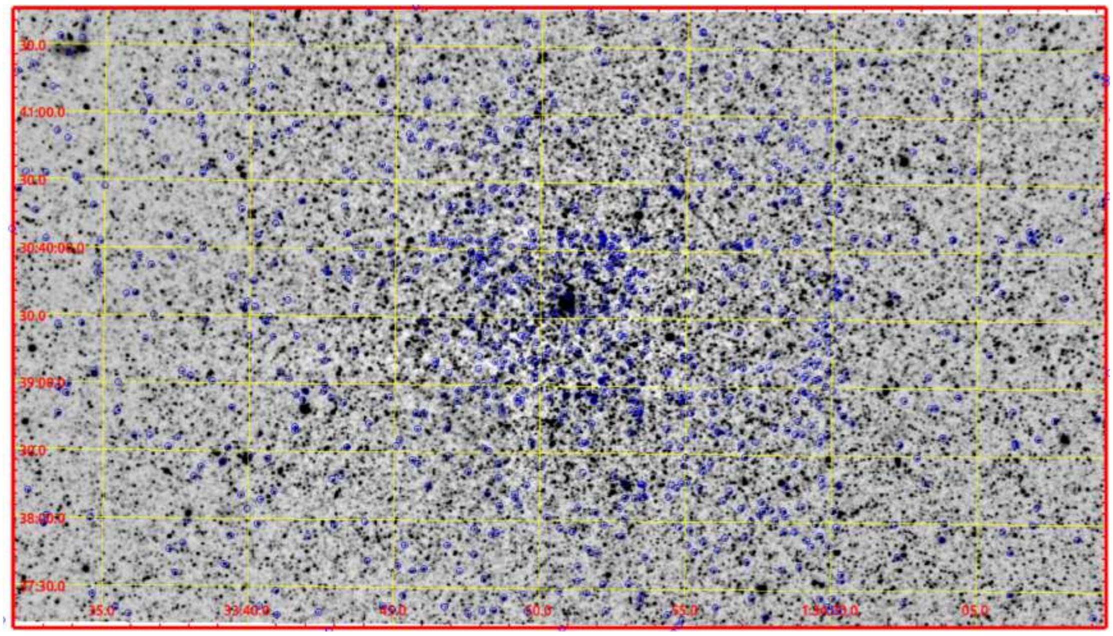

Figure 1. The central region of the M33 with the UIST instrument field of view. Blue circles indicate LPV stars.

2. Data

The data used in this investigation were gathered from three different instruments at the UK Infrared Telescope (UKIRT): the UKIRT Fast-Track Imager (UFTI), the Wide Field Camera (WFCAM), and the UKIRT Imager Spectrometer (UIST). The UFTI conducted K-band observations over three nights in August 2005, enabling high-resolution imaging of M33's center area. A more comprehensive view of star populations may be obtained from the WFCAM data, which were gathered in the J and H bands between 2005 and 2007. This view is further strengthened by the UIST data, which covers the K-band from 2003 to 2007.

Figure 1, shows the M33 galaxy's central region is studied using the UKIRT telescope. This is the field of view of the UIST instrument. Blue circles indicate LPV stars. These datasets work together to provide a thorough analysis of LPV stars, which are essential for comprehending the later phases of a star's life cycle. Previous research by Javadi et al. (2011b) and Saremi et al. (2019) stresses how important it is to combine data from different wavelengths to better understand how stars form in nearby galaxies. Because LPV stars are crucial for monitoring the SFH, we concentrate our inquiry on AGB and red supergiant (RSG) stars

doi: https://doi.org/10.52526/25792776-24.71.2-389

in particular. Point-spread function (PSF) techniques were used to thoroughly calibrate the observational data to ensure precision in photometric measurements. This technique is based on the methods described by Abdollahi et al. (2023) and Javadi et al. (2015), who showed how well infrared measurements work for locating and describing variable stars in the galactic central region. Our objective in using these datasets is to further our understanding of star populations in the center region of M33 and to contribute to broader discussions on galactic evolution.

The AGB stars, classified as LPV pulsating stars, encompass a diverse spectrum of ages, ranging from young stars to those that are significantly older. These stars serve as robust indicators of stellar populations due to their position in the final stages of stellar evolution, where there exists a direct relation between their luminosity and initial mass. As a result, an adequate population of LPVs is essential to derive the SFH of the M33 galaxy. Javadi et al. (2011a) and Saremi et al. (2020).

Owing to the concentration of stars in the M33 galactic central region, photometric technologies capable of determining the stars in this region with great resolution are of interest. Consequently, to enhance the precision of the task, we employed the PSF approach, previously utilized by Javadi et al. (2010). Figure 2 illustrates the differences in magnitude between the WSA (aperture) and DAOPHOT (PSF) photometry, plotted against the WSA magnitude which shows that the PSF photometry has been done with high accuracy.

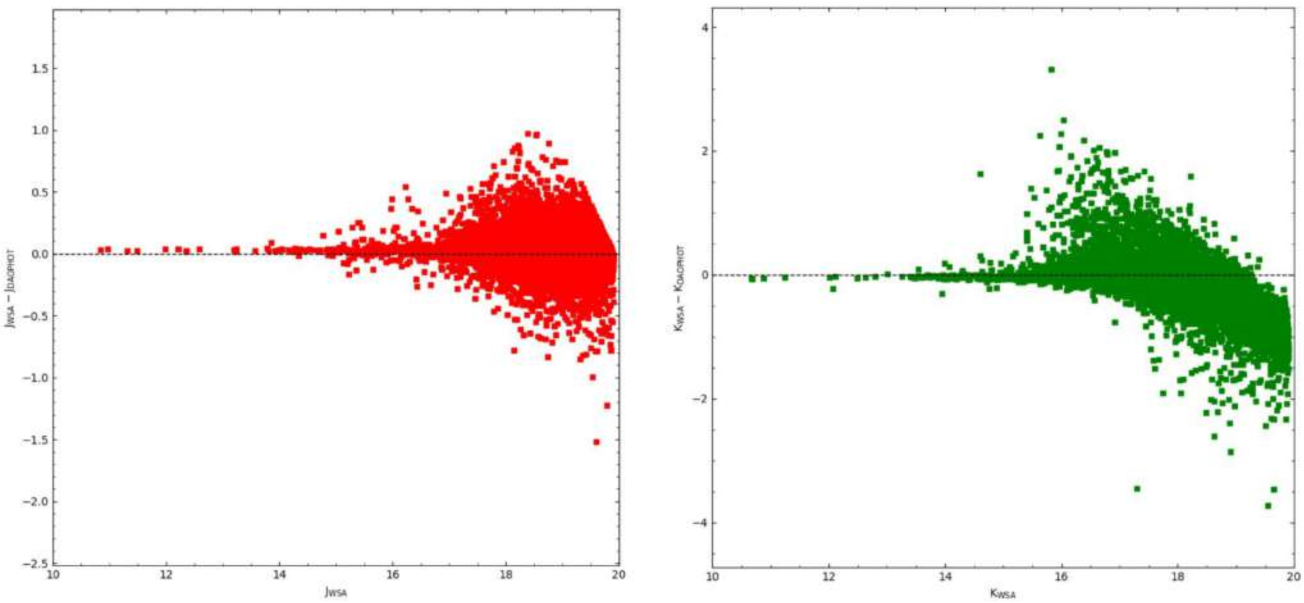

Figure 2. Differences in magnitude between WSA (aperture) and DAOPHOT (PSF) photometry, plotted against WSA magnitude.

3. Methodology

Our approach to studying star formation via isochrone fitting is based on the well-established method described by Javadi et al. (2011b) that has been used to study many galaxies Hamedani Golshan et al. (2017), Abdollahi et al. (2023), Aghdam et al. (2024), Rezai Kh et al. (2014) and Hashemi et al. (2017). To learn more about the SFH of galaxies like M33, we look at LPV stars, especially AGB and RSG stars, which are crucial for finding their paths. We can estimate star formation rates (SFRs) and determine stellar ages by fitting theoretical isochrones from the Padova group (Marigo et al., 2017).

As shown in the work of Saremi et al. (2019, 2020), this method enables us to link the measured luminosities and colors of LPV stars with their evolutionary phases, thus offering insight into the temporal distribution

doi: https://doi.org/10.52526/25792776-24.71.2-389

of star formation activities in the center area of the galaxy. We use an approach that incorporates Kroupa (2001) Initial Mass Function (IMF) to help determine the mass distribution of stars in our sample, ensuring robust findings.

In this investigation, we analyze the mass-loss rates and dust production from evolved stars located within the central square kiloparsec of the galaxy M33. We combine near-infrared (NIR) and mid-infrared (MIR) photometric data using the spectral energy distribution (SED) fitting method to investigate how evolved stars, particularly AGBs and RSGs, contribute to the enrichment of the interstellar medium (ISM). This occurs through their intense mass-loss processes and the subsequent formation of dust production, including carbonaceous and silicate compounds, which are ejected into the ISM via stellar winds. These expelled materials provide essential building blocks for future star and planet formation, highlighting their pivotal role in the chemical and physical evolution of galaxies Javadi et al. (2011b). Some of the UKIRT data that we use to study the SEDs of long-period variable stars are UFTI, WFCAM, and UIST. This plan is based on the work of Javadi et al. (2013), which shows how important dust feedback is in the formation of galaxies.

4. Discussion and On-going Work

In this study, we performed PSF photometry on data collected from the central region of the M33 galaxy using the WFCAM camera. By combining data across different wavelengths, we aim to improve the cadence of observations and accurately identify LPVs. These variables are pivotal for reconstructing the star formation history of the central region of M33, providing insights into the galaxy's evolutionary processes.

Acknowledgements

We thank the staff at UKIRT for their support during the observations. This research made use of the UKIRT Wide Field Camera (WFCAM) and the UKIRT Fast-Track Imager. We acknowledge the support of the Institute for Research in Fundamental Sciences (IPM) and the University of Zanjan.

References

Abdollahi H., et al., 2023, The Astrophysical Journal, 948, 63

Aghdam S. T., et al., 2024, The Astrophysical Journal, 972, 47

Alizadeh M., Javadi A., Van Loon J., Abedini Y. A., Abdollahi H., 2024, in EAS2024, European Astronomical Society Annual Meeting. p. 912

Benjamin R. A., et al., 2005, The Astrophysical Journal, 630, L149

Hamedani Golshan R., Javadi A., van Loon J. T., et al., 2017, Monthly Notices of the Royal Astronomical Society, 466, 1764

Hashemi S. A., Javadi A., van Loon J. T., 2017, arXiv preprint arXiv:1712.05963

Ita Y., et al., 2004a, Monthly Notices of the Royal Astronomical Society, 347, 720

Ita Y., et al., 2004b, Monthly Notices of the Royal Astronomical Society, 353, 705

Javadi A., van Loon J. T., Mirtorabi M. T., 2010, Monthly Notices of the Royal Astronomical Society, 411

Javadi A., van Loon J. T., Mirtorabi M. T., 2011a, Monthly Notices of the Royal Astronomical Society, 411, 263

Javadi A., van Loon J. T., Mirtorabi M. T., 2011b, Monthly Notices of the Royal Astronomical Society, 414, 3394

Javadi A., van Loon J. T., Khosroshahi H., Mirtorabi M. T., 2013, Monthly Notices of the Royal Astronomical Society, 432, 2824

Javadi A., et al., 2015, Monthly Notices of the Royal Astronomical Society, 447, 3973

Javadi A., et al., 2017, Monthly Notices of the Royal Astronomical Society, 464, 2103

Kroupa P., 2001, Monthly Notices of the Royal Astronomical Society, 322, 231

Marigo P., et al., 2008, Astronomy & Astrophysics, 482, 883

doi: https://doi.org/10.52526/25792776-24.71.2-389

Marigo P., et al., 2017, The Astrophysical Journal, 835, 77

Navabi M., et al., 2021, The Astrophysical Journal, 910, 127

Rezai Kh S., Javadi A., Khosroshahi H., et al., 2014, Monthly Notices of the Royal Astronomical Society, 445, 2214

Saremi E., Javadi A., van Loon J. T., et al., 2019, in Proceedings of the International Astronomical Union. pp 125–130, doi:10.1017/S1743921318005574

Saremi E., et al., 2020, The Astrophysical Journal, 894, 135

Whitelock P., Feast M., Catchpole R., 1991, Monthly Notices of the Royal Astronomical Society, 248, 276

Wood P. R., 2000, Publications of the Astronomical Society of Australia, 17, 18

van Loon J. T., et al., 2003, Monthly Notices of the Royal Astronomical Society, 338, 857

doi: https://doi.org/10.52526/25792776-24.71.2-389

Communications of BAO, Vol. 71, Issue 2, 2024, pp. 394-397

Star Formation History of the Local Group Dwarf Irregular Galaxy, NGC 6822

Khatamsaz F. *[1], Abdollahi M. †[1], Abdollahi H. ‡[1], Javadi A.§[1], and van Loon J. Th. ¶[2]

[1]School of Astronomy, Institute for Research in Fundamental Sciences (IPM), Tehran, 19568-36613, Iran
[2]Astrophysics Group, Lennard-Jones Laboratories, Keele University, Staffordshire ST5 5BG, United Kingdom

Abstract

NGC 6822 is an isolated dwarf irregular galaxy in the local group at a distance of ∼ 490 kpc. In this paper, we present the star formation history (SFH) within a field with a radius of ∼ 3 kpc, beyond the optical body of the galaxy (∼ 1.2 kpc). We utilized a novel method based on evolved asymptotic giant branch (AGB) stars. We collected the Near-Infrared data of 329 variable stars, including long-period and -amplitude variables and Carbon-rich AGB stars. We used a stellar evolutionary track and theoretical isochrones to obtain the birth mass, age, and pulsation duration of the detected stars to calculate the star formation rate (SFR) and trace the SFH of the galaxy. We studied the history of galaxy star formation for the mean metallicity value of Z ≈ 0.003. We reconstructed the SFH for two regions: the bar region, a central rectangular area, and the outer region, which covers a circular field beyond the bar region and extends to a radius of 3 kpc. Our results show a significant burst of star formation around 2.6 and 2.9 Gyr ago in the bar and outer regions, respectively. Additionally, we observed a notable enhancement in the SFR in the bar region over the past 200 Myr.

Keywords: *stars: AGB and LPV – stars: formation – galaxies: Local Group: Dwarf Irregular; – galaxies: evolution – galaxies: star formation – galaxies: individual: NGC 6822*

1. Introduction

Investigating the star formation history (SFH) of galaxies provides profound insights into their formation and evolution. NGC 6822 is an isolated dwarf irregular (dIrr) galaxy within the local group, located at a distance of ∼ 490 kpc (Lee et al., 1993; Mateo, 1998) in constellation Sagittarius. The exotic structure of NGC 6822 features a central bright bar, stretching from North to South (Hodge, 1977; Hodge et al., 1991). The central bar is embedded in an HI envelope, extending from the northwest (NW) to the southeast (SE); this central structure is surrounded by a extensive elliptical halo located at a radial distance of ∼ 12 kpc (De Blok & Walter, 2000; Hwang et al., 2005; Zhang et al., 2021). Despite its gas-richness, NGC 6822 has a relatively low metallicity. While a wide range of metallicities have been associated with various ages of the galaxy, the studies by Tolstoy et al., 2001 and Davidge, 2003 reported a mean value of [Fe/H] ≈ −1.00 dex (Z ∼ 0.003), derived based on the red giant branch (RGB) Ca II triplet and the slope of RGB (J, K bands), respectively.

The evolved stellar population of NGC,6822, including the asymptotic giant branch (AGB; Marigo et al., 2008) and the red supergiant (RSG) stars, are excellent implements for tracing SFH over periods ranging from a few million to 10 billion years (Ekström et al., 2013). The significant brightness of AGBs ($\sim 10^3-10^4$ $L_\odot$; Höfner & Olofsson, 2018), along with their radial pulsations, makes these stars conveniently detectable at infrared wavelengths. In this work, we apply a method developed by Javadi et. al. (2011a, 2011b, 2013, 2015) based on AGBs that pulsate with periods longer than 100 days, known as long-period variable (LPV) stars (Iben Jr & Renzini, 1983; Whitelock et al., 2003). The SFH of many nearby galaxies in the LG has been derived utilizing this method (Rezaei kh et al., 2014; Javadi et al., 2016, Javadi et al., 2017;

*fate.khatamsaz@gmail.com, Corresponding author
†m.abdollahi@ipm.ir
‡Hediehabdollahi@ipm.ir
§atefeh@ipm.ir
¶j.t.van.loon@keele.ac.uk

doi: https://doi.org/10.52526/25792776-24.71.2-394

Hamedani Golshan et al., 2017; Hashemi et al., 2019; Navabi et al., 2021; Saremi et al., 2021; Abdollahi et al., 2023; Aghdam et al., 2024); in the following, we will apply this method using the evolved stellar population of NGC 6822 to reconstruct its SFH.

2. Data and Method

The sample used for derivation of the SFH contains the data of 329 evolved stars in J, H, and K_s bands, selected and combined from several catalogs published by Kacharov et al., 2012,Whitelock et al., 2013, and Sibbons et. al.(2012, 2015). Most of the stars in the sample, including 228 long-period and long-amplitude variables and spectroscopy-confirmed Carbon-rich AGB stars, are distributed within the bar region. This region is defined as a rectangular area of 9×21 arcmin^2, situated in the center of the galaxy. Meanwhile, the remaining 101 stars are only spectroscopy-confirmed Carbon-rich AGBs dispersed beyond the bar region, extending up to a radius of 3 kpc, which we refer to as the outer region throughout this paper. We must note that due to insufficient available data, the outer region stars are solely spectroscopy-confirmed Carbon-rich AGBs. As a result, this limitation restricts and narrows the age range of the derived SFH associated with this area.

In order to obtain the SFH, we calculated the star formation rate (SFR), $\xi(t)$ ($\mathrm{M}_\odot\,\mathrm{yr}^{-1}$), which is defined as the mass of gas that has converted into stellar mass over a specific time interval. To do so, we used the Padova stellar evolutionary tracks and isochrones (Marigo et al., 2008, 2017), assuming constant metallicities, to relate the magnitude of each star to its birth mass. Similarly, we obtained the age and pulsation duration (when LPVs are in pulsating phase). Subsequently, we sorted the stars based on age and divided them into several bins. Then, we derived the SFR for each bin, with its associated age and mass range, using the following relation:

$$\xi(t) = \frac{\int_{\mathrm{min}}^{\mathrm{max}} f_{\mathrm{IMF}}(m)\, m\, \mathrm{d}m}{\int_{m(t)}^{m(t+\mathrm{d}t)} f_{\mathrm{IMF}}(m)\, \mathrm{d}m} \, \frac{\mathrm{d}n'(t)}{\delta(t)}, \tag{1}$$

where the m is mass, $\mathrm{d}n'$ is the number of observed LPVs in each bins, $\delta(t)$ is the pulsation duration, and f_{IMF} is the initial mass function (IMF) (Kroupa, 2001). We also consider a statistical error for each bin, derived based on the Poisson statistics:

$$\sigma_{\xi(t)} = \frac{\sqrt{N}}{N}\, \xi(t), \tag{2}$$

where N is the number of LPVs in each bin.

3. Results

We calculated the SFRs in two regions of NGC 6822: the bar region and the outer region, using the method and the dataset explained in Section 2. Furthermore, we assumed that the metallicity remained constant over time and derived the SFH adopting the mean metallicity of [Fe/H] $= -1.05$ dex ($Z \approx 0.003$). The model utilized to obtain the parameters required to calculate the SFR was obtained from Khatamsaz et al., 2024 and Khatamsaz et al., in preparation.

The left panel of Fig. 1 shows the results for the bar region. In this area, star formation began as early as ~ 12.7 Gyr ago, with a rate of $1.1 \pm 0.3 \times 10^{-3}$ $\mathrm{M}_\odot\,\mathrm{yr}^{-1}$. Following this, the SFR increases gradually for ~ 10.0 Gyr and peaks at ~ 2.6 Gyr ago, reaching a rate of $5.3 \pm 1.4 \times 10^{-3}$ $\mathrm{M}_\odot\,\mathrm{yr}^{-1}$. The star formation in the bar region then decreases for ~ 1.6 Gyr. However, it has begun to increase once again in the past $\sim$ 1.0 Gyr and experiences a significant enhancement in its rate, reaching the maximum rate of $\sim 17.0 \pm 4.3$ $\times\, 10^{-3}$ $\mathrm{M}_\odot\,\mathrm{yr}^{-1}$ over the past 300 Myr. This rate is in good agreement with the recent SFR of 21.0×10^{-3} $\mathrm{M}_\odot\,\mathrm{yr}^{-1}$ derived by Hodge, 1993 based on the Hα luminosity.

As we mentioned previously, the dataset of the outer region, as defined in Section 2, is limited to Carbon-rich AGB stars. Therefore, our results are confined to the age range of the used sample, which falls within the range of 15.0 Gyr $<$ look-back time $<$ 620 Myr, considering the mean metallicity of $Z \approx 0.003$. The right panel in Fig 1 presents the results for the outer region. Similar to the bar region, the SFR peaks at ~ 2.9 Gyr ago, reaching the maximum rate of $\sim 2.6 \pm 0.8 \times 10^{-3}$ $\mathrm{M}_\odot\,\mathrm{yr}^{-1}$, which is roughly as half as the rate obtained for the same epoch of star formation burst in the bar region. Following this, the SFR

doi: https://doi.org/10.52526/25792776-24.71.2-394

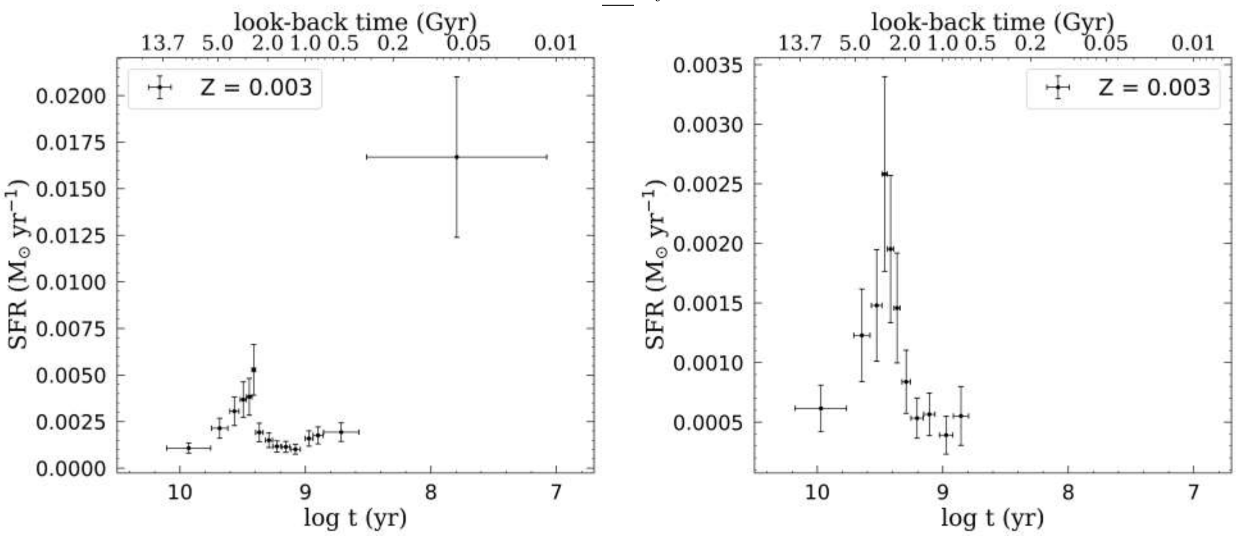

Figure 1. The SFH in NGC 6822 with the adoption of the mean metallicity of Z $\approx$ 0.003. The left panel presents the results for the bar region, and the results for the outer region are displayed on the right panel.

gradually decreases up until $\sim$ 830 Myr ago. However, as mentioned before, due to the limitation of data in the outer region, we cannot retrieve any results for ages younger than $\sim$ 620 Myr ago. Consequently, it remains unclear whether the most recent bin indicates the initiation of a new epoch of star formation similar to the one observed in the bar region.

4. Conclusion

In this paper, we applied a novel method to evolve AGB stars to find the SFH of NGC 6822. Our results show that the SFR in the galaxy has increased significantly during the last 200 Myr in the bar region. Furthermore, star formation bursts and peaks $\sim$ 2.6 and $\sim$ 2.9 Gyr in the bar and outer regions, respectively. The presence of this peak provides evidence for the tidal interaction of NGC 6822 and the Milky Way proposed by Zhang et al., 2021. Furthermore, the non-uniform SFH shows that, despite the noticeable isolation of the galaxy, it has gone under events that triggered the star formation activities. Our upcoming paper on the SFH of NGC 6822 will discuss the subject further and present a new plausible scenario to explain the recent unusual burst of star formation in this galaxy.

References

Abdollahi H., et al., 2023, The Astrophysical Journal, 948, 63

Aghdam S. T., et al., 2024, The Astrophysical Journal, 972, 47

Davidge T., 2003, Publications of the Astronomical Society of the Pacific, 115, 635

De Blok W., Walter F., 2000, The Astrophysical Journal, 537, L95

Efremova B. V., et al., 2011, The Astrophysical Journal, 730, 88

Ekström S., Georgy C., Meynet G., Groh J., Granada A., 2013, EAS Publications Series, 60, 31

Hamedani Golshan R., Javadi A., van Loon J. T., Khosroshahi H., Saremi E., 2017, Monthly Notices of the Royal Astronomical Society, 466, 1764

Hashemi S. A., Javadi A., van Loon J. T., 2019, Monthly Notices of the Royal Astronomical Society, 483, 4751

Hodge P. W., 1977, Astrophysical Journal, Suppl. Ser., Vol. 33, p. 69-82, plates 13-16, 33, 69

Hodge P. W., 1993, ESO Conference and Workshop Proceedings, No. 49, p. 501

Hodge P., Smith T., Eskridge P., MacGillivray H., Beard S., 1991, Astrophysical Journal, Part 1 (ISSN 0004-637X), vol. 379, Oct. 1, 1991, p. 621-630., 379, 621

Höfner S., Olofsson H., 2018, The Astronomy and Astrophysics Review, 26, 1

Hwang N., et al., 2005, Proceedings of the International Astronomical Union, 1, 257

doi: https://doi.org/10.52526/25792776-24.71.2-394

Hwang N., Lee M. G., Lee J. C., Park W.-K., Park H. S., Kim S. C., Park J.-H., 2011, The Astrophysical Journal, 738, 58

Iben Jr I., Renzini A., 1983, IN: Annual review of astronomy and astrophysics. Volume 21 (A84-10851 01-90). Palo Alto, CA, Annual Reviews, Inc., 1983, p. 271-342., 21, 271

Javadi A., van Loon J. T., Mirtorabi M. T., 2011a, Monthly Notices of the Royal Astronomical Society, 411, 263

Javadi A., van Loon J. T., Mirtorabi M. T., 2011b, Monthly Notices of the Royal Astronomical Society, 414, 3394

Javadi A., van Loon J. T., Khosroshahi H., Mirtorabi M. T., 2013, Monthly Notices of the Royal Astronomical Society, 432, 2824

Javadi A., Saberi M., van Loon J. T., Khosroshahi H., Golabatooni N., Mirtorabi M. T., 2015, Monthly Notices of the Royal Astronomical Society, 447, 3973

Javadi A., Van Loon J., Khosroshahi H., 2016, arXiv preprint arXiv:1610.00254

Javadi A., van Loon J. T., Khosroshahi H. G., Tabatabaei F., Hamedani Golshan R., Rashidi M., 2017, Monthly Notices of the Royal Astronomical Society, 464, 2103

Kacharov N., Rejkuba M., Cioni M.-R., 2012, Astronomy & Astrophysics, 537, A108

Khatamsaz F., Abdollahi M., Abdollahi H., Javadi A., Van Loon J., 2024, IAU General Assembly, p. 648

Kroupa P., 2001, Monthly Notices of the Royal Astronomical Society, 322, 231

Lee M. G., Freedman W. L., Madore B. F., 1993, Astrophysical Journal v. 417, p. 553, 417, 553

Marigo P., Girardi L., Bressan A., Groenewegen M. A., Silva L., Granato G. L., 2008, Astronomy & Astrophysics, 482, 883

Marigo P., et al., 2017, The Astrophysical Journal, 835, 77

Mateo M., 1998, Annual Review of Astronomy and Astrophysics, 36, 435

Navabi M., et al., 2021, The Astrophysical Journal, 910, 127

Rezaei kh S., Javadi A., Khosroshahi H., van Loon J. T., 2014, Monthly Notices of the Royal Astronomical Society, 445, 2214

Saremi E., Javadi A., Navabi M., van Loon J. T., Khosroshahi H. G., Arbab B. B., McDonald I., 2021, The Astrophysical Journal, 923, 164

Sibbons L., Ryan S. G., Cioni M.-R., Irwin M., Napiwotzki R., 2012, Astronomy & Astrophysics, 540, A135

Sibbons L., Ryan S. G., Napiwotzki R., Thompson G., 2015, Astronomy & Astrophysics, 574, A102

Tolstoy E., Irwin M. J., Cole A. A., Pasquini L., Gilmozzi R., Gallagher J., 2001, Monthly Notices of the Royal Astronomical Society, 327, 918

Whitelock P. A., Feast M. W., Loon J. T. v., Zijlstra A. A., 2003, Monthly Notices of the Royal Astronomical Society, 342, 86

Whitelock P. A., Menzies J. W., Feast M. W., Nsengiyumva F., Matsunaga N., 2013, Monthly Notices of the Royal Astronomical Society, 428, 2216

Zhang S., Mackey D., Da Costa G. S., 2021, Monthly Notices of the Royal Astronomical Society, 508, 2098

doi: https://doi.org/10.52526/25792776-24.71.2-394

Improving the Efficiency of the AIS System Using Algorithms for Dealing Signal Collisions

S.B. Makarov *[1], S.V. Zavjalov[1], S.V. Volvenko[1], I. Lavrenyuk[1], A.A. Kuznetsova[1], Iu.E. Eremenko[1], A.K. Aharonyan[2], and V.H. Avetisyan[2]

[1]Peter the Great St. Petersburg Polytechnic University, St. Petersburg, Russia
[2]Russian-Armenian University, Yerevan, Armenia

Abstract

The paper considers methods for receiving and processing automatic identification of ships (AIS) signals by a small satellite (CubeSat). A comparison of various methods for reducing the impact of collisions on the reliability of reception is given, such as the choice of orientation and type of the CubeSat receiving antenna, the use of various demodulation algorithms that take into account the presence of Doppler frequency shifts, as well as decollision processing algorithms. Using simulation modeling that takes into account the parameters of the space scenario (orbit altitude, antenna type, etc.), the efficiency of the considered methods in terms of reducing the packet error in the presence of first-order collisions is shown.

Keywords: *CubeSat, AIS, Doppler frequency shift, marine communication systems*

1. Introduction

The growth and development of the domestic segment of small spacecraft have made it possible to form a demand for the creation of a global system for monitoring the activity of marine vessels. To achieve this, it has been proposed to receive and process messages from ground stations on board small satellite (CubeSats).

However, such an application of automatic identification of ships (AIS) is characterized by a high level of signal collisions. In the space segment of AIS, the diameter of satellite coverage is ten times greater than the size of the self-organizing zone of ground stations. At any given time, the input of the receiver may receive messages from several areas that are not in agreement with each other. These messages are not differentiated by the receiver, resulting in a packet collision, which affects the quality of detected messages. This problem is especially significant when trying to receive messages from heavily congested areas and coastal regions. In this regard, studying, evaluating the applicability, and effectiveness of algorithms for de-cluttering AIS signals is a crucial task.

The main purpose of the work was to increase the reliability of receiving messages from the AIS space segment by using decollision processing algorithms. An increase in confidence means a decrease in the packet error rate. It was decided to conduct a comprehensive study of methods for minimizing signal collisions, including: the study of various antennas and their location, algorithms for demodulating AIS signals (according to the degree of complexity: a simple frequency detector, an average receiver based on the Laurent decomposition and the most computationally expensive based on the Viterbi algorithm), as well as the development of an additional decollision algorithm (Colavolpe et al. (2016), Eriksen et al. (2020) Clazzer et al. (2016)).

2. Space AIS Simulation model

To test the effectiveness of the algorithms, an imitation model was developed. The model generates an AIS message flow taking into account the real parameters of the transmitting stations, their location,

*makarov@cee.spbstu.ru, Corresponding author

doi: https://doi.org/10.52526/25792776-24.71.2-398

and location relative to the spacecraft. Radiation timestamps are used to simulate packet collisions. Regarding the space scenario, the model supports loading file or manual adjustment of the spacecraft's orbital parameters. The location of the station relative to the spacecraft makes it possible to take into account the real Doppler displacement, the receiving angle, and the received signal power. The model evaluates the real signal-to-noise value in the AWGN channel, as well as estimates the magnitude of the signal-to-noise of conflicting signals.

The model (see the left top part of Figure 1) is universal, and any parameters can be entered into it. In the right part of Figure 1 is shown the field of view of a spacecraft located in an orbit of 500 km.

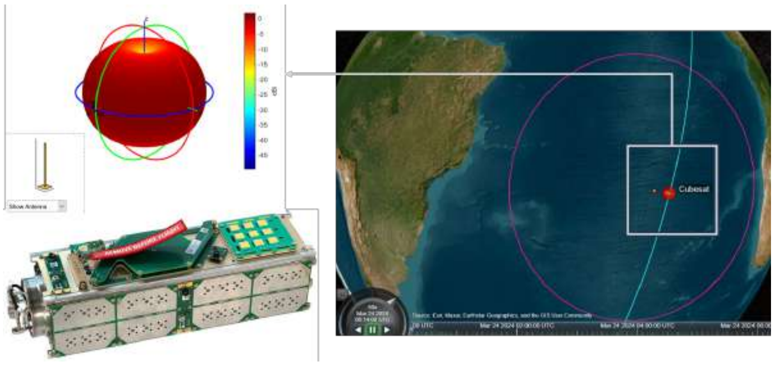

Figure 1. Field of View borders of a spacecraft Polytech Universe-3.

The real power distribution of the received signal in the field of view of the spacecraft for a monopole antenna in the nadir position is shown on the Figure 2. The power of the received signal is calculated using the formula, and depends on the power of the transmitter, the center frequency, the noise coefficient of the receiver, the angle of reception of the signal and propagation losses in free space:

$$(P_R)\text{dB} = (P_T)\text{dB} + (G_T)\text{dB} + (G_R)\text{dB} + (L_s)\text{dB} + (L_a)\text{dB}. \tag{1}$$

were P_R – received signal power in dB, P_T – transmitter power in dB, G_T, G_R– antenna gains, L_s – propagation in free space, L_a – additional loss factor. Propagation in free space could be writte as

$$L_s = \left(\frac{\lambda}{4\pi d}\right)^2. \tag{2}$$

Taken simulation parameters were: transmitter power $P_T = 12$ W, central frequency $f = 162$ MHz, bit rate $R_B = 9600$ bit/s, receiver noise figure 10 dB, receiver attitude: 500 km, antenna type = 'monopole'.

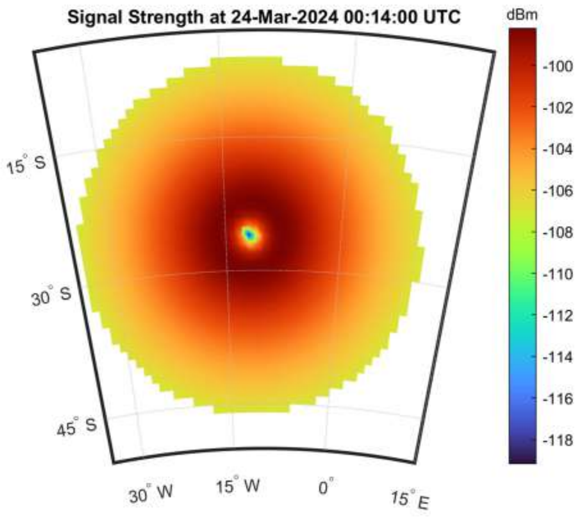

Figure 2. Power distribution of received signals in the spacecraft field of view.

The system does not have the ability to spend resources on accurate frequency and time synchronization, so the implementation of multi-channel processing is necessary. Reception algorithms were analyzed to determine the channel pitch by frequency and character delay.

doi: https://doi.org/10.52526/25792776-24.71.2-398

For a receiver based on the $Viterbi$ algorithm, it was found that for a fixed value of the bit error BER=10^{-3}, a 100 Hz Doppler shift gives a loss of 1 dB. A 1/6 T character synchronization shift gives a loss of 1 dB.

For a receiver based on the $Laurent$ decomposition, with the same bit error of 10^{-3}, a frequency shift of 200 Hz gives a loss of < 1 dB, and a character synchronization shift of 1/6 T gives a loss of 2 dB.

So, depending on the type of demodulator in the receiver circuit, it will be necessary to implement from 6 (for a frequency detector) to 456 (for a receiver based on the $Viterbi$ algorithm) parallel processing channels. Each channel has its own frequency and time delay.

An iterative interference suppression method with repeated modulation was developed as a decollision algorithm (see Figure 3). The input record defines the signal with the maximum power. The signal is demodulated, and the CRC is calculated. If the CRC has converged, then the frequency and time synchronization values corresponding to this channel are saved. The signal is re-modulated and subtracted from the total recording. After that, the operation is repeated for the remaining packet in the record.

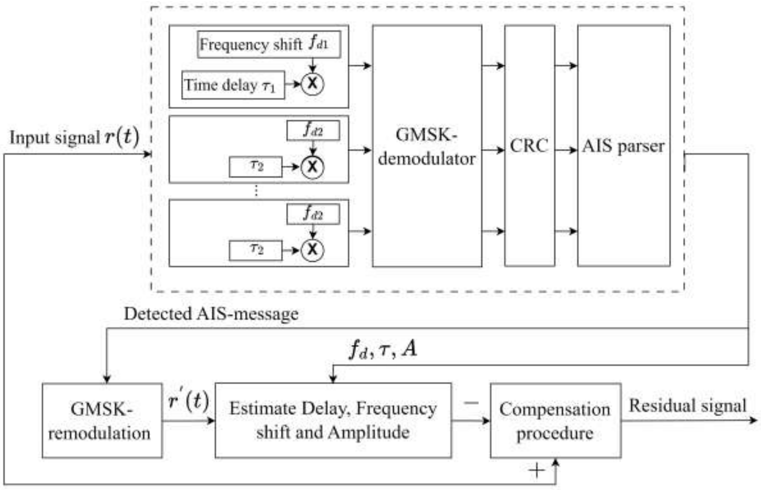

Figure 3. Structural diagram of the parallel demodulator block.

A numerical estimation of the packet error of two conflicting signals was performed depending on the signal-to-noise ratio for different demodulation algorithms with and without the proposed iterative decollision processing. As the signal-to-noise ratio increases, the packet error decreases. The smallest packet error is achieved by the receiver based on the $Viterbi$ algorithm and is equal to 0.22 without decolonizing and 0.09 with decolonizing processing.

A study of the packet error in the case of a collision was conducted depending on the type and orientation of the antenna. The smallest packet error is achieved when the monopole is oriented perpendicular to the spacecraft motion with a pitch angle of 135 or 90 degrees.

The smallest packet error is achieved when the Uda-Yaga antenna is oriented in the nadir position and perpendicular to the motion of the spacecraft with a pitch of 45.

In summary, on average, iterative processing gives a gain of 45%. The transition from the currently implemented frequency detector to more complex receivers gives an increase in correct detection of more than 60%. The smallest packet error is achieved when using a demodulator based on the Viterbi algorithm, however, such an implementation requires the largest number of parallel tuning channels. The orientation of the antenna strongly affects the number of correctly detected messages. The choice in favor of the Uda-Yaga antenna gives an average increase of 15%.

3. Conclusion

The following methods were chosen to study the decollision signal processing in the space segment of AIS: different AIS-demodulators (frequency detector, noncoherent receiver based on Viterbi algorithm, serial receiver based on Laurent decomposition), different receiver antennas: Yagi-Uda and monopole (depending on orientation). An iterative interference cancellation algorithm with signal re-modulation is developed.

A simulation model has been developed that takes into account the orbital parameters of the spacecraft, the characteristics of ground and space antennas, the distribution of ground transmitting stations, and their

doi: https://doi.org/10.52526/25792776-24.71.2-398

radiation power. Using the model and orbital parameters of the Polytech Universe-3 satellite, numerical values of the parameters of the signals arriving at the spacecraft input from the receiver's field of view were obtained for two antennas of the monopole and Yagi-Uda.

The study of applicability of the algorithms showed the need for additional multichannel processing for frequency and time synchronization: for the frequency detector extra 6 channels of processing, for the receiver based on the Loran decomposition - 228, for the receiver based on the Viterbi algorithm - 456 channels.

The average gain from the decollision processing is 45%. For the monopole antenna, the gain for the first packet is 61%, for the second packet by a factor of 12; for the Uda-Yaga antenna, the gain for the first packet is 27%, for the second packet by a factor of 38. The smallest packet error is observed when the monopole is oriented perpendicular to the direction of motion with a pitch of 90 degree and nadir for the Uda-Yaga antenna. The benefit of using the Uda-Yaga antenna is 15%. The receiver based on the Viterbi algorithm has the best packet resolution, with signal-to-interference ratio C/I=12 dB detecting $<$ 90% of the first packets. For the Laurent decomposition based algorithm, $<$ 75% is detected at C/I=12 dB.

Acknowledgements

This work was supported by Ministry of Science and Higher Education of the Russian Federation (state assignment № 075-03-2024-004/5).

References

Clazzer F., Lázaro F., Plass S., 2016, CEAS Space Journal, 8, 257

Colavolpe G., Foggi T., Ugolini A., Lizarraga J., Cioni S., Ginesi A., 2016, International Journal of Satellite Communications and Networking, 34, 57

Eriksen T., Helleren Ø., Skauen A. N., Storesund F. A., Bjørnevik A., Åsheim H., Blindheim E. V., Harr J., 2020, CEAS Space Journal, 12, 503

doi: https://doi.org/10.52526/25792776-24.71.2-398

Combining Bispectral Analysis with the Levenberg–Marquardt Algorithm for Enhanced Non-linear Signal Processing in Astronomy

E. Sivolenko *[1], N. Gasparyan[1], A. Aharonyan[1], V. Avetisyan[1], and M. Vinnichenko[2]

[1]Russian-Armenian University, Yerevan, Armenia
[2]Peter the Great St. Petersburg Polytechnic University, St. Petersburg, Russia

Abstract

The understanding of intricate, non-linear phenomena within astronomical data is pivotal for the progression of our knowledge of the universe. This paper introduces an innovative method that merges bispectral analysis with the Levenberg–Marquardt (LM) algorithm for processing astronomical signals. The LM algorithm is renowned for its effectiveness in non-linear parameter estimation and model fitting. At the same time, bispectral analysis is adept at identifying and measuring non-linear interactions and phase coupling within signals. By integrating these two techniques, our approach facilitates a comprehensive analysis of astronomical signals, encompassing both modeled and unmodeled non-linearities. This integrated methodology is particularly advantageous in fields such as the exploration of pulsars, binary star systems, exoplanet detection, and active galactic nuclei, where non-linear dynamics exert significant influence. The findings illustrate that this collaborative approach amplifies the identification and delineation of non-linear processes, leading to more precise models and profound insights into complex astronomical phenomena.

Keywords: *bispectral analysis, Doppler effect, Levenberg–Marquardt algorithm*

1. Introduction

Astronomical signal processing frequently involves the analysis of complex, non-linear phenomena that arise from the intricate interactions between celestial objects and their environments. Signals originating from sources such as pulsars, black holes, and stellar oscillations often contain subtle modulations and harmonics intricately embedded within background noise. To effectively uncover the hidden dynamics of these signals, the application of advanced processing techniques is crucial.

Bispectral analysis, recognized as a higher-order spectral method, has emerged as a powerful tool for identifying non-linearities and phase coupling in signals. Unlike traditional Fourier-based methods, bispectral analysis emphasizes the interrelationships between frequency components, thereby revealing interactions that linear techniques might overlook. However, extracting precise information from bispectral data requires robust optimization techniques to address the inherent complexity associated with astronomical signals.

The Levenberg–Marquardt (LM) algorithm is a hybrid optimization method that adeptly combines elements of gradient descent and least-squares approaches. Its efficacy in solving non-linear least-squares problems renders it particularly suitable for refining parameter estimates within non-linear signal models. By integrating bispectral analysis with the LM algorithm, researchers can attain enhanced accuracy in characterizing non-linear phenomena in the field of astronomy.

This paper presents an integrated approach that capitalizes on the strengths of both bispectral analysis and the Levenberg–Marquardt algorithm to improve the processing of non-linear astronomical signals. The proposed framework enhances the detection of phase-coupled frequencies and optimizes model parameters, thereby providing fresh insights into complex astrophysical processes [Randall et al. (2016), Smith & Randall (2016), Wang et al. (2019), Sivolenko et al. (2019a), Medvedev et al. (2022)].

*eduard.sivolenko@gmail.com, corresponding author

doi: https://doi.org/10.52526/25792776-24.71.2-402

2. The Micro-Doppler Effect: A Deep Technical Overview

The micro-Doppler effect is a refined aspect of the Doppler effect, focusing on frequency changes due to small-scale motions within a system. Unlike the classical Doppler effect, which looks at overall motion, the micro-Doppler effect results from oscillatory movements of substructures like rotating surfaces or vibrating components. It plays a significant role in astronomy, helping to analyze the dynamics of stars, planetary systems, and compact objects.

For a source moving with velocity v along the observer's line of sight, the observed frequency shift Δf is given by:

$$f_{obs} = f_0 \times \left(1 + \frac{v}{c}\right). \tag{1}$$

Here f_0 – frequency of the emitted wave, v – radial velocity of the source, c – speed of light.

This relationship captures the bulk motion but does not account for internal dynamics, such as rotation or oscillations. For a rotating star, the surface exhibits differential velocities due to rotation. The radial velocity of a point on the star's surface relative to the observer is:

$$v_m\,(t) = R \times \omega \times \sin(\theta) \times \cos(\varphi + \omega \times t). \tag{2}$$

Where R – radius of the star, ω – angular velocity, θ – inclination angle of the rotation axis, φ – the initial phase of rotation. The resulting micro-Doppler shift is:

$$\Delta f_{micro}(t) = f_0 \times \frac{2R \times \omega \times \sin(\theta) \times \cos(\varphi + \omega \times t)}{c}. \tag{3}$$

This produces a periodic modulation in the observed frequency, which can be used to infer the star's rotational parameters and surface features (e.g., star spots).

In pulsating stars, such as Cepheids or RR Lyrae, radial oscillations of the stellar surface generate periodic velocity components:

$$v_m\,(t) = A \times \sin(2\pi \times f_p \times t). \tag{4}$$

Here A – amplitude of oscillation, f_p – frequency of the pulsation. The micro-Doppler shift is:

$$\Delta f_{micro}(t) = f_0 \times \frac{2A \times \sin(2\pi \times f_p \times t)}{c}. \tag{5}$$

This oscillatory modulation is key to asteroseismology, providing detailed information about the star's interior structure and dynamics.

In compact binaries, orbital motion introduces time-dependent micro-Doppler effects. If a binary companion induces oscillations in the primary star's radial velocity, the total velocity becomes:

$$v\,(t) = v_0 + v_{binary}\,(t) + v_{oscillation}(t). \tag{6}$$

Here, $v_{binary}\,(t)$ is the periodic velocity from orbital motion, and $v_{oscillation}(t)$ arises from internal stellar pulsations. The observed frequency shift is:

$$f_{obs}\,(t) = f_0 \times \left(1 + \frac{v_0 + v_{binary}\,(t) + v_{oscillation}(t)}{c}\right). \tag{7}$$

The combined micro-Doppler signature provides a powerful diagnostic of orbital and intrinsic stellar properties.

doi: https://doi.org/10.52526/25792776-24.71.2-402

3. Levenberg–Marquardt algorithm

The Levenberg–Marquardt algorithm (LMA) serves as an optimization technique utilized for addressing non-linear least-squares problems. It is particularly effective in fitting models to data when the models exhibit non-linear dependencies on their parameters. The LMA integrates the gradient-descent method with the Gauss-Newton algorithm, dynamically adjusting between these two methodologies to optimize both convergence speed and robustness.

Mathematical foundation includes non-linear last-squares problem.

$$S(\theta) = \sum_{i=1}^{n} \Big(y_i - f(x_i;\theta) \Big)^2 \tag{8}$$

where $\theta = [\theta_1, \theta_2, ..., \theta_p]$ is a vector of model parameters, $f(x_i;\theta)$ is a non-linear model function, y_i is observed data, x_i is an independent variable. The objective is to find θ that minimizes $S(\theta)$.

Using a first-order Taylor expansion, the model $f(x_i;\theta)$ around an initial estimate θ_k is approximated as:

$$f(x_i;\theta) = f(x_i;\theta_k) + \sum_{j=1}^{p} (J_{ij} \Delta\theta_j) \tag{9}$$

where $\Delta\theta = \theta - \theta_k$, $J_{ij} = \frac{\partial f(x_i;\theta)}{\partial \theta_j}$ is a Jacobian matrix of partial derivatives.

4. Higher Ordered Statistics

The utilization of Higher-Order Statistics (HOS) is essential in the detection of non-Gaussian signals in radar, sonar, and communication systems. Traditional second-order methods, which are based on mean and variance, are not effective in capturing non-Gaussian signals such as radar echoes from clutter and impulsive noise. HOS is instrumental in identifying these challenging signals.

Moreover, higher-order statistics are crucial in system identification, particularly in detecting system non-linearities. They are effective in identifying mechanical faults, such as cracks or misalignments in structures.

Source Separation: HOS methods are employed in blind source separation techniques, facilitating the separation of multiple signal sources in communication systems.

Bispectral and Trispectral Analysis: These analyses are utilized in target detection, non-linear system identification, and vibration analysis, providing a more robust characterization of signals with inherent non-linearities (see Figure 1).

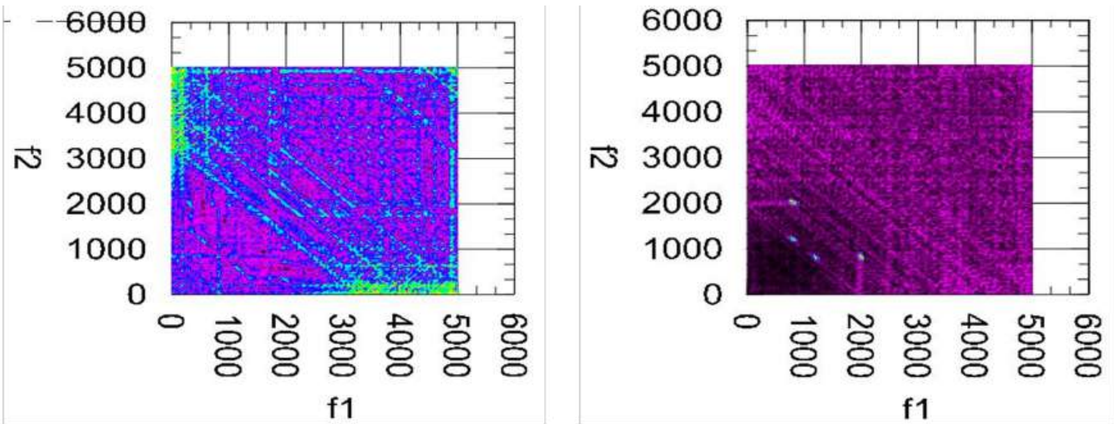

Figure 1. Quadratic phase coupling between frequencies.

With consideration of the bispectrum properties for a real-valued stationary discrete process $\{x^{(m)}(i)\}$ with finite sample number $i = 1, ..., N-1$ and with a finite set of $m = 1, 2, ..., M$ independent realizations $x^{(m)}(i)$ [Grigoryan et al. (2022)]. The autocorrelation function can be written:

doi: https://doi.org/10.52526/25792776-24.71.2-402

$$R_x(k) = \left\langle \sum_{i=0}^{N-1} [x^m(i) - E][x^m(i+k) - E] \right\rangle_\infty \tag{10}$$

where $k = -N+1, ..., N-1$ is shift index, $\left\langle ... \right\rangle_\infty$ denotes ensemble averaging for infinite realization number, i.e. for $M \to \infty$; $E = \left\langle \frac{1}{N} \sum_{i=0}^{N-1} x^m(i) \right\rangle_\infty$ is the mean value; $R_x(0) = \sigma_x^2 = \left\langle \sum_{i=0}^{N-1} [x^m(i) - E]^2 \right\rangle_\infty$ is the variance.

The autocorrelation function is one variable function. Spectral density $P_x(p)$ is defined from the Wiener-Khinchin theorem using direct Fourier transfer:

$$P_x(p) = \left\langle \sum_{k=-\infty}^{k=+\infty} R_x(k) exp(-j2\pi kp) \right\rangle_\infty \tag{11}$$

or by

$$P_x(p) = \left\langle X_{((m)}(p) X^{(*m)}(p) \right\rangle_\infty \tag{12}$$

where $p = -N+1, ..., N-1$ is the frequency sample index; $X_{(m)}(p) \left\langle \sum_{i=0}^{N-1} x^{((m)}(i) exp(-j2\pi ip) \right\rangle_\infty$ is Fourier transform for m-th realization; $*$ is complex conjugation. In equation (3) due to the multiplication of the complex conjugated functions, the phase information is lost.

$R_x(k,l)$ triple autocorrelation function and $\dot{B}_x(p,q)$ bispectrum are functions of two variables, in opposite to autocorrelation function and spectral density. $R_x(k,l)$ the triple autocorrelation function is set as:

$$R_x(k,l) = \left\langle \sum_{i=0}^{N-1} [x^m(i) - E][x^m(i+k) - E] \times [x^m(i+l) - E] \right\rangle_\infty \tag{13}$$

where $k = -N+1, ..., N_1$ and $l = -N+1, ..., N-1$ are the independent shift indexes. Unlike spectral density, $\dot{B}_x(p,q)$ the bispectrum is a complex-valued function of two independent frequencies p and q. It can be written as a 2-D discrete Fourier transform of triple autocorrelation function:

$$\dot{B}_x(p,q) = \left\langle \sum_{k=-N+1}^{N-1} \sum_{l=-N+1}^{N-1} R_x(k,l) exp[-j2\pi(kp + lq)] \right\rangle \tag{14}$$

or as

$$\dot{B}_x(p,q) = \left\langle X^{(m)}(p) X^{(m)}(q) X^{*(m)}(p+q) \right\rangle_\infty \left\langle X^{(m)}(p) X^{(m)}(q) X^{*(m)}(-p-q) \right\rangle_\infty \tag{15}$$

where $\dot{B}_x(p,q) = |\dot{B}_x(p,q)| exp[j\gamma_x(p,q)]$, $\dot{B}_x(p,q)$ and $\lambda_x(p,q)$ are the magnitude bispectrum (bimagnitude) and phase bispectrum (biphase), respectively $p = -N+1, ..., N-1$ and $q = -N+1, ..., N-1$ are the frequency indices. The power spectrum, from (3), is the ensemble averaging of the multiplication of two complex conjugated functions of one variable.

From (15), this bispectrum is a composite average of three complex-valued functions corresponding to different frequency values. As such, spectral density only provides information about amplitude, whereas bispectrum can provide information about phase and amplitude. For one of the main properties, joint phase information storage [Sivolenko et al. (2019b), Peloso & Pietroni (2013), Muthuswamy et al. (1999)], we use bispectral estimation.

5. Main Results

In various scientific disciplines, including astronomy, the complex interactions between celestial phenomena frequently exhibit non-linear characteristics in observational data. Two significant methodologies—bispectral analysis and the Levenberg–Marquardt algorithm (LMA)—provide distinct approaches for identifying and characterizing these non-linearities.

This article accentuates their comparative effectiveness, specifically highlighting scenarios where bispectral analysis encounters limitations (see Fig. 2) and where LMA demonstrates superior performance in detecting Gaussian signals (see Fig. 3).

doi: https://doi.org/10.52526/25792776-24.71.2-402

Table 1. Aspect comparision

Aspect	Bispectral Analysis	Levenberg–Marquardt Algorithm
Signal Type	Periodic, harmonic signals	Any signal with a defined model structure
Gaussian Signals	Ineffective (blind, as in Fig. 1)	Effective (detected in Fig. 2)
Noise Sensitivity	High (struggles with low SNR)	Moderate (handles noise with good models)
Model Dependence	No explicit model required	Requires a well-defined parametric model
Computational Efficiency	Faster (analyzes frequency relationships)	Requires a well-defined parametric model

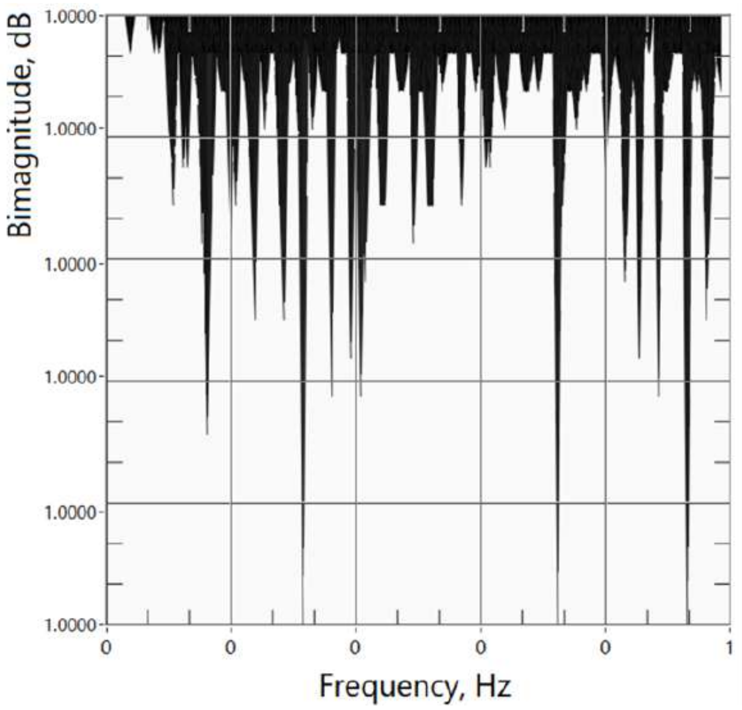

Figure 2. Bispectral analysis of Gaussian signals.

Bispectral Strengths:

- Bispectral analysis is effective for identifying phase coupling and non-linear interactions where specific harmonics interact
- It excels in detecting non-linearities in structured and periodic signals with clear frequency-phase relationships.

Bispectral Blind Spots:

- In cases of Gaussian signals or non-periodic, stochastic non-linearities (as shown in fig.2), the bispectrum often fails because it relies on coherent phase relationships. Gaussian signals, being inherently random, do not produce significant bispectral peaks.
- If the signal-to-noise ratio (SNR) is low, bispectral methods can struggle to extract weak non-linear features buried in noise.

doi: https://doi.org/10.52526/25792776-24.71.2-402

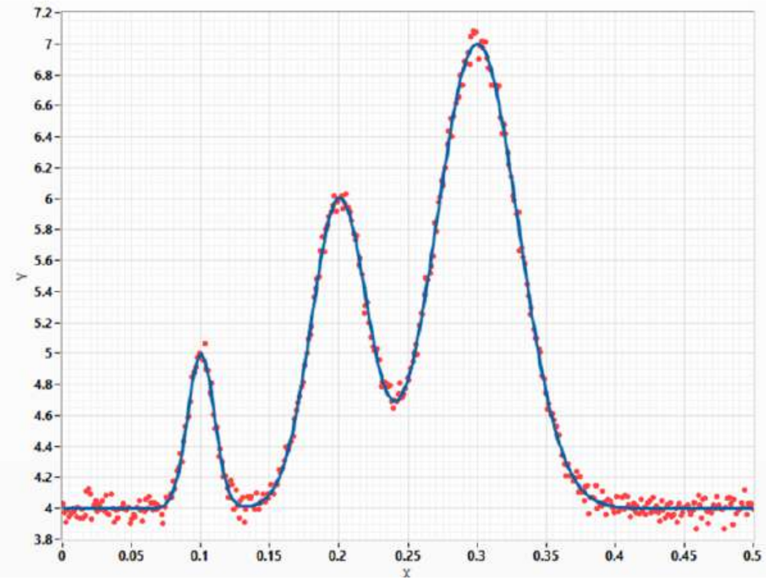

Figure 3. LMA demonstrates superior performance in detecting Gaussian signals.

LMA Strengths:

- LMA, as an iterative optimization tool, can recover non-linear signal parameters even when the bispectrum is ineffective. For instance, Gaussian signals, which appear featureless in bispectral analysis, can still be modeled if a proper parametric model is assumed.
- The LMA can adapt to non-periodic or stochastic non-linearities by fitting a model to data, as illustrated in Fig.3.
- The algorithm's dynamic damping ensures convergence even for highly non-linear problems.

LMA Limitations:

- LMA requires a good initial guess and a well-defined model structure. Without an approximate understanding of the underlying system, the algorithm may converge to a local minimum or fail to provide meaningful results.
- Computationally more expensive compared to the bispectrum, as it involves iterative Jacobian evaluations and matrix inversions. Additionally, the article presents partial code implementations to elucidate these methodologies (see Fig.4.).

6. Conclusion

A comprehensive comparative analysis of bispectral analysis and the Levenberg–Marquardt algorithm elucidates their respective strengths as well as their complementary capabilities in the realm of signal processing. Bispectral analysis is particularly adept at identifying phase-coupled harmonic nonlinearities, which are critical for understanding certain signal characteristics. However, it encounters limitations when tasked with detecting stochastic or Gaussian signals, rendering it less effective in scenarios where such signals are prominent.

In contrast, the Levenberg–Marquardt algorithm is renowned for its robustness and versatility, excelling in the modeling of a wide spectrum of nonlinearities. This algorithm is particularly valuable as it can effectively address complexities that remain undetected by bispectral analysis. By leveraging the strengths of both methodologies, researchers and practitioners can establish a more holistic analytical framework. This integration not only enhances the capability to process and interpret nonlinear signals but also contributes significantly to advancements in fields such as astronomy and various scientific disciplines where nuanced signal characteristics are pivotal.

Ultimately, the combination of bispectral analysis and the Levenberg–Marquardt algorithm presents an enriched toolkit that empowers researchers to undertake comprehensive analyses of nonlinear signals, thereby fostering deeper insights and facilitating progress in their respective fields.

doi: https://doi.org/10.52526/25792776-24.71.2-402

$$y = a_1 e^{-\frac{(x-m_1)^2}{2\sigma_1^2}} + a_2 e^{-\frac{(x-m_2)^2}{2\sigma_2^2}} + a_3 e^{-\frac{(x-m_3)^2}{2\sigma_3^2}} + offset$$

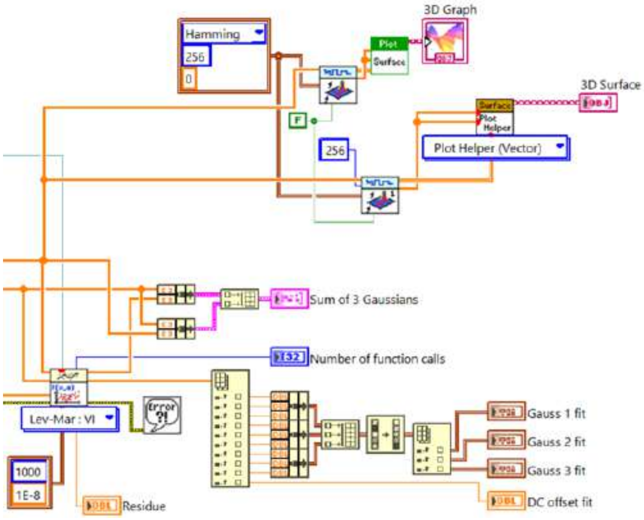

Figure 4. Implemented code in LabVIEW .

Acknowledgments

N.G., E.S., A.A., and V.A. thanks a financial support from the Science Committee of RA, in the frames of the research project 23DP-2B022. M.V. thanks a financial support from the Ministry of Science and Higher Education of the Russian Federation (state assignment 075-03-2024-004/5).

References

Grigoryan M., Sivolenko E., Manasyan A., Aharonyan A., 2022, in International Conference on Microwave & THz Technologies, Wireless Communications and OptoElectronics (IRPhE 2022). pp 22–25

Medvedev A., Temkina V., Makaryan A., Sivolenko E., Hovhannisyan B., Ayvazyan H., 2022, in International Youth Conference on Electronics, Telecommunications and Information Technologies: Proceedings of the YETI 2021, St. Petersburg, Russia. pp 183–190

Muthuswamy J., Sherman D. L., Thakor N. V., 1999, IEEE Transactions on Biomedical Engineering, 46, 92

Peloso M., Pietroni M., 2013, Journal of Cosmology and Astroparticle Physics, 2013, 031

Randall R. B., Coats M. D., Smith W. A., 2016, Mechanical Systems and Signal Processing, 79, 3

Sivolenko E., Hovhannisyan B., Medvedev A., 2019a, in 2019 IEEE International Conference on Electrical Engineering and Photonics (EExPolytech). pp 117–119

Sivolenko E., Hovhannisyan B., Medvedev A., 2019b, in 2019 IEEE International Conference on Electrical Engineering and Photonics (EExPolytech). pp 117–119

Smith W. A., Randall R. B., 2016, Mechanical systems and signal processing, 79, 30

Wang Y., Cao J., Xu C., Cheng Y., Cheng X., Hao Q., 2019, IEEE Photonics Journal, 11, 1

doi: https://doi.org/10.52526/25792776-24.71.2-402

Communications of BAO, Vol. 71, Issue 2, 2024, pp. 409-411

Techniques for Locating GPS Jammers using GNU Radio

M. Sahakyan[1], V. Mkhoyan[1], E. Sivolenko[2], B. Hovhannisyan[2], A. Aharonyan *[2], and S. Makarov[3]

[1]Yerevan State university, Yerevan, Armenia
[2]Russian-Armenian University, Yerevan, Armenia
[3]Peter the Great St. Petersburg Polytechnic University, St. Petersburg, Russia

Abstract

Detecting GPS jammers is crucial for ensuring the integrity and reliability of Global Positioning System (GPS) signals, particularly in environments where jamming devices disrupt navigation and communication systems. These jammers emit radio frequency signals that interfere with legitimate GPS signals, leading to significant disruptions.

To locate these jammers, advanced techniques such as Angle of Arrival (AOA) and Time Difference of Arrival (TDOA) are utilized. AOA uses phased array antennas to determine the direction of the jamming signal, with algorithms like Multiple Signal Classification (MUSIC) and Minimum Variance Distortionless Response (MVDR) enhancing accuracy. TDOA, on the other hand, triangulates the jammer's location by measuring the time difference between signal arrival at multiple sensors.

The integration of unmanned aerial vehicles (UAVs) equipped with directional antennas and sophisticated algorithms further improves the real-time detection of GPS jammers. These UAVs can cover large areas quickly and provide precise bearing measurements, making them invaluable in both military and civilian applications.

Keywords: *GPS, Signal analysis, Jammer, GNSS, Angle of Arrival*

1. Introduction

The necessity for GPS signal jammers and defense against them has grown in importance in the twenty-first century due to the growing usage of GPS signals for worldwide positioning. Our research's goal was to find solutions for GPS locating and jamming issues. Standard GPS antennas, which normally operate in the L1 band at 1575.42 MHz and the L2 band at 1227.6 MHz (newer satellites also broadcast on L5 at 1176 MHz), are frequently used to record GPS signals. This indicates that noise transmissions in these bands are used by jammers to cause disruption.

Even in the absence of additional noise, the amplitudes of the GPS signal are extremely low, making it difficult for receivers to detect the signal [Ferreira et al. (2020)]. When further noise is added, the combined signal is lost due to amplifier cascades. The receiver system was created and tested using a variety of GPS antenna types in a range of weather and terrain circumstances in order to address this problem. We added more noise after making sure that signal detection was reliable enough. The noise was removed from the signal using signal processing techniques and mathematical modifications.

2. Methodology

Several crucial elements were included in the process for identifying and preventing GPS jamming: - Signal Acquisition: We recorded live raw GPS signals using the GPS antennas and USRP N310 receivers. Following digitization, the signals were fed into the processing chain of GNU Radio.

Pre-processing: The first step in signal pre-processing was to improve the signal-to-noise ratio (SNR) and filter out noise. In order to separate the authentic GPS signals from any jamming sources, this step was essential.

*aharon.aharonyan@rau.am, corresponding author

doi: https://doi.org/10.52526/25792776-24.71.2-409

- Jammer Detection: To identify and localize jamming signals, sophisticated algorithms like MUSIC and MVDR were used. The system triangulated the jammers' position by examining the angle of arrival (AOA) and time difference of arrival (TDOA).

- Noise Mitigation: After identifying the jamming signals, other signal processing methods were used to lessen their effects. Adaptive filtering and interference cancellation techniques were among them. -Validation: Extensive field testing was used to confirm the efficacy of the system. In order to assess the precision and dependability of jammer identification and mitigation, the processed signals were compared with ground truth data.

3. Test Setup

We used a thorough test setup that included both hardware and software components to solve the problem of GPS jamming [Moussa et al. (2019),Ferreira et al. (2022)]. The USRP N310, a versatile software-defined radio (SDR) platform with high-fidelity signal processing capabilities and the ability to handle a wide range of frequencies, served as the main piece of hardware in our configuration. With a frequency range of 10MHz to 6GHz and a bandwidth of up to 100MHz, the device can acquire the required signals without experiencing any overflows or underruns due to its 16-bit ADC and 4RX channels. SFP+ 10Gigabit connectors have been used to link it to the host computer. Figure 1 depicts the test configuration.

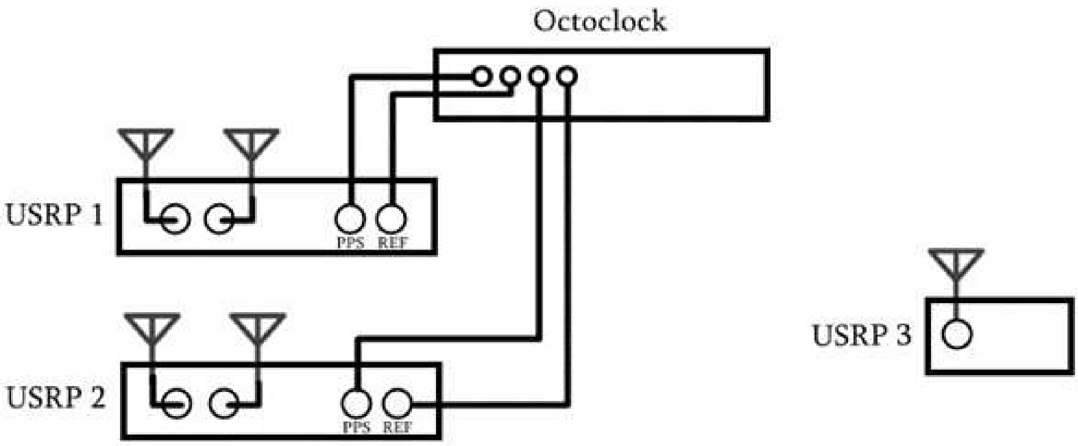

Figure 1. Test Setup: USRP N310s connected to the clock source for receiving external clock and PPS signal for synchronization. USRP N210 used as a jammer.

The software backbone of our system was GNU Radio, an open-source toolkit that allows the development of highly customized signal processing flows. The application is shown in Figure 2. Here

1) USRP Source Configuration: A block called USRP Source is used in the first phase of our signal processing loop. Through the use of the UHD driver, this block connects to our USRP hardware and sets it up to function at the L1 frequency band (1575.42 MHz) with a bandwidth of 200 kHz.

2) Phase Difference Detection: The next step involves processing the three-channel signal that was obtained in order to identify the phase difference between the receivers.

3) Angle and Distance Calculation: To determine the target's angles and distances from our system, a specially designed Python block is used.

4) Data Visualization: Visualizing the processed data is the last step in our procedure.

To make sure the system was reliable, tests were carried out in various terrains and weather situations. This covered rural, suburban, and urban environments, each of which presented different difficulties in processing and detecting signals.

doi: https://doi.org/10.52526/25792776-24.71.2-409

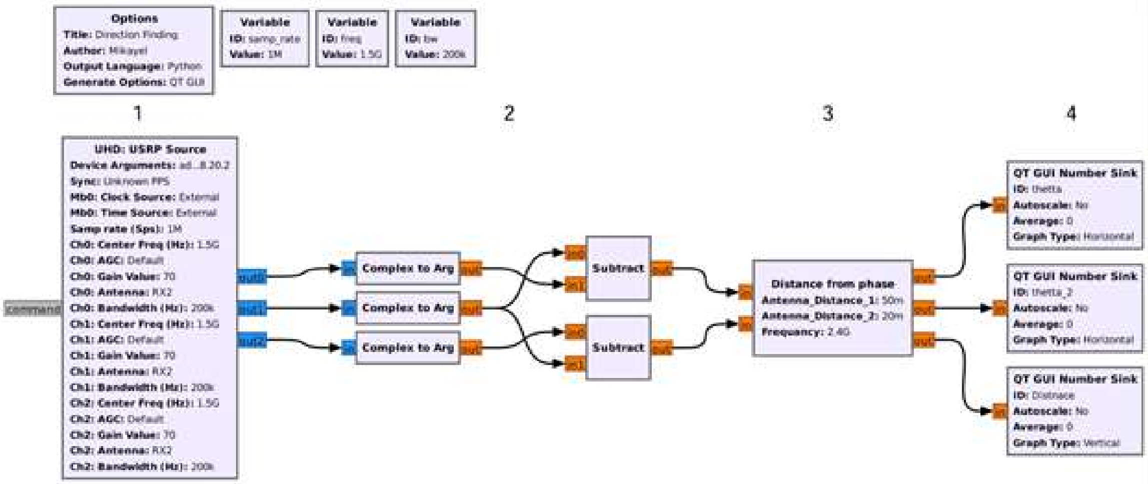

Figure 2. GNU Radio flowgraph.

4. Results

The accuracy of jammer identification was greatly increased by integrating sophisticated algorithms with GNU Radio and USRP N310 receivers. Even under difficult conditions, the system was able to detect jammers with reliability. Following signal processing and computations, Figure 3 shows the results.

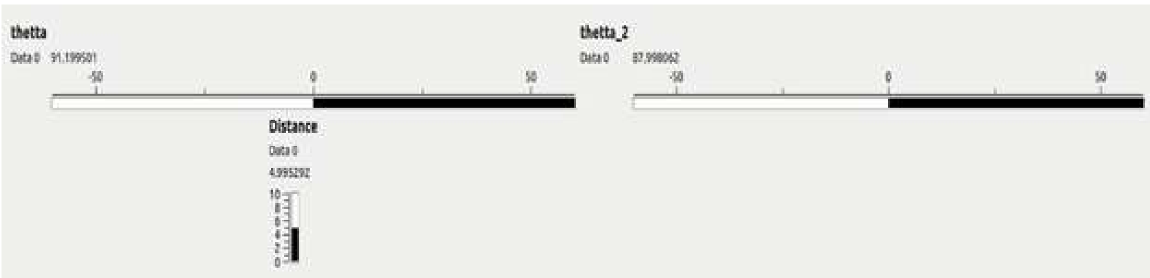

Figure 3. Test results.

5. Conclusion

Maintaining the integrity and dependability of GPS signals requires the detection of GPS jammers, particularly in settings where jamming devices interfere with communication and navigation systems. These jammers cause major disturbances by emitting radio frequency signals that obstruct genuine GPS signals.

Antijamming systems can effectively use sophisticated approaches like the ones we have used to locate these jammers.

Acknowledgements

Authors thank a financial support from the Ministry of Science and Higher Education of the Russian Federation (state assignment 075-03-2024-004/5).

References

Ferreira R., Gaspar J., Sebastiao P., Souto N., 2020, Wireless Personal Communications, 115, 2705

Ferreira R., Gaspar J., Sebastião P., Souto N., 2022, Sensors, 22, 1487

Moussa M., Osman A., Tamazin M., Korenberg M. J., Noureldin A., 2019, Sensors, 19, 5532

doi: https://doi.org/10.52526/25792776-24.71.2-409